Energy, Environment, and Sustainability

Shantanu Bhattacharya
Avinash Kumar Agarwal
Nripen Chanda
Ashok Pandey
Ashis Kumar Sen *Editors*

Environmental, Chemical and Medical Sensors

Springer

Energy, Environment, and Sustainability

This books series publishes cutting edge monographs and professional books focused on all aspects of energy and environmental sustainability, especially as it relates to energy concerns. The Series is published in partnership with the International Society for Energy, Environment, and Sustainability. The books in these series are editor or authored by top researchers and professional across the globe. The series aims at publishing state-of-the-art research and development in areas including, but not limited to:

- Renewable Energy
- Alternative Fuels
- Engines and Locomotives
- Combustion and Propulsion
- Fossil Fuels
- Carbon Capture
- Control and Automation for Energy
- Environmental Pollution
- Waste Management
- Transportation Sustainability

More information about this series at http://www.springer.com/series/15901

Shantanu Bhattacharya · Avinash Kumar Agarwal
Nripen Chanda · Ashok Pandey
Ashis Kumar Sen
Editors

Environmental, Chemical and Medical Sensors

Springer

Editors
Shantanu Bhattacharya
Department of Mechanical Engineering
Indian Institute of Technology Kanpur
Kanpur, Uttar Pradesh
India

Avinash Kumar Agarwal
Department of Mechanical Engineering
Indian Institute of Technology Kanpur
Kanpur, Uttar Pradesh
India

Nripen Chanda
Micro Systems Technology Laboratory
CSIR-CMERI
Durgapur, West Bengal
India

Ashok Pandey
Department of Biotechnology
CSIR-Indian Institute of Toxicology Research
Lucknow, Uttar Pradesh
India

Ashis Kumar Sen
Department of Mechanical Engineering
Indian Institute of Technology Madras
Chennai, Tamil Nadu
India

ISSN 2522-8366 ISSN 2522-8374 (electronic)
Energy, Environment, and Sustainability
ISBN 978-981-10-7750-0 ISBN 978-981-10-7751-7 (eBook)
https://doi.org/10.1007/978-981-10-7751-7

Library of Congress Control Number: 2017961498

Printed on acid-free paper

This Springer imprint is published by Springer Nature
The registered company is Springer Nature Singapore Pte Ltd.
The registered company address is: 152 Beach Road, #21-01/04 Gateway East, Singapore 189721, Singapore

Preface

Energy demand has been rising remarkably due to increasing population and urbanization. Global economy and society are significantly dependent on the energy availability because it touches every facet of human life and its activities. Transportation and power generation are major examples of energy. Without the transportation by millions of personalized and mass transport vehicles and availability of 24×7 power, human civilization would not have reached contemporary living standards.

The first international conference on 'Sustainable Energy and Environmental Challenges' (SEEC-2017) was organized under the auspices of 'International Society for Energy and Environmental Sustainability' (ISEES) by the 'Center of Innovative and Applied Bioprocessing' (CIAB), Mohali, from 26 to 28 February 2017. ISEES was founded at IIT Kanpur in January 2014 with an aim of spreading knowledge in the fields of energy, environment, sustainability and combustion. The society's goal is to contribute to the development of clean, affordable and secure energy resources and a sustainable environment for the society and to spread knowledge in the above-mentioned areas and awareness about the environmental challenges, which the world is facing today. ISEES is involved in various activities such as conducting workshops, seminars, conferences in the domains of its interest. The society also recognizes the outstanding work done by the young scientists and engineers for their contributions in these fields by conferring those awards under various categories.

This conference provided a platform for discussions between eminent scientists and engineers from various countries including India, USA, South Korea, Norway, Malaysia and Australia. In this conference, eminent speakers from all over the world presented their views relating to different aspects of energy, combustion, emissions and alternative energy resource for sustainable development and clean environment through accurate monitoring and control. The conference started with four mini-symposiums on very topical themes, which included (i) New Fuels and Advanced Engine Combustion, (ii) Sustainable Energy, (iii) Experimental and Numerical Combustion and (iv) Environmental Remediation and Rail Road Transport. The conference had 14 technical sessions of topics related to energy and

environmental sustainability and a panel discussion on 'Challenges, Opportunities and Directions of Technical Education and Research in the Area of Energy, Environment and Sustainability' to wrap up the three-day technical extravaganza. The conference included 2 plenary talks, 12 keynote talks, 42 invited talks from prominent scientists, 49 contributed talks and 120 posters. A total of 234 participants and speakers attended this three-day conference, which hosted Dr. V. K. Saraswat, Member, NITI Aayog, India, as a chief guest for the award ceremony of ISEES. This conference laid out the road map for technology development, opportunities and challenges in this technology domain. The technical sessions in the conference included Advances in IC Engines and Fuels; Conversion of Biomass to Biofuels; Combustion Processes; Renewable Energy: Prospects and Technologies; Waste to Wealth—Chemicals and Fuels; Energy Conversion Systems; Numerical Simulation of Combustion Processes; Alternate Fuels for IC Engines; Sprays and Heterogeneous Combustion of Coal/Biomass; Biomass Conversion to Fuels and Chemicals—Thermochemical Processes; Utilization of Biofuels; and Environmental Protection and Health Through Sensory Systems for Monitoring and Control . All these topics have been very relevant for our country and the world in the present context. The society is grateful to Prof. Ashok Pandey for organizing and hosting this conference, which led to the germination of this series of monographs, which included 16 books related to different aspects of energy, environment and sustainability. This is the first time that such a voluminous and high-quality outcome has been achieved by any society in India from one conference.

The editors would like to express their sincere gratitude to the authors for submitting their work in a timely manner and revising it appropriately at short notice. We would like to express our special thanks to Prof. Nripen Chanda, Prof. Ashis Kumar Sen, Dr. Ankur Gupta, Dr. Rishi Kant, Mr. Pankaj Singh Chauhan, Prof. Shantanu Bhattacharya, etc., who have reviewed various chapters of this monograph and provided their valuable suggestions to improve the quality of the manuscripts. We acknowledge the support received from various funding agencies and organizations for successfully conducting the first ISEES conference SEEC-2017, where these monographs germinated. These include Department of Science and Technology, Government of India (special thanks to Dr. Sanjay Bajpai); TSI, India (special thanks to Dr. Deepak Sharma); Tesscorn, India (special thanks to Sh. Satyanarayana); AVL India; Horiba, India; Springer (special thanks to Swati Mehershi); CIAB (special thanks to Dr. Sangwan).

Almost all aspects related to environmental monitoring and control heavily rely on sensory systems which are critical to the maintainability of a good and safe environment with respect to time. This becomes more relevant and an important research theme as environment is being continuously challenged by emission and pollution from power systems, mobility sector, industrial sector, medical sector, etc. In short, wherever there is an issue related to waste management and disposability, the detrimental nature of such waste and their improper management needs to be sustainably monitored. If not monitored and addressed appropriately, such hazards may cause severe challenges for the health and well-being of living systems.

Technology emerged in different length scales has today led to the realization of precise and accurate sensory systems which are easily deployable and rapid in multitasking. In fact, the state-of-the-art research evolved the sensor domain into one where even the very minuscule and trace quantity of an analyte almost up to the level of a single molecule which may otherwise pose an environmental threat can be monitored through sensitive instrumentation and well-thought-out detection scheme.

This monograph is intended for researchers related to sensor design, fabrication and its various applications for the purpose of health and environment monitoring in a very large domain. We hope that the book would be of great interest to the professionals and postgraduate students involved in research related to advanced sensing techniques, fabrications and experimentation. The main objective of this monograph is to promote a better and more accurate understanding of sensing mechanisms and recent progress across all length scales in this domain.

Kanpur, India — Shantanu Bhattacharya
Kanpur, India — Avinash Kumar Agarwal
Durgapur, India — Nripen Chanda
Lucknow, India — Ashok Pandey
Chennai, India — Ashis Kumar Sen

Contents

Part IV Medical Sensors

Editors and Contributors

About the Editors

Prof. Shantanu Bhattacharya is currently a Professor in Department of Mechanical Engineering and also the Head of Design Program at IIT Kanpur, India. He received his BS degree in Industrial and Production Engineering from the University of Delhi, New Delhi, India, in 1996, MS degree in Mechanical Engineering from Texas Tech University, Lubbock, TX, USA, in 2003 and Ph.D. degree in Bioengineering from the University of Missouri, Columbia, MO, USA, in 2006. He served as a Senior Engineer with Suzuki Motors Corporation from 1996 to 2002. He completed his postdoctoral research from the Birck Nanotechnology Center, Purdue University, West Lafayette, IN, USA. He has around 70 international journal publications in areas related to sensor systems, nanotechnology, nanomaterials, advanced functional materials, etc. He serves on the editorial board of several journals. He has been awarded IEI Young Engineer Award in 2010, ISSS Young Scientist Award in 2013, NDRF Design Award from IEI in Mechanical Engineering in 2014 and holds a fellow position of IEI from 2016. His research interests include design and development of microfluidics and MEMS platforms, nanotechnology, nanomaterials, advanced functional materials, sensors for various engineering applications.

Prof. Avinash Kumar Agarwal joined IIT Kanpur in 2001 and is currently a Poonam and Prabhu Goyal Endowed Chair Professor. He was at ERC, University of Wisconsin-Madison, USA, as a Postdoctoral Fellow (1999–2001). His areas of interest are IC engines, combustion, alternative fuels, hydrogen, conventional fuels, lubricating oil tribology, optical diagnostics, laser ignition, HCCI, emission and particulate control and large bore engines. He has published more than 160 peer-reviewed international journals and conference papers. He is Associate Editor of ASME Journal of Energy Resources Technology and International Journal of Vehicle Systems Modelling and Testing. He has edited 'Handbook of Combustion' (5 volumes; 3168 pages), published by Wiley VCH, Germany. He is a Fellow of SAE (2012), Fellow of ASME (2013) and a Fellow of INAE (2015). He is the recipient of several prestigious awards such as NASI-Reliance Industries Platinum Jubilee Award-2012; INAE Silver Jubilee Young Engineer Award-2012; Dr. C. V. Raman Young Teachers Award-2011; SAE International's Ralph R. Teetor Educational Award-2008; INSA Young Scientist Award-2007; UICT Young Scientist Award-2007; INAE Young Engineer Award-2005. He is the recipient of prestigious Shanti Swarup Bhatnagar Award-2016 in Engineering Sciences. He is the first combustion/IC engine researcher to get this honour.

Dr. Nripen Chanda is currently a Senior Scientist at Central Mechanical Engineering Research Institute, Durgapur, India. He has received his Ph.D. degree from IIT Bombay and MS degree from University of Burdwan, West Bengal, India. He has also worked at University of Missouri, Columbia, USA, as Postdoctoral Fellow and a Research Scientist (2007–2012). His research interests are in the areas of micro–nanoscale process technologies, micro–nano systems and devices, lab-on-chip (microfluidics), nanosensors (microfluidics), self-cleaning patterned surfaces, textured solar cell and energy storage applications.

Prof. Ashok Pandey, DPhil, FBRS, FNASc, FIOBB, FISEES, FAMI is Eminent Scientist at the Center of Innovative and Applied Bioprocessing, Mohali, and former Chief Scientist and Head of Biotechnology Division at CSIR's National Institute for Interdisciplinary Science and Technology, Trivandrum. He is Adjunct Professor at MACFAST, Thiruvalla, Kerala, and Kalasalingam University, Krishnankoil, Tamil Nadu. His major research interests are in the areas of microbial, enzyme and bioprocess technology, which span over various programmes, including biomass to fuels and chemicals, probiotics and nutraceuticals, industrial enzymes, solid-state fermentation, etc. He has more than 1150 publications/communications, which include 16 patents, more than 50 books, 140 book chapters, 423 original and review papers, etc., with *h* index of 78 and approximately 25,000 citations (Google Scholar). He is the recipient of many national and international awards and fellowships, which include Fellow of Royal Society of Biology, UK; Academician of European Academy of Sciences and Arts, Germany; Fellow of International Society for Energy, Environment and Sustainability; Fellow of National Academy of Science, India; Fellow of the Biotech Research Society, India; Fellow of International Organization of Biotechnology and Bioengineering; Fellow of Association of Microbiologists of India; Thomson Scientific India Citation Laureate Award, USA; Lupin Visiting Fellowship; Visiting Professor in the Universite Blaise Pascal, France; Federal University of Parana, Brazil; and EPFL, Switzerland; Best Scientific Work Achievement Award, Government of Cuba; UNESCO Professor; Raman Research Fellowship Award, CSIR; GBF, Germany Fellowship and CNRS, France Fellowship; Young Scientist Award, etc. He obtained his honorary doctorate degree from Universite Blaise Pascal, France. He was Chairman of the International Society of Food, Agriculture and Environment, Finland (Food and Health), during 2003–2004. He is Founder President of the Biotech Research Society, India (www.brsi.in); International Coordinator of International Forum on Industrial Bioprocesses, France (www.ifibiop.org); Chairman of the International Society for Energy, Environment and Sustainability (www.isees.org); and Vice-President of All India Biotech Association (www.aibaonline.com). He is Editor-in-Chief of *Bioresource Technology*, Honorary Executive Advisors of *Journal of Water Sustainability* and *Journal of Energy and Environmental Sustainability*, Subject Editor of *Proceedings of National Academy of Sciences, India*, editorial board member of several international and Indian journals and also member of several national and international committees.

Assoc. Prof. Ashis Kumar Sen received his Ph.D. degree from the University of South Carolina, USA, in 2007. Earlier, he received his ME from the Indian Institute of Science, Bangalore, and BE from the National Institute of Technology Rourkela. Before joining IIT, during 2008–2010, he worked as a Microfluidics Engineer at Epigem Ltd, UK, and subsequently as a Research Associate and R&D Engineer at the University of Southampton. His research interests are in the areas of microfluidics, microscale transport phenomena and lab-on-chip development.

Contributors

Avinash Kumar Agarwal Department of Mechanical Engineering, Indian Institute of Technology Kanpur, Kanpur, Uttar Pradesh, India

Ravi Kumar Arun Micro System Technology Laboratory, CSIR-Central Mechanical Engineering Research Institute, Durgapur, India; Academy of Scientific and Innovative Research (AcSIR), CSIR Campus, CSIR Road, Taramani, Chennai, India

Gautam Bacher Department of Electrical and Electronics Engineering, BITS Pilani K.K. Birla Goa Campus, Zuarinagar, Goa, India

Pouriya Bayat Department of Mechanical Engineering, York University, Toronto, ON, Canada

Sunil Bhand Department of Chemistry, Biosensor Lab, BITS Pilani K.K. Birla Goa Campus, Zuarinagar, Goa, India

Geeta Bhatt Microsystems Fabrication Laboratory, Department of Mechanical Engineering, Indian Institute of Technology, Kanpur, India

Shantanu Bhattacharya Microsystems Fabrication Laboratory, Mechanical Engineering Department, Design Program, Indian Institute of Technology Kanpur, UP, Kanpur, India

Pulak Bhushan Microsystems Fabrication Laboratory, Department of Mechanical Engineering, Indian Institute of Technology Kanpur, Kanpur, India

Nripen Chanda Micro System Technology Laboratory, CSIR-Central Mechanical Engineering Research Institute, Durgapur, India

Manosree Chatterjee Micro System Technology Laboratory, CSIR-Central Mechanical Engineering Research Institute, Durgapur, India; Department of Biotechnology, National Institute of Technology, Durgapur, India

Sina Dibaji Department of Mechanical Engineering, York University, Toronto, ON, Canada

Ravindra S. Gaikwad Department of Mechanical Engineering, Department of Electrical Engineering, IIT Madras, Chennai, India

Ankur Gupta School of Mechanical Sciences, Indian Institute of Technology Bhubaneswar, Bhubaneswar, Odisha, India

Namita Jaiswal Micro System Technology Laboratory, CSIR-Central Mechanical Engineering Research Institute, Durgapur, India; Department of Biotechnology, National Institute of Technology, Durgapur, India

Abhiram Hens Micro System Technology Laboratory, CSIR-Central Mechanical Engineering Research Institute, Durgapur, India

Rishi Kant Microsystems Fabrication Laboratory, Mechanical Engineering Department, Indian Institute of Technology Kanpur, Kanpur, Uttar Pradesh, India

Sanjay Kumar Microsystems Fabrication Laboratory, Department of Mechanical Engineering, Indian Institute of Technology Kanpur, Kanpur, India

Nibedita Mahata Department of Biotechnology, National Institute of Technology, Durgapur, India

Dindyal Mandal School of Biotechnology, KIIT University, Patia, Bhubaneswar, Odisha, India

Soumen Mandal Micro System Technology Laboratory, CSIR-Central Mechanical Engineering Research Institute, Durgapur, India; Academy of Scientific and Innovative Research (AcSIR), CSIR Campus, CSIR Road, Taramani, Chennai, India

H. Manisha Nanomaterials Research Laboratory (NMRL), Nano Division—Yenepoya Research Centre, Yenepoya University, Mangalore, India

Kapil Manoharan Microsystems Fabrication Laboratory, Mechanical Engineering Department, Indian Institute of Technology Kanpur, UP, Kanpur, India

Sourav Mishra School of Biotechnology, KIIT University, Patia, Bhubaneswar, Odisha, India

Nagahanumaiah Micro System Technology Laboratory, CSIR-Central Mechanical Engineering Research Institute, Durgapur, India

Peuli Nath Micro System Technology Laboratory, CSIR-Central Mechanical Engineering Research Institute, Durgapur, India; Academy of Scientific and Innovative Research (AcSIR), CSIR Campus, CSIR Road, Taramani, Chennai, India

Chetan A. Nayak Department of Chemical Engineering, BMS College of Engineering, Bengaluru, Karnataka, India

Suraj K. Nayak Rourkela, India

Kunal Pal Rourkela, India

Pramod Pal School of Mechanical Sciences, Indian Institute of Technology Bhubaneswar, Bhubaneswar, Odisha, India

Ashok Pandey Department of Biotechnology, CSIR-Indian Institute of Toxicology Research, Lucknow, Uttar Pradesh, India

Pratyush K. Patnaik Rourkela, India

Amir Reza Peimani Department of Mechanical Engineering, York University, Toronto, ON, Canada

H. N. Pradeep Department of Chemical Engineering, BMS College of Engineering, Bengaluru, Karnataka, India; Department of Chemical Engineering, Dayananda Sagar College of Engineering, Bengaluru, Karnataka, India

K. S. Prasad Nanomaterials Research Laboratory (NMRL), Nano Division–Yenepoya Research Centre, Yenepoya University, Mangalore, India

Nivedita Priyadarshni Micro System Technology Laboratory, CSIR-Central Mechanical Engineering Research Institute, Durgapur, India; Academy of Scientific and Innovative Research (AcSIR), CSIR Campus, CSIR Road, Taramani, Chennai, India

P. D. Priya Shwetha Nanomaterials Research Laboratory (NMRL), Nano Division—Yenepoya Research Centre, Yenepoya University, Mangalore, India

A. Raj Department of Mechanical Engineering, Indian Institute of Technology Madras, Chennai, India

Sirsendu S. Ray Rourkela, India

Pouya Rezai Department of Mechanical Engineering, York University, Toronto, ON, Canada

Anubhuti Saha Microsystems Fabrication Laboratory, Mechanical Engineering Department, Indian Institute of Technology Kanpur, UP, Kanpur, India

A. K. Sen Department of Mechanical Engineering, Indian Institute of Technology Madras, Chennai, India

Ashis Kumar Sen Department of Mechanical Engineering, Indian Institute of Technology Madras, Chennai, Tamil Nadu, India

Ankit Sharma Rourkela, India

Preeti Singh Micro System Technology Laboratory, CSIR-Central Mechanical Engineering Research Institute, Durgapur, India; Academy of Scientific and Innovative Research (AcSIR), CSIR Campus, CSIR Road, Taramani, Chennai, India

Rohit Kumar Singh School of Biotechnology, KIIT University, Patia, Bhubaneswar, Odisha, India

Seemadri Subhadarshini Rourkela, India

Poonam Sundriyal Department of Mechanical Engineering, Indian Institute of Technology, Kanpur, India

D. N. Tibarewala Rourkela, India

Khaled Youssef Department of Mechanical Engineering, York University, Toronto, ON, Canada

Part I
General

Chapter 1
Introduction to Environmental, Chemical, and Medical Sensors

Shantanu Bhattacharya, Avinash Kumar Agarwal, Nripen Chanda, Ashok Pandey, Ashis Kumar Sen, Sanjay Kumar and Poonam Sundriyal

Abstract Sensory systems are available today at all length scales and formulate an important mandate in sustainability of environment and health. They use a wide spectrum of transduction mechanisms and signal conversion approaches with different levels of accuracy and rapidity. Sensors as deployed in various ranges of applications span from relatively simple temperature measurement bimetallic thermocouple structures to the detection of specific entities using advanced physical principles. The best example of sensors emanates from nature itself. Almost all living beings are blessed with sensory systems to sense and act to various environmental stimuli. There is a lot of inferential learning from such systems which can be translated to modern day sensor research. Within the environmental,

S. Bhattacharya (✉)
Department of Mechanical Engineering, Indian Institute of Technology Kanpur Mechanical Engineering, Kanpur, Uttar Pradesh, India
e-mail: bhattacs@iitk.ac.in

A. K. Agarwal
Department of Mechanical Engineering, Indian Institute of Technology Kanpur, Kanpur, Uttar Pradesh, India

N. Chanda
Microsystem Technology Laboratory, CSIR-Central Mechanical Engineering Research Institute, Durgapur, West Bengal, India

A. Pandey
Department of Biotechnology, CSIR-Indian Institute of Toxicology Research, Mohali, Punjab, India

A. K. Sen
Department of Mechanical Engineering, Indian Institute of Technology Madras Department of Mechanical Engineering, Chennai, Tamil Nadu, India

S. Kumar
Microsystems Fabrication Laboratory, Department of Mechanical Engineering, Indian Institute of Technology Kanpur, Kanpur, India

P. Sundriyal
Department of Mechanical Engineering, Indian Institute of Technology, Kanpur 208016, India

S. Bhattacharya et al. (eds.), *Environmental, Chemical and Medical Sensors*, Energy, Environment, and Sustainability, https://doi.org/10.1007/978-981-10-7751-7_1

chemical, and medical domains sensing can be carried out across a variety of length scales like the macroscale, microscale, or nanoscale. In a very organized manner a sensory system can be simplified into an analyte of interest (external to the sensor), a detection element (which is fixated to the sensory surface), a single transduction mechanism (to record measurable signal coming out from the change of analyte concentration), an analyzer and a decision tool. Further, the sensory systems can be using mechanical, microelectronic, micromechanical or electromechanical, optical, electrochemical, colorimetric, and other means to perform rapid sensing in the physical, chemical, and biological types of analytes. This book describes the basic mechanisms, fabrication techniques, and recent advancements in developments related to environmental, chemical, and medical sensors.

Keywords Nanoparticles · Nanofabrication · Impedance sensor
Paper-based sensors · Flexible sensors

We live in an era of persistent and accelerating transformation, driven by demographic, social, and economic development. Every day, there are more of us consuming the limited natural resources of the planet. Our impact on the earth is increasing through urbanization, energy consumption, waste creation, and so on, and this impact is not without consequences. Levels of pollution are cumulative in our environment, with deleterious effects on the health and well-being of living systems. Major changes are observable in our way of life in current times with respect to that in the previous century. This also means that living systems are more and more driven toward increased consumerism and the hunger for more easy and lethargic lifestyles. This has resulted in many consequences like rising public health issues like flabbiness, diseased states with some common recurrents like tumors, clots (atherosclerosis), liver diseases, lifestyle diseases. Coupled to all this is also the increased risk of attack from viruses and other pathogenic biological entities due to mismanagement of the waste mitigated through aids to support the more fashionable lifestyle. Increased life expectancy among living beings places a greater pressure on our healthcare systems as the world's population continues toward a higher average age. Governments are being enforced to amend programs such as home healthcare assistance and also provisions related to real-time threat identification and elimination if necessary at reduced costs. Systems that provide easy access to data on exercise, diet, ambient environment, and so forth, along with intelligent processing and presentation of the data, are critical to supporting viable behavioral change. Technologies such as sensors can give us the tools to help address many of the remarkable global challenges of the twenty-first century. Sensors play a significant role in augmenting safety and improving the quality of life in general. The importance level of such tools gets elevated to several folds when it comes to healthcare sector. A very pertinent example can be sensors which enhance the intelligence of life-supporting implants. They can be used in many different ways that would support a better quality of life for all human beings. In addition, the sensors can be employed for detection of arsenic, heavy metals in

environment, identify advanced symptoms, and avoid severe illnesses through early diagnostics and therapeutics wherever possible.

The recognition of chemical and biological entities is a very important step in biomedical, forensic, and environmental sciences. The generation of extremely sensitive and cost-effective sensors needs sophisticated equipments coupled with basic understanding of chemistry, biology, material science, and engineering. Recognition can be carried out at all different length scales where the domain for most of the attention as of now is at the nanoscale. Nanoparticles especially noble metal nanoparticles (gold and silver) have drawn great attention in this area due to their distinctive physicochemical properties, extremely high surface area, unique electrical or mechanical properties, etc. Nanoscale sensors can be used in constructing innovative identification and transduction processes for chemical and biological sensors. The use of toxic chemicals in traditional synthesis restricts their use in the real samples. Thus, to overcome the limitation green synthetic pathways of nanoparticles have gained tremendous attention, which provide some important features including easy fabrication and high biocompatibility. Herein, potential applications of green-synthesized nanoparticles such as silver nanoparticles, gold nanoparticles, and carbon dots are well visited.

Nanosensors have also been proven to be a powerful tool in sensing various target analytes such as proteins, DNA, RNA, and small molecules like toxins, drugs, metabolites, biomarkers, environmental pollutants with high specificity and selectivity. Among various environmental pollutants, heavy metal pollution is one of the most serious issues in current global scenario because of its potential toxicity toward human and aquatic life. Conventional methods of detecting such toxic ions include inductively coupled plasma mass spectroscopy (ICP-MS) and atomic absorption spectroscopy (AAS). These methods are accurate in trace-level detection, but still possess some drawbacks such as high time consumption, involvement of toxic chemicals, and requirement of sophisticated laboratory setup. Therefore, there is need for low-cost, simple, rapid, and portable methods for detection of these toxic ions. Efforts are being made in developing gold nanosensors for easy monitoring of heavy metal toxins in environmental samples. Due to unique optical, electrical, and mechanical properties, gold nanoparticles render improved performance as sensor probe for better sensitivity, selectivity, portability, and multi-load detection capability. During sensing process, the nanoparticles aggregate in the presence of specific metal ions and show visible color change from red to blue to colorless. The qualitative color change detected using naked eyes shows the presence of targeted heavy metal ions. Apart from the qualitative analysis, the quantitative estimation can be achieved with the help of gold nanoparticles by various techniques such as CCD or CMOS sensors, photodetectors, and color light sensors. Other than the various detection techniques and nano-structured material synthesis, we have also focused on development of smart and thin film flexible sensors for compact sensing devices using inkjet printing and other recent fabrication methods.

This research monograph presents both fundamental science and applied innovations on several keys and emerging technologies involving mechanical, microelectromechanical systems (MEMS), optical, electrochemical, semiconductor, fiber-

optic transducers, colorimetric biosensors. We cover the following specific topics in this manuscript:

- Fabrication of nanostructures with bottom-up approach and their utility in diagnostics, therapeutics, and others;
- Green-synthesized nanoparticles as potential nanosensors;
- Miniaturized sensors and actuators for biological studies on small model organisms of disease;
- Nanoparticles-based diagnostics
- Designing of a low-cost optical density meter for medical applications;
- Low-cost paper analytical devices for environmental and biomedical sensing applications;
- Sensing using microfluidic platform;
- DNA-based sensors;
- The microflow cytometer;
- Gold nanostructure in sensor technology: detection and estimation of chemical pollutants;
- Impedimetric sensors in environmental analysis: an overview;
- Inkjet-printed sensors on flexible substrates;
- Sensors for air monitoring;
- Polymeric-patterned surface for biomedical applications;
- Microfluidic sensors for mechanophenotyping of biological cells;
- Flexible sensors for biomedical application.

The topics are organized into three different sections: (i) environmental sensors, (ii) chemical sensors, and (iii) medical sensors.

This monograph is intended for graduate level researchers, industry professionals and product developers working in the sensor domain. It provides a unique synergy between fabrication protocols and challenges, transduction types and integration, and also for multi domain analytes.

Part II
Environmental Sensors

Chapter 2
Sensors for Air Monitoring

Rishi Kant and Shantanu Bhattacharya

Abstract Monitoring and diagnosis of air quality are essential for providing clean and safe air for breathing. In the current scenario, the air around us contains different types of pollutants such as CO (carbon monoxide), methane (CH_4), sulphur dioxide (SO_2), nitrogen oxides (NO_x), ammonia (NH_3), ozone (O_3), volatile organic compounds (VOCs), heavy metals [Pb (lead), Hg (mercury), etc.] and particulate matter [mixture of suspended particles in air ($PM_{2.5}$ and PM_{10})] leading to severe respiratory disorders within all age groups. These pollutants put threat to life in general by affecting living beings through respiratory system, digestive system, urinary system, nervous system, etc. Thus, it is important that proper diagnostic techniques to be developed for their quick identification and quantification in whole air samples and if possible their immediate remediation through air filtration methods. The present air monitoring stations (comprising sensors) are scattered and fixed in one area which are generally unable to detect most polluted area in one city. So, there is a lot of scope for the development of miniaturized air sensors based on MEMS/NEMS technologies. This chapter presents brief review on MEMS-/NEMS-based air sensors for collecting real-time data in quick time with higher sensitivity and selectivity. Apart from this, a summary of the various technologies like the semiconducting metal oxide, optical, calorimetric, surface acoustic wave, gas chromatography, chemiluminescence is presented in view of air sensor development.

Keywords Air pollutants · Air sensors · Diagnostics · MEMS/NEMS Particulate matter · Human health

R. Kant (✉) · S. Bhattacharya
Microsystems Fabrication Laboratory, Mechanical Engineering Department, Indian Institute of Technology Kanpur, Kanpur 208016, Uttar Pradesh, India
e-mail: dsrishikant@gmail.com

S. Bhattacharya
e-mail: bhattacs@iitk.ac.in

S. Bhattacharya et al. (eds.), *Environmental, Chemical and Medical Sensors*, Energy, Environment, and Sustainability, https://doi.org/10.1007/978-981-10-7751-7_2

1 Introduction

A healthy human inhales around 10^3 L of air every day. The clean air is a basic requirement for the survival of humans in this planet. The current trend of modernization and industrialization of human civilization has led the human life to go into a critical situation as air pollutants are increasing day by day. These air pollutants can go directly into human systems affecting the organs like lungs, kidneys, heart, nervous system. The pollutants can enter into blood–air barrier (alveolar–capillary barrier) creating deleterious effects to the human body which in turn may create respiratory diseases (Beelen et al. 2008), cardiopulmonary mortality (Filleul 2005), asthma exacerbations (Guarnieri and Balmes 2014), etc.

The surrounding air mainly consists of air pollutants like nitrogen oxides (NO_x), ammonia (NH_3), CO (carbon monoxide), methane (CH_4), sulphur dioxide (SO_2), ozone (O_3), cigarette smoke, volatile organic compounds (VOCs) and particulate matter (mixture of suspended particles in air ($PM_{2.5}$ and PM_{10})). Table 1 summarizes the effects of different air pollutants on human health. Since these air pollutants put a threat to human life, so their diagnostics and control become a grand challenge to scientists and technologists. In 2005, World Health Organization (WHO) has released guidelines on these air pollutants which are summarized in Table 1. Through a review conducted by WHO for air quality in 2015, it has been found that 92% of world population is currently living in polluted environment with respect to standard guidelines of the World Health Organization (WHO 2015). We can categorize environmental pollutants based on their physical and chemical characteristics as follows:

(i) Air pollutants (such as NO_x, CO, O_3, VOC, SO_2, CO, NH_3).
(ii) Persistent organic pollutants (such as dioxins).
(iii) Heavy metals [such as Pb (lead), Hg (mercury)].
(iv) Particulate matter (PM) (such as $PM_{2.5}$ and PM_{10}).

We will be focusing on the detection of air pollutants in this particular chapter. Air pollutants' sources and their effect on human body have been summarized in Table 1.

The air monitoring has now been primary task for human beings as air pollution has become threat to the whole human civilization. It is an urgency of today's world to monitor and control air pollutants precisely. For identification and quantification of air pollutants precisely, sensors must have high sensitivity, selectivity, response time, reversibility, low fabrication cost, low energy consumption, portability of instruments, etc. The monitoring of air quality by conventional techniques which commonly utilize networks of air monitoring stations is unable to detect most polluted areas in quick and real time with high sensitivity and specificity which create the need for the evolution of real-time monitoring micro-/nanosystems. Recently, MEMS (microelectromechanical systems)-/NEMS (nanoelectromechanical systems)-based technologies have shown promising outcome for the development of real-time-based sensors for air monitoring (White et al. 2012).

Table 1 Various air pollutants with their effect on human health (Kampa and Castanas 2008), effect on environment, source and WHO guidelines

Air pollutant	Effect on environment	Effect on human health	Source	WHO guidelines
O_3	Greenhouse effect, damaging forest and crop growth	Asthma, pulmonary inflammation, lung disease, etc.	Photochemical reaction of VOC, NO_x and CO under the ultraviolet (UV) light illumination	100 μg/m^3 8-h mean
CO	Causing effect on greenhouse gases	Can cause dizziness, headache, nausea and vomiting	Incomplete combustion of gasoline, charcoal, wood, coal, etc.	10 mg/m^3 24-h mean
NO_2	Causing acid rain and making hazy air	Can damage lung tissue and respiratory organs	Combustion using automobile engines, thermal power plants, chemical refineries, etc.	200 μg/m^3 1-h mean
SO_2	Causing acid rain and deforestation	Nose irritation, shortening of breath, coughing and wheezing, etc.	Combustion of coals and petroleum in power plants, refinery facilities and household fireplaces	20 μg/m^3 24-h mean
NH_3	Causing acidification of groundwater	Burning sensation in nose, throat and respiratory system. Can be cause of respiratory system failure	Agriculture-related chemicals, food industry and by dead animal's body decomposition, etc.	17 mg/m^3 8-h exposure
PM2.5 (particle size less than 2.5 μm)	Causing depletion of nutrients in the soil, acidic rain, etc.	Can damage alveolar wall, lung and throat region of the respiratory track	Soil, rock, emission by automobile and burning plants	25 μg/m^3 24-h mean
PM10 (particle size less than 10 μm)	Harmful to plants and soil, may cause global warming	Bronchitis, lung cancer, asthma and cardiovascular diseases	Construction sites, agriculture, landfills, motor vehicles and waste burning in open environment, etc.	50 μg/m^3 24-h mean

Today, the pervasive air monitoring is being envisioned due to the developments that have taken place in the area of MEMS/NEMS technologies and wireless sensing network. The conventional air monitoring systems have kept challenges as they are bulky in size, remain fixed at one location, and contain heavy weight and higher price. In today's world of extreme human activities, the air monitoring in urban areas requires quick and reliable technological solution which can generate pollution maps in the real time. This enables the people to be more aware of surrounding air condition.

In order to deal emerged problems, the researchers are trying to couple the portable air sensor and wireless sensor network. Combining these two components (portable air sensor and wireless sensor network) enables the person to visualize updated information at every second (Ma et al. 2008). The portability of low-cost

air sensors enables the large-scale arrangement of sensor nodes which in turn increase the spatial and temporal resolution of most polluted areas in the city. The real-time monitoring of air quality with good space and time resolution provides useful information to the people which enable them to take precautions as per their health condition.

In the present chapter, first, we will focus on various MEMS-/NEMS-based technologies that are being utilized for robust air sensor development and their mechanisms for diagnostics of different air pollutants. Further, we will discuss different air pollutant sensors and their capability to detect air pollutants which are presently available in the markets and their limitations.

2 Sensors Based on Various Sensing Techniques

A sensor essentially contains an element which can respond to any alteration in physical/chemical properties. Such response is recorded and then converted in the form of electrical signals with the help of transducers. There exist different techniques for the detection of air pollutants, based on which various sensors can be classified. The different sensor can also be categorized on the basis of sensing materials such as metal oxide semiconductor, nanostructured materials, graphene, carbon nanotube (CNT), polymers, nanofibres. The different sensing techniques can detect air pollutants by measuring the change in electrical conductivity, work function, optical parameters (such as absorption, refractive index, fluorescence, reflection), temperature and the electric current of the sensing material. These techniques have their advantages and disadvantages; for example, metal oxide-based technologies can provide portability to sensor but the same time, they have limitations on sensitivity and selectivity in comparison with optical-based technologies, while optical-based technologies such as Fourier transform infrared spectroscopy (FTIR), differential optical absorption spectroscopy (DOAS), non-dispersive infrared (NDIR) spectroscopy hinder the portability of air sensor. Figure 1 demonstrates various changes happening during sensing of air pollutant by metal oxide-based sensor. The different types of air sensor which can be categorized on the technological basis have been detailed in the following section.

2.1 Semiconducting Metal Oxide Sensors (SMOS)

Sensors based on semiconducting metal oxide find a wide range of applications (such as in automobile, gas sensing, biomedical research, electronic nose). These sensors are suitable candidates for commercialization as they possess high sensitivities, reversibility and have low fabrication cost and also provide ease of portability to instruments. Generally, metal oxide-based sensors include electrodes, sensing elements and the heating elements. For detecting air pollutants, the change

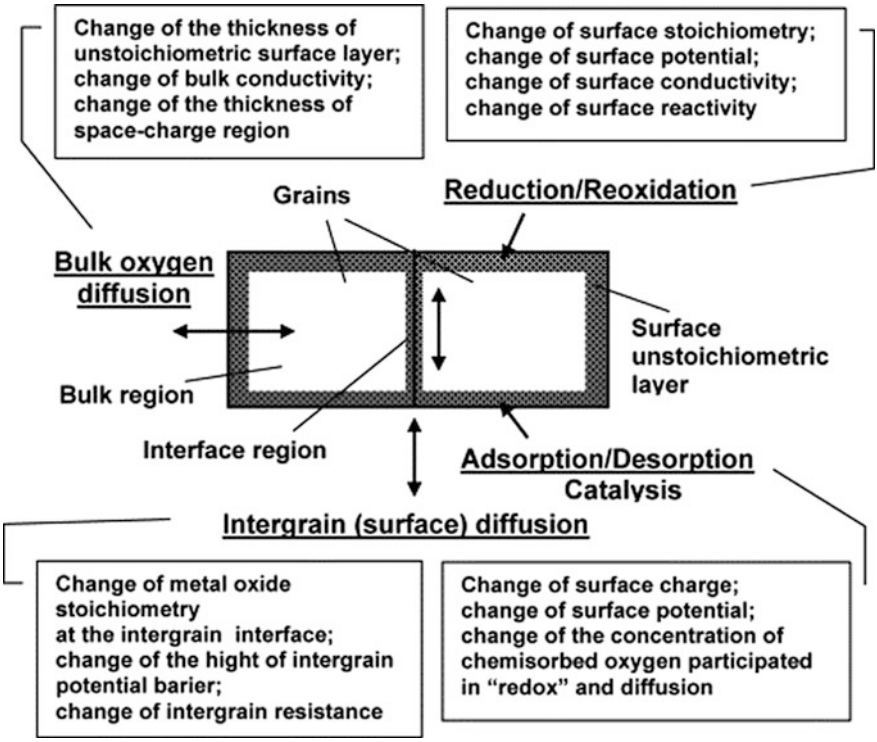

Fig. 1 Changes occurring in semiconductor metal oxides' properties during sensing. Reprinted with permission from Korotcenkov (2007)

of resistance of sensing elements is measured over electrodes. These sensors can perform the detection of air pollutants under adverse environmental conditions.

Their mechanism of sensing can be described in four steps which are as follows:

(i) Pre-adsorption of oxygen on metal oxide surfaces.
(ii) Air pollutant adsorption.
(iii) Adsorbed air pollutant and oxygen reaction.
(iv) Desorption of reaction products of reactions (i.e. previous step).

During above steps, the transfer of electrons between air pollutant and metal oxide yields higher sensitivity of the sensor. When the sensor's surface reacts with air pollutants, its conductivity increases due to the adsorbed surface oxygen which acts as acceptors while a decrease in conductivity of oxygen molecules occurs by virtue of their electron-donating capability (Gardner 1989). In the world of nanotechnology, the characterization of nanostructured metal oxide sensors is being carried out by FET (field-effect transistor), conductometric and impedometric sensors. These nanostructured metal oxides such as TiO_2, Fe_2O_3, GeO_2, MoO_3, Nb_2O_5, CuO, Mn_2O_3, Cr_2O_3, Co_3O_4, Ta_2O_5, La_2O_3 offer their applicability for

sensing of air pollutants by conductive measurements (Kanazawa et al. 2001). In the literature, the numerous work for detecting NO_2 (air pollutants) has been reported by various researchers as NO_2 is considered to be a very dangerous gas for affecting the health of living organisms (Gardner 1989). A sensor based on WO_3 (tungsten oxide) fabricated with thin film deposition techniques (like electrostatic spray) was utilized to detect NO_2 at considerably lower amounts (below 1 ppm) (Ghimbeu et al. 2010). Heidari et al. (2010) reported the synthesis of WO_3 nanoparticles which were deposited over alumina substrates by AC electrophoresis methods. The fabricated sensor shows a response with NO_2 detection limit ($\sim$50 ppb) at 200 °C. ZnO (zinc oxide) has also shown its applicability as a sensing element for NO_2 detection, and the synthesis of ZnO nanopowder was performed by aerosol methods (Baratto et al. 2004). This sensor showed limit of detection for NO_2 up to 0.1 ppm at 200 °C.

Furthermore, there exist a wide variety of air pollutants (NO_2, CO, NH_3, SO_2 and CH_4) sensors which were reported time to time in the literature. They have been summarized in the following section in tabular form (Tables 2, 3, 4, 5 and 6). The tabular form consists of the details about sensing element, fabrication method limit of detection, etc.

In current practice, there has been more attention to explore the possibility of sensing through nanostructured sensing elements such as graphene (Yuan and Shi 2013), ZnO nanobundles (Gupta et al. 2014), TiO_2 (Kirner et al. 1990) to provide a large surface area for coming air pollutant molecules. Recently, inkjet printing has been heavily utilized to fabricate graphene-based flexible NH_3 sensor which contained poly(3,4-ethylenedioxythiophene): poly(styrenesulfonate)-grapheme (PEDOT: PSS) film for sensing. Fig. 2 shows different steps for fabricating graphene-based air sensor which contains (a) an electrode fabrication process, (b) inkjet printing process, (c) deposition of graphene-based sensing film and (d) real picture of the fabricated sensor.

Table 2 Summary of different reported semiconducting metal oxides for NO_2 detection

Sensing element	Fabrication method	Limit of detection/ range (ppm)	References
WO_3	Electrospinning of PVP/TiO_2/Pd composites and calcination	0.8–2.8	Moon et al. (2010)
WO_3	Screen printing	Up to 300	Jo et al. (2009)
ZnO	Hydrothermal	1	Cho et al. (2006)
WO_3	Evaporation of W filament	Up to 1	Meng et al. (2009)

Table 3 Summary of different reported semiconducting metal oxides for CO detection

Sensing element	Fabrication method	Limit of detection/range (ppm)	References
ZnO	Sputtering (via DC magnetron)	1.2–100	Min et al. (2003)
TiO_2	Electrospinning of TiO_2/PVP composites and its calcination	2.6–15	Park et al. (2010)
In/Pd-doped/SnO_2	Solgel	1–10	Zhang et al. (2009b)
ZnO	Evaporation	7.8–100	Lin et al. (1998)
Pt/WO_3	Solgel	1–400	Srivastava and Jain (2008)

Table 4 Summary of different reported semiconducting metal oxides for NH_3 detection

Sensing element	Fabrication method	Limit of detection/range	References
TiO_2	Sputtering (via DC magnetron)	500 ppm	Karunagaran et al. (2007)
CNT/SnO_2	Heat treatment and spin coating	27–200 ppm	Park et al. (2010)
ZnO	Thick films	7.9 ppm	Zhang et al. (2009a)
WO_3	Thick films	0.5 ppm	Sberveglieri et al. (1995)
Graphene	Inkjet printing	25 ppm at room temperature	Seekaew et al. (2014)

Table 5 Summary of different reported semiconducting metal oxides for SO_2 detection

Sensing element	Fabrication method	Limit of detection/range (ppm)	References
WO_3	Pyrolysis	35	Shimizu et al. (2001)
Pt/WO_3	Heat treatment and spin coating	1	
WO_3	Electrostatic spray	3	Ghimbeu et al. (2009)
Ni/SnO_2	Pechini method (based on solgel chemistry)	0.95	Hidalgo et al. (2005)

Table 6 Summary of different reported semiconducting metal oxides for CH_4 detection

Sensing element	Fabrication method	Limit of detection/ range	References
$Pt/SiO_2/SnO_2$	Etching and thin film deposition	100 ppm	Friedberger et al. (2003)
WO_3	Sputtering	0.5 ppm	Sberveglieri et al. (1995)
Pt/SnO_2, Mo/SnO_2, Cu/SnO_2 and Rh/SnO_2	Chemical vapour deposition and evaporation method	NA[a]	Sauvan and Pijolat (1999)

[a]*NA* stands for data not available

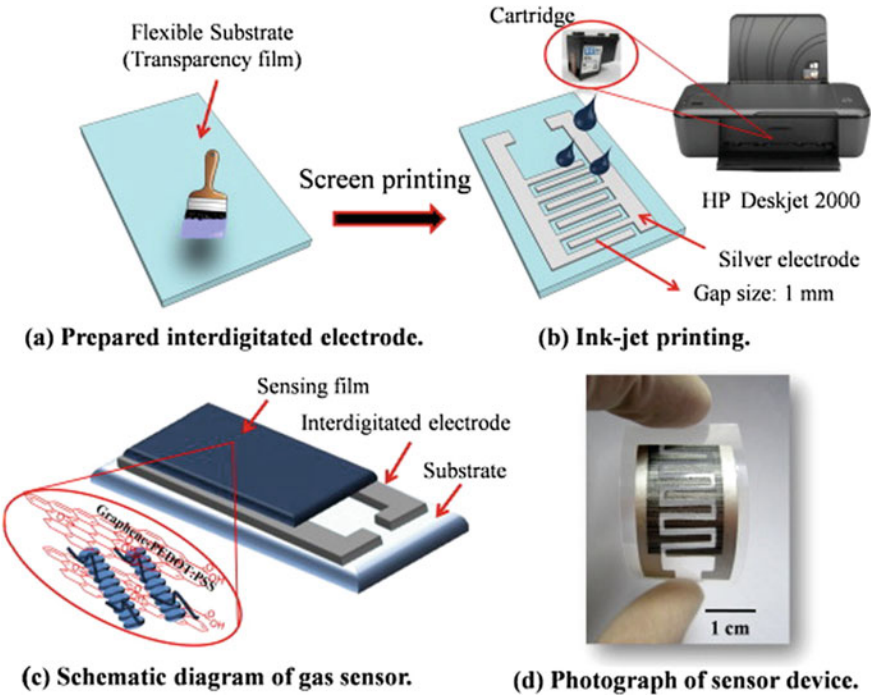

Fig. 2 Schematic representation of steps involving in fabrication of sensor device. Reprinted with permission from Seekaew et al. (2014)

2.2 *Optical Sensors*

Optical sensor majorly utilizes absorption and emission measurement through different techniques such as surface plasma resonance (SPR), differential optical absorption spectroscopy (DOAS), Fourier transform infrared (FTIR) spectroscopy, laser diode absorption spectroscopy (LDAS), cavity ring down spectroscopy

(CRDS), non-dispersive infrared (NDIR) spectroscopy, light detection and ranging (LIDAR), UV fluorescence and chemiluminescence for the detection of air pollutant in air samples. Optical sensors are well known for their selectivity as they do not depend on any chemical reaction or catalytic activity.

Optical detection of air pollutants follows the Beer–Lambert law which is as follows:

$$I = I_0 * e^{-\alpha l}$$

where

I is the light transmitted through the sample, I_0 is incident light, α is absorptivity, l is path length.

The detection of chemical species by spectral transmission method is widely accepted. The detection of air pollutants is realized by utilizing species' optical characteristics such as absorption, Raman scattering. There have been numerous attempts in the literature to carry out optical sensing of air pollutants. Some of them have been discussed below.

Mihalcea et al. (1998) developed a laser diode absorption spectroscopy (LDAS)-based gas sensing system to measure combustion gases (NO, CO, O_2, CO_2 and N_2O). They were able to measure NO in a spectral range 5556–5572 cm^{-1}(at 296° K, 1 atm), N_2O in 6535–6600 cm^{-1} (at 297° K, 272 Torr), H_2O, CO and CO_2 in 6250–6666 cm^{-1} (at 296° K, 1 atm). The limit of detection was found to be 20 ppm for NO, 6 ppm for N_2O, 9 ppm for CO, 7 ppm for CO_2 and 43 ppm for O_2. Archenault et al. reported a low-cost optical fibre chemical sensor for CH_4 gas detection, in which refractive index of medium (acting as the cladding layer) was measured. Their apparatus was able to perform remote sensing of liquid (Archenault et al. 1992). The experimental set-up used by them has been schematically represented in Fig. 3. Further, a sensor based on optical fibre technology was presented, in which the detection of gas and chemical vapours is carried

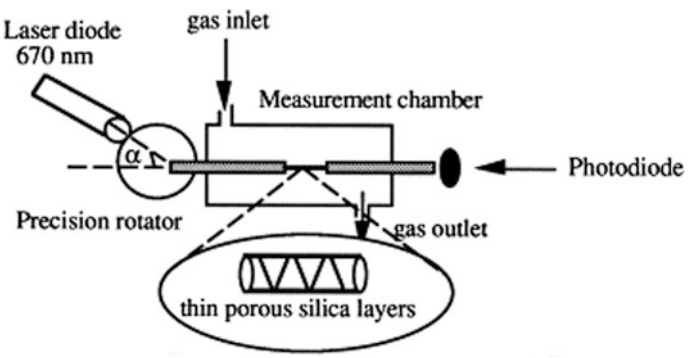

Fig. 3 Schematic representation of used experimental set-up. Reprinted with permission from Archenault et al. (1992)

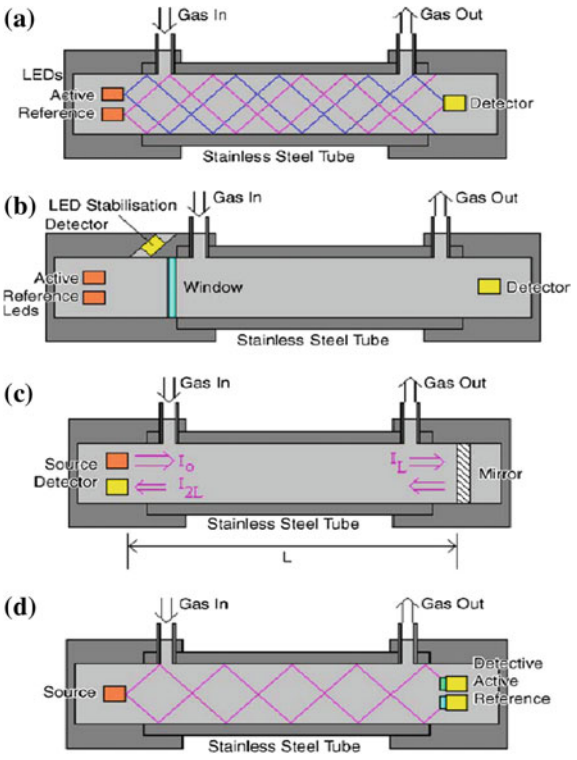

Fig. 4 Different configurations for source and detector of sensor **a** dual source and single detector; **b** dual source and stabilization detector; **c** folded path; **d** single source and dual detector. Reprinted with permission from reference Massie et al. (2006)

out for alkanes and chlorinated hydrocarbons. The detection range varied between 0.6 and 25%. They used a silica fibre with a coating of porous silica fabricated through solgel method (Abdelghani et al. 1997).

For sensing of NH_3, Kondratowicz et al. (2001) demonstrated the detection of ammonia by utilizing electrochromic polymers with fibre optic apparatus in the range of 0–1000 ppm of NH_3 with humidity range (0–100%). Later, Massie et al. presented a portable and low-cost optical sensor for CH_4 sensing with sensitivity up to 1% of the lower limit of exposure (500 ppm). They used near-IR LEDs which were operating on absorption lines of CH_4. They tried different configurations of source and detector in a steel tube (Fig. 4) for getting the enhancement in the sensitivity of the sensor and found out that dual detector system was best suited for providing optimized performance (Massie et al. 2006).

Recently, a LED (light-emitting diode)-based CH_4 gas sensing was performed at minimum explosion limit (4.4 vol.%) (Wittstock et al. 2017). MEMS-based photoacoustic detectors were utilized to monitor methane gas inside an elliptic cell (Fig. 5a). The elliptical cell was designed in such a manner so that whole light could fall (at focal point) onto the detector. The elliptical reflector was made of half ellipsoids which were overlapped (Fig. 5b). The complete sensor design consists of microcontroller coupled with amplifier for controlling LED (mid-IR range), LED

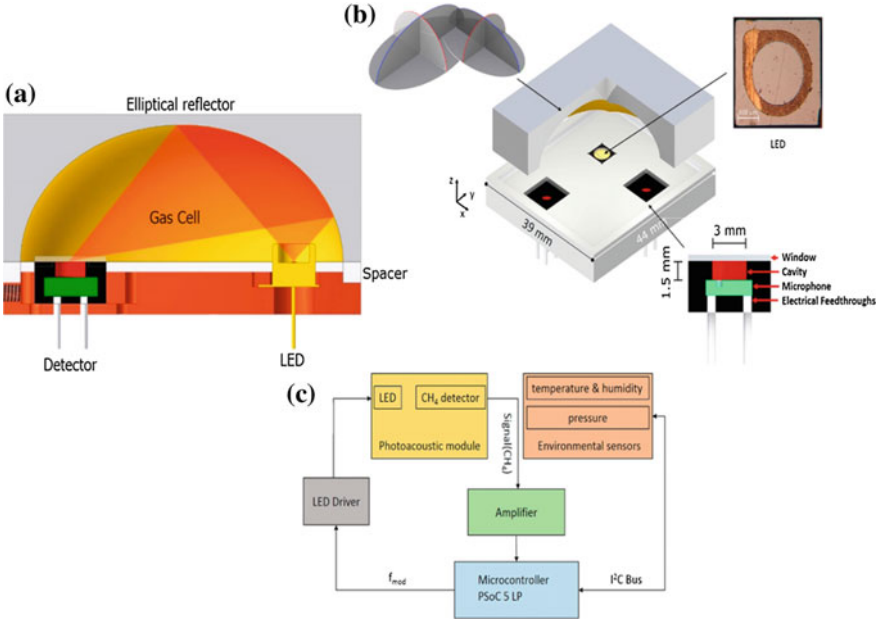

Fig. 5 **a** Schematic representation of single-channel gas sensing set-up of the single-channel sensor set-up for demonstrating focusing of emitted light on photoacoustic detector; **b** schematic representation of sensor design containing photoacoustic detector; **c** schematic diagram for complete set-up consisting of microcontroller, LED driver, photoacoustic detectors and sensors for temperature, humidity, environment and pressure measurements. Reprinted with permission from reference Wittstock et al. (2017)

driver, photoacoustic detectors and sensors for temperature, humidity, environment and pressure measurements (Fig. 5c). The sensor was able to detect methane gas at 2500 ppm detection limit with 12-mm optical path length. The sensor design offered its suitability for working as sensor node in wireless gas sensing network. This would allow real-time monitoring of methane in particular zone of interest.

There have been several other techniques based on optical gas sensors which are utilized for detecting gases like CO_2, CH_4, CO, NO, SO_2, NO_2, N_2O, NH_3 in the literature. A summary has been presented in Table 7, which comprises different techniques, detectable gases and their limit of detection.

2.3 Calorimetric Sensors

The calorimetric sensors utilize change in temperature (due to chemical reaction) of a catalytic surface to perform any sensing event. Their sensing element has the capability to carry out signal transduction, in which any temperature change is converted into readable electrical signals. Even today, these sensors are best suited

Table 7 Summary of different optical detection techniques with their detection capability and limit of detection

Optical detection techniques	Detectable gases	Limit of detection
SPR	N_2, CO_2, NH_3, Cl_2, CH_4, H_2S	N_2, CO_2, NH_3 [$(2 \times 10^{-7}$ (refractive index units)] (Phan et al. 2015), CO_2, NH_3, Cl_2, CH_4, H_2S(10 ppm) (Mishra and Gupta 2015)
LIDAR	O_3, CO_2, NO_2, N_2O, NO, CH_4, H_2S, SO_2	Low ppb range (Bogue 2015)
FTIR	CO_2, CH_4, CO, NO, SO_2, NO_2, N_2O, NH_3,	CO (13 ppb), N_2O (3 ppb), CH_4 (24 ppb) (Grutter 2002)
NDIR	CO_2, N_2O, NH_3, CO and CH_4	CO_2 (70 ppb), N_2O (20 ppb), NH_3 (40 ppb), CO(100 ppm), CH_4 (100 ppm) (Dinh et al. 2016)
CRDS	C_2H_2, CH_4, CO_2, CO, NH_3 and other greenhouse gases	C_2H_2 (0.37 ppbv), CO_2 (10 ppbv), CO (174 ppbv), NH_3 (1.0 ppbv[a]) (He and Orr 2006), CO_2 and other greenhouse gases (Fiddler et al. 2009)
DOAS	NO_2, O_3, SO_2, NH_3 and NO	SO_2 (5 ppb), NH_3 (0.7 ppb), NO (2.8 ppb) (Edner et al. 1993)
LDAS	NO, N_2O, O_2, CO and CO_2	NO (20 ppm), N_2O (6 ppm), CO (9 ppm), CO_2 (7 ppm), O_2 (43 ppm) (Mihalcea et al. 1998), CO (0.1 ppm) (Wang et al. 2000)

[a]*ppbv* parts per billion by volume

for carrying out the measurement of combustion products. A lot of attempts have been made in the development of calorimetric sensors in the literature. Bartlett and Guerin (2003) demonstrated micromachined calorimetric gas sensors for the detection of CH_4, whose detection limit was in the range of 0–2.5%. The sensors were developed using KOH etching route to fabricate the sensor diaphragm made up of a thin Si_3N_4 (silicon nitride) deposited layer which was added through chemical vapour deposition technique (Fig. 6). They utilized surfactant $C_{16}EO_8$ (octaethyleneglycol monohexadecyl ether) and $(NH_4)_2PdCl_4$ (ammonium tetrachloropalladate) for the deposition of a nanostructured palladium thin film electrochemically (Bartlett and Guerin 2003). Later, Park et al. reported a miniaturized calorimetric sensing device for sensing CH_4, H_2 and other mixed gases. They used different catalysts on hot side (Pd/θ–Al_2O_3) and cold side (Pt/α–Al_2O_3) of the device for getting accurate temperature measurements. The sensor had a thermoelectric gas sensing element combined with a catalytic combustion technique (Park et al. 2014).

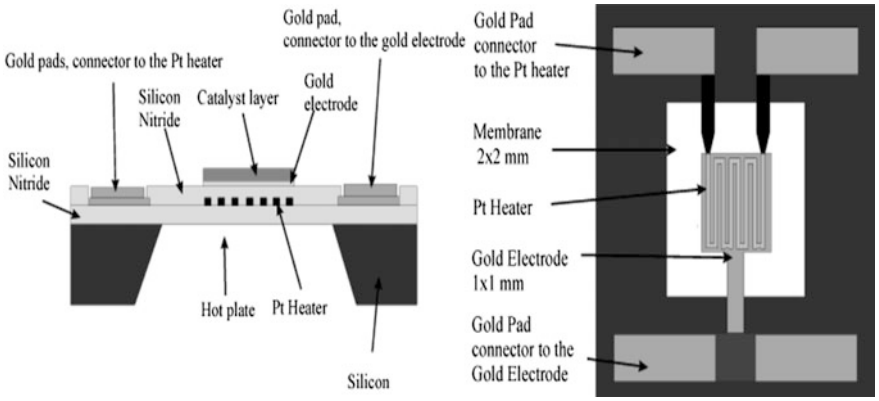

Fig. 6 Micromachined pellistor substrate: cross-sectional image (right side) and top view image (left side). Reprinted with permission from reference Bartlett and Guerin (2003)

2.4 Surface Acoustic Wave-Based Sensors (SAW)

The wave travelling on a material surface which exhibits elastic properties changes the wave properties due to surface adsorption, while the wave reflects off the surface during its traverse. This is generally termed as surface acoustic waves. This phenomenon was first described by Lord Rayleigh. If the absorption of air pollutants by the sensor's thin film occurs during travelling of surface wave in the nearby region then whole wave characteristics changes and this change can be detected with proper instrumentation. Figure 7 shows a schematic piezoelectric substrate on which a thin film of sensor is deposited interacting with the gas molecules. The literature shows that there have been a lot of efforts in the realization of SAW-based gas/air pollutants sensor. Jakubik et al. carried out H_2 detection on a bilayer structure of copper phthalocyanine (CuPc) and a thin palladium (Pd) film using SAW sensors. The working frequency range of the sensor was 200–400 kHz, while oscillator (made of $LiNbO_3$) had frequency range 0.5–43.6 MHz. They were able to detect 0.5–3% hydrogen concentration in nitrogen (Jakubik et al. 2002). Further, Varghese et al. presented a NH_3 sensor by utilizing surface acoustic wave principle. They used alumina nanoporous film to create pores (size 13.6–48 nm) for sensing ammonia

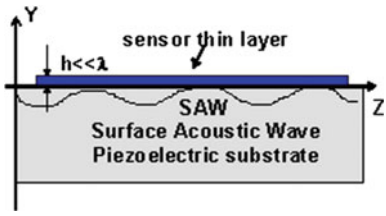

Fig. 7 Principle of surface acoustic wave-based sensor (h—layer thickness and λ—wavelength of travelling wave). Reprinted with permission from Jakubik (2011)

from gas samples. The alumina films were deposited over the surface having travelling wave of frequency 98.5 MHz. They were able to find a frequency shift by 0.001% per ammonia unit percentage increase (Varghese et al. 2003).

2.5 Gas Chromatography (GC)-Based Sensing

The principles of chromatography rely on physical equilibrium between movable sample and stationary phase (solid surface containing particulate). The movable sample can be either gas or liquid. While passing through solid phase, the sample (containing mixture of different components) interacts with stationary phase in different manner which results in the separation of different components (Fig. 8) as each component possesses different distribution coefficients which are the ratio of solute's molar concentration in solid phase to movable phase's molar concentration. Gas chromatography is a most common technique for gas sensing with more sensitivity and selectivity, but still it is at laboratory scale with higher cost.

Although the efforts have been made in the past decade towards its miniaturization, Terry et al. (1979) first presented fabrication of miniaturized GC on silicon wafer with three times size reduction in comparison with laboratory GC. They were able to separate hydrocarbon mixtures within 10 s via thermal conductivity detection system, but detection limit is not high enough as compared to conventional GC instrument. Since then people are trying to fabricate portable GC by utilizing different sensing techniques. In such quest, Zhong et al. (2009) reported a portable GC (Fig. 9) with chemiresistor sensor array for detecting volatile organic compounds (VOCs) mixture (31 different VOCs) in the ppt range. This sensor was able to perform sensing of VOCs within 7 min.

Recently, Akbar et al. (2015) fabricated chip-scale GC (Fig. 10) utilizing MEMS technologies (micropump and valve) for detecting dangerous VOCs (toluene, chlorobenzene, bromobenzene, *p*-xylene, *n*-dodecane, etc.). The miniaturized fabrication contained micromachined separation column (1 m × 190 μm × 240 μm deep with 20 μm circular pillars), sample injection section (2 mm × 250 μm),

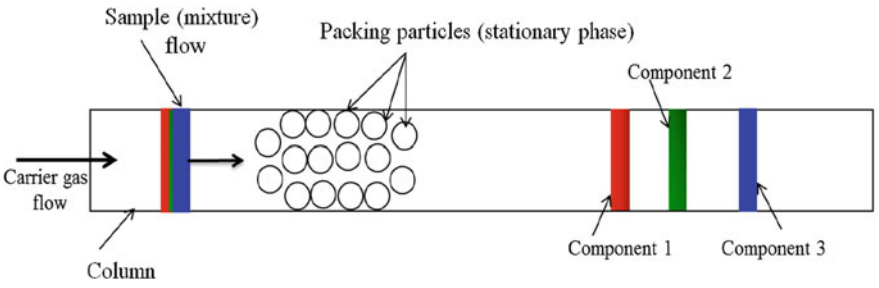

Fig. 8 Schematic representation of basic principle of gas chromatography

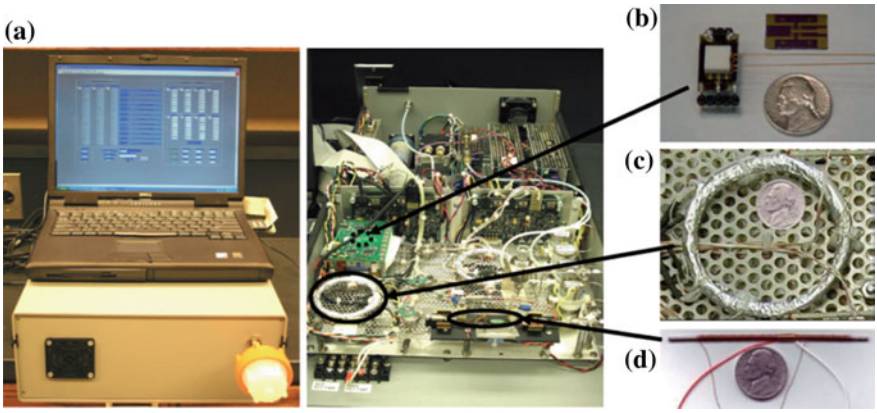

Fig. 9 **a** Portable GC prototype with computer (left) and prototype's cover removed (right); **b** chemiresistive sensor array without assembling in prototype; **c** GC column with heating coil and thermocouple; **d** multistage adsorbent injector with thermocouple and heater. Reprinted with permission from reference Zhong et al. (2009)

microdischarge photoionization detector (μDPID) for helium discharge, T-shaped microchannel, micropump and valves. In order to quantify flow rate fluctuations and estimate loading time (in few seconds), the sample injection unit was characterized in terms of FWHM (full width at half maximum), at different pressure conditions. The μGC laboratory on chip device was able to detect different VOCs (in lower ppm range) having boiling point in a range (110–216 °C) within one minute at optimized flow and temperature conditions. Such robust laboratory on chip device could be directly applied for real-time monitoring of VOCs at industrial or residential sites.

2.6 Chemiluminescence-Based Sensing

The concept of luminescence relies on spontaneous emission of radiation produced from a vibrationally or electronically excited species. Chemiluminescence obtains its energy from the chemical reactions of two chemicals which react to each other to achieve an excited state and emits the light. The popularity of chemiluminescence-based gas sensing is quiet obvious from some of reviews (Aboul-Enein et al. 2000), (Zhang et al. 2005) and (Toda and Dasgupta 2007). The gases such as CO, NO_2, NO, H_2S, Cl_2, NH_3 and gas vapour (acetone, methanol, ethanol, benzaldehyde, acetic acid) can be detective using chemiluminescence-based techniques. Table 8 summarizes detection limit of some gases which can be sensed by chemiluminescence-based techniques.

Further, miniaturization of chemiluminescence-based sensor has been envisioned. In this regard, Gao et al. (2008) have reported microfluidically inspired gas

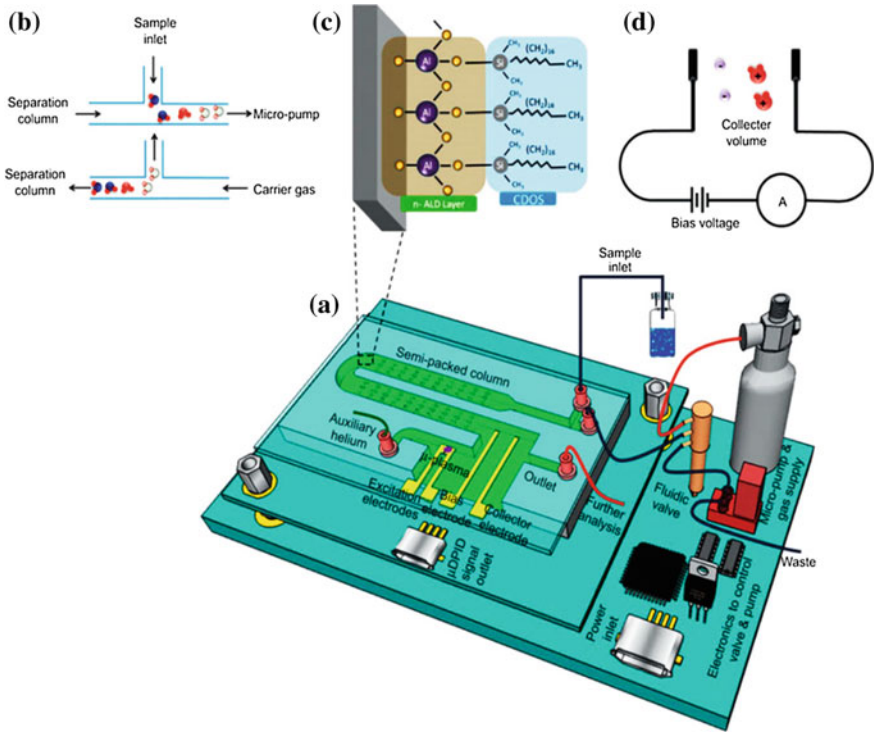

Fig. 10 Schematic representation of miniaturized gas chromatography platform on chip: **a** complete set-up for fluidics (valve and micropump) on chip with carrier gas; **b** loading phase and injection phase; **c** depiction of coating mechanism of microscale semi-packed separation column; **d** electrical interconnects for signal measurement of VOCs' ionization. Reprinted with permission from reference Akbar et al. (2015)

Table 8 Summary of gas sensing by chemiluminescence techniques and limit of detection

Sensing gas	Detection limit	Technique	References
CO	1.0 ppm	Cataluminescence-based sensing	Sadanaga et al. (2008)
NO_2	5.5 pptv (parts per trillion by volume)	Ozone-induced chemiluminescence	Lee et al. (2009)
NO	1.8 pptv	Ozone-induced chemiluminescence	Lee et al. (2009)
NH_3	14 ppb	Cataluminescence-based sensing	Shi et al. (2003)
H_2S	3 ppm	Cataluminescence-based sensing	Zhang et al. (2004)
Cl_2	0.2 ppm	Chemiluminescence sensing	Gao et al. (2008)

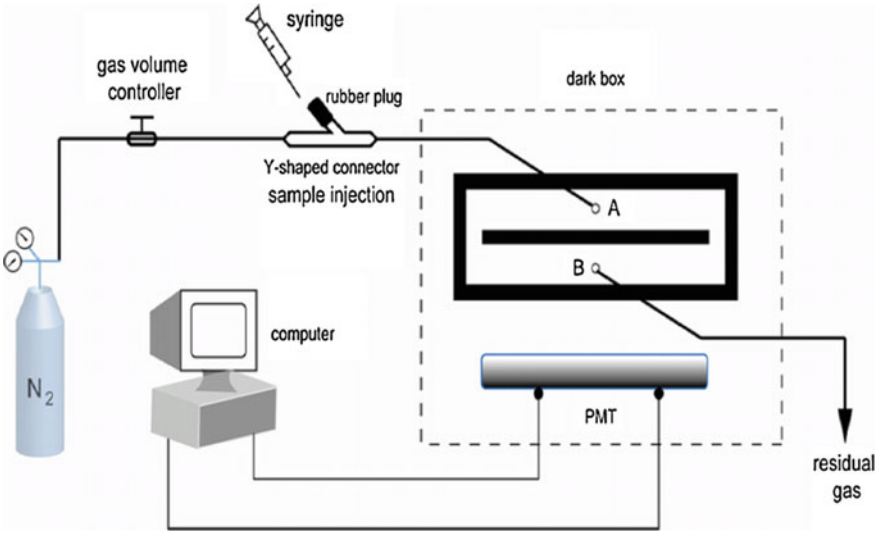

Fig. 11 Schematic representation of miniaturized chemiluminescence-based sensing system. Port A used for sample injection and Port B for residual gases after detection. Reprinted with permission from reference Gao et al. (2008)

sensor for chlorine detection using chemiluminescence technique. They used luminol ($C_8H_7N_3O_2$) solution which was mounted on microchannel [containing two parts (upper and lower)]. After insertion of Cl_2 in the microchannel utilizing surface tension, the luminol solution transmits ClO^- ion and emits chemiluminescence which was further detected by photomultiplier tube (PMT). Fig. 11 represents complete set-up used for chlorine detection utilizing microfluidic platform which consisted of N_2 gas, PMT coupled with computer and microfluidic device.

3 Commercially Available Sensor for Detection of Air Pollutants

Apart from high sensitivity, selectivity, response time, recovery time and low cost, the portability of air monitoring sensor has been the main concern for commercialization. SnO_2-based sensors are available in the market with the capability of detecting CO_2, CO, NH_3, O_3, H_2 gases in the environment. For example, MQ-135 sensor (of Air Quality Click™ and mikroBUS™) operable at 5 V DC provides the detection of NH_3, C_6H_6, NOx, smoke, CO_2 (Fig. 12a). It can detect NH_3 and C_6H_6 in the range of 10–300 ppm. Another sensor (MG-811) has the capability of detecting CO_2, CO, CH_4 and C_2H_5OH in 350–10^3 ppm range (Fig. 12b). The sensor works on principle of solid-state cell electrolyte which is operable at 6 V DC. Moreover, there are sensors available in the market which do not require any additional circuitry to

Fig. 12 **a** Air pollutant sensor for NH_3, NO_x, smokes, CO_2 detection, and model: MQ-135 **b** sensor for detecting CO_2, model: MG-811; **c** VOC formaldehyde and PM2.5 Air Quality Monitoring Tester. *Courtesy* BSIDE EET100

operate, i.e. they have in-house PWM (pulse width modulator), analog or digital signal for connection to microcontroller. Although, the sensitivity and selectivity of these sensors are not high enough to get accurate results in real time environment testing, yet they can provide a rough approximation of air pollutants.

Automobiles generate $PM_{2.5}$ particles in air which are responsible for damaging human respiratory track, and BSIDE's tester is commercially available in the market which can measure VOC and $PM_{2.5}$ particles in air in the range of 0–10 ppm and 0–500 $\mu g/m^3$, respectively. It is operable at 3.7 VDC battery (Fig. 12c). An Indian product (Fig. 13) for monitoring VOC gases (formaldehyde (HCHO), benzene (C_6H_6), toluene ($C_6H_5CH_3$), petrol/diesel and smoke, etc.) up to a range of 0–5 ppm is available in market, and its specification are depicted in Fig. 13.

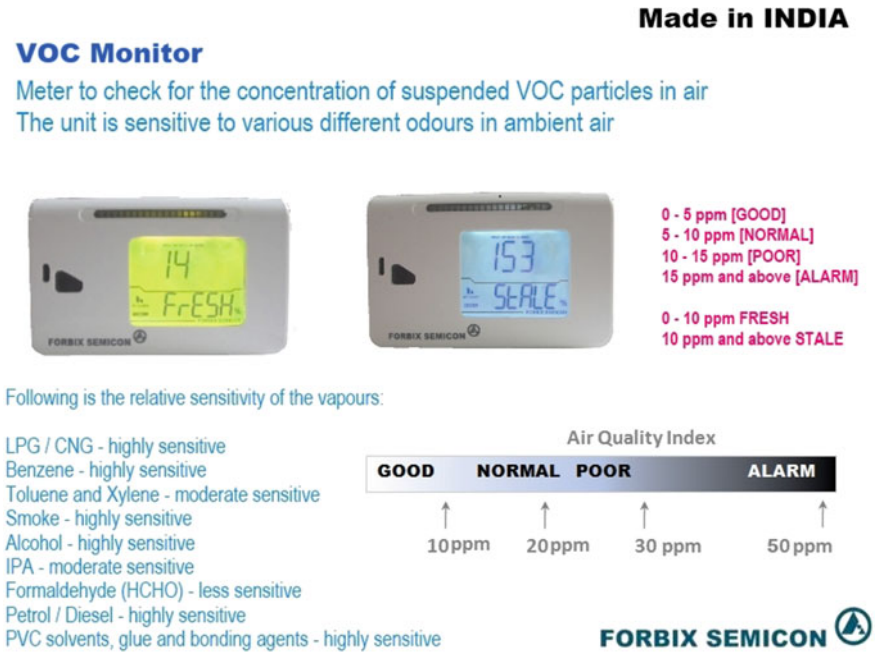

Fig. 13 Detection of VOC gases (formaldehyde, benzene, toluene, petrol/diesel and smoke, etc.) up to a range of 0–5 ppm. *Courtesy* FORBIX SEMICON Co.

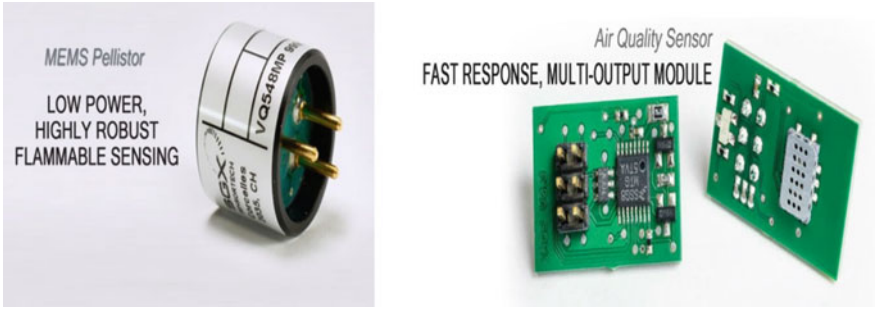

Fig. 14 Model: EC4-500-CO detector. *Courtesy* SGX Sensortech

For CO detection, SGX Sensortech provided infrared-based gas sensor, which can detect carbon monoxide, in the range of 0–500 ppm limit of detection (Fig. 14), while its limit of detection is 0.1 ppm. And it can also detect sulphur dioxide (5 ppm), nitric oxide (25 ppm), nitrogen oxide (5 ppm) and hydrogen (100 ppm).

4 Conclusion

We have outlined the need for air monitoring by sensors coupled with wireless sensing networks. The effects of air pollutants (CO, NH_3, NO_2, SO_2, CH_4, etc.) on human health and environmental condition are discussed in detail with prescribed guidelines provided by WHO. Further, different types of sensor based on various MEMS/NEMS technologies such as semiconducting metal oxide, optical fibre, calorimetric, gas chromatography have been discussed in depth with supporting literature. By keeping the view of miniaturization of sensors for air monitoring, the commercialized air sensors have also been discussed. Despite technological development of robust sensors presented in this chapter, there is utmost need for the development of portable air sensor combined with wireless sensor networks which could give real-time air pollutants' data in selective space and time with high sensitivity and selectivity. MEMS-/NEMS-based technologies are envisioned to fulfil these requirements.

References

Abdelghani A, Chovelon JM, Jaffrezic-Renault N et al (1997) Optical fibre sensor coated with porous silica layers for gas and chemical vapour detection. Sens Actuators B Chem 44:495–498

Aboul-Enein HY, Stefan R-I, van Staden JF et al (2000) Recent developments and applications of chemiluminescence sensors. Crit Rev Anal Chem 30:271–289

Akbar M, Restaino M, Agah M (2015) Chip-scale gas chromatography: from injection through detection. Microsyst Nanoeng 1:15039

Archenault M, Gagnaire H, Goure JP, Jaffrezic-Renault N (1992) A simple intrinsic optical-fibre chemical sensor. Sens Actuators B Chem 8:161–166

Baratto C, Sberveglieri G, Onischuk A et al (2004) Low temperature selective NO_2 sensors by nanostructured fibres of ZnO. Sens Actuators B Chem 100:261–265

Bartlett PN, Guerin S (2003) A micromachined calorimetric gas sensor: An application of electrodeposited nanostructured palladium for the detection of combustible gases. Anal Chem 75:126–132

Beelen R, Hoek G, van den Brandt PA et al (2008) Long-term effects of traffic-related air pollution on mortality in a Dutch cohort (NLCS-AIR study). Environ Health Perspect 116:196–202

Bogue R (2015) Detecting gases with light: a review of optical gas sensor technologies. Sens Rev 35:133–140

Cho P-S, Kim K-W, Lee J-H (2006) NO2 sensing characteristics of ZnO nanorods prepared by hydrothermal method. J Electroceramics 17:975–978

Dinh TV, Choi IY, Son YS, Kim JC (2016) A review on non-dispersive infrared gas sensors: Improvement of sensor detection limit and interference correction. Sens Actuators B Chem 231:529–538

Edner H, Ragnarson P, Spännare S, Svanberg S (1993) Differential optical absorption spectroscopy (DOAS) system for urban atmospheric pollution monitoring. Appl Opt 32:327–333

Fiddler MN, Begashaw I, Mickens MA et al (2009) Laser spectroscopy for atmospheric and environmental sensing. Sensors 9:10447–10512

Filleul L (2005) Twenty five year mortality and air pollution: results from the French PAARC survey. Occup Environ Med 62:453–460

Friedberger A, Kreisl P, Rose E et al (2003) Micromechanical fabrication of robust low-power metal oxide gas sensors. Sens Actuators B Chem 93:345–349

Gao ZX, Li HF, Liu J, Lin JM (2008) A simple microfluidic chlorine gas sensor based on gas-liquid chemiluminescence of luminol-chlorine system. Anal Chim Acta 622:143–149

Gardner JW (1989) Electrical conduction in solid-state gas sensors. Sens Actuators 18:373–387

Ghimbeu CM, Lumbreras M, Schoonman J, Siadat M (2009) Electrosprayed metal oxide semiconductor films for sensitive and selective detection of hydrogen sulfide. Sensors 9:9122–9132

Grutter M (2002) Multi-gas analysis of ambient air using FTIR spectroscopy over Mexico City. Atmósfera 16:1–13

Guarnieri M, Balmes JR (2014) Outdoor air pollution and asthma. Lancet 383:1581–1592

Gupta A, Pandey SS, Nayak M et al (2014) Hydrogen sensing based on nanoporous silica-embedded ultra dense ZnO nanobundles. RSC Adv 4:7476–7482

He Y, Orr BJ (2006) Detection of trace gases by rapidly-swept continuous-wave cavity ringdown spectroscopy: pushing the limits of sensitivity. Appl Phys B Lasers Opt 85:355–364

Heidari EK, Zamani C, Marzbanrad E et al (2010) WO_3-based NO_2 sensors fabricated through low frequency AC electrophoretic deposition. Sens Actuators B Chem 146:165–170

Hidalgo P, Castro RH, Coelho AC, Gouvêa D (2005) Surface Segregation and Consequent SO_2 Sensor Response in SnO_2- NiO. Chem Mat 17:4149–4153

Jakubik WP (2011) Surface acoustic wave-based gas sensors. Thin Solid Films 520:986–993

Jakubik WP, Urbańczyk MW, Kochowski S, Bodzenta J (2002) Bilayer structure for hydrogen detection in a surface acoustic wave sensor system. Sens Actuators B Chem 82:265–271

Jo SE, Kang BG, Heo S et al (2009) Gas sensing properties of WO_3 doped rutile TiO_2 thick film at high operating temperature. Curr Appl Phys 9:e235–e238

Kampa M, Castanas E (2008) Human health effects of air pollution. Environ Pollut 151:362–367

Kanazawa E, Sakai G, Shimanoe K et al (2001) Metal oxide semiconductor N_2O sensor for medical use. Sens Actuators B Chem 77:72–77

Karunagaran B, Uthirakumar P, Chung SJ et al (2007) TiO_2 thin film gas sensor for monitoring ammonia. Mater Charact 58:680–684

Kirner U, Schierbaum KD, Göpel W et al (1990) Low and high temperature TiO_2 oxygen sensors. Sens Actuators B Chem 1:103–107

Kondratowicz B, Narayanaswamy R, Persaud KC (2001) An investigation into the use of electrochromic polymers in optical fibre gas sensors. Sens Actuators B Chem 74:138–144

Korotcenkov G (2007) Metal oxides for solid-state gas sensors: what determines our choice? Mater. Sci Eng B Solid-State Mater Adv Technol 139:1–23

Lee JD, Moller SJ, Read KA et al (2009) Year-round measurements of nitrogen oxides and ozone in the tropical North Atlantic marine boundary layer. J Geophys Res Atmos 114:1–14

Lin HM, Tzeng SJ, Hsiau PJ, Tsai WL (1998) Electrode effects on gas sensing properties of nanocrystalline zinc oxide. Nanostructured Mater 10:465–477

Ma Y, Richards M, Ghanem M et al (2008) Air pollution monitoring and mining based on sensor Grid in London. Sensors 8:3601–3623

Massie C, Stewart G, McGregor G, Gilchrist JR (2006) Design of a portable optical sensor for methane gas detection. Sens Actuators B Chem 113:830–836

Matei Ghimbeu C, Lumbreras M, Siadat M, Schoonman J (2010) Detection of H_2S, SO_2, and NO_2 using electrostatic sprayed tungsten oxide films. Mater Sci Semicond Process 13:1–8

Meng D, Yamazaki T, Shen Y et al (2009) Preparation of WO_3 nanoparticles and application to NO_2 sensor. Appl Surf Sci 256:1050–1053

Mihalcea RM, Baer DS, Hanson RK (1998) A diode-laser absorption sensor system for combustion emission measurements. Meas Sci Technol 9:327–338

Min Y, Tuller HL, Palzer S et al (2003) Gas response of reactively sputtered ZnO films on Si-based micro-array. Sens Actuators B Chem 93:435–441

Mishra SK, Gupta BD (2015) Surface plasmon resonance-based fiber optic chlorine gas sensor utilizing indium-oxide-doped tin oxide film. J Light Technol 33:2770–2776
Moon J, Park JA, Lee SJ et al (2010) Pd-doped TiO_2 nanofiber networks for gas sensor applications. Sens Actuators B Chem 149:301–305
Park JA, Moon J, Lee SJ et al (2010) Structure and CO gas sensing properties of electrospun TiO_2 nanofibers. Mater Lett 64:255–257
Park NH, Akamatsu T, Itoh T et al (2014) Calorimetric thermoelectric gas sensor for the detection of hydrogen, methane and mixed gases. Sensors 14:8350–8362
Phan QH, Yang PM, Lo YL (2015) Surface plasmon resonance prism coupler for gas sensing based on Stokes polarimetry. Sens Actuators B Chem 216:247–254
Sadanaga Y, Yuba A, Kawakami JI et al (2008) A gaseous nitric acid analyzer for the remote atmosphere based on the scrubber difference/NO-ozone chemiluminescence method. Anal Sci 24:967–971
Sauvan M, Pijolat C (1999) Selectivity improvement of SnO_2 films by superficial metallic films. Sens Actuators B Chem 58(1–3):295–301
Sberveglieri G, Depero L, Groppelli S, Nelli P (1995) WO_3 sputtered thin films for NOx monitoring. Sensors Actuators B Chem 26(1–3):89–92
Seekaew Y, Lokavee S, Phokharatkul D et al (2014) Low-cost and flexible printed graphene-PEDOT: PSS gas sensor for ammonia detection. Org Electron phys, Mater Appl
Shi J, Yan R, Zhu Y, Zhang X (2003) Determination of NH_3 gas by combination of nanosized $LaCoO_3$ converter with chemiluminescence detector. Talanta 61:157–164
Shimizu Y, Matsunaga N, Hyodo T, Egashira M (2001) Improvement of SO_2 sensing properties of WO_3 by noble metal loading. Sens Actuators B Chem. https://doi.org/10.1016/S0925-4005(01)00669-4
Srivastava V, Jain K (2008) Highly sensitive NH_3 sensor using Pt catalyzed silica coating over WO_3 thick films. Sens Actuators B Chem 133:46–52
Terry SC, Herman JH, Angell JB (1979) A gas chromatographic air analyzer fabricated on a silicon wafer. IEEE Trans Electron Devices 26:1880–1886
Toda K, Dasgupta PK (2007) New applications of chemiluminescence for selective gas analysis. Chem Eng Commun 195:82–97
Varghese OK, Gong D, Dreschel WR et al (2003) Ammonia detection using nanoporous alumina resistive and surface acoustic wave sensors. Sens Actuators B Chem 94:27–35
Wang J, Maiorov M, Baer DS et al (2000) In situ combustion measurements of CO with diode-laser absorption near 2.3 microm. Appl Opt 39:5579–5589
White RM, Paprotny I, Doering F et al (2012) Sensors and "apps" for community-based: atmospheric monitoring. EM Air Waste Manag Assoc Mag Environ Manag 5:36–40
WHO (2015) World Health Assembly closes, World Health Organization. (2015). World Health Assembly closes, passing resolutions on air pollution and epilepsy. WHO. Retrieved from http://www.who.int/mediacentre/news/releases/2015/wha-26-may2015/en/passingresolutions
Wittstock V, Scholz L, Bierer B et al (2017) Design of a LED-based sensor for monitoring the lower explosion limit of methane. Sens Actuators B Chem 247:930–939
Yuan W, Shi G (2013) Graphene-based gas sensors. J Mater Chem A 1:10078
Zhang J, Wang S, Wang Y et al (2009a) ZnO hollow spheres: Preparation, characterization, and gas sensing properties. Sens Actuators B 139:411–417
Zhang T, Liu L, Qi Q et al (2009b) Development of microstructure In/Pd-doped SnO_2 sensor for low-level CO detection. Sens Actuators B Chem 139:287–291
Zhang Z, Jiang H, Xing Z, Zhang X (2004) A highly selective chemiluminescent H_2S sensor. Sens Actuators B Chem 102:155–161
Zhang Z, Zhang S, Zhang X (2005) Recent developments and applications of chemiluminescence sensors. Anal Chim Acta 541:37–47
Zhong Q, Steinecker WH, Zellers ET (2009) Characterization of a high-performance portable GC with a chemiresistor array detector. Analyst 134:283–293

Chapter 3
Gold Nanostructure in Sensor Technology: Detection and Estimation of Chemical Pollutants

Peuli Nath, Nivedita Priyadarshni, Soumen Mandal, Preeti Singh, Ravi Kumar Arun and Nripen Chanda

Abstract Nanosensors have been proven to be a powerful tool in sensing various targeting analytes such as proteins, DNA, and RNA and small molecules such as toxins, drugs, metabolites, biomarkers, and environmental pollutants with high specificity and selectivity. Among various environmental pollutants, pollution by contamination of heavy metal is one of the most serious issues in current global scenario because of its potential toxicity toward human and aquatic life. Conventional methods of detecting such toxic ions include inductively coupled plasma mass spectroscopy (ICP-MS) and atomic absorption spectroscopy (AAS). These methods are accurate in minute-level detection, but still possess some drawbacks such as high time consumption, involvement of toxic chemicals, and requirement of sophisticated laboratory setup. Therefore, there is a need for inexpensive, user-friendly, quick, and portable methods for detection of these toxic ions. Efforts are being made in developing gold nanosensors for easy monitoring of heavy metal toxins in environmental samples. Due to unique optical, electrical, and mechanical properties, gold nanoparticles render improved performance as sensor probe for better sensitivity, selectivity, portability, and multi-load detection capability. During sensing process, the nanoparticles aggregate in the presence of specific metal ions and show visible color change from red to blue to colorless. The qualitative color change detected using naked eyes shows the presence of targeted heavy metal ions. Apart from the qualitative analysis, the quantitative estimation can be achieved with the help of gold nanoparticles by various techniques such as CCD or CMOS sensors, photodetectors, and color light sensors. This chapter deals with various synthesis processes, potential colorimetric-based sensing applications of gold-based nanosensor, and associated electronic circuitry, which could be employed for detection and quantification of various heavy metal toxins.

P. Nath · N. Priyadarshni · S. Mandal · P. Singh · R. K. Arun · N. Chanda (✉)
Micro System Technology Laboratory, CSIR-Central Mechanical Engineering Research Institute, Mahatma Gandhi Avenue, Durgapur 713209, India
e-mail: n_chanda@cmeri.res.in

P. Nath · N. Priyadarshni · S. Mandal · P. Singh · R. K. Arun · N. Chanda
Academy of Scientific and Innovative Research (AcSIR), CSIR Campus, CSIR Road, Taramani, Chennai 600113, India

S. Bhattacharya et al. (eds.), *Environmental, Chemical and Medical Sensors*, Energy, Environment, and Sustainability, https://doi.org/10.1007/978-981-10-7751-7_3

Keywords Gold nanosensors · Photophysical properties · Chemical pollutants Heavy metal ions · Detection and estimation

1 Introduction

Gold is always considered as a special element both historically and economically. Bulk gold is shiny yellow metal widely used in jewelry and dentistry and for decoration in paintings, in ceramics, and in tapestries. However, when bulk gold is broken down to nanometer size range, the yellow metal color is converted into red-colored suspension in aqueous medium termed as colloidal gold (Fig. 1). Michael Faraday first chemically synthesized it in 1847 by reduction of aqueous chloroaurate ions using phosphorous in carbon disulfide (CS_2) (Heiligtag and Niederberger 2013). Since then, it gained profound interest as an important nanostructure material. Colloidal gold of different shapes and sizes possesses strong vibrant color and thus introduced as a colorant for decorative paintings and in stained glass preparation used in windows. The colloidal gold contains gold element in a nanoscale form called "gold nanoparticle" (AuNP) and remains in highly dispersed phase in colloidal state (Mody et al. 2010). Among various noble metal nanoparticles, gold nanoparticles (AuNPs) provide an excellent platform for designing novel analytical sensors having a wide range of applications from sensing biological to chemical analytes (Saha et al. 2012). AuNPs are extensively studied due to their unique tunable optical, electronic, catalytic, biocompatibility, and thermal properties, unlike bulk gold which is inert in nature (Yeh et al. 2012). The unique optical properties of AuNPs come from the collective oscillation of electrons at their surface called surface plasmon resonance (SPR) which is responsible for its vibrant color in colloidal state. As AuNPs of size 1–100 nm have a high surface-to-volume ratio, their SPR frequency is highly sensitive to the dielectric

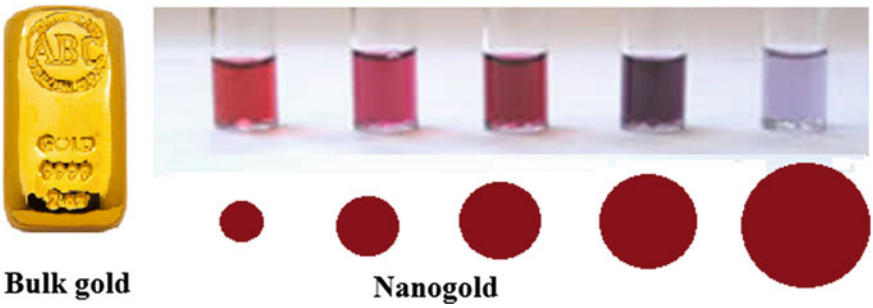

Fig. 1 Yellow-colored metal gold in bulk form (left) and color from red to blue of gold nanoparticle respective to their increasing size

nature of its surrounding medium which makes them a suitable candidate for sensing various analytes such as DNA, RNA, biomolecules, proteins, and heavy metal ions (Fig. 2) (Amendola et al. 2017).

Gold nanoparticle-based sensors can be classified into optical sensor (Yuan et al. 2016), electrochemical sensor (Shams et al. 2016) and piezoelectric sensor (Ding et al. 2014), among which AuNP-based optical sensor gained immense attention due to its interesting optical properties and has been used as colorimetric sensor material (Jongjinakool et al. 2014; Chah et al. 2005; Hung et al. 2010; Kumar et al. 2016). The optical and electronic properties of gold nanoparticles arise from their size confinement of electrons. As the size of gold nanoparticles increases, the SPR frequency redshifts to higher wavelength and the color changes from red (∼15 nm) to pink (∼40 nm) and to blue (∼100 nm) (El-Brolossy et al. 2008) as shown in Fig. 1. AuNPs are synthesized by reduction of gold salts using reducing agents in the presence of appropriate capping agents to prevent aggregation (Kumar and Ganesan 2011). The size of AuNPs can be varied by altering the salt concentration, temperature and rate of addition of reductants. The most common method of gold nanoparticle synthesis is reduction of gold salts using trisodium citrate in aqueous medium. AuNPs of size range from 10 to 25 nm are formed in this method. Other methods of preparation include phase transfer using tetraoctylammoniumbromide as phase transferring agent and sodium borohydride as reducing and stabilizing agent in organic medium like toluene (Cheng and Wang 2004). Gold nanoparticles formed by this method are insoluble in water and often require stronger capping agents such as thiol for their stabilization. AuNPs of size less than diameter 3.0 nm

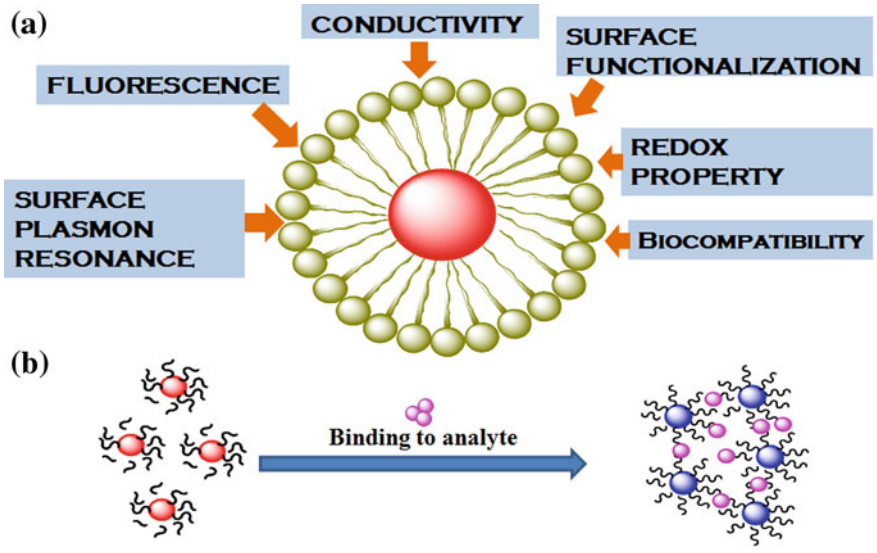

Fig. 2 Schematic illustrations showing **a** various physical properties of gold nanoparticle and **b** AuNP-based detection system

exhibit excellent fluorescence properties and are called fluorescent gold nanoclusters (AuNCs), also known as gold nanodots (Sumi et al. 2015; Chen et al. 2013). AuNCs are highly stable, non-toxic, and biocompatible and can easily enter into various cells, which make them suitable candidature for detection of metal ions inside cell due to metal–ligand interaction leading to either enhancement or quenching of fluorescence (Qu et al. 2015; Durgadas et al. 2011). Fluorescent gold nanoparticles can be encapsulated and stabilized by polyamidoamine (PAMAM) dendrimers or polyethyleneimine (PEI) (Huang et al. 2007) to produce strong fluorescence with high quantum yields. Several methods are applied for synthesis of fluorescent gold nanocluster such as template-based method with DNA, dendrimers, proteins, and polymers and ligand-protected method with thiol or phosphine ligand (Govindaraju et al. 2017). Most common method for preparation of AuNCs is with bovine serum albumin where Au^{3+} is converted into Au^{+} with the help of tyrosine, aspartate, asparagines present in the protein (Xie et al. 2009). For gold nanoparticles to remain stable and dispersed in colloidal state, various stabilization agents such as citrate, borohydride, phenols, and alkenethiols (Comeau and Meli 2012) are used in their synthesis process or surface functionalization is done with suitable coordinating species such as thiol (Moon et al. 2010), PEG (polyethylene glycols) (Manson et al. 2011), or surfactants (Benkovičová et al. 2013). Stabilized tiny gold nanoparticles have electric double layer, which provide strong repulsive force to maintain the nanoparticle in dispersed phase without aggregating in solution (Polte 2015). Thus, stable gold nanostructures with proper surface modification can find several applications from drug delivery (Ghosh et al. 2008) to cell imaging and photothermal therapeutics (McQuaid et al. 2016). In this chapter, the main focus has been given to highlight the synthesis, properties, and the importance of functionalization of gold nanoparticles toward sensing of heavy toxic metal ions which is one of the main sources of the environmental pollution and discuss the recent advances in developing gold-based nanosensors in environmental pollutants monitoring for the benefit of the society.

Chemical pollution in water is one of the major environmental problems nowadays as it possesses threats to human health and welfare and has harmful impact on both society and economy. Chemical pollutants such as chemical toxins, heavy metal ions, and other organic and inorganic pollutants pollute water by various natural or artificial processes that need to be monitored regularly for safe supply of drinking water and also to clean our environment and ecosystem. Heavy metal ions such as arsenic, lead, copper, and mercury are highly toxic in nature. Consumption of these heavy metal toxin-contaminated water leads to several life-threatening diseases such as liver and kidney disease, skin disease, renal failure, cancer, and even death (Moreira and Moreira 2004; Hong et al. 2014; Desai and Kaler 2008). Conventional methods of detecting toxic metal ions are based on chromatographic or spectroscopic techniques such as inductively coupled plasma mass spectroscopy (ICP-MS), atomic absorption spectroscopy (AAS), and high-performance liquid chromatography (HPLC). Though these methods are highly sensitive and provide accurate measurement, they require highly sophisticated instruments, technical expertise, long time for analysis, handling of toxic

chemicals, dedicated laboratory setup, and periodical electrode maintenance making the analysis highly expensive (Yuan et al. 2011). To overcome these challenges, there is a need of inexpensive, portable, simple, rapid user-friendly technique for detection of these toxic ions. In this context, the colorimetric methods are promising as they are simple and inexpensive and need less detection time. Colorimetric sensors are generally based on dyes or involve the use of surface-modified nanoparticles (Yan et al. 2014). Gold nanoparticle-based colorimetric sensor for metal ion detection requires the incorporation of chelating agent on its surface (Priyadarshini and Pradhan 2017). The presence of metal ions induces nanoparticle aggregation by forming complex with the chelating agent, and the color of stabilized nanoparticle changes from red to blue. Recently, many researchers have explored functionalized gold nanoparticles as potential sensors in both colorimetric and fluorometric assays exploiting their unique photophysical properties which make them sensitive to binding with toxic metal ions (Chai et al. 2010; Fang et al. 2010; Jongjinakool et al. 2014; Nath et al. 2014). Detailed study of gold nanoparticle's property and their applications is discussed in consequent segments.

2 Properties of Gold Nanoparticles Toward Sensing Applications

Gold nanoparticles are of great interest because of their size-dependent photophysical properties as compared to its bulk (Link and El-Sayed 1999; Eustis and El-Sayed 2006). The properties of gold nanoparticles change as size decreases, because the number of active atoms on their surface increases unlike present in interior of the particles. They have large surface area that helps them to form suspension (colloidal gold) within the solvent which is strong enough to exceed density differences and otherwise could result in either floating of materials or precipitate formation in the medium (Nguyen Ngoc et al. 2009).

2.1 Photophysical Properties

The photophysical properties of gold nanoparticles arise due to localized surface plasmon resonance phenomenon (LSPR), i.e., collective oscillations of free electrons at a metal–dielectric interface when the frequency of incident light coincides with the frequency of electron oscillations and thus highly influenced by nanoparticle's size, shape, dispersion, and composition (Fig. 3) (Hutter and Fendler 2004). Among noble metal nanoparticles, gold nanoparticles show strong SPR band than any other metal nanosuspension and possess unique optical, physical, and electronic properties, which makes them ideal tool for sensing, imaging, and therapeutic applications in sensitive, easy, simpler, and cost-effective ways

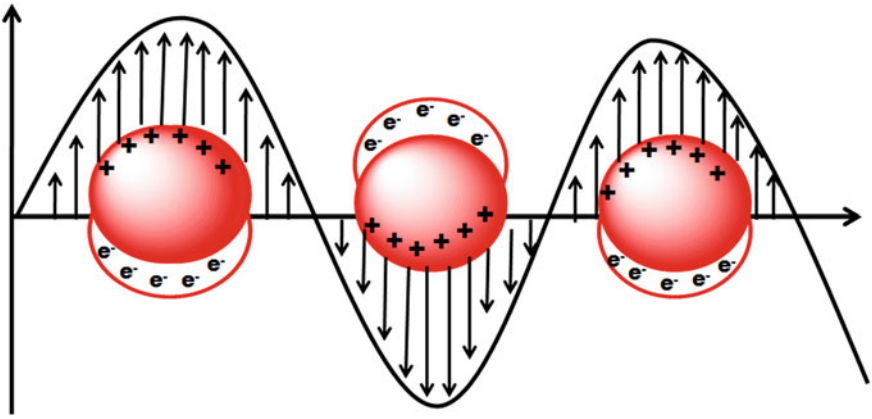

Fig. 3 Schematic representation of the SPR phenomenon showing interactions of the incident electromagnetic wave with the electrons at the surface of the gold nanoparticles

(Homola 2008). The surface plasmon resonance (SPR) of gold nanoparticles primarily depends on the factors such as particle size, shape, composition, and physical–chemical environment including the interparticle distance and dielectric constant of the surrounding medium, which affect electron charge density on the particle surface. Spherical gold nanoparticles exhibit a vibrant range of colors (brown, orange, red, purple) in colloidal state as its size increases from 1 to 100 nm and show a size-relative absorption peak maximum in the span of 520–550 nm (Fig. 4) (Kelly et al. 2003; He et al. 2005). The absorption band at ~520 nm is highly uncertain for particles less than 10 nm and almost absent for particles less than 3.0 nm (fluorescent gold nanoparticles) and for bulk material. This is due to increase rate of electron–surface collisions compared to larger particles. This phenomenon is well described by Mie theory (Huang and El-Sayed 2010). The effects of size on SPR are divided into intrinsic and extrinsic ones. The extrinsic size effect is an electromagnetic phenomenon, which appears in the optical absorption spectrum due to broadening or redshift of SPR on increasing the gold nanoparticle size that causes the change of color from red to blue, also called aggregation of nanoparticle or interparticle plasmon coupling. Intrinsic size effect is due to the modification of metal optical constants when size is below 30 nm (Ghosh and Pal 2007).

The shape of the nanoparticle as explained by Richard Gans in 1912 also determines the number of SPR bands, its width, and position. Gans theory states that absorption is only dependent on the aspect ratio of the particle, not on the absolute dimensions. For example, spherical gold nanoparticles have one SPR band at ~520 nm, while gold nanorods have two plasmon bands. A strong band in NIR region referred to the longitudinal band and a weak band at visible region similar to that of spherical gold nanoparticles called as transverse band resonating at different

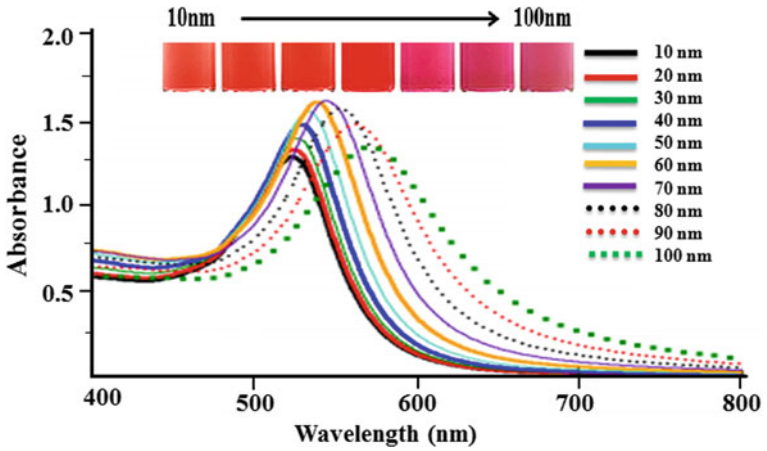

Fig. 4 Variation of UV–Vis absorption spectra of gold nanoparticles with increasing size and respective color change (inset)

wavelengths, which correspond to the collective excitation of conduction electrons along the two axes of nanorod (Hu et al. 2006; Zeng et al. 2010). By further changing the symmetry of nanoparticles, color may change according to the length of the nanorod (Fig. 5) and new plasmon bands may arise which is redshifted compared to that of spheres.

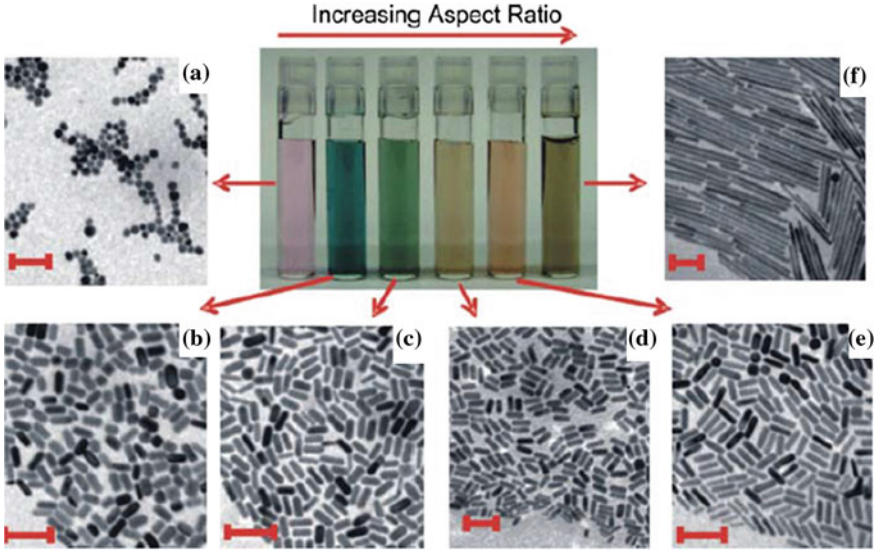

Fig. 5 **a–f** TEM images of gold nanorods respective to their increasing aspect ratios. *Photograph* Showing different color of aqueous solution of gold nanorods with different aspect ratios. All scale bars are 100 nm. Reprinted with permission from Zeng et al. (2010)

The physical–chemical environment influences the SPR bands in many ways: One such mechanism is chemical interface damping (CID). CID is widening of SPR band due to the presence of adsorbates on particle's surface. The photophysical properties of gold nanoparticles are therefore highly dependent on its physical parameters as electronic structure of gold nanoparticles changes with shape and size (Douglas-Gallardo et al. 2016). From this, it is clear that gold nanoparticles exhibit strong SPR absorption band compared to other metal nanoparticles, which makes it a suitable candidate for chemical and biological sensing due to its sensitive spectral response to the surrounding environment. The spectral sensitivity is evident by the relative shift of resonating wavelength with respect to the change in refractive index of the surrounding materials, which depends on the type of metal, its SPR position, width, and shape of the particles (Ghosh and Pal 2007). One of the important features of the sensor is its selectivity, which can be conferred to gold nanoparticle functionalization. The surface of gold nanoparticles can easily be engineered with thiols or disulfides or with a suitable receptor for targeting molecules, enough to produce an appreciable redshift of the SPR band once the nanoparticle binds to the target molecules. All these properties make gold nanoparticle a suitable colorimetric sensor for detection of analytes.

2.2 Colloidal Stability

Nanoparticles' behavior in suspension is highly dependent on particle size, surface composition, and density of the materials used. In nanoscale range below 100 nm, the Brownian motion causes water molecules to collide with particles with high enough force-to-mass ratios, which prevent them from settling, and thus, a true colloidal suspension occurs (Michaelides 2015). However, a particle at such nanometer range becomes highly unstable and tends to aggregate because of their short interparticle distances. At such distances, van der Waals, electrostatic, and magnetic forces come into play and particles are attracted to each other (Rance et al. 2010). Synthesis of metal nanoparticles such as gold is often performed by reduction of gold salts with reducing agents such as sodium citrate, sodium borohydride, and ascorbic acid that also act as stabilizing agents to restrict the aggregation behavior of nanoparticles. The stabilizing agent is adsorbed on the surface and provides a repulsive force for an electrostatic stabilization or steric stabilization. The electrostatically stabilized nanoparticles have one electric double layer due to surface charge (zeta potential) which prevents the nanoparticles from coagulation if the repulsion between the particles is sufficiently high. For preparation of stable nanoparticles, a repulsive interparticle force is required to oppose van der Waals force of attraction, which is provided by the surface charge of the particle.

In solvation state, ions of the solvent surround the ions or molecules of solute to shield their surface charge, which is described by Stern–Gouy–Chapman theory where the surface potential decreases as the ions from first layer move away from the surface of the bulk fluid, and these layers are collectively known as electric

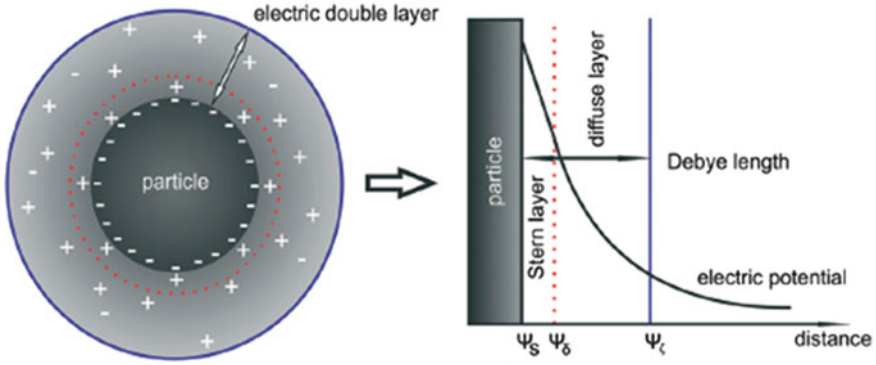

Fig. 6 Electric double layer (EDL) around nanoparticle consisting of inner Stern layer and outer diffuse layer according to Gouy–Chapman model. Reprinted with permission from Polte (2015)

double layer (EDL)—one is the inner compact Stern layer and the other is outer diffused layer. The thickness of EDL is defined as Debye length λ (k^{-1}) and can be quantified using simple electrostatics. A detailed understanding of the distribution of electric surface potential $\psi(x)$ is required to describe the electric double layer effect in colloidal phase (Fig. 6) (Polte 2015). This is well described by two Russian scientists, Derjaguin and Landau, and two Dutch scientists, Verwey and Overbeek, in their stability model known as DLVO theory. The basic assumption of this theory is that the total forces acting on colloidal are the addition of van der Waals force (attraction) and the EDL (repulsion) force acting in between the particles (Polte 2015).

The stability of the nanoparticle depends on the types of ion and their concentration, value of charge density on surface, and size of the particle. When the surface charge (zeta potential) increases, repulsion between the particles is higher. The stable colloidal suspension has zeta potential more than +30 mV or more negative than −30 mV. The van der Waals interaction is relatively independent of ion concentration, but repulsive force depends on it since the counterions are dominant in the Stern and diffused layers. On the other hand, the particle size influences both attractive and repulsive forces of the total interaction energy. As the particle size increases, the total interaction potential (TIP) increases proportionally which is represented in DLVO theory (Polte 2015).

3 Synthesis and Characterization of Gold Nanoparticles

Design and synthesis of nanoscale materials is an important aspect for any sensing applications. Synthesis of nanomaterials involves two main approaches: top-down and bottom-up approaches (Wang and Xia 2004). Top-down approach involves breaking down of bulk material to nanometer scale and is mainly accomplished by

lithography techniques such as electron-beam lithography or soft lithography. Human have been following this approach since beginning of the civilization and mastered the art of breaking materials to sub-micron size, although physical constraint has limited the applications of this approach to nanorange. The bottom-up approach relies on conjugation of several molecules to build nanoconstruct. Various techniques are employed in bottom-up synthesis such as chemical synthesis or chemical self-assembly, where different atoms and molecules are conjugated to form a well-defined stable nanostructure. The most common example of such chemical syntheses is the synthesis of noble metal nanoparticle from their precursor salts. Some common chemical routes for nanoparticles synthesis are the sol–gel method (Epifani et al. 2000), solvothermal synthesis (Choi et al. 2013), micelles-based synthesis (Liebig et al. 2016), and galvanic replacement (Ramos et al. 2011), but the most popular route is by chemical reduction, which provides nanoparticles with controlled size and shape. Controlled size, shape, and stability of nanoparticles are achieved by using different capping agents, solvents, and templates. Although, over the past few decades, physical and chemical methods have dominated the synthesis of nanoparticles, nowadays synthesis by using the biological system has gained great attention. For example, magnetite nanoparticles are found in magnetosomes of the magnetic bacteria which are functional nanoparticles used by the microorganisms to navigate the Earth's geomagnetic field (Yan et al. 2012). This has arisen interest among researchers to understand the underlying mechanism used by the microorganism and to explore the biomimetic approach toward the synthesis of nanoparticles. To date, several bacteria, algae, fungi, and plant materials have been used for the synthesis of nanoparticles including gold one. The details of few well-known bottom-up synthesis procedures of gold nanoparticles are discussed below.

3.1 Turkevich–Frens Method

Turkevich et al. described the first method for gold nanoparticle synthesis in 1951. In this method, gold chloride salt is reduced by sodium citrate forming monodispersed gold nanoparticle suspension in an aqueous medium (Fig. 7) (Kimling et al. 2006). This method is later modified by Frens who produces gold nanoparticles of different sizes from 10 to 100 nm by varying the ratio of gold chloride salts and sodium citrate solution, which is being used as both reducing agent and electrostatic stabilizer. The reaction temperature is kept optimum at $\sim$90 °C, which is important for the formation of gold nanoparticles as both reaction kinetics and oxidation potential are dependent on temperature. The citrate anions form a complex multilayer around nanoparticles preventing it from aggregation and providing a net negative charge. The advantage of citrate layer is its weak coordination with the gold nanoparticle that makes it amenable to functionalization with thiols (Zhu et al. 2003), proteins, or other biomolecules (Thi Ha Lien et al. 2010). Citrate-stabilized gold nanoparticles are more sensitive to change in pH, ionic strength of the

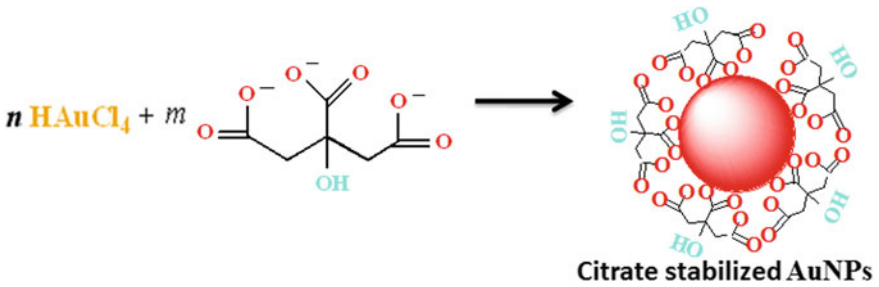

Fig. 7 Reaction mechanism for formation of citrate-stabilized gold nanoparticles

medium, and the presence of other organic and inorganic molecules and thus can directly be used as sensor materials for various sensing applications (Nam et al. 2009).

3.2 *Brust–Schiffrin Method*

Brust and Schiffrin first explored in 1994 that gold nanoparticle can be produced in an organic medium, which is not miscible in water (Perala and Kumar 2013). The synthesis involves the reaction of the chloroauric acid with tetraoctylammonium bromide (TOAB) solution in toluene and sodium borohydride as reducing and anti-coagulant agent. Tetraoctylammonium bromide is used as phase transfer catalyst and as the stabilizing agent. The gold salt is transferred from aqueous medium to organic medium using TOAB followed by reduction with sodium borohydride in the presence of alkanethiols. The reactions involved are shown in Fig. 8.

Gold nanoparticles formed by this method are of the 5–6 nm size range. One of the disadvantages of this method is that the formed gold nanoparticles tend to aggregate over the course of time, as TOAB does not bind to the nanoparticles strongly. In addition, some of the phase transfer agents may remain bound to the nanoparticles, which may affect the physical properties of the gold nanoparticles like solubility.

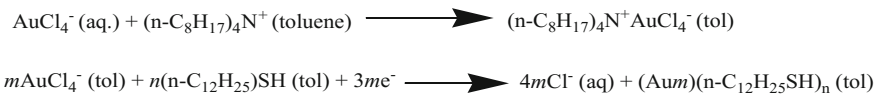

Fig. 8 Reaction mechanisms for formation of gold nanoparticles in organic medium

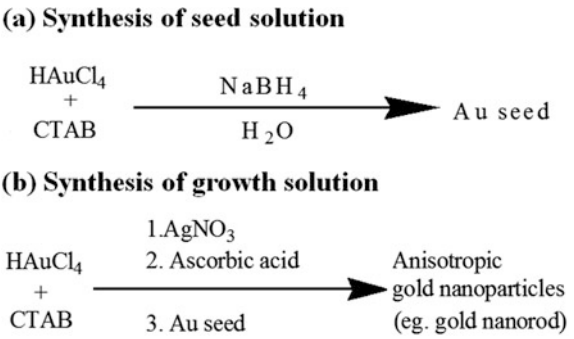

Fig. 9 Reactions illustrate synthesis of gold nanoparticles by seed-mediated growth method

3.3 Seed-Mediated Growth Method

The seed-mediated method is a widely preferred technique for fabricating gold nanoparticle of different shapes. The basic principles of this technique are first to prepare seed particles by reducing gold salts with a strong reducing agent such as sodium borohydride. Then, this seed solution is added to the solution of metal salt in the presence of weak reducing agent (ascorbic acid) and surfactant agent (cetrimonium bromide) to prevent nucleation and accelerate the anisotropic growth of gold nanoparticles (Fig. 9) (Leng et al. 2015).

3.4 Sodium Borohydride Reduction Method

This is "one-pot" synthesis method, which involves reduction of gold salts by sodium borohydride. The method generally produces particle of size range between 4 and 25 nm (Fig. 10a). Sodium borohydride is a strong reducing agent capable of producing small nanoparticles (Deraedt et al. 2014).

3.5 Biosynthesis of Gold Nanoparticles

Chemically synthesized gold nanoparticles generate toxic byproducts and may be harmful for biological applications. Therefore, nowadays, new strategies to synthesize gold nanoparticles without toxic chemicals are developed which attract significant attention among the researchers. This new procedure of producing gold nanoparticle, also referred as "GREEN chemistry," involves the use of biodegradable agents, low toxicity of the final products, and synthesis at ambient temperature and pressure. Different plant extracts are being used to synthesize AuNPs in a clean, reliable, and biofriendly way. Various biocomponents present in plants such as flavonoids, phytosterols, and quinones possess functional groups for

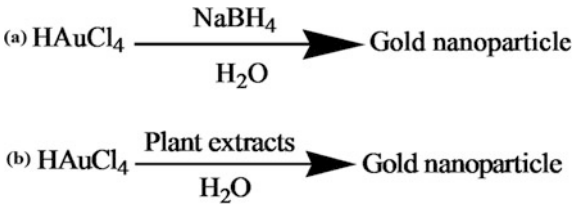

Fig. 10 **a** Reaction mechanism of formation of sodium borohydride-induced gold nanoparticle; **b** biosynthesis of gold nanoparticles using plant extracts

reducing gold salts and also provide stability to the nanoparticle (Lee et al. 2016; He et al. 2007). The procedure involves mixing of gold salts with plant extracts in ambient temperature, pH, conditions to produce AuNPs of different shapes and sizes (Fig. 10b). Biosynthesis of AuNPs using carbohydrate (Shervani and Yamamoto 2011), proteins (Shi et al. 2015), lipids (Nam et al. 2016), and nucleic acid is a fast growing research area as it produces gold nanoparticles in a non-toxic, clean, and eco-friendly way.

3.6 Synthesis of Fluorescent Gold Nanoclusters (AuNCs)

Gold nanoclusters of sub-nanometer size range emit strong fluorescence and are thus suitable for biosensing inside living cells. Several methods such as template-based method, i.e., with polymers, proteins, DNA, dendrimers, and ligand-protected method with phosphine or thiol, are used to synthesize AuNCs. Among these, the most common method of AuNCs synthesis involves bovine serum albumin protein (BSA). The glutamate, aspartate, asparagines, and tyrosine of BSA convert Au^{3+} to Au^{+} ions. Sodium hydroxide (NaOH) is then added which reduces the Au^{+} ions to Au^{0} to form clusters, which is confirmed by the color change from yellow to dark brown (Fig. 11) (Aziz et al. 2015; Xie et al. 2009). In this process, BSA acts as reducing and stabilizing agent. NaOH increases the pH, which further improves the reducing power of BSA. The concentration of gold atoms increases during the reaction, and homogeneous nucleation occurs at the supersaturating level of gold atoms leading to the formation of BSA-stabilized AuNCs. TEM image shows about 1–3 nm size AuNPs are formed in this method.

3.7 Characterization of Gold Nanoparticles

Determination of size, shape, and presence of surface functional molecules on AuNPs is required before any sensing applications and is achieved by several techniques such as atomic force microscopy (AFM), transmission electron microscopy (TEM), field emission scanning electron microscopy (FESEM), X-ray diffraction (XRD), X-ray photoelectron spectroscopy (XPS), UV–Vis absorption

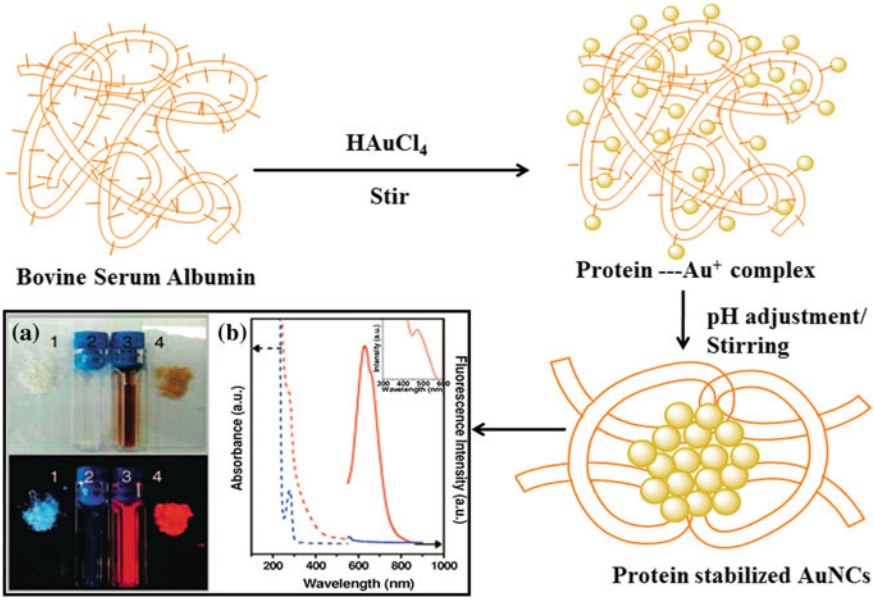

Fig. 11 Schematic illustration of synthesis of fluorescent gold nanoclusters (AuNCs) using protein BSA as reducing agent. Inset (*a*) represents the AuNCs under visible light (above) and shows red fluorescence of AuNCs under UV light of 360 nm wavelength (below). Inset (*b*) demonstrates the UV–Vis and fluorescence graphs in aqueous medium. Reprinted with permission Xie et al. (2009)

spectroscopy, FT-IR spectroscopy, Raman spectroscopy, dynamic light scattering (DLS), electrochemistry and fluorescence spectroscopy. AFM permits for 3D visualization of nanoparticles with sub-nanometer resolution. TEM image allows seeing any self-organization and core-to-core spacing in thin nanoparticle assembly, also interparticle edge-to-edge distance that is ideally equal to the length of the capping agent. X-ray diffraction (XRD) measurements provide information on the crystallographic structure of the nanoparticles. The Fourier transform-infrared spectroscopy is performed to establish the interaction between gold nanoparticles and surface molecules. The electronic states and chemical composition of the nanoparticles are determined using cyclic voltammogram and X-ray photoelectron spectroscopy. The UV–Vis absorption spectra determine the position and the intensity of the SPR band that serves as evidence for changes in the gold nanoparticle structure. Among the various methods, the Raman spectroscopy deserves special mention as it indicates the structure of molecules on the surface of modified gold nanoparticles. For functionalization of gold nanoparticles with either individual organic ligands or coordination compounds, the surface Raman scattering is noticeably enhanced due to surface-enhanced Raman scattering (SERS) from the molecules that are adsorbed on the AuNP surface (Philip 2008; Singh et al. 2016; Nath et al. 2015).

4 Functionalization of Gold Nanoparticles

Surface coating of gold nanoparticles with capping ligands is necessary for stabilization of gold nanoparticle and for functionalization of the particles enabling them to use as sensors by targeting specific analytes. Functionalization can modify the surface, dispersibility, and size of the nanoparticles. Above all, surface modification provides a protective layer on the surface, thus increasing the overall stability of the nanoparticles.

4.1 Thiol-Functionalized Gold Nanoparticles

Thiol (–SH) group binds to gold nanoparticles with high affinity (126–146 kJ/mol) by forming covalent bonds. Organic thiolates such as dihydrolipoic acid have been widely used as surface functionalization ligands because of high stability of Au–S bonds. For example, gadolinium chelates are attached to gold nanoparticles via dithiolated derivatives of diethylenetriaminepenta acetic acid (Spampinato et al. 2016). It provides a protective monolayer around the AuNPs. The exact nature of bond between the Au–S was not known until 2007. A report of single-crystal X-ray diffraction study of a sample of monodispersed gold particles with mercaptobenzoic acid (MBA) reveals a core containing 102 gold atoms that is surrounded by 44 MBA ligands in $Au_{102}(p\text{-MBA})_{44}$ (Levi-Kalisman et al. 2011). The gold core comprises of 89 Au atoms, 49 of which are arranged in Marks decahedron with two 20-atoms caps. The remaining 13 atoms form a band around the equator of the core forming a protective shell with the thiolates. The shell consists of RS(AuSR)*n* units with $n = 1,2$ generally indicated as "staples." Monomeric staples if $n = 1$ (–RS–Au–SR–) or dimeric staples $n = 2$ (–RS–Au–SR–Au–SR–) are bonded to gold through the terminal sulfur atom. A significant finding is that the MBA ligands not only bind to the gold through Au–S bonds but also interact with each other through a series of face-to-face and face-to-edge interactions between adjacent phenyl rings and also by phenyl sulfur interactions. These findings are also in line with recent advances on the study of gold sulfur interfaces in 2D-SAMs of alkanethiols on Au (111), to which the gold–sulfur interaction contributes with about 208 kJ/mol and the van der Waals interaction between methylene groups contributes with an average energy of 6.24 kJ/mol (Bourg et al. 2000). One of the important chemical properties of Au–S bond is the possibility to undergo an exchange reaction, i.e., replacing a ligand with another without affecting the structural integrity of the particle. Compared to other compounds, thiol compound efficiently improves the stability and dispersibility of AuNPs in aqueous medium. Currently used thiol compound includes glutathione (GSH) (Chai et al. 2010), mercaptopropionic acid (MPA), cysteine, cystamine, dihydrolipoic acid (DHLA), thiol ending PEG (PEG-SH) for various applications including sensing of metal toxins (Fig. 12a) (Gao et al. 2012).

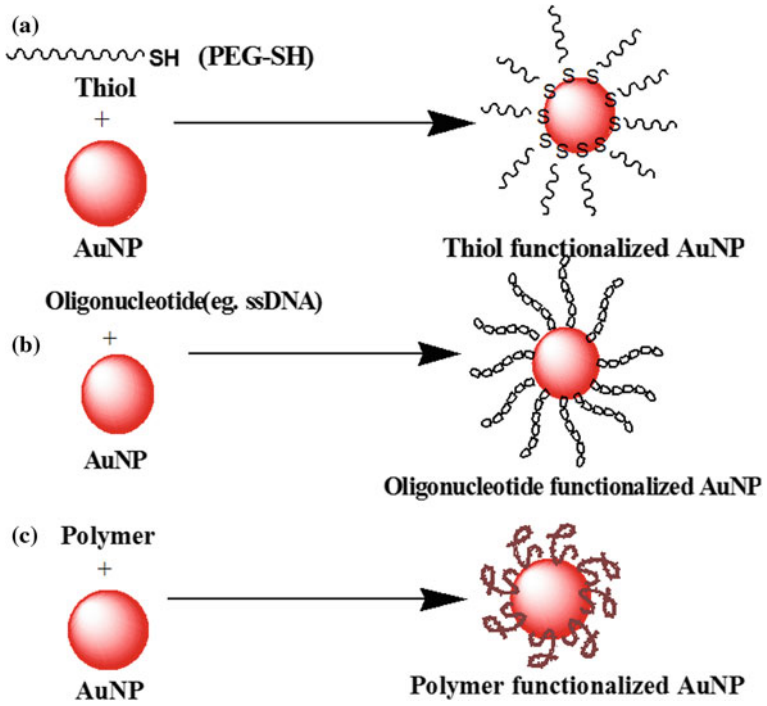

Fig. 12 Schematic presentation of gold nanoparticle functionalization with various moles such as thiols, oligonucleotide (ssDNA), and polymers

4.2 Oligonucleotide Functionalized Gold Nanoparticles

Functionalization of gold nanoparticles with oligonucleotide is another approach toward sensing applications. The gold nanoparticles are generally functionalized with oligonucleotides like DNA in a controlled manner either by attaching modified single-stranded DNA molecules through thiol groups or by saturating the surface of AuNPs with DNA molecules (Fig. 12b). Thermodynamics and kinetics study of DNA-conjugated AuNPs have shown that ssDNA first attaches to the AuNPs and then slowly get adsorbed on its surface (Tan et al. 2011). The DNA hairpin secondary structure inhibits interaction between AuNPs and DNA further thus increasing the overall stability of DNA-functionalized gold nanoparticles. Recently, Mirkin et al. developed DNA-functionalized AuNPs to selectively detect Hg^{2+} ion with high sensitivity. In this study, thiolated DNA-based AuNPs exploit the coordination of thymidine-Hg^{2+}-thymidine complex and related melting temperature (T_m) of the DNA aggregates is monitored (Lee et al. 2007). In this experiment, AuNPs are functionalized with two different DNA probes modified with different thiol groups (probe 1 and probe 2). Probe 1 and probe 2 form aggregates when mixed leading to lower T_m value which corresponds to the mismatch in *T*–*T* base

pair sequences. However in the presence of mercury in the system, the T_m of the AuNP aggregates increases through selective coordination forming stable *T*-Hg^{2+}–T base pairs. This system successfully detects mercury up to 100 nM concentration. Major drawback of this system is the incorporation of an electronic heating device attached with the sensor part for close monitoring of T_m during the detection process. To eliminate this disadvantage, Liu and co-worker investigate and optimized the number of *T*-units to be incorporate on DNA strands so that the system works in ambient temperature (Liu et al. 2013). Recently, a much simpler thymine functionalized AuNPs are designed for colorimetric detection of mercury. The sensor works on the principle of specific interaction of mercury with thymine residue forming the aggregation of AuNPs and indicates corresponding color change. Liu et al. demonstrated DNAzyme base AuNP biosensor for sensitive detection of Pb^{2+} ion. In this sensor, Pb^{2+} ion-specific DNAzyme is chosen as probe for target recognition and AuNPs as the signaling element (Liu and Lu 2004b). The Pb^{2+}-specific DNAzyme comprises of an enzyme strand and its corresponding substrate strand; in the presence of Pb^{2+} ion, the enzyme strand undergoes catalytic reaction cleaving the substrate strand hydrolytically. Incubation of enzyme strand with DNAzyme, DNA-functionalized AuNPs form aggregates according to Watson–Crick base-pairing model giving blue color solution. In the presence of Pb^{2+} ion, DNAzyme is activated further cleaving the substrate strand, thus disassembling AuNPs which results in blue to red color change. The sensor detects up to 100 nM Pb^{2+} ion in less than 10-min time. Other competent metal ions such as Ca^{2+}, Co^{2+}, Ni^{2+}, and Cd^{2+} do not show any color change proving selectivity toward Pb^{2+} ion. Recently, DNA-based AuNPs for uranyl ion detection in living cells is reported. In this experiment, uranyl ion-specific DNAzyme with 3′thiol end for conjugation with AuNP and Cy3 fluorophore at 5′ end and a molecular quencher at 3′ end is fabricated. In the absence of uranyl, the fluorophore is quenched by both AuNPs and molecular quencher, while in the presence of uranyl ion, the DNAzyme cleaves the fluorophore-based molecular strand releasing shorter fragments of Cy3, thus increasing fluorescence intensity. This DNA probe can readily enter living cells making it suitable for intracellular metal ion sensing system (Wu et al. 2013). Such methods are used to detect several metal ions using DNA-functionalized AuNPs in in vivo and in vitro environment.

4.3 Polymer-Functionalized Gold Nanoparticle

Dispersed gold nanoparticles are mostly thermodynamically unstable due to high surface energy and tend to form precipitation under the influence of external stimuli. In order to prevent the self-assembly of AuNPs, conjugation with water-soluble polymer decreases the surface energy of the particles and inhibits interparticle interaction (Fig. 12c) (Iatridi and Bokias 2009). Faraday prepared red-colored gold nanoparticle which is stabilized by gelatin, a water-soluble biopolymer (Neupane et al. 2011). Since then, the polymer is used as an effective

agent to functionalize gold nanoparticles. Polymer-functionalized AuNPs are investigated by many research groups and can be achieved by three techniques:

(a) "Grafting from" fabrication technique: In this method, polymer chains are attached to gold nanoparticles (Huo and Worden 2007; Popelka et al. 2007). This technique provides specific control over the molecular weight of the polymer, flexibility in structural design of polymer layer, and effective introduction of high density polymer. Mostly, artificial polymers are introduced by this technique, like thiol-attached primers, ssDNA. For example, to grafting peptides on AuNPs surfaces, sulfhydryl amines are introduced onto nanoparticle surface followed by elongation of peptide chain with ring opening polymerization.
(b) "Grafting to" fabrication technique: In this technique, the gold salt is reduced in polymer aggregates forming polymer-modified gold nanoparticles (Liu et al. 2007; Liang et al. 2010). This is one-pot synthesis process. Polymer ending with sulfur-containing group such as dithioester, thioether, trithioester, and thiol and with sulfur-free group is used in this method. The thiol-containing polymer forms a shell layer well bounded around the gold core.
(c) Post-modification technique: Here as synthesized gold nanoparticles and as synthesized polymer are mixed together, eliminating uncertain factors such as dispersion of AuNPs and molecular weight of the polymer. Polymer with thiol group is covalently attached to the AuNP surface, while polymer without thiol group is physically adsorbed in the gold nanocomposite.

Hydrophilic polymers such as polypeptides, nucleic acids and polysaccharides, exhibit various unique analytical properties that play important roles in specific detection of homeostasis processes (Siigur and Siigur 2000). Thermoresponsive polymers such as poly(*n*-isopropyl acrylamide) and poly(methyl vinyl ether) are used as functional materials in many chemical analyses. They exhibit a conformational change when subjected to different solution temperatures. This thermoresponsive property facilitates the use of these polymers as key materials in fabricating actuators, micro-TAS, drug delivery systems, and sensors. Conjugation of AuNPs with functional polymers is used to recognize analytes which results in a morphological change in the gold cores and a colorimetric change (Sugunan et al. 2005).

Destabilization of polymer-functionalized AuNPs is a potential approach for developing colorimetric sensors. The negative charge stabilizes the gold nanoparticle which upon binding to metal ions causes the cancellation of negative charge surrounding the AuNPs or shrinkage of electric double layer and resulted in spontaneous aggregation of AuNPs (Uehara 2010). Chen and co-worker synthesize chitosan-functionalized gold nanoparticles that act as signaling probe for metal ion detection. Metal ion Hg^{2+} induces aggregation of AuNPs through a chelation reaction between chitosan and Hg^{2+} ion leading to a strong decrease of the absorbance as the color changes from red to blue. The sensing system is quite sensitive and detects Hg^{2+} ion over other metal ions as low as 1.35 μM which is lower than the WHO level of safe limit for mercury in drinking water (Chen et al. 2015).

5 Applications of Gold Nanoparticles in Sensing Heavy Metal Ions

Functionalized gold nanoparticles are used in wide range of sensing applications because of its unique size-dependent optical properties, SPR. During sensing process, the shift in SPR band happens due to the formation of aggregates of AuNPs that leads to a visual color change in the solution. The benefit of AuNP-based optical colorimetric detection is that a rapid visual assays can be performed which require less or no instrumentation for detection of biomolecules, small molecules including various toxic metal ions. AuNPs have been exploited in the development of biosensors for the detection of specific biomolecules that are significant in disease etiology (Tansil and Gao 2006). For example, uric acid is an important end product of purine metabolism. Abnormal level of UA indicates various metabolic diseases such as gout, hyperuricemia, pneumonia, kidney damage (Kutzing and Firestein 2008). Several methods including colorimetric (Lu et al. 2015), electrochemical (Sakamoto et al. 2011), and enzymatic methods (Cunningham and Keaveny 1978) have been developed for uric acid detection in human fluids. Functionalized AuNPs can also calorimetrically detect uric acid in blood serum and urine with a detection limit as low as 8 ppm (Kumar et al. 2015). Similarly, bimetallic gold–silver nanoparticle-based sensor is developed for glucose detection in blood sample. In this work, silver ions are reduced on gold nanoparticle surface in the presence of glucose forming a new bimetallic gold–silver nanosystem which leads to a direct SPR shift in the UV–Vis spectrum (Li et al. 2017). Correspondingly, another colorimetric-based gold nanosensor is developed using gelatin-coated AuNPs with 6-mercaptohexane-1-ol (MCH) for proteinase activity assay where gelatin serves as proteinase substrate. Proteinase digestion separates the gelatin and brings the nanoparticles closer due to the presence of MCH, therefore forming an aggregation of AuNPs, and change in surface plasmon resonance band is observed which is determined by the change in absorbance ratio (van Hengel et al. 2017). There are many reports on sensing biomolecules using gold nanoparticles; however, as this chapter is focused on detection of chemical pollutants, the following sections are emphasized only on toxic metal ion detections using functionalized AuNPs as sensor probes.

5.1 Detection of Heavy Metal Ions Using Gold Nanoparticle

Arsenic—Arsenic is a heavy metal toxin responsible for causing chronic diseases in human including skin cancer, abdominal pain, renal failure, lungs, and liver diseases (Hong et al. 2014). Colorimetric-based detection of As^{3+} ion using AuNPs is mainly based on the intrinsic property of strong binding affinity of As^{3+} ion toward thiol compounds attached to AuNPs (Al-Sid-Cheikh et al. 2015). Kalluri and co-workers develop gold nanosensor functionalized with thiol-based compound

glutathione (GSH), dithiothreitol (DTT), and cysteine (CYST) for colorimetric detection of As^{3+} ion. The minimal detection is reported 5 ppb for DTT-capped AuNPs, 20 ppb for GSH-capped AuNPs, and 25 ppb for CYST-conjugated AuNPs. The comparative lower detection in DTT is because of binding of As^{3+} ion to DTT via As–S linkage unlike other where As^{3+} ion binds to ligand via As–O linkage. Dynamic light scattering analysis further improves the detection up to 10 ppt limit, suggesting DLS technique as a more sensitive detection method (Fig. 13) (Kalluri et al. 2009). Recently, citrate AuNPs functionalized with GSH-DTT-Cys in one setup and GSH-DTT-Cys-PDCA in another are demonstrated for As^{5+} ion detections. PDCA is used to avoid interference with Hg^{2+} ion. DTT converts As^{5+} to As^{3+}, which binds to AuNP leading to aggregation followed by a color change and SPR shift. It is observed that GSH-DTT-Cys-PDCA is more sensitive in detecting $As^{3+}/^{5+}$ than GSH-DTT-Cys-functionalized AuNPs with a detection limit of 2 ppb which is lower than WHO level of 10 ppb (Dominguez-Gonzalez et al. 2014). Wu et al. detect As^{3+} ion using an As^{3+} ion-specific aptamer and a water-soluble cationic polymer poly(diallyldimethylammonium) (PDDA). In the absence of As^{3+} ion, aptamer forms a duplex complex with PDDA preventing its binding to AuNPs; thus, stabilized AuNPs remain red in color in the colloidal state. However, in the presence of As^{3+} ion, the aptamer forms a complex with the ion leaving PDDA molecules free which binds to the surface of AuNPs causing aggregation and corresponding color change from red to purple (Wu et al. 2012). Similarly, Zhan et al. developed aptamer-based detection method without the involvement of any polymer. Here, the aptamer-functionalized AuNPs remain stabilized and red in color in ionic solution. In the presence of As^{3+} ion, As–aptamer complex is formed which destabilize the AuNPs, resulting in an aggregation with a detection limit of 1.26 ppb (Yu 2014). Xia and co-workers reported a novel detection system using unmodified AuNPs and a phytochelatin-like peptide (g-Glu-Cys)$_3$-Gly-Arg (PC3R) for the detection of As^{3+} ion. PC3R is an oligomer of glutathione, and in the presence of As^{3+} ion, it forms a chemical complex as arsenic has a strong affinity toward thiol compound, thus preventing the aggregation of AuNPs and retaining its red color in solution. In the absence of As^{3+}, the peptide molecules bind to AuNPs surface forming aggregates and change in color from red to blue is observed (Saha et al. 2012).

Copper—Copper is another vital biologically important element, but elevated concentration has an adverse effect on human health. Its accumulation causes reactive oxidation stress and several neural diseases (Desai and Kaler 2008). Various AuNP-based colorimetric methods have been employed in the detection of Cu^{2+} ion. Ye and co-workers use AuNP-stabilized with polyvinylpyrrolidone (PVP) for copper ion detection in solution. In the detection process, 2-mercaptobenzimidazole (MBI) is used to cause aggregation of PVP-stabilized AuNPs by the formation of mercapto-ligand self-assembly of AuNPs leading to a color change from red to blue. However, Cu^{2+} ion, which has an exclusive affinity toward MBI prevents the mercapto-ligand self-assembly of AuNPs and the color remains red due to monodispersity of AuNPs in solution. The detection limit of this colorimetric "purple-to-red" sensor is 5 μM through naked eye and 0.5 μM through

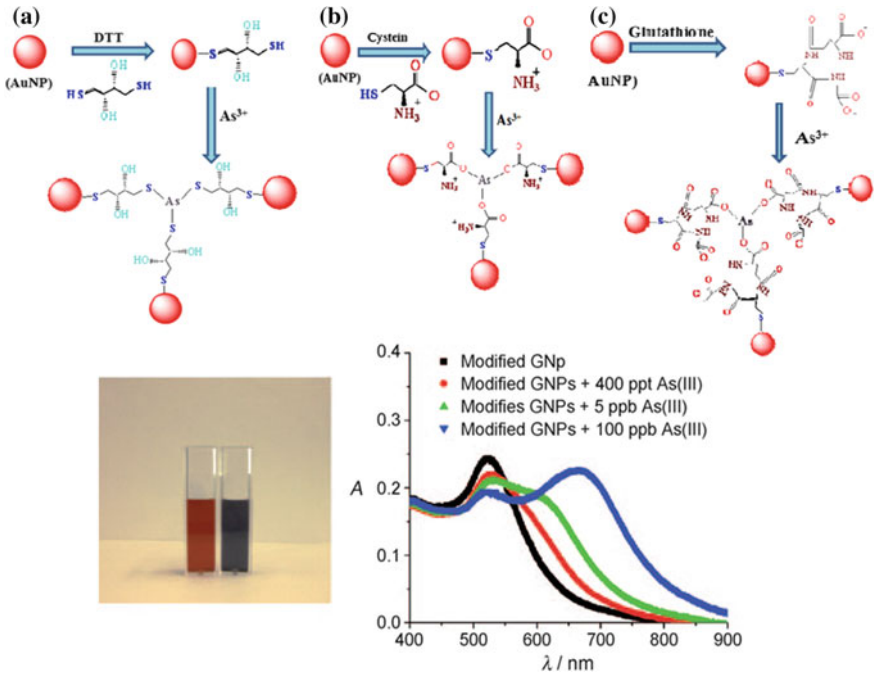

Fig. 13 (Above) Schematic illustration of DTT-AuNPs (**a**), Cys-AuNPs (**b**), GSH-AuNPs (**c**), and their respective interaction with As^{3+} ions. (Below) Image showing colorimetric change of gold nanosensor before and after addition of arsenic ions from red to blue and their corresponding UV–Vis absorption peak. Reprinted with permission from Kalluri et al. (2009)

UV–Vis spectroscopy (Fig. 14) (Yen et al. 2015). Wang et al. synthesize cysteamine-functionalized AuNPs for Cu^{2+} ion detection based on aggregation technique. AuNPs are conjugated with thiol compound cysteamine via Au–S linkage, and thereafter, salicylaldehyde is linked to cysteamine with the help of Schiff base reaction. The Schiff base reacts specifically to Cu^{2+} ion forming aggregation of AuNPs followed by a color change of the sensor from red to blue and SPR shift from 520 to 625 nm (Wang et al. 2012). Another group, Yang, and co-workers develop L-cysteine-functionalized AuNPs for rapid visual detection of copper ion in aqueous solution. In the presence of Cu^{2+} ion, functionalized AuNPs aggregate with a change in color from red to blue and corresponding SPR absorption shift. The Cu^{2+} ion coordinates with the –COOH and $–NH_2$ functional group of L-cysteine molecule forming the aggregates. The minimal detection limit (MDL) of this sensor is up to 10^{-5}M (Yang et al. 2007). Copper-specific DNAzyme-functionalized gold nanoparticles is also fabricated by Wang et al. for colorimetric biosensing of copper. In the presence of Cu^{2+} ion, the Cu^{2+}-specific DNAzymes are cleaved to short ssDNA, which are easily adsorbed on AuNP surface enhancing the stability of AuNPs against salt-induced aggregation; thus, the color remains red in solution. However, in the absence of Cu^{2+} ion long strand of

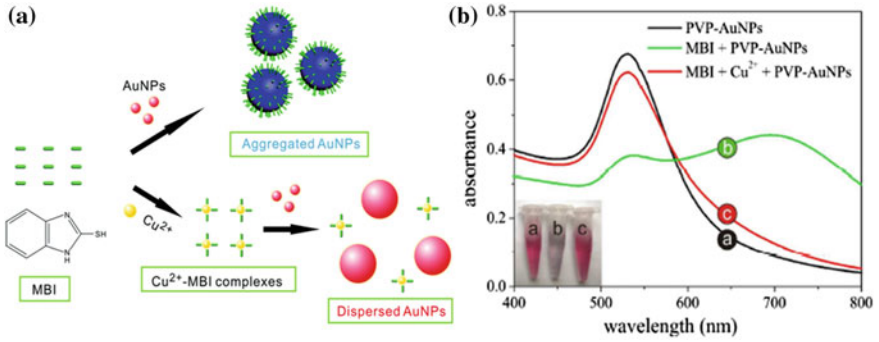

Fig. 14 **a** Schematic showing colorimetric detection of Cu^{2+} ions using PVP-stabilized gold nanoparticles, **b** UV–Vis spectrum of PVP-AuNPs (*a*), MBI-PVP-AuNPs (*b*), MBI + Cu^{2+} + PVP-AuNPs (*c*). Inset photograph showing corresponding color changes. Reprinted with permission Ye et al. (2015)

DNA is slowly adsorbed on AuNP surface leading to aggregation on addition of salt due to diminishing electrostatic repulsion of AuNPs and the color changed to blue. The MDL of this method is as low as 290 nM against other common metal ions (Wang et al. 2010).

Lead—Contamination of water with lead ion is a common problem having adverse effects on living beings. It causes anemia, high blood pressure, and renal disease and affects the central nervous systems (CNS) (Moreira and Moreira 2004). Colorimetric sensor for detection of lead is developed by Chai et al. GSH-functionalized gold nanoparticles are synthesized which show color change from red to blue due to aggregation in the presence of Pb^{2+} ion with the lowest detection limit of 100 nM over other metal ions (Fig. 15) (Chai et al. 2010). Highly sensitive colorimetric sensor and maleic acid-functionalized gold nanoparticles for detection of Pb^{2+} ion are developed by Nalin and co-workers. Maleic acid has –COOH groups that are present on AuNP surface and have a strong affinity toward Pb^{2+} ion forming an aggregation of AuNPs, and color changes from red to blue. The detection limit is 0.5 ppb through naked eye within a period of 15 min (Ratnarathorn et al. 2015). There is a huge development for detection of Pb^{2+} ion using DNAzymes and unmodified gold nanoparticles. DNAzymes are specific to metal ions and form the core of many detection studies. Liu et al. use lead-dependent DNAzyme-functionalized AuNPs for sensitive and selective detection of lead ion in an aqueous environment. In this method, gold nanoparticles are cross-linked by DNAzyme substrates through DNA hybridization forming blue color aggregates with absorption at 700 nm. In the presence of lead, the DNA substrates are cleaved and dispersed gold nanoparticle shows red color with an absorption peak at 522 nm. However, the sensor is time-consuming and requires 2 h to observe the color change (Liu and Lu 2004a).

Mercury and other toxic metal ions—Mercury (II) is the most toxic ion among all heavy metal-based pollutants. Aqueous mercury solution is easily absorbed by

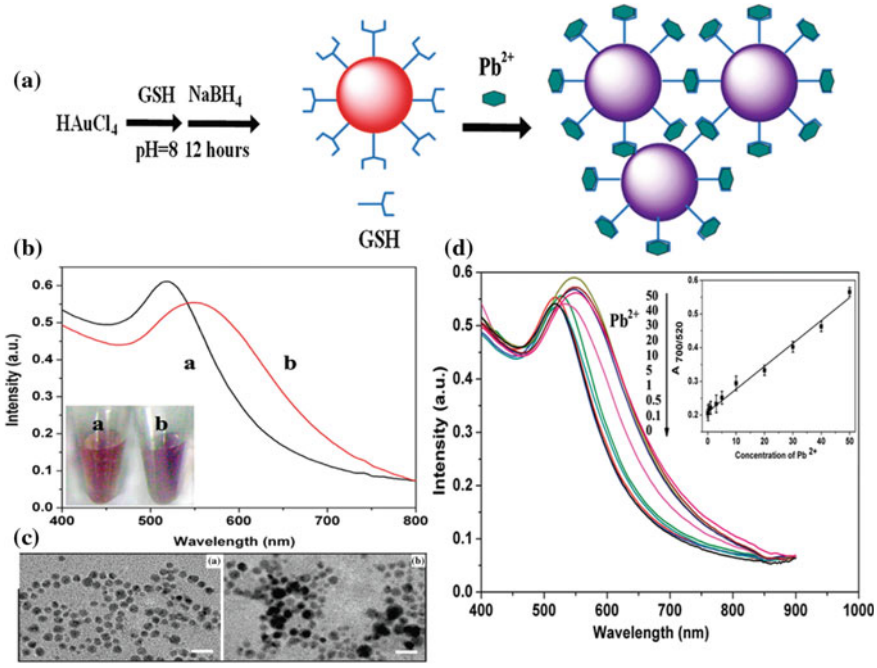

Fig. 15 **a** Binding mechanism of Pb^{2+} ion with GSH-functionalized gold nanoparticles. **b** UV–Vis spectra of GSH-functionalized gold nanoparticle with (*b*) and without (*a*) Pb^{2+} ion and their respective TEM images (**c**). **d** UV–Vis spectra of gold nanosensor with increase concentration of Pb^{2+} ions. Reprinted with permission Chai et al. (2010)

fish or shell fish which then enter human body via food chain causing severe brain, liver, and kidney damage. Several AuNP-based colorimetric methods are employed for mercury (II) detection (Wu and Sun 2016). Among them, DNA-functionalized gold nanoparticles are successfully used in mercury ion detection which are discussed in Sect. 4.2 (Fig. 16) (Lee et al. 2007). Among non-DNA-functionalized gold nanosensor, Kim and co-workers develop 11-mercaptoundecanoic acid (MUA) capped gold nanoparticles using Au–S chemistry for binding 11-MUA with AuNPs which have absorption peak at 526 nm. In the presence of mercury (II) ion, the color of the nanosensor is changed from red to blue due to aggregation. Similarly, 3-mercaptopropionic acid-functionalized AuNPs are developed with 2, 6-pyridinedicarboxylic acid (PDCA) for detecting mercury (II) ion with a minimal detection limit up to 20 ppb (Huang and Chang 2007). L-cysteine-stabilized gold nanoparticles are synthesized to detect Hg^{2+} ion up to a concentration less than 20 μM forming analyte-induced aggregation (Fang et al. 2010). Su et al. report the synthesis of thioctic acid-modified AuNPs for mercury (II) ion detection. Thioctic acid binds to AuNPs via strong Au–S bond and Hg^{2+} ion by free carboxyl groups forming aggregation of nanoparticles and showing redshift of SPR with a minimum detection limit of 10 nM (Su et al. 2013). Fu et al. fabricated array of 3D gold micro-/

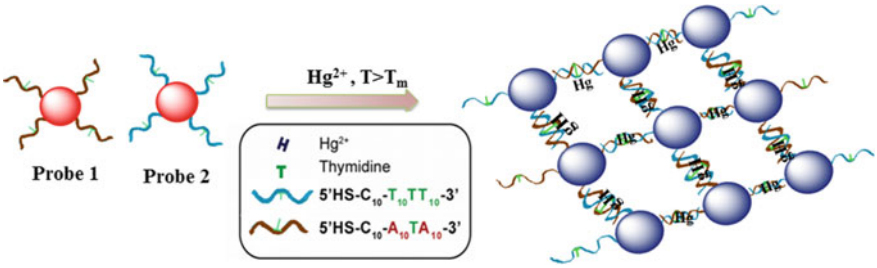

Fig. 16 Colorimetric detection of Hg^{2+} using DNA-functionalized AuNPs exploiting thymidine–Hg^{2+}–thymidine coordination chemistry. Reprinted with permission from Lee et al. (2007)

nanopore structures on gold substrate for the electrochemical determination of mercury in water. Gold is electroplated onto the SiO_2 spheres followed by etching of the template in hydrogen fluoride forming three-dimensional gold microarray electrodes. For selective detection of mercury ion, 2-mercaptobenzothiazole is adsorbed on the electrode surface which precisely detects Hg^{2+} ion up to a trace level of 0.02 nM using square wave anodic stripping voltammetry (Fu et al. 2010). In similar fashion, other toxic species such as chromium and cadmium including some anions such as AcO^- and HPO_4^{2-} are detected with functionalized gold nanoparticles (Liu et al. 2011). It is reported that Cr^{3+} ion have strong affinity toward citrate, and based on this observation, Liu and Wang et al. demonstrate Cr^{3+} ion detection using citrate-capped gold nanoparticles which aggregate in the presence of Cr^{3+} and exhibit a clear-cut color change from red to blue (Wang 2015). AuNPs co-conjugated with L-Cysteine and 6-mercaptonicotinic acids are studied for sensitive colorimetric detection of Cd^{2+} ion. Co-functionalization with these two ligands, L-Cysteine and 6-mercaptonicotinic acid, shows better sensitivity toward Cd^{2+} ion detection forming aggregation and SPR shift to 620 nm (Xue et al. 2011).

5.2 *Heavy Metal Ions Detection Using Fluorescent Gold Nanoclusters (AuNC)*

Detection of heavy metal ions using fluorescent gold nanoclusters has gained attention nowadays. A fluorescent gold nanocluster emits strong fluorescence with high quantum yields, which are increased by tenfolds with the use of alkanethiols, dendrimers, or polyethyleneimine as stabilizing agent. Chang et al. synthesize fluorescent gold nanoparticle using 11-mercaptoundecanoic acid, 2-mercaptoethanol, and 6-mercaptohexanol for selective detection of Hg^{2+} ion. Among all fluorescent AuNPs, 11-MUA-stabilized AuNPs is more sensitive toward Hg^{2+} ion with a minimal detection limit of 5 nM (Fig. 17) (Huang et al. 2007). Guo et al. demonstrate the synthesis of glutathione-capped fluorescent gold nanoparticle, which is highly sensitive for detection of copper ions. In both the cases, the fluorescent gold nanoclusters

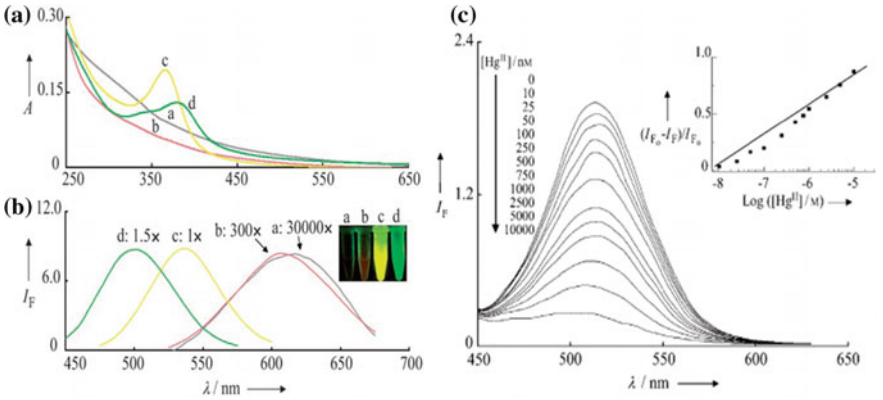

Fig. 17 **a** UV–Vis absorbance spectra and **b** fluorescence spectra of AuNPs (*a*), 2-ME-Au NPs (*b*), 6-MH-AuNPs (*c*), and 11-MU-AuNPs (*d*). Photograph of the fluorescence of the various AuNPs upon excitation under a handheld UV lamp (365 nm) (inset). **b** Their respective fluorescence intensities excited at wavelength 365 nm. **c** Fluorescence spectra showing quenching effect of 11-MUA-functionalized AuNPs on addition of increase concentration of Hg^{2+} ion. Reprinted with permission from Huang et al. (2007)

show quenching effect in the presence of mercury and copper ions up to a low limit of 5 and 8 nM, respectively (Chen et al. 2009).

All these above methods based on either colorimetric or fluorometric approach are exploiting the optical properties of gold nanoparticles, but they are time-consuming and requires handling of toxic chemicals or proper safety for biological substrate for any detection. Recently, there is a thrust for developing miniature devices for detection of these heavy metal ions (Zhao et al. 2016), wherein nanoparticles are immobilized on some substrates like paper and used for sensing applications. Developing such "lab-on-chip" devices for sensitive detection of heavy metal ions opens up new areas toward sensing applications that also allow quantitative analysis of metal ions for monitoring environmental toxicity and providing safety consciousness to human health and welfare (Am et al. 2011).

5.3 *Heavy Metal Ion Detection on Paper Substrate*

As discussed in Sect. 1, traditional methods for the detection of heavy metal ions include ICP-MS, AAS, X-Ray diffraction, and other electrochemical techniques. These methods are highly sensitive, precise, and specific giving accurate result. However, the major drawbacks of these methods include requirement dedicated laboratory setup with trained personnel, sophisticated instruments, involvement of toxic chemicals, and laborious operations which make the analysis highly expensive (Zhao et al. 2016). In developing countries, there is a high demand of simple, rapid, cost-effective sensor device as they lack infrastructure, professional experts

for detection of heavy metals in metal toxin monitoring. In last two decades, microfluidics has emerged as a promising technology in providing rapid "point-of-care" sensing applications. Recently, paper has been explored as a potential candidate for fabricating "lab-on-chip" sensing device (Yang et al. 2017). "Paper-based microfluidic" device works on the capillary flow of actions on the paper substrate. The use of paper also makes the cost of detection device extremely low. Chromatography paper, filter paper, and nitrocellulose paper are used as substrate for paper-based microfluidic device fabrication. In this section, several paper-based microfluidic devices are demonstrated for the detection of heavy metal toxins that require environment monitoring. Conventional colorimetric paper-based kits for detection of metal ions involve the release of toxic gases during operation (Das et al. 2014; Wang et al. 2017). So researchers have come up with the idea of immobilizing colorimetric AuNP-based sensor on paper substrate. Recently developed paper-based device immobilized with gold nanosensor for detection of heavy metal ions is listed in Table 1 (Fig. 18) (Elavarasi et al. 2013; Nath et al. 2014, 2015; Fang et al. 2015; Vijitvarasan et al. 2015). The embedded microstructures of the paper substrate help to pump the fluid due to capillary action. As the sensor comes in contact with the analytes, there is a visual color change of the immobilized gold nanosensor providing a semiquantitative result (Nath et al. 2014). It is worth noting that such paper-based materials have extensively been investigated in microfluidic research on various sensing applications and widely used in point-of-care (POC) diagnostics.

5.4 *Quantification of Heavy Metal Ions Using AuNP-Based Electronic Color Sensor Module*

As discussed in previous section, exposure to heavy metal ions shows distinct change in color of gold nanosensor adsorbed on paper-based substrates. The change in color renders a qualitative detection of particular heavy metal ion in sample. In case of real-time applications such as testing the quality of drinking water or monitoring the amount of pollutants in industrial wastewater, quantification of heavy metal ions is essential. This is owing to the limits set by the WHO and other regulatory bodies in order to check the amount of toxins in the sample. Precise quantitative detection with respect to change in color can be conducted employing color or image sensors along with proper calibration and display module. In one of the arsenic detection techniques, μPAD (microfluidic paper-based analytical device) housing AuNPs functionalized with α-lipoic acid and thioguanine is developed. The change in color of the μPAD on arsenic exposure is recorded using a desktop scanner, and the image is further processed to extract the intensities of red, green, and blue colors. However, quantification of arsenic is not conducted in this work (Chowdury et al. 2017).

Table 1 Recently developed paper-based microfluidic device for sensing heavy metal toxins as chemical pollutants

Nanoconstructs	Metal ions	Paper-based detection techniques	References
Citrate AuNPs	Chromium (III)	Colorimetric (red to blue)	Elavarasi et al. (2013)
DNAzyme-functionalized AuNPs	Lead(II)	Scanometric assay Colorimetric	Vijitvarasan et al. (2015)
Fluorescent AuNCs	Copper(II)	Fluorescent quenching	Fang et al. (2015)
Dansylhydrazine-functionalized AuNPs (Au-TA-DNS)	Lead(II) and Copper(II)	Fluorescent quenching colorimetric	Nath et al. (2015)
Thioguanine-functionalized AuNPs (Au-TA-TG)	Arsenic(III)	Colorimetric	Nath et al. (2014)

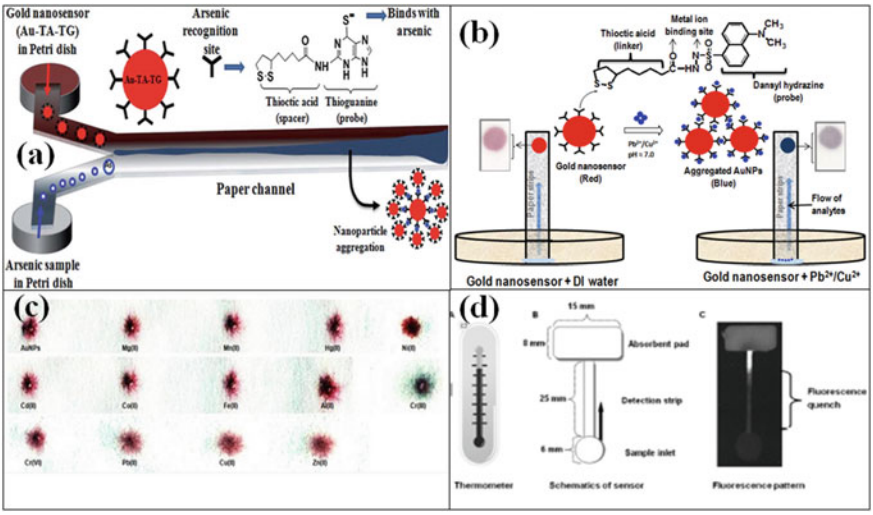

Fig. 18 **a** Schematic showing paper-based microfluidic device for arsenic detection using gold nanosensor Au-TA-TG. **b** Schematic illustration of lead detection in paper-based channel using Au-TA-DNS gold nanosensor. **c** Photograph showing paper strips with gold nanosensor spots for selective detection of chromium ion. **d** Thermometer-like biosensor for detection of copper ion using quenching mechanism of fluorescence gold nanosensor. Reprinted with permission from Nath et al. (2014, 2015), Elavarasi et al. (2013), Fang et al. (2015)

Though systems pertaining precise quantification of heavy metal toxins are limited, approach toward quantitative estimation employing color sensors has been initiated for other chemicals and biomolecules (Shen et al. 2011, 2012; Cho et al. 2010). The generic schematic of the devices used for color-based sensing is shown in Fig. 19. As shown in Fig. 19, the device consists of a color sensor module, a light source, and associated microcontroller-based circuitry for processing,

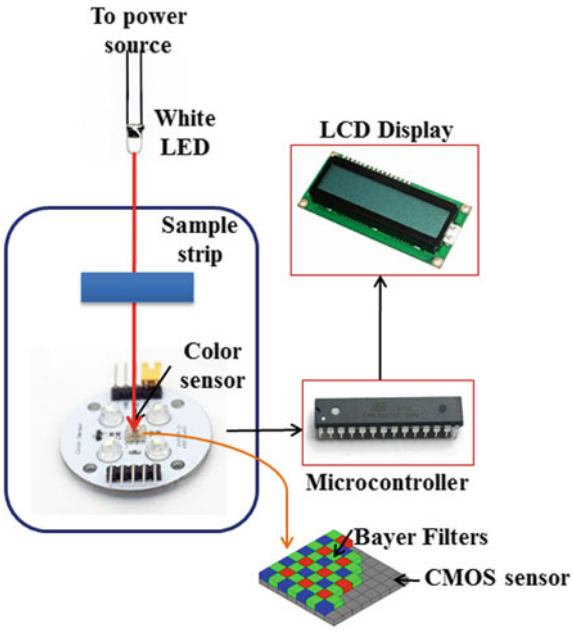

Fig. 19 Generalized schematic for color sensor module used for detecting heavy metal ion induced color change in test strip

inference, and display. The light source incidents white light on the strip. The color of the transmitted light is dependent on the color of the strip. The color sensor module consists of a CMOS-based image sensor, which houses array of Bayer filters. Bayer filters are array of red-, green-, and blue-colored filters, which can absorb a specific wavelength of light and can transmit the rest. It is obvious that the filter will block specific color according to the array configuration and will allow others leading to variation in intensity of the transmitted light based on variation in color. A signal proportional to light intensity will be generated by the CMOS sensor, which is further processed to map the amount of color on the incident light. An approach to quantify heavy metal ions by observing change in color of a test strip is conducted by Ruiz et al. (Cho et al. 2010). In this research, the authors develop a handheld colorimeter for determination of heavy metal concentrations. A microcamera is used to capture the image of the test strip. The HSV (hue, saturation, value)-based color model is used for analysis of the image. The hue component for every image is recorded pixel by pixel. Color change in the test strip due to exposure to particular heavy metal ion renders a different value of hue. The test strips are also scanned for their images employing a desktop scanner. The scanned images are subjected to HSV processing using MATLAB. The hue values obtained from camera images and scanner images are matched for verification.

6 Conclusion

The unique photophysical properties of gold nanoparticles ease of their synthesis and functionalization have made gold nanoparticles a versatile platform for designing various chemical sensors. The optoelectronic properties of AuNPs make them highly selective and sensitive to any binding analytes such as heavy metal toxins. Functionalization of AuNPs improves the sensor performance as they act as both molecular receptor and signal transducer in a single unit.

Detection of heavy metal toxins such as arsenic, mercury, lead, and copper to minute level is mandatory to monitor environmental toxicity, thus helping in providing safe water for consumption which otherwise could have a deleterious effect on human health. Traditional methods of detection of these toxic metal ions are expensive, especially for developing countries. Nanoparticle-based detection system provides simple, rapid, low-cost identification of these toxic ions. AuNP-based colorimetric sensor could provide detection limit from micromolar to picomolar depending on the target species and sensor design. In order to develop efficient "point-of-testing" device, paper-based microfluidics has emerged as a growing platform. In this technique, functionalized gold nanoparticles are immobilized on paper substrate and analytes are passed through exploiting the capillary flow actions of the paper. The paper-based device increases the efficiency of the colorimetric method as miniaturization increases the number of recognition elements. Quantitative analysis of heavy metal ions using gold nanoparticle-based sensor is still in demand and encourages researchers for further innovations for real sample analysis around the corner.

Acknowledgements The authors thank Dr. Harish Hirani, Director, and Dr. Nagahanumaiah, Head, Micro System Technology Laboratory, CSIR-CMERI, Durgapur, for their encouragement. Support from DBT and CSIR grants under project no. GAP-101612 and ESC0112, respectively, is gratefully acknowledged.

References

Al-Sid-Cheikh M, Pédrot M, Dia A, Guenet H, Vantelon D, Davranche M, Gruau G, Delhaye T (2015) Interactions between natural organic matter, sulfur, arsenic and iron oxides in re-oxidation compounds within riparian wetlands: NanoSIMS and X-ray adsorption spectroscopy evidences. Sci Total Environ 515:118–128. https://doi.org/10.1016/j.scitotenv.2015.02.047

Am J, Zhiwei Z, Kang Kug L, Chong HA, Paul LB (2011) State-of-the-art lab chip sensors for environmental water monitoring. Meas Sci Technol 22(3):032001

Amendola V, Pilot R, Frasconi M, Marago OM, Iati MA (2017) Surface plasmon resonance in gold nanoparticles: a review. J Phys: Condens Matter 29(20):203002. https://doi.org/10.1088/1361-648X/aa60f3

Aziz MA, Kim J-P, Shaikh MN, Oyama M, Bakare FO, Yamani ZH (2015) Size-controlled preparation of fluorescent gold nanoparticles using pamoic acid. Gold Bull 48(1):85–92. https://doi.org/10.1007/s13404-015-0164-2

Benkovičová M, Végsö K, Šiffalovič P, Jergel M, Majková E, Luby Š, Šatka A (2013) Preparation of sterically stabilized gold nanoparticles for plasmonic applications. Chem Papers 67. https://doi.org/10.2478/s11696-013-0315-y

Bourg M-C, Badia A, Lennox RB (2000) Gold–sulfur bonding in 2D and 3D self-assembled monolayers: XPS characterization. J Phys Chem B 104(28):6562–6567. https://doi.org/10.1021/jp9935337

Chah S, Hammond MR, Zare RN (2005) Gold nanoparticles as a colorimetric sensor for protein conformational changes. Chem Biol 12(3):323–328. https://doi.org/10.1016/j.chembiol.2005.01.013

Chai F, Wang C, Wang T, Li L, Su Z (2010) Colorimetric detection of Pb2 + using glutathione functionalized gold nanoparticles. ACS Appl Mater Interfaces 2(5):1466–1470

Chen W, Tu X, Guo X (2009) Fluorescent gold nanoparticles-based fluorescence sensor for Cu^{2+} ions. Chem Commun 13:1736–1738. https://doi.org/10.1039/B820145E

Chen W-Y, Chen L-Y, Ou C-M, Huang C-C, Wei S-C, Chang H-T (2013) Synthesis of fluorescent gold nanodot-liposome hybrids for detection of phospholipase C and its inhibitor. Anal Chem 85(18):8834–8840. https://doi.org/10.1021/ac402043t

Chen Z, Zhang C, Tan Y, Zhou T, Ma H, Wan C, Lin Y, Li K (2015) Chitosan-functionalized gold nanoparticles for colorimetric detection of mercury ions based on chelation-induced aggregation. Microchim Acta 182(3):611–616. https://doi.org/10.1007/s00604-014-1365-8

Cheng W, Wang E (2004) Size-dependent phase transfer of gold nanoparticles from water into toluene by tetraoctylammonium cations: a wholly electrostatic interaction. J Phys Chem B 108(1):24–26. https://doi.org/10.1021/jp036522t

Cho SH, Qiao W, Tsai FS, Yamashita K, Lo Y-H (2010) Lab-on-a-chip flow cytometer employing color-space-time coding. Appl Phys Lett 97(9):093704. https://doi.org/10.1063/1.3481695

Choi J, Park S, Stojanović Z, Han H-S, Lee J, Seok HK, Uskoković D, Lee KH (2013) Facile solvothermal preparation of monodisperse gold nanoparticles and their engineered assembly of ferritin-gold nanoclusters. Langmuir 29(50):15698–15703. https://doi.org/10.1021/la403888f

Chowdury M, Walji N, Mahmud M, MacDonald B (2017) Paper-based microfluidic device with a gold nanosensor to detect arsenic contamination of groundwater in Bangladesh. Micromachines 8(3):71

Comeau KD, Meli MV (2012) Effect of alkanethiol chain length on gold nanoparticle monolayers at the air-water interface. Langmuir 28(1):377–381. https://doi.org/10.1021/la202895n

Cunningham SK, Keaveny TV (1978) A two-stage enzymatic method for determination of uric acid and hypoxanthine/xanthine. Clin Chim Acta 86(2):217–221

Das J, Sarkar P, Panda J, Pal P (2014) Low-cost field test kits for arsenic detection in water. J Environ Sci Health Part A Toxic/Hazard Subst Environ Eng 49(1):108–115. https://doi.org/10.1080/10934529.2013.824764

Deraedt C, Salmon L, Gatard S, Ciganda R, Hernandez R, Ruiz J, Astruc D (2014) Sodium borohydride stabilizes very active gold nanoparticle catalysts. Chem Commun 50(91):14194–14196. https://doi.org/10.1039/C4CC05946H

Desai V, Kaler SG (2008) Role of copper in human neurological disorders. Am J Clin Nutr 88(3):855s–858s

Ding J, Lu Z, Wang R, Shen G, Xiao L (2014) Piezoelectric immunosensor with gold nanoparticles enhanced competitive immunoreaction technique for 2,4-dichlorophenoxyacetic acid quantification. Sens Actuators B: Chem 193:568–573. https://doi.org/10.1016/j.snb.2013.11.079

Dominguez-Gonzalez R, Gonzalez Varela L, Bermejo-Barrera P (2014) Functionalized gold nanoparticles for the detection of arsenic in water. Talanta 118:262–269. https://doi.org/10.1016/j.talanta.2013.10.029

Douglas-Gallardo OA, Berdakin M, Sánchez CG (2016) Atomistic insights into chemical interface damping of surface plasmon excitations in silver nanoclusters. J Phys Chem C 120(42):24389–24399. https://doi.org/10.1021/acs.jpcc.6b08519

Durgadas CV, Sharma CP, Sreenivasan K (2011) Fluorescent gold clusters as nanosensors for copper ions in live cells. Analyst 136(5):933–940. https://doi.org/10.1039/C0AN00424C

Elavarasi M, Rajeshwari A, Chandrasekaran N, Mukherjee A (2013) Simple colorimetric detection of Cr(iii) in aqueous solutions by as synthesized citrate capped gold nanoparticles and development of a paper based assay. Anal Methods 5(21):6211–6218. https://doi.org/10.1039/C3AY41435C

El-Brolossy TA, Abdallah T, Mohamed MB, Abdallah S, Easawi K, Negm S, Talaat H (2008) Shape and size dependence of the surface plasmon resonance of gold nanoparticles studied by Photoacoustic technique. Eur Phys J Spec Topics 153(1):361–364. https://doi.org/10.1140/epjst/e2008-00462-0

Epifani M, Giannini C, Tapfer L, Vasanelli L (2000) Sol-gel synthesis and characterization of Ag and Au nanoparticles in SiO_2, TiO_2, and ZrO_2 thin films. J Am Ceram Soc 83(10):2385–2393. https://doi.org/10.1111/j.1151-2916.2000.tb01566.x

Eustis S, El-Sayed MA (2006) Why gold nanoparticles are more precious than pretty gold: noble metal surface plasmon resonance and its enhancement of the radiative and nonradiative properties of nanocrystals of different shapes. Chem Soc Rev 35(3):209–217. https://doi.org/10.1039/B514191E

Fang C, Chungang W, Tingting W, Zhanfang M, Zhongmin S (2010) L-cysteine functionalized gold nanoparticles for the colorimetric detection of Hg^{2+} induced by ultraviolet light. Nanotechnology 21(2):025501

Fang X, Zhao Q, Cao H, Liu J, Guan M, Kong J (2015) Rapid detection of Cu^{2+} by a paper-based microfluidic device coated with bovine serum albumin (BSA)-Au nanoclusters. Analyst 140 (22):7823–7826. https://doi.org/10.1039/C5AN01016K

Fu X-C, Chen X, Guo Z, Kong L-T, Wang J, Liu J-H, Huang X-J (2010) Three-dimensional gold micro-/nanopore arrays containing 2-mercaptobenzothiazole molecular adapters allow sensitive and selective stripping voltammetric determination of trace mercury (II). Electrochim Acta 56 (1):463–469. https://doi.org/10.1016/j.electacta.2010.09.025

Gao J, Huang X, Liu H, Zan F, Ren J (2012) Colloidal stability of gold nanoparticles modified with thiol compounds: bioconjugation and application in cancer cell imaging. Langmuir 28 (9):4464–4471. https://doi.org/10.1021/la204289k

Ghosh SK, Pal T (2007) Interparticle coupling effect on the surface plasmon resonance of gold nanoparticles: from theory to applications. Chem Rev 107(11):4797–4862. https://doi.org/10.1021/cr0680282

Ghosh P, Han G, De M, Kim CK, Rotello VM (2008) Gold nanoparticles in delivery applications. Adv Drug Deliv Rev 60(11):1307–1315. https://doi.org/10.1016/j.addr.2008.03.016

Govindaraju S, Ankireddy SR, Viswanath B, Kim J, Yun K (2017) Fluorescent gold nanoclusters for selective detection of dopamine in cerebrospinal fluid. 7:40298. https://doi.org/10.1038/srep40298

He YQ, Liu SP, Kong L, Liu ZF (2005) A study on the sizes and concentrations of gold nanoparticles by spectra of absorption, resonance Rayleigh scattering and resonance non-linear scattering. Spectrochim Acta Part A Mol Biomol Spectrosc 61(13):2861–2866. https://doi.org/10.1016/j.saa.2004.10.035

He S, Guo Z, Zhang Y, Zhang S, Wang J, Gu N (2007) Biosynthesis of gold nanoparticles using the bacteria *Rhodopseudomonas capsulata*. Mater Lett 61(18):3984–3987. https://doi.org/10.1016/j.matlet.2007.01.018

Heiligtag FJ, Niederberger M (2013) The fascinating world of nanoparticle research. Mater Today 16(7):262–271. https://doi.org/10.1016/j.mattod.2013.07.004

Homola J (2008) Surface plasmon resonance sensors for detection of chemical and biological species. Chem Rev 108(2):462–493. https://doi.org/10.1021/cr068107d

Hong Y-S, Song K-H, Chung J-Y (2014) Health effects of chronic arsenic exposure. J Prevent Med Public Health 47(5):245–252. https://doi.org/10.3961/jpmph.14.035

Hu M, Chen J, Li Z-Y, Au L, Hartland GV, Li X, Marquez M, Xia Y (2006) Gold nanostructures: engineering their plasmonic properties for biomedical applications. Chem Soc Rev 35 (11):1084–1094. https://doi.org/10.1039/B517615H

Huang C-C, Chang H-T (2007) Parameters for selective colorimetric sensing of mercury(ii) in aqueous solutions using mercaptopropionic acid-modified gold nanoparticles. Chem Commun 12:1215–1217. https://doi.org/10.1039/B615383F

Huang X, El-Sayed MA (2010) Gold nanoparticles: optical properties and implementations in cancer diagnosis and photothermal therapy. J Adv Res 1(1):13–28. https://doi.org/10.1016/j.jare.2010.02.002

Huang C-C, Yang Z, Lee K-H, Chang H-T (2007) Synthesis of highly fluorescent gold nanoparticles for sensing mercury(II). Angew Chem Int Ed 46(36):6824–6828. https://doi.org/10.1002/anie.200700803

Hung Y-L, Hsiung T-M, Chen Y-Y, Huang Y-F, Huang C-C (2010) Colorimetric detection of heavy metal ions using label-free gold nanoparticles and alkanethiols. J Phys Chem C 114 (39):16329–16334. https://doi.org/10.1021/jp1061573

Huo Q, Worden JG (2007) Monofunctional gold nanoparticles: synthesis and applications. J Nanopart Res 9(6):1013–1025. https://doi.org/10.1007/s11051-006-9170-x

Hutter E, Fendler JH (2004) Exploitation of localized surface plasmon resonance. Adv Mater 16 (19):1685–1706. https://doi.org/10.1002/adma.200400271

Iatridi Z, Bokias G (2009) Temperature-sensitive water-soluble hybrid organic/inorganic nanoparticles formed through complexation of Cu^{2+} ions with poly(sodium acrylate)-g-poly (N-isopropylacrylamide) comb-type copolymers in aqueous solution. Langmuir 25(13):7695–7703. https://doi.org/10.1021/la900390y

Jongjinakool S, Palasak K, Bousod N, Teepoo S (2014) Gold nanoparticles-based colorimetric sensor for cysteine detection. Energy Procedia 56:10–18. https://doi.org/10.1016/j.egypro.2014.07.126

Kalluri JR, Arbneshi T, Afrin Khan S, Neely A, Candice P, Varisli B, Washington M, McAfee S, Robinson B, Banerjee S, Singh AK, Senapati D, Ray PC (2009) Use of gold nanoparticles in a simple colorimetric and ultrasensitive dynamic light scattering assay: selective detection of arsenic in groundwater. Angewandte Chemie Int Ed 48(51):9668–9671. https://doi.org/10.1002/anie.200903958

Kelly KL, Coronado E, Zhao LL, Schatz GC (2003) The optical properties of metal nanoparticles: the influence of size, shape, and dielectric environment. J Phys Chem B 107(3):668–677. https://doi.org/10.1021/jp026731y

Kimling J, Maier M, Okenve B, Kotaidis V, Ballot H, Plech A (2006) Turkevich method for gold nanoparticle synthesis revisited. J Phys Chem B 110(32):15700–15707. https://doi.org/10.1021/jp061667w

Kumar SV, Ganesan S (2011) Preparation and characterization of gold nanoparticles with different capping agents. Int J Green Nanotechnol 3(1):47–55. https://doi.org/10.1080/19430892.2011.574538

Kumar A, Hens A, Arun RK, Chatterjee M, Mahato K, Layek K, Chanda N (2015) A paper based microfluidic device for easy detection of uric acid using positively charged gold nanoparticles. Analyst 140(6):1817–1821

Kumar S, Bhushan P, Bhattacharya S (2016) Development of a paper-based analytical device for colorimetric detection of uric acid using gold nanoparticles–graphene oxide (AuNPs–GO) conjugates. Anal Methods 8(38):6965–6973. https://doi.org/10.1039/c6ay01926a

Kutzing MK, Firestein BL (2008) Altered uric acid levels and disease states. J Pharmacol Exp Ther 324(1):1–7. https://doi.org/10.1124/jpet.107.129031

Lee J-S, Han MS, Mirkin CA (2007) Colorimetric detection of mercuric ion (Hg^{2+}) in aqueous media using DNA-functionalized gold nanoparticles. Angew Chem Int Ed 46(22):4093–4096. https://doi.org/10.1002/anie.200700269

Lee SY, Krishnamurthy S, Cho C-W, Yun Y-S (2016) Biosynthesis of gold nanoparticles using ocimum sanctum extracts by solvents with different polarity. ACS Sustain Chem Eng 4 (5):2651–2659. https://doi.org/10.1021/acssuschemeng.6b00161

Leng W, Pati P, Vikesland PJ (2015) Room temperature seed mediated growth of gold nanoparticles: mechanistic investigations and life cycle assesment. Environ Sci Nano 2(5):440–453. https://doi.org/10.1039/C5EN00026B

Levi-Kalisman Y, Jadzinsky PD, Kalisman N, Tsunoyama H, Tsukuda T, Bushnell DA, Kornberg RD (2011) Synthesis and characterization of Au_{102}(p-MBA)44 Nanoparticles. J Am Chem Soc 133(9):2976–2982. https://doi.org/10.1021/ja109131w

Li M, Shi L, Xie T, Jing C, Xiu G, Long Y-T (2017) An ultrasensitive plasmonic nanosensor for aldehydes. ACS Sens 2(2):263–267. https://doi.org/10.1021/acssensors.6b00769

Liang M, Lin IC, Whittaker MR, Minchin RF, Monteiro MJ, Toth I (2010) Cellular uptake of densely packed polymer coatings on gold nanoparticles. ACS Nano 4(1):403–413. https://doi.org/10.1021/nn9011237

Liebig F, Sarhan RM, Prietzel C, Reinecke A, Koetz J (2016) "Green" gold nanotriangles: synthesis, purification by polyelectrolyte/micelle depletion flocculation and performance in surface-enhanced Raman scattering. RSC Adv 6(40):33561–33568. https://doi.org/10.1039/C6RA04808K

Link S, El-Sayed MA (1999) Size and temperature dependence of the plasmon absorption of colloidal gold nanoparticles. J Phys Chem B 103(21):4212–4217. https://doi.org/10.1021/jp984796o

Liu J, Lu Y (2004a) Accelerated color change of gold nanoparticles assembled by dnazymes for simple and fast colorimetric Pb^{2+} detection. J Am Chem Soc 126(39):12298–12305. https://doi.org/10.1021/ja046628h

Liu J, Lu Y (2004b) Colorimetric biosensors based on DNAzyme-assembled gold nanoparticles. J Fluoresc 14(4):343–354

Liu Y, Shipton MK, Ryan J, Kaufman ED, Franzen S, Feldheim DL (2007) Synthesis, stability, and cellular internalization of gold nanoparticles containing mixed peptide–poly(ethylene glycol) monolayers. Anal Chem 79(6):2221–2229. https://doi.org/10.1021/ac061578f

Liu D, Wang Z, Jiang X (2011) Gold nanoparticles for the colorimetric and fluorescent detection of ions and small organic molecules. Nanoscale 3(4):1421–1433. https://doi.org/10.1039/C0NR00887G

Liu P, Yang X, Sun S, Wang Q, Wang K, Huang J, Liu J, He L (2013) Enzyme-free colorimetric detection of DNA by using gold nanoparticles and hybridization chain reaction amplification. Anal Chem 85(16):7689–7695. https://doi.org/10.1021/ac4001157

Lu J, Xiong Y, Liao C, Ye F (2015) Colorimetric detection of uric acid in human urine and serum based on peroxidase mimetic activity of MIL-53(Fe). Anal Methods 7(23):9894–9899. https://doi.org/10.1039/C5AY02240A

Manson J, Kumar D, Meenan BJ, Dixon D (2011) Polyethylene glycol functionalized gold nanoparticles: the influence of capping density on stability in various media. Gold Bull 44 (2):99–105. https://doi.org/10.1007/s13404-011-0015-8

McQuaid HN, Muir MF, Taggart LE, McMahon SJ, Coulter JA, Hyland WB, Jain S, Butterworth KT, Schettino G, Prise KM, Hirst DG, Botchway SW, Currell FJ (2016) Imaging and radiation effects of gold nanoparticles in tumour cells. 6:19442. https://doi.org/10.1038/srep19442. http://dharmasastra.live.cf.private.springer.com/articles/srep19442#supplementary-information

Michaelides EE (2015) Brownian movement and thermophoresis of nanoparticles in liquids. Int J Heat Mass Transf 81:179–187. https://doi.org/10.1016/j.ijheatmasstransfer.2014.10.019

Mody VV, Siwale R, Singh A, Mody HR (2010) Introduction to metallic nanoparticles. J Pharm Bioallied Sci 2(4):282–289. https://doi.org/10.4103/0975-7406.72127

Moon S, Tanaka S, Sekino T (2010) Crystal growth of thiol-stabilized gold nanoparticles by heat-induced coalescence. Nanoscale Res Lett 5(5):813–817. https://doi.org/10.1007/s11671-010-9565-6

Moreira FR, Moreira JC (2004) Effects of lead exposure on the human body and health implications. Rev Panam Salud Publica 15(2):119–129

Nam J, Won N, Jin H, Chung H, Kim S (2009) pH-induced aggregation of gold nanoparticles for photothermal cancer therapy. J Am Chem Soc 131(38):13639–13645. https://doi.org/10.1021/ja902062j

Nam J, Kim Y-T, Kang A, Kim K-H, Lee K, Yun WS, Kim YH (2016) Lipid reconstitution-enabled formation of gold nanoparticle clusters for mimetic cellular membrane. J Nanomaterials 2016:7. https://doi.org/10.1155/2016/2860859

Nath P, Arun RK, Chanda N (2014) A paper based microfluidic device for the detection of arsenic using a gold nanosensor. RSC Adv 4(103):59558–59561. https://doi.org/10.1039/C4RA12946F

Nath P, Arun RK, Chanda N (2015) Smart gold nanosensor for easy sensing of lead and copper ions in solution and using paper strips. RSC Adv 5(84):69024–69031. https://doi.org/10.1039/C5RA14886C

Neupane MP, Lee SJ, Park IS, Lee MH, Bae TS, Kuboki Y, Uo M, Watari F (2011) Synthesis of gelatin-capped gold nanoparticles with variable gelatin concentration. J Nanopart Res 13 (2):491–498. https://doi.org/10.1007/s11051-010-9971-9

Nguyen Ngoc L, Le Van V, Chu Dinh K, Sai Cong D, Cao Thi N, Pham Thi H, Nguyen Duy T, Luu Manh Q (2009) Synthesis and optical properties of colloidal gold nanoparticles. J Phys Conf Ser 187(1):012026

Perala SRK, Kumar S (2013) On the mechanism of metal nanoparticle synthesis in the Brust-Schiffrin method. Langmuir 29(31):9863–9873. https://doi.org/10.1021/la401604q

Philip D (2008) Synthesis and spectroscopic characterization of gold nanoparticles. Spectrochim Acta Part A Mol Biomol Spectrosc 71(1):80–85. https://doi.org/10.1016/j.saa.2007.11.012

Polte J (2015) Fundamental growth principles of colloidal metal nanoparticles—a new perspective. CrystEngComm 17(36):6809–6830. https://doi.org/10.1039/C5CE01014D

Popelka Š, Lk Machová, Rypáček F (2007) Adsorption of poly(ethylene oxide)–block–polylactide copolymers on polylactide as studied by ATR-FTIR spectroscopy. J Colloid Interface Sci 308 (2):291–299. https://doi.org/10.1016/j.jcis.2006.12.022

Priyadarshini E, Pradhan N (2017) Gold nanoparticles as efficient sensors in colorimetric detection of toxic metal ions: a review. Sens Actuators B Chem 238:888–902. https://doi.org/10.1016/j.snb.2016.06.081

Qu X, Li Y, Li L, Wang Y, Liang J, Liang J (2015) Fluorescent gold nanoclusters: synthesis and recent biological application. J Nanomaterials 2015:23. https://doi.org/10.1155/2015/784097

Ramos M, Ferrer DA, Chianelli RR, Correa V, Serrano-Matos J, Flores S (2011) Synthesis of Ag-Au nanoparticles by galvanic replacement and their morphological studies by HRTEM and computational modeling. J Nanomaterials 2011:5. https://doi.org/10.1155/2011/374096

Rance GA, Marsh DH, Bourne SJ, Reade TJ, Khlobystov AN (2010) van der Waals interactions between nanotubes and nanoparticles for controlled assembly of composite nanostructures. ACS Nano 4(8):4920–4928. https://doi.org/10.1021/nn101287u

Ratnarathorn N, Chailapakul O, Dungchai W (2015) Highly sensitive colorimetric detection of lead using maleic acid functionalized gold nanoparticles. Talanta 132:613–618. https://doi.org/10.1016/j.talanta.2014.10.024

Saha K, Agasti SS, Kim C, Li X, Rotello VM (2012) Gold nanoparticles in chemical and biological sensing. Chem Rev 112(5):2739–2779. https://doi.org/10.1021/cr2001178

Sakamoto H, Hatsuda R, Miyamura K, Shiraishi H, Sugiyama S (2011) Electrochemical selective detection of uric acid using a copper-modified carbon electrode. Anal Sci Int J Japan Soc Anal Chem 27(3):333–335

Shams N, Lim HN, Hajian R, Yusof NA, Abdullah J, Sulaiman Y, Ibrahim I, Huang NM (2016) Electrochemical sensor based on gold nanoparticles/ethylenediamine-reduced graphene oxide for trace determination of fenitrothion in water. RSC Adv 6(92):89430–89439. https://doi.org/10.1039/C6RA13384C

Shen L, Ratterman M, Klotzkin D, Papautsky I (2011) A CMOS optical detection system for point-of-use luminescent oxygen sensing. Sens Actuators B Chem 155(1):430–435. https://doi.org/10.1016/j.snb.2011.01.001

Shen L, Hagen JA, Papautsky I (2012) Point-of-care colorimetric detection with a smartphone. Lab Chip 12(21):4240–4243. https://doi.org/10.1039/C2LC40741H

Shervani Z, Yamamoto Y (2011) Carbohydrate-directed synthesis of silver and gold nanoparticles: effect of the structure of carbohydrates and reducing agents on the size and morphology of the composites. Carbohyd Res 346(5):651–658. https://doi.org/10.1016/j.carres.2011.01.020

Shi C, Zhu N, Cao Y, Wu P (2015) Biosynthesis of gold nanoparticles assisted by the intracellular protein extract of *Pycnoporus sanguineus* and its catalysis in degradation of 4-nitroaniline. Nanoscale Res Lett 10:147. https://doi.org/10.1186/s11671-015-0856-9

Siigur J, Siigur E (2000) Polypeptides and proteins active in the coagulation process. In: Rochat H, Martin-Eauclaire M-F (eds) Animal toxins: facts and protocols. Birkhäuser Basel, Basel, pp 319–346. https://doi.org/10.1007/978-3-0348-8466-2_20

Singh P, Nath P, Arun RK, Mandal S, Chanda N (2016) Novel synthesis of a mixed Cu/CuO-reduced graphene oxide nanocomposite with enhanced peroxidase-like catalytic activity for easy detection of glutathione in solution and using a paper strip. RSC Adv 6(95):92729–92738. https://doi.org/10.1039/C6RA20882G

Spampinato V, Parracino MA, La Spina R, Rossi F, Ceccone G (2016) surface analysis of gold nanoparticles functionalized with thiol-modified glucose SAMs for biosensor applications. Front Chem 4(8). https://doi.org/10.3389/fchem.2016.00008

Su D, Yang X, Xia Q, Chai F, Wang C, Qu F (2013) Colorimetric detection of Hg^{2+} using thioctic acid functionalized gold nanoparticles. RSC Adv 3(46):24618–24624. https://doi.org/10.1039/C3RA43276A

Sugunan A, Thanachayanont C, Dutta J, Hilborn JG (2005) Heavy-metal ion sensors using chitosan-capped gold nanoparticles. Sci Technol Adv Mater 6(3–4):335

Sumi T, Motono S, Ishida Y, Shirahata N, Yonezawa T (2015) Formation and optical properties of fluorescent gold nanoparticles obtained by matrix sputtering method with volatile mercaptan molecules in the vacuum chamber and consideration of their structures. Langmuir 31(14):4323–4329. https://doi.org/10.1021/acs.langmuir.5b00294

Tan YN, Lee KH, Su X (2011) Study of single-stranded DNA binding protein-nucleic acids interactions using unmodified gold nanoparticles and its application for detection of single nucleotide polymorphisms. Anal Chem 83(11):4251–4257. https://doi.org/10.1021/ac200525a

Tansil NC, Gao Z (2006) Nanoparticles in biomolecular detection. Nano Today 1(1):28–37. https://doi.org/10.1016/S1748-0132(06)70020-2

Thi Ha Lien N, Thi Huyen L, Xuan Hoa V, Viet Ha C, Thanh Hai N, Quang Huan L, Emmanuel F, Quang Hoa D, Hong Nhung T (2010) Synthesis, capping and binding of colloidal gold nanoparticles to proteins. Adv Nat Sci Nanosci Nanotechnol 1(2):025009

Uehara N (2010) Polymer-functionalized gold nanoparticles as versatile sensing materials. Anal Sci 26(12):1219–1228. https://doi.org/10.2116/analsci.26.1219

van Hengel IAJ, Riool M, Fratila-Apachitei LE, Witte-Bouma J, Farrell E, Zadpoor AA, Zaat SAJ, Apachitei I (2017) Selective laser melting porous metallic implants with immobilized silver nanoparticles kill and prevent biofilm formation by methicillin-resistant *Staphylococcus aureus*. Biomaterials 140:1–15. https://doi.org/10.1016/j.biomaterials.2017.02.030

Vijitvarasan P, Oaew S, Surareungchai W (2015) Paper-based scanometric assay for lead ion detection using DNAzyme. Anal Chim Acta 896:152–159. https://doi.org/10.1016/j.aca.2015.09.011

Wang X (2015) Red-to-blue colorimetric detection of chromium via Cr (III)-citrate chelating based on Tween 20-stabilized gold nanoparticles. Colloids Surf A hysicochemical Eng Aspects 472:57–62. https://doi.org/10.1016/j.colsurfa.2015.02.033

Wang Y, Xia Y (2004) Bottom-up and top-down approaches to the synthesis of monodispersed spherical colloids of low melting-point metals. Nano Lett 4(10):2047–2050

Wang Y, Yang F, Yang X (2010) Label-free colorimetric biosensing of copper(II) ions with unimolecular self-cleaving deoxyribozymes and unmodified gold nanoparticle probes. Nanotechnology 21(20):205502. https://doi.org/10.1088/0957-4484/21/20/205502

Wang Y, Li X, Zhou Y, Liu C (2012) Colorimetric detection of copper (II) based on the self-assembly of Schiff's base-functionalized gold nanoparticles. 4(4). https://doi.org/10.5539/ijc.v4n4p90

Wang Y, Wan W, Qiu S, Luo L, Li Y, Guo L, Lin Z, Chen G (2017) Colorimetric probe for copper (ii) ion detection based on cost-effective aminoquinoline derivative. Anal Methods 9(11):1727–1731. https://doi.org/10.1039/C6AY03428D

Wu ZH, Sun S (2016) A review on colorimetric detection of mercury in water using gold nanoparticles. IAEJ 25(2):75–83

Wu Y, Liu L, Zhan S, Wang F, Zhou P (2012) Ultrasensitive aptamer biosensor for arsenic(iii) detection in aqueous solution based on surfactant-induced aggregation of gold nanoparticles. Analyst 137(18):4171–4178. https://doi.org/10.1039/C2AN35711A

Wu P, Hwang K, Lan T, Lu Y (2013) A DNAzyme-gold nanoparticle probe for uranyl ion in living cells. J Am Chem Soc 135(14):5254–5257. https://doi.org/10.1021/ja400150v

Xie J, Zheng Y, Ying JY (2009) Protein-directed synthesis of highly fluorescent gold nanoclusters. J Am Chem Soc 131(3):888–889. https://doi.org/10.1021/ja806804u

Xue Y, Zhao H, Wu Z, Li X, He Y, Yuan Z (2011) Colorimetric detection of Cd^{2+} using gold nanoparticles cofunctionalized with 6-mercaptonicotinic acid and l-Cysteine. Analyst 136 (18):3725–3730. https://doi.org/10.1039/C1AN15238F

Yan L, Zhang S, Chen P, Liu H, Yin H, Li H (2012) Magnetotactic bacteria, magnetosomes and their application. Microbiol Res 167(9):507–519. https://doi.org/10.1016/j.micres.2012.04.002

Yan Z, Yuen M-F, Hu L, Sun P, Lee C-S (2014) Advances for the colorimetric detection of Hg^{2+} in aqueous solution. RSC Adv 4(89):48373–48388. https://doi.org/10.1039/C4RA07930B

Yang W, Gooding JJ, He Z, Li Q, Chen G (2007) Fast colorimetric detection of copper ions using L-cysteine functionalized gold nanoparticles. J Nanosci Nanotechnol 7(2):712–716

Yang Y, Noviana E, Nguyen MP, Geiss BJ, Dandy DS, Henry CS (2017) Paper-based microfluidic devices: emerging themes and applications. Anal Chem 89(1):71–91. https://doi.org/10.1021/acs.analchem.6b04581

Ye Y, Lv M, Zhang X, Zhang Y (2015) Colorimetric determination of copper(ii) ions using gold nanoparticles as a probe. RSC Advances 5 (124):102311–102317

Yeh YC, Creran B, Rotello VM (2012) Gold nanoparticles: preparation, properties, and applications in bionanotechnology. Nanoscale 4(6):1871–1880. https://doi.org/10.1039/c1nr11188d

Yen C-W, de Puig H, Tam JO, Gómez-Márquez J, Bosch I, Hamad-Schifferli K, Gehrke L (2015) Multicolored silver nanoparticles for multiplexed disease diagnostics: distinguishing dengue, yellow fever, and Ebola viruses. Lab Chip 15(7):1638–1641

Yu M (2014) Colorimetric detection of trace arsenic(III) in aqueous solution using arsenic aptamer and gold nanoparticles. Aust J Chem 67(5):813–818. https://doi.org/10.1071/CH13512

Yuan X, Chapman RL, Wu Z (2011) Analytical methods for heavy metals in herbal medicines. Phytochem Anal 22(3):189–198. https://doi.org/10.1002/pca.1287

Yuan Z, Hu C-C, Chang H-T, Lu C (2016) Gold nanoparticles as sensitive optical probes. Analyst 141(5):1611–1626. https://doi.org/10.1039/C5AN02651B

Zeng J, Ma Y, Jeong U, Xia Y (2010) AuI: an alternative and potentially better precursor than AuIII for the synthesis of Au nanostructures. J Mater Chem 20(12):2290–2301. https://doi.org/10.1039/B922571D

Zhao L, Gu W, Zhang C, Shi X, Xian Y (2016) In situ regulation nanoarchitecture of Au nanoparticles/reduced graphene oxide colloid for sensitive and selective SERS detection of lead ions. J Colloid Interface Sci 465:279–285

Zhu T, Vasilev K, Kreiter M, Mittler S, Knoll W (2003) Surface modification of citrate-reduced colloidal gold nanoparticles with 2-mercaptosuccinic acid. Langmuir 19(22):9518–9525. https://doi.org/10.1021/la035157u

Chapter 4
Impedimetric Sensors in Environmental Analysis: An Overview

Sunil Bhand and Gautam Bacher

Abstract In recent years, there has been a great need for rapid, reliable, specific and sensitive techniques for environmental monitoring. Conventional analytical techniques for environmental monitoring involves high cost, skilled personnel and also often are not available for online detection. On the other hand, impedance-based electrochemical sensing has the advantages of low cost, ease of use, portability and ability to perform both screening and online monitoring. Impedance-based detection technique is very powerful tool for the analysis of interfacial properties related to biosensing and chemical sensing at the modified electrode surfaces. Impedance method is less destructive as compared to other electrochemical methods for bio and chemical analysis. Impedance sensing gives direct electrical signals and does not require a label or other pre-treatment process. Label-free detection for biological and chemical analysis has been widely reported to detect environmental toxins. This chapter describes basic concepts in sensor design and construction and also covers recent developments in the field of impedimetric sensing applied to environmental analysis. Selected examples are discussed with respect to mycotoxins (aflatoxin M1, aflatoxin B1, ochratoxin A), antibiotic and pesticide residue analysis.

Keywords EIS · Biosensor · Electrodes · Antibody · Aptamer
Mycotoxin · Immunosensor

S. Bhand (✉)
Department of Chemistry, Biosensor Lab,
BITS Pilani K.K. Birla Goa Campus, Zuarinagar 403726, Goa, India
e-mail: sunilbhand@goa.bits-pilani.ac.in

G. Bacher
Department of Electrical and Electronics Engineering,
BITS Pilani K.K. Birla Goa Campus, Zuarinagar 403726, Goa, India
e-mail: ggb@goa.bits-pilani.ac.in

S. Bhattacharya et al. (eds.), *Environmental, Chemical and Medical Sensors*, Energy, Environment, and Sustainability, https://doi.org/10.1007/978-981-10-7751-7_4

1 Introduction

Biosensors have emerged as a promising toll to the traditional methods for the detection of pathogens and toxins (Alocilja and Radke 2003; Arora et al. 2006). Biosensors cover the wide range of analyte detection in complex matrices and have shown great potential in areas such as clinical, food analysis, bioprocess and environmental monitoring. Biosensors are of great interest because of their several advantages over the conventional techniques in the field of environmental analysis. The main advantages in the use of biosensors as compared to conventional methods are the short analysis time, low-cost detection, their suitability for automated analysis and the possibility to perform in real time. Direct monitoring of antibody-antigen interaction facilitates label-free detection, which will have many advantages such as high sensitivity, ease of detection, lower sample cost and short analysis time. Among the several types of transducers, label-free biosensors based on impedance have received considerable attention in recent years. These sensors have various attractive features associated with the use of specifically the electrochemical transducers, such as scalability of production, low cost and scope for miniaturization. Electrochemical impedance spectroscopy (EIS)-based sensors are considered as promising candidates for real-time applications. Moreover, the label-free nature of EIS has major advantages over amperometric and potentiometric sensors. Hence, impedimetric biosensors have potential for simple, rapid, label-free and low-cost detection of biomolecules in the environmental analysis.

2 Impedimetric Biosensor

Impedimetric detection is predominantly based on affinity biosensors (Van Emon 2007). It is used to capture and quantify immunological binding events such as antibody-antigen interaction on an electrode surface. This binding results into impedance change which is proportional to the concentration of the target analyte specific to the receptor. Lorenz and Schulze in 1975 (Lorenz and Schulze 1975) explained EIS by measuring resistive and capacitive properties of materials, when a small amplitude sinusoidal ac excitation signal typically of 2–10 mV is applied to a system (Bartlett 2008; Suni 2008). The impedance response is obtained by varying frequency over a wide range. In impedance measurement, a suitable ac voltage is applied to the electrode system and the corresponding response current is measured. The resistive and capacitive components of impedance are extracted from in-phase and out-of-phase current. Impedance methods are very useful because it can capture electron transfer process at high frequency and mass transfer activity at low-frequency range. The change in electron transfer resistance or change in capacitance is observed at the electrode/electrolyte interface as a result of antibody-antigen binding. The electron transfer resistance or capacitance change depends on faradaic or non-faradaic impedance measurement.

2.1 Electrochemical Impedance Spectroscopy (EIS)

EIS is an efficient tool for the analysis of bio-interfacial properties associated with bio-recognition occurring at the modified electrode surfaces. EIS is less destructive method for analysis of biological interactions (Bogomolova et al. 2009) compared to other electrochemical methods such as cyclic voltammetry (CV) or differential pulse voltammetry (DPV) and facilitates easy diagnostics (Daniels and Pourmand 2007). EIS analyses in terms of electrical components such as resistance and capacitance change that occurs at the electrode surface. Such components enable capturing of very sensitive biological binding events such as antibody-antigen interaction. Till date, several immunosensors based on EIS have been reported (Lisdat and Schäfer 2008; Qi et al. 2010). Specifically, label-free detection method for biological and chemical analysis has been reported for detection of marine bio-toxins (Syaifudin et al. 2009) and characteristics of food products (Li et al. 2011).

2.1.1 Fundamentals of EIS

The impedance (Z) of an electrochemical system is determined by applying a suitable voltage with small amplitude and measuring the corresponding current response. Thus, Z is the ratio of the voltage–time function $V(t)$ to the resulting current–time function $I(t)$ as given by Eq. 2.1

$$Z = \frac{V(t)}{I(t)} = \frac{V_0 \sin(2\pi ft)}{I_0 \sin(2\pi \mathrm{ft} + \varphi)} \tag{2.1}$$

where

V_0 and I_0	are the amplitude of voltage and current signals
f	is the applied frequency
t	is time and
φ	is the phase shift between the voltage and current

In an electrochemical cell, the impedance 'Z' represents the total opposition offered by all the components (resistors, capacitors and or inductors) to the flow of electrons and ions present. In an ac circuit, the electrode kinetics, redox processes, diffusion phenomena and other molecular interactions at the electrode surface also oppose the flow of electrons (Macdonald 1987). Impedance measurement gives information in terms of resistance/capacitance, upon changes at the electrode surface. However, the contribution from inductance is significant at high frequency in impedance spectra. Whereas, in EIS-based sensors, the contribution from inductance is of less significance.

Generally, Impedance is a complex number, with ohmic resistance as real component and the capacitive reactance as imaginary component. The data are

usually analysed using Nyquist and Bode plots. In the Nyquist plot, the imaginary component Z'' (out-of-phase) of impedance is plotted against the real component Z' (in-phase) of impedance for each excitation frequency as presented in Fig. 1a. A distinctive shape of faradaic impedance spectrum is presented with Nyquist plot (Fig. 1b). This comprises of a semicircle region and a straight line. The straight line (linear part, $\phi = 45°$), observed at the low-frequency range, represent a mass transfer limited process and the semicircle portion observed at high frequency range, denotes a charge transfer limited process. Whereas, in Bode plot, the absolute impedance data is plotted against frequency as shown in Fig. 1c. In non-faradaic impedance measurement, redox probe is absent in the electrolyte and electrode surface is covered only with dielectric layer resembling perfect insulator. Hence electrode setup works as a capacitor. Thus, in such situation the antibody-antigen interaction causes change in capacitance resulting in impedance change. Usually, Bode plot is used to represent impedance data against frequency for analysis of Ab–Ag interaction and quantification in terms of impedance '*Z*'.

Capacitive immunosensors are mainly based on measurement of the change in dielectric properties and/or thickness of the dielectric layer. An electrolytic capacitor is represented by two plates, where the first plate is represented by sensing

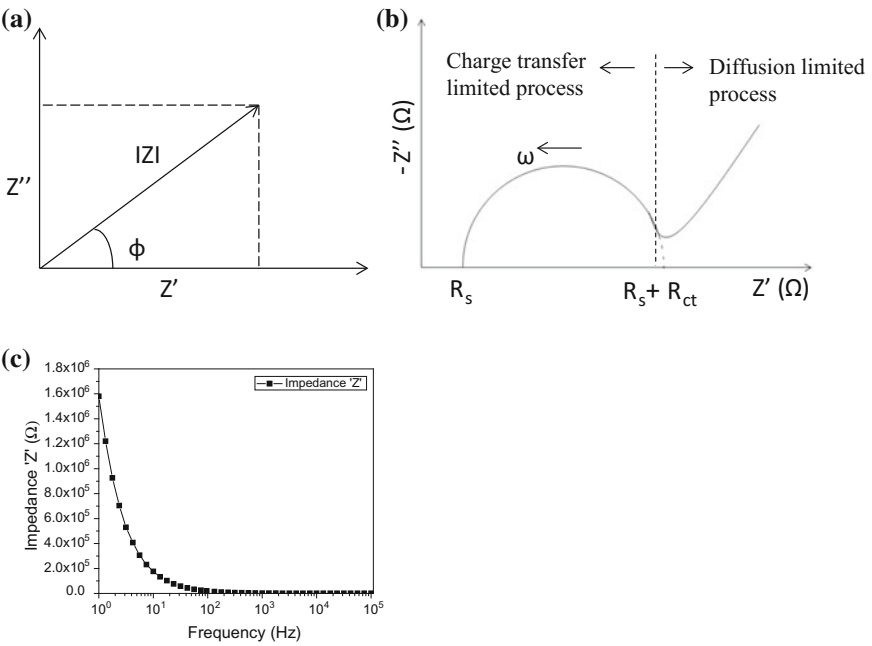

Fig. 1 **a** Phasor diagram of impedance **b** Nyquist plot for faradaic EIS (R_s: electrolyte resistance, R_{ct}: charge-transfer resistance, C_{dl}: double-layer capacitance, ω: angular frequency, Z': real component of Z and Z'': imaginary component of Z) **c** Bode plot for faradaic EIS

electrode and the second plate is represented by electrolyte. This allows the detection of an analyte specific to the bioreceptor that has been already immobilized on the insulating dielectric layer (Berggren et al. 2001; Katz and Willner 2003; K'Owino and Sadik 2005). Generally, this configuration resembles as capacitor having charge storage ability, and hence, the capacitance between the sensing electrode and the electrolyte is represented by Eq. 2.2.

$$C = \frac{\varepsilon_0 \in A}{d} \tag{2.2}$$

where

'ε' is the dielectric constant of the medium between the plates,
'ε_0' is the permittivity of free space,
'A' is the surface area of the plates in square metre, m^2,
'd' is the thickness of the insulating layer in metre, m.

2.1.2 EIS Measurement

EIS measurement is generally carried out using either three electrodes or a two electrode setup, which is a part of an electrochemical cell. In a three-electrode setup, the working electrode should be chemically stable, conductive and solid materials such as Pt, Ag, or graphite is used. Conventionally, the reference electrode is a silver metal coated with a layer of silver chloride (Ag|AgCl) and the auxiliary electrode a platinum wire. The advantage of a three electrode system is its stable half cell potential due to the greater charge flow through auxiliary instead of the reference electrode; this in turn helps in maintaining its half-cell potential (Ronkainen et al. 2010). A two-electrode system consists of a working and reference electrode. In two-electrode system, the need for a counter electrode is eliminated since the reference electrode can carry the charge with no adverse effects when current density is low. Both three-electrode systems as well as two-electrode systems are reported for biosensing. Since a disposable biosensor system does not require long-term stability, hence two electrode system may be preferable. In impedance biosensors, the applied voltage should be quite small, usually up to 10 mV in amplitude for several reasons. First, the current–voltage relationship is linear only for small perturbations (Barbero et al. 2005), and impedance is strictly defined for linear region only. The second reason for using a small perturbation is to avoid disturbing the probe layer since the covalent bond energies are usually in the order of 1–3 eV (Daniels and Pourmand 2007), but probe–target and electrode–probe binding energies can be much less. Correctly performed EIS does not damage or even disturb the biomolecular probe layer; this is a major advantage over voltammetry or amperometry where extreme voltages are usually applied. A schematic of EIS measurement setup is shown in Fig. 2a–f.

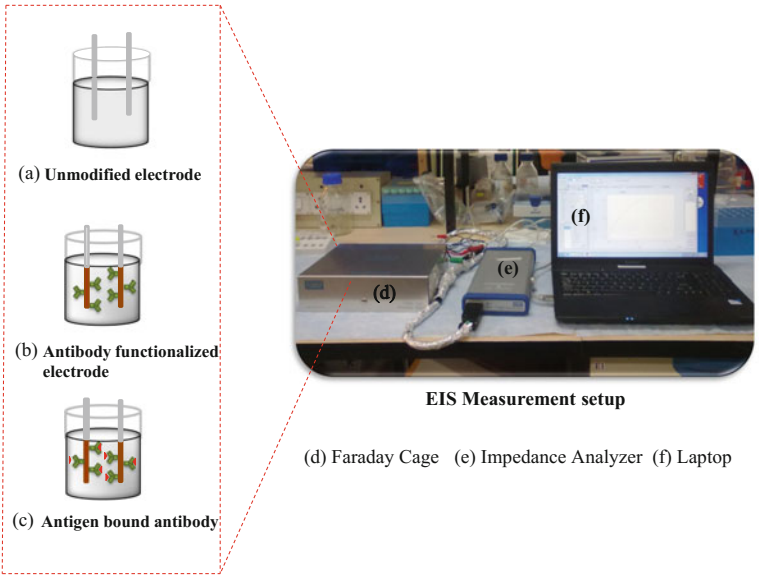

Fig. 2 Schematic diagram of EIS measurement setup

2.1.3 Interpretation of EIS Data

In EIS technique, a sinusoidal voltage is applied across the electrode and corresponding current signal is measured. The impedance is calculated by applying Ohm's law as given in Eq. 2.3.

$$Z = \frac{V}{I} = Z' + jZ'' \tag{2.3}$$

where Z is impedance, real term Z' (real component of Z) and Z'' (imaginary component of Z). An equivalent circuit is used to analyse impedance data. An equivalent circuit is the representation of the physical system parameters in terms of electrical components, mainly resistors, capacitors or constant phase elements. These electrical components are connected in series or in parallel depending on how and when different events occur in the system under study. The data interpretation and analysis by equivalent circuits is broadly accepted.

2.1.4 Labelled Versus Label-Free Detection

In labelled biosensors, a label is attached to the target and the amount of label detected corresponds to the number of bound targets (Daniels and Pourmand 2007). The labels mostly used are fluorophores or an enzyme. Labelling needs extra steps for sample preparations and hence adds extra time and cost. However, labelling a

target can significantly alter its binding properties and also might result in highly variable coupling efficiency (Haab 2003). These problems are very serious when a protein target is used. Therefore, for protein target, an indirect labelling is used. Indirect labelling requires two probes that bind to the target. The first probe is immobilized on the solid support, the analyte is introduced and then a secondary probe is introduced after washing. This second probe is labelled or can be detected by introducing yet another labelled probe that binds to all the secondary probes. This method increases selectivity with higher development cost and hence limited use in research. In label-free system, the interaction between target molecule and probe results changes in electrical properties of the surface due to the presence of the target molecule only. Moreover, label-free operation facilitates real-time detection of target-probe binding (Skládal 1997) which is not possible with labelled systems.

2.1.5 Faradaic Versus Non-faradaic Response

EIS can be divided into two categories: faradaic and non-faradaic EIS (Yang et al. 2004). In faradaic measurement, the charge is transferred across the electrode/electrolyte interface. Whereas, in a non-faradaic EIS, transient currents can flow without actual charge transfer (e.g. as in charging a capacitor). For electrical circuit analysis, a non-faradaic interface is characterized by a capacitor, and a faradaic interface is characterized by a resistor. Actual electrode–solution interfaces can have both faradaic and non-faradaic components. Faradaic impedance measurement requires a redox probe, while non-faradaic impedance measurement can be performed in the absence of a redox probe. When an electrode is immersed in electrolyte without having redox probe, the interfacial capacitance at the electrode can be used as a sensitive function of surface change associated with a binding event (Berggren et al. 2001). The change in capacitance due to binding of analyte is mainly because of changes in dielectric constant, charge distribution; electrolyte or water penetration. This is practically simple since no redox probe needs to be added to the electrolyte and hence very useful from an end-user perspective. A non-faradaic impedance biosensor using high-density microelectrode array was reported for *E.coli* O157:H7 detection (Radke and Alocilja 2005). AFM1 detection in the ppt range was reported by non-faradaic impedance measurement (Vig et al. 2009). The capacitive biosensor usually defines a sensor based on non-faradaic system and refers to one that makes measurements at a single frequency.

2.1.6 Equivalent Circuit Analysis for EIS

The interfacial phenomena of electrochemical cell are represented by an equivalent circuit and behave same as the real cell under given excitation (Yang et al. 2003). The electrochemical phenomena at the electrode/electrolyte interface can be modeled with electrical components used in equivalent circuit corresponding to

Table 1 Reported equivalent circuit design for impedimetric biosensor

Recognition element	Analyte	Circuit design	Detection limit	References
Anti-serum	Serum with Johne's disease	RC	10 $ngmL^{-1}$	Li et al. (2014)
Anti-HSA antibody	HSA	R(RC)	$2.4 \pm 0.1 \times 10^{-8}$ to $84.3 \pm 1.2 \times 10^{-8}$ M	Wongkittisuksa et al. (2011)
Antibody	AFM1	R_s, $C_{dl(ol)}$ ($R_{dl}C_{dl\ (il)}$)	6.25–100 pg mL^{-1}	Bacher et al. (2012)
IgG antibodies	Ciprofloxacin	R(RC)(RC)	10 $pgmL^{-1}$ to 100 $ngmL^{-1}$	Ionescu et al. (2007)
Anti-salmonella antibodies	Salmonella	R(C(RW))	100–10,000,000 $cfumL^{-1}$	Dong et al. (2013)
Anti-IL-6 antibodies	IL-6	(RC)(C(RW))	0.01 $fgmL^{-1}$	Yang et al. (2013)
Anti-CEA antibodies	CEA	R_DC_DL	10 μM	Jin et al. (2016)
Anti-OTA antibody	Ochratoxin A (OTA)	R(C(RW))	0.01–5 $ngmL^{-1}$	Malvano et al. (2016)

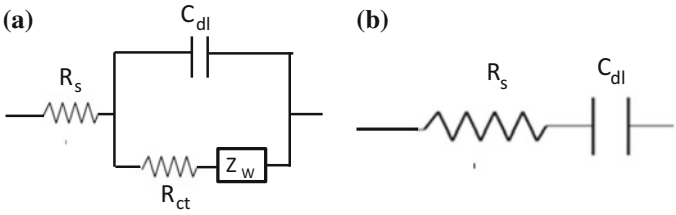

Fig. 3 Electrical equivalent circuit models for **a** faradaic impedance measurement and **b** non-faradaic impedance measurement

experimental impedance data. The electrical components used in equivalent circuit include the ohmic resistance of electrolyte solution R_s, the Warburg impedance Z_W, which represent diffusion of ions from bulk electrolyte to the electrode, the double-layer capacitance C_{dl}, and charge-transfer resistance R_{ct}, when redox probe is present in the electrolyte solution. Usually, more than one circuit model can fit the experimental data, but a unique equivalent circuit is selected based on the one best describing the physical characteristics of electrochemical cell. A simple equivalent circuit was reported having resistor and capacitor in series to show the behaviour of the impedance test using two electrodes setup (Yang and Bashir 2008). A summary of reported equivalent circuits for impedimetric immunosensors is presented as Table 1. In case of faradaic impedance measurement, Randles circuit (Fig. 3a) is commonly used to fit the EIS experimental data. A simple electrical equivalent circuit model was reported for non-faradaic impedance measurement to detect *Salmonella typhimurium* (Yang et al. 2003). For non-faradaic impedance measurement, a simple equivalent circuit consists of a series combination of medium resistance (R_s) and the double-layer capacitance (C_{dl}) was presented as shown in Fig. 3b.

2.1.7 Double-Layer Capacitance (C_{dl})

When the electrodes are polarized as compared to electrolyte, it attracts ions of opposite charge. This attractive tendency is countered by the randomizing thermal motion of the ions but results in a build-up of ions with opposite charge near the surface. This local charge imbalance prevents the electric field generating from the charged surface from penetrating very far into solution. The characteristic length of this spatial decay of the electric field is called the Debye length. The locally enhanced populations of ions act like the second plate of a capacitor; hence, it is termed as double-layer capacitance or diffuse layer capacitance (Fig. 4).

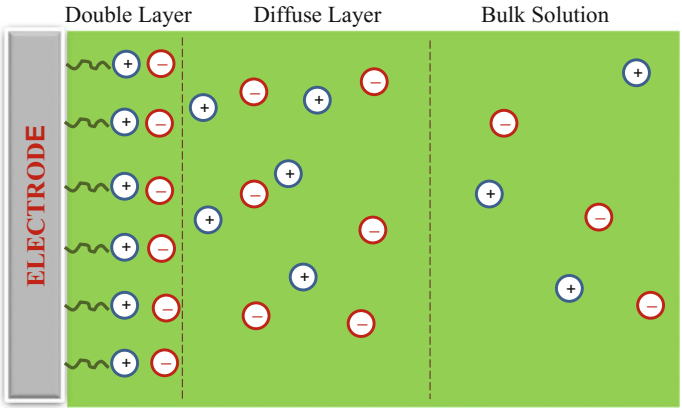

Fig. 4 Schematic diagram of electric double layer with distribution of +ve and −ve charge species

2.1.8 Constant Phase Element (CPE)

The electrode| electrolyte impedance change is also influenced by the frequency dispersion. This frequency dispersion is generally attributed to a 'capacitance dispersion' expressed in terms of a constant phase element (CPE). CPE behaviour is generally attributed to distributed surface reactivity, surface inhomogeneity, roughness or fractal geometry, electrode porosity, and current and potential distributions associated with electrode geometry (Jorcin et al. 2006). CPE is generally used to model double-layer capacitance of electrodes over simple capacitor (Gawad et al. 2004). The complex impedance of a CPE is given by Eq. 2.4.

$$Z_{\mathrm{CPE}} = \frac{1}{(j\omega)^m A} \tag{2.4}$$

where 'A' is analogous to a capacitance, ω is the frequency expressed in rad/sec and m is the CPE phase parameter. It can easily be seen that $m = 1$ corresponds to a capacitor.

2.2 Impedimetric Immunosensor Constructions

An impedimetric biosensor consists of a pair of bio-functionalized electrodes, integrated with an insulating cross-linking layer connected to a transducer. The selection of electrode material and the appropriate surface modification of electrode are crucial for achieving the desired function and performance.

2.2.1 Selection of Electrode Material

The choice of electrode material is crucial in construction of impedimetric immunosensor for better performance in terms of sensitivity and selectivity. Metals such as Pt, Au (Kim et al. 2000), Ag (Brunelle 2001) and stainless steel have been reported as electrode materials owing to their excellent electrical and mechanical properties. The choice of materials was based on biocompatibility, low cost and ease of construction or fabrication of sensors.

2.2.2 Micro-interdigitated Electrode (μ-IDEs)

μ-IDEs are widely used for the development of biosensors. They present advantages in terms of low ohmic drop and increased signal-to-noise ratio (Maruyama et al. 2006). μ-IDEs have been investigated in varying shapes, size and structures and number of alternate fingers. Since μ-IDEs does not require a reference electrode, the measurement setup is quite simple and easy to perform compared to a conventional electrochemical setup (Nebling et al. 2004). μ-IDEs are generally fabricated by using photolithography techniques on silicon (Si) substrates with a features size varying from nanometres (nm) to tens of microns. Most commonly used metals for the fabrication of electrodes are Au, Ti and Pt. A summary of μ-IDEs with various metals with dimensions is presented as Table 2.

2.2.3 Self-Assembled Monolayers (SAMs)

Self-assembled monolayers (SAMs) of organic cross-linkers are widely used to attach specific bioprobes to the electrode. In impedance-based sensors, SAMs also act as an insulating layer. The common linkers are based on thiols (–SH) bound to electrode surfaces (Love et al. 2005). The use of proper SAMs helps in oriented and repeatable immobilization of biomolecules (Cheng et al. 2008). SAMs are also used

Table 2 Summary of reported fabricated μ-IDEs with various metals

Material	Substrate	Fabrication techniques	References
Gold (Au)	Silicon	Photolithography	Baccar et al. (2014)
Titanium (Ti), nickel (Ni) and gold (Au)	Pyrex	Photolithography	Laczka et al. (2008)
Platinum (Pt)	Borosilicate glass	Photolithography	Yang et al. (2011)
Silver (Ag)	Epoxy-glass fibre PCB	Photolithography	Cortina et al. (2006)
Aluminium (Al)	Silicon	Photolithography	Moreno-Hagelsieb et al. (2007)

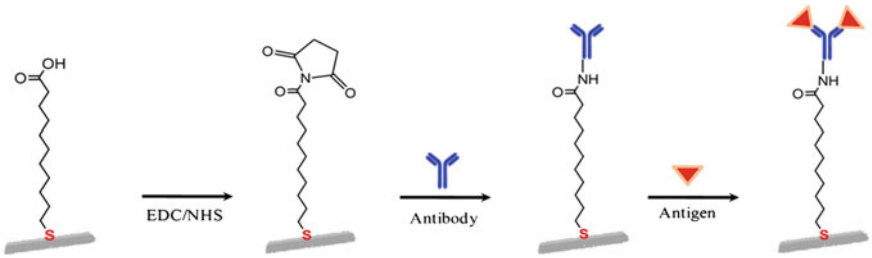

Fig. 5 Schematic showing functionalization of electrode surface by SAMs and binding of antibody-antigen on a metal substrate

to prevent protein denaturation at electrode surface and for improving stability of biomolecules (Kafi et al. 2007). A tightly packed (high leakage resistance, R_{leak}) SAM is desired for non-faradaic sensor, in contrast with faradaic sensors where the electrode surface needs to be accessible to the redox species (Lai et al. 2006).

2.2.4 Immobilization of Receptor

The bioreceptor is an integral component of the biosensor device. It is essential that the bioreceptor should be selective and sensitive towards specific target analyte. It should prevent interference by another substance from the sample matrix. For construction of a biosensor, immobilization of a biomolecules on a SAMs surface is an important requirement (Arya et al. 2009). Different immobilization strategies were employed and compared for selective and sensitive detection of biomolecule (dos Santos et al. 2009). An affinity biosensor is prepared by immobilizing antibodies onto a substrate of conducting or semiconductor material. A typical example of surface modification of a metal electrode and antibody coupling via SAMs is presented in Fig. 5. Noble metal substrates are very suitable for this purpose (Hou et al. 2004). The immobilization method also affects the immune-recognition event of antibodies towards antigens (Sassolas et al. 2012).

3 Materials and Instrumentation

All the chemicals used were of analytical grade and were used as received. Ag wire (diameter = 0.25 mm) was procured from ACROS Organics, USA. Anti-AFM1 and AFB1-fractionated anti-serum primary monoclonal antibody (mAb) were purchased from AbCam (UK). AFM1 standard, AFB1 standard, Tween20, 11-MUA, 1-ethyl-3-[3-dimethylaminopropyl] carbodiimide hydrochloride (EDC), *N*-hydroxysuccinimide (NHS), certified reference material (CRM) ERM-BD 282 (AFM1 in whole milk powder < 0.02 μg kg^{-1}) were purchased from

Sigma–Aldrich, USA. Ethyl alcohol 200 proof was purchased from TEDIA, USA. Hydrogen peroxide (H_2O_2) 30% (w/v), acetonitrile (ACN) HPLC grade, disodium hydrogen phosphate (Na_2HPO_4), sodium dihydrogen phosphate (NaH_2PO_4) from MERCK (Germany) and sodium hypochlorite (4%) solution were purchased from Fisher Scientific (India). For sample handling, micropipettes (eppendorf®, Germany) were used. Centrifugation of milk sample was done by minispin (eppendorf®, Germany). Shaking and filtration of the samples were done by Spinix shaker (Tarsons, India). For the handling of AFM1 standard solution, glove box (Cole Parmer, USA) was used. For preparing all the solutions, water produced in a Milli-Q system (Millipore, Beford, MA, USA) was used. Impedance measurements were carried out using IVIUM CompactStat impedance analyser, Netherland. The required protocols and detailed procedures for the preparation of solutions, reagents and standards are as described (Bacher et al. 2012).

4 Experimental Setup for Aflatoxin Analysis

The measurement setup consisting of a pair of functionalized metal electrode with an appropriate diameter was immersed in the analyte solution confined in glass cell and separated by an optimal distance. The measurement setup is kept in an enclosed chamber. The anti-aflatoxin M1 monoclonal antibodies (mAb) were covalently coupled on a metal wire electrode through SAMs. The functionalized wire electrodes were connected to an impedance analyser. The schematic diagram of measurement setup is presented in Fig. 6.

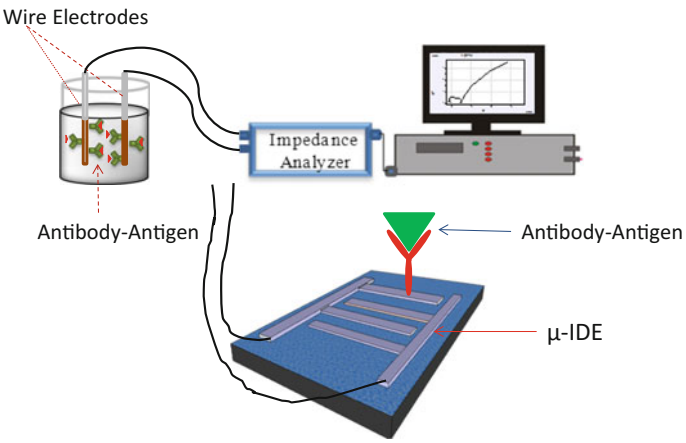

Fig. 6 Schematic connection diagram of impedance measurement setup

4.1 EIS Study for Aflatoxin M1 Analysis

The quantification of the interaction of anti-AFM1 and AFM1 was carried out using EIS. For non-faradaic impedance measurement, the impedance of the interface is measured at a single frequency. Figure 7 shows the impedance response of antibody-antigen interaction on for a blank (without AFM1 and a sample with 50 ppt AFM1). A distinctive change in impedance was observed over the blank which can be correlated with the presence of AFM1 in the low-frequency region. Such response can be measured for higher concentrations of the analyte under consideration.

4.2 Construction of Calibration Curve (AFB1 Analysis)

As another typical example for analytical purposes, non-faradaic impedance measurements were conducted using functionalized electrodes for AflatoxinB1 (AFB1) with increasing concentration (0.1–100 $pgmL^{-1}$). The impedance data were recorded at a frequency of 1 Hz with applied ac potential of 5 mV. A significant impedance change was observed at 1 Hz frequency. The specific interaction of anti-AFB1 and AFB1 at the electrode/electrolyte interface results in an overall increase in impedance change from baseline response for AFB1. The percentage

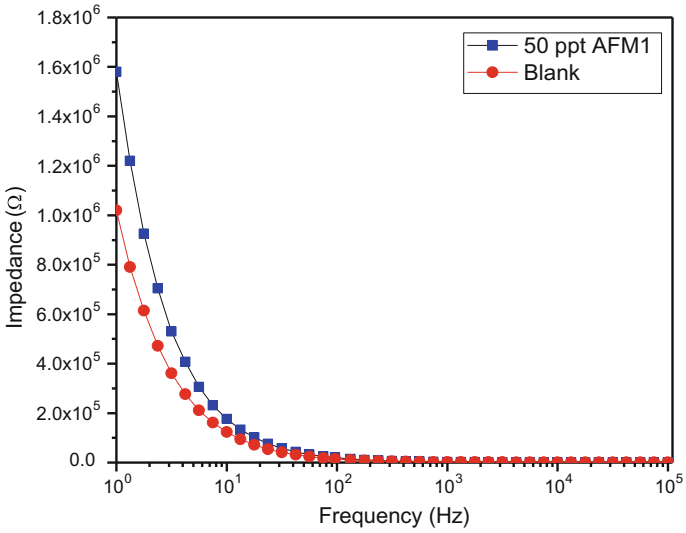

Fig. 7 Impedance response of the immunosensor before and after antibody-antigen interaction (50 ppt AFM1) at room temperature (0.01 M PBS medium, frequency range 1 Hz to 100 kHz at ac potential of 10 mV)

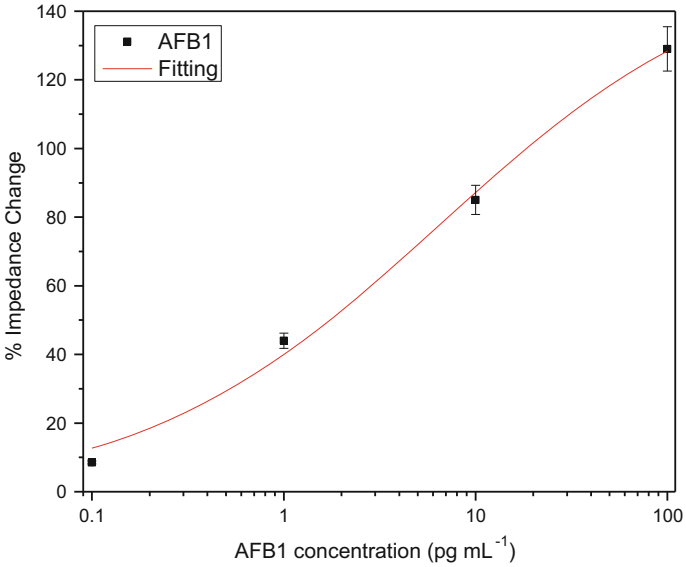

Fig. 8 Calibration curve of AFB1 (0.1–100 pgmL^{-1}) at a frequency range of 1–100 kHz), 5 mV ac potential

impedance change was determined corresponding to various concentrations of AFB1. The resulting calibration curve is presented in Fig. 8. A linear range for AFB1 detection 1–100 pgmL^{-1} with SD = 0.15 and R^2 = 0.99 was achieved. Limit of detection (LOD) was found to be 0.1 pg mL^{-1}.

5 Recent Developments in Impedimetric Sensing

It has been established that impedimetric immunosensor provides a platform for detection of various contaminants including food toxin in the environment. One of the important challenges in the analytical sciences is to develop the devices and methods capable of detecting carcinogenic or highly toxic chemical contaminants requiring detection at levels as low as 1–50 ngL^{-1} range or below. The development of impedimetric sensors has gained advances with application in various environmental matrices spanning from water to food and even to the cellular level. For instance, impedimetric immunosensor for detection of aflatoxin M1 (AFM1) is reported with a detection limit of 1 pgmL^{-1} within 20 min. This technique has also been extended to milk product such as flavoured milk and yogurt (Kanungo et al. 2014). In the recent years, the use of screen-printed three electrode as well as interdigitated electrodes in impedimetric sensors has gained significant attention in environmental analysis (Rivas et al. 2015; Istamboulié et al. 2016; Li et al. 2016; Gu et al. 2015; López Rodriguez et al. 2015; Liu et al. 2015; Sharma et al. 2017).

Table 3 Recently reported impedimetric biosensor for different analytes

Analyte	Matrix	Transducer	LOD	References
Ochratoxin A (OTA)	White wine	Screen-printed carbon electrode (SPCE)	5.65 ng kg^{-1}	Rivas et al. (2015)
AFM1	Milk	SPCE	1.15 ng L^{-1}	Istamboulié et al. (2016)
AFB1	Rice	Screen-printed interdigitated microelectrodes	5 ng mL^{-1}	Li et al. (2016)
Deoxynivalenol (DON)	Cell toxicity	Gold microelectrode	0.03 μg mL^{-1}	Gu et al. (2015)
Lindane	Bacterial culture	Stainless steel elctrodes	120 μg L^{-1}	López Rodriguez et al. (2015)
Carbofuran	Water	Gold electrode	0.1 ng mL^{-1}	Liu et al. (2015)
Kanamycin	Milk	SPCE	0.11 ng mL^{-1}	Sharma et al. (2017)
DNA molecules	Deionized water	Gold microelectrode	Nano molar	Liu et al. (2008)

In addition to the use of bioreceptor (antibodies, enzymes and aptamer) as sensing element, the impedimetric sensors devices based on interdigitated electrodes have also been demonstrated for the detection of DNA concentration and length in deionized water (Liu et al. 2008). Further developments in label-free detection using EIS incorporated integration of nonmaterial in detection of DNA sequences as well as to confirm the signal amplification in peptide-based nucleic acid and as genosensors (Bonanni and Del Valle 2010). The use of nucleic acid receptors such as aptamer is also gaining significant attention owning to their selectivity and better stability over antibody-based receptors. Recently reported impedimetric biosensors for antibiotic residue analysis in milk and pesticide residue analysis as well as mycotoxins analysis are summarized in Table 3 with the reported limit of detection achieved using EIS.

Acknowledgements This work was financially supported under NAIP project of ICAR, Govt. of India No. C4/C10125.

References

Alocilja EC, Radke SM (2003) Market analysis of biosensors for food safety. Biosens Bioelectron 18(5):841–846

Arora K, Chand S, Malhotra B (2006) Recent developments in bio-molecular electronics techniques for food pathogens. Anal Chim Acta 568(1):259–274

Arya SK, Solanki PR, Datta M, Malhotra BD (2009) Recent advances in self-assembled monolayers based biomolecular electronic devices. Biosens Bioelectron 24(9):2810–2817

Baccar H, Mejri M, Prehn R, del Campo R, Baldrich E, Rosemonde M, Abdelghani A (2014) Interdigitated microelectrode arrays integrated in microfluidic cell for biosensor applications. J Nanomedicine Nanotechnol 5(6):1

Bacher G, Pal S, Kanungo L, Bhand S (2012) A label-free silver wire based impedimetric immunosensor for detection of aflatoxin M1 in milk. Sens Actuators B Chem 168:223–230

Barbero G, Alexe-Ionescu A, Lelidis I (2005) Significance of small voltage in impedance spectroscopy measurements on electrolytic cells. J Appl Phys 98(11):113703

Bartlett PN (2008) Bioelectrochemistry: fundamentals, experimental techniques and applications. Wiley. https://doi.org/10.1002/9780470753842

Berggren C, Bjarnason B, Johansson G (2001) Capacitive biosensors. Electroanalysis 13(3): 173–180

Bogomolova A, Komarova E, Reber K, Gerasimov T, Yavuz O, Bhatt S, Aldissi M (2009) Challenges of electrochemical impedance spectroscopy in protein biosensing. Anal Chem 81 (10):3944–3949

Bonanni A, Del Valle M (2010) Use of nanomaterials for impedimetric DNA sensors: a review. Analytica chimic aacta 678(1):7–17

Brunelle S (2001) Electro immunoassay technology for foodborne pathogen detection. IVD Technol 6(2001):55

Cheng F, Gamble LJ, Castner DG (2008) XPS, TOF-SIMS, NEXAFS, and SPR characterization of nitrilotriacetic acid-terminated self-assembled monolayers for controllable immobilization of proteins. Anal Chem 80(7):2564–2573

Cortina M, Esplandiu M, Alegret S, Del Valle M (2006) Urea impedimetric biosensor based on polymer degradation onto interdigitated electrodes. Sens Actuators B Chem 118(1):84–89

Daniels JS, Pourmand N (2007) Label-free impedance biosensors: opportunities and challenges. Electroanalysis 19(12):1239–1257

Dong J, Zhao H, Xu M, Ma Q, Ai S (2013) A label-free electrochemical impedance immunosensor based on AuNPs/PAMAM-MWCNT-Chi nanocomposite modified glassy carbon electrode for detection of Salmonella typhimurium in milk. Food Chem 141(3):1980–1986

dos Santos MB, Sporer C, Sanvicens N, Pascual N, Errachid A, Martinez E, Marco M-P, Teixeira V, Samiter J (2009) Detection of pathogenic bacteria by electrochemical impedance spectroscopy: influence of the immobilization strategies on the sensor performance. Proc Chem 1(1):1291–1294

Gawad S, Cheung K, Seger U, Bertsch A, Renaud P (2004) Dielectric spectroscopy in a micromachined flow cytometer: theoretical and practical considerations. Lab Chip 4(3):241–251

Gu W, Zhu P, Jiang D, He X, Li Y, Ji J, Zhang L, Sun Y, Sun X (2015) A novel and simple cell-based electrochemical impedance biosensor for evaluating the combined toxicity of DON and ZEN. Biosens Bioelectron 70:447–454

Haab BB (2003) Methods and applications of antibody microarrays in cancer research. Proteomics 3(11):2116–2122

Hou Y, Tlili C, Jaffrezic-Renault N, Zhang A, Martelet C, Ponsonnet L, Errachid A, Bausells J (2004) Study of mixed Langmuir-Blodgett films of immunoglobulin G/amphiphile and their application for immunosensor engineering. Biosens Bioelectron 20(6):1126–1133

Ionescu RE, Jaffrezic-Renault N, Bouffier L, Gondran C, Cosnier S, Pinacho DG, Marco MP, Sánchez-Baeza FJ, Healy T, Martelet C (2007) Impedimetric immunosensor for the specific label free detection of ciprofloxacin antibiotic. Biosens Bioelectron 23(4):549–555

Istamboulié G, Paniel N, Zara L, Granados LR, Barthelmebs L, Noguer T (2016) Development of an impedimetricaptasensor for the determination of aflatoxin M1 in milk. Talanta 146:464–469

Jin Y, Mao H, Jin Q, Zhao J (2016) Real-time determination of carcinoembryonic antigen by using a contactless electrochemical immunosensor. Anal Methods 8(24):4861–4866

Jorcin J-B, Orazem ME, Pébère N, Tribollet B (2006) CPE analysis by local electrochemical impedance spectroscopy. Electrochim Acta 51(8):1473–1479

Kafi A, Lee D-Y, Park S-H, Kwon Y-S (2007) Development of a peroxide biosensor made of a thiolated-viologen and hemoglobin-modified gold electrode. Microchem J 85(2):308–313

Kanungo L, Bacher G, Bhand S (2014) Flow-based impedimetricimmunosensor for aflatoxin analysis in milk products. Appl Biochem Biotechnol 174(3):1157–1165

Katz E, Willner I (2003) Probing biomolecular interactions at conductive and semiconductive surfaces by impedance spectroscopy: routes to impedimetric immunosensors, DNA-sensors, and enzyme biosensors. Electroanalysis 15(11):913–947

Kim J-H, Cho J-H, Cha GS, Lee C-W, Kim H-B, Paek S-H (2000) Conductimetric membrane strip immunosensor with polyaniline-bound gold colloids as signal generator. Biosens Bioelectron 14(12):907–915

K'Owino IO, Sadik OA (2005) Impedance spectroscopy: a powerful tool for rapid biomolecular screening and cell culture monitoring. Electroanalysis 17(23):2101–2113

Laczka O, Baldrich E, Muñoz FX, del Campo FJ (2008) Detection of Escherichia coli and *Salmonella typhimurium* using interdigitated microelectrode capacitive immunosensors: The importance of transducer geometry. Anal Chem 80(19):7239–7247

Lai RY, Seferos DS, Heeger AJ, Bazan GC, Plaxco KW (2006) Comparison of the signaling and stability of electrochemical DNA sensors fabricated from 6-or 11-carbon self-assembled monolayers. Langmuir 22(25):10796–10800

Li X, Toyoda K, Ihara I (2011) Coagulation process of soymilk characterized by electrical impedance spectroscopy. J Food Eng 105(3):563–568

Li S, Cui H, Yuan Q, Wu J, Wadhwa A, Eda S, Jiang H (2014) AC electrokinetics-enhanced capacitive immunosensor for point-of-care serodiagnosis of infectious diseases. Biosens Bioelectron 51:437–443

Li Z, Ye Z, Fu Y, Xiong Y, Li Y (2016) A portable electrochemical immunosensor for rapid detection of trace aflatoxin B1 in rice. Anal Methods 8(3):548–553

Lisdat F, Schäfer D (2008) The use of electrochemical impedance spectroscopy for biosensing. Anal Bioanal Chem 391(5):1555

Liu Y-S, Banada PP, Bhattacharya S, Bhunia AK, Bashir R (2008) Electrical characterization of DNA molecules in solution using impedance measurements. Appl Phys Lett 92(14):143902

Liu L, Xu D, Hu Y, Liu S, Wei H, Zheng J, Wang G, Hu X, Wang C (2015) Construction of an impedimetric immunosensor for label-free detecting carbofuran residual in agricultural and environmental samples. Food Control 53:72–80

López Rodriguez ML, Benimeli C, Madrid RE, Giacomelli CE (2015) A simple Streptomyces spore-based impedimetric biosensor to detect lindane pesticide. Sens Actuators B Chem 207:447–454

Lorenz W, Schulze K (1975) Zuranwendung der transformations—impedanzspektrometrie. J Electroanal Chem Interfacial Electrochem 65(1):141–153

Love JC, Estroff LA, Kriebel JK, Nuzzo RG, Whitesides GM (2005) Self-assembled monolayers of thiolates on metals as a form of nanotechnology. Chem Rev 105(4):1103–1170

Macdonald JR (1987) Impedance spectroscopy, vol 11. Wiley, New York

Malvano F, Albanese D, Pilloton R, Di Matteo M (2016) A highly sensitive impedimetric label free immunosensor for Ochratoxin measurement in cocoa beans. Food Chem 212:688–694

Maruyama K, Ohkawa H, Ogawa S, Ueda A, Niwa O, Suzuki K (2006) Fabrication and characterization of a nanometer-sized optical fiber electrode based on selective chemical etching for scanning electrochemical/optical microscopy. Anal Chem 78(6):1904–1912

Moreno-Hagelsieb L, Foultier B, Laurent G, Pampin R, Remacle J, Raskin J-P, Flandre D (2007) Electrical detection of DNA hybridization: three extraction techniques based on interdigitated Al/Al_2O_3 capacitors. Biosens Bioelectron 22(9):2199–2207

Nebling E, Grunwald T, Albers J, Schäfer P, Hintsche R (2004) Electrical detection of viral DNA using ultra microelectrode arrays. Anal Chem 76(3):689–696

Qi H, Wang C, Cheng N (2010) Label-free electrochemical impedance spectroscopy biosensor for the determination of human immunoglobulin G. Microchim Acta 170(1–2):33–38

Radke SM, Alocilja EC (2005) A high density microelectrode array biosensor for detection of *E. coli* O157: H7. Biosens Bioelectron 20(8):1662–1667

Rivas L, Mayorga-Martinez CC, Quesada-González D, Zamora-Gálvez A, de la Escosura-Muñiz A, Merkoçi A (2015) Label-free impedimetric aptasensor for ochratoxin—a detection using iridium oxide nanoparticles. Anal Chem 87(10):5167–5172

Ronkainen NJ, Halsall HB, Heineman WR (2010) Electrochemical biosensors. Chem Soc Rev 39 (5):1747–1763

Sassolas A, Blum LJ, Leca-Bouvier BD (2012) Immobilization strategies to develop enzymatic biosensors. Biotechnol Adv 30(3):489–511

Sharma A, Istamboulie G, Hayat A, Catanante G, Bhand S, Marty JL (2017) Disposable and portable aptamer functionalized impedimetric sensor for detection of kanamycin residue in milk sample. Sens Actuators B Chem 245:507–515

Skládal P (1997) Advances in electrochemical immunosensors. Electroanalysis 9(10):737–745

Suni II (2008) Impedance methods for electrochemical sensors using nanomaterials. TrAC Trends Anal Chem 27(7):604–611

Syaifudin AM, Jayasundera K, Mukhopadhyay S (2009) A low cost novel sensing system for detection of dangerous marine biotoxins in seafood. Sens Actuators B Chemical 137(1):67–75

Van Emon JM (2007) Immunoassay and other bioanalytical methods. CRC Press, Boca Raton

Vig A, Radoi A, Munoz-Berbel X, Gyemant G, Marty J-L (2009) Impedimetric aflatoxin M 1 immunosensor based on colloidal gold and silver electrodeposition. Sens Actuators B Chem 138(1):214–220

Wongkittisuksa B, Limsakul C, Kanatharana P, Limbut W, Asawatreratanakul P, Dawan S, Loyprasert S, Thavarungkul P (2011) Development and application of a real-time capacitive sensor. Biosens Bioelectron 26(5):2466–2472

Yang L, Bashir R (2008) Electrical/electrochemical impedance for rapid detection of foodborne pathogenic bacteria. Biotechnol Adv 26(2):135–150

Yang L, Ruan C, Li Y (2003) Detection of viable Salmonella typhimurium by impedance measurement of electrode capacitance and medium resistance. Biosens Bioelectron 19(5): 495–502

Yang L, Li Y, Erf GF (2004) Interdigitated array microelectrode-based electrochemical impedance immunosensor for detection of *Escherichia coli* O157: H7. Anal Chem 76(4):1107–1113

Yang L, Guiseppi-Wilson A, Guiseppi-Elie A (2011) Design considerations in the use of interdigitated microsensor electrode arrays (IMEs) for impedimetric characterization of biomimetic hydrogels. Biomed Microdevice 13(2):279–289

Yang T, Wang S, Jin H, Bao W, Huang S, Wang J (2013) An electrochemical impedance sensor for the label-free ultrasensitive detection of interleukin-6 antigen. Sens Actuators B Chem 178:310–315

Part III
Chemical Sensors

Chapter 5
Inkjet-Printed Sensors on Flexible Substrates

Poonam Sundriyal and Shantanu Bhattacharya

Abstract Printing processes are gaining much prominence in sensing technologies through which smart materials can be deposited over flexible substrates. The attractive features of inkjet printing processes to replace other material deposition techniques are in terms of simplicity, low cost, environment friendliness, high resolution, less waste generation and mass production. This chapter presents a summary of various thin-film smart sensors as developed by inkjet printing processes over flexible substrates. The critical parameters for the printable ink, materials for the sensing applications, substrates for flexible electronics, advantages and challenges of inkjet printing method and its exploration for future flexible electronics sensors are visited through this chapter.

Keywords Inkjet printing · Smart sensors · Flexible substrates
Smart material ink

1 Introduction

Recently, a lot of attention is provided to find out efficient methods and materials for low-cost flexible sensors and electronics. Inkjet printing is a mature and versatile micromanufacturing tool which has assisted and revolutionized the rapidly increasing field of flexible sensors by providing a simple and cost-effective solution for their realization (Komuro et al. 2013). The important features associated with the printing process like simplicity, low waste generation, mask-free approaches, reduced usage of toxic chemicals, low cost, shape and size flexibility, no contact

P. Sundriyal (✉) · S. Bhattacharya
Department of Mechanical Engineering, Indian Institute of Technology, Kanpur 208016, Uttar Pradesh, India
e-mail: poonams@iitk.ac.in

P. Sundriyal · S. Bhattacharya
Microsystems Fabrication Laboratory, Indian Institute of Technology, Kanpur 208016, Uttar Pradesh, India

S. Bhattacharya et al. (eds.), *Environmental, Chemical and Medical Sensors*, Energy, Environment, and Sustainability, https://doi.org/10.1007/978-981-10-7751-7_5

with substrate and many others make it suitable for flexible sensor manufacturing (Singh et al. 2010). Also, the emergence of desktop printers for sensor and electronics device fabrication has drastically reduced sensor costs by several orders (Zheng et al. 2013; Andò and Baglio 2013; Sundriyal and Bhattacharya 2017). Due to the advancement of compact, on-chip and flexible sensors, thin-film flexible sensor markets are continuously growing. Initially, Kimura et al. reported inkjet printing of biosensors by enzyme deposition on the surface of a field effect transistor (Kimura et al. 1989). Recently, several research groups have reported many inkjet-printed sensors such as strain sensor (Andò and Baglio 2013), gas sensors (Stempien et al. 2016a), vapour sensors (Belsey et al. 2017), touch sensors (Ma et al. 2015), glucose sensors (Song et al. 2017) and wearable sensors (Morse et al. 2016).

Compatibility of inkjet printers with various flexible substrates (like paper, polymer, textile fabric and metal foils) (Ma et al. 2015; Wang et al. 2016; Stempien et al. 2016b) and sensor material inks (such as metallic ink, conducting polymer ink and carbon-based ink) (Stempien et al. 2016b; Arrese et al. 2017; Qin et al. 2016; Lee et al. 2016) has boosted its applications for printed sensor technologies. Despite many efforts and several advantages, some limitations of inkjet printing process still hinder its full utilization. One major challenge is the requirement of ink with rigid physical properties controllable by surface tension, viscosity and density of the ink. The range of these properties, their effect on print quality and optimum range of required physical properties have previously been reported by several researchers (Jang et al. 2009; Fromm 1984; Derby and Reis 2003).

All the components of sensor devices can be deposited on flexible substrates by inkjet printing. A sensor device has three main components: the conducting layer, the active sensing layer and the insulating layer. With the development of conducting material's ink, semiconducting material's ink and dielectric material's ink, the complete sensor can now be fabricated by using printing-assisted deposition in extremely short-time scales just by selecting different ink cartridges. The reported materials for conducting inks are silver (Arrese et al. 2017), copper (Lee et al. 2016), graphene (Das et al. 2016), carbon nanotube (CNT) (Qin et al. 2016) and conducting polymers (Crowley et al. 2008; Hwang et al. 2011). Inks used for active sensing layers are basically metal oxides (Kukkola et al. 2012; Rieu et al. 2015; Tsangarides et al. 2016), and dielectric material inks are based on polyvinyl alcohol, poly (methyl methacrylate), polyimide, poly (4-vinylphenol), polystyrene and terephthalate (Hamad et al. 2016; Pease and Chou 2008). Development of ink based on organic and inorganic materials for sensing applications still needs active research efforts. Another important component of flexible sensing devices is the substrate material over which the printing is carried out. The role of the substrate to be inked is very prominent due to adhesion issues between the ink and the substrates and also other mechanical properties associated with the device development. Some of the properties involved are flexibility, mechanical strength, wettability and stability of the substrates. Some investigations have been carried out for printing of sensors and other associated electronics in substrates like polymers (Ma et al. 2015; Rieu et al. 2015), paper (Wang et al. 2016), metal foils

(MacDonald et al. 2007) thin glasses (Zardetto et al. 2011) and textile fabrics (Stempien et al. 2016a). The choice of a substrate depends on the type of material deposited over it and also the required post-treatment temperature needed for settling and adhering the print to the substrate and also on sensing applications related to the concerned device (Lee et al. 2016; Das et al. 2016). The rapidly growing market of flexible electronics needs a high level of flexibility of involved substrates, high operational temperature ranges, wettability and long-term stability of devices. The main reason for their exploration is the emerging trend associated with flat and light weight electronic consumer goods and also the general market need for aesthetics and better form factors of electronic products. Also, the direct use of this technology for the development of microfluidic channels (Bhatt et al. 2016) can drastically increase the market of low-cost diagnostic devices and biosensors.

This chapter is an overview of this very new area of flexible electronics using printing technology and is organized as a series of basic technical issues related to the device development using flexible printed substrates. These issues are a thorough study of required physical properties of the printable inks, the inkjet printable materials constituting the ink required for sensor fabrication such as conductive materials, semiconductive materials, dielectric materials, substrates for printed sensors along with their compatibility and limitation for a particular application, advantages and limitations and future scope of inkjet-printed sensors.

2 Required Physical Properties of the Printable Ink

Most of the inkjet printing patterns as used by the industry are based on drop-on-demand (DOD) method which demands optimum physical properties of the ink for good quality printing. The droplet generation in DOD printers is a complex process which is governed by viscosity, surface tension and density of the printing ink (Fromm 1984). These properties affect the drop formation process and the drop size at a given injection voltage. Performance parameters that are involved in the drop formation process for inkjet printing can be characterized by the following dimensionless numbers:

Reynolds number (Re): It is the ratio of inertial to viscous forces.

$$\mathrm{Re} = \frac{\text{Inertia force}}{\text{Viscous force}} = \frac{va\rho}{\eta} \tag{1}$$

Weber number: It is the ratio of inertial force and surface tension forces.

$$\mathrm{We} = \frac{\text{Inertia force}}{\text{Surface tension}} = \frac{v^2 a\rho}{\gamma} \tag{2}$$

Ohnesorge number: It is the ratio of square root of Weber number and Reynolds number.

$$\mathrm{Oh} = \frac{\sqrt{\text{Weber number}}}{\text{Reynolds number}} = \frac{\eta}{\sqrt{a\rho\gamma}} \tag{3}$$

where v, a, ρ, η and γ represent average velocity, characteristic length (diameter of the printing nozzle), density, dynamic viscosity and surface tension of the fluid, respectively. The suitability of a fluid for inkjet printing is evaluated by finding out the Z number, which is the inverse of the Ohnesorge number.

At the initial stages of understanding the drop formation process, Fromm et al. (1984) suggested $Z > 2$ for a stable drop formation in DOD printers. This range was further refined by Reis and Derby as $1 < Z < 10$, and it was further observed that lower limit of Z depends on fluid viscosity which prevents droplet ejection while upper limit is restricted by the formation of satellite drops rather than a single droplet (Derby and Reis 2003). Again, Jang et al. (2009) have proposed this range

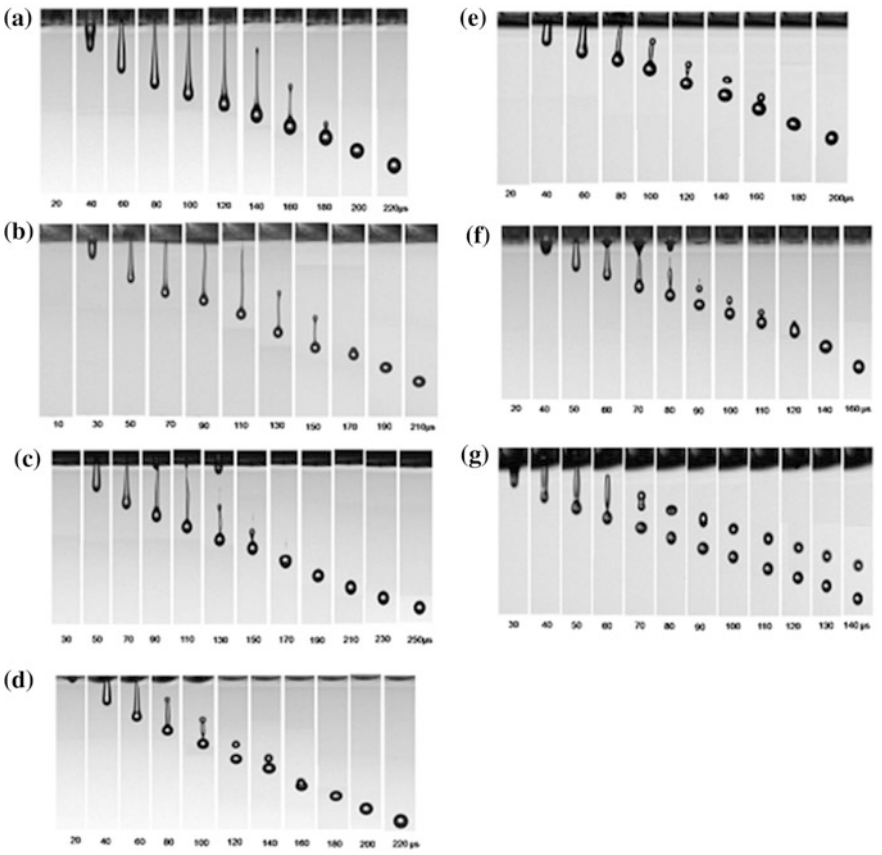

Fig. 1 Images of inkjet-printed droplet formulation for inks with Z value: **a** 2.17; **b** 3.57; **c** 4.08; **d** 6.57; **e** 7.32; **f** 13.68 and **g** 17.32. Reproduced from Jang et al. (2009) with permission from the American Chemical Society

as $4 < Z < 14$ by considering various factors like single drop formation, jet frequency, positional accuracy and required stand-off distance. Figure 1 shows image of inkjet-printed droplet formation for Z number variation from 2 to 17 at a constant voltage of 25 V.

3 Materials for Printed Sensors

Material choice is an important determinant of the sensor performance. To make a low-cost and flexible printed sensor, various materials (organic and inorganic) have been widely explored. Printing ink of the selected material must fulfil the requirement of specific rheological properties which is the most challenging task in the fabrication of printed sensor technology, and it is a limiting factor for the selection of the ink material. The sensor materials could be classified as follows: (i) conducting; (ii) semiconducting and (iii) dielectric, respectively.

3.1 Conducting Materials

Conducting materials play an important role in all electronic devices as a fundamental material due to its application in generating interconnects and other device layers. Inkjet printing provides an attractive feature of controlling the overall thickness, resolution and shape of the conducting patterns. Some conducting materials are used extensively for printing technology and have gained much attention by research community as they satisfy the physical properties of the printable ink (surface tension, viscosity, particle size, good colloidal dispersion, etc.). These are metal-based, carbon-based and conducting polymer-based inks as detailed in subsequent sections.

3.1.1 Metal-Based Ink

Among all the explored metallic inks, silver-based ink is the most dominating choice for printed electronics due to its excellent electrical conductivity, resistance to oxidation and other suitable physical properties enabling such ink to have good adhesion with substrates. Silver paste has been explored from almost time immemorial for developing interconnects for MEM grade sensorwork, printed circuit boards, etc. The high cost of silver limits its use for low cost flexible electronics and thus utilization of other inexpensive materials is required for its replacement. Aresse et al. (2017) have studied inkjet-printed silver patterns and compared them to conventional silver epoxy and solders. The printed silver circuit patterns and their conductivity change with different substrates, and processes are demonstrated in Fig. 2.

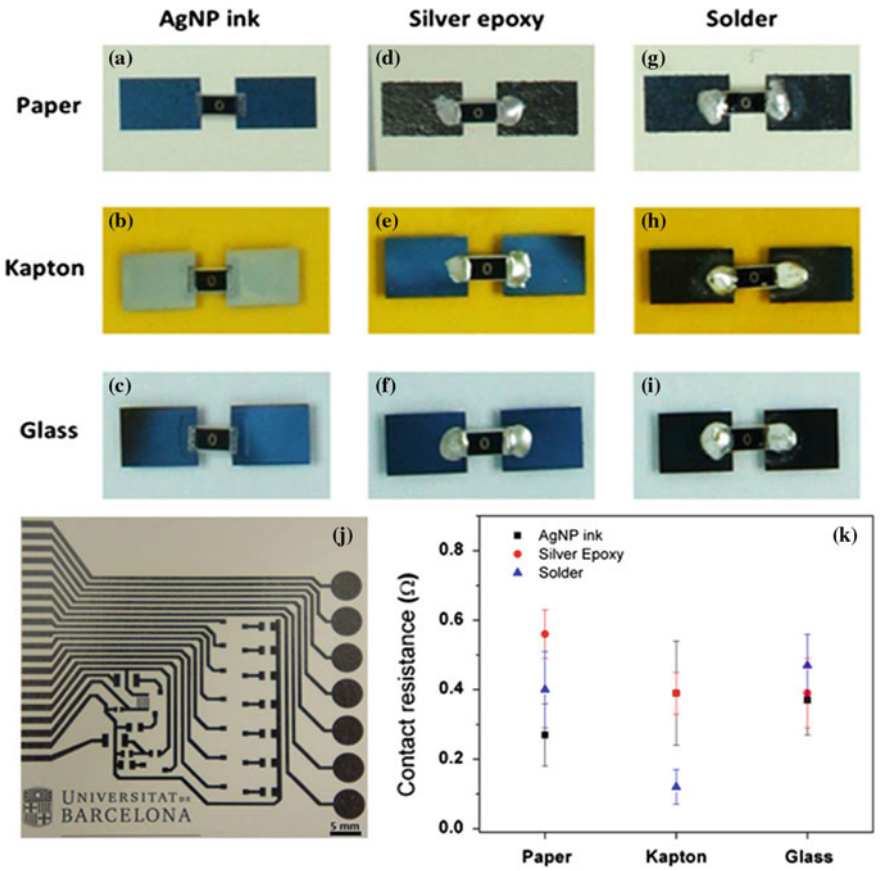

Fig. 2 Shows **a–i** the silver pattern on flexible substrate (paper and kapton) and glass by inkjet printing, silver epoxy and soldering; **j** printed circuit pattern and **k** dependence of electrical resistance on material and substrate used. Reproduced from Arrese et al. (2017) with permission from the American Institute of Physics

Copper-based ink has also been investigated for printed electronics; however, its oxidation after printing makes it highly unsuitable for high-performance devices (Kim et al. 2011). Recently, Lee et al. (2016) have reported copper patterns with good electrical performance (resistivity $\sim 15.18\ \mu\Omega$) by using hydrazine treatment at low temperature. Using post-treatments with such chemicals, the printing can enable the metallic ink to be suitable for flexible sensors. Other than copper, aluminium-based ink is also a good choice for conducting patterns on flexible substrates, but its poor conductivity due to Al_2O_3 layer formation in air limits its use although the inexpensive nature of this material may provide a good solution if it can be coated by another anti-oxidation material layer to prevent oxidation (Foley et al. 2005). Future research is required to make conducting Al ink patterns by

optimizing its processing parameters and using multilevel ink layers of different materials.

3.1.2 Carbon-Based Ink

Carbon-based materials like graphene and CNT have secured their place quite prominently in inkjet technology due to their excellent electrical conductivity, mechanical properties and ease of forming good dispersing inks (Qin et al. 2016; Das et al. 2016). Due to their superior electrical and mechanical properties, these materials have gained much attention in the area of fabrication of flexible electronics and also studied as possible replacement of indium tin oxide (ITO) printing. Though these materials have been extensively explored for printing, still more efforts are required to utilize the green chemistry based or biowaste extracted carbon materials (Sundriyal and Bhattacharya 2017) for printed electronics and sensors.

Recently, Das et al. (2016) have reported a laser irradiation technique to improve the performance of a printed graphene pattern and used this pattern for detection of H_2O_2. They have explained graphene ink formation by sonication and filtration processes and printed the prepared ink on flexible polyimide sheets by using a dimatix materials printer. These printed patterns have been further annealed through laser irradiation which has been found to significantly improve the electrical conductivity of the printed patterns. Figure 3 shows a schematic of ink formation, printing, annealing, variation of sheet resistance with laser energy and flexibility of the studied substrate.

CNT-based ink is also widely applied to printed electronics. Qin et al. (2016) have reported inkjet printing of single-walled carbon nanotubes (SWCNT) as both conducting interconnects and pH sensing layers. A constant increase of electrical conductivity has been observed up to 200 passes of printing, with a response time of 7 s. They have also observed pH sensitivity of 48.1 mV as shown in Fig. 4.

3.1.3 Conducting Polymer-Based Ink

Beside metals and carbon-based materials, conducting polymers like polyaniline, polypyrole, polyacetylene, PEDOT: PSS (3, 4-polyethylenedioxythiphene—polystyrene sulfonic acid), etc., have also been explored for inkjet-printed sensors (Crowley et al. 2008; Hwang et al. 2011; Mabrook et al. 2006). Previously, Crowley et al. (2008) showed an inkjet-printed polyaniline electrode for ammonia sensing using amperometric techniques. The electrode performance was recorded to be excellent with four printing layers at neutral pH. Relationship of amperometric response with a number of printing layers and ammonia concentration and stability of electrodes were thoroughly characterized as shown in Fig. 5.

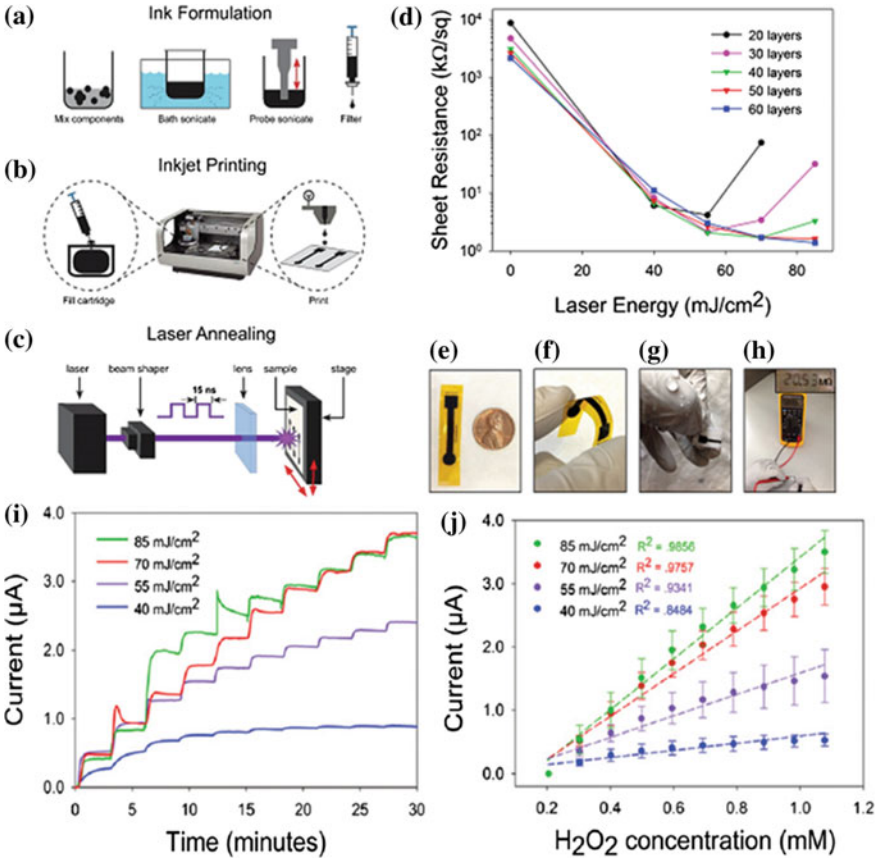

Fig. 3 **a** Schematic diagram of graphene ink formation; **b** inkjet printing of graphene ink; **c** schematic of post-printing laser annealing of printed electrodes; **d** variation of sheet resistance with laser energy density and thickness of the printed layer; **e** printed electrode in flat position; **f** printed electrode in bend position; **g** printing on paper and after DI water and detergent washing; **h** electrical conductivity after 100 washing and bending cycles; **i** H_2O_2 sensing of printed electrodes using amperometry and **j** linear regression analysis of current versus concentration. Reproduced from Das et al. (2016) with permission from the Royal Society of Chemistry

Inkjet-printed PEDOT electrodes have also been widely studied by various researchers (Hwang et al. 2011; Mabrook et al. 2006). Mabrook et al. have investigated sensing of organic vapours using PEDOT-printed patterns. AFM microscopy of one printed layer of PEDOT-PSS hybrid ink before and after exposure to methanol vapours have been studied in great detail. The sensitivity of the printed layers after exposure to methanol and ethanol vapours and the comparative response of printed layers at different methanol concentrations were also investigated (Mabrook et al. 2006).

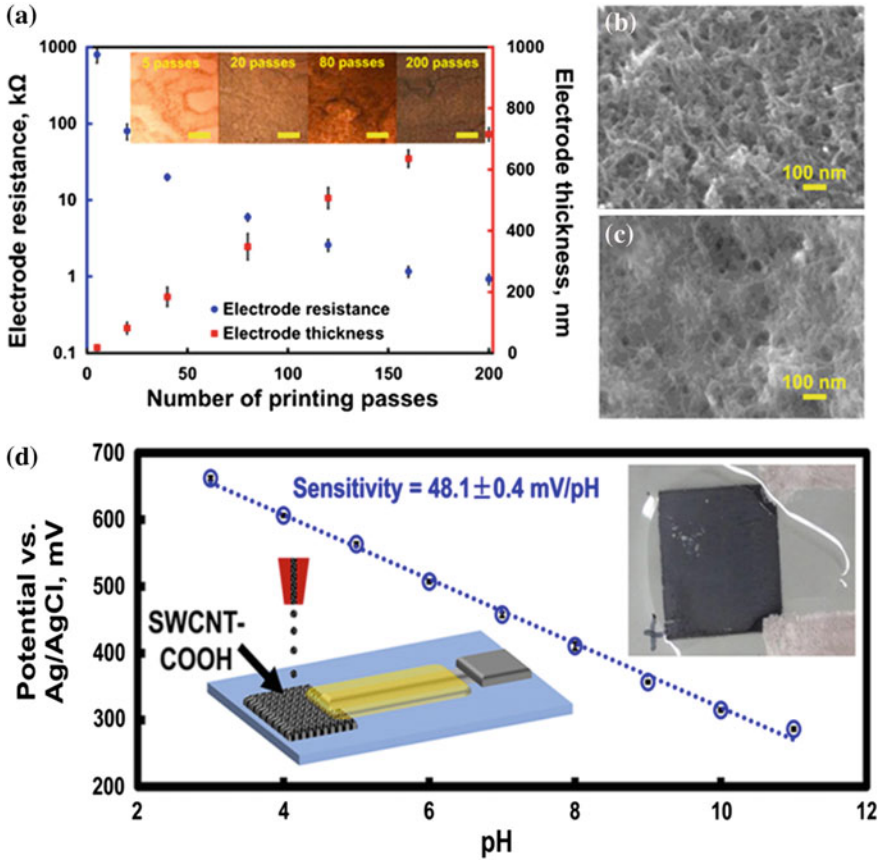

Fig. 4 **a** Variation of electrical resistance and electrode thickness with number of printing layers (inset shows optical microscope image of printed films with different number of passes on 100-mm scale bar); SEM image of CNT film using **b** 20 passes; **c** 200 passes and **d** printed CNT pH sensing electrode calibration curve. Reproduced from Qin et al. (2016) with permission from the Elsevier

3.2 Semiconducting Materials

Semiconducting materials work as an acting sensing layer, and this sensing layer is a critical component for a sensing device. Their electronic properties and hence sensitivity largely depends on the doped impurities, and desired properties can be obtained by changing doping levels in a controlled way. Till date, the materials that are utilized under this category are metal oxides (Kukkola et al. 2012; Rieu et al. 2015; Tsangarides et al. 2016) and silicon (Pi et al. 2012; Drahi et al. 2014).

Pi et al. (2012) have efficiently used Si quantum dots for solar cells by inkjet printing methods. There has been no recordable deterioration in device efficiency even after 30 days which shows high stability of the printed patterns. It has been

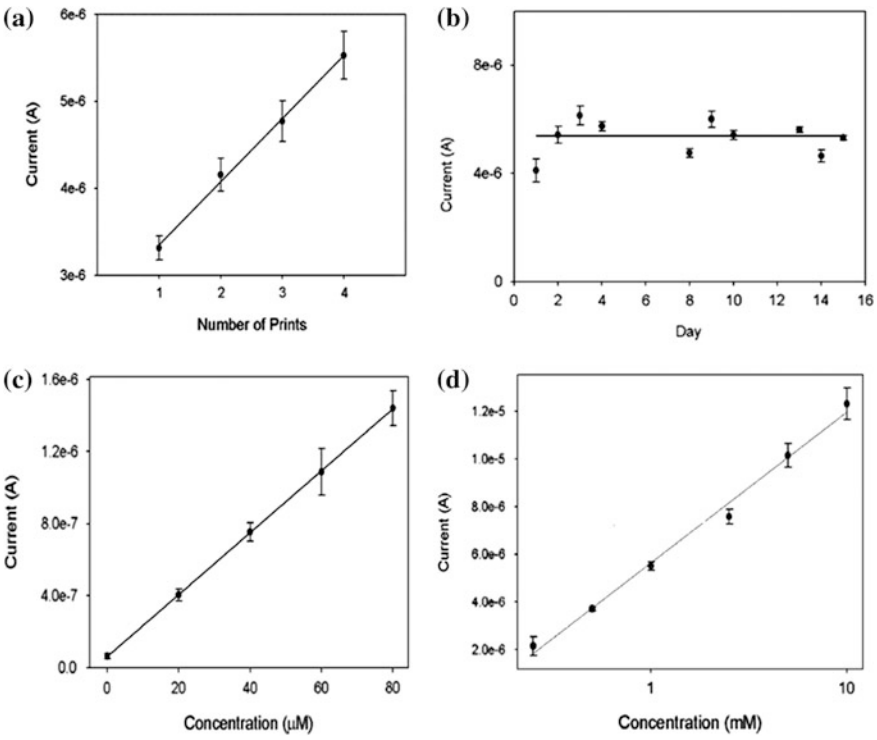

Fig. 5 **a** Dependence of amperometric response with printing layer thickness of PANI electrode; **b** stability of the printed PANI electrodes to 18 ppm ammonium as ammonium chloride; amperometric response of electrodes to the ammonium concentration; **c** 0–1.44 ppm and **d** 1.8–450 ppm. (Potential applied was −0.3 V vs. AgCl reference electrode.) Reproduced from Crowley et al. (2008) with permission from the Royal Society of Chemistry

reported that the printed quantum dots were highly resistant to the air oxidation due to hydrosilylation reaction which resulted in no change of printed layer properties for a long time. Figure 6 shows schematic of Si ink printing on Si surface and dependence of layer thickness and porosity with drop spacing while Fig. 7 shows variation of different performance parameters of solar cell with the drop spacing. Drahi et al. (2014) have characterized inkjet-printed Si nanoparticles for thin-film devices and investigated change in its properties with varying sintering temperature. Si has been explored for the inkjet printing processes by some researchers, but its high sintering temperature makes it unfit for use in most of the flexible substrates. Also, its high cost makes it unsuitable for low-cost electronics.

Carbon-based materials have also been investigated as semiconducting active layers in inkjet-printed sensor devices. These materials have already been introduced in the above section. Other important class of materials for the printed sensors is metal oxides although such materials necessitate a post-printing sintering (300–500 °C) step to get optimum performance. Tsangarides et al. (2016) have reported the effect of

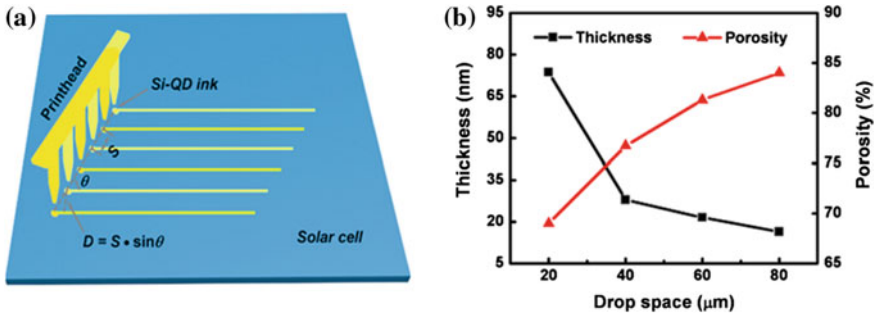

Fig. 6 **a** Schematic of inkjet-printed Si quantum dots on Si solar cell surface (*D*—drop space, *S*—step of printhead movement, θ—angle between printhead and edge of solar cell) and **b** variation of porosity and thickness with drop space. Reproduced from Pi et al. (2012) with permission from the American Chemical Society

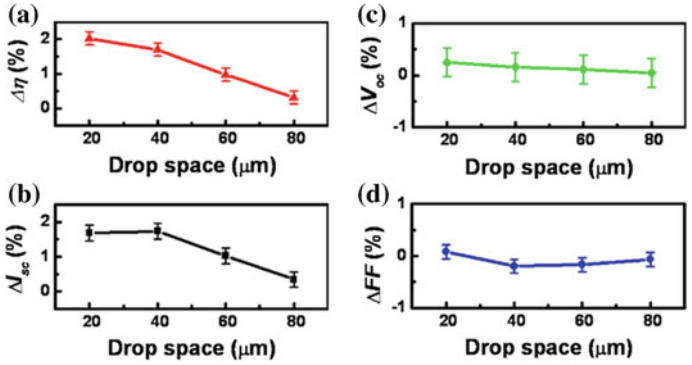

Fig. 7 Variation of **a** efficiency (η); **b** short-circuit current (I_{sc}); **c** open-circuit voltage (V_{oc}) and **d** fill factor (FF) of solar cell after Si quantum dot printing. Reproduced from Pi et al. (2012) with permission from the American Chemical Society

temperature on the growth, layer uniformity and morphology of ZnO nanowires from inkjet-printed patterns of zinc acetate dehydrate. Uniform layers of ZnO were obtained at 60 °C, which are suitable for all flexible substrates. Also, there is no coffee-ring effect on the printed layers at this temperature. Thus, this method can be used for the inkjet-printed flexible sensors based on ZnO nanostructures. Figure 8 shows particle distribution mechanism on drying drops and SEM images of ZnO nanowire arrays grown over one printed layer at different temperatures.

Kukkola et al. (2012) have investigated gas-sensing properties of inkjet-printed WO_3 nanoparticles on Si substrates decorated with various metal particles. Inkjet-printed patterns with different layers and different drying times are shown in Fig. 9, and gas-sensing responses of the printed sensors were found to be highly dependent on the metal modified surface as shown in Fig. 10. In yet another work, Riet et al. (2015) have developed inkjet-printed SnO_2 gas sensors on polyimide foil

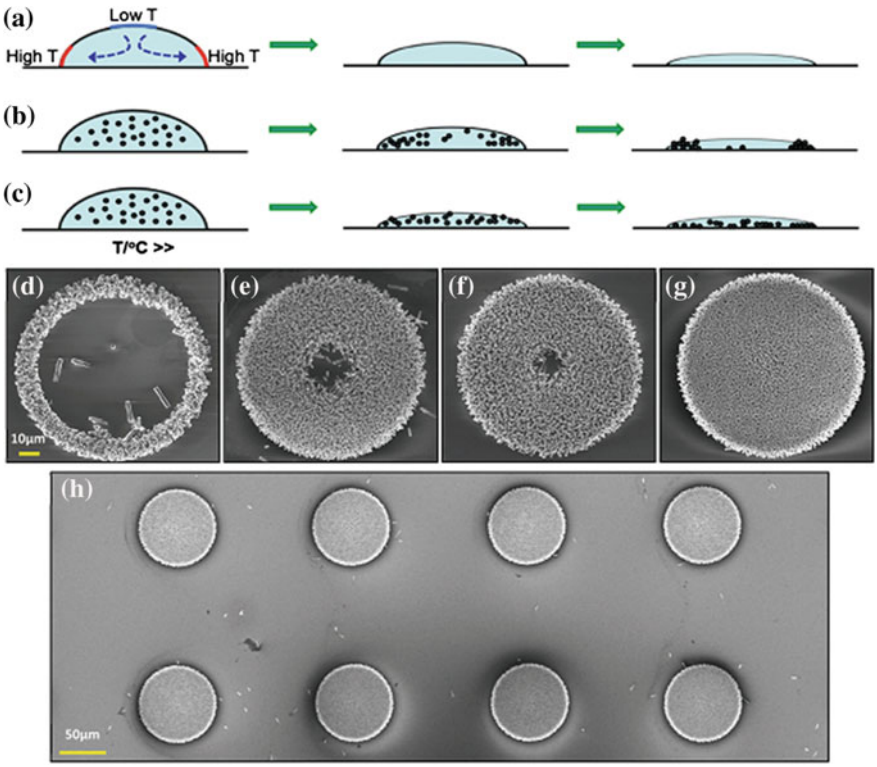

Fig. 8 Schematic of particle distribution mechanism of drying drops: **a** thermo-capillary flow due to temperature gradient; **b** particles follow the flow and attach to the droplet contact line; **c** uniform dispersion of particles at high temperatures. SEM images of ZnO nanowires with single printing layer at temperature: **d** 25 °C; **e** 40 °C; **f** 50 °C; **g** 60 °C; **h** ZnO nanowire dots (60 °C). Reproduced from Tsangarides et al. (2016) with permission from the Royal Society of Chemistry

with an annealing temperature of 400 °C. This sensor has been used for sensing of CO and NO gases under dry and wet air conditions. Bernacka-Wojcik et al. have investigated the electrical properties of the inkjet-printed TiO_2 layers and found that these films have more porosity and surface area and hence higher efficiency than the doctor blade-made films of the same material with the same thickness. The printed layers also have better transport properties due to increased diffusion lengths (Bernacka-Wojcik et al. 2016).

Till date some metal oxides have been explored for inkjet printing and successfully used for various electronic applications. However, their wide acceptability for flexible sensors is limited because of their requirement of high post treatment temperatures. This is not suitable for low temperature substrates. Hence, further research is needed to fully utilize such material ink for inkjet-printed sensor devices and also metal oxide-based sensor devices that are based on green chemistry approach (Patel et al. 2017).

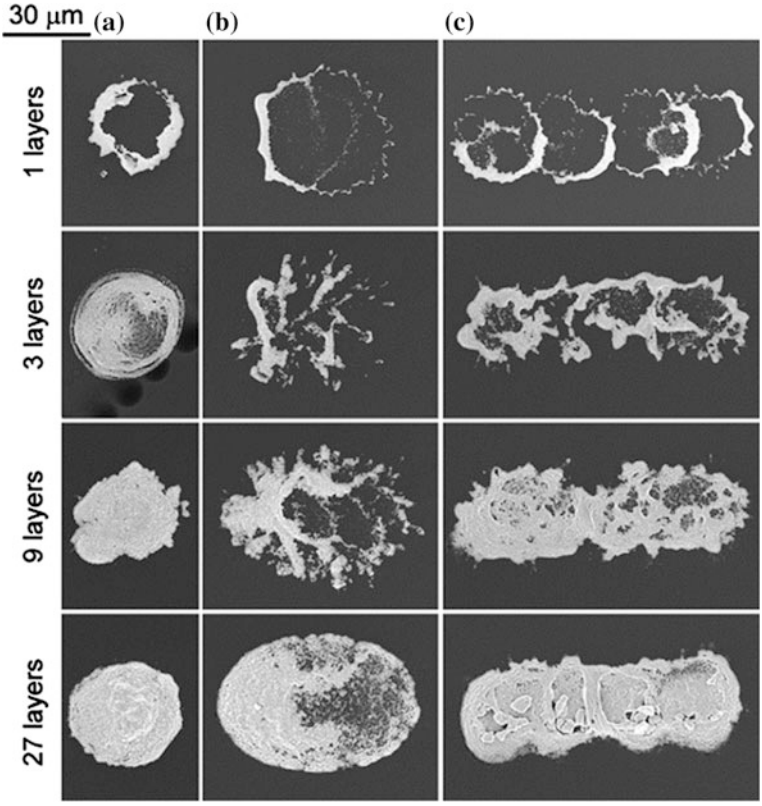

Fig. 9 Inkjet-printed patterns of WO_3 nanoparticles: **a** printed droplet at a single location. Inkjet printing of four drops with 25 mm spacing using drying time of: **b** 0.2 ms and **c** 1.8 s between two subsequent printing drops. Reproduced from Kukkola et al. (2012) with permission from the Royal Society of Chemistry

3.3 Dielectric Materials

Dielectric materials are required in high-capacitance multilayer devices as an insulating layer to prevent leakage currents particularly in low-voltage applications. Both organic and inorganic (silica, alumina, etc.) materials are used as dielectric materials; however, inorganic materials have not yet been explored as dielectric layers for printed devices. Some organic materials have been explored for the printed electronics such as: polyvinyl alcohol, poly (methyl methacrylate), polyimide, poly (4-vinylphenol), polystyrene and terephthalate (Hamad et al. 2016; Pease and Chou 2008).

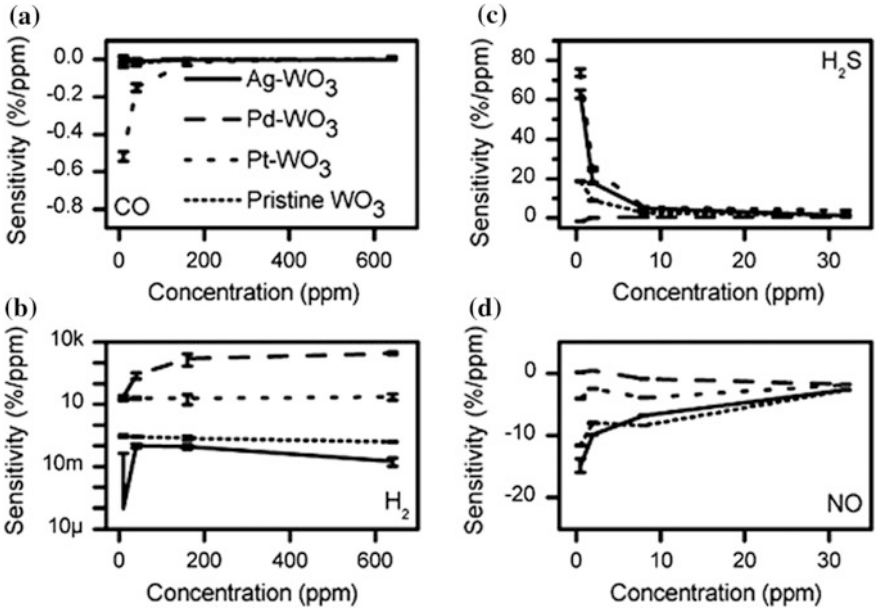

Fig. 10 Gas-sensing response of metal modified WO_3 printed sensors to **a** CO, **b** H_2, **c** H_2S and **d** NO. Reproduced from Kukkola et al. (2012) with permission from the Royal Society of Chemistry

4 Substrates for Flexible Sensors

The requirement of foldable, bendable, malleable, smart and compact sensor devices has emerged from the requirements posed by printable flexible electronics. Fortunately, a lot of low-cost flexible substrates are available which are suitable for inkjet printing. The essential properties of a substrate which can be employed for flexible sensors are as follows: thermal stability, low coefficient of thermal expansion, flexibility, low cost, resistant to moisture and gases, transparency and high surface area to volume ratio. To date, flexible substrates used for inkjet-printed sensors are thin glasses (Zardetto et al. 2011), metal foils (MacDonald et al. 2007), papers (Wang et al. 2016), polymer sheets (Mabrook et al. 2006) and textile fabrics (Stempien et al. 2016a). Thin glass structures with good bending properties may also serve as a good choice, but their brittleness limits their utility for making flexible electronic devices. On the other hand, metal foils and tapes have good flexibility and high temperature resistance thus providing the possibility for practical use of inkjet-printed inorganic materials which need high sintering temperature, but their high cost, high material density and surface roughness make them unsuitable for low-cost flexible electronics.

Table 1 Properties of polymer substrates (MacDonald et al. 2007; Zardetto et al. 2011; Choi et al. 2008)

S. No.	Property	PET	PI	PC	PEN
1.	Glass transition temperature (°C)	70	270	145	120
2.	Transparency (%)	90	35–60	92	88
3.	Young's modulus (GPa)	2–2.7	2.5	2.6	0.1–0.5
4.	Upper processing temperature (°C)	115	250–320	115–160	268
5.	Coefficient of thermal expansion (ppm/°C)	33	8–20	75	20
6.	Dimensional stability	Good	Fair	Fair	Good
7.	Surface roughness	Poor	Good	Good	Poor
8.	Solvent resistance	Good	Good	Poor	Good

4.1 Polymer-Based Substrates

Polymer-based materials have gained much attention for low-cost printed flexible electronics due to their suitable chemical, physical, mechanical and optical performance as depicted in Table 1. Despite the above suitable properties of polymers for printed electronics, its low glass transition temperature hinders its use for inorganic materials. Glass transition temperatures for various polymer substrates are shown in Fig. 11.

Polymer substrates for printable electronic structures can be divided as:

(i) Semicrystalline substrate such as polyethylene terephthalate (PET), polyetheretherketone (PEEK) and polyethylene napthalate (PEN) (MacDonald et al. 2007; Zardetto et al. 2011; Choi et al. 2008).
(ii) Amorphous substrates such as polyethersulphone (PES), polycarbonate (PC), polyimide (PI), polyaraylate (PAR), etc., (MacDonald et al. 2007; Zardetto et al. 2011; Choi et al. 2008).

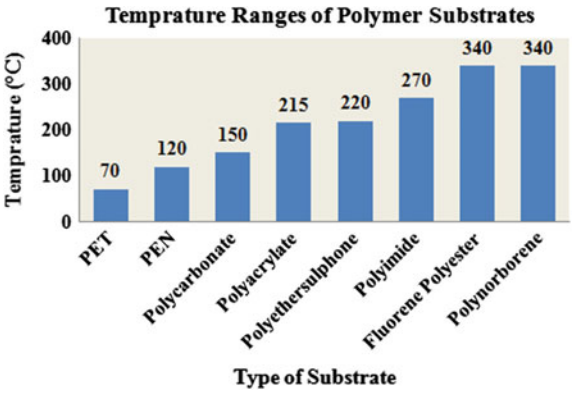

Fig. 11 Glass transition temperatures of commonly used plastic substrates in printed sensors and electronics (MacDonald et al. 2007; Zardetto et al. 2011)

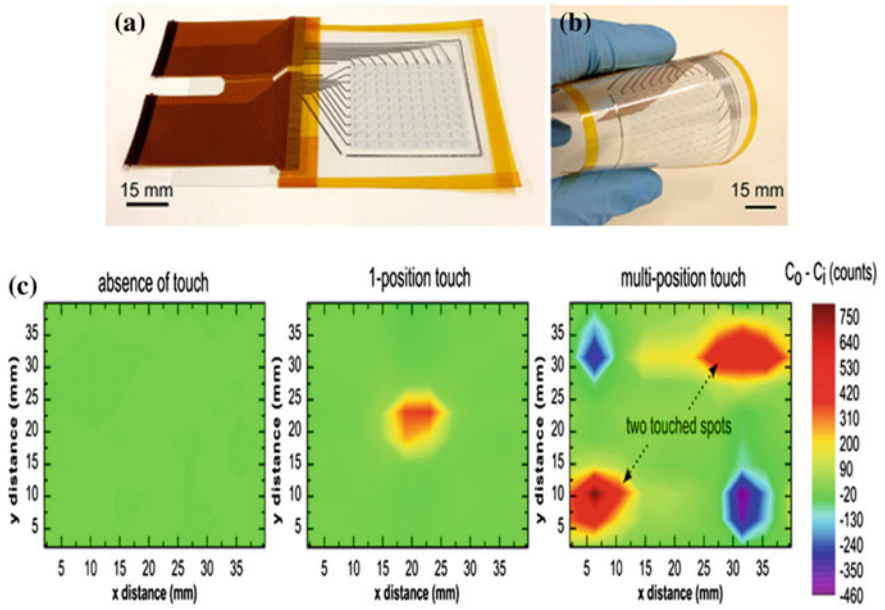

Fig. 12 Images of inkjet-printed sensor on PET substrate with one printing layer under: **a** flat position; **b** bend position and **c** touch sensing visualization of the printed sensor. Reproduced from Ma et al. (2015) with permission from the American Chemical Society

One example of inkjet-printed patterns on flexible PET substrate is shown in Fig. 12 as developed by Ma et al. for application in touch sensors (Ma et al. 2015). Electrical resistance and transparency of the device decreased with increasing printing passes.

4.2 Paper-Based Substrates

Paper has also been an attractive choice for inkjet-printed electronics due to its easy availability, environment friendliness, low cost, light weight and flexibility. It is a biodegradable and renewable substrate, and its surface properties can be easily modified by some chemical and other treatments which add extra flexibility to the structure (Sundriyal and Bhattacharya 2017). Although it is a potential candidate for the inkjet-printed electronics, however, its incapability to sustain high temperatures required for sintering of most of the metal-based inks limits its utility. Recently, Wang et al. (2016) have shown pre-treated papers with stannous chloride to decrease the ink absorption levels and have reported inkjet-printed copper patterns for disposable RFID tags and three-dimensional flexible and foldable devices as shown in Fig. 13.

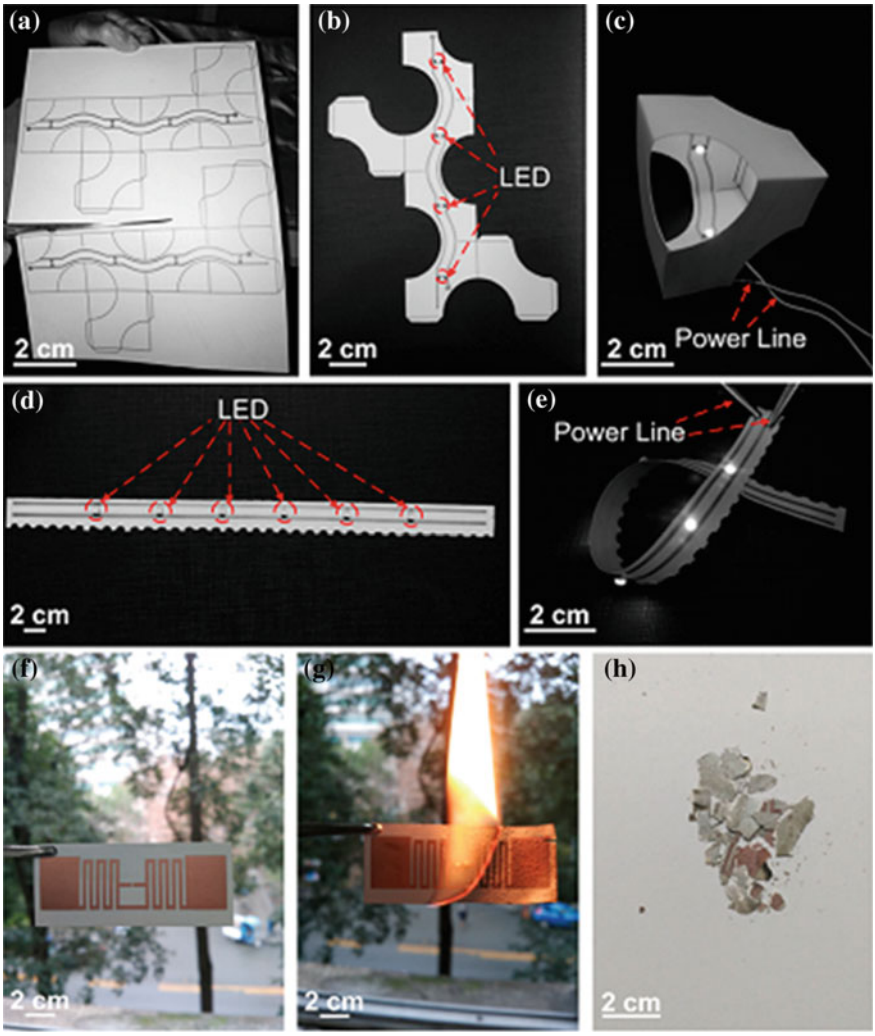

Fig. 13 **a** Printed circuit on paper. **b** Clipping of paper circuit with LED's. **c** Working LED's with folded paper circuit. Paper-based LED device in: **d** flat position and **e** bend position. **f** Optical image of disposable RFID tag on paper substrate. **g** Burning of RFID tag. **h** Burned RFID tag. Reproduced from Wang et al. (2016) with permission from the American Chemical Society

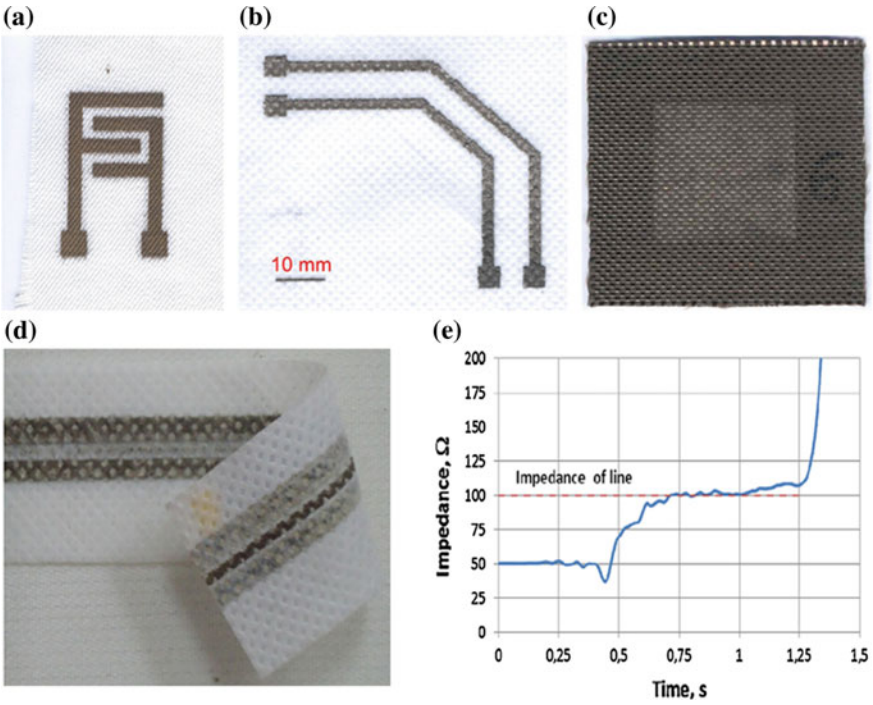

Fig. 14 Digital images of inkjet-printed silver electrodes on: **a** polyacrylonitrile, **b** polypropylene and **c** basalt fabric. **d** Inkjet-printed silver transmission line on polypropylene textile and **e** impedance behaviour of printed transmission line. Reproduced from Stempien et al. (2016b) with permission from the Elsevier

4.3 Textile-Based Substrates

Another class of substrates for inkjet-printed sensors are textile-based substrates which are an active topic of research for various applications in sectors like health care, military and aerospace for smart, wearable and disposable sensors. The special feature of this substrate is its wear-ability and biocompatibility. Wearable sensors have the ability to automatically detect the various life processes and activities and physical status of its own user, and any change in the surrounding environment will be able to provide feedback accordingly. An example of inkjet-printed textile for transmission lines is shown in Fig. 14 (Stempien et al. 2016b).

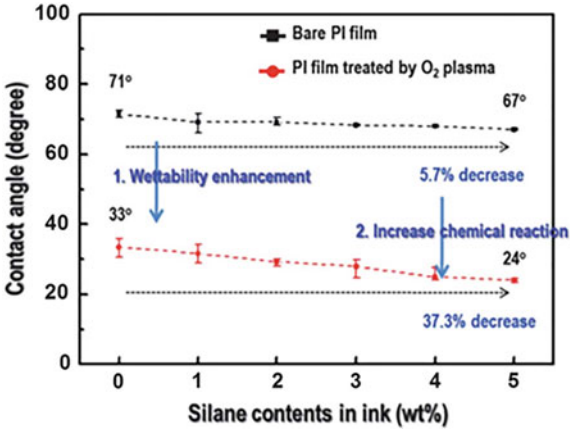

Fig. 15 Contact angle variation between ink and polyimide substrate before and after oxygen plasma treatment. Reproduced from Lee et al. (2012) with permission from the Royal Society of Chemistry

4.4 Adhesion of Printable Ink with Substrate

Till date, various research groups have optimized several key factors of inkjet printing process like jet stability, physical properties of ink and post-printing treatments of the printed patterns to obtain good performance of the printed sensors. However, one of the unresolved issues is improper adhesion between printed patterns and the substrate which affects the overall performance and reliability of the printed sensors. Adhesion is the ability of a film to remain bonded to its substrate and depends on the morphology, chemical properties and interfacial properties of the interacting surfaces. Surface energies of the contacting surfaces and interface play an important role for adhesion control and governed by the Young's equation (Young 1805) as follows:

$$\gamma_s = \gamma_{sl} + \gamma_l \cos\theta \tag{4}$$

where γ_s is the surface energy of substrate, γ_l is the surface energy of the ink droplet and γ_{sl} is the interfacial free energy and θ is the contact angle between the interacting surfaces. For good adhesion, γ_s should be very high than γ_l.

Adhesion can be improved by modification of substrate's surface using physical or chemical treatments, using an adhesion enhancing layer of Ni or Cr metals and by using silane coupling agents (Agina et al. 2015; Lee and Choa 2012). Lee et al. have used oxygen plasma treatment to generate hydrophilic groups to promote adhesion between the polyimide substrates and printed Cu patterns. Figure 15 shows comparative variation in contact angle before and after oxygen plasma treatment (Lee and Choa 2012). A drastic decrease in contact angle after substrate treatment exhibits incremental hydrophilic groups on the surface of the substrate, thus promotes the adhesion between interacting surfaces.

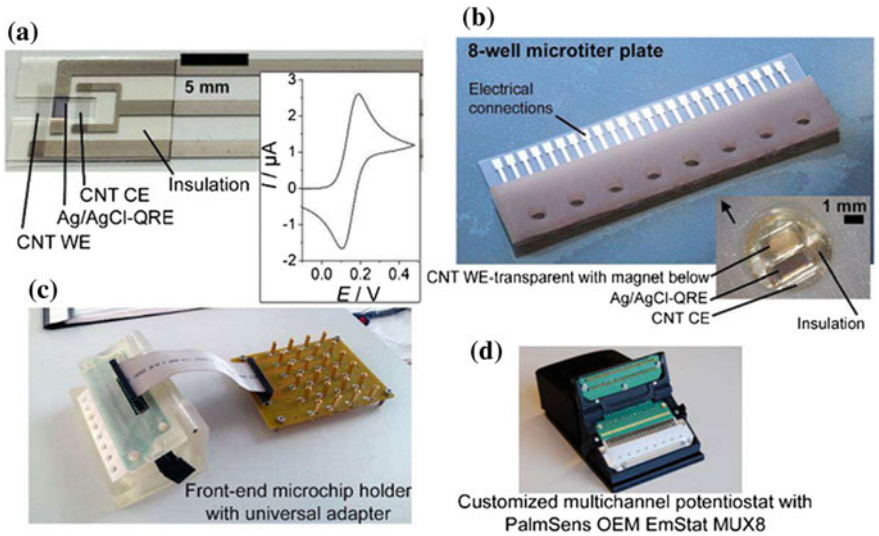

Fig. 16 **a** Inkjet-printed CNT sensor (inset shows cyclic voltammogram of the three-electrode sensor in 2 mM FcMeOH and 0.1 M KCl at a scan rate of 50 mV/s), **b** microtitre plate with eight wells or eight units each with a sample capacity of 50 µL and an individual electrode cell (below image shows magnet location to fix magnetic beads for immunoassay-based detection), **c** plate holder with universal potentiostatic adapter and **d** multichannel for immunoassay-based detection. Reproduced from Lesch et al. (2017) with permission from the Electrochemical Society

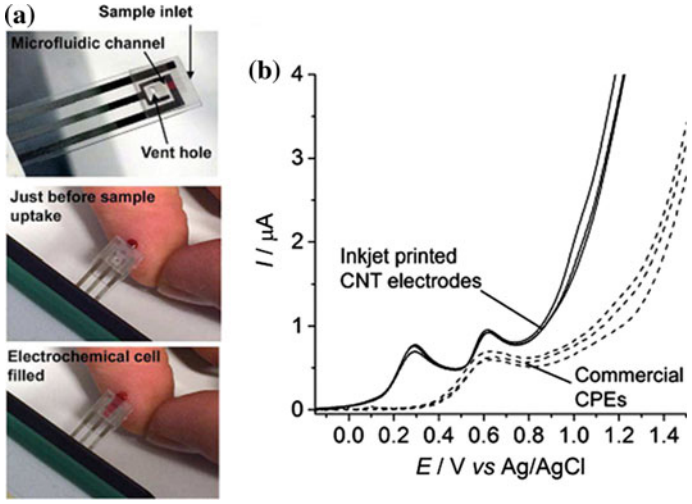

Fig. 17 **a** Blood sample uptake in the printed three-electrode sensor with a microfluidic channel and **b** comparative linear sweep voltammogram for inkjet-printed CNT electrode and commercial carbon paste at a scan rate of 100 mV/s. Reproduced from Lesch et al. (2017) with permission from the Electrochemical Society

5 Inkjet-Printed Sensors for Health care

One of the important applications of printed flexible electronics along with wireless networking is the development of smart health monitoring sensors. Recently, a number of inkjet-printed healthcare sensors have been reported for point-of-care diagnostics (Lesch et al. 2017), wireless monitoring of chronic wounds (Farooqui and Shamim 2016; Zhang et al. 2016), bacterial detection (Creran et al. 2014), detection of human chorionic gonadotropin by ELISA (Apilux et al. 2013) and wearable sensor for monitoring human physiological performance (Wang and Loh 2017). Lesch et al. (2017) reported an inkjet-printed microchip consisting carbon nanotube (CNT) as working and counter electrode while Ag/AgCl as reference electrode for point-of-care diagnostics application. The sample volume capacity of the developed sensor was 50 μL, and sensor can be used up to 20 times when using complex samples like blood. It is also reported that the printed CNT sensor shows better electrochemical response than the commercial carbon paste electrodes. Figure 16 shows inkjet-printed CNT sensor and its electrochemical response while Fig. 17 shows inkjet-printed sensor with a microfluidic channel for the measurement of blood sample and comparative linear sweep voltammograms of inkjet-printed CNT electrode and commercial carbon paste.

6 Advantage, Limitation and Future Scope of Inkjet Printing Technology for Printed Sensors

Inkjet printing technology is a promising tool for flexible printed electronics including sensors. Its advantages, limitation and future scopes are as following:

6.1 Advantages

- **Simple and low cost**: It is a simple method which is at a mature stage in industry for a variety of applications. Its comparative low cost other than competing deposition methods like photolithography, microcontact printing, etc., makes it attractive for printed electronics.
- **Material Saving**: It is a direct deposition tool with negligible wastage of material. Unlike other processes, it does not require any mask, and material can be deposited only at the required area on the substrates.

- **Good resolution**: It provides high-resolution printing.
- **Non-contact deposition**: As it is a non-contact printing process thus eliminating/minimizing any contamination and distortion issues of the print layers.
- **Flexibility**: Any shape or pattern can be easily printed by this process, and also patterns can be changed just by modifying the drawing in the software of the printer system.

6.2 Limitation

- **Rigid physical properties of ink**: One of the major limitations of inkjet-printed sensor is the requirement of ink which follows strict rheological conditions with small range of viscosity and surface tension. It also limits concentration of sensing material in an ink and leads to the requirement of multiple printing cycles to achieve adequate packing density of the deposited material.
- **Requirement of additives and stabilizers**: Additional materials like additives required to control the surface tension and viscosity and need for stabilizing agents to prevent agglomeration of nanoparticles that can negatively affect the sensing behaviour of the printed devices.
- **Coffee-ring patterns**: Uneven drying of deposited materials lead to the coffee-ring effects which are undesirable for the sensing performance.
- **Slow speed**: High printing speed is desired to compete with other processes. Speed can be increased by modifying drop frequency, number of nozzles, material concentration in ink and stand-off distance. However, modification of these parameters is very complex.

6.3 Future Scope

For the future of the electronics industry, inkjet printing is considered as an effective tool for compact, low cost and disposable flexible sensors. Its cost effectiveness and utility in combination to low-cost substrates may significantly shift the economy levels of the modern electronics industry. Its combination with other printing tools can efficiently develop the highly sensitive and low-cost sensors. Its compatibility with functional materials paves the path for further material research for inkjet-printed sensors. It can possibly replace the requirement of high-cost materials for sensing application and boosts the low-cost printed electronics market.

7 Conclusion

In summary, inkjet printing approach for flexible sensors is gaining much attention due to its suitability for large area flexible electronics. Researchers are in continuous surge to benefit sensor and other electronics from this micromanufacturing tool and have established a strong base for printed flexible electronics. Although some inherent limitations of this technology exist still with the advancement of this process, exploration of improved ink and new flexible substrates can certainly overcome the existing challenges.

References

Agina EV, Sizov AS, Yablokov MY, Borshchev OV, Bessonov AA, Kirikova MN, Bailey MJ, Ponomarenko SA (2015) Polymer surface engineering for efficient printing of highly conductive metal nanoparticle inks. ACS Appl Mater Interfaces 7(22):11755–11764

Andò B, Baglio S (2013) All-inkjet printed strain sensors. IEEE Sens J 13(12):4874–4879

Apilux A, Ukita Y, Chikae M, Chailapakul O, Takamura Y (2013) Development of automated paper-based devices for sequential multistep sandwich enzyme-linked immunosorbent assays using inkjet printing. Lab Chip 13(1):126–135

Arrese J, Vescio G, Xuriguera E, Medina-Rodriguez B, Cornet A, Cirera A (2017) Flexible hybrid circuit fully inkjet-printed: Surface mount devices assembled by silver nanoparticles-based inkjet ink. J Appl Phys 121(10):104904

Belsey K, Parry A, Rumens C, Ziai M, Yeates S, Batchelor JC, Holder SJ (2017) Switchable disposable passive RFID vapour sensors from inkjet printed electronic components integrated with PDMS as a stimulus responsive material. J Mater Chem C 5(12):3167–3175

Bernacka-Wojcik I, Wojcik P, Aguas H, Fortunato E, Martins R (2016) Inkjet printed highly porous TiO_2 films for improved electrical properties of photoanode. J Colloid Interface Sci 465:208–214

Bhatt G, Kumar S, Sundriyal P, Bhushan P, Basu A, Singh J, Bhattacharya S (2016) Microfluidics overview. Microfluidics for biologists. Springer, Berlin, pp 33–83

Choi M-C, Kim Y, Ha C-S (2008) Polymers for flexible displays: from material selection to device applications. Prog Polym Sci 33(6):581–630

Creran B, Li X, Duncan B, Kim CS, Moyano DF, Rotello VM (2014) Detection of bacteria using inkjet-printed enzymatic test strips. ACS Appl Mater Interfaces 6(22):19525–19530

Crowley K, O'Malley E, Morrin A, Smyth MR, Killard AJ (2008) An aqueous ammonia sensor based on an inkjet-printed polyaniline nanoparticle-modified electrode. Analyst 133(3): 391–399

Das SR, Nian Q, Cargill AA, Hondred JA, Ding S, Saei M, Cheng GJ, Claussen JC (2016) 3D nanostructured inkjet printed graphene via UV-pulsed laser irradiation enables paper-based electronics and electrochemical devices. Nanoscale 8(35):15870–15879

Derby B, Reis N (2003) Inkjet printing of highly loaded particulate suspensions. MRS Bull 28(11):815–818

Drahi E, Gupta A, Blayac S, Saunier S, Benaben P (2014) Characterization of sintered inkjet-printed silicon nanoparticle thin films for thermoelectric devices. Phys Status Solidi A 211(6):1301–1307

Farooqui MF, Shamim A (2016) Low cost inkjet printed smart bandage for wireless monitoring of chronic wounds. Sci Rep 6:28949

Foley TJ, Johnson CE, Higa KT (2005) Inhibition of oxide formation on aluminum nanoparticles by transition metal coating. Chem Mater 17(16):4086–4091

Fromm J (1984) Numerical calculation of the fluid dynamics of drop-on-demand jets. IBM J Res Dev 28(3):322–333

Hamad E, Bilatto S, Adly N, Correa D, Wolfrum B, Schöning MJ, Offenhäusser A, Yakushenko A (2016) Inkjet printing of UV-curable adhesive and dielectric inks for microfluidic devices. Lab Chip 16(1):70–74

Hwang H, Kim S-H, Kim T-H, Park J-K, Cho Y-K (2011) Paper on a disc: balancing the capillary-driven flow with a centrifugal force. Lab Chip 11(20):3404–3406

Jang D, Kim D, Moon J (2009) Influence of fluid physical properties on ink-jet printability. Langmuir 25(5):2629–2635

Kim DS, Khan A, Rahman K, Khan S, Kim HC, Choi KH (2011) Drop-on-demand direct printing of colloidal copper nanoparticles by electrohydrodynamic atomization. Mater Manuf Process 26(9):1196–1201

Kimura J, Kawana Y, Kuriyama T (1989) An immobilized enzyme membrane fabrication method using an ink jet nozzle. Biosensors 4(1):41–52

Komuro N, Takaki S, Suzuki K, Citterio D (2013) Inkjet printed (bio) chemical sensing devices. Anal Bioanal Chem 405(17):5785–5805

Kukkola J, Mohl M, Leino A-R, Tóth G, Wu M-C, Shchukarev A, Popov A, Mikkola J-P, Lauri J, Riihimäki M (2012) Inkjet-printed gas sensors: metal decorated WO3 nanoparticles and their gas sensing properties. J Mater Chem 22(34):17878–17886

Lee Y-I, Choa Y-H (2012) Adhesion enhancement of ink-jet printed conductive copper patterns on a flexible substrate. J Mater Chem 22(25):12517–12522

Lee Y-I, Kwon Y-T, Kim S, Lee K-J, Choa Y-H (2016) Hydrazine vapor-based rapid and low temperature post-processing for inkjet printed conductive copper patterns. Thin Solid Films 616:260–264

Lesch A, Jović M, Baudoz M, Zhu Y, Tacchini P, Gumy F, Girault HH (2017) Point-of-care diagnostics with inkjet-printed microchips. ECS Trans 77(7):73–81

Ma S, Ribeiro F, Powell K, Lutian J, Møller C, Large T, Holbery J (2015) Fabrication of novel transparent touch sensing device via drop-on-demand inkjet printing technique. ACS Appl Mater Interfaces 7(39):21628–21633

Mabrook MF, Pearson C, Petty MC (2006) Inkjet-printed polymer films for the detection of organic vapors. IEEE Sens J 6(6):1435–1444

MacDonald WA, Looney M, MacKerron D, Eveson R, Adam R, Hashimoto K, Rakos K (2007) Latest advances in substrates for flexible electronics. J Soc Inform Display 15(12):1075–1083

Morse J, Zhao Y, Rotello V, Nugen S, Watkins J (2016) Wearable microfluidic biomarker sensor for human performance assessment. In: Electronic system-integration technology conference (ESTC), 2016 6th, IEEE, pp 1–3

Patel V, Sundriyal P, Bhattacharya S (2017) Aloe-vera vs. poly (ethylene) glycol-based synthesis and relative catalytic activity investigations of ZnO nanorods in thermal decomposition of potassium perchlorate. Part Sci Tech 35:1–8

Pease RF, Chou SY (2008) Lithography and other patterning techniques for future electronics. Proc IEEE 96(2):248–270

Pi X, Zhang L, Yang D (2012) Enhancing the efficiency of multicrystalline silicon solar cells by the inkjet printing of silicon-quantum-dot ink. J Phys Chem C 116(40):21240–21243

Qin Y, Kwon H-J, Subrahmanyam A, Howlader MM, Selvaganapathy PR, Adronov A, Deen MJ (2016) Inkjet-printed bifunctional carbon nanotubes for pH sensing. Mater Lett 176:68–70

Rieu M, Camara M, Tournier G, Viricelle J, Pijolat C, de Rooij N, Briand D (2015) Inkjet printed SnO_2 gas sensor on plastic substrate. Procedia Engineering 120:75–78

Singh M, Haverinen HM, Dhagat P, Jabbour GE (2010) Inkjet printing—process and its applications. Adv Mater 22(6):673–685

Song E, da Costa TH, Choi J-W (2017) A chemiresistive glucose sensor fabricated by inkjet printing. Microsys Tech 23(8):1–7

Stempien Z, Kozicki M, Pawlak R, Korzeniewska E, Owczarek G, Poscik A, Sajna D (2016a) Ammonia gas sensors ink-jet printed on textile substrates. In: Sensors, 2016 IEEE, pp 1–3

Stempien Z, Rybicki E, Rybicki T, Lesnikowski J (2016b) Inkjet-printing deposition of silver electro-conductive layers on textile substrates at low sintering temperature by using an aqueous silver ions-containing ink for textronic applications. Sens Actuators B Chem 224:714–725

Sundriyal P, Bhattacharya S (2017) Inkjet-Printed Electrodes on A4 Paper Substrates for Low-Cost, Disposable, and Flexible Asymmetric Supercapacitors. ACS Applied Materials & Interfaces 9(44):38507–38521

Tsangarides CP, Ma H, Nathan A (2016) ZnO nanowire array growth on precisely controlled patterns of inkjet-printed zinc acetate at low-temperatures. Nanoscale 8(22):11760–11765

Wang L, Loh KJ (2017) Wearable carbon nanotube-based fabric sensors for monitoring human physiological performance. Smart Mater Struct 26(5):055018

Wang Y, Guo H, Chen J-J, Sowade E, Wang Y, Liang K, Marcus K, Baumann RR, Feng Z-S (2016) Paper-based inkjet-printed flexible electronic circuits. ACS Appl Mater Int 8 (39):26112–26118

Young T (1805) An essay on the cohesion of fluids. Philos Trans R Soc Lond 95:65–87

Zardetto V, Brown TM, Reale A, Di Carlo A (2011) Substrates for flexible electronics: a practical investigation on the electrical, film flexibility, optical, temperature, and solvent resistance properties. J Polym Sci Part B Polym Phys 49(9):638–648

Zhang X, Wasserberg D, Breukers C, Terstappen LW, Beck M (2016) Temperature-switch cytometry releasing antibody on demand from inkjet-printed gelatin for on-chip immunostaining. ACS Appl Mater Interfaces 8(41):27539–27545

Zheng Y, He Z, Gao Y, Liu J (2013) Direct desktop printed-circuits-on-paper flexible electronics. Scientific reports 3

Chapter 6
Sensing Using Microfluidic Platform

Chetan A. Nayak and H. N. Pradeep

Abstract Microfluidic devices have emerged as prevailing and reliable microscale total analysis devices that offer minimum reagent consumption, high throughput, and control of multiple processes in a single smallest device. This book chapter discusses about sensing on microfluidic platform, its flow physics, which is very important for microflow systems and its potential applications. It discusses about manufacture methods and materials used for microfluidic platform that effect the flow systems. Further, the droplet-based microfluidics, drop dynamics, as well as formation of droplet mechanism for handling of chemical and/or biological samples for its sensors application are discussed. The developed sensing using microfluidic platform can show a scaled solution for future analysis.

Keywords Microfluidics · Microfluidic sensors · Analysis

1 Introduction

Sensors are very important essential part of all measurement and control systems. The need for portable inexpensive sensors in medical, consumer products, automated manufacturing, and processing industries is in great demand. A numerous variety of convenient and useful parameters are to be sensed or analyzed. Such parameters analyzers are to be developed. Sensor applications and sensor technology have become multidisciplinary and interdisciplinary field of endeavor.

Sensors, sophisticated analytical devices that convert the response of physical, chemical, or biological property or condition like temperature, pressure, biological

C. A. Nayak (✉) · H. N. Pradeep
Department of Chemical Engineering, BMS College of Engineering,
Bull Temple Road, P B NO. 1908, Bengaluru 560019, Karnataka, India
e-mail: canayak.che@bmsce.ac.in

H. N. Pradeep
Department of Chemical Engineering, Dayananda Sagar College of Engineering, Shavige Malleshwara Hills, Kumaraswamy Layout, Bengaluru 560078, Karnataka, India

S. Bhattacharya et al. (eds.), *Environmental, Chemical and Medical Sensors*, Energy, Environment, and Sustainability, https://doi.org/10.1007/978-981-10-7751-7_6

response, humidity, speed are frequently used to detect and respond as electrical or optical signals. Definition about sensor usually leads to ambiguity. The terms "sensor" and "transducer" are used in similar ways. The standardized definition of transducer is "*a device which provides a usable output in response to a specific measurand*". Whereas an output is an "*electrical quantity*" and while a measurand is "*a physical quantity, property, or condition which is measured*" (ANSI 1975). Sensors are the most worldwide term used by scientific literature work worldwide.

In early 1800s, the temperature response of different materials to electrical resistance was noted. This initiated Wilhelm von Siemens in early 1860s to develop a sensors response to a temperature based on copper resistance. In the year 1980, sensors applications started when Warren S. Johnson, USA, invented regulating heating systems by electric thermostat (Johnson 1883).

Sensors are classified on the basis of simple sensor or a complex sensor. A better way of classifying a sensor is on the basis of its characteristic properties such as material, stimulus, specifications, physical phenomenon, conversion, and application field (Middelhoek et al. 1983).

Extremely thorough and careful attempt for organizing sensors was undertaken and represented by its input and output energy. Figure 1 depicts the sensors representation by various input energy.

1.1 Classification of Sensors

Sensors are advanced devices which are commonly used to detect and act in response to electrical or optical signals received. A sensor converts the operating parameters into electrical signals which are measured. The sensing devices are classified by their

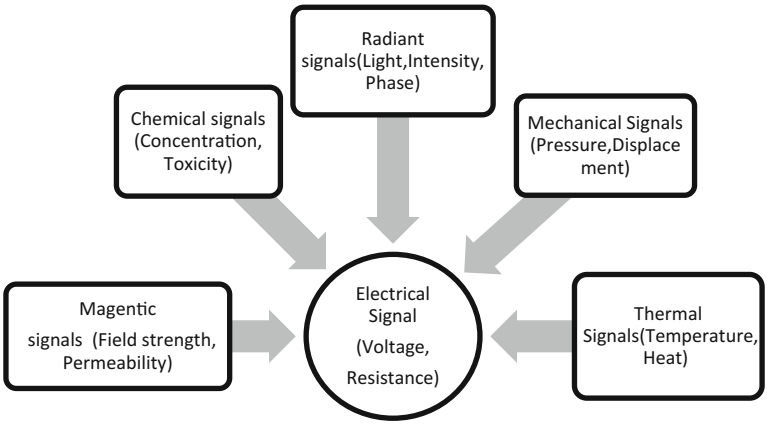

Fig. 1 Sensors representation by various input energy

- Operation type—analog or digital sensors;
- Quantity measured—direct or indirect sensors;
- Operation medium—optical or electrical etc.
- Application field.

Classification based on its applications and its measurands, technical aspects, detection means, sensor materials (White 1987), is shown in Table 1.

2 Microfluidics

Microfluidics is a multidisciplinary subject applicable to science and technology which connects various branches such as chemistry, biology, physics, and engineering (Wang et al. 2009). Microfluidics involves the designing, manufacturing, formulating devices, and processes. It deals with fluid volume in the range of microliters (10^{-6}) to picoliters (10^{-12}). A microfluidic device can be identified by the fact that it has one or more channels with at least one dimension which is less than 1 μm or orifice diameter is typically in the order of micrometer (Whitesides 2006).

The important length of a scale is not the overall device size but rather the length scale of the channel which determines the flow behavior (Stone et al. 2004). During 1970s, the development of machining, mechanical microdevices, microelectromechanical systems [MEMS] began. Further, in late 1980s, development of micropumps, microvalve, and microflow sensors initiated the era of microfluidics. Microfluidics developed rapidly after the innovation of solid-state sensors and actuators. Many researchers have made use of this innovation and developed sensors for its applications in life science and chemistry (Manz et al. 1990).

In microfluidics, fluid-based devices and transport phenomena are at microscopic scale length. Regardless of the size of device, only the space where the fluid is processed and quantity of fluid is important in microfluidics. Various scales of microfluidic devices are tabulated in Table 2.

Based on the end use, microfluidics can be classified according to flow, droplet of a fluid, and digitalization. In flow devices, channels are permanently etched. Secondary accessories such as micropumps and microvalves are used to control and manage the flow of fluid in these devices (Henares et al. 2008). Droplet microfluidics uses droplets for sensing applications, whereas in digital microfluidics most of manipulation of flow is carried out digitally (Najah et al. 2012).

2.1 Physics of Microfluidics

Handling and analyzing of fluid at micrometer scale can be diverse from the conventional scales. In microscale flow, physics of flow and forces dominating on fluid

Table 1 Classification based on applications of sensors

Measurands	Technological aspects of sensors	Detection means used in sensors	Sensor conversion phenomena	Sensor materials	Fields of application
Acoustic Biological Chemical Electrical Magnetic Thermal Mechanical Radiation Optical	Sensitivity Measurand range Stability Resolution Selectivity Speed of response Ambient conditions Overload characteristics Output format Cost Size Weight	Biological Chemical Electric Magnetic Electromagnetic wave Heat, temperature Mechanical Displacement Radioactivity	Biological Biochemical transformation Physical transformation	Inorganic Organic Conductor Insulator Semiconductor Liquid, gas plasma Biological substance	Automotive Domestic appliances Energy, power security Health, telecommunications Manufacturing Marine Scientific measurement

Table 2 Various scales of microfluidic devices

Microfluidic devices	Length scale	Volume scale
Micro-filter/micro-reactor	≤ 1 mm	<1 ml
Conventional microfluidic device	<1 mm	<μl
Nanotechnology/nanodevice	1 μm–1 nm	<fl

is very different. Laminar flow, diffusion, fluidic resistance, surface area to volume ratio, and surface tension are the important properties that dominate in microfluidics (Meyvantsson and Beebe 2008; Squires and Quake 2005).

Flow physics: Dimensionless numbers are important parameters which evaluate and clarify physical phenomena occurring at micrometer scales.

Reynolds number (N_{Re}) is most frequently used dimensionless number in microfluidics; it compares inertial effects with viscous effects and is expressed as a function of density (ρ), velocity (U), characteristic length (L), hydraulic diameter (D_h), and dynamic viscosity (μ).

$$\text{Reynolds number } (N_{Re}), \quad N_{Re} = \frac{\rho UL}{\mu} \tag{1}$$

The Reynolds number should be in the order of unity or less than unity. Usually the fluid flow rate in microfluidics will be in the order of μm/s so that the flow will be in laminar range (Das and Chakraborty 2010).

Surface to volume ratio: It is one of the parameters which helps during dimensional scaling. When the dimension of device is decreased, the surface area of the device will become relatively large. Parameter of fluid such as wetting performance and surface charges significantly increases due to change in the surface area. These parameters become important than inertia which is based on volume and mass.

Surface Tension: In macroscale, pressure, gravity, and inertial force dominate; as a result, the surface tension and capillary forces are generally negligible in fluid dynamics. But in microscale as volume reduced to microliter range the behavior is reversed. Surface tension and capillary forces become important properties in microfluidics.

Surface tension or free energy at surface is more important than that of its bulk. According to the basic principle, "*the system will try to decrease its free energy to a minimum value.*" Hence, the boundary between immiscible fluids will try to shrink and minimize the surface. Therefore, surface tension and contact angle are affected by dimensional scaling.

Bond number, Webber number, and Capillary number: These are the dimensional numbers which are important for low-speed microfluidic, micro-droplet applications, and dynamics study which are evaluated by surface tension with buoyancy force, fluid's inertia, and viscous forces, respectively.

$$\text{Bond number } (N_{Bo}), \quad N_{Bo} = \frac{\Delta\rho g^2 L}{\sigma} \tag{2}$$

$$\text{Webber number } (N_{We}), \quad N_{We} = \frac{\rho u^2 L}{\sigma} \tag{3}$$

$$\text{Capillary number } (N_{Ca}), \quad N_{Ca} = \frac{\eta u}{\sigma} \tag{4}$$

Diffusion: Microfluidic application requires control over particle concentration or molecule. Diffusion is one of the primary phenomena that influence the functionality of microfluidic devices. It has an important role compared to convection and bulk flow. Smaller particles in suspended liquid have higher values for diffusion coefficient than larger particles. This property helps in separation processes.

$$J = -D\left(\frac{\mathrm{d}c}{\mathrm{d}x}\right) \tag{5}$$

The ratio of convection to diffusion is given as Peclet number (Pe), a dimensionless number. It is the ratio of flow velocity (U), a characteristic length (L) to diffusion coefficient (D).

$$\text{Peclet number } (N_{Pe}), \quad N_{Pe} = \frac{UL}{D} \tag{6}$$

2.2 Materials for Fabrication of Microfluidics

Materials properties are very important for fabrication and the design of a microfluidic device. It affects both functionality and manufacturability. The major materials used in fabrication of microfluidic devices such as silicon, glass, metals, and polymers are discussed below.

Silicon: Silicon is an important and commercially successful material used in the fabrication of microelectronicmechanical system (MEMS). It has effective mechanical properties, high melting temperature, low coefficient of thermal expansions, which are essential for reliable and successful accelerometer as well as pressure sensors (Petersen 1982). Its semiconductor property helps in selection of silicon for fabrication of pumps valves and mixers. Use of silicon can be easily fabricated to high surface–volume ratio of microfluidic devices. These characteristics of silicon are used for catalysis adsorption/or desorption and other surface reaction sensing application (Camara et al. 2007). In electrostatic diaphragm and heating element, polycrystalline micro-pump can be doped with silicon and used. This can be utilized for development of various micro-machined sensors and actuators for various functionalities (Jang et al. 2004).

Glass: Glass is very easily and economically available material for fabrication of microfluidic device. Important property of glass is it's optically transparent, rigid, and is dimensionally stable. This makes microfluidic device convenient for imaging and detection for fluids. Glass can form into flat slides and cut into required designed channels for several sensor applications. Commercially borosilicate glass is available in a variety of forms that can be used in different microfabrication applications (Diepold and Obermeier 1996). Mainly amorphous silicon oxide (SiO_2) known as silica is used as the basic raw material in glass manufacturing. But the properties of glass can be modified by combining with sodium carbonate, calcium oxide, and boron oxide to get varieties of optical, thermal, mechanical properties (Khan Malek et al. 2007).

Metals and other materials: Metals are significantly high in electrical conductivity and mechanical strength. Its high thermal conductivity helps in microfluidic devices for functional electrical components like conducting lines, electrodes, heat spreader, and high pressure applications (Kang et al. 2004). Electroplating and electroforming use some commonly used metals like gold, nickel, and copper. One of the important metal-based microfluidic structures is ink-jet print head made of single nickel electroforming step. Other compounds, such as silicon dioxide, silicon carbide, silicon nitrides, are extensively used in microfabrication (Hamblin et al. 2007). A piezoelectric effect in electromechanical actuation is exhibited by lead zirconate titanate (Doll et al. 2007).

Polymers: Extensive variety of commercially available polymer materials initiated the development of polymer-based microfluidic devices. The fabrication difficulties of silicon- and glass-based microfluidic devices also aided the investigation of economic and reliable fabrication materials (Becker and Locascio 2002). The polymers offer low mechanical strength, low melting, and high electrical resistance. One of the important advantages of the polymer is that they can be engineered or synthesized to exhibit properties for targeted functionality. Polymers used in microfluidics are polydimethylsiloxane (PDMS), polymethylmethacrylate (PMMA), polyamide, epoxy-based negative photoresist polymer called SU-8, etc. PDMS is a nontoxic, chemically stable, optically transparent material fabricated by soft lithography. A simple schematic representation is shown in Fig. 2.

Polymethylmethacrylate (PMMA) a thermoplastic material easily patterned with desired microchannels structures by fast embossing or by laser cutting (Hong et al. 2010). Its opaque to light transmission in the ultraviolet range limits its applicability to sensing application, but it can integrate with metal electrode for electrochemical sensing application (Chen et al. 2006). Among the polymers, polyamide shows higher mechanical strength, heat resistance, and dielectric strength (Wilson et al. 1990). It has been widely used in MEMS sensors, and as multifunctional chips used in liquid chromatography and electrospray application (Yin et al. 2005). SU-8 is an excellent stable polymer against several concentrated acids and bases. Its thermal stability makes it a very attractive polymer for micro-optics, micromachining, packaging, and analytical microfluidic applications.

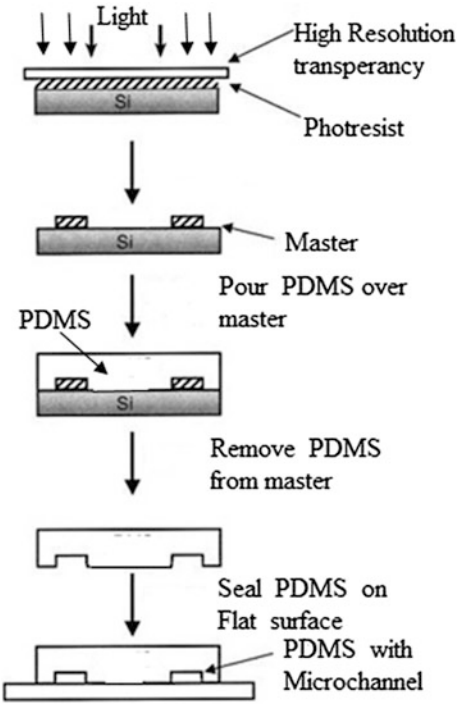

Fig. 2 Schematic representation of fabrication steps of PDMS microfluidics

2.3 Properties of Material

Selection of materials for microfluidic fabrication is very important parameter. Electrical, thermal, mechanical, optical, chemical, and magnetic properties are considered during fabrication. Elastic properties like fatigue life, flexural strength, and modulus of rupture are some of the important mechanical properties that should be considered for smooth functioning of a microfluidic device.

For manufacturing of a microfluidic device, thermal properties such as melting point, glass transition temperature, coefficient of thermal expansion, specific heat, and thermal conductivity are significant. Electrical properties are important during manufacturing of microfluidic components such as microvalves and micropumps. This property is used for the functioning of electrostatic actuation, electrokinetic pumping, resistive heating, and capacitive sensing. Some of the basic electrical properties are resistivity; dielectric constant and breakdown voltage are to be considered during functionality of the device. Other physical properties such as density, hydrophobicity, water absorption, chemical resistance, and surface conditions always significantly effect on microfluidic functionality (Becker and Locascio 2002).

3 Microfabrication of Microfluidics

Fabrication of the microfluidic devices can be carried out by various methods. The fabrication methods are lithography, soft lithography, etching, and injection molding. The microfabrication of microfluidics is well documented in various literatures (Leester-Schädel et al. 2016; Saem et al. 2017; Wang et al. 2017a, b). One of the important microfabrication is by photolithography which is discussed below.

Photolithography: It is the most important process step used more than one time in fabrication of microfluidic devices. In this process, following steps are included: (1) coating of photoresist on to a substrate, (2) selectively exposing regions to UV radiation through a photomask, (3) removing the region that remains soluble by developing. The basic steps are shown in Fig. 3.

Micromachining of silicon and glass usually involves the use of various methods like wet and dry etching, photolithography, electron beam lithography, and variety of other methods. All these methods require the use of clean room facilities. Various literatures have explained in detail about the micromachining of silicon and glass (Diepold and Obermeier 1996; Khan Malek et al. 2007; Leester-Schädel et al. 2016; Wang et al. 2017a; Iliescu et al. 2012; Faustino et al. 2016).

Photolithography is not a suitable method for fabrication of basic polymer microfluidic devices for several reasons. An inexpensive and simple non-lithographic method is required for fabrication of polymer microfluidic platform. A wide non-photolithography method has been developed in replacement of photolithography techniques (Pradeep and Nayak 2016). Microfluidic device fabricated by non-photolithography method is shown in Fig. 4. CO_2 laser can be used

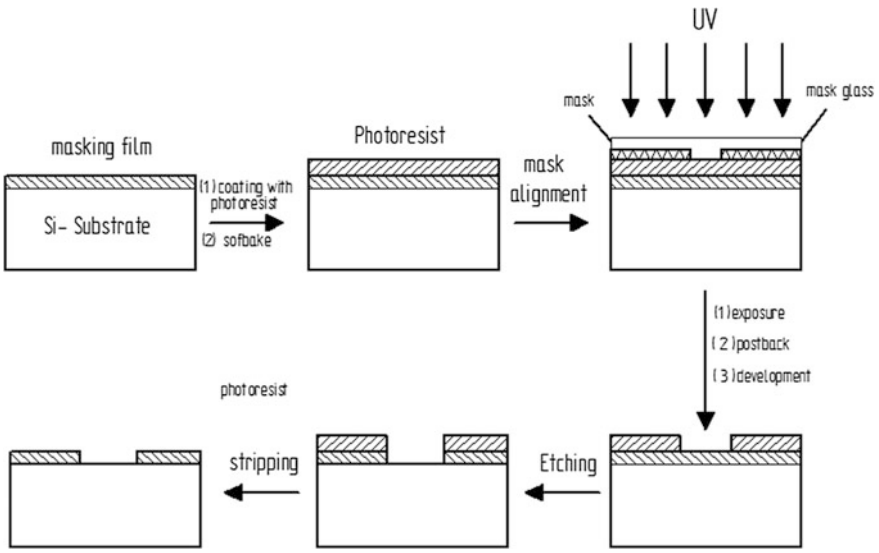

Fig. 3 Fabrication steps for photolithography

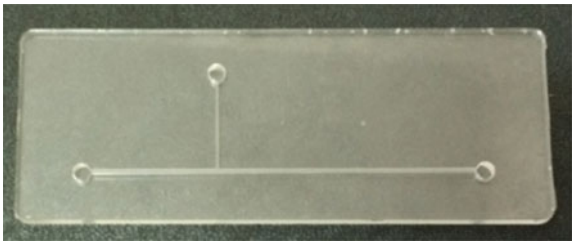

Fig. 4 Photograph of cross-channel microfluidic device by laser cutting

to fabricate PMMA with 10 to several hundred micrometer microchannels (Hong et al. 2010). Microinjection molding is one of the most promising methods suitable for mass production of disposable polymeric devices (Attia and Alcock 2010). Fabrication conditions during molding process have large effect on the width and depth of a microfluidic channel. Hot embossing with the mold is also used for several types of microfluidic devices (Mathur et al. 2009).

4 Droplet-Based Microfluidics

Surface area to volume ratio of devices is one of the most important properties for on-site testing. The high surface area to volume ratio benefits insignificant decrease of the consumption of sample and reagents for assays. This reduces the size of the microfluidic device. Microfluidic technology also enhances high throughput, cost of the device, and speed of biological/chemical assays. This technology has also been used for polymerase chain reaction (Sun et al. 2009), protein crystallization, DNA/blood analysis (Song et al. 2006). Generating uniform and high throughput droplets is an important step in achieving micro-droplet functionalities. Droplet-based microfluidic systems are established on creating or manipulation of droplets in microchannels or in a device. Droplet can be mixed, separated, or combined, and these are transported and analyzed for biological assays and chemical reactions (Faustino et al. 2016; Zhu and Wang 2017; Zhu and Fang 2013). Digital microfluidic systems are fundamentally different compared to droplet-based microfluidic systems as they provide process automation of discrete droplets through electrostatically actuated electrodes.

In droplet-based microfluidics, droplets formations are categorized as active method and passive method. In active method, the use of additional energy input in promoting interfacial instabilities is considered during the droplet generation and whereas, in passive method, droplets without external actuation are considered (Zhu and Fang 2013). Dielectrophoresis (DEP) and electrowetting on dielectric (EWOD) are examples for active droplet generator, whereas T-junction, cross-junction, and flow focusing methods fall under the passive method (Sharma et al. 2013). Most common methods for droplet generation are achieved with either T-junction, cross-junction, or co-flow microfluidic channel by hydrodynamic means. In these

channel geometric configuration, immiscible fluids at required flow rate are sent into separate channels by external pump or pressure sources. These two immiscible fluids form two phases, a continuous phase and disperse phase. These two phases meet at the junction and due to shear force created by one fluid makes other fluid to extend to some finger shape and finally pinched off as droplet.

A droplet of dispersed phase is formed due to the instability of the interface. Size and high throughput of droplet depend upon channel geometry and dimensions of the microchannels of microfluidic device. It also depends on flow rates of dispersed fluid and continuous fluid, applied pressures used to drive into the channels, fluid properties like viscosity and interfacial tension between two phases. In this chapter, the physics and dynamics of droplet formation in T-junction are discussed. These droplet formations in T-junction are similar to cross-junction and co-flow junction. T-junction is one of the familiar microfluidic channel geometry used over a broad range of flow conditions for generating high throughput droplet (Mathur et al. 2009; Thorsen et al. 2001).

Commonly T-junction consists of two channel situated at right angle to each other. Dimensions of channel are in the range of micrometers. Depending on the size and frequency of droplet, channel size and cross-section can be designed. Droplet forming fluid is to be sent as dispersed phase in right-angled channel, and in the continuous phase the fluid which is immiscible to disperse phase is sent through another channel. Figure 5 depicts the droplet generation in a T-junction where Q_c—carrier phase flow rate, Q_d—dispersed phase flow rate, W_c—width of the continuous channel, and W_d—width of the side channels. Droplet formation frequency and size of the droplets in T-junction are influenced by dimensional numbers, capillary number, contact angle, channel geometric configurations, and materials which are used for fabrication of the device.

Regimes of droplet formation: Squeezing, dripping, and jetting are three distinctive flow regimes that occur in flow channels during droplet formation. The various regimes of droplet formation are shown in Fig. 6.

In the squeezing regime, droplet formation is mainly due to the pressure drop across the plug. Dispersed phase enters into main channel and blocks the channel of the continuous phase as shown in Fig. 6a. The pressure starts to increase in the

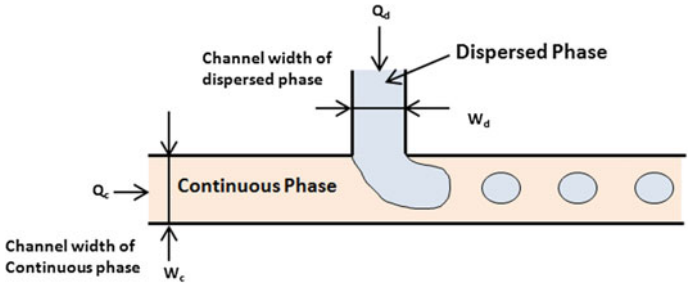

Fig. 5 Droplet formation in T-junction

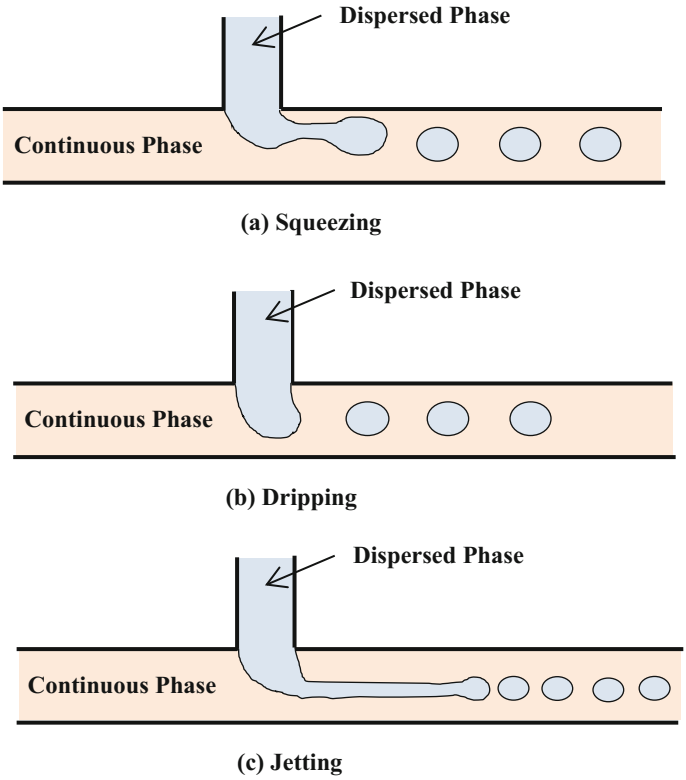

Fig. 6 Droplet formation in T-junction devices: **a** squeezing, **b** dripping, and **c** jetting regimes

upstream of the T-junction which is attributed to the obstruction caused in the flow of continuous phase. Continuous phase fluid starts to squeeze the dispersed phase fluid and pinch-off the plug. Channel junction corner is the generating point of droplet in squeezing regime.

In the dripping regime, continuous phase fluid partially blocks the dispersed phase. When dispersed fluid enters at the two-phase junction, shear force and buildup pressure by continuous phase fluid immediately break dispersed phase into droplets as depicted in Fig. 6b. Droplets are formed at the downstream of the main channel, and size of the droplet is always smaller than the dimensions of the channel. The resulting drops are carried downstream by the continuous phase.

In the jetting regime, the dispersed phases at the junction carried by the continuous phase to long neck resemble a jet as shown in Fig. 6c. Break of jet of dispersed phase begins, and break point is carried downstream. Finally, droplet is pinched off.

Influence of other parameters on droplet formation: Capillary number (Ca) that is a comparison of surface tension force with viscous force is the most important dimensionless number in droplet formation or fission process. Interfacial tension

between the continuous phase and dispersed phase, viscosity, and velocity of continuous phase plays key role in droplet dynamics. Size of the droplet (R) increases with respect to increase in pressure ($R \propto Ca^{-1}$) (Nisisako et al. 2002). When Ca is small, the dispersed phase fluid enters into main channel and tries to occupy full width of it, but incoming continuous phase fluid breaks up it into droplet at downstream side of the main channel. Here, interfacial force dominates the shear stress (Garstecki et al. 2006).

As the capillary number increases, the size of the droplet increases and this change in the size obstructs the continuous phase channel (De Menech et al. 2008). In large capillary number, dispersed phase fluid partially fills the main channel and droplet formed at the neck of dispersed channel. These two regimes are squeezing and dripping, respectively. When capillary numbers cross its critical value, droplet formation shifts from squeezing to droplet regimes.

In addition to capillary number, flow rates of both the phases also have a significant role in droplet generation process. The droplet grows as the rate ratio (dispersed phase/continuous phase) increases, but it reduces as capillary number increases (De Menech et al. 2008). When ratio between flow rates (dispersed phase/continuous phase), is little, the droplets are pinched off at the T-junction corner in any case of the capillary number.

For a larger flow rate ratio, increase in capillary number will detach the droplet from the corner. When capillary number and flow rate ratio increases, the droplet pinches off progressively, moves downwards, and forms a stable jet. In the dripping regime, the influence of the viscosity ratio (dispersed phase/continuous phase) leads to smaller droplet, but in the squeezing regime expected droplet diameter is nearly independent of the viscosity ratio. If the ratio does not influence the diameter of the droplet it indicates that viscous shear force and the capillary force control it. Due to large surface to volume ratio, fluid/surface ratio and contact angle influence the droplet shape, generation frequency, and detachment point. When the contact angle increases droplet diameter becomes smaller.

5 Applications of Sensors

Scientists have developed many cutting-edge technologies to make sensing more convenient for environmental analytical purposes. The microfluidic technology origins are from the micro-analytical techniques as well as methods namely capillary electrophoresis (CE), gas chromatography (GC), and high-pressure liquid chromatography (HPLC). For development of various sensors, these novel technologies are combined with the capability of the optical detection using laser light, impedance measurement, electrochemical, and biochemical reactions. These combined technology sensors have high resolution and high sensitivity using very minute quantity for detection. Recently, many applications of microfluidic sensor

technology are developed. These sensors are mainly in three major domains namely environmental sensors, electrochemical sensors, and medical tests for a diagnostic testing. The following sections discuss about the various microfluidic sensors.

5.1 Environmental Sensors

In the last few decades, the increase in hazardous compounds has made a dent in environment due to industrialization, globalization, and exponential growth in human population. Environmental sensors are used to detect the change in pH, pesticides, and heavy metals to safeguard the environment. These sensors are developed for a quick detection with high sensitivity and high resolution as well as minimum amount of reagent used for analysis.

Microfluidic pH sensor: A microfluidic pH sensor was developed by de Vargas et al. (2016) for in situ pH measurements. It utilizes small volume of samples and reagents. It has an economic detector system that utilizes a light-emitting diode as light source and a photodiode as the detector. The pH microfluidic sensor system has been characterized for various parameters like pH response, reproducibility, and stability. Multisource real water samples were analyzed using the microfluidic pH sensor system which has an error of 3.84% for its applications for the environmental applications (de Vargas et al. 2016). Rérolle et al. (2013) developed a microfluidic pH sensor to analyze the seawater pH. The system is used for optical setup which was robust and miniature of an USB mini-spectrometer. Microfluidic pH sensor used three wavelengths LED when compared to that of a spectrometer (Rérolle et al. 2013). Ges et al. 2005 had also developed planar pH microelectrodes with a dimension less that 500 μm^2 on transparent glass slides using IrO_x selective electrochemical deposition using lithographic technique.

Heavy Metals Sensors: Environmental pollution is mainly attributed to the heavy metal pollution which is a serious concern and threat around the globe. Hazardous heavy metal pollution has posed a greatest threat and challenge to the environment. The present detection of these heavy metals requires expensive instruments and tedious operation for detection which can be taken up in sophisticated diagnostic centers or laboratories. The various sensors are developed for heavy metal detection using microfluidic platform. The most published papers are on the methods of detection using integrated microfluidic paper-based analytical device's (μPAD's). The detection of heavy metals is well tabulated and reported in various reviews (Sharma et al. 2013; Nath et al. 2015; Busa et al. 2016; Lin et al. 2016). The μPAD's uses colorimetric/fluorescence-based gold or silver nanoparticle to develop the microfluidic chip to identify/detect the presence of the heavy metal in polluted water streams. The μPAD's is having the properties of paper and advantages of economic and cost-effective way to detect the pollutant.

Till date, a large variety of detection techniques and methods have been developed and adopted using microfluidic platform. The detection methods are colorimetric, fluorescent, electrochemical, nanoparticles-based, hybrid microfluidic

chip, etc. For a good sensor, the following properties are to be identified: (i) economic and cost effectiveness, (ii) robust, (iii) sensitivity, (iv) specificity, and (v) accuracy.

Chai et al. (2010) developed a microfluidic sensor using glutathione functionalized gold nanoparticles for a cost-effective and sensitive method for detection of lead ions. The method utilizes colorimetric detection using 1 M sodium chloride aqueous solution, and the detection limit is 100 nM. The functionalized gold nanoparticles bound by lead ions showed excellent selectivity with a prominent color change compared to other heavy metal ions. The microfluidic laboratory chip was excellent to detect lead ions in lake water with low interference and high sensitivity (Chai et al. 2010). Nath et al. (2014) developed a paper-based microfluidic device that can rapidly detect very low concentration of arsenic ions using gold nanosensor (Nath et al. 2014). The microfluidic device developed was extremely selective for arsenic with a detection limit of 1.0 ppb which was below the reference of WHO for standard potable water. Nath et al. (2015) also developed a paper-based microfluidic device that can rapidly detect very low concentration arsenic, lead (Pb^{2+}) ions, and Copper (Cu^{2+}) ions. This microfluidic device utilized both colorimetric and fluorometric analysis with a detection limit of ≤ 10.0 ppb for water quality monitoring process (Nath et al. 2015).

5.2 *Electrochemical Microfluidic Sensors*

The first electrochemical-based oxygen sensor was developed in the year 1962 by Clark and Lyons (Clark and Lyons 1962). Rackus et al. (2015) have reported a review paper discussing about the convergence of the electrochemistry, biosensors, and the microfluidics. This review paper discusses most of the electrochemical microfluidic sensor basics. An electrochemical detector comprises three electrodes namely working electrode, reference electrode, and an auxiliary electrode. A working electrode facilitates the electron transfer to and from the analyte when a voltage is applied, whereas a reference electrode facilitates as a reference to measure and control the working electrodes. The auxiliary electrode also known as counter electrode gives the current required to balance the current measured at the working electrode. The ease of integration and fabrication of electrochemical cells with microfluidic devices is the main advantage for developing various microfluidic sensors. There are mainly three categories: (a) current, (b) potential, and (c) impedance; electrochemical sensors based on the detecting parameter and the electrochemical reaction take place during the analysis (Luka et al. 2015).

Satoh et al. (2008) have investigated and developed a device that carries out the transport of fluids and conducts electroanalysis. On the basis of electrowetting principle, various electrochemical sensors were developed to analyze glucose, lactate, glutamic pyruvic transaminase (GPT), glutamic oxaloacetic transaminase (GOT), pH, ammonia, creatinine, and urea. These electrochemical microfluidic sensors showed a quick and distinct response when a sample solution reaches the

respective sensing site (Satoh et al. 2008). Electrochemical techniques are mainly used in microfluidics sensors because they can be miniaturized and has better selectivity and sensitivity compared to other detection techniques.

5.3 *Food Safety Microfluidic Sensors*

Safety of food is to be given the most priority because the food pathogens cause food-borne infections and diseases. The rapid identification of these pathogens can prevent their spread and epidemics. The food safety microfluidic sensors are developed to identify these pathogens (Skurtys and Aguilera 2008). The sensors rely on the recognition of the antigen targets or receptors by antibodies and high-affinity ligands. The food safety microfluidic sensors have a great opportunity to be the rapid, sensitive, and useful for on-site detection of the pathogen (Narsaiah et al. 2012; Adley 2014). Busa et al. (2016) reported a consolidated on the food safety microfluidic paper-based analytical devices using different detectors like colorimetric, fluorescence, electrochemical, chemiluminescence, and electro-chemiluminescence technique, which can identify the food pathogens as well as the potable water contamination.

Many immunoassays are carried out using microfluidic technology for quick and accurate detection of the pathogens. One of the immunoassays is lateral flow assay (LFA) which is a very simple and also well known as dipstick assay. In LFA, it consists of a membrane which is coated with different antibodies which can detect food-borne pathogens. In a LFA, which consists of two lines in the strip, one targeting the food born pathogen like *Escherichia coli* and other with an antibody i.e., gold nanoparticle (Guo et al. 2012). When the sample containing the pathogen is applied in the inlet of the microfluidic sensor, the pathogen and the conjugated antibody travel through capillary action, and later it gets bound with the antibody present in the strip. The antibody–gold nanoparticle absorbs the light to give a pink color; the presence of two bands on the strip indicates the presence of food pathogen, and absence of one band states the non-presence of the target.

Another type of immunoassay sensor which uses electrochemical detection rather than optical detection is known as impedance immunoassay sensor. The antibodies are immobilized on the surface of the electrodes and called as inter-digitated microelectrode (IME). When the sample is injected into the inlet of the sensor, bacterium is attached to the antibodies, and some of the molecules bind between the electrodes decreasing the resistance which in turn change the impedance measured. The schematic diagram is depicted in Fig. 7. If the configuration can be designed, such that the smaller targets can be detectable due to change in the impedance, then smaller species of pathogens like viruses can be targeted. These sensors have been successfully demonstrated the detection of food-borne pathogens like *E. coli* (Guo et al. 2012) and *Salmonella typhimurium* (Yang et al. 2004) in many various food sample matrices.

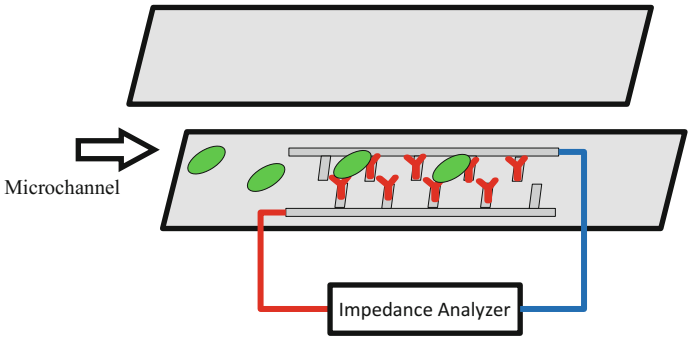

Fig. 7 Schematic food microfluidic sensor (image redrawn from Open Access Journal (Yoon and Kim 2012))

5.4 Biomedical Microfluidic Sensor

Successful application of microfluidic principle for the analysis started with rapid diagnostic test strips for pregnancy, blood glucose, and cardiac markers based on capillary action. Development of paper-based microfluidic devices increased rapidly due to simplicity of the design, less energy consumption, and minimum requirement of accessories and economically viable for on-site tests (Faustino et al. 2016). The presently commercially available paper-based devices cannot predict precise results. The next generation portable devices, which utilize disposable cartridges and analysis, were carried out by portable analyzer. This type of devices had disadvantage of disposable of cartridges and replacement of the analyzer as well as the reagents. The portable device is limited by its unit operation problem, i.e., mixing of the reagents, channeling, and transportation. These disadvantages of portable-based devices initiated the development of new microfluidic-based sensors (Bai et al. 2013). Microfluidic-based sensors were fabricated with microchannel operating in laminar range. These sensors were developed to operate in batch or continuous mode. Droplet-based analysis consists of droplet generation, merging, splitting, sorting, and mixing in microfluidic channel. The analysis includes cell analysis, single organism, DNA assays, drug screening (Yeo et al. 2011), purification of nucleic acids (Bhattacharyya and Klapperich 2006), and protein crystallization (Streets and Huang 2013). The cultivation and analysis of bacteria, yeast, and other type of cells are successfully carried out using droplet-based microfluidic sensor (Henares et al. 2008). An important application of droplet-based sensor is polymerase chain reaction (PCR) integrated microfluidic sensor (Tewhey et al. 2009). In digital PCR droplets were generated, sequentially sorted, and detected for high throughput DNA quantification. This helps in human evaluation studies (Boettger et al. 2012) and rare mutated DNA molecules (Streets and Huang 2014).

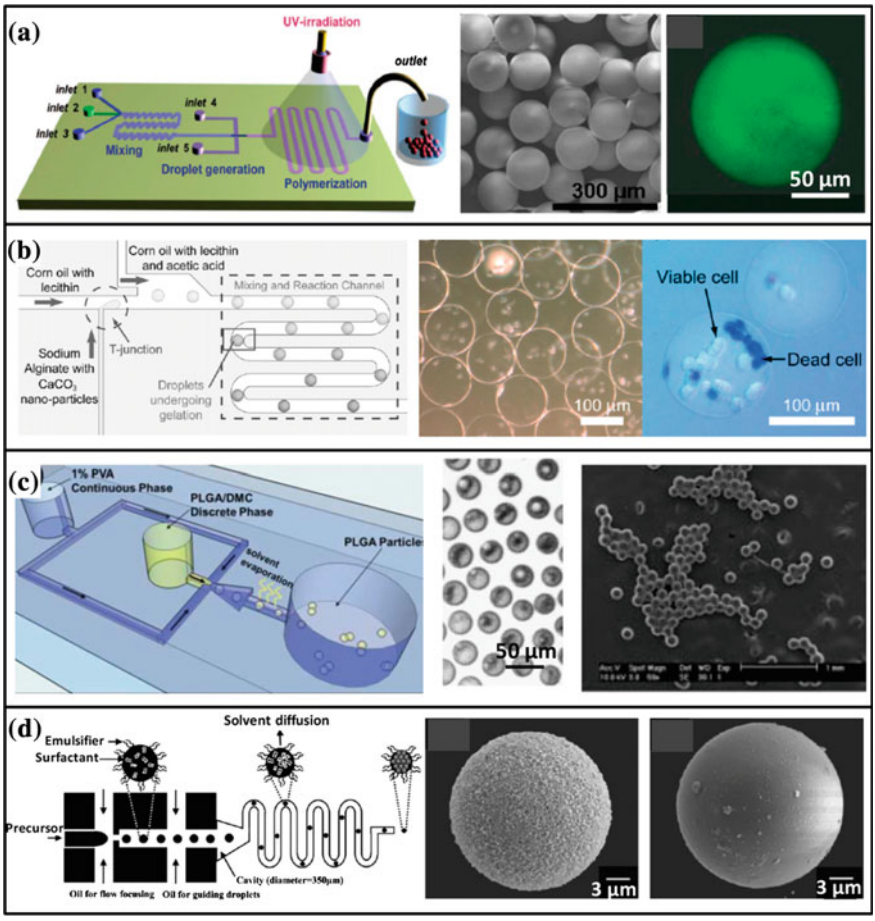

Fig. 8 Droplet-based microfluidics preparation of microspheres: **a** radiation-induced microspheres; **b** live cell encapsulation using sodium alginate; **c** droplet synthesis of PLGA microspheres; **d** solgel microfluidics microspheres. Reproduced from Open source journal (Ma et al. 2017)

Droplets tend to be in spherical shape if there is no external force applied. The droplets can be converted into microspheres by application of ultraviolet light or heat-induced polymerization. These microspheres will help for drug delivery applications (Riahi et al. 2015). The formation of the microspheres using droplet microfluidics is shown in Fig. 8a. Live cells are encapsulated using sodium alginate as dispersed phase and calcium carbonate nanoparticles using the gelation process using T-junction which is depicted in Fig. 8b. Microspheres have extensive applications in medical field for drug release. Microspheres are prepared by the oil–water system. Biocompatible and biodegradable properties adhered polymers are selected like polylactic-co-glycolic acid (PLGA). The size of the microsphere size is

dependent on the size of the droplet formed as well as the polymer concentration. The PLGA microspheres formation is as shown in Fig. 8c. For the biomolecule delivery using microfluidic technology is explored using hydrolysis reaction using inorganic oxide precursor. Synthesis of silicon oxide microspheres is synthesized is as shown in Fig. 8d.

Single cell in droplet provides analytical tool for analyzing the enzyme activity at the single cell level (Huebner et al. 2008). A protein crystallization screening chip can analyze hundreds of parameters with as small amount of microliter volume of droplet. These droplet-based microfluidic sensors have a great potential in biomedical diagnostics (Faustino et al. 2016; Sackmann et al. 2014; Kim et al. 2009).

6 Conclusion

Microfluidic device has been extensively reliable and economical for sensing applications in biological and environmental fields. This book chapter discussed about the sensor classification and its importance in the field of analysis and diagnostics. The microfabrication technique photolithography along with the droplet formations in a T-junction has many applications. The study of various flow regimes and droplet formation initiated the development of droplet-based microfluidic devices. The microfluidic sensors namely environmental, electrochemical, food safety, and medical diagnosis microfluidic sensors have improved exponentially in the recent years. The future of analysis and diagnostic is strongly dependent on these microfluidic sensors.

Acknowledgements The authors thank Dr. G. N. Rameshaiah, Head, Department of Chemical Engineering, B.M.S. College of Engineering, Bengaluru, and Dr. Ravishankar R., Head, Department of Chemical Engineering, Dayananda Sagar College of Engineering, Bengaluru, for constant encouragement and support.

References

Adley CC (2014) Past, present and future of sensors in food production. Foods 3(3):491–510

ANSI (1975) Electrical transducer nomenclature and terminology. ANSI Standard MC6.1-1975 (ISA S37.1). Instrument Society of America, USA

Attia UM, Alcock JR (2010) A process chain for integrating microfluidic interconnection elements by micro-overmoulding of thermoplastic elastomers. J Micromech Microeng 20(5):055017

Bai Y, Patil SN, Bowden SD, Poulter S, Pan J, Salmond GPC, Welch M, Huck WTS, Abell C (2013) Intra-species bacterial quorum sensing studied at single cell level in a double droplet trapping system. Int J Mol Sci 14(5):10570–10581

Becker H, Locascio LE (2002) Polymer microfluidic devices. Talanta 56(2):267–287

Bhattacharyya A, Klapperich CM (2006) Thermoplastic microfluidic device for on-chip purification of nucleic acids for disposable diagnostics. Anal Chem 78(3):788–792

Boettger LM, Handsaker RE, Zody MC, McCarroll SA (2012) Structural haplotypes and recent evolution of the human 17q21.31 region. Nat Genet 44(8):881–885

Busa L, Mohammadi S, Maeki M, Ishida A, Tani H, Tokeshi M (2016) Advances in microfluidic paper-based analytical devices for food and water analysis. Micromachines 7(5):86

Camara EHM, Pijolat C, Courbat J, Breuil P, Briand D, Rooij NFd (2007) Microfluidic channels in porous silicon filled with a carbon absorbent for GAS preconcentration. In: Transducers-2007 international solid-state sensors, actuators and microsystems conference, 10–14 June 2007, pp 249–252

Chai F, Wang C, Wang T, Li L, Su Z (2010) Colorimetric detection of Pb^{2+} using glutathione functionalized gold nanoparticles. ACS Appl Mater Interfaces 2(5):1466–1470

Chen R, Guo H, Shen Y, Hu Y, Sun Y (2006) Determination of EOF of PMMA microfluidic chip by indirect laser-induced fluorescence detection. Sens Actuators B Chem 114(2):1100–1107

Clark LC, Lyons C (1962) Electrode systems for continuous monitoring in cardiovascular surgery. Ann N Y Acad Sci 102(1):29–45

Das T, Chakraborty S (2010) Bio-microfluidics: overview. In: Chakraborty S (ed) Microfluidics and microfabrication. Springer, Boston, pp 131–179

De Menech M, Garstecki P, Jousse F, Stone HA (2008) Transition from squeezing to dripping in a microfluidic T-shaped junction. J Fluid Mech 595:141–161

de Vargas IMP, Fay CD, Cleary J, Nightingale AM, Mowlem MC, Diamond D (2016) Autonomous reagent-based microfluidic pH sensor platform. Sens Actuators B Chem 225: 369–376

Diepold T, Obermeier E (1996) Smoothing of ultrasonically drilled holes in borosilicate glass by wet chemical etching. J Micromech Microeng 6(1):29–32

Doll A, Wischke M, Schrag HJ, Geipel A, Goldschmidtboeing F, Woias P (2007) Characterization of active silicon microvalves with piezoelectric membrane actuators. Microelectron Eng 84 (5):1202–1206

Faustino V, Catarino SO, Lima R, Minas G (2016) Biomedical microfluidic devices by using low-cost fabrication techniques: a review. J Biomech 49(11):2280–2292

Garstecki P, Fuerstman MJ, Stone HA, Whitesides GM (2006) Formation of droplets and bubbles in a microfluidic T-junction-scaling and mechanism of break-up. Lab Chip 6(3):437–446

Ges IA, Ivanov BL, Schaffer DK, Lima EA, Werdich AA, Baudenbacher FJ (2005) Thin-film IrO_x pH microelectrode for microfluidic-based microsystems. Biosens Bioelectron 21(2):248–256

Guo X, Kulkarni A, Doepke A, Halsall HB, Iyer S, Heineman WR (2012) Carbohydrate-based label-free detection of *Escherichia coli* ORN 178 using electrochemical impedance spectroscopy. Anal Chem 84(1):241–246

Hamblin MN, Edwards JM, Lee ML, Woolley AT, Hawkins AR (2007) Electroosmotic flow in vapor deposited silicon dioxide and nitride microchannels. Biomicrofluidics 1(3):034101

Henares TG, Mizutani F, Hisamoto H (2008) Current development in microfluidic immunosensing chip. Anal Chim Acta 611(1):17–30

Hong T-F, Ju W-J, Wu M-C, Tai C-H, Tsai C-H, Fu L-M (2010) Rapid prototyping of PMMA microfluidic chips utilizing a CO_2 laser. Microfluid Nanofluid 9:1125–1133

Huebner A, Olguin LF, Bratton D, Whyte G, Huck WTS, de Mello AJ, Edel JB, Abell C, Hollfelder F (2008) Development of quantitative cell-based enzyme assays in microdroplets. Anal Chem 80(10):3890–3896

Iliescu C, Taylor H, Avram M, Miao J, Franssila S (2012) A practical guide for the fabrication of microfluidic devices using glass and silicon. Biomicrofluidics 6(1):16505–1650516

Jang WI, Choi CA, Jun CH, Kim YT, Esashi M (2004) Surface micromachined thermally driven micropump. Sens Actuators A 115(1):151–158

Johnson WS (1883) Electric tele thermoscope. USA Patent 281884

Kang S-W, Tsai S-H, Ko M-H (2004) Metallic micro heat pipe heat spreader fabrication. Appl Therm Eng 24(2):299–309

Khan Malek C, Robert L, Boy J-J, Blind P (2007) Deep microstructuring in glass for microfluidic applications. Microsyst Technol 13(5):447–453

Kim J, Junkin M, Kim D-H, Kwon S, Shin YS, Wong PK, Gale BK (2009) Applications, techniques, and microfluidic interfacing for nanoscale biosensing. Microfluid Nanofluid 7 (2):149–167

Leester-Schädel M, Lorenz T, Jürgens F, Richter C (2016) Fabrication of microfluidic devices. In: Dietzel A (ed) Microsystems for pharmatechnology: manipulation of fluids, particles, droplets, and cells. Springer International Publishing, Cham, pp 23–57

Lin Y, Gritsenko D, Feng S, Teh YC, Lu X, Xu J (2016) Detection of heavy metal by paper-based microfluidics. Biosens Bioelectron 83:256–266

Luka G, Ahmadi A, Najjaran H, Alocilja E, DeRosa M, Wolthers K, Malki A, Aziz H, Althani A, Hoorfar M (2015) Microfluidics integrated biosensors: a leading technology towards lab-on-a-chip and sensing applications. Sensors 15(12):30011–30031

Ma J, Wang Y, Liu J (2017) Biomaterials meet microfluidics: from synthesis technologies to biological applications. Micromachines 8(8):255

Manz A, Graber N, Widmer HM (1990) Miniaturized total chemical analysis systems: a novel concept for chemical sensing. Sens Actuators B Chem 1(1–6):244–248

Mathur A, Roy SS, Tweedie M, Mukhopadhyay S, Mitra SK, McLaughlin JA (2009) Characterisation of PMMA microfluidic channels and devices fabricated by hot embossing and sealed by direct bonding. Curr Appl Phys 9(6):1199–1202

Meyvantsson I, Beebe DJ (2008) Cell culture models in microfluidic systems. Ann Rev Anal Chem 1(1):423–449

Middelhoek S, Noorlag DJW, Steenvoorden GK (1983) Silicon and hybrid micro-electronic sensors. Electrocomponent Sci Technol 10(4):217–229

Najah M, Griffiths AD, Ryckelynck M (2012) Teaching single-cell digital analysis using droplet-based microfluidics. Anal Chem 84(3):1202–1209

Narsaiah K, Jha SN, Bhardwaj R, Sharma R, Kumar R (2012) Optical biosensors for food quality and safety assurance—a review. J Food Sci Technol 49(4):383–406

Nath P, Arun RK, Chanda N (2014) A paper based microfluidic device for the detection of arsenic using a gold nanosensor. RSC Adv 4(103):59558–59561

Nath P, Arun RK, Chanda N (2015) Smart gold nanosensor for easy sensing of lead and copper ions in solution and using paper strips. RSC Adv 5(84):69024–69031

Nisisako T, Torii T, Higuchi T (2002) Droplet formation in a microchannel network. Lab Chip 2 (1):24–26

Petersen KE (1982) Silicon as a mechanical material. Proc IEEE 70(5):420–457

Pradeep HN, Nayak CA (2016) Microencapsulation of C-phycocyanin by microfluidics. In: Regupathi I, Shetty KV, Thanabalan M (eds) Recent advances in chemical engineering: select proceedings of ICACE 2015. Springer Singapore, Singapore, pp 89–95

Rackus DG, Shamsi MH, Wheeler AR (2015) Electrochemistry, biosensors and microfluidics: a convergence of fields. Chem Soc Rev 44(15):5320–5340

Rérolle VMC, Floquet CFA, Harris AJK, Mowlem MC, Bellerby RRGJ, Achterberg EP (2013) Development of a colorimetric microfluidic pH sensor for autonomous seawater measurements. Anal Chim Acta 786:124–131

Riahi R, Tamayol A, Shaegh SAM, Ghaemmaghami AM, Dokmeci MR, Khademhosseini A (2015) Microfluidics for advanced drug delivery systems. Curr Opin Chem Eng 7:101–112

Sackmann EK, Fulton AL, Beebe DJ (2014) The present and future role of microfluidics in biomedical research. Nature 507(7491):181–189

Saem S, Zhu Y, Luu H, Moran-Mirabal J (2017) Bench-top fabrication of an all-PDMS microfluidic electrochemical cell sensor integrating micro/nanostructured electrodes. Sensors 17(4):732

Satoh W, Hosono H, Yokomaku H, Morimoto K, Upadhyay S, Suzuki H (2008) Integrated electrochemical analysis system with microfluidic and sensing functions. Sensors 8(2): 1111–1127

Sharma S, Srisa-Art M, Scott S, Asthana A, Cass A (2013) Droplet-based microfluidics. Methods Mol Biol 949:207–230

Skurtys O, Aguilera JM (2008) Applications of microfluidic devices in food engineering. Food Biophys 3(1):1–15

Song H, Chen DL, Ismagilov RF (2006) Reactions in droplets in microfluidic channels. Angew Chem Int Ed Engl 45(44):7336–7356

Squires TM, Quake SR (2005) Microfluidics: fluid physics at the nanoliter scale. Rev Mod Phys 77 (3):977–1026

Stone HA, Stroock AD, Ajdari A (2004) Engineering flows in smal devices. Annu Rev Fluid Mech 36(1):381–411

Streets AM, Huang Y (2013) Chip in a lab: microfluidics for next generation life science research. Biomicrofluidics 7(1):011302

Streets AM, Huang Y (2014) Microfluidics for biological measurements with single-molecule resolution. Curr Opin Biotechnol 25:69–77

Sun Y, Kwok YC, Foo-Peng Lee P, Nguyen NT (2009) Rapid amplification of genetically modified organisms using a circular ferrofluid-driven PCR microchip. Anal Bioanal Chem 394 (5):1505–1508

Tewhey R, Warner JB, Nakano M, Libby B, Medkova M, David PH, Kotsopoulos SK, Samuels ML, Hutchison JB, Larson JW, Topol EJ, Weiner MP, Harismendy O, Olson J, Link DR, Frazer KA (2009) Microdroplet-based PCR enrichment for large-scale targeted sequencing. Nat Biotech 27(11):1025–1031

Thorsen T, Roberts RW, Arnold FH, Quake SR (2001) Dynamic pattern formation in a vesicle-generating microfluidic device. Phys Rev Lett 86(18):4163–4166

Wang J, Ren L, Li L, Liu W, Zhou J, Yu W, Tong D, Chen S (2009) Microfluidics: a new cosset for neurobiology. Lab Chip 9(5):644–652

Wang B, Prinsen P, Wang H, Bai Z, Wang H, Luque R, Xuan J (2017a) Macroporous materials: microfluidic fabrication, functionalization and applications. Chem Soc Rev 46(3):855–914

Wang J, Eijkel JCT, Jin M, Xie S, Yuan D, Zhou G, van den Berg A, Shui L (2017b) Microfluidic fabrication of responsive hierarchical microscale particles from macroscale materials and nanoscale particles. Sens Actuators B Chem 247:78–91

White RM (1987) A sensor classification scheme. IEEE Trans Ultrason Ferroelectr Freq Control 34(2):124–126

Whitesides GM (2006) The origins and the future of microfluidics. Nature 442(7101):368–373

Wilson D, Stenzenberger HD, Hergenrother PM (eds) (1990) Polyimides. Chapman and Hall, New York

Yang L, Li Y, Griffis CL, Johnson MG (2004) Interdigitated microelectrode (IME) impedance sensor for the detection of viable *Salmonella typhimurium*. Biosens Bioelectron 19(10): 1139–1147

Yeo LY, Chang H-C, Chan PPY, Friend JR (2011) Microfluidic devices for bioapplications. Small 7(1):12–48

Yin H, Killeen K, Brennen R, Sobek D, Werlich M, van de Goor T (2005) Microfluidic chip for peptide analysis with an integrated HPLC column, sample enrichment column, and nanoelectrospray tip. Anal Chem 77(2):527–533

Yoon J-Y, Kim B (2012) Lab-on-a-chip pathogen sensors for food safety. Sensors 12(8): 10713–10741

Zhu Y, Fang Q (2013) Analytical detection techniques for droplet microfluidics—a review. Anal Chim Acta 787:24–35

Zhu P, Wang L (2017) Passive and active droplet generation with microfluidics: a review. Lab Chip 17(1):34–75

Chapter 7
Green Synthesized Nanoparticles as Potential Nanosensors

Dindyal Mandal, Sourav Mishra and Rohit Kumar Singh

Abstract The recognition of chemical and biological entities is an important step in biomedical, forensic, and environmental sciences. The generation of extremely sensitive and cost-effective sensors needs sophisticated equipment coupled with basic understanding of chemistry, biology, and material science. Nanoparticles especially noble metal nanoparticles (gold, silver) have drawn great attention in this area due to their distinctive physicochemical properties and can be used in constructing innovative identification and transduction process for chemical and biological sensors. The use of toxic chemicals in traditional synthesis restricts their use in the real samples. Thus, to overcome the limitation, green synthetic pathways of nanoparticles have gained tremendous attention, which provide some important features including easy fabrication and high biocompatibility. Herein, potential applications of green synthesized nanoparticles such as silver nanoparticles, gold nanoparticles, and carbon dots have been described.

Keywords Green synthesis · Gold nanoparticles · Silver nanoparticles
Carbon dots · Chemical sensor · Heavy metals · Surface plasmon resonance

1 Introduction

Early detection and estimation of the toxic materials in the environment, aquatic system, and food samples are imperative to prevent severe diseases in human body (Connon et al. 2012). To address this issue, precise analysis of aqueous samples is a challenging task. Several physical, chemical, and biological methods are being used for this purpose, where highly complicated equipments including ICP-MS, AAS have been utilized (Choudhary et al. 2016). However, these processes are time-consuming and costly. Hence, there is a requirement to develop a rapid and

D. Mandal (✉) · S. Mishra · R. K. Singh
School of Biotechnology, KIIT University, Patia,
Bhubaneswar 751024, Odisha, India
e-mail: ddmandal@gmail.com

S. Bhattacharya et al. (eds.), *Environmental, Chemical and Medical Sensors*, Energy, Environment, and Sustainability, https://doi.org/10.1007/978-981-10-7751-7_7

cost-effective protocol for the detection of metal ions. Recently, developing colorimetric detection of toxic chemicals has attracted researchers due to its simplicity and user-friendly nature.

Nanoparticles have gain tremendous popularity in the world owing to their small size and physicochemical properties. Nanoparticles with controlled size, shape, and structures show tremendous potential in optical, magnetic, electronic, and biomedical applications (Nie et al. 2010). Nanotechnology shows promising role in diagnosing diseases which is termed as "nanodiagnostics" (Lin et al. 2013). Owing to their unique properties, they exhibit widespread application as a straightforward and responsive device for the detection of chemical species (Nimbalkar et al. 2014). Advantages of nanoparticles include the tailoring of nanoparticles by suitable chemical compound using advanced technology for the designed applications (Pannopard et al. 2015). Plasmonic metal nanoparticles including gold and silver have tremendous potential for chemical and biological sensors, due to their sensitive spectral change to the local surroundings of the nanoparticle surface and simplicity of monitoring their light signal owing to their strong scattering or absorption (Ray 2010).

Conventional organic dyes and quantum dots (QDs) have some limitations in using as sensor (Resch-Genger et al. 2008). Organic dyes suffer from little fluorescent intensity, photobleaching, and stokes shift. On the other hand, QDs are made of toxic heavy metals including cadmium and lead and harsh conditions are used for synthesis (Mussa Farkhani and Valizadeh 2014). Carbon nanomaterials including carbon nanotubes, grapheme, fullerene, and carbon nanofilms have shown promising results in various fields such as biological markers (Münzer et al. 2013), biochemistry, and biomedicine (Bianco et al. 2005). Fluorescence carbon dots (CDs) represent fascinating class of recently discovered nanocarbons which have attracted considerable interest among the researchers due to their photoluminescence properties, good photostability, biocompatibility, low toxicity, and aqueous solubility (Liu et al. 2007). Thereby, CDs are extensively employed as fluorescence probe in sensing.

Traditionally, the synthesis of nanoparticles involves the use of toxic reagents including sodium borohydride, ascorbic acid, hydrazine hydrate. However, the consumption of hazardous chemicals used in the above-mentioned methods restricts their biocompatibility and application of nanoparticles. Thus, green synthesis of nanoparticles has been triggered and their potential application as sensor has gained significant attention in the field of nanotechnology.

The objective of this chapter is to present recent research trends in the field of green nanotechnology for sensor applications. This chapter focuses on three major nanoparticles (gold nanoparticles, silver nanoparticles, and carbon dots) which have been extensively explored as sensors.

2 Green Synthesized Gold Nanoparticles as Sensors

2.1 Detection of Heavy Metals

Among metallic nanoparticles, gold nanoparticles (AuNPs) have drawn significant interest due to their wide applications starting from catalysis to nanomedicines (Daniel and Astruc 2003). AuNPs offer several advantages over its counterparts as sensors including their inert nature, stability against oxidizing agents, and easy to synthesize using several physicochemical and biological methods (Chen et al. 2011).

The ability of AuNPs as sensors is based on the shifting of surface plasmon resonance (SPR) peak which is attributed to the binding of metal ions with the surface of AuNPs and as a consequence color change of nanoparticle solution occurs (Rex et al. 2006). L-tyrosine has been explored as capping agent in gold nanoparticles synthesis. L-tyrosine-capped AuNPs can efficiently detect Hg^{2+} ions and Pb^{2+} ions in the presence of other heavy and toxic metal ions (Annadhasan et al. 2014). Herein, AuNPs did not exhibit any shift in SPR band and color change in the presence of other metals except Hg^{2+} and Pb^{2+} ions. Blue shift of the SPR peak of AuNPs from 522 to 511 nm was observed in case of Hg^{2+} ions, whereas bathochromic shift from 522 to 552 nm was noticed in case of Pb^{2+} ions, indicating the strong interaction between Pb^{2+} ions and AuNPs compared to that of Hg^{2+} ions and AuNPs. The detection limit of AuNPs for Pb^{2+} ions and Hg^{2+} ions was found to be 16 and 53 nM, respectively. Herein, the adsorption of Hg^{2+} on the surface of gold nanoparticle leads to the development of core–shell structure that also prevents nanoparticle from agglomeration (Fig. 1). The AuNPs-based sensor shows efficiency in real samples like tap water and drinking water.

Hg^{2+} can also be detected by L-arginine functionalized gold nanorods (Guan et al. 2015). Red gold nanorods solution turns to green upon the addition of Hg^{2+} ion to the L-arginine-capped gold nanorods, indicating its ability as sensor. Interestingly, red color of AuNRs without L-arginine functionalization remains unchanged with or without the addition of Hg^{2+} ion, suggesting the role of L-Arginine in the color change process and detection of Hg^{2+} ions. Herein, color change of solution occurs due to the shifting of plasmon band upon the addition of mercuric ion. Out of two plasmon bands exhibited by AuNRs, longitudinal plasmon band emerges in the NIR region and the transverse plasmon band emerges in the visible region. After the addition of mercury a blue shift in both the plasmon band was noticed and blue shift in higher longitudinal band was more prominent with decrease in intensity as compared to the shift in visible plasmon band. The possible reason behind the blue shift with decrease in intensity may be explained from TEM results. TEM images revealed that L-arginine-capped AuNRs showed good dispersity in solution before addition of Hg^{2+} and side-by-side assembly structures were formed; however, after the addition of Hg^{2+} ions side-by-side assembly structures were developed along longitudinal axis and as a matter of fact shifting of

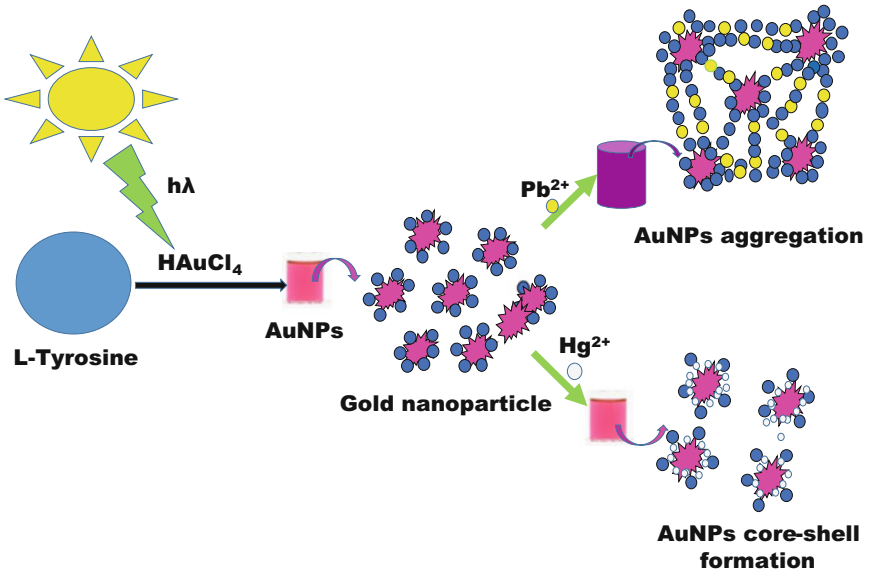

Fig. 1 Schematic representations of the formation route of AuNPs and its color change with metal ions

NIR plasmon band occurred. Significantly, the AuNRs-based sensor can detect up to 5 nM of Hg^{2+} ions.

One of the most hazardous heavy metal arsenic causes threat to ecosystem and health from contaminated water and industrial waste, especially in the developing countries including India, China, Taiwan, and Africa (Moriarty et al. 2009). Therefore, there is an urgency to generate a cost-effective, selective, and sensitive nanosensor system for the detection of arsenic in rural areas and industrial areas. An amino acid, asparagine (ASP) was explored recently for the production of gold nanoparticles (AuNPs) and generated nanoparticles exhibited promising result in the detection of arsenic (Ghodake et al. 2015). The selectivity of arsenic in the presence of other heavy metals was investigated at 1000 ppb concentration by colorimetric assay-based on UV–Vis spectroscopy. The bright red color of AuNPs turned into gray–black color immediately after the addition of As (III), which was not observed in case other metals, indicating strong binding affinity between As (III) and ASP ligands.

From TEM analysis, it was observed that AuNPs formed chain like assemblies and aggregates in the presence of 1000 ppb As (III) without affecting core structures of nanoparticles and, thus, eliminates the possibility of agglomeration. This optical sensing technique for the recognition of heavy metal As (III) can be applied in environment or wastewater treatment without using expensive instrumentation.

2.2 Detection of Aluminum and Fluoride Development of Dual Sensor

Fluoride plays a crucial role in biological and medical processes. It is also used in toothpaste to prevent tooth decay and medicinal component against osteoporosis. However, excessive consumption of fluoride can cause severe diseases. Fluoride within optimum limit is used to decontaminate ground water, nevertheless excess amount could be a problem in drinking water.

Kumar et al. (2017) have developed a straightforward green rout for the synthesis of gold nanoparticle by polyacrylic acids which perform as reducing agent as well as stabilizing agent under sunlight irradiation. These nanoparticles show the ability to detect Al^{3+} selectively and, moreover, Al^{3+}-induced PAA-capped AuNPs also help to detect F^- ions by inspecting the color change and shifting in UV–Vis spectra. In presence of Al^{3+} aggregation of PAA-AuNPs was noticed along with a red shift in absorbance maxima at pH 7.5. The absorbance maxima of AuNPs shifted from 530 to 630 nm upon the addition of Al^{3+}. Within 10 min, the color of the reaction mixture turned to purple from red. Interestingly, when F^- ions were added to the aggregated PAA-AuNPs, the color of the solution reversed back to red. On the other hand, when the reaction was performed in the reverse sequence, i.e., addition of F^- followed by Al^{3+}, no spectral change was observed. The probable mechanism behind this regeneration of color of PAA-AuNPs in case of F^- addition is that Al^{3+} strongly binds with F^- into the aggregated Al^{3+}-PAA-AuNPs, resulting in the formation of Na_3AlF_6 complex. It showed good selectivity even in the presence of various metal ions and anions. The method was further applied for the detection of F^- in various sources of water, even in toothpaste of different brands and satisfactory results were found.

2.3 Detection of Small Molecules

Amino acids play a major role in human physiology and their deficiency causes many diseases. Among amino acids, cysteine plays crucial role in human metabolism and detoxification. It provides cross-linking support for proteins and thus maintains the secondary structures of proteins. Deficiency of cysteine may lead to lethargy and other diseases including hair depigmentation, hematopoiesis, skin lesions, liver damage. (Shahrokhian 2001). Hence, detection of cysteine is important in biomedical system. Recently, AuNPs-based system has been developed for this purpose. Apple juice-mediated synthesized gold nanoparticles exhibit excellent selectivity toward the detection of cysteine (Bagci et al. 2015). Gold nanoparticles have been synthesized at optimum concentration of apple juice to avoid any unwanted aggregation of nanoparticles. Moreover, for the synthesis of AuNPs, alkaline condition was necessary even with mixing of optimal concentration of apple juice and gold salt. The possible explanation in using NaOH might be to

stimulate the phytochemicals present in apple juice and follow alkali driven mechanism to support the nuclei formation during the reduction process. Upon the addition of cysteine, red color of gold nanoparticles turned to purple color along with red shift of SPR band from 518 to 551 nm, indicating the aggregation of AuNPs. It is believed that gold shows significant binding affinity toward sulfur. Herein, thiol group of cysteine is responsible for the aggregation of nanoparticles. Interesting fact is that color of AuNPs remains same when the nanoparticle solution is mixed with another 19 proteinogenic amino acids including methionine which also contains sulfur, thus suggesting the selectivity of AuNPs toward cysteine. This can be attributed to the fact that in methionine sulfur is flanked by two alkyl group, whereas sulfur resides at terminal position in cysteine, thus reducing the reactivity of sulfur in methionine.

Histidine, another important amino acid regulates the transmission of metals in biological bases through the imidazole side chain (Li and Bian 2009). Recent studies indicate that deficiency of histidine may lead to damaged dietetic condition in patients who are suffering from chronic kidney diseases (Watanabe et al. 2008). Therefore, it is important to detect histidine level in plasma. In order to address this issue, there is a need to explore easy-to-use fluorescence sensors for detection of histidine. BSA-capped gold nanocrystals (AuNCs) have been reported for the detection of histidine (He et al. 2012). The fluorescent AuNCs exhibit excitation and emission at 480 and 605 nm, respectively. The fluorescence of AuNC is quenched by the addition of Ni^{2+} ion and quenching is depending upon the concentration of Ni^{2+} ranging from 0 to 20 μm. The fluorescence of AuNC decreases quickly in the presence of Ni^{2+} and become stable within 5 min. As the system is expected to be applied on biological fluids optimum pH (pH 7) has been chosen and salt effect also examined by using 0–0.1 N NaCl where it does not show any affect on the fluorescence of AuNC. The quenched fluorescence of AuNC can be recovered by the addition of histidine in AuNC-Ni^{2+} complex, which is attributed to the binding tendency of Ni^{2+} to histidine. Recovered fluorescence intensity enhances upon the addition of histidine. It was found that the addition of histidine in AuNCs did not affect the fluorescence emission, thus, confirming the enhanced fluorescence from detachment of Ni^{2+} ions from the surface of AuNCs only. The fluorescence restoration can be explained not only on the binding between Ni^{2+} and primary amine and/or carboxylic acids, but also, the role of the imidazole side chain should be considered. The AuNC-based turn on sensor is found to be selective for histidine detection over other amino acids. Histidine was successfully detected in urine samples in the interferences of other metal ions, glutathione, BSA, HSA, MPA. Urea does not affect the detection of certain concentration level of histidine. Nevertheless, the thiol and protein exhibit serious effect at the same concentration of histidine. However, this issue can be eliminated using diluted urine sample.

Physiologically important biomolecule glucose is an essential component of metabolic pathways in living organisms. Abnormal glucose level in human body is a caution sign for health condition. For instance, unbalanced level of glucose in our blood or urine is a marker of diabetes in clinical diagnostics (Wang 2008). Hence, glucose monitoring system is necessary to assess the health condition. There has

been great effort to develop such monitoring system (glucose sensor) using electrochemical (Xiao et al. 2003) fluorescence (Liu et al. 2010), Raman scattering (Shafer-Peltier et al. 2003), etc.

Recently, colorimetric sensor attracted great attention due to their low price, effortlessness, and easy to detect through bare eye (Wei and Wang 2008). However, developed glucose sensors show some limitations including low selectivity and high detection limit. Using human single strand DNA along with AuNPs, Li et al. (2012) have developed more efficient detection system for glucose. The function of the sensor is based on the well-known principle that cytosine base containing DNA strands can construct special packed structures known as i-motif which is formed in slight acidic condition through the base pair formation originated from protonated cytosine–cytosine ($C:C^+$). Using this concept, they have synthesized AuNPs by C-rich DNA which is carrier of normal human telomeric sequence. Once glucose and glucose oxide (GOx) combination is mixed with AuNPs, red AuNPs turns into blue rapidly, indicating the loss of protective effect of C-rich ssDNA. The AuNPs show a absorption band at 522 nm before the addition of glucose and GOx, whereas the intensity of absorbance band is decreased upon the addition of glucose along with the shifting of absorption maxima to 600 nm which is due to the aggregation of AuNPs. The plausible cause behind this aggregation is the generation of gluconic acid which decreases the pH of the reaction mixture. Under this acidic condition, the C-rich ssDNA collapses into quadruplex i-motif structure and base pairs are accommodated inside the anionic phosphate backbone to generate more compact structure. As a consequence, it is unable to provide stability to AuNPs and, thus, leads to aggregation. To confirm their hypothesis another experiment was designed where it was shown that individual addition of gluconic acids into AuNPs directed to the aggregation of AuNPs, whereas glucose or GOx separately did not show any such effects. H_2O_2, one of the oxidized products of glucose, on sole addition without catalyst could not cleave the DNA and also no aggregation was observed, thus, eliminating the effect of H_2O_2 alone. It was noticed that with increase in concentration of glucose, the pH of the reaction mixture decreased from 7 to 5.1, due to generation of gluconic acids. Absorption ratio (A_{600}/A_{522} ratio) showed a drastic change from pH 6.0 to 7.0, indicating the conformational change of i-motif DNA occurred in this pH range, which supports the previous report (Ahmed et al. 1994). Other glucose analogs like fructose, lactose, and saccharose, or some widespread interferents including dopamine, ascorbic acid, and uric acid did not show this effect. This study confirms the potential application of the sensor for the visual recognition of glucose in juice or in human serum.

Another biomolecule, heparin plays a vital role in our physiological and pathological processes (Althaus et al. 2013). Heparin is used as anticoagulant in the clinic. However, overdoses of heparin may lead to severe complications in human body. Optimum concentration of heparin is used during cardiovascular surgery and postoperation period. Therefore, proper monitoring and quantification are necessary for regulation of physiological processes and clinical applications. Till date, a number of fluorescence-based heparin sensors have been developed (Wright et al. 2005), where fluorescence quenching method is mostly used as signal output;

however, this is undesirable in the presence of other interfering components in the surrounding environment.

Chitosan-capped gold nanoparticles have been developed recently based on resonance light scattering (RLS) technique for the detection of heparin (Chen et al. 2013). These nanoparticles exhibit a weak resonance light scattering (RLS) and intense wine red color. The weak resonance light scattering intensity of chitosan-capped AuNPs in aqueous solution increased as the concentration of heparin was increased and the color of the solutions turned blue from red. Such colorimetric observation can be easily utilized for the quantitative estimation of heparin. The addition of polyanionic heparin led to aggregation of nanoparticles because of the electrostatic attraction between positive charge generated by chitosan on surface of AuNPs and negatively charged heparin, resulting in the shifting of spectral band from 520 to 660 nm. In the presence of HA and Chs, negligible change in the RLS intensity of chitosan stabilized AuNPs was observed. Noticeably, other biomolecules such as glucose, cysteine did not affect the sensitivity of AuNPs toward heparin.

Gold nanoparticles show its potential as sensor for the detection of antibacterial agent also. Chloramphenicol is a wide-spectrum antibacterial agent used for the treatment of food producing animals. However, high dose of this antibacterial agent should be avoided to eliminate the possibility of adverse side effects in human. Thus, monitoring of chloramphenicol is important in food samples as far as food safety is concerned. To address this issue, Karthik et al. (2016a) have reported the synthesis of gold nanoparticles by using *Bischofia javanica Blume* leaves as reducing agent. Graphene oxide (GO) has been used to decorate the surface of gold nanoparticle and to make an AuNPs/GO composite film-modified electrode which shows a good electrocatalytic activity toward chloramphenicol (CAP) (Fig. 2). This method has been applied for the detection of chloramphenicol in milk, powder milk, honey, and in pharmaceutical samples like eye drops. The electrochemical activity of CAP (200 μM) was investigated at AuNPs/GO/GCE (glassy carbon electrode) and compared with control electrodes using cyclic voltammetry at scant rate of 50 mV s^{-1}. A reduction peak of CAP is found at −0.689 V for GCE (glassy carbon electrode). Irreversible reduction peaks of CAP are produced by the AuNPs/GCE and GO/GCE composites at cathodic peak potentials of −0.680 and −0.55 V, respectively, whereas AuNPs/GO/GCE composite demonstrate a sharp cathodic peak at −0.544 V in presence of CAP, indicating the reduction of nitro group present in CAP to hydroxylamine. In anodic scan, no oxidation peak is observed, indicating the irreversible nature of the reduction peak. However, a peak corresponding to oxidation at −0.007 V with another peak corresponding to reduction at −0.024 V is appeared during second scan. The reduction process of nitroso compound to hydroxylamine derivative is responsible for the appearance of cathodic peak. On the whole electrochemical steps involved here are provided as Eqs. (1) and (2). Moreover, 1.5 and 2.1 fold higher reduction peak current of CAP at the newly developed electrode (AuNPs/GO/GCE) is observed when compared to that of AuNPs/GCE and GO/GCE, respectively. Additionally, the over potential for CAP reduction at AuNPs/GO electrode is greatly lower when it is compared to that

of control electrodes. The results indicate that AuNPs/GO is a competent electrode matrix for the responsive detection of CAP.

$$R-NO_2 + 4H^+ + 4e^- \rightarrow R-NHOH + H_2O \quad (1)$$

$$R-NO + 2H^+ + 2e^- \rightarrow R-NHOH \quad (2)$$

The modified electrode delivers a well promising amperometric response toward each addition of 100 μM CAP, whereas negligible responses are detected in presence of 500-fold excess concentrations of metal ions, anions, 4-acetaminophenol, 4-aminophenol, 2-nitro aniline, and 4-nitro aniline. Only, 4-nitro phenol and 4-nirobenzene show 11 and 13% of signals (percentage with respect to CAP signal). The results indicate that modified electrode is competent for the detection of CAP in presence of excess amount of regular metal ions and nitro compounds.

Similar application of AuNPs was explored for the detection of pesticides. Red tomato generated gold nanoparticles showed promising result in the detection of methyl parathion, a pesticide used broadly worldwide to manage wide range of insect pests. Citric acid and ascorbic acid, constituents of red tomato, are most likely responsible for the reduction of gold chloride solution (Barman et al. 2013). The surface of the AuNPs was decorated with sodium dodecyl sulfate (sds) as stabilizing agent. Upon the addition of methyl parathion in gold nanoparticle, a new peak around 400 nm was found instead of 532 nm observed only from AuNPs. The

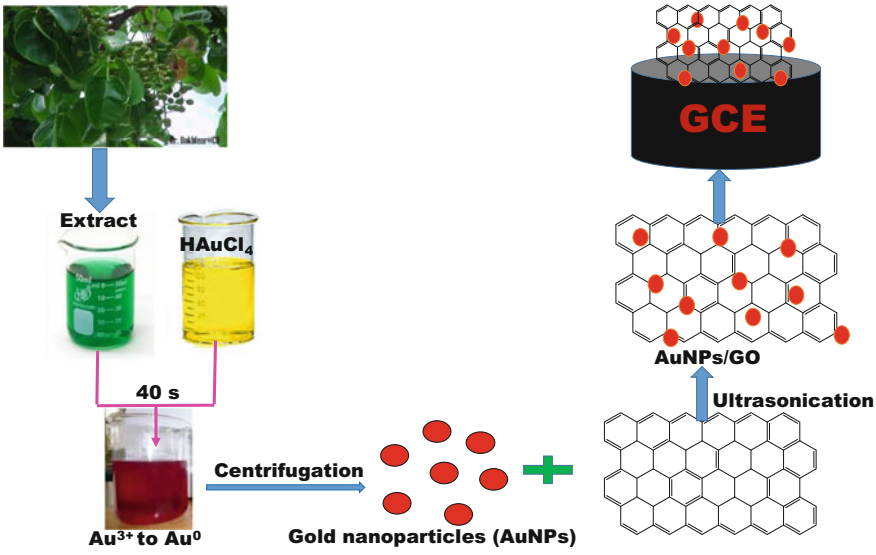

Fig. 2 Green syntheses of gold nanoparticles and their decoration on graphene oxide toward the detection of chloramphenicol

new peak at 400 nm is attributed to the generation of 4-nitrophenolate, the hydrolyzed product of methyl parathion in alkaline condition. Aggregation of AuNPs was observed with the enhanced concentration of methyl parathion and this is because of the generation of sulfur-containing compound, sodium di-*o*-methyl thiophosphate, another product from methyl parathion.

Dopamine (DA) is a biological small molecule, which plays vital role in human metabolism and central nervous system of mammalians. Excess amount of dopamine is cardiotoxic which leads to serious problems including death of heart muscles, high blood pressure, and high heart rate (Vilian 2016). Therefore, it is important to detect low level of dopamine in analytical and biomedical applications. Till date, various electrode-based sensors have been generated for the detection of DA. However, lack of selectivity and sensitivity became barrier for their application in clinic.

A new green approach of preparation of gallic acid supported graphene oxide encapsulated gold nanoparticles (GA-RGO/AuNPs) has been reported very recently (Thirumalraj et al. 2017). Herein, AuNPs-modified electrode was used for the sensitive and selective detection of DA in presence of ascorbic acid and uric acid. The electrooxidation of DA using GA-RGO/AuNPs-modified electrode in 0.05 M PBS (pH 7) was investigated using cyclic voltammetry (CV). It was found that only GCE (without AuNPs) did not show any responses where as electrode with GO displayed a weak irreversible peak toward DA. However, AuNPs-modified electrode displayed a good electrochemical redox behavior toward DA oxidation at 0.218 and 0.167 V, respectively. Similarly, the RGO-modified electrode showed a well defined results toward the redox behavior of DA. This newly constructed GA-RGO/AuNPs-modified electrode showed promising result in the detection and determination of DA in human blood serum and urine samples.

In order to detect nucleic acid, Lin et al. (2015) have proposed a simple, reproducible, UV light-assisted synthesis of gold nanoclustures (AuNCs) in presence of citrate ion using 30 adenosine nucleotides (A_{30}). Herein, UV light has been used for the reduction of gold ion and decomposition of citrate ion and A_{30} was used as stabilizer. The fluorescence of A_{30}-stabilized AuNCs appeared at 475 nm. A single-stranded DNA (ssDNA) composed of an AuNC-nucleation sequence and a hybridization sequence was utilized to made an AuNC-based fluorescent probe in the presence of the double-strand-chelating dye SYBR Green I (SG). Under single wavelength excitation, the combination of AuNC/SG-bearing ssDNA and entirely matched DNA emitted fluorescence at 475 and 525 nm. These AuNC/SG-bearing ssDNA have been involved in selective and sensitive detection of nucleic acid. For the detection of nucleic acid 100 nM SG and entirely matched DNA_{pm} was added to the AuNC-bearing ssDNA, and the formation of double-stranded DNA (dsDNA) interacted with the SG molecules, which caused an increase in their fluorescence intensity at 525 nm. The fluorescence intensities at 475 and 525 nm of AuNC/SG-bearing dsDNA were similar to those of AuNC-bearing ssDNA and SG-labeled dsDNA at the same concentrations. Hence, AuNC/SG-bearing ssDNA was chosen for the recognition of specific nucleic acid targets. As the concentration of DNA_{pm} was increased, the fluorescence intensity at 525 nm (I525 nm) also

enhanced gradually and at the same time 475 nm peak remained unchanged. The limit of detection (LOD) was observed to be 0.3 nM that is incredible. The sensitivity of this probe was also established by comparing the ratio I_{525} nm/I_{475} nm obtained from DNApm and that of obtained from single-base mismatched DNA, double-base mismatched DNA, and non-target DNA. The results indicate that AuNC/SG-bearing ssDNA probe is highly selective toward DNA_{pm}. This probe was further successfully used for the detection and quantification of DNA_{pm} in human plasma.

2.4 Detection of Hazardous Chemicals

Several research groups are involved in developing AuNPs-based sensors for the detection of environmentally hazardous chemicals which include hydrazine, ammonia, and nitrobenzene. For the detection of hydrazine, gold nanoparticles were generated from *Cerasus serrulata* (*C. serrulata*) leave extract. Cyclic voltammetry was used as analytical technique for this detection (Karthik et al. 2016b). The effect of AuNPs/GCE and bare GCE on CV have been examined in presence and absence of 1 M hydrazine. At GCE only any oxidation peak was not observed in presence of hydrazine at +0.24 V and, furthermore, it required over potential value. However, in case of AuNPs/GCE prominent oxidation peak was observed at the potential of +0.24 V. Moreover, greater oxidation current is achieved in case of hydrazine at customized AuNPs/GCE compared to that of at bare GCE. The above results indicate that gold nanoparticles play an important role by providing good electrocatalytic capability toward the oxidation. As the hydrazine concentration was increased the oxidation current peak intensity elevated, which was because of electrooxidation of hydrazine.

The possible mechanism for the oxidation of hydrazine at the AuNPs customized GCE can be depicted as provided in Eqs. (3), (4), and (5).

$$N_2H_4 \rightarrow N_2H_3 + H_3O^+ + e^- \quad \text{(slow)} \tag{3}$$

$$N_2H_4 + 3H_2O \rightarrow N_2 + 3H_3O + 3e^- \quad \text{(fast)} \tag{4}$$

$$N_2H_4 + 4H_2O \rightleftharpoons N_2 + 4H_3O^+ + 4e^- \tag{5}$$

Equations suggest that 4 protons (4 H^+) and 4 electrons (4e^-) are involved in the oxidation process of hydrazine. Besides this, they have evaluated the effect of interferents like metal ion or biological molecule on it. The AuNPs/GCE showed specific response toward every 50 μM hydrazine, whereas no significant responses were observed even in higher concentration of metal ions and 150-fold concentration of glucose, uric acid, ascorbic acid, dopamine. However, the above-mentioned molecules exhibited insignificant response on the customized

electrode, which did not influence the hydrazine response. Therefore, it can be concluded that AuNPs/GCE exhibits a good selectivity and sensitivity for the detection of hydrazine.

Simple sensor for the detection of environmentally hazardous compound ammonia is demonstrated by Pandey et al. (2013) by using the optical properties of gold nanoparticles. For synthesis of gold nanoparticles (AuNPs), they adopted a simple, one pot, eco-friendly rout using guar gum (GG) as reducing agent. The sensing of ammonia solution was conducted by optical instruments. For sensing ammonia, core–shell-structured GG/AuNPs were mixed with different concentration NH_3 (1–2000 ppb) and surface plasmon resonance band (SPR) of AuNPs was monitored. No shifting of SPR band was noticed as the concentration of ammonia was increased but the intensity of 539 nm peak decreased and at the same time a new peak at 408 nm appeared. Herein, most probably, Au^{3+} or Au^{+} formed coordination complex with NH_3 and generate complex compound such as $[Au(NH_3)_2]^{3+}$ and $[Au(NH_3)_2]^{+}$. Lowest detection limit for ammonia sensing was found to be 1 ppb. They also observed that above 1000 ppb the A_{539}/A_{408} absorbance ratio remained constant. To check the selectivity of this nanocomposite, various interferents like methanol, ethanol were added during ammonia sensing and no changes in peak were found, suggesting good selectivity of AuNPs.

Another hazardous pollutant of the environment is nitrobenzene which causes methemoglobinemia. Emmanuel et al. (2014) established gold nanoparticles-based sensor for the detection of nitrobenzene (NB). Gold nanoparticles were synthesized using *Acacia nilotica* twig bark extract at room temperature. Different pulse voltammetry (DPV) was used for the sensor study by using glassy carbon electrode-modified AuNPs. As compared to unmodified electrode, AuNPs-modified electrode displayed significant result for the detection of nitrobenzene. Cyclic voltammetry (CV) was performed in presence of 300 μM nitrobenzene in buffer at a scan rate of 50 mV s^{-1} on both unmodified and AuNPs-modified electrode. No reduction peak response was observed in absence of NB on AuNPs-modified electrode. However, a quick irreversible peak was observed at −0.647 V in presence of 300 μM nitrobenzene, which is attributed to the reduction of nitrobenzene to phenylhydroxylamine. Here four electrons and protons are involved in the process. On the other hand, when scanning is reversed an oxidation peak of weak strength was appeared at 0.274 V. This signal indicates the oxidation of phenylhydroxylamine to nitrobenzene. They also found that the modified electrode showed three times improved current response with −0.08 V negative shifts for nitrobenzene when compared to unmodified GCE. The results suggest that modified AuNPs electrode is more efficient for the detection and estimation of nitrobenzene. The selectivity of the modified electrode in presence of phenol derivative, aromatic nitro compound, and inorganic metal ion by DPV study indicates that metal ion and biologically active compound have no effects on the reduction of NB, whereas a small effect was found in case of phenolic compound.

2.5 Pharmacological Applications

Green synthesized nanoparticles have also been explored as sensor in medical research. Recently, gelatine-stabilized gold nanoparticles have been generated for the detection of cancer cells (Zhang et al. 2009). Herein, green synthesized gold nanoparticles (AuNPs) were conjugated with single-wall carbon nanotubes for the immobilization and sensing of HL-60 cells. The AuNPs-carbon nanotube composites were found to be efficient for the immobilization and sensing of HL-60 cells at electrode. Moreover, the new composite could facilitate the uptake of anticancer drug, adriamycin inside the cells, which could induce the death of leukemia cells. The results indicate that the nanocomposite could be used in cancer diagnosis.

3 Silver Nanoparticles as Sensor

3.1 Detection of Heavy Metals

Currently, silver nanoparticles (AgNPs) have achieved incredible popularity in the world in the field of sensors because of its exceptional optical, electronic, and chemical properties (Schultz et al. 2000). Optical properties of AgNPs have been exploited for the detection of metal ions. Tagad et al. (2017) demonstrated the potential application of AgNPs synthesized by powder extract of panax ginseng for the detection of Hg^{2+}. In this work, detection was performed by obtaining the absorption spectrum of the compound as a function of metal ions concentration, which resulted in the decrease in absorption of peak intensity along with slight blue shift. The AgNPs solution became colorless upon the addition of Hg^{2+} due to formation of Ag–Hg amalgam. Good selectivity was observed even in the presence of heavy metals.

Ravi et al. (2013) developed another method for the production of silver nanoparticles which showed promising result for the detection of Hg^{2+} in a wide pH range. In this work, citrus fruit extracts (lemon, *Citrus limon*) and sweet orange (*Citrus limetta*) have been used for the synthesis of AgNPs. Very recently, we have observed that green tea metabolite, epigallocatechin gallate generated AgNPs also can selectively detect Hg^{2+} in presence of various metal ions (Unpublished result).

Another toxic metal Cu^{2+} can be detected by silver nanoparticles. Basiri et al. have shown that *Cucumis melo* juice-mediated synthesis of AgNPs (R/AgNPs) is potential candidates for the detection of Cu^{2+} ions. The literature reveals that *Cucumis melo* contains polyphenols which can cause reducing the ionic silvers as well as stabilizing of the silver nanoparticles (Prakash and Prakash 2011). Presence of Cu^{2+} and thiosulfate can lead to size reduction of R/AgNPs and a significant color change from light yellow to colorless because thiosulfate ions immediately can interact with R/AgNPs through S–Ag bonding and form $Ag(S_2O_3)^{3-}$ complexes

in the presence of O_2, which results in partial dissolution of R/AgNPs (Chaiyo et al. 2015). R/AgNPs-based sensor offers a remarkable detection limit of 1.12 nM.

3.2 Detection of Hazardous Chemicals

The absorption properties of AgNPs can be used for the detection of hazardous chemicals such as ammonia, hydrogen peroxide, nitrite. Pandey et al. (2012) developed biopolymer-AgNPs nanocomposites for the detection of ammonia. The sensing study of ammonia solution was conducted by using localized SPR (LSPR) of silver nanoparticles. The study indicates that increase in concentration of ammonia (1–100 ppm), the LSPR peak at 440 nm decreased and at the same time new peak at 413 nm enhanced, which can be explained by the interparticle distance between the particles and polarity of the surrounding medium. Concentration of ammonia can be determined by considering the absorbance ration Abs_{413}/Abs_{440} as a function of ammonia concentration. It was observed that beyond 50 ppm the ratio remains constant, suggesting the sensitivity of the current optical sensor.

In order to address the same issue, Dubas and Pimpan (2008) have demonstrated another approach for the synthesis of AgNPs, where UV radiation has been used in presence of poly (methacrylacid) (PMA). Interestingly, generated AgNPs exhibited unusual purple color instead of traditional yellow or brown color. The absorbance of nanoparticles solution showed strong shift upon addition of ammonia and the color of the solution turned from purple to yellow. The results support the hypothesis of using AgNPs as sensor for ammonia.

To detect hazardous chemical hydrogen peroxide, AgNPs-based sensor has been developed by Liu et al. (2013a) where they have demonstrated that *Bacillus subtilis* synthesized AgNPs can be used for the detection of hydrogen peroxide. The electrochemical properties of the resultant AgNPs as sensor revealed that it showed excellent catalytic activity in the reduction of H_2O_2. The activity was found to be in the wide range from 0.05 to 120 mM with a response limit of 8 μM. AgNPs-based sensor also showed good selectivity in determining the concentration of H_2O_2 in the presence of other bio/organic molecules including glucose, acetaminophen, ascorbic acid, and uric acid. Inspiring by this work, later Subramanian et al. demonstrated that cellulose-coated AgNPs can be used for the detection of hydrogen peroxide (Subramanian et al. 2017).

In order to detect nitrite ion (NO_2^-), Ramachandran et al. (2016) have reported biosynthesized silver nanoparticles using piper betel leaves. The detection of nitrite by AgNPs was performed by electrochemical studies using electrodes GCE and Ag/GCE with or without nitrite ions. No significant electrochemical response was noticed in the absence of NO_2^- ions at bare GCE; however, Ag/GCE showed a prominent redox peak at +0.32 and −0.16 v (vs. Ag/AgCl), which can be attributed to the oxidation process of silver to silver ion and reduction process of silver ion to silver, respectively. Naked GCE did not respond to NO_2^- ion due to its inactive nature. The possible mechanism is depicted in Fig. 3.

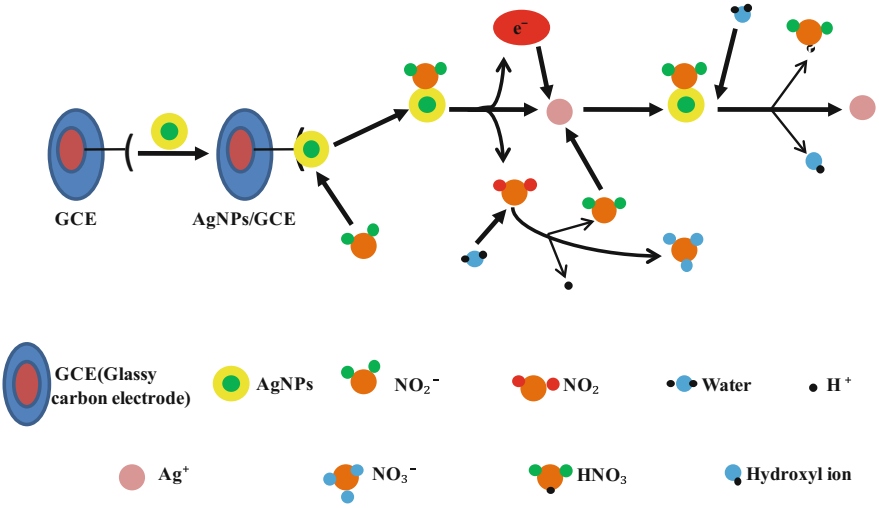

Fig. 3 Schematic illustration of involved mechanism in the electroxidation of NO_2^- at Ag/GCE

3.3 *Detection of Small Molecules*

Development of AuNPs-based sensor for the detection of cysteine is already described in the previous section. Borase et al. (2015a) demonstrated a new green synthetic route for the synthesis of silver nanoparticles using leaf extract of *Calotropis procera* and generated AgNPs were explored for the detection and estimation of cysteine. The as-synthesized silver nanoparticles showed surface plasmon band at 421 nm and upon the addition of cysteine the yellow color AgNPs turned into pink and simultaneously the intensity of band decreased significantly. This color change was due to the aggregation of AgNPs caused by strong interaction between –SH group of cysteine and surface of AgNPs and the change can be visualized by naked eye. Selectivity of AgNPs toward cysteine was evaluated in the presence of other amino acids at 10 times more concentration; however, no other amino acid except cysteine showed any shifting of absorbance peak, indicating the high selectivity of AgNPs for the detection of cysteine.

Melamine (2, 4, 6-triamino-1, 3, 5-triazine) is a white crystalline powder containing great amount of nitrogen (66%) and inexpensive. Melamine is illegally contaminated in food products for presenting higher protein content; however, it has been analyzed that this is an in effective non-protein nitrogen source. Thus, detection/determination of melamine is important to maintain the limit in food products including infant formula. Visual recognition of melamine in raw milk using silver nanoparticles was reported by Borase et al. Synthesis of silver nanoparticles (AgNPs) was performed by using leaves extract of *Jatropha gossypifolia* and generated AgNPs revealed characteristic SPR peak at 419 nm. Previously, for melamine detection AgNPs were made by complicated synthetic

strategy including reduction and functionalization with various chemicals such as dopamine, 1-(2-mercaptoethyl)-1,3,5-triazinane-2,4,6-trione (MTT) (Ai et al. 2009), sodium borohydride (Ping et al. 2012), and *p*-nitroaniline. However, AgNPs synthesized by green route remained unexplored for melamine detection. SPR band of AgNPs at 419 nm decreased gradually upon the addition of melamine and red shifting of the peak was observed along with appearance of a fresh peak at 500 nm (Borase et al. 2015b). The detection limit was found to be 252 ppb. The concentration of melamine was determined by change in absorption ratio (A_{500}/A_{419}) of AgNPs.

4 Carbon Dots as Sensor

4.1 Detection of Heavy Metals

Very recently, emergence of fluorescent carbon dots (CD) has shown incredible impact in the field of sensing. Carbon dots can be used as sensor for the detection of toxic metal such as Hg^{2+}. CDs synthesized by low-cost pomelo peel as carbon source showed potential application in the detection of Hg^{2+} ions (Lu et al. 2012). The detection can be monitored by change in PL intensity. The PL intensity of fluorescent carbon nanoparticle (CDs) in presence of Hg^{2+} ions decreases and shows a quenching of fluorescence of CDs. This is attributed to the fact that Hg^{2+} can quench the fluorescence of CDs by energy transfer. For selective and sensitivity study the PL intensity of CPs at 444 nm decreases with the addition of Hg^{2+} ions concentration at the level in nanoscale where the detection is found to be 0.23 nM. Selectivity study in presence of other metal ions indicates that Hg^{2+} ion has stronger affinity to the carboxylic acid groups in surface of CDs than other metal ions. The CDs were successfully applied for the analysis of lake water sample.

Hg^{2+} detection is also reported by Wang et al., where N-, S-, P-co-doped carbon dots (N/S/P-CDs) have been synthesized using cucumber juice by hydrothermal methods (Wang et al. 2014). The UV–Vis absorption spectra and fluorescence spectra of N/S/P-CDs exhibited red shift with increasing temperature. Different colors from these samples under UV radiation and daylight at different temperature were noticed, indicating different size, shape, and defects of these CDs, which is also consistent with chemically synthesized CDs. Furthermore, it did not lose any fluorescent intensity under UV irradiation for 3 h, suggesting their photostability. Their fluorescence intensity remained unchanged in presence of NaCl and different pH values, indicating its stability in presence of high concentration of ions in the solution. Due to the presence of oxygen on the surface of N/S/P-CDs, it can interact with metal ions. Based on this hypothesis, screening of different metal ions was performed, where Hg^{2+} showed good selectivity in binding, indicating the efficiency of sensor probe toward the detection of Hg^{2+}. It showed good result during the analysis of river samples, suggesting the potentiality as sensor.

Another metal ion Fe^{3+} which is found as contamination in water can be detected by CDs. CDs synthesized by onion waste show promising result for the detection of Fe^{3+} ions in the presence of other metal ions (Bandi et al. 2016). A steady increase in the excitation wavelength from 320 to 540 nm and a red shift in the emission peak from 426 to 570 nm were observed which is used for the selective and sensitive detection of Fe^{3+}. Among the screened, the metal ions only Fe^{2+}, Cu^{2+}, Cr^{3+}, Hg^{2}, Pb^{2+}, Cd^{2+}, Ni^{2+} showed little decrease in fluorescence, which is attributed to the non-specific interaction of these metal ions to the surface of CDs. However, Fe^{3+} displayed a significant decrease in the fluorescence intensity of CDs, which is because of special coordination of Fe^{3+} with the phenolic OH or the amine group present on the surface of CDs. This sensor showed promising result in the detection of Fe^{3+} ions in real water.

Another CD synthesized by sweet potato also shows promising result in the detection of Fe^{3+} ions. These fluorescence carbon dots were made by using sweet potato and normal hydrothermal method (Shen et al. 2017). In this work, the maximum emission peak found from these CDs was 442 nm when it is excited at 360 nm. Like other CDs herein the PL emission peak of CDs was shifted from 406 to 486 nm with the excitation variation from 300 to 410 nm. It was found that Fe^{3+} had significant fluorescence quenching effect on CDs in comparison to other metal ions. These fluorescence quenching is attributed to the charge transfer and restrained excitation. The possible mechanism is that the Fe^{3+} ion specifically coordinate with surface of CDs rather than other ions which contains hydroxyl group leading to the electronic structural change. Therefore, actually the properties of CDs are depending upon the chemical structure which assisted by the main functional group on the CDs surface and there interaction with meal ions. The limit of detection was evaluated at 0.32 μM based on a signal to noise ratio 3, indicating good sensitivity of CD. It is noteworthy to mention that CDs were further explored for cell imaging studies. Interestingly, CD treated cells emit fluorescence under UV light, suggesting the suitability of CDs as probes for cell imaging.

Detection of Fe^{3+} can also be achieved by another method where dopamine and trypsin have been used as precursors for the synthesis of carbon dots (CDs) (Feng et al. 2016). The inner filter effect (IFE) and quenching mechanism have been explored for the detection of Fe^{3+} ion. During the addition of Fe^{3+} ion, it was observed that the fluorescence of CNPs quenched with the increase in concentration of Fe^{3+} ion. A noteworthy linear relationship exists between the quenching efficiency (F_0/F) and the Fe^{3+} concentration in the range of 0.1–500 μM. The detection limit is 30 nM which is remarkable compared to other existing methods. The results indicate that the fluorescence quenching may be due to the inner filter effect (IFE) between CNPs and Fe^{3+} ions. In the presence of other interfering metal ions and amino acids, no obvious fluorescence quenching was noticed, suggesting the selectivity of the CD-based sensor toward Fe^{3+} ions. This sensor successfully detects Fe^{3+} ion in urine and serum samples, confirming its reliability and accuracy for the detection of Fe^{3+} ion in biological samples.

Vikneswaran et al. (2014) have developed another green rout for the synthesis of fluorescent carbon dots using banana peels as a carbon source for the detection of

Fe^{3+} ion. These C-dots also show an intense PL emission peak centered at 462 nm when excited at 360 nm, indicating the fluorescent nature of CDs which exhibit a bright blue fluorescence under UV irradiation. Intensity change in photoluminescence (PL) in presence or absence of other metal ions indicates that only Fe^{3+} induced a noticeable and significant decrement of intensity, whereas other metal ion shows no or slightly changes in PL intensities, indicating the selectivity of the detection of Fe^{3+} ion. The tentative reason behind these quenching of fluorescence could be the affinities between the surfaces of the C-dots and Fe^{3+} ion.

Potato derived CDs also show the efficiency to detect Fe^{3+}. A simple water soluble, well dispersed, green rout has been developed for the synthesis of fluorescence carbon dots using potatoes by hydrothermal process and utilized as a sensing probe for the selective and sensitive detection of Fe^{3+} ion (Xu et al. 2014). Herein, CDs exhibit bright blue fluorescence under UV lamp (365 nm). Fluorescence generated by CDs displayed a high stability under high ionic strength condition which showed no changes in fluorescence even in higher concentration of NaCl. The change in photoluminescence (PL) intensity in presence of various metal ions including Fe^{3+} ion reveals that only Fe^{3+} can reduce PL intensity at 405 nm significantly, offering CDs as sensing device for the detection of Fe^{3+} ion. The possible mechanism could be the affinity of Fe^{3+} ion toward the CDs. Revival of spiked water samples ranges from 93.7 to 101.5% with negligible standard deviation authenticate the accuracy of the method.

Further, N-doped carbon dots (N-CQD) were developed by Lv et al. (2017) for the detection of Fe^{3+} in lake water. The quenching of fluorescence of as-prepared N-CQD was observed upon addition of Fe^{3+} ion due to aggregation (Fig. 4). High affinity of Fe^{3+} ions for O and N which are present on N-CQD surface assists the aggregation by forming N-CQD-Fe^{3+} chelates, and thus, fluorescence quenching occurs. The mechanism of fluorescence quenching of carbon dots by Fe^{3+} ions is proposed in the literature. Mei et al. (2012) describe that coordination of Fe^{3+} with the phenolic hydroxyl groups (−OH) on N-CQD surface occurs, which leads to a stable Fe(III)-complex formation. Then, the excited electrons of the N-CQDs are shifted to the 3d orbitals of Fe^{3+}, thus assisting the non-radiative electron–hole recombination and significant fluorescence quenching occurs, which is depicted in Eq. (6).

$$6\mathrm{CQD{-}OH} + \mathrm{Fe}^{3+} \rightarrow \left[\mathrm{Fe(OCQD)}_6\right]^{3+} + 6\mathrm{H}^{+} \tag{6}$$

Copper ion (Cu^{2+}) is one of the abundant crucial transition metal ion in human body except zinc and iron ions and also plays a very imperative role in living organism (Wu et al. 2009). However, Cu^{2+} is a toxic metal and a big threat to environmental pollution. In order to control Cu^{2+} pollution and Cu^{2+}-induced toxic effect, there is an enormous demand for green, reliable and sensitive approach for Cu^{2+} detection. A green method has been reported for the synthesis of fluorescence carbon quantum dots (CQDs) using bamboo leaves as carbon source and branched polyethylenimine (BPEI) as coating agent (Liu et al. 2014). The coating of PEI

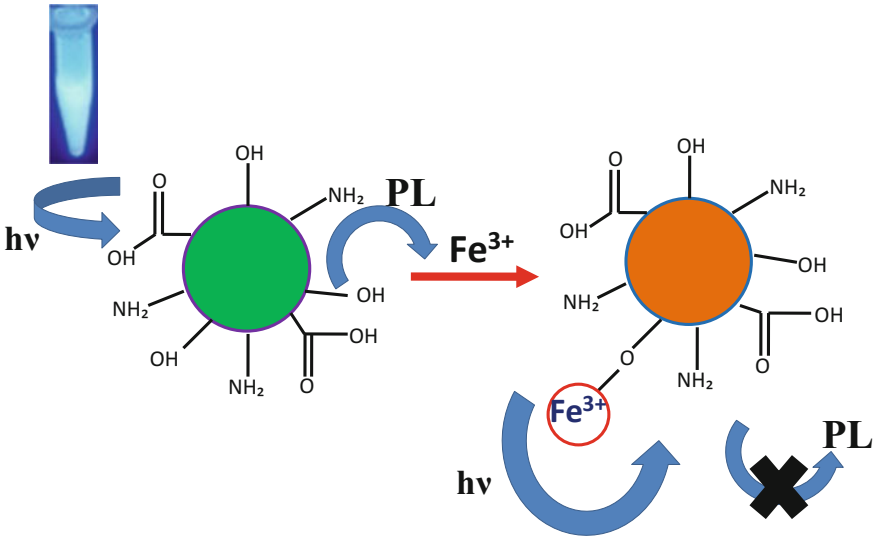

Fig. 4 Schematic illustration of the fluorescence quenching process of N-CQDs in presence of Fe^{3+} ions

leads to the increase in 10 nm red shift of UV–Vis absorption due to the increased size of CQDs. PL emission of CQDs and BPEI-CQDs changes from 440 to 540 nm upon excitation from 365 to 525 nm, which is characteristic of carbon dots. The pH study reveals that under acidic condition (pH $\leq$ 3.0), due to protonation in PEI, no binding occurs between BPEI-CQD and Cu^{2+}, whereas Cu^{2+} is unstable in alkaline pH (>7.0) due to hydrolysis. Selectivity study indicates that Cu^{2+} alone exhibits strong quenching of BPEI-CQDs fluorescence and other metal ions showed negligible quenching at pH 4. Some metal ions exhibit good quenching at pH 5 and pH 6. The results indicate that the detection of Cu^{2+} is pH dependent. The quenching effect is probably due to inner filter effect (IFE) of cupric amine complexes formed at the surface of CQDs. BPEI-CQDs sensor probe has been applied successfully for the detection of Cu^{2+} in river water and environmental water samples.

Chromium contamination generated by industrial techniques including electroplating, textile dyeing, leather tanning, mining, and wood preserving is very detrimental for human body, particularly $Cr^{6+,}$ which is highly poisonous and carcinogenic in nature among all oxidation states of chromium due to greater oxidation potential, small size, and great mobility (Zhitkovich 2011). Sensitive and selective detection of Cr^{6+} in aqueous system is essential for both human health concern and ecological point of view. Many techniques have been developed for the detection of Cr^{6+} such as inductively coupled plasma mass spectrometry (ICP-MS), surface-enhanced Raman scattering (SERS), X-ray absorption spectroscopy, atomic absorption spectrometry (AAS), electroanlytical, and colorimetric detection. However, recently, Tyagi et al. (2016) have reported a simple water soluble green synthesis of fluorescent carbon quantum dots (CQDs) using waste lemon peels by

normal hydrothermal process which have the ability to selectively detect the toxic Cr^{6+} ion. Generated CQDs showed a blue intense luminescence under UV light irradiation. The fluorescence of CQDs is obtained at 441 nm as emission peak at a excitation of 360 nm which on addition of Cr^{6+} metal ion the intensity decreases. The fluorescence quenching of CQDs exhibits a linear relationship with Cr^{6+} ion. Generated fluorescent probe displays a very low detection limit of 73 nM and an excellent selectivity in presence of various metal ions. According to the World Health Organization (WHO), Cr^{6+} concentrations less than 900 nM are tolerable in drinking water. Therefore, this fluorescent-based method is responsive enough to measure Cr^{6+} amount in drinking water. Further, they have demonstrated that immobilization of CQDs on TiO_2 nanofibers can produce 2.5 times more efficient system compared to TiO_2 alone for the photocatalytic degradation of methylene blue (MB) which is a well-known pollutant in the environment. The possible mechanism of MB degradation is depicted in Fig. 5.

4.2 *Detection of Fluorides*

The C-dot-based sensors are described so far to detect the cations like Hg^{2+}, Pb^{2+}, Be^{2+}, Ag^{+}; however, few reports are available for anion detection. Among anions F^{-} ions are considered as one of the key water pollutants. Though F^{-} is essential for our biological system but excess ingestion can damage different organs in our body. According to World Health Organization (WHO), excess F^{-} ingestion can permanently destroy bones, teeth, and kidney. Thus, selective detection of fluoride ion in water is tremendously important and required. To address this issue, an easy, water soluble, cost-effective, environmentally benign synthesis of fluorescence carbon dots (CDs) using easily available starch (*Sabudana* (*Tapioca Sago*)) has been reported recently (Basu et al. 2015). Generated CDs were explored as effective chemo-sensor for the detection of fluoride ion based on photoluminescence (PL) intensity changes. The sensor probe acts like on–off–on mechanism where upon the initial addition of

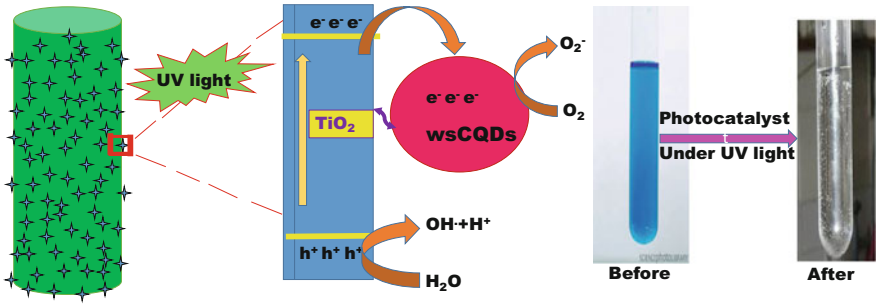

Fig. 5 Schematic diagrams for the photocatalytic degradation of methylene blue on carbon dots nanocomposite under UV light irradiation and images of the dye before and after degradation

Fe^{3+} ion on CDs fluorescence quenching occurs through charge transfer process as Fe^{3+} ion attached to the surface of CDs. Later on the addition of F^- leads to removal of Fe^{3+} ion from the CDs surface and also restored the PL intensity. In sensing study, ferric chloride ($FeCl_3$), nickel nitrate ($Ni(NO_3)_2$), cobalt nitrate ($Co(NO_3)_2$), cadmium nitrate ($Cd(NO_3)_2$), cupric chloride ($CuCl_2$), and manganese chloride($MnCl_2$) have been used as the sources of Fe^{3+}, Ni^{2+}, Co^{2+}, Cd^{2+}, Cu^{2+}, and Mn^{2+}, respectively. Among these metal ions, Cu^{2+} and Fe^{3+} ion exhibit good PL quenching. The effective quenching of PL intensity of CDs is observed due to the charge transfer complex formation of metal ions to the –COOH group present on the surface of CDs. The complex formation based on HSAB (hard soft acid base) principle, the better charge transfer complex formation leads to higher decrease of PL intensity. As Fe^{3+} is a hard acid it forms better stable complex rather than other borderline metal ions. To evaluate the selectivity of the sensor, a comparative study using other anions with F^- was performed and found that F^- displayed a good selectivity for the recovery of fluorescence of QDs. To remove Fe^{3+} from the surface of CDs, the final product should be very much stable in aqueous solution. For instance, the product formed herein is FeF_3 which is very stable in water because the lattice energy (5870 kJ/mol) of FeF_3 is higher than hydration energy (4953 kJ/mol).

4.3 Detection of Small Molecule

Apart from the detection of harmful metal ions and anions, carbon dots have also been explored as sensor for organic small molecules and drugs. Feng et al. (2015) have generated fluorescence carbon dots (CDs) by using rose flower as source of carbon for the first time. The CDs were explored for the detection of tetracycline (TC) which is an effective antibiotic and used in therapy during bacterial infection. However, irrational use of TC may lead to risk to human body. In this work, the fluorescence carbon dots show maximum excitation and emission spectra at 390 and 435 nm, respectively. Based on the strong fluorescence properties it was hypothesized that they can be used as fluorescent probe. Interestingly, 50% decrease in fluorescent intensity was observed at 435 nm upon the addition of tetracycline. When similar experiment was performed with other antibiotics no change of fluorescent intensity was observed, indicating the selectivity of CDs toward the detection of TC. The plausible mechanism may be the interaction between surface group of CDs with TC, which leads to the formation of energy consumed by forming new bonds. This facilitates the quenching of fluorescence of CDs. The CD-based sensor was successfully applied to detect TC in urine sample.

Another organic molecule, glyphosate and herbicide, used for weed control is harmful to human body when it presents at high level in the agriculture products (Wei et al. 2013). CDs developed from wool show good result in the detection of glyphosate (Wang et al. 2016). Glyphosate detection has been demonstrated by the recovery of fluorescence of CDs, which was quenched by the addition of

cysteamine stabilized AgNPs. The intensity of fluorescence of CDs was efficiently quenched in presence of AgNPs. The possible mechanism behind this quenching involves the overlapping of CDs fluorescence spectra with AgNPs which exhibit a broad absorption spectrum in the range 300–600 nm where a strong absorption peak at 402 nm is observed. Fluorescence resonance energy transfer FRET and inner filter effect IFE may take place between AgNPs and CDs in the current system. However to ascribe the quenching mechanism, the UV–Vis spectra of AgNPs has been recorded in presence and absence of carbon dots and no changes in absorption spectrum of AgNPs was found. Therefore, no complex was formed between AgNPs and CDs and thus eliminating the possibility of FRET. Zeta potential study indicates that there is an electrostatic repulsion between AgNPs and CDs as both are positively charged. Therefore due to the distance between these two, chances of FRET are nil. This data suggests that fluorescence of CDs can be recovered in presence of AgNPs and glyphosate which leads to a detection of glyphosate. It was found that there was no fluorescence emission spectral changes of CDs occurred in presence or absence of glyphosate as it did not have any interaction with CDs. The fluorescence of CDs was found to be quenched in presence of AgNPs solution due to IFE effect. However, in presence of small amount of glyphosate a little amount of fluorescence can be recovered. On the contrary, at high concentration of glyphosate, maximum fluorescence can be recovered and the shape of fluorescence emission spectra does not show any changes, which indicates that recovery emission comes from CDs not from other emission centers. Mechanistic study reveals that with increase in the concentration of glyphosate there is a decrease in the 402 nm peak of AgNPs, which is due to aggregation of AgNPs. The reason behind this aggregation is that as the surface of AgNPs is positively charged with $-NH_3^+$ group, absorption of glyphosate occurs on the surface of the AgNPs, leading to an electrostatic interaction between AgNPs and glyphosate. Newly generated CDs show good selectivity toward glyphosate even in the presence of other pesticides. It exhibits perfect result in cereal samples.

Further, the fluorescence property was explored for the detection of methylene blue (MB) which is famous to have carcinogenic, mutagenic, and high coloring effect to the ecosystem when it is released as waste in the surroundings (Tan et al. 2008). Furthermore, methylene blue which is a cationic lethal dye can cause serious problems including mutations, skin disease, cancer, and eye pain in human and animals, thus, it is necessary to detect MB in wastewater for reuse (Liu et al. 2013b). A simple green rout synthesis of fluorescence carbon dots has been reported using lychee seeds, which shows promising result in the detection of methylene blue (MB) (Xue et al. 2015). The CDs exhibit a strong blue fluorescence when irradiated by UV light at 365 nm. Herein, synthesized CDs produce transparent solution, indicating the exceptional aqueous dispersibility of the carbon dots due to the presence of large number of hydrophilic amino groups on the surface. The fluorescence emission peak was observed at 440 nm when excited at 365 nm which showed good photostability by storing it for more than 60 days. The fluorescence quenching mechanism was chosen for the sensing parameter for MB, the intensity of CDs fluorescence decreased by 80% within 5 min at the concentration of

50 μM MB. Furthermore, if the absorbance spectra of MB is analyzed, there is one peak at 663 ascribed as monomer and another shoulder peak at 615 nm attributed as dimer. Spectra of the dye shifted to 658 and 608 nm, respectively, after the addition of MB in CD solution and the same time intensity decreased. This suggests that the MB molecules adsorb on the surface of CDs. Not only that, the absorbance ratio of dimer and monomer was increased in MB–CD mixture, suggesting some dimers formation in presence of CDs, which is consistent with other previous reports. The detection limit was estimated to be 50 nM which is much more lower than previous reports. CDs show good selectivity toward MB in presence of metal ions and some organic dyes including methyl orange and thioflavin-T. Other oxidation products of methylene blue such as azure A, azure B, thionine, thionol, and thionoline do not affect the fluorescence of CDs, eliminating the possibility of their role in fluorescence quenching. When CDs are incubated in cells, it shows significant blue emission under the 405 nm excitation, suggesting the capability of cell penetration of CDs and label cell membrane and cytoplasm. This result reveals that new bioimaging probe based on CDs is efficient to replace the traditional probe.

Tartrazine is the extensively used artificial food colorants which are generally found in some food products including candies, beverages, bakery products, and dairy products (Gan et al. 2012). However, few reports reveal that tartrazine may cause terrible health effects including changes in hepatic and renal parameter, reproductive toxicity, also neurobehavioral poisonousness with excessive uptaking (Amin et al. 2010). To address this issue, Xu et al. (2015) have developed a fluorescence carbon dots utilizing aloe as carbon source and generated carbon dots are useful as a sensor probe for the detection of tartrazine colorant. These C-dots showed an emission peak from 443 to 545 nm with increasing exciting wavelength. The C-dots upon addition of tartrazine exhibit a decrease in fluorescence which is observed at 503 nm when excited at 441 nm. The intensity UV–Vis absorption spectra at 280 nm of CDs increase with a blue shift upon increasing the concentration of tartrazine. The pH study indicates that upon elevation of pH from 4.0 to 6.0, it leads to the enhancement of fluorescence quenching efficiency whereas further increase in pH from 6 to 7.5 directs to a steady decrease, suggesting that the detection of tartrazine is pH sensitive. The detection limit of this sensor is found to be 73 nM. The selectivity of the fluorescence quenching efficiency in presence of metal ions and other organic molecules such as glutamic acid, glutathione (GSH), citric acid, phenylalanine, starch, tartaric acid, vitamin C, glucose, lactose, sunset yellow, erioglaucine disodium salt indicates that tetrazine causes significant quenching compared to other interferents. This approach is further successfully implemented for the trace-level detection of tartrazine in food samples.

5 Conclusion

The present chapter has summarized simple, rapid, and easy-to-use colorimetric assays for the detection of toxic chemicals in aquatic system, environment, and food samples. The exceptional optical properties of nanoparticles have laid the way for the advancement of optical sensor and imaging techniques. All sensing methods reported herein use environmentally friendly approach and provide cost-effective way for detecting toxic materials. Described sensor systems in this chapter generated by "green technology" have enriched this field in two directions (1) easy way of synthesis of efficient nanoparticles for sensor study, (2) based on the molecule present on the surface of nanoparticles, electrochemical sensor, or chemical sensor can be constructed. The assays reported herein may be used in both quantitative as well as qualitative detection of toxic chemicals in the target sample even with the detection limit of nM concentration. Even though the nanoparticles are showing promising results in the application as sensor, they are still in an early stage of development. The surface chemistry of nanoparticles including the capping molecule must be deeply understood to study the interactions with other metal ions or organic small molecules.

Acknowledgements The authors would like to acknowledge Department of Science & Technology, Department of Biotechnology, and Board of Research in Nuclear Sciences, Government of India, for financial support.

References

Ahmed S, Kintanar A, Henderson E (1994) Human telomeric C–strand tetraplexes. Nat Str Mol Biol 1(2):83–88

Ai K, Liu Y, Lu L (2009) Hydrogen-bonding recognition-induced color change of gold nanoparticles for visual detection of melamine in raw milk and infant formula. J Am Chem Soc 131(27):9496–9497

Althaus K, Hron G, Strobel U, Abbate R, Rogolino A, Davidson S, Greinacher A, Backoul T (2013) Evaluation of automated immunoassays in the diagnosis of heparin induced thrombocytopenia. Thromb Res 131:85–90

Amin KA, Hameid HA, Abd Elsttar AH (2010) Effect of food azo dyes tartrazine and carmoisine on biochemical parameters related to renal, hepatic function and oxidative stress biomarkers in young male rats. Food Chem Toxicol 48:2994–2999

Annadhasan M, Muthukumarasamyvel T, Sankar Babu VR, Rajendiran N (2014) Green synthesized silver and gold nanoparticles for colorimetric detection of Hg^{2+}, Pb^{2+}, and Mn^{2+} in aqueous medium. ACS Sus Chem Eng 2(4):887–896

Bagci PO, Wang YC, Gunasekaran S (2015) A simple and green route for room temperature synthesis of gold nanoparticles and selective colorimetric detection of cysteine. J Food Sci 80 (9):2071–2078

Bandi R, Gangapuram BR, Dadigala R, Eslavath R, Singh SS, Guttena V (2016) Facile and green synthesis of fluorescent carbon dots from onion waste and their potential applications as sensor and multicolour imaging agents. RSC Adv 6(34):28633–28639

Barman G, Maiti S, Laha JK (2013) Bio-fabrication of gold nanoparticles using aqueous extract of red tomato and its use as a colorimetric sensor. Nanoscale Res Lett 8(1):181

Basu A, Suryawanshi A, Kumawat B, Dandia A, Guin D, Ogale SB (2015) Starch (Tapioca) to carbon dots: an efficient green approach to an on–off–on photoluminescence probe for fluoride ion sensing. Analyst 140(6):1837–1841

Bianco A, Kostarelos K, Prato M (2005) Applications of carbon nanotubes in drug delivery. Curr Opin Chem Biol 9(6):674–679

Borase HP, Patil CD, Salunkhe RB, Suryawanshi RK, Kim BS, Bapat VA, Patil SV (2015a) Bio-functionalized silver nanoparticles: A novel colorimetric probe for cysteine detection. Appl Biochem and Biotech 175(7):3479–3493

Borase HP, Patil CD, Salunkhe RB, Suryawanshi RK, Salunke BK, Patil SV (2015b) Biofunctionalized silver nanoparticles as a novel colorimetric probe for melamine detection in raw milk. Biotec Appl Biochem 62(5):652–662

Chaiyo S, Siangproh W, Apilux A, Chailapakul O (2015) Highly selective and sensitive paper-based colorimetric sensor using thiosulfate catalytic etching of silver nanoplates for trace determination of copper ions. Anal Chim Acta 866:75–83

Chen L, Lou T, Yu C, Kang Q, Chen L (2011) N-1-2-mercaptoethyl thymine modification of gold nanoparticles: a highly selective and sensitive colorimetric chemosensor for Hg^{2+}. Analyst 136 (22):4770–4773

Chen Z, Wang Z, Chen X, Xu H, Liu J (2013) Chitosan-capped gold nanoparticles for selective and colorimetric sensing of heparin. J Nano Res 15(9):1930

Choudhary R, Patra S, Madhuri R, Sharma PK (2016) Equipment-free single-step rapid on-site kit for visual detection of lead ions in soil water bacteria live cells and solid fruits using fluorescent cube-shaped nitrogen doped carbon dots. ACS Sust Chem Eng 4(10):5606–5617

Connon RE, Geist J, Werner I (2012) Effect-based tools for monitoring and predicting the ecotoxicological effects of chemicals in the aquatic environment. Sensors 12(9):12741–12771

Daniel MC, Astruc D (2003) Gold nanoparticles: assembly, supramolecular chemistry, quantum size-related properties, applications toward biology, catalysis and nanotechnology. Chem Rev 104:293–346

Dubas ST, Pimpan V (2008) Green synthesis of silver nanoparticles for ammonia sensing. Talanta76 (1):29–33

Emmanuel R, Karuppiah C, Chen SM, Palanisamy S, Padmavathy S, Prakash P (2014) Green synthesis of gold nanoparticles for trace level detection of a hazardous pollutant (nitrobenzene) causing Methemoglobin anemia. J Hazard Mater 279:117–124

Feng Y, Zhong D, Miao H, Yang X (2015) Carbon dots derived from rose flowers for tetracycline sensing. Talanta 140:128–133

Feng J, Chen Y, Han Y, Liu J, Ren C, Chen X (2016) Fluorescent carbon nanoparticles: a low-temperature trypsin-assisted preparation and Fe^{3+} sensing. Anal Chim Acta 926:107–117

Gan T, Sun JY, Cao SQ, Gao FX, Zhang YX, Yang YQ (2012) One-step electrochemical approach for the preparation of graphene wrapped-phosphotungstic acid hybrid and its application for simultaneous determination of sunset yellow and tartrazine. Electrochim Acta 74:151–157

Ghodake G, Vassiliadis VS, Choi JH, Jang J, Lee DS (2015) Facile synthesis of gold nanoparticles by amino acid asparagine: selective sensing of arsenic. J Nanosci Nanotechnol 15(9):7235–7239

Guan J, Wang YC, Gunasekaran S (2015) Using L-arginine functionalized gold nanorods for visible detection of mercury (II) ions. J Food Sci 80(4):828–833

He Y, Wang X, Zhu J, Zhong S, Song G (2012) Ni^{2+}-modified gold nanoclusters for fluorescence turn-on detection of histidine in biological fluids. Analyst 137(17):4005–4009

Karthik R, Govindasamy M, Chen SM, Mani V, Lou BS, Devasenathipathy R, Hou YS Elangovan A (2016a) Green synthesized gold nanoparticles decorated graphene oxide for sensitive determination of chloramphenicol in milk, powdered milk, honey and eye drops. J Coll Int Sci 475:46–56

Karthik R, Chen SM, Elangovan A, Muthukrishnan P, Shanmugam R, Lou BS (2016b) Phyto mediated biogenic synthesis of gold nanoparticles using Cerasus serrulata and its utility in detecting hydrazine, microbial activity and DFT studies. J Colloid Interface Sci 468:163–175

Kumar A, Bhatt M, Vyas G, Bhatt S, Paul P (2017) Sunlight induced preparation of functionalized gold nanoparticles as recyclable colorimetric dual sensor for aluminium and fluoride in water. ACS Appl Mater Int 9(20):17359–17368

Li H, Bian Y (2009) Selective colorimetric sensing of histidine in aqueous solutions using cysteine modified silver nanoparticles in the presence of Hg^{2+}. Nanotech 20(14):145502

Li W, Feng L, Ren J, Wu L, Qu X (2012) Visual detection of glucose using conformational switch of i-motif DNA and non crosslinking gold nanoparticles. Chem Eur J 18(40):12637–12642

Lin M, Pei H, Yang F, Fan C, Zuo X (2013) Applications of gold nanoparticles in the detection and identification of infectious diseases and biothreats. Adv Mat 25:3490–3496

Lin ZY, Wu YT, Tseng WL (2015) UV-light-induced improvement of fluorescence quantum yield of DNA-templated gold nanoclusters: application to ratiometric fluorescent sensing of nucleic acids. ACS Appl Mater Interfaces 7(42):23708–23716

Liu H, Ye T, Mao C (2007) Fluorescent carbon nanoparticles derived from candle soot. Angew Chem Int Ed 46(34):6473–6475

Liu Y, Deng C, Tang L, Qin A, Hu R, Sun JZ, Tang BZ (2010) Specific detection of D-glucose by a tetra phenylethene-based fluorescent sensor. J Am Chem Soc 133(4):660–663

Liu R, Wei Y, Zheng J, Zhang H, Sheng Q (2013a) A hydrogen peroxide sensor based on silver nanoparticles biosynthesized by *Bacillus subtilis*. Chinese J Chem 31(12):1519–1525

Liu L, Lin Y, Liu Y, Zhu H, He Q (2013b) Removal of methylene blue from aqueous solutions by sewage sludge based granular activated carbon: adsorption equilibrium, kinetics, and thermodynamics. J Chem Eng Data 58(8):2248–2253

Liu Y, Zhao Y, Zhang Y (2014) One-step green synthesized fluorescent carbon nanodots from bamboo leaves for copper (II) ion detection. Sens Actuators B Chem 196:647–652

Lu W, Qin X, Liu S, Chang G, Zhang Y, Luo Y, Asiri AM, Al-Youbi AO, Sun X (2012) Economical, green synthesis of fluorescent carbon nanoparticles and their use as probes for sensitive and selective detection of mercury (II) ions. Anal Chem 84(12):5351–5357

Lv P, Yao Y, Zho H, Zhang J, Pang Z, Ao K, Cai Y, Wei Q (2017) Synthesis of novel nitrogen-doped carbon dots for highly selective detection of iron ion. Nanotech 28(16):165502

Mei Q, Jiang C, Guan G, Zhang K, Liu B, Liu R, Zhang Z (2012) Fluorescent graphene oxide logic gates for discrimination of iron (3+) and iron (2+) in living cells by imaging. Chem Comm 48:7468–7470

Moriarty MM, Koch I, Gordon RA, Reimer KJ (2009) Arsenic speciation of terrestrial invertebrates. Env Sci Technol 43:4818–4823

Münzer Alexandra M, Michael Zachary P, Star A (2013) Carbon nanotubes for the label-free detection of biomarkers. ACS Nano 7(9):7448–7453

Mussa Farkhani S, Valizadeh A (2014) Review: three synthesis methods of CdX quantum dots. IET Nanobiotech 8(2):59–76

Nie Z, Petukhova A, Kumacheva E (2010) Properties and emerging applications of self-assembled structures made from inorganic nanoparticles. Nat Nano 5(1):15–25

Nimbalkar S, Tagad CK, Sabharwal SG, Kumar RA, Gosavi S, Kim T, Zinjarde S, Kulkarni A (2014) Optical detection of melamine in raw milk. Sens Lett 12(11):1633–1636

Pandey S, Goswami GK, Nanda KK (2012) Green synthesis of biopolymer–silver nanoparticle nanocomposite: an optical sensor for ammonia detection. Int J Biol Macromol 51(4):583–589

Pandey S, Goswami GK, Nanda KK (2013) Green synthesis of polysaccharide/gold nanoparticle nanocomposite: an efficient ammonia sensor. Carb Polym 94(1):229–234

Pannopard P, Boonyuen C, Warakulwit C, Hoshikawa Y, Kyotani T, Limtrakul J (2015) Size-tailored synthesis of gold nanoparticles and their facile deposition on AAO-templated carbon nanotubes via electrostatic self-assembly: application to H_2O_2 detection. Carbon 94:836–844

Ping H, Zhang M, Li H, Li S, Chen Q, Sun C, Zhang T (2012) Food Control 23:191–197

Prakash CVS, Prakash I (2011) Bioactive chemical constituents from pomegranate (*Punica granatum*) juice, seed and peel-a review. Int J Res Chem Environ 1:1–18

Ramachandran K, Kalpana D, Sathish kumar Y, Lee YS, Ravichandran K (2016) A facile green synthesis of silver nanoparticles using *Piper betle* biomass and its catalytic activity toward sensitive and selective nitrite detection. J Ind Eng Chem 35:29–35

Ravi SS, Christena LR, SaiSubramanian N, Anthony SP (2013) Green synthesized silver nanoparticles for selective colorimetric sensing of Hg^{2+} in aqueous solution at wide pH range. Analyst 138(15):4347–4370

Ray PC (2010) Size and shape dependent second order nonlinear optical properties of nanomaterials and their application in biological and chemical sensing. Chem Rev 110 (9):5332–5365

Resch-Genger U, Grabolle M, Cavaliere-Jaricot S, Nitschke R, Nann T (2008) Quantum dots versus organic dyes as fluorescent labels. Nat Meth 5(9):763–775

Rex M, Hernandez FE, Campiglia AD (2006) Pushing the limits of mercury sensors with gold nanorods. Anal Chem 78(2):445–451

Schultz S, Smith DR, Mock JJ, Schultz DA (2000) Single-target molecule detection with nonbleaching multicolor optical immunolabels. Proc Natl Acad Sci 97(3):996–1001

Shafer-Peltier KE, Haynes CL, Glucksberg MR, Van Duyne RP (2003) Toward a glucose biosensor based on surface-enhanced Raman scattering. J Am Chem Soc 125(2):588–593

Shahrokhian S (2001) Lead phthalocyanine as a selective carrier for preparation of a cysteine-selective electrode. Anal Chem 73(24):5972–5978

Shen J, Shang S, Chen X, Wang D, Cai Y (2017) Facile synthesis of fluorescence carbon dots from sweet potato for Fe^{3+} sensing and cell imaging. Mater Sci Eng C 76:856–864

Subramanian L, Sabu T, Obey K (2017) Green synthesis of silver nanoparticles using aqueous plant extracts and its application as optical sensor. Int J Biosen Bioelect 2:22

Tagad C, Seo HH, Tongaonkar R, Yu YW, Lee JH, Dingre M, Kulkarni A, Fouad H, Ansari SA, Moh SH (2017) Green synthesis of silver nanoparticles using *Panax ginseng* root extract for the detection of Hg^{2+}. Sens Mat 29(2):205–215

Tan IAW, Ahmad AL, Hameed BH (2008) Adsorption of basic dye using activated carbon prepared from oil palm shell: batch and fixed bed studies. Desalination 225(1–3):13–28

Thirumalraj B, Rajkumar C, Chen SM, Palanisamy S (2017) One-pot green synthesis of graphene nanosheets encapsulated gold nanoparticles for sensitive and selective detection of dopamine. Sci Rep 7:41213

Tyagi A, Tripathi KM, Singh N, Choudhary S, Gupta RK (2016) Green synthesis of carbon quantum dots from lemon peel waste: applications in sensing and photocatalysis. RSC Adv 6 (76):72423–72432

Vikneswaran R, Ramesh S, Yahya R (2014) Green synthesized carbon nanodots as a fluorescent probe for selective and sensitive detection of iron (III) ions. Mater Lett 136:179–182

Vilian ATE (2016) Fabrication of 3D honeycomb-like porous polyurethane-functionalized reduced graphene oxide for detection of dopamine. Biosens Bioelectron 86:122–128

Wang J (2008) Electrochemical glucose biosensors. Chem Rev 108(2):814–825

Wang C, Sun D, Zhuo K, Zhang H, Wang J (2014) Simple and green synthesis of nitrogen-, sulfur-, and phosphorus-co-doped carbon dots with tunable luminescence properties and sensing application. RSC Adv 4(96):54060–54065

Wang L, Bi Y, Hou J, Li H, Xu Y, Wang B, Ding H, Ding L (2016) Facile, green and clean one-step synthesis of carbon dots from wool: application as a sensor for glyphosate detection based on the inner filter effect. Talanta 160:268–275

Watanabe M, Suliman ME, Qureshi AR, Garcia-Lopez E, Bárány P, Heimbürger O, Stenvinkel P, Lindholm B (2008) Consequences of low plasma histidine in chronic kidney disease patients: associations with inflammation, oxidative stress, and mortality. Am J Clin Nutr 87(6):1860–1866

Wei H, Wang E (2008) Fe_3O_4 magnetic nanoparticles as peroxidase mimetics and their applications in H_2O_2 and glucose detection. Anal Chem 80(6):2250–2254

Wei X, Gao X, Zhao L, Peng X, Zhou L, Wang J, Pu Q (2013) Fast and interference-free determination of glyphosate and glufosinate residues through electrophoresis in disposable microfluidic chips. J Chromatogr A 1281:148–154

Wright AT, Zhong ZL, Anslyn EV (2005) A functional assay for heparin in serum using a designed synthetic receptor. Angew Chem Int Ed 44:5679–5682

Wu SP, Huang RY, Du KJ (2009) Colorimetric sensing of Cu(II) by 2-methyl-3-[(pyridin-2-ylmethyl)-amino]-1,4-naphthoquinone: Cu(II) induced deprotonation of NH responsible for color changes. Dalton Trans 4735–4740

Xiao Y, Patolsky F, Katz E, Hainfeld JF, Willner I (2003) Plugging into enzymes: nanowiring of redox enzymes by a gold nanoparticle. Science 299(5614):1877–1881

Xu J, Zhou Y, Liu S, Dong M, Huang C (2014) Low-cost synthesis of carbon nanodots from natural products used as a fluorescent probe for the detection of ferrum (III) ions in lake water. Anal Methods 6(7):2086–2090

Xu H, Yang X, Li G, Zhao C, Liao X (2015) Green synthesis of fluorescent carbon dots for selective detection of tartrazine in food samples. J Agric Food Chem 63(30):6707–6714

Xue M, Zou M, Zhao J, Zhan Z, Zhao S (2015) Green preparation of fluorescent carbon dots from lychee seeds and their application for the selective detection of methylene blue and imaging in living cells. J Mater Chem B 3(33):6783–6789

Zhang J, Gu M, Zheng T, Zhu J (2009) Synthesis of gelatin-stabilized gold nanoparticles and assembly of carboxylic single-walled carbon nanotubes/Au composites for cytosensing and drug uptake. Anal Chem 81:6641–6648

Zhitkovich A (2011) Chromium in drinking water: sources, metabolism, and cancer risks. Chem Res Toxicol 24(10):1617–1629

Part IV
Medical Sensors

Chapter 8
Fabrication of Nanostructures with Bottom-up Approach and Their Utility in Diagnostics, Therapeutics, and Others

Sanjay Kumar, Pulak Bhushan and Shantanu Bhattacharya

Abstract Nanofabrication has been a critical area of research in the last two decades and has found wide-ranging application in improvising material properties, sensitive clinical diagnostics, and detection, improving the efficiency of electron transport processes within materials, generating high energy densities leading to pulse power, novel therapeutic mechanisms, environmental remediation and control. The continued improvements in the various fabrication technologies have led to realization of highly sensitive nanostructure-based devices. The fabrication of nanostructures is in principle carried out primarily using top-down or bottom-up approaches. This chapter summarizes the important bottom-up nanofabrication processes for realizing nanostructures and also highlights the recent research conducted in the domain of therapeutics and diagnostics.

Keywords Nanofabrication · Bottom-up approach · Diagnostics and therapeutics

Sanjay Kumar and Pulak Bhushan: Both authors have equal contribution in this chapter.

S. Kumar (✉) · P. Bhushan · S. Bhattacharya (✉)
Microsystems Fabrication Laboratory, Department of Mechanical Engineering, Indian Institute of Technology Kanpur, Kanpur, India
e-mail: sanjay21505@gmail.com

S. Bhattacharya
e-mail: bhattacs@iitk.ac.in

P. Bhushan
e-mail: pulakbhushan@gmail.com

S. Bhattacharya
Design Programme, Indian Institute of Technology Kanpur, Kanpur, India

S. Bhattacharya et al. (eds.), *Environmental, Chemical and Medical Sensors*, Energy, Environment, and Sustainability, https://doi.org/10.1007/978-981-10-7751-7_8

1 Introduction

Nanotechnology can be defined as the design, characterization, and fabrication of engineered nanostructures or nanodevices with at least one dimension less than 100 nm (Biswas et al. 2012; Abu-Salah et al. 2010; Wang et al. 2016). A reduction in the overall size of a structure to the nanometer scale results in a substantial change in its properties, e.g., chemical, physical, thermal, mechanical, which may differ entirely from their macroscale equivalents. These nanoparticles possess a high surface-to-volume ratio providing higher binding site density for the adsorption of various biomolecules (Arruebo et al. 2009). Nanoparticles conjugated with antibodies or other biological moieties (e.g., low molecular weight ligands, peptides, proteins, DNA, plasmids) provide highly specific and selective recognition characteristics. One of the distinguished features of nanoparticles is the variation of their physical or chemical properties dependent on their size and shape. For example, by varying the size of metal nanoparticles their radiation and excitation wavelength can be tuned. This unique characteristic can be attributed to an optical phenomenon known as localized surface plasmon resonance (LSPR). LSPR occurs due to the interaction of the incident light with the surface electrons present in the conduction band (Petryayeva and Krull 2011). The phenomenon is generated by entrapped light waves in the conductive metal nanoparticles. Hence, nanoparticles offer specific physical and chemical properties that enable their utilization in a variety of domains like biomedical, energy and environment, manufacturing.

In general, there are three broad classifications of nanomaterials that are, natural, incidental and engineered (Hu et al. 2010). Natural nanomaterials are formed through natural processes and are governed by natural laws. Incidental nanomaterials are the by-products of industries (e.g., coal dust, particulates). Engineered nanomaterials are complex in shape and require specific processes for their fabrication. Based on the number of dimensions of the features, these nanomaterials can be classified into four types: 0-D, 1-D, 2-D, and 3-D (Chopra et al. 2007; Ciesielski et al. 2010; Pashchanka et al. 2010; Song et al. 2010). Zero-dimensional nanostructured materials have nanoscale dimensions in all directions, e.g., nanoparticles, nanospheres, quantum dots. One-dimensional nanostructures have non-nanoscale dimensions in a single direction such as nanorods, nanotubes, nanowires, nanobelts, nanoribbons, nanostars (Kumar et al. 2017). Two-dimensional nanostructures possess two dimensions having non-nanometric size range, e.g., graphene nanosheets, nanoplates, nanobelts, nanodiscs. Three-dimensional nanostructures contain non-nanoscale features in any three dimensions, e.g., nanotetrapods, nanoflowers, nanocombs.

This chapter presents a brief review of the bottom-up fabrication techniques used for fabrication of different shaped nanostructures and nanocomposites. It also covers the recent advancements in fabrication of ZnO-based nanostructures, DNA-based nanostructures, polymer-based nanostructures, and metal-based nanostructures and their widespread applications in the field of diagnostics, therapeutics, and others.

2 Fabrication Techniques

Nanostructures, nanomaterials, and nanocomposites can be fabricated using two different techniques, top-down and bottom-up (Bellah et al. 2012). The top-down approach involves lateral patterning of bulk materials by either subtractive or additive methods to realize nano-sized structures. Several methods are used to fabricate nanostructures using the top-down approach such as photolithography, scanning lithography, laser machining, soft lithography, nanocontact printing, nanosphere lithography, colloidal lithography, scanning probe lithography, ion implantation, diffusion, deposition. (Chi 2010; Kumar et al. 2013a). Although the top-down approach has been playing a vital role in the fabrication of nanostructures, it has several limitations such as development of imperfections in processed materials, high cost (lithographic processes), requirement of high surface finished materials, longer etching times. (Mijatovic et al. 2005; Biswas et al. 2012). In the bottom-up approach, nanostructures are fabricated by building upon single atoms or molecules. In this method, controlled segregation of atoms or molecules occurs as they are assembled into desired nanostructures (2–10 nm size range). In general, there are two basic methods utilizing the bottom-up approach, i.e., gas-phase synthesis and liquid-phase formation. Some of the methods used in bottom-up approach include plasma arcing, chemical vapor deposition process, metal organic decomposition, laser pyrolysis, molecular beam epitaxy, solgel method, wet synthesis, and self-assembly processes.

2.1 Plasma Arcing

Plasma is one of the fundamental states of matter comprising of electrons and molecules in ionic states. It maintains a condition of overall neutrality, although there may be a net positive or negative charge on certain particles. Plasma arcing method requires an ionized state of gas atoms, for which high energy is necessary to peel off the electron from its valence shell to obtain a positively charged atom. An electrical arrangement consisting of an anode and cathode is developed providing sufficient amount of electric field to transform the atoms into ions. Electrodes used are usually made up of conducting materials or mixtures of conducting and non-conducting materials. Generation of contracted plasma uses inert gas as a heat source. Emission of electrons takes place from one electrode due to the presence of high potential difference causing an electrical breakdown. A sudden avalanche of electrons results in the formation of an arc in the zone between the electrodes. Positively charged ions travel at a high velocity and are driven by the applied bias voltage toward the cathode and get deposited as nanoparticles. It is ensured that the depth of deposition consists of a few layers of atoms with each particle of the order of more than 1 nm and all particles so formed are mutually separated. The average temperature of the arc in cold plasmas is generally higher than 104 K.

2.2 Chemical Vapor Deposition (CVD)

Chemical vapor deposition process is mostly used in the semiconductor industry for depositing thin films of various materials. The process involves exposure of the substrate to one or more volatile precursors. These precursors decompose the substrate and react with it to produce the desired deposit. In the process, vaporized precursors are first adsorbed onto a substrate at a high temperature, which then react with one another or decompose and produce crystals. There are three main steps involved in the process: (i) Reactants are transported onto the growth surface by a boundary layer, (ii) chemical reactions take place on the growth surface, and (iii) by-products formed by the gas-phase reaction are removed from the growth surface. Homogeneous nucleation takes place in gas phase, whereas heterogeneous nucleation takes place in the substrate.

2.3 Molecular Beam Epitaxy (MBE)

Molecular beam epitaxy is a physical evaporation process with no chemical reactions involved. The basic difference between MBE and other epitaxy systems is that the former does not involve any chemical reactions and is instead a simple physical evaporation process. This method works on the principle of vacuum evaporation where thermal molecular and atomic beams are directly impinged on a heated substrate under ultra-high vacuum conditions (Cho and Arthur 1975). The first major advantage of the MBE process is it being a comparatively low-temperature process as compared to vapor phase epitaxy. The low-temperature characteristic of this process enables it to reduce autodoping. The second advantage of MBE is that one can have precise control over the doping process. One can achieve a growth rate as low as 0.01 μm per minute up to a maximum of 0.3 μm per minute, allowing for ultra-precise control of layer growth. With the advent of VLSI technology, it is critical to reduce all dimensions to atomic levels and thus the thickness of the epitaxial layer may also reduce further in future.

2.4 Solgel Synthesis

In the solgel process, dispersed solid nanoparticles (sols with diameter of 1–100 nm) are mixed in a homogeneous liquid medium and agglomerated to form a continuous three-dimensional network (gel) with pore diameter in the sub-micrometer domain in the liquid phase (Hench and West 1990). A sol is a liquid in which solid colloidal particles are dispersed, e.g., black inkjet ink (carbon black is dispersed in water), while a gel is a wet solid-like rigid network of interconnected nanostructures in a continuous liquid phase. Generally, there are three

approaches that have been employed to fabricate solgel film: (i) gelation of a solution of solid colloidal particles, (ii) hydrolysis and polycondensation of alkoxides followed by hypercritical drying of gels, and (iii) hydrolysis and polycondensation of alkoxide followed by aging and drying under ambient conditions. Several steps are involved in the process like mixing (formation of suspended colloidal solution by mixing of nanoparticles in water), casting of sol, gelation (formation of three-dimensional network), aging (for increasing the life of cast objects immersed in liquid), drying (removal of liquid from the interconnected continuous pore network), dehydration or chemical stabilization (to improve stability), and densification (heating the solgel at higher temperatures to eliminate pores and enhance the density, e.g., densification of alkoxide gels carried out at a temperature of 1000 °C) (Hench and West 1990). The properties of solgels depend on important parameters such as pH, type of solvent, temperature, time, catalysts and agitation mechanisms.

2.5 Molecular Self-Assembly

In general, four strategies are used for chemical synthesis of nanoparticles, i.e., sequential chemical synthesis, covalent polymerization, self-organizing synthesis, and molecular self-assembly. Molecular self-assembly (MSA) process is an ensemble of the properties of each of the above methods. MSA is a process in which atoms or molecules assemble together in equilibrium conditions to form a stable and well-defined nanophase by non-covalent bonds (Whitesides et al. 1991). All natural materials (organic or inorganic) are processed through a self-assembly route; e.g., in a natural biological process, a DNA double helix is formed through self-assembly. This approach can be used as a basic structuring mechanism to fabricate complex nanostructures (Mijatovic et al. 2005). The molecular self-assembly process is highly capable of fabricating nanostructures in the range of 1–100 nm. In order to create complex nanostructures using self-assembly process, critical parameters such as, the well-defined geometry and the specific interactions between the basic units requisite significant consideration (Rothemund 2005).

2.6 DNA Nanotechnology

Deoxyribonucleic acid (DNA) nanotechnology is the method to fabricate artificial nucleic acid nanostructures which can be utilized as nanofilters, biological scaffolds, fast performing nanowire devices, etc. Owing to its excellent physical and chemical properties, DNA has become the most widely used material for construction of nanostructures. Using nucleotide sequence-directed hybridization, DNA is able to produce duplexes and other secondary structures (Feldkamp and Niemeyer 2006). This property allows DNA molecules to self-assemble and

formulate nanoscale structures which can be employed in scaffolds, nanostructures, and nanodevices. DNA nanotechnology also utilizes the self-recognition properties of a DNA molecule to fabricate nanostructures in a desirable manner. A novel approach known as 'the DNA origami method' has been developed to fabricate two-dimensional DNA nanostructures of arbitrary shapes (Rothemund 2005).

3 Design and Synthesis of Nanostructures

3.1 ZnO-Based Nanostructures

In the recent years, various metal and metal oxide nanoparticles (MONPs) have been synthesized. Among these nanomaterials, the synthesis of metal oxides, especially zinc oxide, tin oxide, titanium dioxide nanostructures has been very prominent. The zinc oxide system in particular has shown many diverse applications owing to its relatively high and customizable band gap. Zinc oxide has been exploited for various applications like sensors (gas, bio, chemical, visible light, and ultraviolet), cosmetics, optical devices, optoelectronic devices, electrical devices, photochemical applications, solar cells, light-emitting displays, optical storages, drug delivery systems. (Gupta et al. 2013, 2014b, 2015a, b; Kumar et al. 2013b; Yao et al. 2002; Vaseem et al. 2010; Tian et al. 2003). ZnO is a semiconductor with a wide band energy gap of 3.37 eV at room temperature and a binding energy of 60 meV (Djurišić et al. 2012; Kumar et al. 2013b). The crystalline structure of ZnO is wurtzite containing hexagonal unit cells. ZnO nanostructures provide large surface area, high aspect ratio, high catalytic activity, and higher number of adsorption sites on their surfaces (Chen and Tang 2007). Also, a numerous variety of electronic and optical properties can be obtained using different ZnO nanostructures because of their rich defect chemistry (Djurišić et al. 2012).

Several fabrication techniques have been described in the literature for fabrication of ZnO nanostructures, such as sputtering, laser ablation, molecular beam epitaxy, physical vapor deposition, thermal evaporation, electrochemical deposition, template-based synthesis, and solgel methods (Yao et al. 2002; Wu et al. 2005; Chiou et al. 2003; Sun et al. 2004; Huang et al. 2001; Heo et al. 2002; Zhang et al. 2009). A variety of ZnO nanostructures such as nanoparticles (Kumar et al. 2013b), nanowires (Baruah et al. 2016; Vayssieres 2003), nanoseeds (Gupta et al. 2014b), nanorods (Vayssieres 2003), nanocombs (Huang et al. 2006), nanobelts (Fig. 1) (Sun et al. 2008), nanotubes (Sun et al. 2005), tetrapods (Qiu and Yang 2007), ribbons (Fan et al. 2009), nanopropellers (Fig. 2) (Gao and Wang 2004) have been fabricated using some of the above-mentioned fabrication technologies. ZnO quantum dots have also been fabricated for applications in bacteria diagnosis (Chen et al. 2015) and electrochemical cells (Daumann et al. 2017). Scanning electron microscopy images of a few of the above morphologies of ZnO nanostructures are shown in Fig. 3.

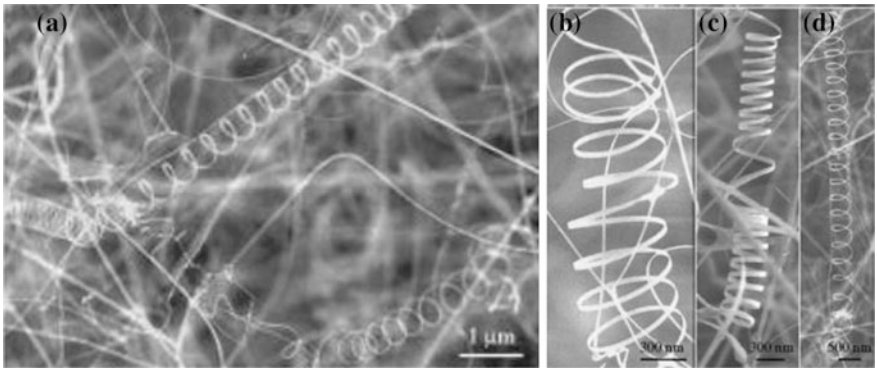

Fig. 1 a–d Image of ZnO helical nanobelts as shown in scanning electron microscope. Reproduced from Kong and Wang (2003), with permission from American Chemical Society

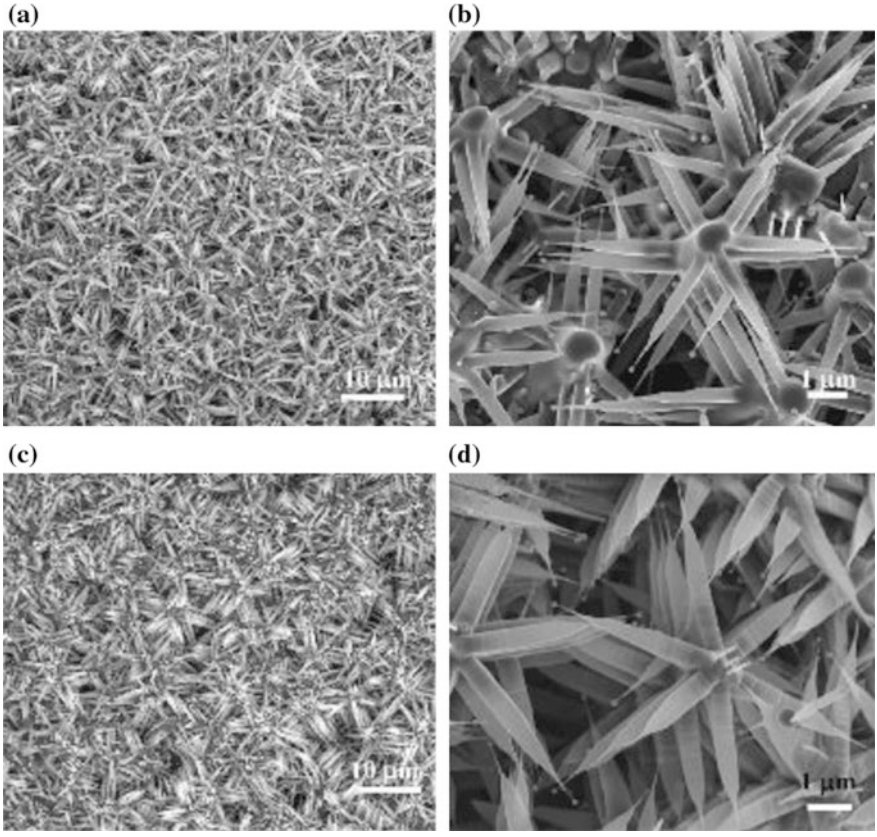

Fig. 2 a–d ZnO nanopropeller arrays as seen through a scanning electron microscope. Reproduced from Gao and Wang (2004), with permission from AIP Publishing LLC

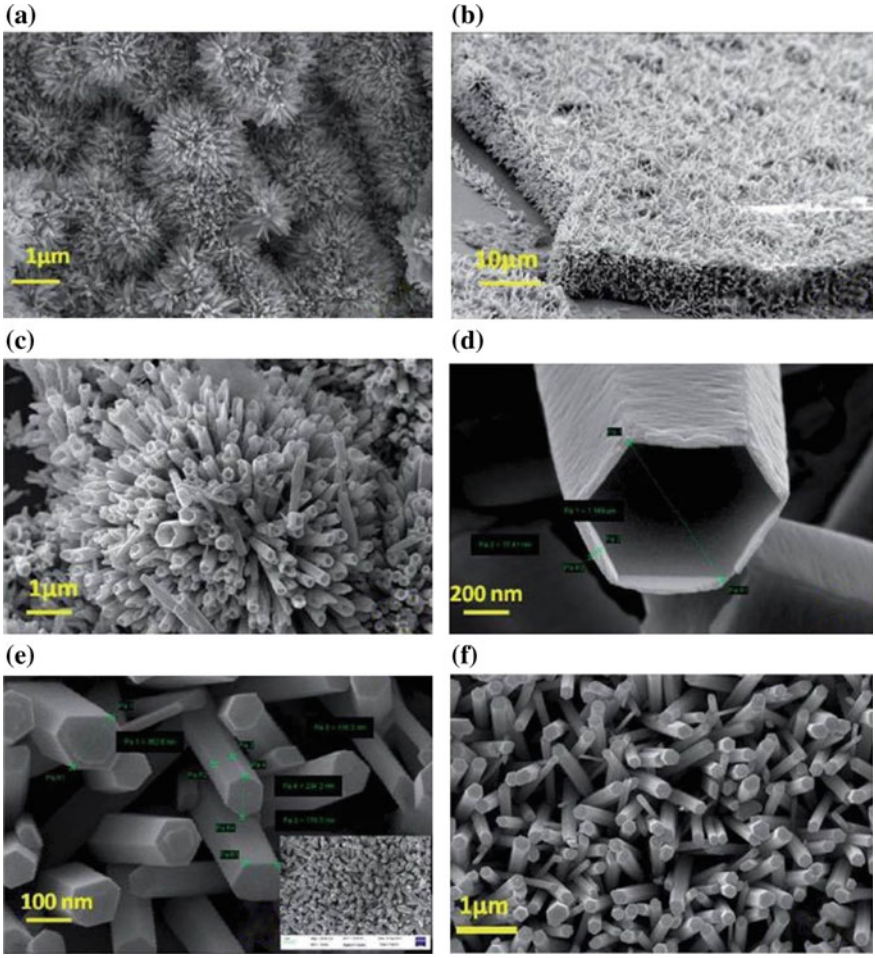

Fig. 3 FESEM images of various ZnO nanostructures morphologies at different concentrations of $Zn(NO_3)_2$. Reproduced from Gupta et al. (2014b), with permission from Royal Society of Chemistry

3.2 Polymer-Based Nanostructures

Polymers are the most extensively used biomaterials in the medical field for applications in implantation, medical devices, medical coatings, tissue engineering, and prostheses, owing to their biocompatibility with human tissues and cells (Jagur-Grodzinski 2003). Polymers are generally categorized as natural or synthetic (Broz 2010). Natural polymers extracted from the Mother Nature are biodegradable and offer excellent biocompatibility. Silk, wool, proteins (Dutta et al. 2004) (e.g., collagen, gelatin), cellulose, and DNA are some examples of naturally occurring

polymers. Due to their complex structures, modification of natural polymers is challenging. While synthetic polymers are fabricated using petroleum oils as the main constituent, there are mainly four types of synthetic polymers which include thermoplastics, thermosets, elastomers, and synthetic fibers (Peacock 2000). Examples of synthetic polymers include polydimethylsiloxane (PDMS), nylon, polypropylene, polyvinyl chloride, polystyrene, Teflon.

The fabrication methods of polymer nanostructures can be divided into two groups, template-based synthesis and template-free synthesis. Template-based synthesis includes conventional hard-template method (Parthasarathy and Martin 1994; Martin 1995; Yin and Zheng 2012), soft-template method (Meng et al. 2007), and novel wire-template method (e.g., water soluble templates, reactive self-degraded wire templates, seeding wire templates, biological wire templates) (Liang et al. 2010). On the other hand, template-free synthesis includes self-assembly method (Wan 2008), electrospinning (Li and Xia 2004), and nanoscale patterning. Template-based synthesis employs nanostructured matters as templates, over which one-dimensional polymer nanostructures can be grown. In a conventional hard-template method, micro-/nanoporous membrane materials, e.g., anodic aluminum oxide and particle track-etched membranes, are used as templates. The growth of polymer nanostructures takes place due to an electrochemical reaction of the loaded monomer solutions within the pores of these templates (Martin 1996). Reaction rate, reaction time, and temperature are vital parameters for controlling the growth of these nanostructures using conventional hard-template methods. In soft-template methods, soft amphiphilic materials like liquid crystals, surfactants, copolymers are utilized as templates. The formation of polymer nanostructures takes place as a result of the aggregation of self-assembled amphiphilic molecules through hydrogen bonding, hydrophilic–hydrophobic interactions and Van der Waals forces (Han and Foulger 2006). Novel wire-template methods are superior compared to hard-template and soft-template methods because they possess combined properties of both the above methods (Liang et al. 2010). The fabricated polymer nanostructures by this process possess high stability. In this process, preexisting one-dimensional nanomaterials are used as templates over which 1D polymer nanocomposites are grown. Template-free methods do not require any templates. Self-assembly is extensively used as a template-free chemical method for fabrication of nanostructures. Polymer nanostructures form by aggregation of nanoparticles through non-covalent bonding such as dipole–dipole interaction, electrostatic interaction, Van der Waals forces, ion–dipole interactions, and π-π stacking. Electrospinning is also a template-free physical method, in which a very high electric field is applied between the syringe containing the polymeric fluid and a conductive collector screen. A liquid jet forms when the applied electric field surpasses the surface tension of the polymeric fluid and accelerates toward the counter electrode. During this movement, the liquids get solidified and accumulate as nanofibers over the collector. Several researchers have reported the fabrication of various polymer nanostructure morphologies. Epoxy-based SU-8 polymer nanostructures with tunable high aspect ratios have been fabricated using electron beam

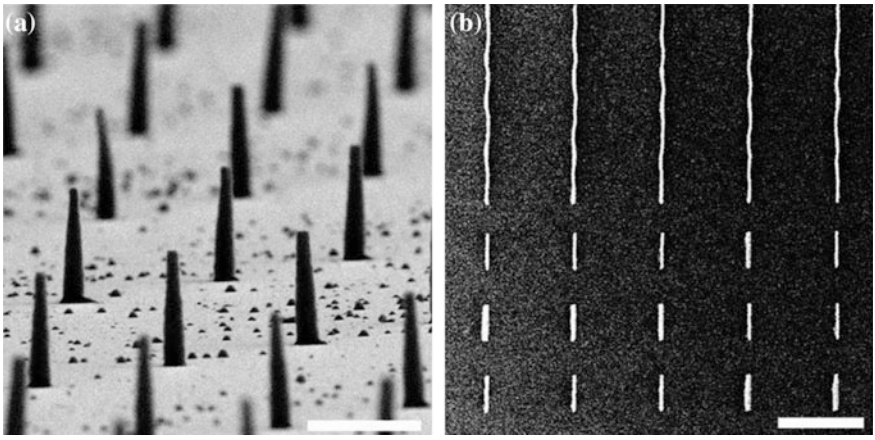

Fig. 4 SEM images of **a** nanopillars and **b** nanolines. Reproduced from Beckwith et al. (2015), with permission from the Royal Society of Chemistry

lithography (Beckwith et al. 2015). These nanostructures were synthesized on glass cover slips. Uniform arrays of SU-8 nanopillars and nanolines are shown in Fig. 4.

Ferroelectric polymer nanostructures have also been synthesized using flexible polyethylene terephthalate substrates (Song et al. 2015). A low-pressure reverse nanoimprint lithography technique has been developed that uses soft polycarbonate molds derived from recordable DVDs to fabricate nanostructures. These nanostructures are highly stable and exhibit switchable piezoelectric response and good crystallinity.

3.3 Metal-Based Nanostructures

Recently, many research fields have focused on the development of metallic nanostructures with complex shapes and various compositions in order to exploit their distinctive qualities (Gentile et al. 2016; Xia et al. 2009). Due to the high surface-to-volume ratios, metal-based nanostructured materials have been used in various domains such as catalysis, sensing, fuel cells, mechanical actuators, electrodes, point-of-care diagnostics, medicine. (Gentile et al. 2016; Jiang et al. 2012).

Various metallic nanostructures have been reported such as porous nanowires (Kolmakov et al. 2008), porous nanotubes (Lévy-Clément et al. 2009), porous nanosheets (Liang et al. 2004; Zhang et al. 2007), quantum dots (Abeyasinghe et al. 2016; Lian et al. 2015), hollow and porous nanospheres (Zhang et al. 2006). Figures 5 and 6 show SEM and TEM images of some nanowires and nanospheres.

Monodispersed bismuth particles have been fabricated by thermally decomposing bismuth acetate in boiling ethylene glycol (Wang and Xia 2004). The size of the nanospheres was varied by varying the concentration of the bismuth precursor

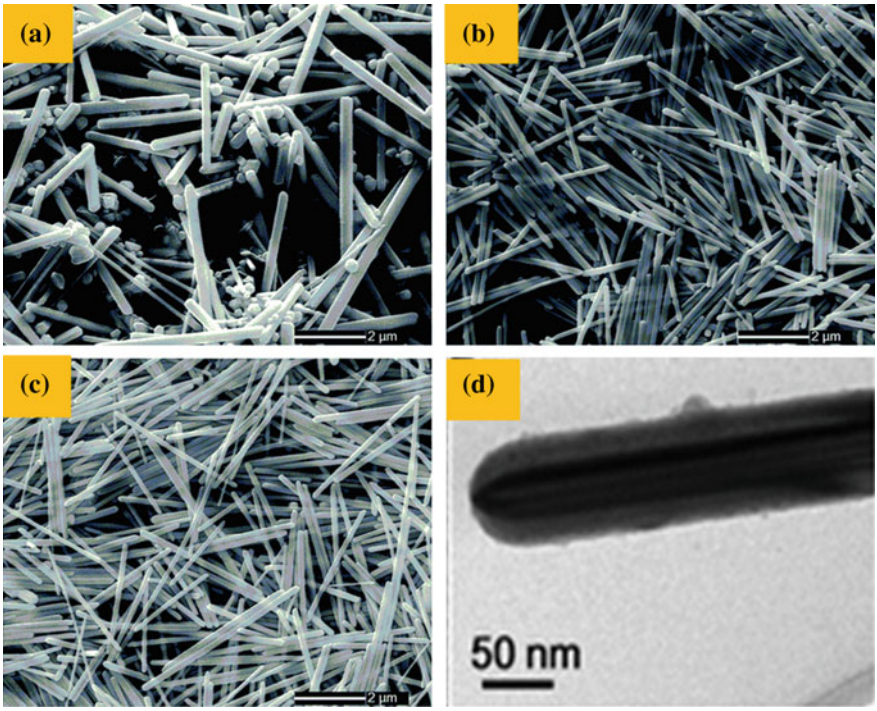

Fig. 5 **a** SEM images of silver nanowires synthesized with different amounts of $FeCl_3$: **a** 0.05 mM, **b** 0.10 mM, and **c** 0.15 mM. Adapted from Ma and Zhan (2014), with permission from the Royal Society of Chemistry. **d** TEM image of a typical silver nanowire. Reproduced from Hu et al. (2012), with permission from the Royal Society of Chemistry

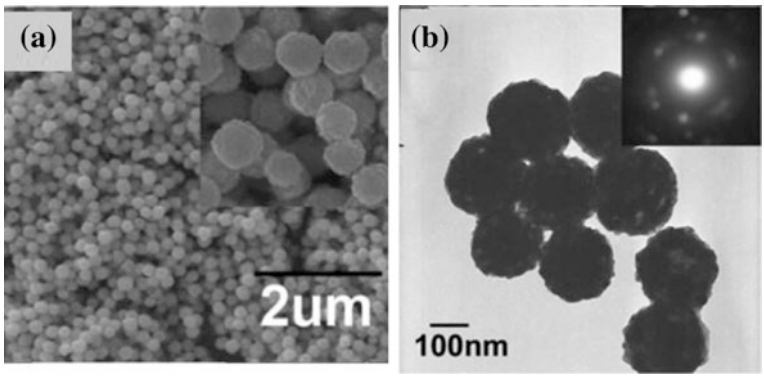

Fig. 6 **a** SEM image of CuO nanospheres. The inset shows the image at a higher resolution, **b** transmission electronic microscope image of the CuO nanospheres with an inset depicting the ED pattern of one nanosphere. Reproduced from Zhang et al. (2006), with permission from American Chemical Society

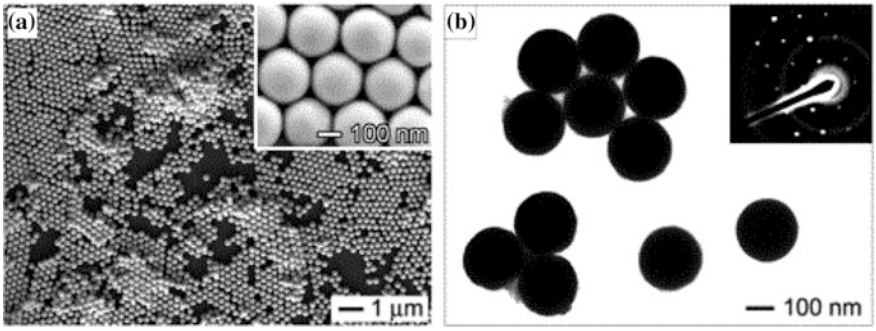

Fig. 7 **a** SEM image of bismuth nanospheres. Inset: higher resolution image, **b** TEM image of the bismuth nanospheres. Inset: SAED pattern of one nanosphere. Reproduced from Wang and Xia (2004), with permission from American Chemical Society

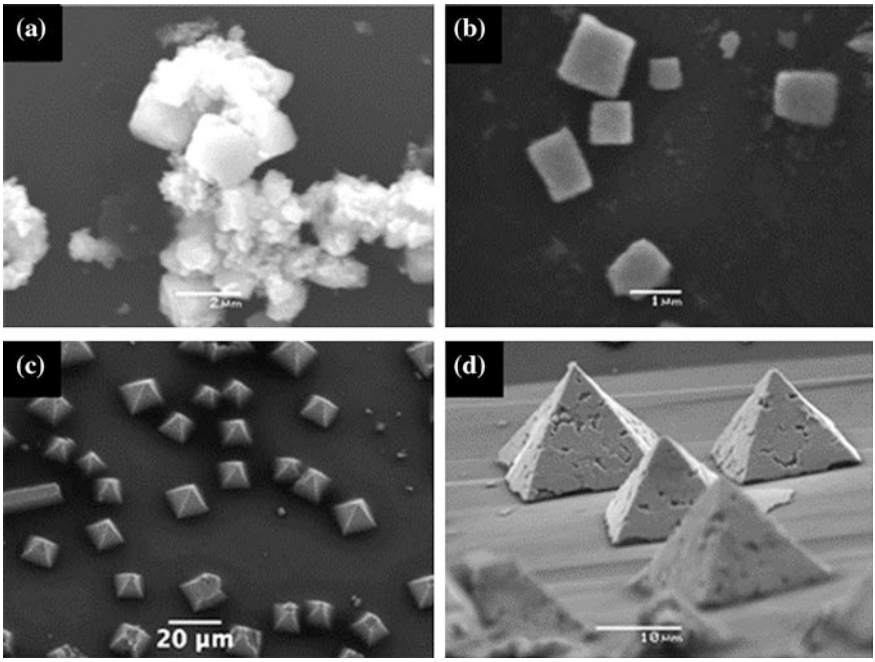

Fig. 8 **a**, **b** SEM image of cubic-shaped superlattices obtained from platinum nanocubes, **c**, **d** SEM images of pyramidal-shaped superlattices obtained from truncated nanocubes. Reproduced from Demortiere et al. (2008), with permission from American Chemical Society

and the stirring rate. The respective SEM and TEM images of the nanospheres are shown in Fig. 7.

Platinum nanocrystals have been synthesized using a liquid–liquid-phase transfer method (Demortiere et al. 2008). By controlling the nucleation and

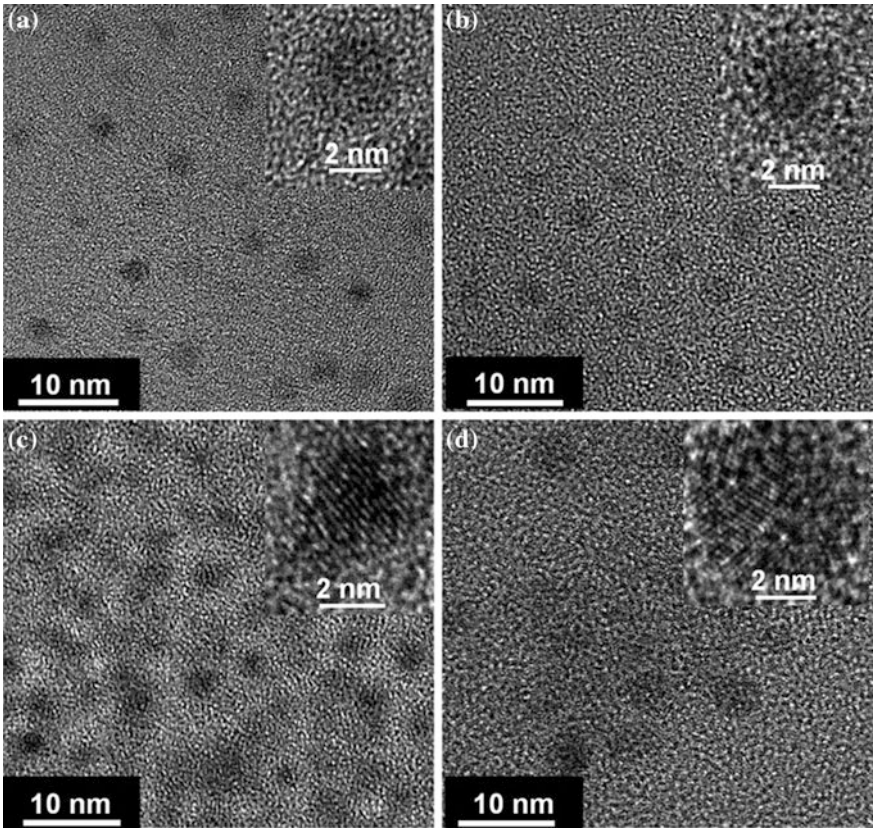

Fig. 9 HRTEM images of carbon dots using different precursors: **a** TMB, **b** DAB, **c** PY, and **d** PHA. Insets show the magnified HRTEM images. Reproduced from Yang et al. (2013), with permission from the Royal Society of Chemistry

growth process parameters, cubic and pyramidal morphologies have been achieved (Fig. 8). Further, the nanocrystals self-assemble to develop 2D and 3D supracrystals.

A soft–hard-template method has been employed for fabrication of monodispersed carbon dots (Yang et al. 2013). In order to obtain different sizes, compositions, and crystallinity, four different precursors have been used that include pyrene (PY), 1,3,5-trimethylbenzene (TMB), phenanthroline (PHA), and diaminebenzene (DAB). The TEM images of the as-synthesized carbon dots have been shown in Fig. 9.

3.4 DNA-Based Nanostructures

Deoxyribonucleic acid (DNA) is a genetic molecule in which hereditary information is encoded. It has an antiparallel double-stranded helical structure which enables its use in fabrication of nanostructures and nanodevices through a self-assembly process (Seeman 2010; Sun and Kiang 2005; Yan et al. 2003). The diameter of each strand of DNA is about 2 nm, and the helical pitch is about 3.5 nm. DNA is composed of a nitrogen-containing nucleobase (adenine, cytosine, guanine, and thymine), a sugar molecule, and a phosphate group. It has several specific characteristics that make it a preferable choice for fabrication of engineered biological nanostructures. First, DNA molecules segregate by self-assembly process so that complex structures can be fabricated with a nanometer resolution (Yan et al. 2003). Second, since the genetic information is encoded by chemical coding process, the intermolecular interaction of molecules can be easily programmed (Sun and Kiang 2005). Third, although double-stranded DNA (dsDNA) is a flexible polymer, it acts as a rigid polymer below the 50 nm size (Feldkamp and Niemeyer 2006). Therefore, the nanostructures (<50 nm) made from dsDNA can be used as rigid nanomaterials. Fourth, single-stranded DNA (ssDNA) is very flexible in comparison with dsDNA. It can be twisted to about 180° and is even capable of forming tight loops in the nanometer size. By combining the properties of dsDNA and ssDNA, complex artificial DNA nanocomposites can be fabricated. The rigidity and flexibility of these tailored nanomaterials can be controlled easily. Fifth, DNA has superior physicochemical stability as compared to proteins. The nanostructures fabricated by DNA exhibit features such as robustness and can be easily processed and synthesized.

Due to their excellent properties, DNA molecules have been used in many applications such as functional DNA nanostructures (suprastructure materials), porous, hexagonal, and 2D DNA arrays (Yan et al. 2003), DNA nanomechanical machines (Bath and Turberfield 2007; Venkataraman et al. 2007; Modi et al. 2009), and molecular computing systems (Benenson 2011; Elbaz et al. 2010; Ran et al. 2009). The fabrication of these nanostructures includes three main steps: hybridization, stably branched DNA, and synthesis of designed sequences. DNA molecules have been used to fabricate λ-DNA duplex, helix ribbon, helix tube, and DNA lattice (Fig. 10) (Lee et al. 2014). A 4 × 4 lattice has been developed by four four-armed DNA-branched junctions. Due to the large cavity size, these lattices can serve as binding sites for other molecules. For self-assembly of protein arrays, developed nanogrids were used to template streptavidin. The atomic force micrograph (AFM) of the self-assembled protein array is shown in Fig. 11. Also, a highly conductive metallic nanoelectrode has been developed by depositing silver nanomaterials on bacteriophage l DNA templates.

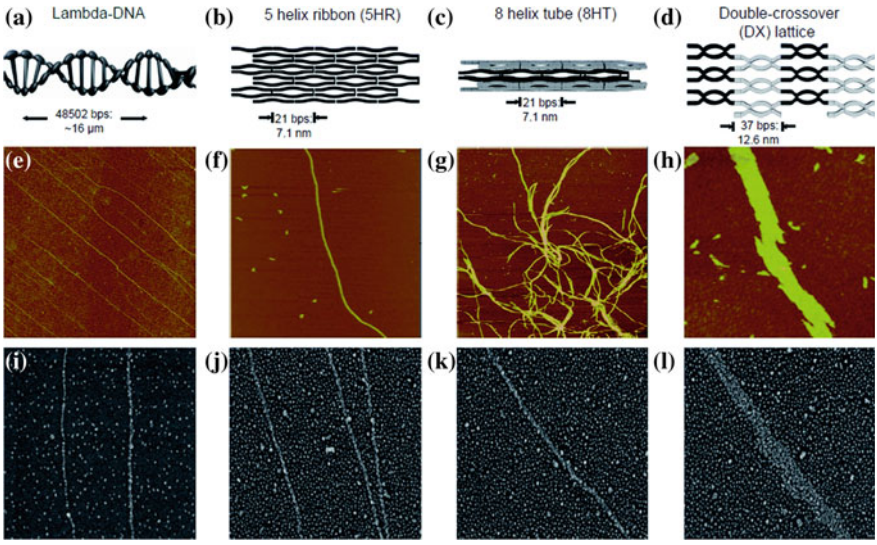

Fig. 10 **a** QD-aligned DNA nanostructures. **a–d** Schematic diagrams of the various DNA templates: **a** a λ-DNA duplex, **b** a five-helix ribbon, **c** an eight-helix tube, and **d** a double crossover (DX) DNA lattice. **e–h** AFM images of the DNA templates. AFM images in the same column as the schematic diagrams of the DNA nanostructures **a–d** correspond to those structures. **i–l** SEM images of Qdots aligned on corresponding DNA templates. Reproduced from Lee et al. (2014), with permission from the Royal Society of Chemistry

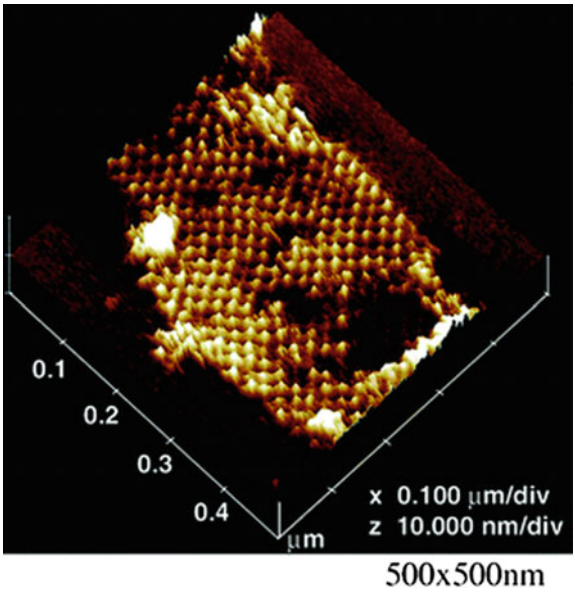

Fig. 11 Self-assembly of streptavidin array at 500 × 500 nm scale as seen through AFM. Reproduced from Christman et al. (2006), with permission from the Royal Society of Chemistry

4 Applications

Nanostructured materials have been used in a wide range of nanotechnology fields such as nanoelectronics, optoelectronics, bioelectronics, nanochemistry, sensing, nanofluidics, point-of-care diagnostics, nanomachines, therapeutics, advanced energy storages. On account of the increasing requirements of real-time sectors such as medical and health care, the diagnostic and therapeutic applications are being developed rapidly.

4.1 Diagnostic Applications

In the recent past, researchers have focused on investigating the relevance of nanostructures for development of clinical diagnostic devices. ZnO nanostructures have been used for various biological applications attributing to their non-toxic and environment-friendly nature (Vaseem et al. 2010; Gupta et al. 2014a, 2015c). ZnO nanowires have been utilized in biosensing applications by immobilization of antibodies on its surface (Gupta et al. 2014a). Goat antisalmonella was used for the immobilization purpose. Owing to the high aspect ratio, the surface of ZnO nanowires provides larger binding sites for the antibodies. For biological applications, the nanomaterials are required to be hydrophilic in nature which can be achieved by modifying the surface of nanostructures with water soluble agents. In this regard, water soluble ZnO–Au nanocomposites have been fabricated (Wang et al. 2007). These composites fulfill two purposes: ZnO provides the fluorescence, and gold nanoparticle delivers the high affinity toward the conjugation of organic

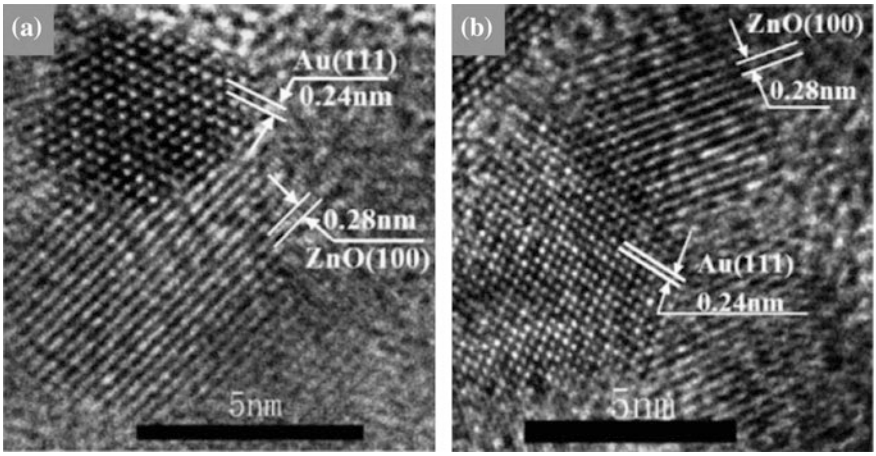

Fig. 12 **a**, **b** High-resolution TEM images of ZnO–Au nanocomposites. Reproduced from Wang et al. (2007), with permission from American Chemical Society

molecules. The transmission electron micrograph of the developed nanocomposite is shown in Fig. 12.

Several authors have reported the green synthesis of ZnO nanoparticles (Bauermann et al. 2006; Wang et al. 2007). ZnO nanoparticles have been synthesized in aqueous solution having a neutral pH (Bauermann et al. 2006). The transmission electron micrograph (TEM) and scanning electron micrograph (SEM) of these nanoparticles are shown in Fig. 13. A non-toxic buffer tris(hydroxymethyl) aminomethane acting as a polydentade ligand is used to improve the adsorption capabilities of ZnO nanoparticles.

A novel biosensor based on ZnO–Au nanocomposite has been developed for rapid and sensitive detection of microorganisms in food and water samples. Nanoporous silica film has been prepared by the traditional porogen method using poly(methylsilsesquioxane) (PMSSQ) (empirical formula: $(CH_3SiO_{1.5})_n$) as the matrix and poly(propylene glycol) (PPG) (empirical formula: $(CH(CH_3)CH_2O)n$ and molecular weight: 20,000 g/mol) as the porogen. Propylene glycol methyl ether acetate was used as a solvent for the preparation of nanoporous silica. ZnO nanostructures were grown using wet chemical synthesis, and the ZnO–Au nanocomposite was prepared by mixing the ZnO and Au nanoparticles.

Viral plant pathogens have also been detected using polypyrrole (PPy) nanoribbons (Chartuprayoon et al. 2013). Cucumber mosaic virus (CMV) has been detected by immobilizing the capture antibodies on PPy nanoribbons. The sensitivity of the device has been enhanced by reducing the thickness of PPy nanoribbons from 100 to 25 nm. The schematic representations of the biofunctionalized PPy nanoribbon and the detection of CMV are shown in Fig. 14.

Food-borne microorganisms have been detected using nucleic acid-based method (q-PCR) in a single integrated polymeric device (Nayak et al. 2013). A gold nanoparticle-assisted conjugation of IgG antibodies was employed for detection of *E. coli* bacteria. Soft lithography and replica molding techniques were used to fabricate microchannels in polydimethylsiloxane (PDMS). The fabricated microchannels are shown in Fig. 15.

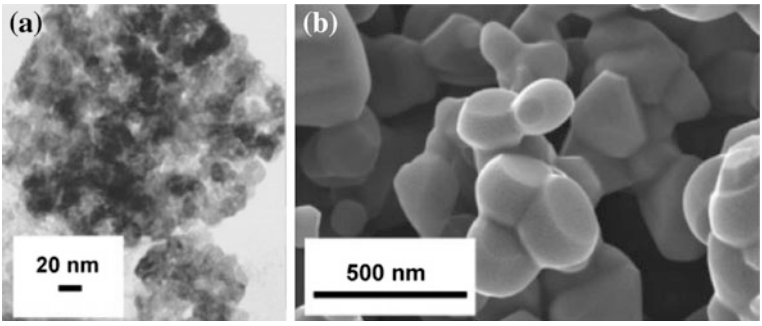

Fig. 13 **a** Transmission electron microscope images of ZnO nanoparticles. **b** SEM images of ZnO nanoparticles sintered at 1000 °C. Reproduced from Bauermann et al. (2006), with permission from American Chemical Society

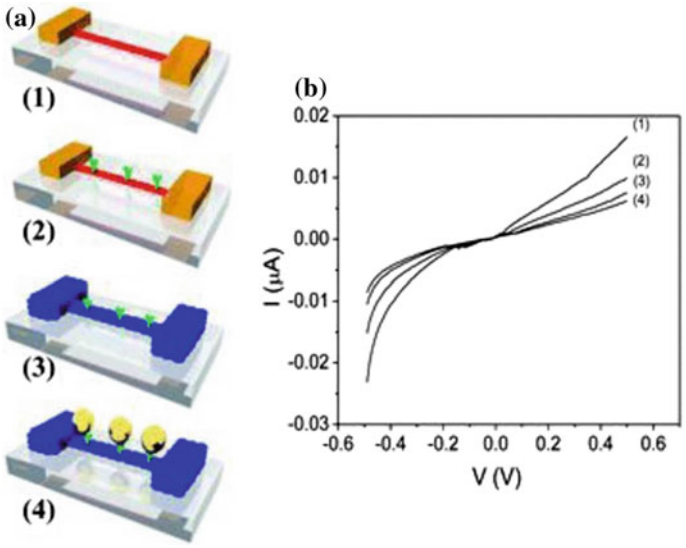

Fig. 14 **a** Schematic representations of the biofunctionalized PPy nanoribbon and the detection of CMV after each step: (1) unfunctionalized PPy nanoribbon, (2) CMV antibody functionalized PPy nanoribbon using EDC/NHS chemistry, (3) prevention of non-specific binding by immobilizing BSA onto the nanoribbon, and (4) chemiresistive detection of CMV using PPy nanoribbon and **b** corresponding I–V characteristics. Reproduced from Chartuprayoon et al. (2013), with permission from the Royal Society of Chemistry

For detection of biomarkers in human blood serum, a hybrid ZnO nanorod poly (oligo(ethylene glycol) methacrylate-*co*-glycidyl methacrylate (POEGMA-*co*-GMA) polymer brush has been reported (Hu et al. 2015). The sensitivity and specificity of an antibody microarray has been improved significantly by development of polymeric nanostructures. ZnO nanorods grown on glass slide behave as the backbone substrate over which polymer brush grows. Also, ZnO nanorods amplify the fluorescence intensity facilitating the detection of biomarkers. The POEGMA-*co*-GMA nanobrush is utilized to retain antibodies with higher densities. The limit of detection (LOD) of biomarkers in human blood serum was reported to be as low as 100 fg mL^{-1}.

In order to perform colorimetric detection of uric acid in human serum, graphene oxide-based gold nanoparticle-embedded networks have been utilized. A paper-based sensing platform has been developed that provides rapid results within 5 min and exhibits a high sensitivity of 4 ppm (Kumar et al. 2016).

Nanocantilevers have a wide range of applications in science (physical and chemical) especially in the field of sensing and point-of-care disease diagnostics. The advantages of using nanocantilevers as sensors over microsensors are that they provide higher sensitivity, are economic in terms of cost, require lower concentration of analytes (in μl), employ label-free detection, have a faster response, and consume lower power. Diagnosis of a variety of analytes for detection of various

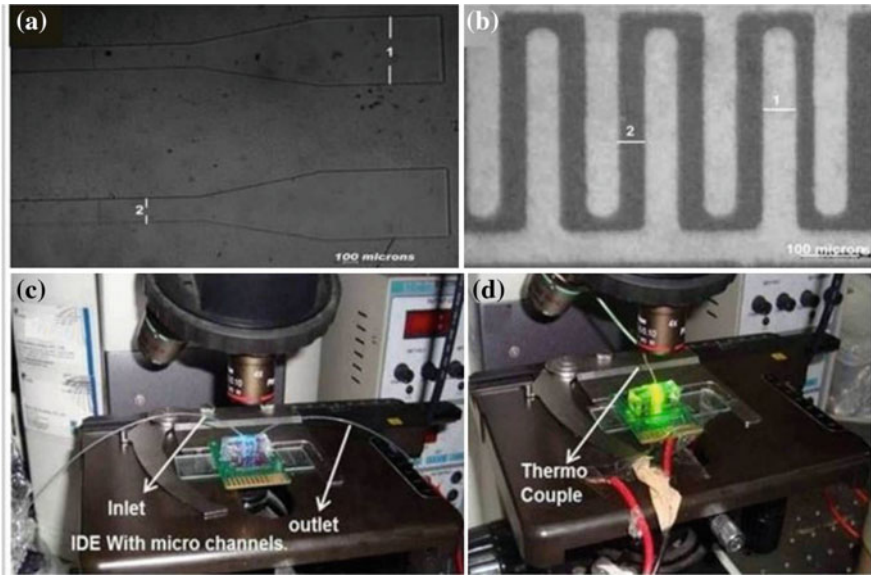

Fig. 15 Images of microchannels fabricated on polydimethylsiloxane (PDMS). **a** Image of microchannel: (1) dimension of inlet/outlet ports is around 650 µm, and (2) the main portion has a dimension of around 225 µm, **b** image of interdigitated electrodes: (1) individual width of 53.562 µm and (2) inter-electrode spacing of 42.322 µm, **c** image of dielectrophoretic capture, and **d** image of RT-PCR-based detection. Reproduced from Nayak et al. (2013), with permission from scientific reports

diseases on array of microcantilevers can be done on a single microcantilever chip leading to a higher throughput and efficiency. The surface functionalization over these cantilevers using bottom-up approaches enables sensing and detection of analytes with higher sensitivity. This methodology holds the future for high-sensitivity next-generation nanocantilever-based sensing for forthcoming point-of-care diagnostics. Single molecule detection will be the aim of researchers necessitating development of highly sensitive sensors. Gupta et al. fabricated an array of silicon nanocantilevers for detection of a single virus particle (Gupta et al. 2004). The nanocantilevers were fabricated on a p-type silicon on insulator wafer. The oxide layer was wet etched using buffered hydrofluoric acid (BHF) up to a 30 nm depth. A hybrid technique comprised of photolithography and reactive ion etching was used to pattern the cantilever beam. The etching was ceased by growing an oxide layer by means of plasma-enhanced chemical vapor deposition. BHF was used to remove the oxide layer from the side to open the windows through which silicon wafer was exposed. Finally, the cantilever beams were released through vapor phase etching using xenon difluoride. Scanning electron micrograph of the nanocantilever loaded with vaccinia virus particle is shown in Fig. 16.

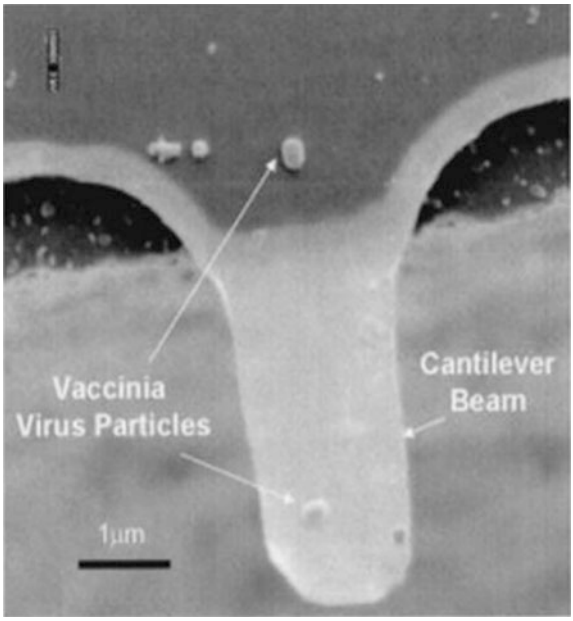

Fig. 16 SEM image of nanocantilever over which vaccinia virus particle is loaded. Reproduced from Gupta et al. (2004), with permission from AIP Publishing LLC

A nonpathogenic insect, baculovirus, has been detected using a nanoelectromechanical cantilever beam (Ilic et al. 2004). Arrays of nanomechanical free standing microcantilevers, coated with polycrystalline silicon and antibodies, were used to sense the binding of varying concentrations of baculovirus. Mechanical resonance on microcantilever-based DNA detection using gold nanoparticles has been reported (Su et al. 2003). A change in the mass of the microcantilever is induced by the DNA hybridization leading to the shift in resonance frequency of the microcantilever beam. This change is further measured. The hybridization is seen to occur through the binding of the gold nanoparticles on the microcantilever surface resulting in a chemical amplification as a result of nucleation of silver. The method reports the limit of detection of target DNA at a concentration of 0.05 nM.

DNA nanostructures have also been predominantly used for diagnostic purposes. Anisotropic, branched, and crosslinkable (ABC monomers) building blocks have been created to construct nanoarchitectures with multifunctional capabilities (Lee et al. 2009). Polymerization processes have been employed to fabricate the ABC polymeric spheres (Fig. 17). These spheres can grow only in the presence of specific target DNA molecule that leads to the detection of highly sensitive pathogens. Each ABC monomer sphere comprises of two specific quantum dots having individual ratios (1G1R). Nanoarchitectures are concocted by a combination of various quantum dots put together, with each having a unique fluorescence code. These exclusive properties enable the detection of multiple pathogens simultaneously. Three pathogens SARS, Ebola, and anthrax have been detected

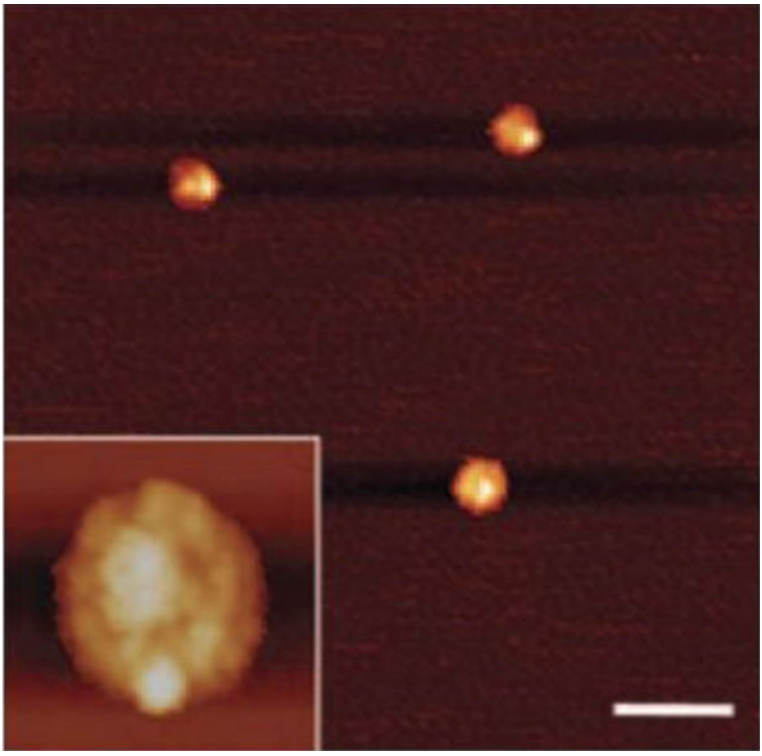

Fig. 17 AFM image of ABC polymeric spheres. A higher magnification image is shown in the inset. Scale bar, 1 μm. Reproduced from Lee et al. (2009), with permission from Macmillan Publishers Limited, part of Springer Nature

simultaneously. Distinguished relative fluorescence intensities can be visualized for detection of each pathogen (Fig. 18a–c). It has been observed that ABC polymer sphere does not construct when some unknown DNA was mixed into it (Fig. 18d).

Recently, researchers have reported the development of DNA machines (nanometer scale) that can diagnose a particular target antibody (Ranallo et al. 2015). A structural change of the DNA stems is observed when an antibody binds with the DNA nanomachines, which can also be sensed by external means or through naked eye. A light-emitting fluorophore and quencher are connected to the two single-stranded DNA stems (weak). The recognition elements capable of binding the target molecule are attached to the ends of the DNA stem. Peptides and oligonucleotides are the two most widely used recognition elements. When these elements (symbolized by the red hexagon in Fig. 19) bind to their specific target molecule, the DNA stem is broken in two parts. It separates the light-emitting fluorophore and quencher which then generate a light signal. DNA nanomachines are highly versatile and can be customized in such a way that many antibodies can

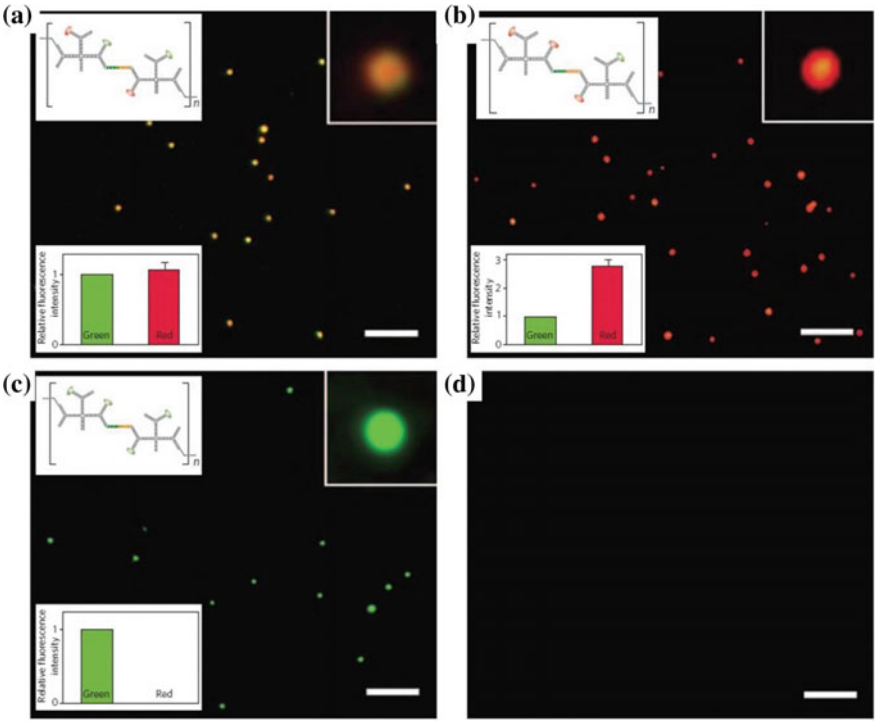

Fig. 18 **a–c** Fluorescence microscopy images of polymers with pathogen DNAs including SARS, Bacillus anthracis, and Ebola, respectively. **d** No polymerized DNA materials were observed on incubating 1G1R ABC monomers with an unrelated pathogen DNA. Scale bars, 5 μm. Reproduced from Lee et al. (2009), with permission from Macmillan Publishers Limited, part of Springer Nature

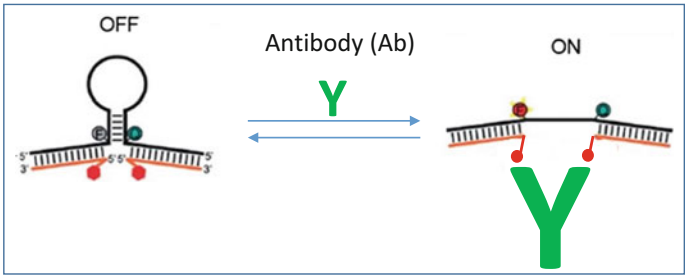

Fig. 19 Schematic diagram of antibody detection using DNA nanomachines, (F—fluorophore, and green circle denotes quencher)

be detected simultaneously with high sensitivity. Other benefits of using DNA nanomachines are that they are rapid, robust, and do not require any reagent chemicals.

Clinical diagnostic devices utilizing nanostructures have shown promise owing to their increased sensitivity, speed, portability, and inexpensive nature as compared to conventional diagnostic techniques.

4.2 Therapeutic Applications

The exponentially growing potential of nanostructures has envisaged several applications in the treatment of numerous medical ailments. ZnO nanoparticles have been used to augment the mechanical and antimicrobial properties of dental filler material (Gupta et al. 2015c). ZnO–HAP nanocomposite was fabricated by mixing ZnO nanoparticles with hydroxyapatite (HAP) using a wet chemical route through ultrasonication process. The antimicrobial properties of this nanocomposite have been investigated for *E. coli* DH5α and Streptococcus mutans, and a substantial enhancement in the antimicrobial activity has been reported. ZnO nanostructures have also been used for anticancer studies and their action against human brain tumor U87 and cervical cancer HeLa (Wahab et al. 2011). Under all effective concentrations, these nanostructures revealed reduced cytotoxicity against normal human HEK cells. ZnO nanoparticles have also shown a strong special capability to destroy cancerous T cells (Hanley et al. 2008). It has also been reported that ZnO nanostructures exhibit excellent ultraviolet blocking characteristics (Smijs and Pavel 2011; Kathirvelu et al. 2009). There are primarily three types of ultraviolet rays contained in natural sunlight, i.e., UV-A (320–400 nm), UV-B (290–320 nm), and UV-C (250–290 nm) (Vaseem et al. 2010). Among all of them, UV-A and UV-B are more dangerous as they may cause skin cancer. In order to protect the human skin from direct exposure of these rays, a ZnO–TiO_2 (titanium dioxide) nanocomposite (Smijs and Pavel 2011) has been developed in which TiO_2 blocks the UV-B rays while ZnO nanoparticles block the UV-A rays. ZnO nanoparticles have been coated on fabrics to make them UV resistant (Kathirvelu et al. 2009). Since the size of ZnO particles is in the nanometer range, it binds very well to the fabric owing to the Van der Waals force of attraction and the adhesion is retained even after multiple washings (Fig. 20).

Self-assembled amphiphilic polymer nanostructures have become efficient nanocarriers for targeted delivery of anticancer therapeutics (Wiradharma et al. 2009). Polysaccharide chitosan-based polymeric nanostructures have been employed in delivery of hydrophilic and lipophilic drugs onto the eye surfaces (de la Fuente et al. 2010). Therapeutic efficiency against pancreatic tumor has been enhanced by using a bundled assembly of helical polymeric nanostructures laden with platinum drugs (Mochida et al. 2014). Due to their structural diversity, biocompatibility, and uniformity in structures, DNA-based nanostructures have been extensively used for therapeutic applications. The growth of cancer cells has been

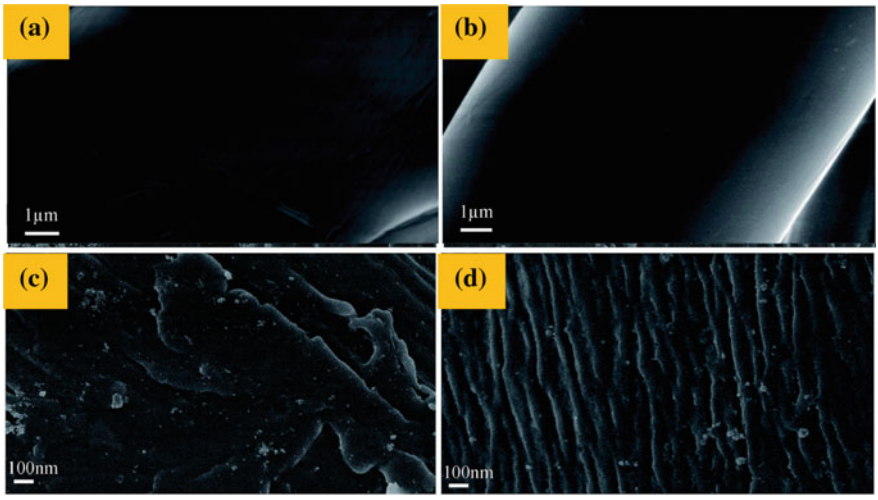

Fig. 20 FESEM images of **a**, **b** 100% cotton and **c**, **d** ZnO nanoparticles embedded fabric. Reproduced from Bușilă et al. (2015), with permission from the Royal Society of Chemistry

inhibited by combining AS1411 aptamers into DNA pyramids without using any transfection reagents (Charoenphol and Bermudez 2014).

Electroporation is a commonly used method for gene delivery, which requires high voltage ($\sim$100–500 k V/m) for DNA transfection. However, a major portion of the exposed cells are completely destroyed as a result of this high voltage. In order to overcome this problem, molecular delivery using shock wave-assisted methods has been widely employed (Lauer et al. 1997; Kodama et al. 2002). These shock waves can be generated using nanoenergetic materials, which can further be utilized for gene transfection purposes (Gangopadhyay et al. 2011; Patel et al. 2015).

The small size of the nanostructures provides the requisite potential in this domain, which is enablement of easy access to the internal parts of the body without affecting other body functions. Although they can be utilized for therapeutics, the materials that they are made of possess a potential danger to the human body. Hence, further research is required to critically analyze the biocompatibility and biodegradability of these materials.

4.3 Miscellaneous Applications

Apart from the mainstream applications of nanostructures, nanostructures have been largely explored for various other outlying areas, e.g., environmental protection, bio-imaging, water purification. For example, ZnO nanoparticles possess capabilities to remove organic dyes and hazardous materials from polluted water.

Dye-sensitized solar cells (DSSCs) utilize ZnO aggregate films as photoelectrodes (Zhang et al. 2008). Polyol-mediated precipitation of zinc acetate in diethylene glycol has been used for synthesis of ZnO aggregates. It has been found that the size of ZnO aggregates can be manipulated by controlling the concentration of zinc acetate, rate of heating, etc. The drop-cast method has been used for the fabrication of photoelectrode film by depositing the ZnO aggregates on the fluorine-doped tin oxide glass substrates. The morphologies of ZnO films at different temperatures are shown in Fig. 21.

For the fabrication of a nonvolatile memory device, conductive polymer nanostructures have been prepared from graphene oxide and poly (3,4-ethylenedioxythiophene)-poly(styrenesulfonate) (PEDOT-PSS)-based composites (Ray et al. 2015). Silver electrodes of thickness 200 nm and diameter 100 μm were deposited on the fabricated composites to examine their electrical properties. The linear voltage–current relationships of polymer nanostructures confirmed its conductive nature. Conductive polymer nanostructures can be used for harvesting energy from solar light using photocatalysis under visible light (Ghosh et al. 2015). One-dimensional nanofibers made of poly(diphenylbutadiyne) (PDPB) have been synthesized by photopolymerization using a novel soft-template approach. These nanofibers are highly efficient for degradation of pollutants under visible light. It has been observed that the nanofibers are very stable and exhibit higher photocatalytic activity than bulk PDPB. The organic pollutants such as methyl orange and phenol are highly toxic and are a threat to the ecosystem. These pollutants have been degraded by photocatalysis process. The nano-PDPB nanofibers possess good photocatalytic activity for methyl orange under visible light. A 75% degradation of methyl orange has been achieved after 240 min of irradiation. The change in morphology of PDPB nanostructures after photocatalysis is shown in Fig. 22.

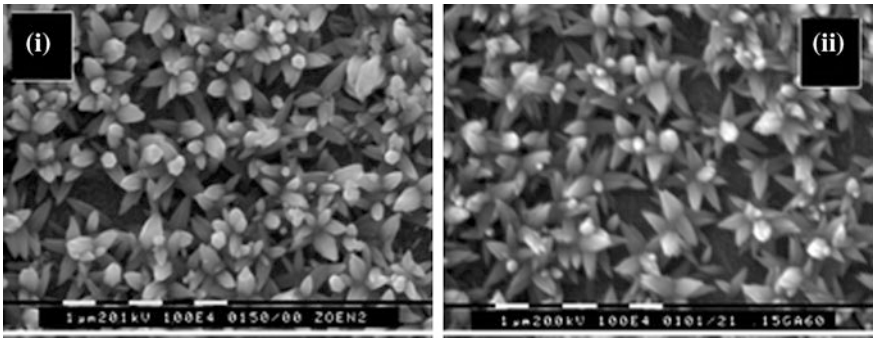

Fig. 21 Scanning electron microscopic images of developed ZnO films from en-baths (70 °C, pH 11) containing: i. zinc acetate; ii. zinc chloride. Reproduced from Govender et al. (2004), with permission from the Royal Society of Chemistry

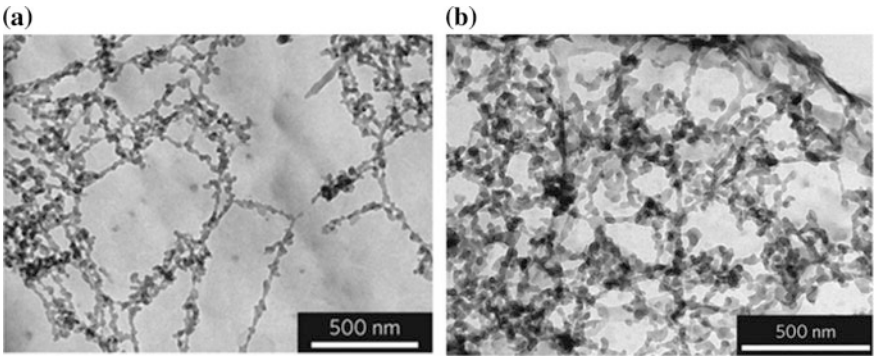

Fig. 22 **a** TEM image of fabricated PDPB nanostructures, **b** TEM image of the PDPB nanofibers after methyl orange degradation under visible light irradiation. Reproduced from Ghosh et al. (2015), with permission from Macmillan Publishers Limited, part of Springer Nature

Studies have yielded fascinating results in these domains for nanostructures made of single as well as composite nanomaterials. Such varied applications of nanostructures have enabled the advancement of the nanotechnology sector to great extents.

5 Conclusion

In this chapter, the fabrication of nanostructures by employing bottom-up approach has been described. Some basic processes used in the bottom-up approach have been discussed in detail. The latest fabrication technologies for the fabrication of ZnO nanostructures, DNA nanostructures, polymer-based nanostructures, and metal-based nanostructures have also been discussed. It is seen that these nanostructures have wide applications as, sensors (gas, bio, chemical, visible light, and ultraviolet), cosmetics, optical devices, optoelectronics, electrical devices, photo-chemistry, solar cells and light-emitting displays separation, optical storages, and drug delivery. DNA nanostructures have been utilized in drug delivery, nanoswitches, computing, etc. Owing to characteristics like high sensitivity, inexpensive, non-hazardous, and faster response to analytes, nanostructures have been employed for sensing, detection, screening of viruses, etc. It is evident that nanotechnology is an emerging field with potential to revolutionize the therapeutics and diagnostics industry. Advancements in the area of nanostructure fabrication have allowed to achieve development of highly sensitive and specific sensors. The integration of these nanostructures for therapeutic and diagnostic purposes could facilitate the engineering of improved nanostructures specific to required biomedical applications.

References

Abeyasinghe N, Kumar S, Sun K, Mansfield JF, Jin R, Goodson T III (2016) Enhanced emission from single isolated gold quantum dots investigated using two-photon-excited fluorescence near-field scanning optical microscopy. J Am Chem Soc 138(50):16299–16307

Abu-Salah KM, Ansari AA, Alrokayan SA (2010) DNA-based applications in nanobiotechnology. Biomed Res Int 2010:15

Arruebo M, Valladares M, González-Fernández Á (2009) Antibody-conjugated nanoparticles for biomedical applications. J Nanomater 2009:37

Baruah S, Thanachayanont C, Dutta J (2016) Growth of ZnO nanowires on nonwoven polyethylene fibers. Sci Technol Adv Mater 9:8

Bath J, Turberfield AJ (2007) DNA nanomachines. Nat Nanotechnol 2(5):275–284

Bauermann LP, Bill J, Aldinger F (2006) Bio-friendly synthesis of ZnO nanoparticles in aqueous solution at near-neutral pH and low temperature. J Phys Chem B 110(11):5182–5185

Beckwith KS, Cooil SP, Wells JW, Sikorski P (2015) Tunable high aspect ratio polymer nanostructures for cell interfaces. Nanoscale 7(18):8438–8450

Bellah MM, Christensen SM, Iqbal SM (2012) Nanostructures for medical diagnostics. J Nanomater 2012:2

Benenson Y (2011) Biocomputing: DNA computes a square root. Nat Nanotechnol 6(8):465–467

Biswas A, Bayer IS, Biris AS, Wang T, Dervishi E, Faupel F (2012) Advances in top–down and bottom–up surface nanofabrication: techniques, applications & future prospects. Adv Colloid Interface Sci 170(1):2–27

Broz P (2010) Contents. In: Polymer-based Nanostructures. pp P009–P015

Buşilă M, Mușat V, Textor T, Mahltig B (2015) Synthesis and characterization of antimicrobial textile finishing based on Ag: ZnO nanoparticles/chitosan biocomposites. RSC Adv 5 (28):21562–21571

Charoenphol P, Bermudez H (2014) Aptamer-targeted DNA nanostructures for therapeutic delivery. Mol Pharm 11(5):1721–1725

Chartuprayoon N, Rheem Y, Ng JC, Nam J, Chen W, Myung NV (2013) Polypyrrole nanoribbon based chemiresistive immunosensors for viral plant pathogen detection. Anal Methods 5 (14):3497–3502

Chen H, Zhang M, Li B, Chen D, Dong X, Wang Y, Gu Y (2015) Versatile antimicrobial peptide-based ZnO quantum dots for in vivo bacteria diagnosis and treatment with high specificity. Biomaterials 53:532–544

Chen J-C, Tang C-T (2007) Preparation and application of granular ZnO/Al 2 O 3 catalyst for the removal of hazardous trichloroethylene. J Hazard Mater 142(1):88–96

Chi L (2010) Nanotechnology: volume 8: nanostructured surfaces, vol 7. Wiley, Weinheim

Chiou W-T, Wu W-Y, Ting J-M (2003) Growth of single crystal ZnO nanowires using sputter deposition. Diamond Relat Mater 12(10):1841–1844

Cho A, Arthur J (1975) Molecular beam epitaxy. Prog Solid State Chem 10:157–191

Chopra N, Gavalas VG, Bachas LG, Hinds BJ, Bachas LG (2007) Functional one-dimensional nanomaterials: applications in nanoscale biosensors. Anal Lett 40(11):2067–2096

Christman KL, Enriquez-Rios VD, Maynard HD (2006) Nanopatterning proteins and peptides. Soft Matter 2(11):928–939

Ciesielski A, Palma CA, Bonini M, Samorì P (2010) Towards supramolecular engineering of functional nanomaterials: pre-programming multi-component 2D self-assembly at solid-liquid interfaces. Adv Mater 22(32):3506–3520

Daumann S, Andrzejewski D, Di Marcantonio M, Hagemann U, Wepfer S, Vollkommer F, Bacher G, Epple M, Nannen E (2017) Water-free synthesis of ZnO quantum dots for application as an electron injection layer in light-emitting electrochemical cells. J Mater Chem C 5(9):2344–2351

de la Fuente M, Raviña M, Paolicelli P, Sanchez A, Seijo B, Alonso MJ (2010) Chitosan-based nanostructures: a delivery platform for ocular therapeutics. Adv Drug Deliv Rev 62(1):100–117

Demortiere A, Launois P, Goubet N, Albouy P-A, Petit C (2008) Shape-controlled platinum nanocubes and their assembly into two-dimensional and three-dimensional superlattices. J Phys Chem B 112(46):14583–14592

Djurišić AB, Chen X, Leung YH, Ng AMC (2012) ZnO nanostructures: growth, properties and applications. J Mater Chem 22(14):6526–6535

Dutta PK, Dutta J, Tripathi V (2004) Chitin and chitosan: chemistry, properties and applications. J Sci Ind Res 63(1):20–31

Elbaz J, Lioubashevski O, Wang F, Remacle F, Levine RD, Willner I (2010) DNA computing circuits using libraries of DNAzyme subunits. Nat Nanotechnol 5(6):417–422

Fan X, Zhang ML, Shafiq I, Zhang WJ, Lee CS, Lee ST (2009) ZnS/ZnO heterojunction nanoribbons. Adv Mater 21(23):2393–2396

Feldkamp U, Niemeyer CM (2006) Rational design of DNA nanoarchitectures. Angew Chem Int Ed 45(12):1856–1876

Gangopadhyay S, Apperson S, Gangopadhyay K, Bezmelnitsyn A, Thiruvengadathan R, Kraus M, Shende R, Hossain M, Subramanian S, Bhattacharya S (2011) Shock wave and power generation using on-chip nanoenergetic material. US Patent U.S. Patent 8,066,831

Gao P, Wang ZL (2004) Nanopropeller arrays of zinc oxide. Appl Phys Lett 84:2883–2885

Gentile A, Ruffino F, Grimaldi MG (2016) Complex-morphology metal-based nanostructures: fabrication, characterization, and applications. Nanomaterials 6(6):110

Ghosh S, Kouamé NA, Ramos L, Remita S, Dazzi A, Deniset-Besseau A, Beaunier P, Goubard F, Aubert P-H, Remita H (2015) Conducting polymer nanostructures for photocatalysis under visible light. Nat Mater 14(5):505–511

Govender K, Boyle DS, Kenway PB, O'Brien P (2004) Understanding the factors that govern the deposition and morphology of thin films of ZnO from aqueous solution. J Mater Chem 14 (16):2575–2591

Gupta A, Akin D, Bashir R (2004) Single virus particle mass detection using microresonators with nanoscale thickness. Appl Phys Lett 84(11):1976–1978

Gupta A, Mondal K, Sharma A, Bhattacharya S (2015a) Superhydrophobic polymethyl-silsesquioxane pinned one dimensional ZnO nanostructures for water remediation through photo-catalysis. RSC Adv 5(57):45897–45907

Gupta A, Nayak M, Singh D, Bhattacharya S (2014a) Antibody immobilization for ZnO nanowire based biosensor application. In: MRS proceedings. Cambridge University Press, pp 33–39

Gupta A, Pandey S, Nayak M, Maity A, Majumder SB, Bhattacharya S (2014b) Hydrogen sensing based on nanoporous silica-embedded ultra dense ZnO nanobundles. RSC Adv 4(15):7476–7482

Gupta A, Pandey SS, Bhattacharya S (2013) High aspect ZnO nanostructures based hydrogen sensing. In: Proceeding of international conference on recent trends in applied physics and material science: RAM 2013, vol 1. AIP Publishing, pp 291–292

Gupta A, Saurav JR, Bhattacharya S (2015b) Solar light based degradation of organic pollutants using ZnO nanobrushes for water filtration. RSC Adv 5(87):71472–71481

Gupta A, Singh D, Raj P, Gupta H, Verma S, Bhattacharya S (2015c) Investigation of ZnO-hydroxyapatite nanocomposite incorporated in restorative glass ionomer cement to enhance its mechanical and antimicrobial properties. J Bionanosci 9(3):190–196

Han MG, Foulger SH (2006) Facile synthesis of poly (3, 4-ethylenedioxythiophene) nanofibers from an aqueous surfactant solution. Small 2(10):1164–1169

Hanley C, Layne J, Punnoose A, Reddy K, Coombs I, Coombs A, Feris K, Wingett D (2008) Preferential killing of cancer cells and activated human T cells using ZnO nanoparticles. Nanotechnology 19(29):295103

Hench LL, West JK (1990) The sol-gel process. Chem Rev 90(1):33–72

Heo Y, Varadarajan V, Kaufman M, Kim K, Norton D, Ren F, Fleming P (2002) Site-specific growth of ZnO nanorods using catalysis-driven molecular-beam epitaxy. Appl Phys Lett 81 (16):3046–3048

Hu H, Onyebueke L, Abatan A (2010) Characterizing and modeling mechanical properties of nanocomposites-review and evaluation. J Miner Mater Charact Eng 9(04):275

Hu M, Gao J, Dong Y, Yang S, Li RK (2012) Rapid controllable high-concentration synthesis and mutual attachment of silver nanowires. RSC Adv 2(5):2055–2060

Hu W, Liu Y, Chen T, Liu Y, Li CM (2015) Hybrid ZnO nanorod-polymer brush hierarchically nanostructured substrate for sensitive antibody microarrays. Adv Mater 27(1):181–185

Huang MH, Wu Y, Feick H, Tran N, Weber E, Yang P (2001) Catalytic growth of zinc oxide nanowires by vapor transport. Adv Mater 13(2):113–116

Huang Y, Zhang Y, Bai X, He J, Liu J, Zhang X (2006) Bicrystalline zinc oxide nanocombs. J Nanosci Nanotechnol 6(8):2566–2570

Ilic B, Yang Y, Craighead H (2004) Virus detection using nanoelectromechanical devices. Appl Phys Lett 85(13):2604–2606

Jagur-Grodzinski J (2003) Biomedical applications of polymers 2001–2002. e-Polymers 3(1):141–176c

Jiang J, Li Y, Liu J, Huang X, Yuan C, Lou XWD (2012) Recent advances in metal oxide-based electrode architecture design for electrochemical energy storage. Adv Mater 24(38):5166–5180

Kathirvelu S, D'souza L, Dhurai B (2009) UV protection finishing of textiles using ZnO nanoparticles. Indian J Fibre Text Res 34(3):267–273

Kodama T, Doukas AG, Hamblin MR (2002) Shock wave-mediated molecular delivery into cells. biochimica et biophysica acta (BBA)-molecular. Cell Res 1542(1):186–194

Kolmakov A, Chen X, Moskovits M (2008) Functionalizing nanowires with catalytic nanoparticles for gas sensing application. J Nanosci Nanotechnol 8(1):111–121

Kong XY, Wang ZL (2003) Spontaneous polarization-induced nanohelixes, nanosprings, and nanorings of piezoelectric nanobelts. Nano Lett 3(12):1625–1631

Kumar S, Bhushan P, Bhattacharya S (2016) Development of a paper-based analytical device for colorimetric detection of uric acid using gold nanoparticles–graphene oxide (AuNPs–GO) conjugates. Anal Methods 8(38):6965–6973. https://doi.org/10.1039/c6ay01926a

Kumar S, Bhushan P, Bhattacharya S (2017) Facile synthesis of Au@Ag–Hemin decorated reduced graphene oxide sheets: a novel peroxidase mimetic for ultrasensitive colorimetric detection of hydrogen peroxide and glucose. RSC Adv 7:37568–37577. https://doi.org/10.1039/c7ra06973a

Kumar S, Dubey AK, Pandey AK (2013a) Computer-aided genetic algorithm based multi-objective optimization of laser trepan drilling. Int J Precis Eng Manuf 14(7):1119–1125

Kumar SS, Venkateswarlu P, Rao VR, Rao GN (2013b) Synthesis, characterization and optical properties of zinc oxide nanoparticles. Int Nano Lett 3(1):1–6

Lauer U, Bürgelt E, Squire Z, Messmer K, Hofschneider P, Gregor M, Delius M (1997) Shock wave permeabilization as a new gene transfer method. Gene therapy 4(7):710–715

Lee J, Lee J, Yeon SM, Min S, Kim J, Choi H, Kim S, Koo J, Kim K, Park SH (2014) Assembling CdSe/ZnS core–shell quantum dots on localized DNA nanostructures. RSC Adv 4(95):53201–53205

Lee JB, Roh YH, Um SH, Funabashi H, Cheng W, Cha JJ, Kiatwuthinon P, Muller DA, Luo D (2009) Multifunctional nanoarchitectures from DNA-based ABC monomers. Nat Nanotechnol 4(7):430–436

Lévy-Clément C, Elias J, Tena-Zaera R (2009) ZnO/CdSe nanowires and nanotubes: formation, properties and applications. physica status solidi (c) 6(7):1596–1600

Li D, Xia Y (2004) Electrospinning of nanofibers: reinventing the wheel? Adv Mater 16 (14):1151–1170

Lian Z, Wang W, Xiao S, Li X, Cui Y, Zhang D, Li G, Li H (2015) Plasmonic silver quantum dots coupled with hierarchical TiO2 nanotube arrays photoelectrodes for efficient visible-light photoelectrocatalytic hydrogen evolution. Sci Rep 5:10461

Liang HW, Liu S, Yu SH (2010) Controlled synthesis of one-dimensional inorganic nanostructures using pre-existing one-dimensional nanostructures as templates. Adv Mater 22(35):3925–3937
Liang Z-H, Zhu Y-J, Hu X-L (2004) β-nickel hydroxide nanosheets and their thermal decomposition to nickel oxide nanosheets. J Phys Chem B 108(11):3488–3491
Ma J, Zhan M (2014) Rapid production of silver nanowires based on high concentration of $AgNO_3$ precursor and use of $FeCl_3$ as reaction promoter. RSC Adv 4(40):21060–21071
Martin CR (1995) Template synthesis of electronically conductive polymer nanostructures. Acc Chem Res 28(2):61–68
Martin CR (1996) Membrane-based synthesis of nanomaterials. Chem Mater 8(8):1739–1746
Meng L, Lu Y, Wang X, Zhang J, Duan Y, Li C (2007) Facile synthesis of straight polyaniline nanostick in hydrogel. Macromolecules 40(9):2981–2983
Mijatovic D, Eijkel J, Den Van, Berg A (2005) Technologies for nanofluidic systems: top-down versus bottom-up—a review. Lab Chip 5(5):492–500
Mochida Y, Cabral H, Miura Y, Albertini F, Fukushima S, Osada K, Nishiyama N, Kataoka K (2014) Bundled assembly of helical nanostructures in polymeric micelles loaded with platinum drugs enhancing therapeutic efficiency against pancreatic tumor. ACS Nano 8(7):6724–6738
Modi S, Swetha M, Goswami D, Gupta GD, Mayor S, Krishnan Y (2009) A DNA nanomachine that maps spatial and temporal pH changes inside living cells. Nat Nanotechnol 4(5):325–330
Nayak M, Singh D, Singh H, Kant R, Gupta A, Pandey SS, Mandal S, Ramanathan G, Bhattacharya S (2013) Integrated sorting, concentration and real time PCR based detection system for sensitive detection of microorganisms. Sci Rep 3:3266
Parthasarathy RV, Martin CR (1994) Synthesis of polymeric microcapsule arrays and their use for enzyme immobilization. Nature 369(6478):298
Pashchanka M, Hoffmann RC, Gurlo A, Schneider JJ (2010) Molecular based, chimie douce approach to 0d and 1d indium oxide nanostructures. Evaluation of their sensing properties towards co and h 2. J Mater Chem 20(38):8311–8319
Patel VK, Saurav JR, Gangopadhyay K, Gangopadhyay S, Bhattacharya S (2015) Combustion characterization and modeling of novel nanoenergetic composites of Co_3O_4/nAl. RSC Adv 5 (28):21471–21479
Peacock A (2000) Handbook of polyethylene: structures: properties, and applications. CRC Press, Boca Raton, FL
Petryayeva E, Krull UJ (2011) Localized surface plasmon resonance: nanostructures, bioassays and biosensing—a review. Anal Chim Acta 706(1):8–24
Qiu Y, Yang S (2007) ZnO nanotetrapods: controlled vapor-phase synthesis and application for humidity sensing. Adv Funct Mater 17(8):1345–1352
Ran T, Kaplan S, Shapiro E (2009) Molecular implementation of simple logic programs. Nat Nanotechnol 4(10):642–648
Ranallo S, Rossetti M, Plaxco KW, Vallée-Bélisle A, Ricci F (2015) A modular, DNA-based beacon for single-step fluorescence detection of antibodies and other proteins. Angew Chem 127(45):13412–13416
Ray SC, Bhunia SK, Saha A, Jana NR (2015) Graphene oxide (GO)/reduced-GO and their composite with conducting polymer nanostructure thin films for non-volatile memory device. Microelectron Eng 146:48–52
Rothemund PW (2005) Design of DNA origami. In: Proceedings of the 2005 IEEE/ACM international conference on computer-aided design, 2005. IEEE Computer Society, pp 471–478
Seeman NC (2010) Nanomaterials based on DNA. Annu Rev Biochem 79:65
Smijs TG, Pavel S (2011) Titanium dioxide and zinc oxide nanoparticles in sunscreens: focus on their safety and effectiveness. Nanotechnol Sci Appl 4:95
Song H, Zhang W, Cheng C, Tang Y, Luo L, Chen X, Luan C, Meng X, Zapien J, Wang N (2010) Controllable fabrication of three-dimensional radial ZnO nanowire/silicon microrod hybrid architectures. Cryst Growth Des 11(1):147–153

Song J, Lu H, Li S, Tan L, Gruverman A, Ducharme S (2015) Fabrication of ferroelectric polymer nanostructures on flexible substrates by soft-mold reverse nanoimprint lithography. Nanotechnology 27(1):015302
Su M, Li S, Dravid VP (2003) Microcantilever resonance-based DNA detection with nanoparticle probes. Appl Phys Lett 82(20):3562–3564
Sun T, Qiu J, Liang C (2008) Controllable fabrication and photocatalytic activity of ZnO nanobelt arrays. J Phys Chem C 112(3):715–721
Sun Y, Fuge GM, Ashfold MN (2004) Growth of aligned ZnO nanorod arrays by catalyst-free pulsed laser deposition methods. Chem Phys Lett 396(1):21–26
Sun Y, Fuge GM, Fox NA, Riley DJ, Ashfold MN (2005) Synthesis of aligned arrays of ultrathin ZnO nanotubes on a Si wafer coated with a thin ZnO film. Adv Mater 17(20):2477–2481
Sun Y, Kiang C-H (2005) DNA-based artificial nanostructures: Fabrication, properties, and applications. vol 2. American Scientific Publishers, Houston, TX
Tian ZR, Voigt JA, Liu J, Mckenzie B, Mcdermott MJ, Rodriguez MA, Konishi H, Xu H (2003) Complex and oriented ZnO nanostructures. Nat Mater 2(12):821–826
Vaseem M, Umar A, Hahn Y-B (2010) ZnO nanoparticles: growth, properties, and applications, vol 5. American Scientific Publishers, New York
Vayssieres L (2003) Growth of arrayed nanorods and nanowires of ZnO from aqueous solutions. Adv Mater 15(5):464–466
Venkataraman S, Dirks RM, Rothemund PW, Winfree E, Pierce NA (2007) An autonomous polymerization motor powered by DNA hybridization. Nat Nanotechnol 2(8):490–494
Wahab R, Kaushik NK, Verma AK, Mishra A, Hwang I, Yang Y-B, Shin H-S, Kim Y-S (2011) Fabrication and growth mechanism of ZnO nanostructures and their cytotoxic effect on human brain tumor U87, cervical cancer HeLa, and normal HEK cells. J Biol Inorg Chem 16(3):431–442
Wan M (2008) A template-free method towards conducting polymer nanostructures. Adv Mater 20 (15):2926–2932
Wang L, Sun Y, Li Z, Wu A, Wei G (2016) Bottom-up synthesis and sensor applications of biomimetic nanostructures. Materials 9(1):53
Wang X, Kong X, Yu Y, Zhang H (2007) Synthesis and characterization of water-soluble and bifunctional ZnO-Au nanocomposites. J Phys Chem C 111(10):3836–3841
Wang Y, Xia Y (2004) Bottom-up and top-down approaches to the synthesis of monodispersed spherical colloids of low melting-point metals. Nano Lett 4(10):2047–2050
Whitesides GM, Mathias JP, Seto CT (1991) Molecular self-assembly and nanochemistry: a chemical strategy for the synthesis of nanostructures. Science 254(5036):1312–1319
Wiradharma N, Zhang Y, Venkataraman S, Hedrick JL, Yang YY (2009) Self-assembled polymer nanostructures for delivery of anticancer therapeutics. Nano Today 4(4):302–317
Wu G, Xie T, Yuan X, Li Y, Yang L, Xiao Y, Zhang L (2005) Controlled synthesis of ZnO nanowires or nanotubes via sol–gel template process. Solid State Commun 134(7):485–489
Xia Y, Xiong Y, Lim B, Skrabalak SE (2009) Shape-controlled synthesis of metal nanocrystals: simple chemistry meets complex physics? Angew Chem Int Ed 48(1):60–103
Yan H, Park SH, Finkelstein G, Reif JH, LaBean TH (2003) DNA-templated self-assembly of protein arrays and highly conductive nanowires. Science 301(5641):1882–1884
Yang Y, Wu D, Han S, Hu P, Liu R (2013) Bottom-up fabrication of photoluminescent carbon dots with uniform morphology via a soft–hard template approach. Chem Commun 49 (43):4920–4922
Yao B, Chan Y, Wang N (2002) Formation of ZnO nanostructures by a simple way of thermal evaporation. Appl Phys Lett 81(4):757–759
Yin Z, Zheng Q (2012) Controlled synthesis and energy applications of one-dimensional conducting polymer nanostructures: an overview. Adv Energy Mater 2(2):179–218
Zhang B, Liu J, Guan S, Wan Y, Zhang Y, Chen R (2007) Synthesis of single-crystalline potassium-doped tungsten oxide nanosheets as high-sensitive gas sensors. J Alloys Compd 439 (1):55–58

Zhang J, Liu J, Peng Q, Wang X, Li Y (2006) Nearly monodisperse Cu_2O and CuO nanospheres: preparation and applications for sensitive gas sensors. Chem Mater 18(4):867–871
Zhang Q, Chou TP, Russo B, Jenekhe SA, Cao G (2008) Aggregation of ZnO nanocrystallites for high conversion efficiency in dye-sensitized solar cells. Angew Chem 120(13):2436–2440
Zhang Q, Dandeneau CS, Zhou X, Cao G (2009) ZnO nanostructures for dye-sensitized solar cells. Adv Mater 21(41):4087–4108

Chapter 9
Miniaturized Sensors and Actuators for Biological Studies on Small Model Organisms of Disease

Khaled Youssef, Pouriya Bayat, Amir Reza Peimani, Sina Dibaji and Pouya Rezai

Abstract The process of discovering a drug is extremely time consuming and expensive, requiring extensive biochemical screening assays on cells and animal models of human diseases. Small organisms such as *Caenorhabditis elegans* (worm), *Drosophila melanogaster* (fruit fly), and *Danio rerio* (zebrafish) are among the top models used for investigation of disease pathology and the search for therapeutics. These model organisms offer many advantages including simplicity, genetic homology to humans, body transparency, and amenability to genetic manipulation which are desirable for investigation of various neurobehavioral processes in a whole biological system. However, the conventional manual or equipment-intensive methods for organism-based assays are slow, low-throughput and mostly qualitative, due to the lack of technologies to facilitate automation, control and quantitative analysis on these models. In this chapter, we will review the microsystems developed to date for worm, fruit fly, and zebrafish studies with a focus on providing basic information about these model organisms, followed by an introduction of microfluidic devices developed for studying the organisms'

The authors Pouriya Bayat and Amir Reza Peimani contributed equally to this chapter.

K. Youssef · P. Bayat · A. R. Peimani · S. Dibaji · P. Rezai (✉)
Department of Mechanical Engineering, York University, BRG 433B, 4700 Keele Street, M3J 1P3 Toronto, ON, Canada
e-mail: prezai@yorku.ca

K. Youssef
e-mail: kyoussef@yorku.ca

P. Bayat
e-mail: pouriya@yorku.ca

A. R. Peimani
e-mail: peimani@yorku.ca

S. Dibaji
e-mail: sdibaji@yorku.ca

S. Bhattacharya et al. (eds.), *Environmental, Chemical and Medical Sensors*, Energy, Environment, and Sustainability, https://doi.org/10.1007/978-981-10-7751-7_9

neuronal and behavioral responses to various environmental cues such as chemicals, electrical signals, mechanical forces and light, to name a few. It is anticipated that these microfluidic devices will play a major role in facilitating fundamental disease investigations and drug discovery assays involving small-scale model organisms.

Keywords Organism-on-a-chip · Microfluidics · Microsystems
Caenorhabditis elegans · *Drosophila melanogaster* · *Danio rerio*
Neuronal screening · Behavioral screening

1 Introduction

The process of discovering a drug is extremely time consuming and expensive. The optimized lead chemicals that are developed during preclinical in vitro assays in drug discovery usually fail at in vivo stages of screening, mainly due to the toxicity effects. So far, the search for in vitro and in vivo models that better recapitulate disease pathology has resulted in the introduction of 3D cell cultures, organoids, and small-scale whole biological organisms that have a great potential to fill in the gap in between conventional 2D cell cultures and complex animal models in drug discovery.

The most widely used small-scale group of model organisms is *Caenorhabditis elegans* (worm), *Drosophila melanogaster* (fruit fly), and *Danio rerio* (zebrafish). These organisms offer several advantages such as cellular and neuronal simplicity, genetic homology to humans, rapid and low-cost growth and maintenance in labs, body transparency for microscopy, and amenability to genetic manipulation for the investigation of various neurobehavioral processes in a whole biological organism. Models of these organisms for studying human diseases have already been developed and helped to expand the fundamental understanding of disease pathology and the search for drugs (Bilen and Bonini 2005; Kaletta and Hengartner 2006; Seth et al. 2013). Nonetheless, despite many advantages offered by these organisms, technological deficiencies in achieving automated, high throughput, simple and low-cost screening assays have hindered the widespread use of these models in the drug discovery arena.

Microfluidics is the science and technology of handling fluids at the micrometer to millimeter scale using microfabricated and micromachined components such as channels, chambers, valves, and pumps (Whitesides 2006). It has successfully led to the introduction of major scientific and technological breakthroughs in studying various molecular, cellular, and behavioral processes in the above-mentioned organisms. Some of the advantages provided by microfluidic devices are precise control on handling the organisms and chemicals, automation of assays, enhancement of throughput, lowering the consumption of biochemicals, and making complex biological experiments simple, and convenient for the end users. By the

integration of various actuation and sensing mechanisms on these microfluidic devices, researchers have been able to perform laboratory-based manual assays automatically on a chip with enhanced precision and accuracy in quantifying complex behaviors or cellular processes in model organisms.

In this chapter, we introduce the above-mentioned miniaturized microsystems, with a focus on microfluidic-based sensors and actuators that have been developed over the past two decades, to facilitate neurobehavioral screening of model organisms including *C. elegans*, *D. melanogaster,* and *D. rerio*. We categorize the chapter based on the organism type, then introduce the advantages offered by each model, followed by a review of microsystems developed to date for studying each model's responses to various environmental cues including chemicals, mechanical forces, thermal actuations, optical stimulations, and acoustic waves. We report the major findings with respect to the nature of responses that can have neuron, organ and/or behavior basis for each model organism. We hope that the content of the chapter will shed light on the state-of-the-art microsystem technologies developed for the investigation of biological processes and disease pathologies in simple model organisms, hence, providing advanced platforms for implementation in the cycle of drug discovery to search for therapeutics in a faster and more efficient way.

2 Microsystems for *Caenorhabditis elegans* Studies

C. elegans or the roundworm is a versatile model organism which offers many experimental advantages such as small size (<1 mm length), rapid growth, and body transparency which enhance its amenability to high-throughput screening and cellular and molecular visualization using fluorescent imaging (Rezai et al. 2012a; Bakhtina and Korvink 2014; Spieth et al. 2014; Gupta and Rezai 2016; Mackinnon 2016; Muthaiyan Shanmugam and Subhra Santra 2016). In contrast to mammalian animals, *C. elegans* reproduces in a short life cycle of approximately 3 days and it is easier to be maintained in the laboratory conditions. This makes the worm one of the most cost-effective whole model organisms for system biology and disease studies. Moreover, the worm's genome has been fully sequenced showing a high degree of genetic similarity to humans. *C. elegans* has a simple nervous system with various sensory neurons which are affected by the environmental stimuli such as chemicals, electrical signals, temperature, and light. Accordingly, *C. elegans* has been proven to be a powerful tool for understanding of the neuronal pathways underlying these sensory mechanisms. In addition, phenotypic screening of *C. elegans'* dynamic behavior and locomotion provides a comprehensive tool for studying different diseases that involve motor output dysfunctions. Therefore, it is inevitable that a variety of microsystems have been developed to manipulate and analyze the neurobehavioral responses of *C. elegans* to various external stimulations. These advancements are reviewed in this section.

2.1 *Microsystems for* C. elegans *Manipulation*

Due to the small-sized worm's continuous crawling and swimming behavior, its manipulation poses a significant challenge in performing accurate and high-throughput assays. Some of the most challenging unit operations during the manipulation process are immobilization, body orientation, spatiotemporal stimulus exposure, and sorting of the worms. Conventionally, researchers restrain the worm's motion by glue (Kerr et al. 2000) or in between two coverslips coated with agarose while adding M9 buffer solution containing anesthetics (Carr et al. 2011; Chung et al. 2011; Mondal et al. 2011; Liu et al. 2013). Despite their common use, these low-throughput methods are slow, irreversible, and inapplicable for long-term immobilization of the worm. Many microfluidic devices, involving a variety of mechanical, chemical, and electrical approaches, have been developed to address the above challenges in *C. elegans* manipulation (Gupta and Rezai 2016).

Mechanical immobilization of *C. elegans* has been conducted through application of pressure on the worm's body and trapping it in a microchannel. A method used by Hulme et al. (2007) and Lee et al. (2014) was to insert the worm into a tapered microchannel to restrict its motion in a reversible manner. However, because of the complications created as a result of the high-level pressure applied on the worm and the amenability of tapered channels to clogging, researchers have successfully developed an alternate technique involving the deflection of a flexible polydimethylsiloxane (PDMS) membrane onto the worm's body to immobilize it at the side of a microchannel (Guo et al. 2008; Chokshi et al. 2009; Crane et al. 2009; Ma et al. 2009; Gilleland et al. 2010; Mondal et al. 2011). Generally, these devices consist of two PDMS layers separated by a flexible PDMS membrane (Fig. 9.1a). One layer contains the immobilization channel, and the other holds the pneumatic actuation channels for spatial control over the membrane deflection to immobilize the worm at the side of microchannel. Despite providing more control on immobilization, the multilayer nature of the device and the required pneumatic pressure impose some challenges in fabricating and operating the devices. Another mechanical immobilization technique, introduced by Rohde et al. (2007) and McCormick et al. (2011), utilized tiny side channels with negative actuation pressure along the main microchannel to immobilize *C. elegans* longitudinally (Fig. 9.1b). In addition, several researchers have developed hybrid microfluidic chips integrating suction channels with a flexible membrane (Rohde et al. 2007; Zeng et al. 2008; Gilleland et al. 2010) or a tapering channel (Ardeshiri et al. 2016b) to be able to carry on precise immobilization of the worm during the investigation periods. Another mechanical approach recently introduced by Dong et al. (2017) involves two microfluidics devices for worm immobilization. One device took advantage of PDMS elasticity by applying tensile stresses perpendicular to the channel in order to securely immobilize and align the worm in the deflecting channel. The second device relied on a height adjustable chip involving compressive stress applied to a PDMS crescent-shaped micropillar array. By

adjusting the height and spacing between the pillars, the authors were able to tightly immobilize the worms at all development stages.

Chemicals have been commonly used for worm immobilization. Chokshi et al. (2009) and Mondal et al. (2011) studied the effect of carbon dioxide (CO_2) on worm motility by developing a simple microfluidic device for single worm immobilization. Owing to the porosity of PDMS and diffusion of CO_2 through it, the researchers succeeded in ceasing the worm's movement for longer terms (1–2 h) without harming the animal compared to short-term (minutes) purely mechanical immobilization (Fig. 9.1a). However, the lethality rate for CO_2-based immobilization extending beyond 3 h was reported to be high. Recently, Wang et al. (2017) showed the possibility of applying nitrogen (N_2) gas to gently dehydrate the worm's surface, and hence creating a quiescent state to immobilize the worm. By investigating the survival rate and analyzing DAF-16 distribution, this method proved to be viable for immobilizing the worm for up to 20 min.

Krajniak and Lu (2010) and Aubry et al. (2015) introduced the use of Pluronic F127, a biocompatible polymer, for the worm immobilization. In this technique, the gel was passed into the worm-containing culture chambers to immobilize *C. elegans* by controlling the gel's temperature and mechanical properties using hot water. Other techniques used for immobilization include using a 4 °C cooling liquid through a control layer over the worm (Chung et al. 2008; Chung and Lu 2009) and increasing the body temperature of worm up to 37 °C using an optoelectric microchip (Chuang et al. 2013). In the later microchip, laser irradiation in presence of electric field was used to induce a sublethal temperature, referred to as knock-down temperature (31–37 °C), on the worm body which resulted in a temporary shutdown of worm's neuronal functions and reversible contact-free immobilization. One of the other very commonly used vehicles that have been used to encapsulate and manipulate *C. elegans* is microdroplets. A variety of microfluidic-based methods such as co-flow and flow focusing techniques have been used to generate microdroplets in which worms can be encapsulated, chemically treated, and assayed either at individual organism or high-throughput multi-organism levels (Clausell-Tormos et al. 2008; Shi et al. 2008; Neuži et al. 2012).

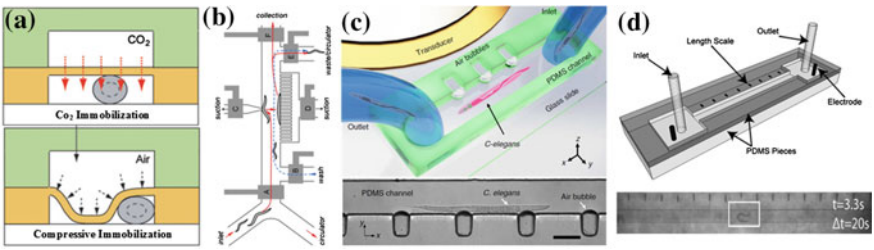

Fig. 9.1 *C. elegans* manipulation approaches in microfluidic devices involving **a** gas infusion and flexible membrane (Chokshi et al. 2009) and **b** side channel suction (Rohde et al. 2007) for immobilization; and **c** acoustic waves (Ahmed et al. 2016), and **d** alternating current electrical fields (Rezai et al. 2010c) for lateral and longitudinal orientation, respectively

In addition to immobilization, orienting the worm in the desired longitudinal and lateral directions has also been a focus of several studies. For instance, using a piezoelectric transducer (Fig. 9.1c), an acoustic-based on-chip manipulation approach was developed to trap and rotate the worm without inducing any physiological defects (Ding et al. 2012; Ahmed et al. 2016). We also achieved lateral orientation of the worm by a rotatable glass capillary that was integrated with a tapering *C. elegans* trap channel for multidirectional imaging of the worm (Ardeshiri et al. 2016b). Furthermore, we (Rezai et al. 2010c) demonstrated that direct and alternate current electric fields at various frequencies in a microchannel (Fig. 9.1d) can also be applied to orient the worm longitudinally or stop its locomotion for any desired period of time.

All in all, it is presumed that orientation and immobilization will continue to be inevitable unit operations for *C. elegans* studies. Nevertheless, the choice of proper manipulation technique heavily depends on the desired assay and the post-manipulation readout signals, as described in the next sections.

2.2 Electrical Screening Microsystems

Microfluidic devices have been used for investigating the response of *C. elegans* to electric field, dubbed electrotaxis, or galvanotaxis. Electrotaxis of the worm in a straight microchannel (Fig. 9.1d) toward the negative pole of direct and asymmetric-alternating current electrical fields were demonstrated by us (Rezai et al. 2010b, c). We showed that electrotaxis is mediated by certain sensory neurons. Recently, multiple microfluidic platforms have been developed to help either sort the worms electrotactically based on their age and mutation (Manière et al. 2011; Rezai et al. 2012b; Han et al. 2012; Wang et al. 2015) or screen the effects of various chemicals on them using electrotaxis readout (Rezai et al. 2010a; Salam et al. 2013; Tong et al. 2013; Chuang et al. 2016; Liu et al. 2016; Shanmugam 2017).

We successfully designed two side-by-side microfluidic chambers (Rezai et al. 2012b), interconnected with small microchannels, and applied an electric field between the chambers (Fig. 9.2a). A mixed population of worms injected into one of the chambers was stimulated electrotactically to move toward the microchannels. Inside the microchannels, the electric field was elevated to a certain level that was intolerable to the older worms, while younger ones could pass through and get sorted in the device. This device was effectively used for age- and mutant-based sorting of *C. elegans*. Han et al. (2012) also demonstrated the electrotactic sorting of the worms in a microfluidic device. Applying an electric field along the channel, this device consisted of parallel arrays of micro-bump channels (Fig. 9.2b) optimized to only allow a targeted size of the worms swim continuously. To simultaneously separate worm mixtures, Wang et al. (2015) exploited a phenomenon called "deflecting electrotaxis" in a device including a loading chamber and multiple symmetric sorting channels with different angles (Fig. 9.2c). Depending on their

size, the worms moved in specific angles, determined by the strength of electric field, and got sorted based on their developmental stages in the device.

Jung et al. (2016) designed a microfluidic device to assess the undulatory motion of *C. elegans* by measuring the average speed of the worms using the change in resistance of a flexible electrode. The device included three PDMS layers, irreversibly bonded with O_2 plasma. The first layer contained a main sinusoidal channel conforming to the wavy motion of the worm. The electrode was located on the second layer which was fabricated by Cr and Au sputtering. The third layer included a simple channel to allow the deflection of electrode caused by the worm motion. The velocity of worm was correlated with changes in the electrical resistance of channel which could easily be recorded with this device.

2.3 Chemical Screening Microsystems

C. elegans has the ability to sense and differentiate among a wide range of chemical compounds via two types of organs, i.e., amphids and phasmids which are located near the anterior and posterior regions of the worm. To investigate the chemosensation of *C. elegans*, several microfluidic devices have been developed to date that facilitate the analyzes of the worm's sensory-motor responses to different compounds which are precisely controlled within these devices. Sensory responses have been studied using microscopic imaging of transient fluorescent signals in various neurons (Zimmer et al. 2009) and electrophysiological screening of neuromuscular events (Lockery et al. 2012). Behavioral assessments have mostly involved investigation of *C. elegans* locomotion inside the channel by quantifying various subtle phenotypes such as speed, body bend frequency, omega turn time, and many more.

Different chemicals such as a variety of anesthetics (e.g., levamisole ad sodium azide) (Carr et al. 2011; Chung et al. 2011; Mondal et al. 2011; Liu et al. 2013), odors (Zhang et al. 2005b; Chronis et al. 2007; Chalasani et al. 2008; Luo et al. 2008; Albrecht and Bargmann 2011), zinc ion (Zn^{2+}), and glucose (Song et al. 2015) have been carefully examined to investigate their effects on the worm movement

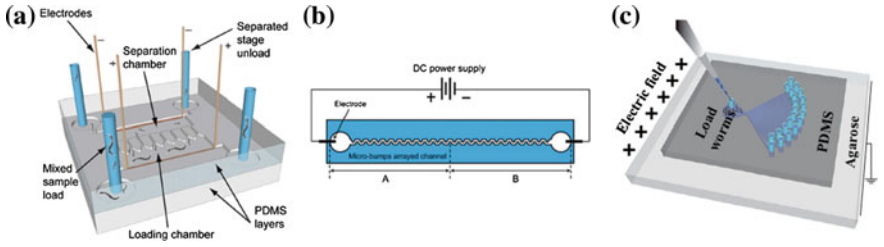

Fig. 9.2 Schematic illustration of different electric microfluidic devices for *C. elegans* sorting (Rezai et al. 2012b; Han et al. 2012; Wang et al. 2015)

behavior. The electrotaxis method introduced in the previous section has been used as a tool to induce movement on-demand for behavior investigations (Carr et al. 2011; Salam et al. 2013). These devices can find applications in high-throughput chemical screening in toxicological assays and drug discovery. For instance, researchers have used *C. elegans* to facilitate the discovery of various disease inhibition and therapeutic drugs by investigating chemical compounds such as anticancer drugs (Cornaglia et al. 2015), antibiotics (Chalasani et al. 2008), sodium chloride (NaCl) (Yang et al. 2013; Hu et al. 2015b), manganese (Zhang et al. 2014), and glycerol (Chronis et al. 2007; Chokshi et al. 2010; Wang et al. 2011, 2013a).

Chronis et al. (2007) developed an olfactory microfluidic chip to monitor calcium changes in ASH neuron under exposure to different chemicals by trapping the worm's body inside a narrow tapered channel while protruding its nose into a chemical exposure channel (Fig. 9.3a). Using this device, Chalasani et al. (2008) studied the activities of *C. elegans* olfactory neurons (AWC) in response to attractive odors, such as benzaldehyde and isoamyl alcohol, and concluded that odor removal results in the activation of AWC neurons. Hu et al. (2015b) studied the chemosensory behavior of *C. elegans* in response to chemical gradients by achieving eight different concentrations (0–300 mM) of NaCl using mixing microchannels designed in a monolayer tree-like microfluidic chip (Fig. 9.3b). Using this design, the authors observed that chemotaxis behavior is not consistent for all larval stages, since low concentration of NaCl induced a strong chemotactic response on L3 stage worms. Moreover, the same group designed a precise stimulus delivery system for neuronal investigations in response to different gases (O_2, CO_2) and odors (1-Octanol) (Hu et al. 2015a). Their device (Fig. 9.3c) consisted of a T-junction stimulus delivery system and a tapered channel for worm immobilization, enhanced by a comb-shaped microvalve structure on top. Their investigations indicated that CO_2 anesthetizes the worm by inhibiting BAG neuronal activities while increased O_2 levels stimulate URX neuronal responses. Some of these results were confirmed by Zimmer et al. (2009).

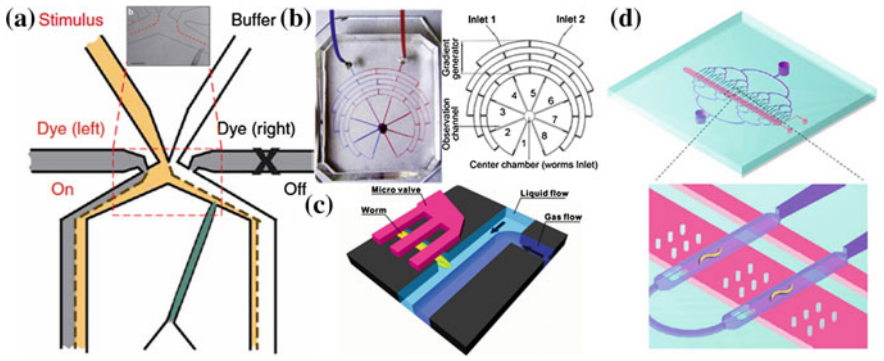

Fig. 9.3 Microfluidic devices for analysis of *C. elegans* chemotaxis behavior (Chronis et al. 2007; Ma et al. 2009; Hu et al. 2015a, b)

Owing to the unique features of *C. elegans* nervous system, worm models of neurodegenerative diseases have been developed to facilitate the discovery of pathological mechanisms underpinning these diseases and to screen for therapeutic drugs (Ma et al. 2009; Shi et al. 2010; Salam et al. 2013). As an example, Parkinson's disease (PD) is a progressive neurodegenerative disease known for the loss of dopaminergic neurons (DNs) in the brain. DNs degeneration in *C. elegans* has been mimicked using different neurotoxins [e.g., 6-hydroxydopamine (6-OHDA)] that induce several symptoms of PD, such as tremor and slow crawling. By developing a microchip to immobilize individual mutant worms in parallel channels using controlled microvalves (Fig. 9.3d), Ma et al. (2009) demonstrated that neurotoxins, such as MPP+, could induce neuron degeneration and mobility defects, for instance slow and coiled movements, in *C. elegans*. Shi et al. (2010) developed a droplet-based device to study the effect of MPP+ and 6-OHDA on mutant worms by encapsulating them within droplets. Their findings supported the results of Ma et al. (2009) on MPP+ and concluded that 6-OHDA was also able to degenerate DNs due to increased oxidative stress. Furthermore, Salam et al. (2013) utilized electrotactic screening to investigate the movement behavior of worms under exposure to neurotoxins. Their studies revealed that PD-like movement disorder symptoms could be induced using neurotoxin chemical compounds and could be suppressed using known neuroprotective chemicals such as acetaminophen.

2.4 Mechanical Screening Microsystems

Responses to mechanical stimulation are critical for the survival of *C. elegans*. Worms use their mechanosensory neurons to control their locomotion and other behaviors. Neuronal and behavioral responses of *C. elegans* to mechanical forces have been studied in microfluidic devices, taking advantage of the high level of animal and stimulus control and manipulation that is provided by these technologies.

In various microfluidic devices, mechanical stimulation has been achieved by using micropillars in a channel which can induce force on worms' body. Park et al. (2008) used a microfluidic device consisting of agar microposts to simulate the soil environment for the worms. They observed that the microposts helped the worms move faster and more efficiently in their structured device comparing to their movement on a smooth agar surface. They also studied the effect of post-spacing to find the optimum grid microstructure design and finally concluded that this phenomenon can be attributed to *C. elegans* mechanosensory behavior, since, compared to wild-type worms, the mutants lacking this ability (e.g., mec-4 and mec-10) had trouble moving between the posts. Wang et al. (2013b) used PDMS micropillars to model the crowding stress caused by other worms in a population. They observed that by decreasing the micropillar distance (i.e., increasing crowding stress), an increase in DAF-16 nuclear localization occurs. Micropillars have also

been utilized as tools for sensing the body forces of mobile worms (Doll et al. 2009; Johari et al. 2013).

Recently, Nekimken et al. (2017) developed a microfluidic device to study the response of mechanoreceptor neurons of *C. elegans* to mechanical stimulation. In their device, worms were first immobilized in a tapered channel, and then a mechanical force generated by a pneumatic actuator was transferred to the worm's body at three different positions (i.e., head, tail, and middle body) through a thin PDMS membrane at the side of trap. Activation of the individual touch receptive neurons (TRNs) by these spatial stimulations in the device was then captured using calcium-sensitive fluorescence imaging.

2.5 Other Screening Microsystems

In addition to the chemical, electrical, and mechanical stimuli that were presented in the previous sections, *C. elegans* responses to other cues, such as light and temperature differences, have also been studied using microfluidic devices.

C. elegans usually lives in the soil darkness and is known to lack any light-sensitive organs such as eyes (Brenner 1974). Therefore, one may assume that worms do not respond to light, known as a behavior called phototaxis. However, Ward et al. (2008) demonstrated that *C. elegans* show negative phototaxis by avoiding the light and attempting to remain in the darkness, potentially for survival purposes. They concluded that a group of ciliary sensory neurons are responsible for negative phototaxis.

Several researchers have also studied the optical activation of neurons (optogenetic) and induced synaptic functions and behaviors using light-activated channelrhodopsin-2 (ChR2) (Nagel et al. 2005; Liewald et al. 2008; Guo et al. 2009). In all of the above-mentioned studies, the stimulation of neurons was conducted manually on freely moving worms. This makes the investigation time consuming and low throughput. Besides that, in most cases, the freely moving worm coils its body under exposure to light, making it challenging to perform imaging, image processing, and data analysis on the samples. Microfluidic techniques are good assets to address these issues since the throughput can be increased by parallelization and the worms can be immobilized using different techniques already introduced in the manipulation section.

Stirman et al. (2010) designed a microfluidic device and combined it with automated image processing to perform synaptic function studies on *C. elegans* using optogenetics. Their device included eight parallel channels between two inlet and outlet chambers. The worms were trapped and immobilized in these channels using two valves at the beginning and end of each channel. The width of the channel was set slightly larger than the width of the adult worms to let them move across the channel while preventing them from coiling. After loading and partial immobilization of the worms in the channels, they could only react to blue light stimulus by increasing or decreasing their body lengths which were recorded in

videos and analyzed quantitatively before and after illuminating. The study was performed on wild-type and mutant worms, and the effect of different chemicals on *C. elegans* during optogenetic experiments was studied at throughputs as high as 100 worms per 5 min.

C. elegans response to light can also be used as a behavioral readout to investigate the effect of various experimental methods on the worms. For instance, Chuang et al. (2011) investigated the nematodes' response to light to reveal the effect of dielectrophoresis on *C. elegans*. In their device, animal's tail was trapped and the head position was plotted after illumination with blue and green lights on top of partially trapped worm. Observing that the trapped worms avoided the blue light by changing the position of their heads but remained oblivious to green light, they concluded that light-sensitive neurons were not impaired during dielectrophoresis.

Similar to phototaxis, response toward temperature gradients or thermotaxis is also critical for worms' survival. Negative and positive thermotaxis behaviors in the worms have been investigated by researchers (Garrity et al. 2010). It is a challenge to study the spatial orientation of freely moving worms, since analysis of their movement is difficult and the initial position of the worms affects their eventual response to thermal stimuli. Therefore, McCormick et al. (2011) developed a microfluidic device to investigate the spatial orientation behavior of *C. elegans* in response to various stimulations, including a temperature gradient. In their device, a worm was immobilized with two vacuum ports restraining its mid body while leaving the head and tail free to move in a channel. In order to create the thermal gradient, two laminar fluids flowing along the worm axis were used and the fluids' temperatures were controlled and monitored by Peltier devices and thermistors. The results revealed that the worms moved their heads toward the flow with a preferred temperature of 20 °C rather than 25 °C. The worms also chose the cooler stream, when they were exposed to two different temperatures, equally distanced from their preferred temperatures (e.g., 15 and 25 °C).

3 Microsystems for *Drosophila melanogaster* Studies

D. melanogaster is one of the fly species that has been used as a model organism at all developmental stages, including embryonic, larval, and adult ages. Advantages of *D. melanogaster* such as inexpensive and easy culturing, short life cycle, amenability to genetic modification, and reasonably transparent body during early larval stages as well as scientists' knowledge of its genome sequence and functionality have made *Drosophila* a great candidate for genetic, physiology, neuroscience, and disease pathology studies for over a century now (Bilen and Bonini 2005; Pandey and Nichols 2011). Various microfluidic and lab-on-a-chip devices have been developed in the past decade to facilitate and automate the scientific investigations on *Drosophila*, majorly at the larval stage due to its size suitability for microfluidic studies.

3.1 *Microsystems for* D. melanogaster *Manipulation*

The first major step for investigating the effects of various stimuli on *Drosophila* larva is immobilizing the animal. A variety of techniques have been developed to date for on-chip immobilization of *Drosophila*. Mondal et al. (2011) focused on developing a reliable method to immobilize *Drosophila* larvae in a PDMS chip for neuronal imaging. They utilized a two-layer PDMS channel in which the larva was introduced through the bottom layer and immobilized by applying pressure to a flexible membrane located on the top of screening channel. Their method was proved efficient for immobilizing *Drosophila* larva with a minimum pressure of 7 psi. Ghannad-Rezaie et al. (2012) introduced two microfluidic chips for short-term (SI chip) and long-term (LI chip) immobilization of *Drosophila* larvae. The SI chip consisted of a microchamber with 1.5 mm width and 140 μm height over which a vacuum was applied to immobilize a larva for close to 1 h at a time. The LI chip was a two-layer microfluidic chip made of PDMS that was employed for immobilizing the larvae for longer periods of up to 12 h. In this device, mechanical force, along with exposure to CO_2, was used to immobilize the animal, which helped achieve longer immobilization periods. Major advantages of this technique were eliminating the recovery time after immobilization, simplicity of fabrication and repeatability. To immobilize *Drosophila* larva, Ghaemi and Selvaganapathy (2016) also invested in the application of tapering microchannels. Their results demonstrated that simple narrow channels, as used for *C. elegans*, are not optimal and efficient for immobilizing *Drosophila's* internal organs, such as central nervous system. The process was optimized by adding primary and secondary clamps inside the tapered channel.

3.2 *Mechanical Screening Microsystems*

Mechano-receptors in *Drosophila* are capable of responding to various mechanical stimuli that make disturbance in the form of touching, imbalance, and hearing to the animal (Walker et al. 2000). Mondal et al. (2011) used a two-layer deflectable membrane PDMS microfluidic chip that enabled them to immobilize and take images of *Drosophila* larvae without the use of anesthetics. Their technique has the potential to be used for subcellular imaging of axonal, intraflagellar, and dendritic transport. They claimed that this method could be a powerful tool for imaging cellular and subcellular events in organisms such as *Drosophila*, *C. elegans*, and *D. rerio*.

Ghannad-Rezaie et al. (2012) employed their LI and SI chips, introduced earlier, for neuronal imaging and collecting the subcellular responses of *Drosophila* after dendrite injury and axotomy. Using fluorescent imaging, they demonstrated that their device could indeed be used for imaging the intracellular Ca^{2+} dynamics in *Drosophila* larvae. Khare et al. (2015) took another approach to investigate the

mechanosensory mechanism of *Drosophila* and focused on measuring the force that the animal experiences during its movement in a microchannel. For this, they fabricated a PDMS straight microchannel with embedded colored micropillars. By measuring the deflection of micropillars while the larvae crawled on top of them, they could calculate the total average force per animal (32.61 ± 8.68 μN), average force applied per pillar (1.58 ± 0.39 μN), and maximum force on a single pillar (5.84 ± 1.03 μN). Their technique simulated the natural habitat situation for the larvae and allowed stimulating them with a relatively uniform force distribution.

Delubac et al. (2012) fabricated a LabVIEW-controlled microfluidic device in which *Drosophila* embryos were automatically directed toward an embedded needle in a channel for microinjection of reagents. They evaluated the embryos' survival rate under mechanical stress in their device. For this, they circulated the embryos through the device and stored them off chip inside Klearol white oil where they measured the number of embryos that developed mouth hooks after 24 h. Their findings showed that for flow rates of higher than 500 μL/min, embryos cannot survive, while the survival rate for flow rates of 150–300 μL/min was reported to be almost 50–70%.

3.3 Chemical Screening Microsystems

Drosophila larvae are strong and reliable models for investigating various chemosensory pathways (Adams et al. 2000; Gerber and Stocker 2007; Makos et al. 2009). We fabricated a microfluidic chip for screening the cardiac response of *Drosophila* larvae upon exposure to various chemicals (Ardeshiri et al. 2016a). In this device (Fig. 9.4a), the larva was oriented in the desired direction using a glass capillary and immobilized using a side suction channel. Afterward, the larva was exposed to sodium azide (NaN_3), oxygen (O_2), and carbon dioxide (CO_2) with various concentrations and the animal's heartbeat was counted. We revealed that increasing the concentration of CO_2 and NaN_3 will increase the rate of heartbeat reduction. Also, the animal's heart rate declined drastically when oxygen was removed from the channel (anoxia), while exposure to higher than normal oxygen (hyperoxia) did not change the heart rate significantly. In addition, we concluded that, upon removing the stimuli, the larvae could recover to the pre-exposure heart rate state for all the cases except sodium azide.

We also investigated the effect of chemicals on egg laying or oviposition behavior of adult *Drosophila* (Leung et al. 2015, 2016). Oviposition can be an important measure in determining the behavioral responses and biological fitness of *Drosophila*. For this purpose, we designed two separate devices for toxicity and multiple choice assays. In both devices, we used a layer of agar integrated with a PDMS microfluidic layer and a ring that facilitated installation of a stock bottle in which the adult flies were stored (Fig. 9.4b). In the toxicity chip, the effect of a single dose of a chemical was studied while the multiple choice device enabled us

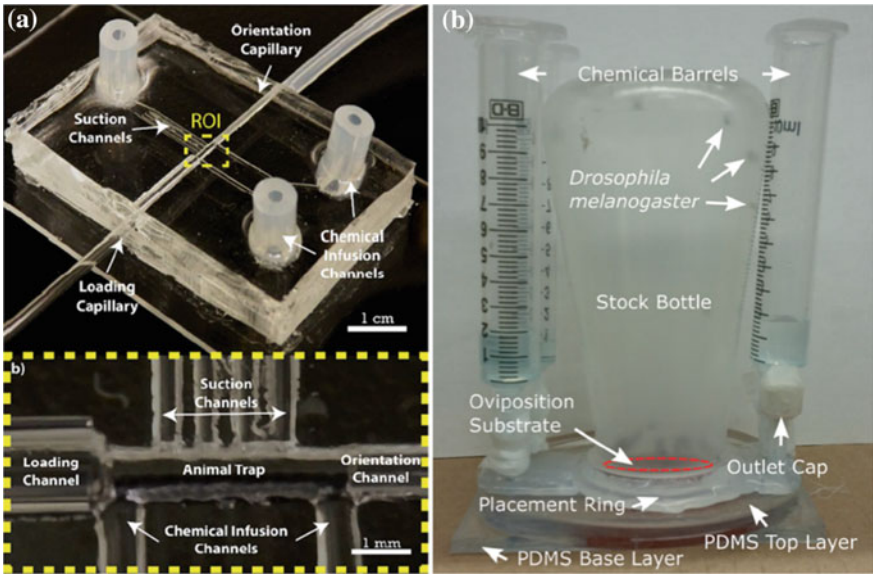

Fig. 9.4 Microfluidic devices developed by us for the investigation of *Drosophila melanogaster* **a** heart rate (Ardeshiri et al. 2016a) and **b** oviposition (Leung et al. 2016) under exposure to various chemicals

to study dosing with three different chemicals. Zinc and acetic acid with concentrations of 0–70 mM and 0–15%, respectively, were tested in the toxicity chip, and no effect on survival rate was observed. However, the maximum oviposition rate was shown to occur at 20 mM zinc and 5% acetic acid. Multiple choice assay confirmed that 20 mM Zn and 5% acetic acid were more attractive to the animals than the other concentrations, although some variations were observed in attractiveness of the lower concentrations.

3.4 Thermal Screening Microsystems

Thermoreceptor cells in *Drosophila* aid the animal with their body orientation in response to thermal stimulus (Liu et al. 2015). Lucchetta et al. (2005) introduced a device with a T-shape channel to co-flow two streams of water at controlled temperatures on top of an embryo with the objective of observing the effect of thermal perturbation in time and space on the dynamics of *Drosophila* embryonic patterning network. They first ran two fluids with uniform temperatures around the embryo, manually positioned between the streams, and demonstrated that uniform temperature is not capable of disrupting the development of embryos, provided that the shear rate was maintained within a biological range (700 s^{-1}). In order to produce

temporal and spatial thermal perturbations, they exposed *Drosophila* embryo to a temperature gradient with various amplitudes and exposure times. Monitoring the density of nuclei in the warm and cold halves of embryos, the study revealed that temperature gradient can affect the development of embryos. The ones in the warmer half developed faster and with more nuclei formed. Also, a greater difference in the development rate was observed when the temperature difference between the halves' and the exposure time was increased. Later on, Lucchetta et al. (2006) added a numerical scheme to the above experiments to quantify the effect of position of the embryo in the microchannel on the temperature gradient inside the embryo. They discovered that the temperature distribution within the embryo was not significantly affected by embryo positioning, and they provided a protocol for microfluidic devices to precisely control the temperature of biological systems. In 2007, Dagani et al. (2007) attempted to improve the above device by increasing its throughput rate. The major challenge in their work was to develop an automated technique for immobilizing the embryo. For this, they employed a previously established technique by Zhang et al. (2005a) for positioning the *Drosophila* embryo. Briefly, they introduced the embryos, immersed in water, into the microchannel, where they came into contact with an adhesive pad and were stuck to the bottom of the channel. Next, a buffer solution was run over the glued embryos to clear the remaining water inside the channel. This step was proved to be crucial for a firm bonding since water has high interfacial tension with the adhesive pad and could decrease the bonding quality. The authors could optimize this method to increase the working flow rate by three orders of magnitude.

3.5 Auditory Screening Microsystems

We developed two microfluidic chips (pneumatic chip and flexi chip) to investigate the activity of central nervous system (CNS) of *Drosophila* larvae under the effect of sound stimulation (Ghaemi et al. 2015). In the pneumatic chip, we employed a narrow channel, followed by introducing a primary gate, a secondary gate and a stopper to facilitate automated loading, unloading and immobilization of the larva. The narrow channel helped with the encapsulation of body, while the primary and secondary gates were responsible for pinning the larva in the channel. The flexi chip was used for manual and convenient loading of the larva, but not very optimal for high-throughput experiments. In these studies, we mounted a speaker on top of the chips and sealed the whole setup from the surrounding to reduce the noise from the ambient. The speaker was connected to a function generator to expose the larva to sound frequencies of 50–5000 Hz and intensities of 95–115 dB. The results revealed that CNS activity (measured using transient GCaMP fluorescence imaging) increased upon exposure to sound. The largest fluorescent intensity variation (corresponding to the optimal response) was observed at 200 Hz and 115 dB.

4 Microsystems for *Danio rerio* Studies

D. rerio or zebrafish is one of the simplest and most advantageous vertebrate model organisms on which many biological and disease studies have been conducted to date (Yang et al. 2016). It offers several unique characteristics including small size during embryonic and larval stages, body transparency, and genetic similarity to humans. These characteristics make the organism ideal for biological investigations such as neural (Lin et al. 2015) and behavioral (Rudin-Bitterli et al. 2014) screening, human disease modeling (Yang et al. 2016), and drug discovery (Candelier et al. 2015; Lin et al. 2016). As such, researchers have developed microfluidic devices to facilitate the investigation of neurobehavioral responses in zebrafish to various stimuli such as chemicals (Lin et al. 2015, 2016, Akagi et al. 2012, 2013; van Noort et al. 2012; Bischel et al. 2013; Rudin-Bitterli et al. 2014; Zhu et al. 2015a, b; Candelier et al. 2015), sound (Kwon et al. 2014), electrical (Peimani et al. 2017a), and flow (Peimani et al. 2017b, c). These studies have been mostly conducted on zebrafish embryos and larvae due to their size compatibilities with microfluidic components.

4.1 Microsystems for D. rerio *Manipulation*

To conduct the above-mentioned studies, zebrafish larva should be manipulated in a way that its favorable organs such as the brain, spinal cord, heart, and tail can be imaged effectively. This has proved challenging due to the high level of body activities in zebrafish larvae. There has been several distinguished microfluidic approaches offered for the manipulation of zebrafish larvae such as the use of physical obstacles in a channel (Bischel et al. 2013; Erickstad et al. 2015; Hong et al. 2016), tapered channels (similar to *C. elegans* and *Drosophila*) (Akagi et al. 2012; Lin et al. 2015, 2016), agarose-based immobilization (Candelier et al. 2015) and magnetic particle-based handling (Chen and Cheng 2014).

Erickstad et al. (2015) fabricated a microfluidic device (Fig. 9.5a) with a PDMS obstacle created inside a channel for the manipulation of zebrafish larva. The larva was loaded into the channel hydrodynamically, and the obstacle acted as a barrier in front of its head to help immobilize the animal relying on hydrodynamic forces (Fig. 9.5b). Bischel et al. (2013) also employed a similar barrier-based technique in their PDMS device to trap and immobilize the larvae for further drug treatment studies (Fig. 9.5c). Using a slightly different technique, Hong et al. (2016) designed a series of microchannels with narrowed ends in which the larvae's heads were immobilized for electrophysiological monitoring after they voluntarily swam into these screening channels (Fig. 9.5d).

Candelier et al. (2015) integrated the agarose gel inside a PDMS device to partially immobilize a zebrafish larva while leaving the mouth and tail regions free for chemical exposure and behavioral monitoring, respectively (Fig. 9.5e). Their

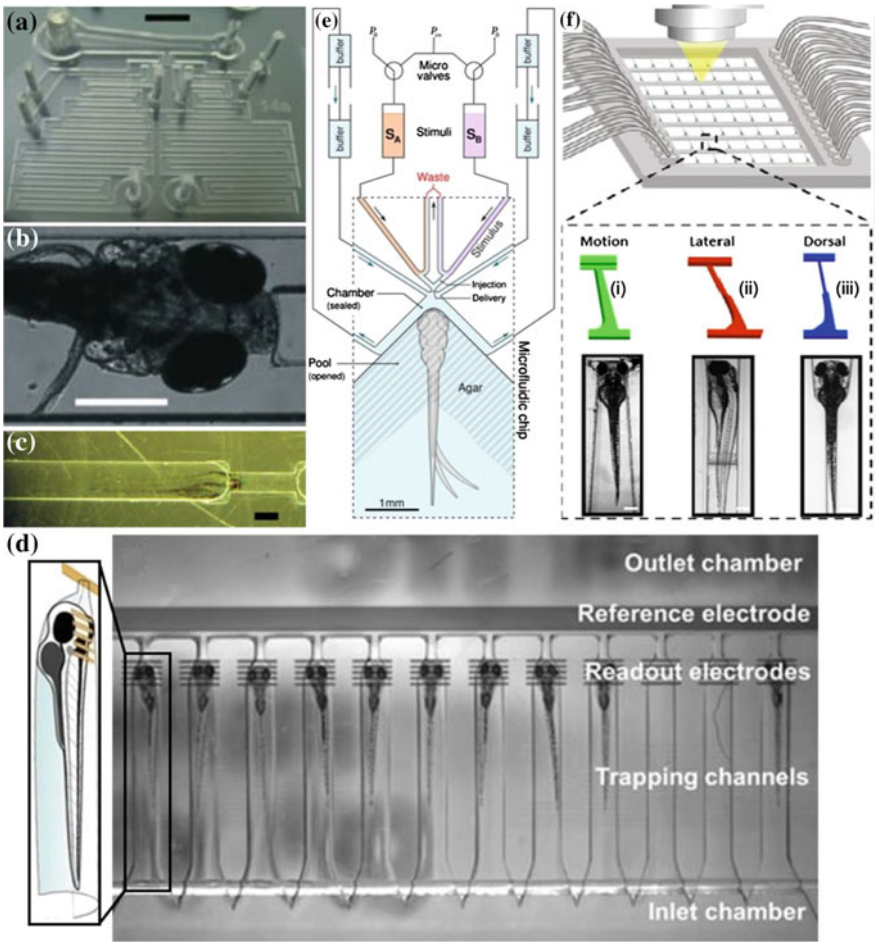

Fig. 9.5 Microfluidic devices for manipulation and screening of zebrafish larvae. **a** Micro-device for oxygen deprivation studies, scale bar: 4 mm (Erickstad et al. 2015), **b** real image of a zebrafish larva trapped by a barrier, scale bar: 0.35 mm (Erickstad et al. 2015), **c** narrow-ended channel for the larva's head trapping, scale bar: 0.5 mm (Bischel et al. 2013), **d** real picture of multiple trapped zebrafish larvae in the electrophysiology microfluidic system (Hong et al. 2016), **e** schematic design of the microfluidic device where the larva is immobilized by agarose and its mouth and tail is free to be drug exposed and recorded, respectively (Candelier et al. 2015), and **f** scheme of the chip with the real images of immobilized fish in the end-tapered channels of (i) motion, (ii) lateral, and (iii) dorsal chips. Larva is exposed to chemical by the horizontal channel which is perpendicular to the trapping channel, scale bar: 0.2 mm (Lin et al. 2016)

microfluidic device consisted of a V-shaped chamber inside which the larva was placed with its mouth facing the edge of V-chamber, located in front of the chemical exposure channels. The larva's body, except for the tail and mouth, was then embedded in agarose for partial immobilization.

Lin et al. (2016) developed a high-throughput microfluidic device made of PDMS with tapered channels which were used for trapping tens of zebrafish larvae simultaneously inside the device (Fig. 9.5f). They came up with three different designs of motion, lateral and dorsal chips for their tapered channel. In the motion chip, the channel was designed narrower at one end where the head of larva was trapped and wider at the other end where the behavioral imaging took place (Fig. 9.5f-i). In the lateral chip, the channel was straight but its width was designed to match the thickness of larva to load it with a lateral side-up orientation in the trap (Fig. 9.5f-ii). In the dorsal chip, the channel mimicked the shape of larva to perfectly trap it with restraining the body from movements and providing accessibility to larva's head for neural imaging (Fig. 9.5f-iii). The concept of tapered channels has been employed for embryo trapping as well, where a U-shaped chamber was used with a suction channel at its base to trap the embryo inside a channel for imaging (Akagi et al. 2012).

There has also been a hypothetical microfluidic approach proposed for the manipulation of zebrafish larvae and embryos employing magnetic field as a stimulus (Chen and Cheng 2014). Magnetic particles aggregated around the body of the fish and the application of magnetic forces in three orthogonal directions, using three pairs of coils, have been proposed to orient zebrafish larva and embryo in a desired direction in the channel.

4.2 Chemical Screening Microsystems

Candelier et al. (2015) developed a microfluidic device made of transparent acrylic (PMMA) slabs to partially immobilize and to expose zebrafish larvae to chemicals. The device (Fig. 9.5e) included an open pool where the larva was partially immobilized with agar while its head was positioned in front of the chemical infusion channels and its tail was free to move for behavioral screening. In this study, different flavors of critic acid (CA), as a sour aversive chemical, and L-proline (LP), as an appetitive tastant, were delivered in step pulses to examine the gustatory neuronal responses and the tail movement behavior of larva. It was shown that the majority of dorsal, medial, and ventral neurons respond to either CA or LP while a few reacted to both. Furthermore, the monitored tail motions proved that whenever there was a behavioral response, the neuronal reactions induced by the chemicals were also large. By comparing the neuronal responses with and without the association of tail motions, the authors showed that sensory and gustatory-induced responses were related to different regions of the brain.

In order to study the behavior of zebrafish in exposure to oxygen deprivation (i.e., hypoxia), Erickstad et al. (2015) developed a microfluidic device which allows the users to manipulate the oxygen doses of zebrafish medium. Their PDMS device contained a zebrafish channel in which a larva was loaded and trapped utilizing the

microfabricated obstacle and hydrodynamic force approach (Fig. 9.5a, b). Two sets of zigzag microchannels were designed to integrate two different gases A and B with two medium streams used in this study. Permeability of PDMS channel walls to the gases made it possible to manipulate the oxygen level in the exposure media. The results suggested that the body movement rate and pectoral fin beats significantly increase with the strongest hypoxia treatment (i.e., $[O_2] = 1.8\%$), in comparison to the control group.

Lin et al. (2016) designed three microchips (Fig. 9.5f) in which zebrafish larvae were trapped in different positions and orientations, i.e., partially free for movement monitoring (Fig. 9.5f-i), laterally immobilized for cardiac screening (Fig. 9.5f-ii), and dorsally immobilized for brain function monitoring (Fig. 9.5f-iii), under exposure to ethanol. The larvae were loaded through a channel into the device and immobilized one by one inside the tapered channels due to the continuously applied hydrodynamic forces. For behavioral analysis of zebrafish larvae, their pectoral fin beats, eye saccades, and body movements were quantified under exposure to ethanol with different concentrations. At low ethanol concentration of 0.75%, the fin beats and eye movements were increased, whereas a significant drop in the fin, eye, and body movements was observed at the high concentration of 3% ethanol. These results suggested that ethanol may cause impairment in the motor coordination and vision function of zebrafish larvae. The larvae's heart rate plummeted after being treated by all doses of ethanol (0.75, 1.5, and 3%), which showed that ethanol of up to 3% concentration negatively affected the evoked cardiac function in the larvae. This study was expanded down to the neuronal level where brain-wide GCaMP activities in the nervous systems were recorded during larva's exposure to ethanol. The dose-dependent effect of ethanol on neural activities was also observed. At low ethanol concentration, neuron responses initiated from caudal hindbrain and then continued to grow into the cerebellum, ventral midbrain, and forebrain. As opposed to the results obtained for weak behavioral activities at high ethanol dosages, the forebrain neuronal activities were reported to be high and most intensely induced at that dosage.

Hong et al. (2016) proposed a novel technique for neural recording with a microfluidic-based electrophysiology platform for zebrafish screening (Fig. 9.5d). They designed a multichannel platform made of PDMS with narrowing-end channels in which several larvae were trapped for monitoring. Electrophysiological recording of the brain activities was achieved using an array of readout electrodes positioned on the top of immobilized larvae heads and a reference electrode in front of their mouths. For chemical screening, media in the device was infused with valproic acid (VPA) and topiramate (TOP), followed by the recording of electroencephalogram (EEG) activities in the immobilized larvae. In the treatment with VPA, all nine treated mutants could successfully respond to the drug while seven of them only showed a successful response once treated successively with TOP.

4.3 Auditory Screening Microsystems

Despite a significant attention given to zebrafish chemical screening with microfluidic devices in the literature, there are a few studies of the auditory function using microfluidics, one of which is reviewed here. Kwon et al. (2014) designed a microfluidic device to induce hearing damage to the hair cells of zebrafish lateral line. Because the sensory hair cells in zebrafish's lateral line system, which are located on the surface of their body, are the cells for detecting sound stimuli, the authors targeted damaging these cells with the aid of high shear flows close to the boundaries in a microchannel containing the larva. The device consisted of a main channel, small enough to restrain the fish from escaping the region of interest, and multiple side-angled channels, as the inlets and outlets for flow. Side channel flows were applied in order to maximize the flow velocity and shear on the lateral line hair cells to induce a permanent damage. The design was optimized employing computational fluid dynamics (CFDs) modeling to study the effect of side channel angles and sizes so that only the hair cells would be impaired without damaging the fish itself. Aside from the optimized sizes, the simulation results revealed that by angling the side inlet/outlet channels at 60°, the pressure could be lowered to 0.3 Pa to minimize damage to the brain while a reasonably strong shear stress of 1.9 Pa could be achieved for removal of the lateral line hair cells.

4.4 Other Screening Microsystems

A very recent study by us focused on using a microfluidic device to extensively investigate the electrotaxis behavior of zebrafish larva (Peimani et al. 2017a, c). We were able to develop a PDMS device in which the larva's activity was confined to swimming longitudinally in a channel with electrodes at its two ends. We applied various electric currents along the channel axis (and the larva), and any potential responses were examined. We observed that the larva tends to swim toward the anode pole, as opposed to *C. elegans* hermaphrodites that swim to the cathode when exposed to electrical currents of 3–25 μA.

Another interesting behavior in zebrafish larva is rheotaxis which is defined as orientation against flow direction. This behavior has mainly been investigated using complex and inaccurate experimental setups. We used the same unidirectional motion electrotaxis device described above to study rheotaxis among zebrafish larvae in a simple, accurate, and repeatable manner (Peimani et al. 2017b). Replacing electrical stimuli with water flow, we investigated the effect of flow rate on rheotaxis response rate and time. The results showed that rheotaxis behavior is strongly influenced by the flow velocity and direction.

5 Conclusions and Future Trends

Small-scale model organisms such as *C. elegans* (worm), *D. melanogaster* (fly), and *D. rerio* (zebrafish) are among the most advantageous model organisms for studying human diseases, from understanding disease pathology to screening for drugs and therapeutics. To achieve higher levels of automation, throughput, and accuracy in assays as well as quantitative analyzes, a wide variety of microfluidic devices and Lab-on-Chips for organism studies have been developed over the past decade. Majority of these devices have focused on developing advanced techniques to enhance organism manipulation in terms of loading, orientation, exposure to stimuli, immobilization, imaging, sorting and recovery for the post-experimental assays. An assessment of organism-on-a-chip literature reveals that the focus of these technological advancements has been mostly placed on achieving automation, high-throughput screening, and quantitative analysis while adopting biological assays that are somewhat established in their respective fields. Considering the fact that many of these technologies have been matured over the past decade, it is expected for them to be more widely adopted by biologists for application-driven assays such as studying the fundamentals of diseases or toxicological assays. For this, the tradeoff between technological complexity and ease-of-use demand by the end users must be carefully considered.

6 Compliance with Ethical Standards

York University and the Natural Sciences and Engineering Research Council of Canada (NSERC) have financially supported the authors of this article.

References

Adams MD, Celniker SE, Holt RA, Evans CA, Gocayne JD, Amanatides PG, Scherer SE, Li PW, Hoskins RA, Galle RF, George RA, Lewis SE, Richards S, Ashburner M, Henderson SN, Sutton GG et al (2000) The genome sequence of *Drosophila melanogaster*. Science (80-) 287:2185–2195. https://doi.org/10.1126/science.287.5461.2185

Ahmed D, Ozcelik A, Bojanala N et al (2016) Rotational manipulation of single cells and organisms using acoustic waves. Nat Commun 7:1–11. https://doi.org/10.1038/ncomms11085

Akagi J, Khoshmanesh K, Evans B et al (2012) Miniaturized embryo array for automated trapping, immobilization and microperfusion of zebrafish embryos. PLoS ONE 7:12–15. https://doi.org/10.1371/journal.pone.0036630

Akagi J, Khoshmanesh K, Hall CJ et al (2013) Fish on chips: microfluidic living embryo array for accelerated in vivo angiogenesis assays. Sens Actuators, B Chem 189:11–20. https://doi.org/10.1016/j.snb.2012.11.036

Albrecht DR, Bargmann CI (2011) High-content behavioral analysis of *Caenorhabditis elegans* in precise spatiotemporal chemical environments. Nat Methods 8:599–605. https://doi.org/10.1038/nmeth.1630

Ardeshiri R, Hosseini L, Amini N, Rezai P (2016a) Cardiac screening of intact *Drosophila melanogaster* larvae under exposure to aqueous and gaseous toxins in a microfluidic device. RSC Adv 6:65714–65724. https://doi.org/10.1039/C6RA14159E

Ardeshiri R, Mulcahy B, Zhen M, Rezai P (2016b) A hybrid microfluidic device for on-demand orientation and multidirectional imaging of *C. elegans* organs and neurons. Biomicrofluidics. https://doi.org/10.1063/1.4971157

Aubry G, Zhan M, Lu H (2015) Hydrogel-droplet microfluidic platform for high-resolution imaging and sorting of early larval *Caenorhabditis elegans*. Lab Chip 15:1424–1431. https://doi.org/10.1039/C4LC01384K

Bakhtina NA, Korvink JG (2014) Microfluidic laboratories for *C. elegans* enhance fundamental studies in biology. RSC Adv 4:4691–4709. https://doi.org/10.1039/C3RA43758B

Bilen J, Bonini NM (2005) Drosophila as a model for human neurodegenerative disease. Annu Rev Genet 39:153–171. https://doi.org/10.1146/annurev.genet.39.110304.095804

Bischel LL, Mader BR, Green JM et al (2013) Zebrafish Entrapment By Restriction Array (ZEBRA) device: a low-cost, agarose-free zebrafish mounting technique for automated imaging. Lab Chip 13:1732–1736. https://doi.org/10.1039/c3lc50099c

Brenner S (1974) The genetics of *Caenorhabditis elegans*. Genetics 77:71–94. https://doi.org/10.1002/cbic.200300625

Candelier R, Sriti Murmu M, Alejo Romano S et al (2015) A microfluidic device to study neuronal and motor responses to acute chemical stimuli in zebrafish. Sci Rep 5:12196. https://doi.org/10.1038/srep12196

Carr JA, Parashar A, Gibson R et al (2011) A microfluidic platform for high-sensitivity, real-time drug screening on *C. elegans* and parasitic nematodes. Lab Chip 11:2385–2396. https://doi.org/10.1039/c1lc20170k

Chalasani SH, Chronis N, Tsunozaki M et al (2008) Dissecting a circuit for olfactory behaviour in *Caenorhabditis elegans*. Nature 451:102–103. https://doi.org/10.1038/nature06540

Chen C-Y, Cheng C-M (2014) Microfluidics expands the zebrafish potentials in pharmaceutically relevant screening. Adv Healthc Mater 3:940–945. https://doi.org/10.1002/adhm.201300546

Chokshi TV, Ben-Yakar A, Chronis N (2009) CO_2 and compressive immobilization of *C. elegans* on-chip. Lab Chip 9:151–157. https://doi.org/10.1039/B807345G

Chokshi TV, Bazopoulou D, Chronis N (2010) An automated microfluidic platform for calcium imaging of chemosensory neurons in *Caenorhabditis elegans*. Lab Chip 10:2758–2763. https://doi.org/10.1039/c004658b

Chronis N, Zimmer M, Bargmann CI (2007) Microfluidics for in vivo imaging of neuronal and behavioral activity in *Caenorhabditis elegans*. Nat Methods 4:727–731. https://doi.org/10.1038/nmeth1075

Chuang H-S, Raizen DM, Lamb A et al (2011) Dielectrophoresis of *Caenorhabditis elegans*. Lab Chip 11:599. https://doi.org/10.1039/c0lc00532k

Chuang H-S, Chen H-Y, Chen C-S, Chiu W-T (2013) Immobilization of the nematode caenorhabditis elegans with addressable light-induced heat knockdown (ALINK). Lab Chip 13:2980. https://doi.org/10.1039/c3lc50454a

Chuang H-S, Kuo W-J, Lee C-L et al (2016) Exercise in an electrotactic flow chamber ameliorates age-related degeneration in *Caenorhabditis elegans*. Sci Rep 6:28064. https://doi.org/10.1038/srep28064

Chung K, Lu H (2009) Automated high-throughput cell microsurgery on-chip. Lab Chip 9:2764–2766. https://doi.org/10.1039/b910703g

Chung K, Crane MM, Lu H (2008) Automated on-chip rapid microscopy, phenotyping and sorting of *C. elegans*. Nat Methods 5:637–643. https://doi.org/10.1038/nmeth.1227

Chung K, Zhan M, Srinivasan J et al (2011) Microfluidic chamber arrays for whole-organism behavior-based chemical screening. Lab Chip 11:3689. https://doi.org/10.1039/c1lc20400a

Clausell-Tormos J, Lieber D, Baret JC et al (2008) Droplet-based microfluidic platforms for the encapsulation and screening of mammalian cells and multicellular organisms. Chem Biol 15:427–437. https://doi.org/10.1016/j.chembiol.2008.04.004

Cornaglia M, Mouchiroud L, Marette A et al (2015) An automated microfluidic platform for *C. elegans* embryo arraying, phenotyping, and long-term live imaging. Sci Rep 5:10192. https://doi.org/10.1038/srep10192

Crane MM, Chung K, Lu H (2009) Computer-enhanced high-throughput genetic screens of *C. elegans* in a microfluidic system. Lab Chip 9:38–40. https://doi.org/10.1039/B813730G

Dagani GT, Monzo K, Fakhoury JR et al (2007) Microfluidic self-assembly of live *Drosophila* embryos for versatile high-throughput analysis of embryonic morphogenesis. Biomed Microdevices 681–694. https://doi.org/10.1007/s10544-007-9077-z

Delubac D, Highley CB, Witzberger-krajcovic M et al (2012) Microfluidic system with integrated microinjector for automated *Drosophila* embryo injection. Lab Chip 4911–4919. https://doi.org/10.1039/c2lc40104e

Ding X, Lin S-CS, Kiraly B et al (2012) On-chip manipulation of single microparticles, cells, and organisms using surface acoustic waves. Proc Natl Acad Sci 109:11105–11109. https://doi.org/10.1073/pnas.1209288109

Doll JC, Harjee N, Klejwa N et al (2009) SU-8 force sensing pillar arrays for biological measurements. Lab Chip 9:1449. https://doi.org/10.1039/b818622g

Dong L, Zhang J, Cornaglia M et al (2017) *C. Elegans* immobilization using deformable microfluidics for in vivo studies of early embryogenesis and intestinal microbiota, MEMS Conference, Las Vegas, USA, Jan 22–26 2017, 616–619

Erickstad M, Hale LA, Chalasani SH, Groisman A (2015) A microfluidic system for studying the behavior of zebrafish larvae under acute hypoxia. Lab Chip 15:857–866. https://doi.org/10.1039/C4LC00717D

Garrity PA, Goodman MB, Samuel AD, Sengupta P (2010) Running hot and cold: behavioral strategies, neural circuits, and the molecular machinery for thermotaxis in *C. elegans* and *Drosophila*. Genes Dev 24:2365–2382. https://doi.org/10.1101/gad.1953710

Gerber B, Stocker RF (2007) The *Drosophila* larva as a model for studying chemosensation and chemosensory learning : a review. Chem Senses 65–89. https://doi.org/10.1093/chemse/bjl030

Ghaemi R, Selvaganapathy PR (2016) Microfluidic devices for automation of assays on *Drosophila melanogaster* for applications in drug discovery and biological studies. Curr Pharm Biotechnol 17:822–836

Ghaemi R, Rezai P, Iyengar BG, Selvaganapathy PR (2015) Microfluidic devices for imaging neurological response of *Drosophila melanogaster* larva to auditory stimulus. Lab Chip 15:1116–1122. https://doi.org/10.1039/C4LC01245C

Ghannad-Rezaie M, Wang X, Mishra B et al (2012) Microfluidic chips for in vivo imaging of cellular responses to neural injury in *Drosophila* larvae. PLoS ONE 7:e29869. https://doi.org/10.1371/journal.pone.0029869

Gilleland CL, Rohde CB, Zeng F, Yanik MF (2010) Microfluidic immobilization of physiologically active *Caenorhabditis elegans*. Nat Protoc 5:1888–1902. https://doi.org/10.1038/nprot.2010.143

Guo SX, Bourgeois F, Chokshi T et al (2008) Femtosecond laser nanoaxotomy lab-on-a-chip for in vivo nerve regeneration studies. Nat Methods 5:531–533. https://doi.org/10.1038/nmeth.1203

Guo ZV, Hart AC, Ramanathan S (2009) Optical interrogation of neural circuits in *Caenorhabditis elegans*. Nat Methods 6:891–896. https://doi.org/10.1038/nmeth.1397

Gupta BP, Rezai P (2016) Microfluidic approaches for manipulating, imaging, and screening *C. elegans*. Micromachines. https://doi.org/10.3390/mi7070123

Han B, Kim D, Ko UH et al (2012) A sorting strategy for *C. elegans* based on size-dependent motility and electrotaxis in a micro-structured channel. Lab Chip 12:4128–4134. https://doi.org/10.1039/c2lc40209b

Hong S, Lee P, Baraban SC, Lee LP (2016) A novel long-term, multi-channel and non-invasive electrophysiology platform for Zebrafish. Sci Rep 6:28248. https://doi.org/10.1038/srep28248

Hu L, Wang J, Feng X et al (2015a) Microfluidic device for analysis of gas-evoked neuronal sensing in *C. elegans*. Sens Actuators, B Chem 209:109–115. https://doi.org/10.1016/j.snb.2014.11.081

Hu L, Ye J, Tan H et al (2015b) Quantitative analysis of *Caenorhabditis elegans* chemotaxis using a microfluidic device. Anal Chim Acta 887:155–162. https://doi.org/10.1016/j.aca.2015.07.036

Hulme SE, Shevkoplyas SS, Apfeld J et al (2007) A microfabricated array of clamps for immobilizing and imaging *C. elegans*. Lab Chip 7:1515. https://doi.org/10.1039/b707861g

Johari S, Nock V, Alkaisi MM, Wang W (2013) On-chip analysis of *C. elegans* muscular forces and locomotion patterns in microstructured environments. Lab Chip 13:1699. https://doi.org/10.1039/c3lc41403e

Jung J, Nakajima M, Takeuchi M et al (2016) Microfluidic device to measure the speed of *C. elegans* using the resistance change of the flexible electrode. Micromachines. https://doi.org/10.3390/mi7030050

Kaletta T, Hengartner MO (2006) Finding function in novel targets: *C. elegans* as a model organism. Nat Rev Drug Discov 5:387–398. https://doi.org/10.1038/nrd2031

Kerr R, Lev-Ram V, Baird G et al (2000) Optical Imaging of Calcium Transients in Neurons and Pharyngeal Muscle of *C. elegans*. Neuron 26:583–594. https://doi.org/10.1016/S0896-6273(00)81196-4

Khare SM, Awasthi A, Venkataraman V (2015) Colored polydimethylsiloxane micropillar arrays for high throughput measurements of forces applied by genetic model organisms. Biomicrofluidics 14111:1–20. https://doi.org/10.1063/1.4906905

Krajniak J, Lu H (2010) Long-term high-resolution imaging and culture of *C. elegans* in chip-gel hybrid microfluidic device for developmental studies. Lab Chip 10:1862. https://doi.org/10.1039/c001986k

Kwon H-J, Xu Y, Solovitz Sa et al (2014) Design of a microfluidic device with a non-traditional flow profile for on-chip damage to zebrafish sensory cells. J Micromech Microeng 24:17001. https://doi.org/10.1088/0960-1317/24/1/017001

Lee H, Kim SA, Coakley S et al (2014) A multi-channel device for high-density target-selective stimulation and long-term monitoring of cells and subcellular features in *C. elegans*. Lab Chip 14:4513–4522. https://doi.org/10.1039/C4LC00789A

Leung JCK, Taylor-Kamall RW, Hilliker AJ, Rezai P (2015) Agar-polydimethylsiloxane devices for quantitative investigation of oviposition behaviour of adult drosophila melanogaster. Biomicrofluidics. https://doi.org/10.1063/1.4922737

Leung JCK, Hilliker AJ, Rezai P (2016) An integrated hybrid microfluidic device for oviposition-based chemical screening of adult *Drosophila melanogaster*. Lab Chip 16:709–719. https://doi.org/10.1039/C5LC01517K

Liewald JF, Brauner M, Stephens GJ et al (2008) Optogenetic analysis of synaptic function. Nat Methods 5:895–902. https://doi.org/10.1038/nmeth.1252

Lin X, Wang S, Yu X, Liu Z, Wang F, Li WT, Cheng SH, Dai Q, Shi P (2015) High-throughput mapping of brain-wide activity in awake and drug-responsive vertebrates. Lab Chip 15(3):680–689. https://doi.org/10.1039/c4lc01186d

Lin X, Li VWT, Chen S et al (2016) Autonomous system for cross-organ investigation of ethanol-induced acute response in behaving larval zebrafish. Biomicrofluidics 10:24123. https://doi.org/10.1063/1.4946013

Liu P, Martin RJ, Dong L (2013) Micro-electro-fluidic grids for nematodes: a lens-less, image-sensor-less approach for on-chip tracking of nematode locomotion. Lab Chip 13:650–661. https://doi.org/10.1039/c2lc41174a

Liu WW, Mazor O, Wilson RI (2015) Thermosensory processing in the *Drosophila* brain. Nature 519:353–357. https://doi.org/10.1038/nature14170

Liu D, Gupta B, Selvaganapathy PR (2016) An automated microfluidic system for screening *Caenorhabditis elegans* behaviors using electrotaxis. Biomicrofluidics. https://doi.org/10.1063/1.4941709

Lockery SR, Hulme SE, Roberts WM et al (2012) A microfluidic device for whole-animal drug screening using electrophysiological measures in the nematode *C. elegans*. Lab Chip 12:2211–2220. https://doi.org/10.1039/c2lc00001f

Lucchetta EM, Lee JH, Fu LA, Patel NH, Ismagilov RF (2005) Dynamics of *Drosophila* embryonic patterning network perturbed in space and time using microfluidics. Nature 434 (7037). https://doi.org/10.1038/nature03509

Lucchetta EM, Munson MS, Ismagilov RF (2006) Characterization of the local temperature in space and time around a developing *Drosophila* embryo in a microfluidic device. Lab Chip 185–190. https://doi.org/10.1039/b516119c

Luo L, Gabel CV, Ha H-I et al (2008) Olfactory behavior of swimming *C. elegans* analyzed by measuring motile responses to temporal variations of odorants. J Neurophysiol 99:2617–2625. https://doi.org/10.1152/jn.00053.2008

Ma H, Jiang L, Shi W et al (2009) A programmable microvalve-based microfluidic array for characterization of neurotoxin-induced responses of individual *C. elegans*. Biomicrofluidics. https://doi.org/10.1063/1.3274313

Mackinnon N (2016) Advanced microfluidic assays for *Caenorhabditis elegans*

Makos MA, Kuklinski NJ, Berglund EC et al (2009) Chemical measurements in *Drosophila*. Trends Anal Chem 28:1223–1234. https://doi.org/10.1016/j.trac.2009.08.005

Manière X, Lebois F, Matic I et al (2011) Running worms: *C. elegans* self-sorting by electrotaxis. PLoS One. https://doi.org/10.1371/journal.pone.0016637

McCormick KE, Gaertner BE, Sottile M et al (2011) Microfluidic devices for analysis of spatial orientation behaviors in semi-restrained *Caenorhabditis elegans*. PLoS ONE. https://doi.org/10.1371/journal.pone.0025710

Mondal S, Ahlawat S, Rau K et al (2011) Imaging in vivo neuronal transport in genetic model organisms using microfluidic devices. Traffic 12:372–385. https://doi.org/10.1111/j.1600-0854.2010.01157.x

Muthaiyan Shanmugam M, Subhra Santra T (2016) Microfluidic devices in advanced *Caenorhabditis elegans* research. Molecules 21:1–16. https://doi.org/10.3390/molecules21081006

Nagel G, Brauner M, Liewald JF et al (2005) Light activation of channelrhodopsin-2 in excitable cells of *Caenorhabditis elegans* triggers rapid behavioral responses. Curr Biol 15:2279–2284. https://doi.org/10.1016/j.cub.2005.11.032

Nekimken AL, Fehlauer H, Kim AA et al (2017) Pneumatic stimulation of *C. elegans* mechanoreceptor neurons in a microfluidic trap. Lab Chip 17:1116–1127. https://doi.org/10.1039/C6LC01165A

Neuži P, Giselbrecht S, Länge K et al (2012) Revisiting lab-on-a-chip technology for drug discovery. Nat Rev Drug Discov 11:620–632. https://doi.org/10.1038/nrd3799

Pandey UB, Nichols CD (2011) Human disease models in *Drosophila melanogaster* and the role of the fly in therapeutic drug discovery. Drug Deliv 63:411–436. https://doi.org/10.1124/pr.110.003293.411

Park S, Hwang H, Nam SW et al (2008) Enhanced *Caenorhabditis elegans* locomotion in a structured microfluidic environment. PLoS ONE 3:1–5. https://doi.org/10.1371/journal.pone.0002550

Peimani AR, Zoidl G, Rezai P (2017a) A microfluidic device to study electrotaxis and dopaminergic system of zebrafish larvae. Biomicrofluidics

Peimani AR, Zoidl G, Rezai P (2017b) A microfluidic device for quantitative investigation of zebrafish larvae's rheotaxis. Biomed Microdevices 19(4):99. https://doi.org/10.1007/s10544-017-0240-x

Peimani AR, Zoidl G, Rezai P (2017c) Zebrafish larva's cyclic electrotaxis behavior and its dependency on dopamine level enabled by a novel microfluidic assay, international conference on miniaturized systems for chemistry and life sciences (MicroTAS 2017), Georgia, USA, Oct 22–26, 1094–1095

Rezai P, Salam S, Selvaganapathy PR, Gupta BP (2010a) Transport, localization and separation of *Caenorhabditis elegans* using electrotaxis for movement based behavioral assays in drug discovery, international conference on miniaturized systems for chemistry and life sciences (MicroTAS 2010), Groningen, The Netherlands, 160–162

Rezai P, Siddiqui A, Selvaganapathy PR, Gupta BP (2010b) Electrotaxis of *Caenorhabditis elegans* in a microfluidic environment. Lab Chip 10:220–226. https://doi.org/10.1039/b917486a

Rezai P, Siddiqui A, Selvaganapathy PR, Gupta BP (2010c) Behavior of *Caenorhabditis elegans* in alternating electric field and its application to their localization and control. Appl Phys Lett 96:2010–2013. https://doi.org/10.1063/1.3383223

Rezai P, Salam S, Selvaganapathy PR, Gupta BP (2012a) 27 Microfluidic systems to study the biology of human diseases and identify potential therapeutic targets in *Caenorhabditis elegans*

Rezai P, Salam S, Selvaganapathy PR, Gupta BP (2012b) Electrical sorting of *Caenorhabditis elegans*. Lab Chip 12:1831. https://doi.org/10.1039/c2lc20967e

Rohde CB, Zeng F, Gonzalez-Rubio R et al (2007) Microfluidic system for on-chip high-throughput whole-animal sorting and screening at subcellular resolution. Proc Natl Acad Sci 104:13891–13895. https://doi.org/10.1073/pnas.0706513104

Rudin-Bitterli TS, Tills O, Spicer JI et al (2014) Combining motion analysis and microfluidics—a novel approach for detecting whole-animal responses to test substances. PLoS ONE 9: e113235. https://doi.org/10.1371/journal.pone.0113235

Salam S, Ansari A, Amon S et al (2013) A microfluidic phenotype analysis system reveals function of sensory and dopaminergic neuron signaling in *C. elegans* electrotactic swimming behavior. Worm 2:e24558. https://doi.org/10.4161/worm.24558

Seth A, Stemple DL, Barroso I (2013) The emerging use of zebrafish to model metabolic disease. Dis Model Mech 6:1080–1088. https://doi.org/10.1242/dmm.011346

Shanmugam MM (2017) Galvanotaxis of *Caenorhabditis elegans*: current understanding and its application in improving research. Biol Eng Med 2:1–5. https://doi.org/10.15761/BEM.1000111

Shi W, Qin J, Ye N, Lin B (2008) Droplet-based microfluidic system for individual *Caenorhabditis elegans* assay. Lab Chip 8:1432–1435. https://doi.org/10.1039/b808753a

Shi W, Wen H, Lu Y et al (2010) Droplet microfluidics for characterizing the neurotoxin-induced responses in individual *Caenorhabditis elegans*. Lab Chip 10:2855. https://doi.org/10.1039/c0lc00256a

Song P, Zhang W, Sobolevski A et al (2015) A microfluidic device for efficient chemical testing using *Caenorhabditis elegans*. Biomed Microdevices 17:1–10. https://doi.org/10.1007/s10544-015-9939-8

Spieth J, Lawson D, Davis P, Williams G, Howe K (2014) Overview of gene structure in *C. elegans*. WormBook 1–18. https://doi.org/10.1895/wormbook.1

Stirman JN, Brauner M, Gottschalk A, Lu H (2010) High-throughput study of synaptic transmission at the neuromuscular junction enabled by optogenetics and microfluidics. J Neurosci Methods 191:90–93. https://doi.org/10.1016/j.jneumeth.2010.05.019

Tong J, Rezai P, Salam S et al (2013) Microfluidic-based electrotaxis for on-demand quantitative analysis of *Caenorhabditis elegans* locomotion. J Vis Exp. https://doi.org/10.3791/50226

van Noort S, Choudhury D, Danny van Noort A et al (2012) Fish and Chips: a microfluidic perfusion platform for monitoring zebrafish development. Lab Chip 12:892–900. https://doi.org/10.1039/c1lc20351g

Walker RG, Willingham AT, Zuker CS (2000) A *Drosophila* mechanosensory transduction channel. Science 287(5461):2229–2234

Wang J, Feng X, Du W, Liu BF (2011) Microfluidic worm-chip for in vivo analysis of neuronal activity upon dynamic chemical stimulations. Anal Chim Acta 701:23–28. https://doi.org/10.1016/j.aca.2011.06.007

Wang J, Li Z, Xu Z et al (2013a) Development of an integrated microfluidic device for evaluating of in vivo chemo-sensing of intact *Caenorhabditis elegans*. Sens Actuators, B Chem 178:343–349. https://doi.org/10.1016/j.snb.2012.12.102

Wang X, Tang L, Xia Y et al (2013b) Stress response of *Caenorhabditis elegans* induced by space crowding in a micro-column array chip. Integr Biol 5:728. https://doi.org/10.1039/c3ib20289e

Wang X, Hu R, Ge A et al (2015) Highly efficient microfluidic sorting device for synchronizing developmental stages of *C. elegans* based on deflecting electrotaxis. Lab Chip 15:2513–2521. https://doi.org/10.1039/C5LC00354G

Wang X, Ge A, Hu L et al (2017) A novel on-chip immobilization strategy for imaging analysis of neuronal response to gas cues in *C. elegans*. Sens Actuators, B Chem 244:1152–1159. https://doi.org/10.1016/j.snb.2017.01.083

Ward A, Liu J, Feng Z, Xu XZS (2008) Light-sensitive neurons and channels mediate phototaxis in *C. elegans*. Nat Neurosci 11:916–922. https://doi.org/10.1038/nn.2155

Whitesides GM (2006) The origins and the future of microfluidics. Nature 442:368–373. https://doi.org/10.1038/nature05058

Yang J, Chen Z, Yang F et al (2013) A microfluidic device for rapid screening of chemotaxis-defective *Caenorhabditis elegans* mutants. Biomed Microdevices 15:211–220. https://doi.org/10.1007/s10544-012-9719-7

Yang F, Gao C, Wang P et al (2016) Fish-on-a-chip: microfluidics for zebrafish research. Lab Chip. https://doi.org/10.1039/C6LC00044D

Zeng F, Rohde CB, Yanik MF (2008) Sub-cellular precision on-chip small-animal immobilization, multi-photon imaging and femtosecond-laser manipulation. Lab Chip 8:653. https://doi.org/10.1039/b804808h

Zhang X, Chen C, Bernstein RW et al (2005a) Microoptical characterization and modeling of positioning forces on *Drosophila* embryos self-assembled in two-dimensional arrays. Journal of Microelectromech Syst 14:1187–1197

Zhang Y, Lu H, Bargmann CI (2005b) Pathogenic bacteria induce aversive olfactory learning in *Caenorhabditis elegans*. Nature 438:179–184. https://doi.org/10.1038/nature04216

Zhang B, Li Y, He Q et al (2014) Microfluidic platform integrated with worm-counting setup for assessing manganese toxicity. Biomicrofluidics 8:1–13. https://doi.org/10.1063/1.4896663

Zhu F, Hall CJ, Crosier PS, Wlodkowic D (2015a) Interfacing lab-on-a-chip embryo technology with high-definition imaging cytometry. Zebrafish 12:315–318. https://doi.org/10.1089/zeb.2015.1105

Zhu F, Wigh A, Friedrich T et al (2015b) Automated lab-on-a-chip technology for fish embryo toxicity tests performed under continuous microperfusion (μFET). Environ Sci Technol 49:14570–14578. https://doi.org/10.1021/acs.est.5b03838

Zimmer M, Gray JM, Pokala N et al (2009) Neurons detect increases and decreases in oxygen levels using distinct guanylate cyclases. Neuron 61:865–879. https://doi.org/10.1016/j.neuron.2009.02.013

Chapter 10
Polymeric-Patterned Surface for Biomedical Applications

Namita Jaiswal, Abhiram Hens, Manosree Chatterjee, Nibedita Mahata, Nagahanumaiah and Nripen Chanda

Abstract Polymeric-patterned surfaces are finding significant importance in various biomedical applications such as screening and diagnostic assays, tissue engineering, biosensors, and in the study of fundamental cell biology. A wide variety of methods, involving photolithography, inkjet printing, soft lithography, and dip-pen lithography, have emerged for protein or polymer patterning on various substrates. For directional immobilization or adsorption of protein, surface requires pre-defined regions to which protein molecules can be immobilized. The most common techniques to introduce defined protein immobilization are soft lithography and photolithography. However, these techniques have some associated limitations. In soft lithography, stamps with well-defined structures are required, and the migration of ink during and after printing needs to be well controlled. In photolithography, a polymeric photoresist and a mask are needed which require expensive setup to fabricate. Therefore, facile and economic techniques are worth exploring. The dewetting of a thin polymeric film is a spontaneous and self-organized process that forms an array of microscale and nanoscale droplets on a substrate. This is a facile approach of patterning polymer on glass substrate providing a reliable surface for specific, dense, and uniform immobilization of desired molecules to pre-designed patterns. Since antibody orientation is very important in antibody-based surface capture assays, patterned polymer surfaces are of great importance with respect to an increasing number of biosensor applications. Apart from protein patterning, such polymeric-patterned surface can be effectively used in specific type of cell isolation and detection. Indeed, it is found that circulating tumor cells (CTCs) are easily

N. Jaiswal · A. Hens (✉) · M. Chatterjee · Nagahanumaiah · N. Chanda (✉)
Micro System Technology Laboratory, CSIR-Central Mechanical Engineering Research Institute, Mahatma Gandhi Avenue, Durgapur 713209, India
e-mail: a_hens@cmeri.res.in

N. Chanda
e-mail: n_chanda@cmeri.res.in

N. Jaiswal · M. Chatterjee · N. Mahata
Department of Biotechnology, National Institute of Technology, Mahatma Gandhi Avenue, Durgapur 713209, India

S. Bhattacharya et al. (eds.), *Environmental, Chemical and Medical Sensors*, Energy, Environment, and Sustainability, https://doi.org/10.1007/978-981-10-7751-7_10

isolated using such patterned structures either on a flat plate or inside a microfluidic environment.

Keywords Patterned surface · Polymers · Proteins · Biosensors
Cell isolation · Detection

1 Introduction

The last two decades have witnessed a rapid development of broad range of techniques such as photolithography, inkjet printing, soft lithography, and dip-pen lithography employed to pattern polymers. The diversity of the existing synthetic and biological polymers is critical to the extensive development of polymer patterning strategies. Moreover, great versatility of patterned polymer films in terms of chemical composition, properties, and the ease of processing are the key factors responsible for the growing demand of these surfaces. Polymers due to their low cost, good mechanical properties, and compatibility with most of the patterning techniques are ideal choice for patterning-based applications. Thus, patterned polymeric surfaces are widely used in many fields, including (1) the fabrication of light-emitting displays (LEDs), semiconductor microelectronics, and plastic-electronics (Black et al. 2007; Shimoda et al. 2003; Singh and Sariciftci 2006); (2) biomedical research including the study of cells and tissue engineering (Théry et al. 2005, 2006; Hollister 2005); (3) the generation of masks and templates (Park et al. 1997; Kane et al. 1996); (4) the production of optical components such as gratings or photonic crystals (Valkama et al. 2004; Campbell et al. 2000); and (5) fundamental research in surface science and combinatorial synthesis (Fodor et al. 1991; Seemann et al. 2005a). The present chapter will focus on different routes of fabricating polymeric-patterned surfaces and their applications related to the biomedical field, specifically in protein patterning, cell isolation, and other sensing-related applications.

Micropatterned polymer surfaces with chemical and topographical features have gained much popularity in biomedical research. For example, biosensor, where biomolecules (such as enzyme) immobilized onto a conductive or semiconductive-patterned surface, is used to convert the biological functions into electronic information/signals (Willner and Katz 2000). In the field of drug discovery and development, as most drug-targets are composed of proteins, these studies greatly influence the process of new drug development and precisely locating new possible targets. Patterned protein surfaces allow parallel screening of protein functions with ease and simplicity (Satoh et al. 2009). Additionally, protein patterns can be used to select and characterize novel antibodies from phage display libraries and for identification of antigens (Büssow et al. 2001). The technique of patterning proteins is also indispensable in microfluidic devices involved in concentration and identification of specific cells and biomolecules (Nagrath et al. 2007).

Proteins, unlike oligonucleotides, have diverse characteristics related to charge, structure hydrophobicity, and other biochemical properties which affect their stability and interfacial behavior. Protein-patterned surfaces which are also known as protein microarrays need well-defined immobilization strategies capable of maintaining protein structure–property relationships. An unique possibility for exploration and progress of a variety of biomedical and biotechnological applications especially in the areas of screening and diagnostic assay (Chen et al. 2008; Hartmann et al. 2009; Caiazzo et al. 2009), biosensor technology (Willner and Katz 2000), proteomics (Poliness et al. 2004), drug delivery (Riepl et al. 2005), tissue engineering (Riepl et al. 2005), and fundamental cell biology studies (Suh et al. 2004) are offered by protein microarrays.

The performance of polymeric-patterned surface depends mainly on the properties of the substrate, including homogeneity of chemical and physical structures, surface energies, and surface morphologies (Valkama et al. 2004). The base substrates used for protein patterning can be metals, silicon-based substrates (glass and silicon wafer), and polymers. Metal surfaces such as gold, palladium, silver, platinum, copper, and nickel are routinely used, as they are easy to modify. Gold is the most frequently utilized substrate for protein immobilization in the form of microarrays because of its specific properties, such as inertness to oxygen and biocompatibility (Karthaus et al. 1999). However, the high cost of the noble metal surfaces has necessitated the development of alternative surfaces such as polymeric ones. The goal of this chapter is to present the recent developments in the field of polymer patterning techniques and the various biomedical applications of these patterned surfaces including cell isolation and detection in vitro.

2 Methods for Developing Polymeric-Patterned Surfaces

2.1 Photolithography

Photolithography is one of the most traditional and widely used techniques for patterning of polymers (Ito and Okazaki 2000; Bates et al. 2001). The key requirements of this technique are an UV light, a photoresist (a light-sensitive organic polymer), and a mask. The substrate to be patterned is spin coated with a thin homogeneous layer of UV-sensitive monomer or polymer (photoresist) and selectively exposed this layer to photoirradiation followed by removal of the selected areas of the film via chemical etching using appropriate solvent. Selective irradiation with ultraviolet light is obtained by exciting the film through an ultraviolet mask which triggers various chemical reactions such as photopolymerization, photocrosslinking, and functionalization or decomposition reactions (Ghezzi 2015). Photolithographically patterned polymer surfaces are widely used as substrates for protein patterning. For this, photoresist pattern is further modified with the protein adhesion-promoting molecules and removal of the residual photoresist is done by

sonication in organic solvent. Finally, backfilling the surface with a protein-resistant molecules followed by incubation in a protein solution results in proteins patterned on the surface (Yap and Zhang 2007). The process is quite tedious and requires clean room facilities and expensive equipment. Above all, enhancing the resolution of patterning without raising the cost of the process could be a major challenge. Maintaining the structural integrity and function of biomolecules may be compromised due to sensitivity to UV irradiation, solvents used or photoinitiators. Patterning using this technique can only be done on flat surfaces, thereby making other types of modified surfaces unsuitable for this type of approach. Thus, facile, inexpensive, high-throughput methods which can be operated on a regular laboratory bench top with less processing steps are desirable.

2.2 Soft Lithography

A set of biocompatible techniques for patterning biomolecules have recently been developed by Whitesides and colleagues, collectively known as "soft lithography." It is so named because a soft elastomeric stamp with patterned relief structures is used for generation of patterns of size in the range of 30 nm–100 μm (Kane et al. 1999; Xia and Whitesides 1998). The elastomeric stamp is fabricated by casting a liquid pre-polymer (e.g., poly (dimethylsiloxane) or PDMS) against a master having desired patterned release structure. Fabrication of protein patterns is done either by directly patterning proteins or by first patterning protein adhesion-promoting molecules and then by subsequent protein immobilization. It is a more user-friendly, convenient, and inexpensive method as compared to photolithography because of reusability of stamps or masters (Kane et al. 1999), minimization of clean room requirement, and suitability for patterning over non-planer surfaces. Among various soft lithographic techniques, stencil patterning is the most common technique that is used for micropatterning of proteins and biomolecules. The main disadvantage of soft lithography is that it uses photolithography during the fabrication of the masters that are used for casting PDMS stamps. Moreover, stamps with well-defined structures are required in this case, and the migration of ink during and after printing needs to be precisely controlled as it decreases the fidelity of patterns (Lau et al. 2008).

2.3 Direct Writing Techniques

Patterning by delivery of molecules through a nozzle or a probe tip to the targeted areas of the substrate is the underlying principle of direct writing technique. Dip-pen nano-lithography and inkjet printing are the patterning approaches associated with direct writing. Dip-pen nano-lithography (DPN) is a scanning probe microscopy-based technique where selective deposition of the patterning material

on the substrate is done by the tip of an atomic force microscope (AFM) (Piner et al. 1999). Scanning of the substrate by the AFM tip loaded with the patterning material results in the formation of a liquid meniscus between the tip and the substrate, followed by transferring the patterning materials. DPN can "write" patterns as small as 15 nm which is way below the smallest size achieved by lithography-based techniques.

Microarrays and nano-arrays of proteins and DNA have been generated utilizing DPN patterning technique, showing promising applications in biological recognition and diagnostics studies (Lee et al. 2002, 2006). The major drawback of DPN is the slow rate of patterning and its inability to pattern large areas, despite the recent attempts to accelerate the process by using massive parallel method (Bietsch and Michel 2000; Sirringhaus et al. 2000). Similarly, in inkjet printing, polymer droplets are deposited on a substrate by using ink jet printers. A jet of polymer solution breaks up into small droplets and gets deposited on the substrate, thereby forming polymer patterns upon evaporation of the solvent (Cai 2009). The printing done through this method is inexpensive, simple, and flexible. However, the size of the pattern (typically ~ 100 μm) is larger than the lithography-based techniques (Geoghegan and Krausch 2003).

2.4 *Self-organization of Thin Film*

Dewetting is defined as a phenomenon where a thin film reorganizes on a substrate into an ensemble of separated objects such as droplets, pillars, or stripes. It is a common phenomenon and can be observed in everyday life, such as the rupture of a water layer into droplets on a hydrophobic teflon-coated surface (Gentili et al. 2012). Thin films made from polymer solutions are ideal for dewetting experiments. The thin polymeric films are obtained by spin coating the polymeric solution on a solid substrate. When this thin polymeric film is either heated or kept under a solvent vapor chamber, dewetting takes place. Basically, it arises due to the instability at the liquid—vapor interface caused by surface tension and intermolecular forces. When extent of this instability crosses a certain critical limit, initiation of dewetting takes place via rupturing of the film. The ruptured film further organizes based on surface tension and finally produces an array of droplets or patterned structures (Reiter 1992; Sharma and Reiter 1996; Seemann et al. 2001a, 2005b; Redon et al. 1991; Wyart et al. 1993) (Fig. 1).

Dewetting may proceed by either homogeneous or heterogeneous mode of hole nucleation. In case of heterogeneous mode of nucleation which is characteristic of most unstable and metastable films, dewetting is initiated with random nucleation of holes at sites of local heterogeneity in the liquid film or on the substrate, usually the defect sites (e.g., dust particles) or sites with high residual stress in the case of thin polymer films (Jacobs et al. 1998; Reiter et al. 2005).

Minimization of the contact area between the liquid film and solid substrate is achieved by lateral growth in the size of the nucleated holes on the polymeric film.

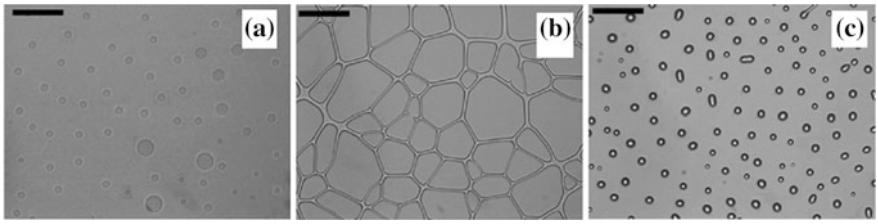

Fig. 1 Morphological evolution at different stages of solvent (toluene) vapor-induced dewetting of PS film **a** hole formation, **b** growth of holes, and **c** formation of isolated droplets. Reprinted with permission from Mukherjee et al. (2010)

Hole growth accompanied by material displacement from the center of the nuclei leads to accumulation of material into a rim surrounding the hole. In the late stage of dewetting, the holes cannot grow any further and coalesce with neighboring holes. Coalescence causes overlapping of the rims of the two holes, thereby forming a liquid cylinder, which eventually decays into single droplets due to Rayleigh–Plateau instability. In the final state, isolated droplets of liquid are found throughout the solid substrate as spherical caps, with Young's equilibrium contact angle (Fig. 2) (Seemann et al. 2001b).

Dewetting is an undesirable phenomenon in several situations, as in case of rupture of protective coating films or paints. However, dewetting becomes desirable when it is used as a powerful tool for surface micropatterning. Dewetting mediated surface patterning is fundamentally a scalable process. By tuning the annealing conditions (temperature and time), patterned structures of controllable sizes could be produced. Dewetting at any stage of hole growth can be stopped by reducing the temperature. Larger holes are obtained by providing the dewetting process to continue over longer periods of time (or the higher annealing temperature). Thus, dewetting is inexpensive, facile, high-throughput technique, wherein the number of processing steps for fabrication of a micropatterned surface is low and independent

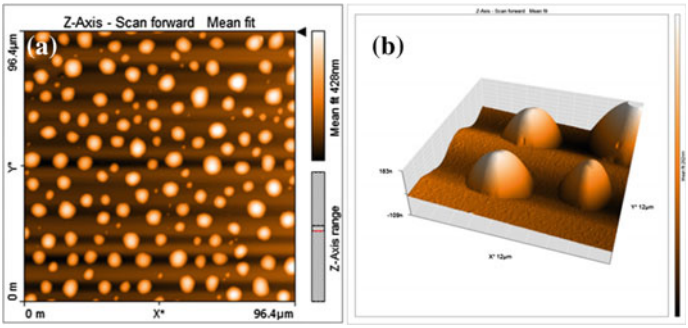

Fig. 2 **a** AFM image of dewetted PLGA structures; **b** 3D rendering of an AFM topography image illustrating the final stage of dewetting of poly (D,L-lactide-co-glycolide) (PLGA) on a glass substrate. Reprinted with Permission from Jaiswal (2017)

of surface size. Micropatterns generated by this technique can be one of the regular laboratory benchtop methods without the necessity of expensive instrumentation or a sophisticated environment. Dewetting has been suggested as an important process for patterning biological molecules for biological/biomedical applications. Telford et al. (2012) reported the use of surface patterns produced by dewetting of thin polymer films for site-selective protein adsorption and cell immobilization.

3 Applications of Polymeric-Patterned Surfaces

3.1 Protein Patterning

Protein micropatterns refer to highly ordered arrays of proteins spatially immobilized on a pretreated solid support while the neighboring regions being resistant to non-specific adsorption of proteins (Yap and Zhang 2007). Protein microarrays mainly find applications for identification, quantification, and functional analysis of proteins, which are of interest for proteomic research in basic and applied biology and diagnostic applications. They are also employed in pharmaceutical industries where the validation of potential target molecules is of main concern (Stoll et al. 2004). The history of protein patterns can be dated back to 1978, when the micropatterning technique was first used by Macaler and Wehrung for creating a bioelectronic microcircuit pattern (McAlear and Wehrung 1978). Unlike nucleic acids which have predictable sequence-specific hybridization chemistry, proteins have numerous differences in their functional groups, affinities, secondary and tertiary structures. The complex tertiary structures of proteins are highly sensitive to environmental and interfacial conditions, thus most proteins usually require customized attachment solutions in order to preserve their conformation and activity. This is further complicated by the diversity of proteins in terms of structure, function, expression level, and stability (Wagner and Kim 2002). Moreover, the post-translational modification such as acetylation, glycosylation, phosphorylation, and the tendency of multi-merization further makes the protein structure more diverse and complex. Though protein patterning is governed by the same fundamental concept as DNA patterning, the low stability and greater complexity of proteins (Schena 2005; Müller and Nicolau 2005) make protein patterning more challenging than DNA patterning. Antibodies are glycoproteins belonging to the immunoglobulin super family (Schramm et al. 1993). These molecules, due to their high specificity and affinity for epitope, a small region on target protein (Saerens et al. 2008; Blažek and Celer 2003), can make exceptional probes and hence have multiple applications in various fields of biological research such as biosensors and diagnostics.

Valsesia et al. (2008) use an alternative fabrication methodology combining colloidal lithography (CL) with plasma-enhanced chemical vapor deposition (PE-CVD) of functional polymers for preparation of chemically nano-structured

surfaces (Valsesia et al. 2004, 2006). This method enables the fabrication of nano-patterned surfaces with contrasted adhesive properties: Particularly, COOH-functionalized nano-areas are surrounded by a poly (ethylene oxide) (PEO)-like anti-adherent matrix. Such surface allows selective immobilization of biomolecules on the adhesive regions leaving the background free of biomolecules. The immune-reaction efficiency between uniformly functionalized and chemically nano-patterned surfaces for antigen/antibody interactions with and without the use of an orienting protein, viz. protein-A, is compared in this study.

Briefly, the steps involved in the formation of the nano-structured surfaces are as follows: First, poly (acrylic acid) (PAA) layers, with carboxylic functional groups, are deposited on the substrate by means of PE-CVD. A nano-mask is obtained by spin coating COOH-functionalized polystyrene (PS) nanoparticles in colloidal suspension. This allows the formation of a homogeneous monolayer of PS beads over the entire active area of the sample. The substrate used is a quartz crystal resonator and the process is accurately controlled so bead multilayers formation could be avoided. Oxygen (O_2) plasma etching enables the transfer of the nano-mask pattern to the PAA layer. After the formation of polymeric nano-structures on the surface, plasma deposition of the PEO-like coating (anti-adhesive layer) as chemical contrast through the nano-mask is done. An ultrasonic treatment of the surfaces in ultrapure water enables the lifting-off of the residual nano-sphere mask. The final surface comprises of nano-areas of carboxylic functionalities surrounded by the anti-adhesive layer. The morphology of the resulting surface is shown in Fig. 3.

Further, quartz crystal resonator microbalance-based real-time monitoring of the immunoreaction between human IgG and Ab-human IgG is done. The two different surfaces used in the study are as follows: a homogeneously functionalized surface by COOH moieties obtained by PE-CVD, and the other is COOH-functionalized nano-domes immersed in a non-adhesive matrix. The study applies two routes of IgG immobilization: Direct immobilization of IgG on the platforms is done in the

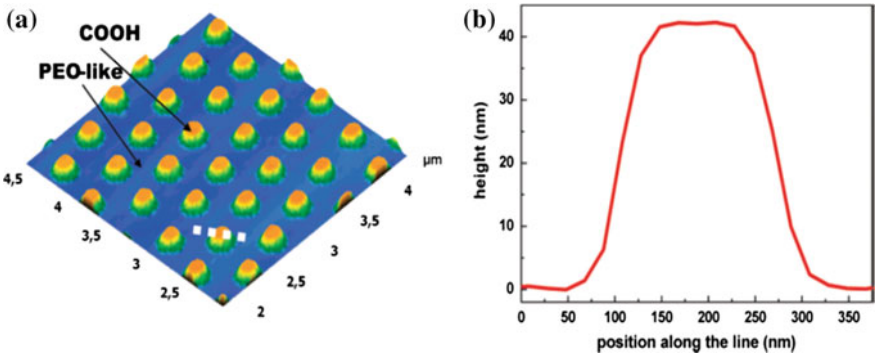

Fig. 3 **a** Atomic force microscope (AFM) image of the COOH-functionalized nano-patterned surface **b** profile along the dotted line in (**a**). Reprinted with permission from Valsesia et al. (2008)

first route, while in the second route, prior immobilization of protein-A is carried out for directional capture of IgG molecules. A 30% increase in reaction efficiency with Ab-IgG is observed on surfaces containing protein-A as it helps the orientation of the IgG molecules.

The nano-patterned platform without protein-A pre-treatment shows highest IgG/Ab-IgG reaction efficiency, demonstrating the capability of the adhesives/anti-adhesives nano-patterned surface for immobilization of molecules in a reactive state. This "increased availability" is attributed to the reduction of the steric hindrance of the immobilized molecules due to the artificial separation levied by the adhesive-non-adhesive surface pattern. This type of nano-patterned surfaces can be extremely advantageous when used as immuno- and biosensors, as optimum values for the immunoreaction efficiency could be achieved without the use of orienting proteins such as protein-A, which are usually very expensive and difficult to synthesize. Moreover, the easy fabrication of such nano-patterned surfaces makes them excellent candidates for immobilization of diverse biomolecules.

In another work, by Ghezzi et al. (2014), dewetting-assisted micropatterning of poly (D,L-lactide-co-glycolide) (PLGA) thin films on top of polystyrene (PS) thin films are grafted with poly (ethylene glycol) (PEG) brushes. The so obtained micropatterned surface is used for selective adsorption of proteins, and the presence of dense PEG brushes help in repelling the unwanted proteins.

In their approach, PLGA micropatterns were obtained via dewetting process. Surface patterns consisting of randomly nucleated polystyrene (PS) holes in the bulk of PLGA matrix were formed by annealing above glass transition temperature (T_g). Functionalization of PLGA micropattern is done by a two-step method involving aminolysis or hydrolysis followed by grafting of PEG molecules. The advantages associated with this type of functionalization procedure are the flexibility (use of different chemical reactions for antibody immobilization on aminolyzed surfaces), the limited synthetic effort involved (commercially-available chemicals are used), and the eco-friendly nature (reactions are performed mostly in water or PBS). Selective protein adsorption on micropatterned substrates is achieved due to the difference in protein adsorption affinity on PEG brushes and PS holes. PLGA films grafted with PEG show very low protein adsorption. Passivation of the PEG-grafted PLGA (PEG-g-PLGA) due to PEG coating results in resistance to hydrolytic degradation of the PEG-g-PLGA films in PBS as compared to the untreated PLGA films. High protein adsorption along with the low cytotoxicity of PLGA makes these surfaces an promising platform for biomedical applications such as studying single-cell assays, targeted cell capture studies, development of high sensitivity ELISA surfaces.

A non-photolithography-based approach for patterning FITC-tagged bovine serum albumin (BSA) is proposed by Cai and Newby (2008) utilizing dewetted polystyrene (PS) droplets. A poly (ethylene glycol) (PEG) silane-modified surface is spin coated with thin film of polystyrene (PS) followed by annealing at 120 °C for 2 h. Upon evaporation of a dilute PS solution in chloroform (100 μg/mL) between the PEG-silane-modified silicon surface and moving parallel glass surface, isolated PS droplets are formed which selectively adsorb protein molecules, thereby

exposing the PEG-silane-modified surface, capable of resisting the adsorption of protein. More protein adsorption takes place on the dewetted structures as compared to the flat undewetted PS surfaces (Fig. 4). The possible explanations for this type of observation could be attributed to the fact that the area of the droplet or the curved rim is greater than that of its planar projection, thus an increased area for protein adsorption is available (Yap and Zhang 2005). Another possible explanation

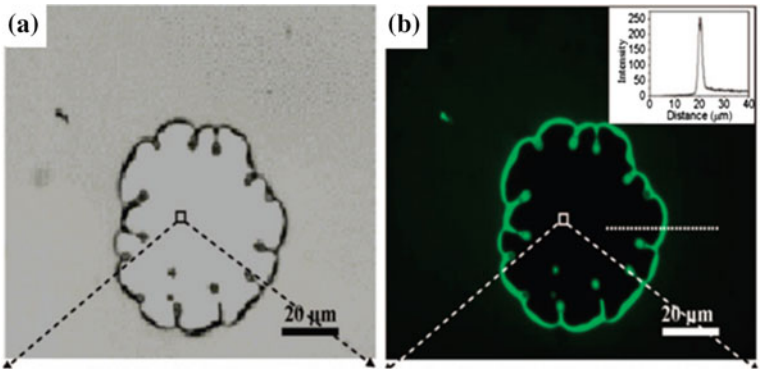

Fig. 4 **a** Optical microscopic view of polystyrene (PS) thin film after 2 h annealing at 120 °C in vacuum. **b** Fluorescence view of image (**a**) after 20 min incubation of the sample in FTIC-BSA solution (inset) white line indicating the fluorescence intensity profile. Reprinted with permission from Cai and Newby (2008)

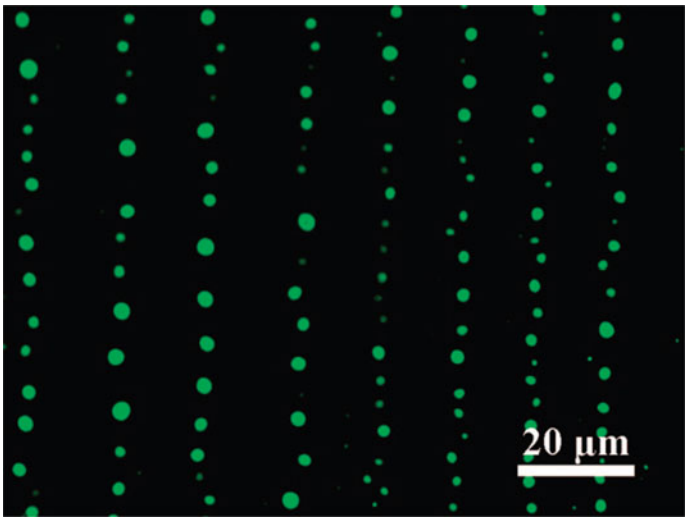

Fig. 5 Fluorescent view of protein patterns on ordered PS droplets obtained after dewetting. Reprinted with permission from Cai and Newby (2008)

is the increased surface roughness. It is well established that an increased effective surface area is provided by a rougher surface, thereby facilitating the deposition of protein multi-layers (Rechendorff et al. 2006; Lee and Vilgis 2003) (Fig. 5).

Thus, higher protein density is found to be adsorbed on rough PS droplets which eventually facilitate easy detection of the PS particles. Thus, enhanced biosensor sensitivity and improved detection capability can be expected from sensors utilizing this type of protein patterns (Mehrvar and Mustafe 2004). By simply controlling the thickness of the film, the method allowed the fabrication of a wide range of sizes of PS droplet patterns, which in turn could be utilized for patterning of protein over a large area within a short period of time and on a regular laboratory bench top.

3.2 Cell Isolation and Detection

Tumor cells present in blood stream are denoted as circulating tumor cells (CTC). Their presence and number in the blood stream closely correlate with the development, disease progress, and treatment response of metastatic cancer in patients (Cristofanilli et al. 2004; Danila et al. 2011; Riethdorf et al. 2007, 2010). The isolation and detection of CTC from blood, frequently called "liquid biopsy," is a field attracting tremendous scientific and clinical interest, as the method offers potential to replace the existing tissue biopsy that is invasive in nature and technically quite challenging (van de Stolpe et al. 2011). However, due to the low frequency of CTCs among blood cells (one in 10^6–10^9 hematologic cells), clinically significant detection of CTCs still remains a highly challenging task. A number of detection methods, viz. size-/density-based detection, nucleic acid-based detection, and antibody-based detection against tumor cell surface markers, are investigated, so as to achieve sensitive and efficient CTC detection. The routinely used surface markers in such studies include epithelial cell adhesion molecule (EpCAM) (Allard et al. 2004; Momburg et al. 1987), carcino-embryonic antigen (CEA) (Balasubramanian et al. 2011), EpCAM/cytokeratin combinations (Deng et al. 2008), and human epidermal growth factor receptor-2 (HER-2) (Mi et al. 2011; Xu et al. 2011).

Polymers have played a pivotal role in most of the CTC detection and isolation techniques mentioned above including separation based on physical properties using polymeric-patterned structures (Zheng et al. 2011), targeted detection in solution using polymer-coated inorganic nanoparticles (Balasubramanian et al. 2011; Galanzha et al. 2009), and capturing based on polymer-immobilized surfaces (Myung et al. 2011). Although the recent advances in CTC detection have been summarized in many reviews (Paterlini-Brechot and Benali 2007; Mostert et al. 2009; Yu et al. 2011), the central role played by polymers yet needs revisiting. This section therefore focuses on the utilization of polymeric materials for CTC isolation and detection, also emphasizing on current developments in related technologies, thereby providing a detailed overview for the use of polymer patterns in enhanced CTC isolation and detection methodologies.

Oxygen plasma treatment of polystyrene (PS) has long been used to create optimal surface for tissue culture (Zeiger et al. 2013). The resulting hydrophilic nano-structured PS surface provides an efficient binding platform for adherent cells (Ishizaki et al. 2010). Based on this observation, Wan et al. (2014) report a marker-free integrated approach for CTC detection combining high-throughput total content screening technology, which significantly increases tumor cell binding on standard tissue culture polystyrene well plates (Wan et al. 2014). The procedure involves a single 5 min high-power oxygen plasma treatment of standard tissue culture polystyrene substrates resulting in homogeneously nano-structured surfaces (Fig. 6).

These patterned surfaces are further employed to establish the effect of nanoscale roughness on tumor cell binding using 5×10^5 T98G (glioblastoma cell line) cells suspended in DMEM. At 2 h time point, it is observed that 94 ± 2% of the cells adhered onto the nano-structured PS surfaces while only 73 ± 2.5 and 34 ± 4% cells are bound onto the untreated PS and glass surfaces, respectively. Further improvement of the binding yield of tumor cells on the nano-structured PS is obtained by adsorption of poly-L-lysine (PLL) layer resulting in excess positive charges on the structured surface, which significantly enhanced the tumor cell binding yields above 97% at 2 h as shown in Fig. 7. Studies of binding yields of various cancerous and non-cancerous cell lines demonstrate that the tumor cell lines used in the study have efficient, strong, and rapid attachment onto nano-structured tissue culture PS surfaces as compared to the non-cancerous cells, which showed relatively low binding.

In another study, clinically significant concentrations of highly metastatic variant of human breast cancer cell line MDA-MBA-231 expressing green fluorescent protein and spiked into healthy human blood are reliably detected on the nano-structured PS surfaces using the operetta automated high-content analysis system. In order to demonstrate the feasibility of the approach in real-life situation, detection of CTCs in the blood of a stage-IIIc colorectal cancer patients is carried

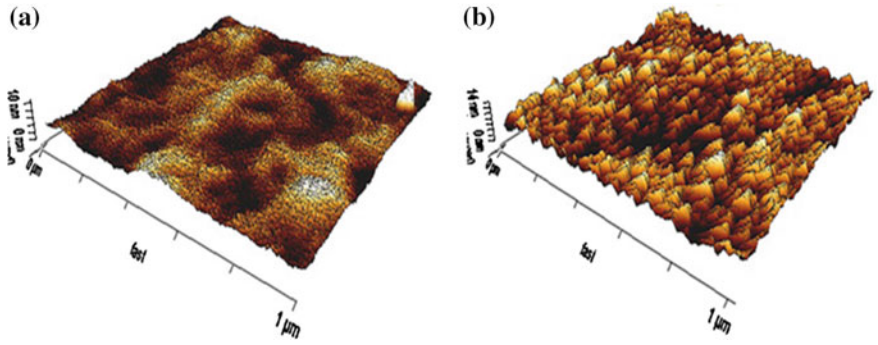

Fig. 6 Representative atomic force microscope (AFM) images (1 × 1 µm) of **a** untreated PS and **b** treated PS (500 W oxygen plasma treatment for 5 min). Reprinted with permission from Wan et al. (2014)

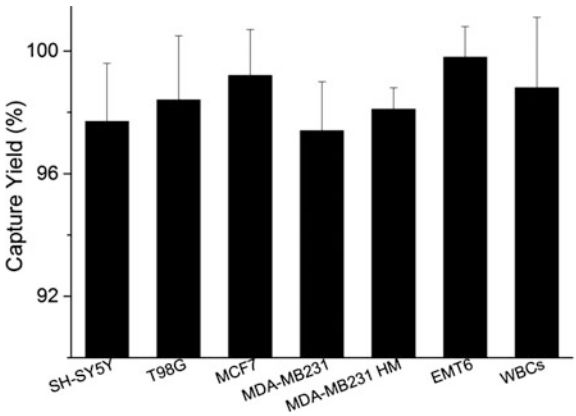

Fig. 7 Binding yields for different cell lines (cancerous and non-cancerous) on PLL-treated rough PS surface. Reprinted with permission from Wan et al. (2014)

out. 3.5 mL of blood is analyzed, and 21 CTCs are unambiguously identified (Fig. 8). The proposed approach therefore enables rapid, unbiased, and marker-free detection and molecular analysis of tumor cells. The tumor cell isolation substrates reported in this study could readily be used after clinical validation, on a large scale in any center equipped with automated microscopy facilities. The approach is potentially cost-effective and efficient solution toward large-scale clinical implementation of CTC-based diagnostic and prognostic approaches.

It is well established that nano-structures offer high specific surface area, thereby allowing immobilization of more immune-sensitive molecules onto their surface. Hierarchical structures provide additional physical cues which interact with the cancer cells. Therefore, with the objective of utilizing the combined advantage of both nano-structures and microfluidics, several groups have attempted the integration of nano-structures into microfluidics channels (Han et al. 2009; Wang et al. 2013). For example, nano-wires (Chen et al. 2011), three-dimensional nano-pillars (Hsiao et al. 2014), and other nano-materials/arrays (Han et al. 2009; Meng et al. 2014; Liu et al. 2013; Mattila and Lappalainen 2008) are integrated with microfluidics. However, aforesaid hierarchical structures, due to complicated fabrication

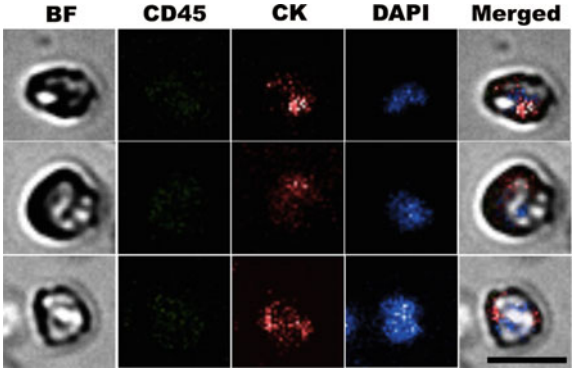

Fig. 8 CTCs isolated from a colorectal cancer patient after DAPI, CD45, and anti-cytokeratin staining. The image was taken using the 20 × objective lens. BF = bright field. The scale bar equals 10 μm. Reprinted with permission from Wan et al. (2014)

process and mostly based on silicon, result in poor optical transparency (Chen et al. 2011; Zhang et al. 2013).

A soft lithography-based fabrication of a "Rhipsalis (Cactaceae)"—a micropillar array-based device (Rm-chip) for efficient capture of cancer cells in three dimensions (X, Y, and Z planes) with high optical transparency is proposed by Yan et al. (2016) and shown in Fig. 9.

Fabrication of PDMS micropillar array (dimensions of the channel: 40 mm in length and 20 mm in width, and 100 μm in diameter) is carried out by conventional soft lithography. The device is plated with gold layer following a previously reported electroless plating procedure (Bai et al. 2009). Modification of the device surface with EpCAM antibody is achieved through the thiol-oligonucleotide linkers employing avidin–biotin conjugation.

In order to determine the cell capture efficiency of the Rm-chip, cell suspension of human breast cancer (MCF-7), non-small-cell lung cancer (NSCLC, NCI-H1650), and cervical cancer (HeLa) cell lines pre-labeled with fluorescence are spiked into phosphate buffered saline (PBS) or whole blood and pumped through the chip with the help of Micro4 syringe pump. In this study, EpCAM expressing cell lines (MCF-7 and NCI-H1650) are easily captured with higher efficiency as compared with the non-EpCAM (HeLa) cells. The capture efficiency of Rm-chip for MCF-7 spiked in PBS is found to be 88% and that for NCI-H1650

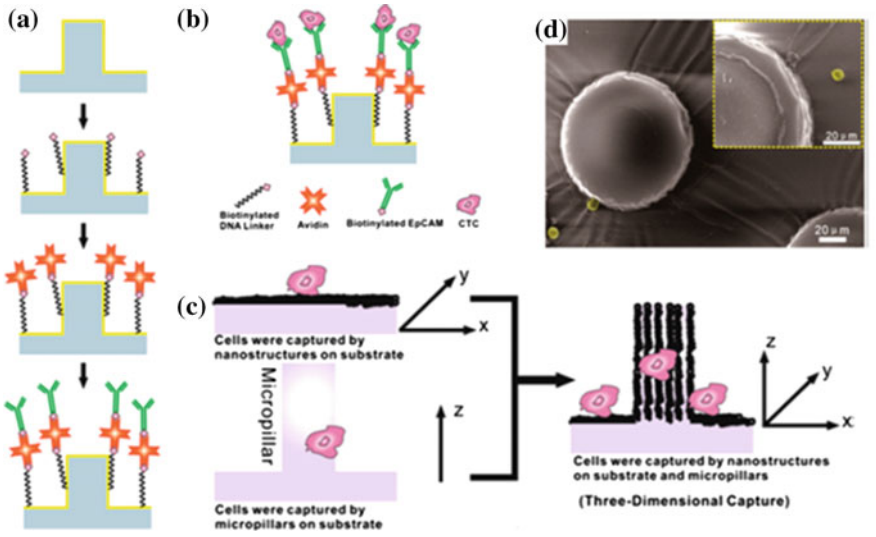

Fig. 9 Schematic of the micropillar functionalization and cancer-cell capture principle of the Rm-chip. **a** Modification procedures of micropillar array. **b** Schematic of the antibody conjugation chemistry and the cell capture. **c** Schematic of cancer-cell capture principle on the nano-structured substrate, conventional micropillar, and modified micro-/nano-structured-micropillar. **d** Scanning electron microscope (SEM) image of captured MCF-7 cell on the micropillar and bottom. Inset: magnified SEM image of the captured MCF-7 cell on the bottom. Reprinted with permission from Yan et al. (2016)

cell spiked in whole blood samples is found to be 83.7%. The high capture yield of Rm-chip is attributed to the thorn-like topological structures of the micropillars and over the substrate. Enhanced interaction between the cells and Rm-chip occurs due to the hierarchical structures, leading to high capture efficiency.

As the anti-EpCAM antibodies are immobilized through DNA linker, exonuclease-I is used to hydrolyze DNA linkers, thereby releasing the captured cancer cell (Fig. 10). The efficient release of cancer cells from the device channel could aid in implementing subsequent molecular and functional analyses of the cells, demonstrating the potential applicability of the patterning strategy used in Rm-chip in CTC studies and clinical diagnosis.

In a recent study, Dou et al. (2017) develop a novel bioinspired surface with hierarchical microscale and nanoscale topographic structures capable of efficient capture and release of circulating tumor cells (CTCs). Fabrication of the hierarchically structured PDMS substrates is done using red rose petals as a template (Fig. 11) as the sizes of their microstructures are analogous to that of a CTC. A facile imprint-pattern transfer procedure is employed for the preparation of hierarchical rose petal-derived PDMS surface. The replicated structures are observed to be closely packed arrays of concave cavities and almost hemispherical micropapillae with diameters and depths/heights of the microstructures about 20–30 μm and typical widths of about 500–600 nm on the surface. A five-step modification process achieves immobilizations of EpCAM on the surfaces. APTES is coupled on the oxygen (O_2) plasma-activated substrates in order to introduce $-NH_2$ (primary amine) groups on the surfaces. Then, grafting of NHS-(S–S)-biotin linker on the substrates is achieved by reaction of the $-NH_2$ groups and the NHS esters. Classic biotin−avidin interaction is employed for conjugation of streptavidin to the biotin-modified substrates. Finally, attachment of biotinylated anti-EpCAM molecules is done onto the substrates before the cell capture experiments.

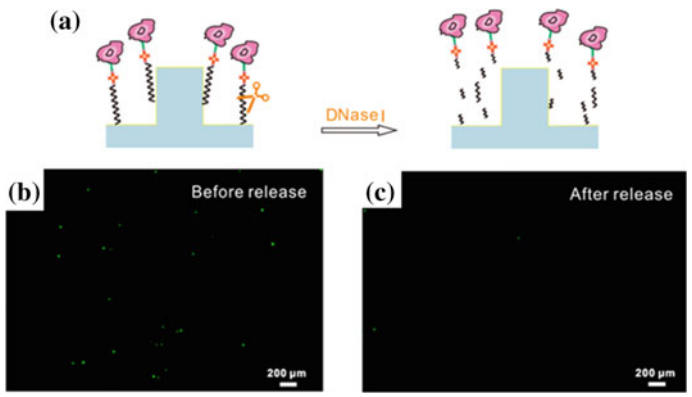

Fig. 10 Release of captured NCI-H1650. **a** Cell release schematic after using exonuclease-I. **b** Images of fluorescence microscopy of captured cells pre-stained with calcein-AM before exonuclease-I treatment. **c** Fluorescence microscopy image of (**b**) after exonuclease-I treatment at 37 °C for 50 min. Reprinted with permission from Yan et al. (2016)

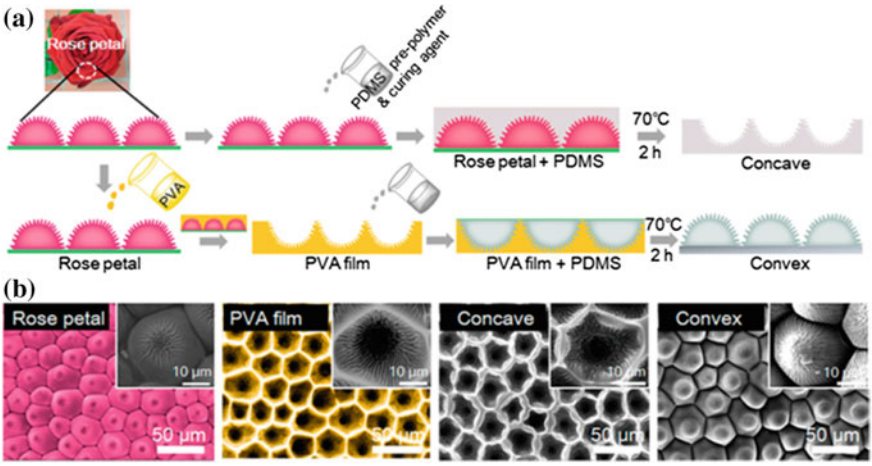

Fig. 11 **a** Schematic for the fabrication of PDMS replicas and inverse replicas of the rose petal (Dou et al. 2015). **b** Scanning electron microscope (SEM) images of an original rose petal, a replicated PVA film, a replicated PDMS substrate with concave hierarchical structures, and a PDMS substrate replicated from the PVA exhibiting convex hierarchical structures. Reprinted with permission from Dou et al. (2017)

The maximal cell capture on the anti-EpCAM-modified PDMS substrates is achieved after about 60 min while 120 min of incubation is required for the same on tissue culture polystyrene (TCP) surfaces.MCF7, an EpCAM-positive cell line when captured on anti-EpCAM-modified hierarchical structures, shows up to four times higher capture efficiency than that on the flat surface.

Treatment of the patterned surface with the biocompatible reductant glutathione (GSH) releases up to 85% of the captured cells (Fig. 12). More than 98% cell

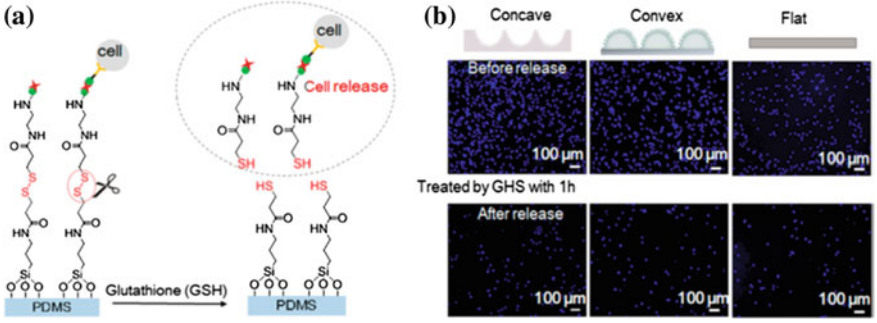

Fig. 12 Release of captured PaTu 8988t cells via cleavable disulfide bonds. **a** Schematic of cell release by cleavage of the disulfide bonds with glutathione (GSH). **b** Fluorescence microscopy images of PaTu 8988t cells after capture on the substrates, before and after GSH treatment, respectively. Hoechst 33258 blue fluorescent dye was used to stain cell nuclei. Reprinted with permission from Dou et al. (2017)

viability is observed when the released cells are cultured in tissue culture polystyrene plate (TCP) for 24 h. Therefore, these bioinspired hierarchically structured and functionalized substrates have been successfully applied for capture as well as release of CTCs, which is important for subsequent analysis.

3.3 Biomolecule Adhesion

It is a well-established fact that cells respond to their microenvironment. Microscale features are comparable in size to the cells themselves and usually are responsible for whole-cell contact guidance. The cell alignment with patterned topography is called contact guidance and was first reported in 1911 (Harrison 1911; Weiss and Garber 1952; Curtis and Varde 1964). In contrast, the nanoscale features are several orders of magnitude below the cells, similar to dimensions of individual cell receptors and thus cell response can be modulated by targeting the receptor-driven pathways.

Integrins are the receptors associated with cellular adhesion and serve as the communication channels for the cells to interact with neighboring surfaces. The interaction outside the cell is mediated by transmembrane, heterodimeric protein receptors binding to peptide ligands (mostly to arginine, glycine, aspartic acid (RGD) sequence) and by cell's signaling machinery and cytoskeleton within the cell. Many integrin molecules gather together (on nano-scale) to mediate adhesions (on microscale) (Riveline et al. 2001). Thus, the impact of nano-pattern on cell can be evaluated by studying the interaction and gathering of integrin with resulting cell adhesion. The enhanced understanding of cell–nano-topography interactions from these studies aids to the accelerated development of implant interfaces, next-generation stem cell culture materials, and toward advancement of stem cell therapeutics discovery to support regenerative therapies. Several methods have subsequently been developed for surfaces patterning at nanometer resolution which gives control of the peptide clusters position or that of single adhesive ligands.

In a study by Spatz group, influence of surface patterning of bioactive materials and their subsequent organization at nano-level for mimicking the geometric organization and physical and chemical signaling moieties of extracellular matrix (ECM) responsible for controlling cell adhesion has been elucidated. A nano-colloidal assembly mediated control of the number density of integrin-adhesive RGD ligands with a density threshold corresponding to $\sim$70 nm spacing of RGD ligands was achieved (Cavalcanti-Adam et al. 2007, 2008). Higher RGD ligand density (RGD ligands with less than 70 nm separation) enabled formation of focal adhesions and polymerization of contractile actin cytoskeletal stress fibers (Cavalcanti-Adam et al. 2007). Low cell adhesion was observed (more rounded cells with small focal adhesions) at low densities of RGD ligands (more than 70 nm separation) (Cavalcanti-Adam et al. 2007, 2008). These findings suggested that a threshold density of RGD ligands is crucial for the formation of stable integrin adhesions, which again promotes the effective spreading of cell and

formation of focal adhesions. Low adhesion was observed to be potentially unfavorable for cell proliferation as it resulted in cell quiescence or even apoptosis mediated by programed cell death through "homelessness" (Cavalcanti-Adam et al. 2008).

3.4 Other Sensing Applications

The uniquely engineered and multi-functional biological structures and processes are being constantly studied and investigated so as to mimic them which might aid in solving a host of problems. The present-day understanding of biological structures and functions associated with complex physiological systems has provided with tools for development of new therapeutics. Development of biologically inspired materials such as polymers, synthetic hydrogels, artificial pathogens, and biomimetic adhesives is greatly attributed to the enhanced understanding of biological microenvironments, macromolecular assemblies, and biological nano-particulate interactions at molecular level.

Plant and animal tissues are composed of hydrogels which are formed by crosslinking of polymers creating an insoluble network capable of absorbing water without dissolving in the system. Proteins and proteoglycans are the natural polymers that make up the building blocks of hydrogels in biological systems, which in turn form tissues. Many tissue properties can be mimicked by synthetic, thereby finding wide range of applications in biomedical field such as serving as vessels for cells culture and as scaffolds for tissue engineering, contributing largely in rebuild and repair of tissues in vivo. The physical properties of the artificial hydrogels including mechanical strength, elasticity, and water content can be controlled readily by changing the chemistry and crosslinking density of the polymers so as to mimic those of specific natural tissue or elicit a desired biological outcome (Fig. 13a, b, c, d) (Rosales and Anseth 2016). For instance, use of hard or soft hydrogels for stem cell culture directs them to proliferate into brain-like or bone-like cells (Engler et al. 2006). Modification of the hydrogels can be done in such a manner so as to create specific patterned geometries mimicking particular biological structure or for controlling cell shape and functions. It has been shown that restraining the mammary epithelial cells into confined three-dimensional (3D) micropatterned spaces of varying shapes has significant effects on mammary epithelial branching morphogenesis including formation of complex developmental structures (Nelson et al. 2006). Synthetic mimic of natural extracellular matrix (ECM)—the structural and biological framework for all body tissues— may be achieved by covalent and/or non-covalent immobilization of active biological species such as proteins, peptides, and proteoglycans into hydrogels. Highly biocompatible hydrogel structures made of appropriate polymeric materials such as silk-based materials (Ye et al. 2015) find widespread applications for cell culture or mimicking biological microenvironments.

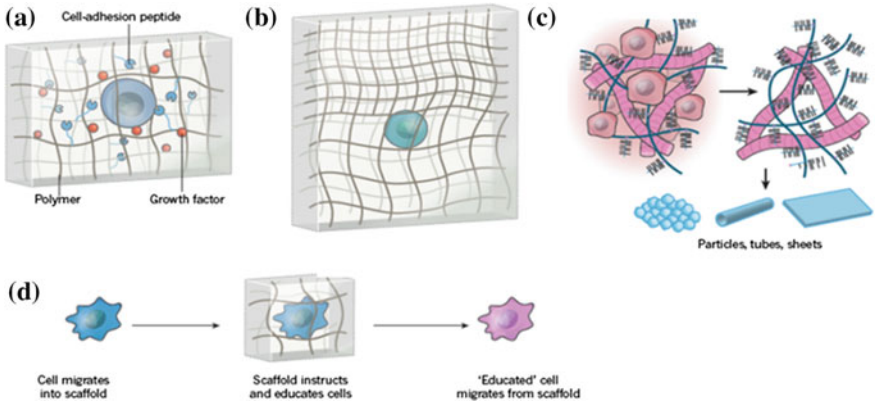

Fig. 13 Strategies involved in creation of tissue mimicking synthetic environments. **a** Native tissue extracellular matrix (ECM) mimics by synthetic polymeric hydrogels modified with peptides or proteins (such as growth factors) (Rosales and Anseth 2016). **b** Controlling the mechanical properties of the hydrogel by varying the crosslinking density or chemically: utilizing metal ligand chemistry from the mussel (Lee et al. 2007). **c** The natural ECM from tissues can be processed into different scaffold forms, such as particles, tubes, and sheets after removing cells. **d** A cell after migrating into a polymeric material can be "educated" to perform a particular function in the body by specific signals embedded in the scaffold. Reprinted with permission from Green and Elisseeff (2016)

The incorporation of large intact biomolecules, or their active regions, or biological small molecules and chemical entities into hydrogels were one of the earliest strategies used to mimic the natural tissue environment. Hydrogels formed by chemically modified poly (ethylene glycol) (PEG) with tethered functional groups such as t-butyl, phosphate, or carboxylic acid were used as a patterned three-dimensional (3D) matrix for encapsulation of human mesenchymal stem cells (hMSCs) (Benoit et al. 2008). Controlling the 3D environment of the hydrogel matrix with the tethered small molecules induced the differentiation of hMSCs into adipogenic and osteogenic pathways. The study demonstrates a powerful technique wherein induction of multiple hMSC lineages was achieved through the interaction of functional groups of small moieties associated with the hydrogel material. Production of therapeutics can thus become cheaper and simpler.

In addition to the above-mentioned application, patterned protein surfaces also find promising applications in other areas. Loeffler et al. (2012) use a combination of different peptides with the CMOS device in order to design multiple peptide-patterned surface, which is used for in situ synthesis of peptides. The method allows parallel synthesis of 16,384 different peptides (10,000 spots cm^{-2}) onto the surface of a microelectronic chip which is among the first of its kind to be reported in this field.

In another study, Borteh et al. (2011) use patterned proteins and peptides for deposition of gold nanoparticles on polymer substrates. The idea to prepare biomolecule-induced gold-patterned surface is realized for the first time and thus

provides a new avenue for preparation of inorganic-patterned surface. Besides these, patterned protein surfaces also find significant applications in the field of genomics, proteomics and diagnosis (Chan and Nie 1998), drug discovery and synthetic biology (Tian et al. 2004), bioreactor and biotransformation (Mao et al. 2004).

4 Conclusion

Patterning of polymers for immobilization of proteins and cells has taken a great leap since its first demonstration a few decades ago. The key techniques involved in patterning of biomolecules include photolithography, soft lithography, and direct writing techniques. However, these techniques have some limitations associated with them; therefore, facile, inexpensive, and flexible methods such as self-organization of thin films via dewetting are rapidly being explored. The promising applications of polymer patterns in the development of protein microarray, biosensors, Circulating tumor cells (CTCs) capture platforms, and fundamental studies in cell biology have kindled strong interest among researchers for continuous improvement of patterning techniques. The incorporation of microparticles or nanoparticles arrays generates a non-planar topography thus providing an increased effective surface area for protein adsorption. Higher densities of biomolecules are thus attached to the non-planar surface which is vital for improving the sensitivity of detection in biosensors. Furthermore, nanoscale features of substrate having similar dimension as that of proteins result in better adsorption of the protein molecules with low interaction and thus helps retain structural and biological activity of the proteins. Successful immobilization of proteins retaining their structural and functional integrity opens new arenas for highly sensitive isolation and identification of biomolecules, specific cells like CTC from blood samples.

Acknowledgements The authors greatly acknowledge Director, CSIR-CMERI, Durgapur, for the support and encouragement. Support from CSIR 12th FYP project no. ESC0112 is gratefully acknowledged.

References

Allard WJ, Matera J, Miller MC, Repollet M, Connelly MC, Rao C, Tibbe AG, Uhr JW, Terstappen LW (2004) Tumor cells circulate in the peripheral blood of all major carcinomas but not in healthy subjects or patients with nonmalignant diseases. Clin Cancer Res 10 (20):6897–6904

Bai H-J, Shao M-L, Gou H-L, Xu J-J, Chen H-Y (2009) Patterned Au/poly (dimethylsiloxane) substrate fabricated by chemical plating coupled with electrochemical etching for cell patterning. Langmuir 25(17):10402–10407

Balasubramanian S, Kagan D, Jack Hu CM, Campuzano S, Lobo-Castañon MJ, Lim N, Kang DY, Zimmerman M, Zhang L, Wang J (2011) Micromachine-enabled capture and isolation of cancer cells in complex media. Angew Chem Int Ed 50(18):4161–4164

Bates AK, Rothschild M, Bloomstein TM, Fedynyshyn TH, Kunz RR, Liberman V, Switkes M (2001) Review of technology for 157-nm lithography. IBM J Res Dev 45(5):605–614

Benoit DS, Schwartz MP, Durney AR, Anseth KS (2008) Small functional groups for controlled differentiation of hydrogel-encapsulated human mesenchymal stem cells. Nat Mater 7(10): 816–823

Bietsch A, Michel B (2000) Conformal contact and pattern stability of stamps used for soft lithography. J Appl Phys 88(7):4310–4318

Black CT, Ruiz R, Breyta G, Cheng JY, Colburn ME, Guarini KW, Kim H-C, Zhang Y (2007) Polymer self assembly in semiconductor microelectronics. IBM J Res Dev 51(5):605–633

Blažek D, Celer V (2003) The production and application of single-chain antibody fragments. Folia Microbiol 48(5):687–698

Borteh HM, Ferrell NJ, Butler RT, Olesik SV, Hansford DJ (2011) Peptide-induced patterning of gold nanoparticle thin films. Appl Surf Sci 258(1):230–235

Büssow K, Konthur Z, Lueking A, Lehrach H, Walter G (2001) Protein array technology. Am J Pharmacogenomics 1(1):37–43

Cai Y (2009) Simple alternative patterning techniques for selective protein adsorption. University of Akron, Akron

Cai Y, Newby B-mZ (2008) Dewetting of polystyrene thin films on poly (ethylene glycol)-modified surfaces as a simple approach for patterning proteins. Langmuir 24(10):5202–5208

Caiazzo RJ, Maher AJ, Drummond MP, Lander CI, Tassinari OW, Nelson BP, Liu BCS (2009) Protein microarrays as an application for disease biomarkers. PROTEOMICS-Clin Appl 3 (2):138–147

Campbell M, Sharp D, Harrison M, Denning R, Turberfield A (2000) Fabrication of photonic crystals for the visible spectrum by holographic lithography. Nature 404(6773):53–56

Cavalcanti-Adam EA, Volberg T, Micoulet A, Kessler H, Geiger B, Spatz JP (2007) Cell spreading and focal adhesion dynamics are regulated by spacing of integrin ligands. Biophys J 92(8):2964–2974

Cavalcanti-Adam EA, Aydin D, Hirschfeld-Warneken VC, Spatz JP (2008) Cell adhesion and response to synthetic nanopatterned environments by steering receptor clustering and spatial location. HFSP J 2(5):276–285

Chan WC, Nie S (1998) Quantum dot bioconjugates for ultrasensitive nonisotopic detection. Science 281(5385):2016–2018

Chen H, Yuan L, Song W, Wu Z, Li D (2008) Biocompatible polymer materials: role of protein–surface interactions. Prog Polym Sci 33(11):1059–1087

Chen L, Liu X, Su B, Li J, Jiang L, Han D, Wang S (2011) Aptamer-mediated efficient capture and release of T lymphocytes on nanostructured surfaces. Adv Mater 23(38):4376–4380

Cristofanilli M, Budd GT, Ellis MJ, Stopeck A, Matera J, Miller MC, Reuben JM, Doyle GV, Allard WJ, Terstappen LW, Hayes DF (2004) Circulating tumor cells, disease progression, and survival in metastatic breast cancer. N Engl J Med 351(8):781–791

Curtis A, Varde M (1964) Control of cell behavior: topological factors 2. J Natl Cancer Inst 33 (1):15–26

Danila DC, Pantel K, Fleisher M, Scher HI (2011) Circulating tumors cells as biomarkers: progress toward biomarker qualification. Cancer J (Sudbury, Mass) 17(6):438

Deng G, Herrler M, Burgess D, Manna E, Krag D, Burke JF (2008) Enrichment with anti-cytokeratin alone or combined with anti-EpCAM antibodies significantly increases the sensitivity for circulating tumor cell detection in metastatic breast cancer patients. Breast Cancer Res 10(4):R69

Dou X-Q, Zhang D, Feng C, Jiang L (2015) Bioinspired hierarchical surface structures with tunable wettability for regulating bacteria adhesion. ACS Nano 9(11):10664–10672

Dou X, Li P, Jiang S, Bayat H, Schönherr H (2017) Bioinspired hierarchically structured surfaces for efficient capture and release of circulating tumor cells. ACS Appl Mater Interfaces 9 (10):8508–8518
Engler AJ, Sen S, Sweeney HL, Discher DE (2006) Matrix elasticity directs stem cell lineage specification. Cell 126(4):677–689
Fodor SP, Read JL, Pirrung MC, Stryer L, Lu AT, Solas D (1991) Light-directed, spatially addressable parallel chemical synthesis. Science 251(4995):767–773
Galanzha EI, Shashkov EV, Kelly T, Kim J-W, Yang L, Zharov VP (2009) In vivo magnetic enrichment and multiplex photoacoustic detection of circulating tumour cells. Nat Nanotechnol 4(12):855–860
Gentili D, Foschi G, Valle F, Cavallini M, Biscarini F (2012) Applications of dewetting in micro and nanotechnology. Chem Soc Rev 41(12):4430–4443
Geoghegan M, Krausch G (2003) Wetting at polymer surfaces and interfaces. Prog Polym Sci 28 (2):261–302
Ghezzi M (2015) Functional surface micropatterns by dewetting of thin polymer films, Ph.D Thesis, School of Chemistry, University of Sydney
Ghezzi M, Thickett SC, Telford AM, Easton CD, Meagher L, Neto C (2014) Protein micropatterns by PEG grafting on dewetted PLGA films. Langmuir 30(39):11714–11722
Green JJ, Elisseeff JH (2016) Mimicking biological functionality with polymers for biomedical applications. Nature 540(7633):386–394. https://doi.org/10.1038/nature21005
Han W, Allio BA, Foster DG, King MR (2009) Nanoparticle coatings for enhanced capture of flowing cells in microtubes. ACS Nano 4(1):174–180
Harrison RG (1911) On the stereotropism of embryonic cells. Science 34(870):279–281
Hartmann M, Roeraade J, Stoll D, Templin MF, Joos TO (2009) Protein microarrays for diagnostic assays. Anal Bioanal Chem 393(5):1407–1416
Hollister SJ (2005) Porous scaffold design for tissue engineering. Nat Mater 4(7):518–524
Hsiao YS, Luo SC, Hou S, Zhu B, Sekine J, Kuo CW, Chueh DY, Yu Hh, Tseng HR, Chen P (2014) 3D Bioelectronic interface: capturing circulating tumor cells onto conducting polymer-based micro/nanorod arrays with chemical and topographical control. Small 10 (15):3012–3017
Ishizaki T, Saito N, Takai O (2010) Correlation of cell adhesive behaviors on superhydrophobic, superhydrophilic, and micropatterned superhydrophobic/superhydrophilic surfaces to their surface chemistry. Langmuir 26(11):8147–8154
Ito T, Okazaki S (2000) Pushing the limits of lithography. Nature 406(6799):1027–1031
Jacobs K, Herminghaus S, Mecke KR (1998) Thin liquid polymer films rupture via defects. Langmuir 14(4):965–969
Jaiswal N (2017) Development and functionalization of polymeric patterned surface for biomedical applications, MTech Thesis, National Institute of Technology Durgapur (India)
Kane R, Cohen R, Silbey R (1996) Synthesis of PbS nanoclusters within block copolymer nanoreactors. Chem Mater 8(8):1919–1924
Kane RS, Takayama S, Ostuni E, Ingber DE, Whitesides GM (1999) Patterning proteins and cells using soft lithography. Biomaterials 20(23):2363–2376
Karthaus O, Gråsjö L, Maruyama N, Shimomura M (1999) Formation of ordered mesoscopic polymer arrays by dewetting. Chaos Interdisc J Nonlinear Sci 9(2):308–314
Lau K, Bang J, Kim DH, Knoll W (2008) Self-assembly of protein nanoarrays on block copolymer templates. Adv Funct Mater 18(20):3148–3157
Lee N-K, Vilgis TA (2003) Preferential adsorption of hydrophobic-polar model proteins on patterned surfaces. Phys Rev E 67(5):050901
Lee K-B, Park S-J, Mirkin CA, Smith JC, Mrksich M (2002) Protein nanoarrays generated by dip-pen nanolithography. Science 295(5560):1702–1705
Lee SW, Oh BK, Sanedrin RG, Salaita K, Fujigaya T, Mirkin CA (2006) Biologically active protein nanoarrays generated using parallel dip-pen nanolithography. Adv Mater 18(9):1133–1136

Lee H, Lee BP, Messersmith PB (2007) A reversible wet/dry adhesive inspired by mussels and geckos. Nature 448(7151):338

Liu X, Chen L, Liu H, Yang G, Zhang P, Han D, Wang S, Jiang L (2013) Bio-inspired soft polystyrene nanotube substrate for rapid and highly efficient breast cancer-cell capture. NPG Asia Mater 5(9):e63

Loeffler F, Schirwitz C, Wagner J, Koenig K, Maerkle F, Torralba G, Hausmann M, Bischoff FR, Nesterov-Mueller A, Breitling F (2012) Biomolecule arrays using functional combinatorial particle patterning on microchips. Adv Func Mater 22(12):2503–2508

Mao C, Solis DJ, Reiss BD, Kottmann ST, Sweeney RY, Hayhurst A, Georgiou G, Iverson B, Belcher AM (2004) Virus-based toolkit for the directed synthesis of magnetic and semiconducting nanowires. Science 303(5655):213–217

Mattila PK, Lappalainen P (2008) Filopodia: molecular architecture and cellular functions. Nat Rev Mol Cell Biol 9(6):446–454

McAlear JH, Wehrung JM (1978) Microsubstrates and method for making micropattern devices. Google Patents

Mehrvar M, Mustafe A (2004) Recent developments, characteristics, and potential applications of electrochemical biosensors. Anal Sci 20(8):1113–1126

Meng J, Liu H, Liu X, Yang G, Zhang P, Wang S, Jiang L (2014) Hierarchical biointerfaces assembled by leukocyte-inspired particles for specifically recognizing cancer cells. Small 10 (18):3735–3741

Mi Y, Li K, Liu Y, Pu K-Y, Liu B, Feng S-S (2011) Herceptin functionalized polyhedral oligomeric silsesquioxane–conjugated oligomers–silica/iron oxide nanoparticles for tumor cell sorting and detection. Biomaterials 32(32):8226–8233

Momburg F, Moldenhauer G, Hämmerling GJ, Möller P (1987) Immunohistochemical study of the expression of a Mr 34,000 human epithelium-specific surface glycoprotein in normal and malignant tissues. Can Res 47(11):2883–2891

Mostert B, Sleijfer S, Foekens JA, Gratama JW (2009) Circulating tumor cells (CTCs): detection methods and their clinical relevance in breast cancer. Cancer Treat Rev 35(5):463–474

Mukherjee R, Das S, Das A, Sharma SK, Raychaudhuri AK, Sharma A (2010) Stability and dewetting of metal nanoparticle filled thin polymer films: control of instability length scale and dynamics. ACS Nano 4(7):3709–3724

Müller UR, Nicolau DV (2005) Microarray technology and its applications. Springer

Myung JH, Gajjar KA, Saric J, Eddington DT, Hong S (2011) Dendrimer-mediated multivalent binding for the enhanced capture of tumor cells. Angew Chem Int Ed 50(49):11769–11772

Nagrath S, Sequist LV, Maheswaran S, Bell DW, Irimia D, Ulkus L, Smith MR, Kwak EL, Digumarthy S, Muzikansky A, Ryan P, Balis UJ, Tompkins RG, Haber DA, Toner M (2007) Isolation of rare circulating tumour cells in cancer patients by microchip technology. Nature 450(7173):1235–1239

Nelson CM, VanDuijn MM, Inman JL, Fletcher DA, Bissell MJ (2006) Tissue geometry determines sites of mammary branching morphogenesis in organotypic cultures. Science 314 (5797):298–300

Park M, Harrison C, Chaikin PM, Register RA, Adamson DH (1997) Block copolymer lithography: periodic arrays of ~ 1011 holes in 1 square centimeter. Science 276(5317):1401–1404

Paterlini-Brechot P, Benali NL (2007) Circulating tumor cells (CTC) detection: clinical impact and future directions. Cancer Lett 253(2):180–204

Piner RD, Zhu J, Xu F, Hong S, Mirkin CA (1999) "Dip-pen" nanolithography. Science 283 (5402):661–663

Poliness AE, Healey MG, Brennecke SP, Moses EK (2004) Proteomic approaches in endometriosis research. Proteomics 4(7):1897–1902

Rechendorff K, Hovgaard MB, Foss M, Zhdanov V, Besenbacher F (2006) Enhancement of protein adsorption induced by surface roughness. Langmuir 22(26):10885–10888

Redon C, Brochard-Wyart F, Rondelez F (1991) Dynamics of dewetting. Phys Rev Lett 66(6):715

Reiter G (1992) Dewetting of thin polymer films. Phys Rev Lett 68(1):75

Reiter G, Hamieh M, Damman P, Sclavons S, Gabriele S, Vilmin T, Raphaël E (2005) Residual stresses in thin polymer films cause rupture and dominate early stages of dewetting. Nat Mater 4(10):754–758

Riepl M, Östblom M, Lundström I, Svensson SC, Denier van der Gon AW, Schäferling M, Liedberg B (2005) Molecular gradients: an efficient approach for optimizing the surface properties of biomaterials and biochips. Langmuir 21(3):1042–1050

Riethdorf S, Fritsche H, Müller V, Rau T, Schindlbeck C, Rack B, Janni W, Coith C, Beck K, Jänicke F (2007) Detection of circulating tumor cells in peripheral blood of patients with metastatic breast cancer: a validation study of the CellSearch system. Clin Cancer Res 13 (3):920–928

Riethdorf S, Müller V, Zhang L, Rau T, Loibl S, Komor M, Roller M, Huober J, Fehm T, Schrader I (2010) Detection and HER2 expression of circulating tumor cells: prospective monitoring in breast cancer patients treated in the neoadjuvant GeparQuattro trial. Clin Cancer Res 16(9):2634–2645

Riveline D, Zamir E, Balaban NQ, Schwarz US, Ishizaki T, Narumiya S, Kam Z, Geiger B, Bershadsky AD (2001) Focal contacts as mechanosensors. J Cell Biol 153(6):1175–1186

Rosales AM, Anseth KS (2016) The design of reversible hydrogels to capture extracellular matrix dynamics. Nat Rev Mater 1:15012

Saerens D, Ghassabeh GH, Muyldermans S (2008) Antibody technology in proteomics. Briefings Funct Genomics Proteomics 7(4):275–282

Satoh J, Obayashi S, Misawa T, Sumiyoshi K, Oosumi K, Tabunoki H (2009) Protein microarray analysis identifies human cellular prion protein interactors. Neuropathol Appl Neurobiol 35 (1):16–35

Schena M (2005) Protein microarrays. Jones & Bartlett Learning

Schramm W, Paek S-H, Voss G (1993) Strategies for the immobilization of antibodies. Immunomethods 3(2):93–103

Seemann R, Herminghaus S, Jacobs K (2001a) Gaining control of pattern formation of dewetting liquid films. J Phys: Condens Matter 13(21):4925

Seemann R, Jacobs K, Blossey R (2001b) Polystyrene nanodroplets. J Phys: Condens Matter 13 (21):4915

Seemann R, Brinkmann M, Kramer EJ, Lange FF, Lipowsky R (2005a) Wetting morphologies at microstructured surfaces. Proc Natl Acad Sci USA 102(6):1848–1852

Seemann R, Herminghaus S, Neto C, Schlagowski S, Podzimek D, Konrad R, Mantz H, Jacobs K (2005b) Dynamics and structure formation in thin polymer melt films. J Phys: Condens Matter 17(9):S267

Sharma A, Reiter G (1996) Instability of thin polymer films on coated substrates: rupture, dewetting, and drop formation. J Colloid Interface Sci 178(2):383–399

Shimoda T, Morii K, Seki S, Kiguchi H (2003) Inkjet printing of light-emitting polymer displays. MRS Bull 28(11):821–827

Singh TB, Sariciftci NS (2006) Progress in plastic electronics devices. Annu Rev Mater Res 36:199–230

Sirringhaus H, Kawase T, Friend R, Shimoda T, Inbasekaran M, Wu W, Woo E (2000) High-resolution inkjet printing of all-polymer transistor circuits. Science 290(5499):2123–2126

Stoll D, Bachmann J, Templin MF, Joos TO (2004) Microarray technology: an increasing variety of screening tools for proteomic research. Drug Discovery Today: TARGETS 3(1):24–31

Suh KY, Seong J, Khademhosseini A, Laibinis PE, Langer R (2004) A simple soft lithographic route to fabrication of poly (ethylene glycol) microstructures for protein and cell patterning. Biomaterials 25(3):557–563

Telford A, Meagher L, Glattauer V, Gengenbach T, Easton C, Neto C (2012) Micropatterning of polymer brushes: grafting from dewetting polymer films for biological applications. Biomacromol 13(9):2989–2996

Théry M, Racine V, Pépin A, Piel M, Chen Y, Sibarita J-B, Bornens M (2005) The extracellular matrix guides the orientation of the cell division axis. Nat Cell Biol 7(10):947–953

Théry M, Racine V, Piel M, Pépin A, Dimitrov A, Chen Y, Sibarita J-B, Bornens M (2006) Anisotropy of cell adhesive microenvironment governs cell internal organization and orientation of polarity. Proc Natl Acad Sci 103(52):19771–19776

Tian J, Gong H, Sheng N, Zhou X, Gulari E, Gao X, Church G (2004) Accurate multiplex gene synthesis from programmable DNA microchips. Nature 432(7020):1050–1054

Valkama S, Kosonen H, Ruokolainen J, Haatainen T, Torkkeli M, Serimaa R, ten Brinke G, Ikkala O (2004) Self-assembled polymeric solid films with temperature-induced large and reversible photonic-bandgap switching. Nat Mater 3(12):872–876

Valsesia A, Colpo P, Manso Silvan M, Meziani T, Ceccone G, Rossi F (2004) Fabrication of nanostructured polymeric surfaces for biosensing devices. Nano Lett 4(6):1047–1050

Valsesia A, Colpo P, Meziani T, Bretagnol F, Lejeune M, Rossi F, Bouma A, Garcia-Parajo M (2006) Selective immobilization of protein clusters on polymeric nanocraters. Adv Func Mater 16(9):1242–1246

Valsesia A, Colpo P, Mannelli I, Mornet S, Bretagnol F, Ceccone G, Rossi F (2008) Use of nanopatterned surfaces to enhance immunoreaction efficiency. Anal Chem 80(5):1418–1424

van de Stolpe A, Pantel K, Sleijfer S, Terstappen LW, den Toonder JM (2011) Circulating tumor cell isolation and diagnostics: toward routine clinical use. Cancer Res 71(18):5955–5960

Wagner P, Kim R (2002) Protein biochips: an emerging tool for proteomics research. Curr Drug Discov 23–28

Wan Y, Winter M, Delalat B, Hardingham JE, Grover PK, Wrin J, Voelcker NH, Price TJ, Thierry B (2014) Nanostructured polystyrene well plates allow unbiased high-throughput characterization of circulating tumor cells. ACS Appl Mater Interfaces 6(23):20828–20836

Wang L, Asghar W, Demirci U, Wan Y (2013) Nanostructured substrates for isolation of circulating tumor cells. Nano Today 8(4):374–387

Weiss P, Garber B (1952) Shape and movement of mesenchyme cells as functions of the physical structure of the medium contributions to a quantitative morphology. Proc Natl Acad Sci 38 (3):264–280

Willner I, Katz E (2000) Integration of layered redox proteins and conductive supports for bioelectronic applications. Angew Chem Int Ed 39(7):1180–1218

Wyart FB, Martin P, Redon C (1993) Liquid/liquid dewetting. Langmuir 9(12):3682–3690

Xia Y, Whitesides GM (1998) Soft lithography. Annu Rev Mater Sci 28(1):153–184

Xu H, Aguilar ZP, Yang L, Kuang M, Duan H, Xiong Y, Wei H, Wang A (2011) Antibody conjugated magnetic iron oxide nanoparticles for cancer cell separation in fresh whole blood. Biomaterials 32(36):9758–9765

Yan S, Zhang X, Dai X, Feng X, Du W, Liu B-F (2016) Rhipsalis (Cactaceae)-like hierarchical structure based microfluidic chip for highly efficient isolation of rare cancer cells. ACS Appl Mater Interfaces 8(49):33457–33463

Yap FL, Zhang Y (2005) Protein micropatterning using surfaces modified by self-assembled polystyrene microspheres. Langmuir 21(12):5233–5236

Yap F, Zhang Y (2007) Protein and cell micropatterning and its integration with micro/nanoparticles assembly. Biosens Bioelectron 22(6):775–788

Ye C, Nikolov SV, Calabrese R, Dindar A, Alexeev A, Kippelen B, Kaplan DL, Tsukruk VV (2015) Self-(Un) rolling biopolymer microstructures: rings, tubules, and helical tubules from the same material. Angew Chem 127(29):8610–8613

Yu M, Stott S, Toner M, Maheswaran S, Haber DA (2011) Circulating tumor cells: approaches to isolation and characterization. J Cell Biol 192(3):373–382

Zeiger AS, Hinton B, Van Vliet KJ (2013) Why the dish makes a difference: quantitative comparison of polystyrene culture surfaces. Acta Biomater 9(7):7354–7361

Zhang P, Chen L, Xu T, Liu H, Liu X, Meng J, Yang G, Jiang L, Wang S (2013) Programmable fractal nanostructured interfaces for specific recognition and electrochemical release of cancer cells. Adv Mater 25(26):3566–3570

Zheng S, Lin HK, Lu B, Williams A, Datar R, Cote RJ, Tai Y-C (2011) 3D microfilter device for viable circulating tumor cell (CTC) enrichment from blood. Biomed Microdevice 13(1): 203–213

Chapter 11
Nanoparticles-Based Diagnostics

Kapil Manoharan, Anubhuti Saha and Shantanu Bhattacharya

Abstract Nanoparticles can be described as a particulate material whose dimensional range lies in nanoscale (i.e., 1–100 nm). Nanoparticles of various shapes such as spheres, rods, wires, planes, stars, cages, multipods can be tailored using different nanochemical procedures. Efforts are being applied in fashioning different hybridized shapes like core–shell nanostructures, spheres dispersed in nanosheets to exploit the physical and chemical properties of the different chemical entities used as well as their varying surface chemistry with change in geometry of the particulate. The unique advantageous properties exhibited by the nanoparticles unlike their bulk counter parts include high surface-to-volume ratio, higher surface energy, and unique mechanical, thermal, electrical, magnetic, and optical behaviors. Nanomaterials are considered to have a commendable potential in the field of biosensors for its capability of efficient signal capture of the biological recognition event (transduction) at nanoscale level. Efficient transduction at such a low length scale is the defining parameter of an efficient and robust biomedical sensor. Translation of the interaction of the biological analytes with that of the bioinspired receptors (nanomaterial) into molecular level range is the key of high sensitivity of any biosensor, and this property can be further exploited for medical diagnosis of cancer at very initial stages and many other physiological ailments. This chapter will be mainly dealing with nanoparticles-based diagnostics and correspondingly their sensitivity validated by their physical and chemical characterization. It will also include a section with a discussion on related recent advancements and future prospects which are to be explored on the field of nanoparticles-based diagnostics.

Keywords Nanoparticles · Diagnostics · Analytes · Biomedical sensor

K. Manoharan · A. Saha (✉) · S. Bhattacharya
Microsystems Fabrication Laboratory, Mechanical Engineering Department,
Indian Institute of Technology Kanpur, UP 208016 Kanpur, India
e-mail: anusaha@iitk.ac.in

S. Bhattacharya et al. (eds.), *Environmental, Chemical and Medical Sensors*, Energy, Environment, and Sustainability, https://doi.org/10.1007/978-981-10-7751-7_11

1 Introduction

Nanoparticles can be described as particulate materials which lie in the nanoscale dimensional range (i.e., 1–100 nm). Different nanochemical/electrochemical and mechanical procedures are used to generate various nanoparticles such as nanospheres, rods, wires, planes, stars, cages, multipods. Basically, two approaches are followed for generation of these nanomaterials:

1. Top-down approach: refers to development of nanoscale structures by machining, lithography, or templating techniques.
2. Bottom-up approach: also known as molecular nanotechnology, which uses self-assembly or self-organization of atom with atom or molecule with molecule.

Currently, the top-down approach is followed the most but slowly the shift is toward bottom-up approach as it has advantages like less wastage, better control on chemical, physical, and structural properties of the nanostructures generated.

The physical and chemical properties change with the change in shape and size of each nanoparticle, and these properties are being used in sensing and diagnostic purposes. Unique mechanical, thermal, electrical, magnetic, and optical behaviors as well as high surface-to-volume ratio and high surface energy are some of the properties which are being used for diagnosis of highly infectious diseases as well as detection of cancers and tumors. Drug delivery on targeted sites is also one of the emerging areas where nanoparticles are used.

This chapter will be mainly dealing with the types of nanoparticles and some of the synthesis methods, nanoparticles-based diagnostics techniques in the medical field and future prospects and applications of nanomaterials in field of medicine.

2 Brief Introduction to Nanoparticles Used for Medical Diagnostics and Their Synthesis Methods

Efficient level of specificity of a bioreceptor unit toward its corresponding analyte in a biosensor is the key to designing a medical diagnostic with precise readouts. Binding or interaction of bioreceptor with the target analytes is the vital step to achieve such meticulous level of transduction. In order to achieve molecular level immobilization of bioanalytes (like DNAs of bacteria or viruses, proteins like antigen and antibodies, or simple molecules like glucose, cholesterol), nanoparticles can be considered a prime choice for a biosensing platform. Constant research is being continued in synthesis of nanoparticles with varying shapes to modulate its surface and physical chemistry in order to refine their specificities toward a bioanalyte. Morphological changes in nanoparticles also result in modified transduced readouts. This section discusses different categories of nanoparticles with varying

shapes mostly used in medical diagnostics and their corresponding synthesis methods.

2.1 Metallic Nanoparticles

These nanomaterials include nanogold, nanosilver and metal oxides, such as titanium dioxide. Recently, with the advent of point-of-care medical diagnostics, metallic nanoparticles are extensively experimented as a substitute for peroxidase mimetics. Monometallic nanoparticles or bimetallic composites act as a catalyst for the oxidation of a particular substrate by hydrogen peroxide. It can be also used as hydrogen peroxide detector. Gold- and silver-based nanostructures have also been explored. Surface plasmon resonance effect of Au and Ag has been exploited in the area of colorimetric assay. It has been observed that Ag nanoparticles exhibit much stronger SPR characteristics compared to Au nanoparticles. But Ag NPs are environmentally sensitive as it possesses easy oxidation. Conjugating the advantages of both Ag and Au, Zhang et al. (2016) proposed a core–shell bimetallic nanoparticle peroxidase mimetic platform bearing a good plasmonic sensitivity as well as chemical stability. Yu et al. (2011), Che et al. (2009) developed bimetallic Au/Pt sensors for H_2O_2 and noted the superiority of the same over monometallic nanoparticles-based sensors. The bimetallic construct provided a facile way of electron transfer with enhanced catalytic activity. Similarly, both Pt/Pd and Au/Pt NPs (Safavi and Farjami 2011; Cao et al. 2013) and TiO_2-/graphene-supported Pt/Pd nanocomposites are being explored for cholesterol sensing.

Synthesis of metallic nanoparticles through chemical method is an inexpensive route facilitating self-assembly or patterning possible. Nanoparticles are generally synthesized using chemical methods. The respective synthesis procedure mainly involves the following two steps: (1) reduction of the metal salt and (2) stabilization of nanoparticles by generating repulsive coulombic interactions using capping/stabilizing agents. For example, the gold salt is first reduced with trisodium citrate and then stabilization is done using thiols or capping agents like polyethylene glycols or cetyltrimethylammonium bromide (CTAB).

Synthesis of gold nanoparticles with varying morphologies

The most efficient and preferred method for synthesizing gold nanoparticles are chemical reduction methods. The primary step involves nucleation or formation of gold seeds. Generation of gold particles with varying morphologies and dimensionalities by chemical reduction method were experimented by Sau and Murphy (2004). The ingredients of the synthesis procedure consist of gold salt ($HAuCl_4 \cdot 3H_20$), $NaBH_4$, $AgNO_3$, CTAB, and ascorbic acid. Firstly, an amount of 10-ml seed solution was prepared by adding 0.6 mM $NaBH_4$ to a reaction mixture of 0.25 mM ($HAuCl_4 \cdot 3H_2O$) and 0.75 mM CTAB. The resulting seed was approximately 4 nm in diameter. Larger seed size could be produced by increasing the CTAB concentration. Further, the growth reaction involved mixing of 0.01 ml

of gold seed solution to a reaction mixture of 0.20 ml of $HAuCl_4$ solution, 4.75 mL of 0.10 M CTAB, 0.03 mL of 0.01 M $AgNO_3$, and 0.032 ml of 0.10 M ascorbic acid. The resultant product was gold nanorod-like structures. Silver nitrate was found to be the factor responsible for the absence of any nanospherical structures in the final colloid. It was observed that the morphology of the final gold nanostructure obtained was a function of gold seed size, concentration of seed solution, concentration of stabilizing agent, i.e., CTAB and ascorbic acid. Simply by modulating any of the reagent concentration and reaction time, the size and shape of the gold nanostructure could be controlled. It was observed that in comparison with increase in the concentration of reagents used during preparation of gold nanorods, if the concentration of ascorbic acid is increased, it resulted in formation of hexagonal nanostructures. If ascorbic acid concentration is further increased, cube-shaped particles are formed. Various TEM images for different shaped gold nanostructures are shown in Fig. 1.

2.1.1 Synthesis of Gold–Silver Core and Shell Nanostructure

Synthesis of gold–silver core–shell particles involved the preparation of gold (Au) seed particles, followed by in situ growth of silver (Ag) shell over the gold seed. Gold seeds were prepared by conventional citrate reduction method. An

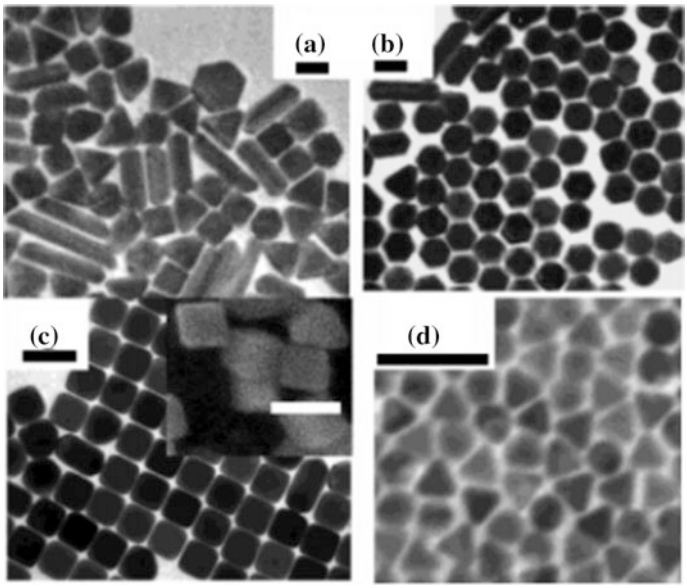

Fig. 1 TEM images of Au nanoparticles synthesized under different conditions of varying concentration of ascorbic acid and seed concentration (scale bar = 100 nm). Reprinted with the permission from Sau and Murphy (2004)

amount of 50 ml of 1 mM $HAuCl_4$ was prepared by mixing the gold salt ($HAuCl_4 \cdot 4H_2O$) into 50 ml of ultrapure water. The reaction mixture is continuously stirred and heated to boiling temperature. The reaction is preferably carried out in round bottom flask to avoid evaporation. Once the mixture starts boiling, 5 ml of 38.8 mM of sodium citrate is added dropwise. Then, the solution is refluxed for about 15 min during which it undergoes a color change from yellow to wine red. Once the solution turns wine red, the solution is cooled to room temperature. The prepared gold colloid will comprise of spherical gold nanoparticles with an average diameter of 20 nm. An in situ growth of silver shell around the prepared gold seeds was obtained by adding 60 μl of 100 mM ascorbic acid, 15 μl of 100 mM of $AgNO_3$, and 75 μl of 100 mM of NaOH to 10 ml of the Au seed solution. The reaction mixture was slowly stirred for 30 min, followed by a second cycle of addition. After a selected number of additions after every 30 min, the resulting core–shell particles were centrifuged for 20 min at 1800 rpm and redispersed in ultrapure water. The respective TEM image of the fabricated core–shell particles is shown in Fig. 2.

2.2 *Magnetic Nanoparticles*

Morphological modulations are vital depending upon the application of corresponding magnetic nanoparticles in biomedical diagnostics (in vivo or vitro). In vivo applications generally, demand is for particle size smaller than 100 nm to attain higher effective surface areas, lower sedimentation rates, and improved tissular diffusion. Encapsulation of nanoparticles with biocompatible polymer is also essential to prevent formation of large aggregates or biodegradation, when exposed to biological environments. The core containing the magnetic component (such as magnetite, iron, nickel, and cobalt), the outer polymeric shell, and the corresponding shape and size are the deciding factors for the toxicity of manufactured magnetic nanoparticles (Akbarzadeh et al. 2012). Unlike in vivo, the size restrictions are not that severe in vitro. Rather, a particulate size resulting in long

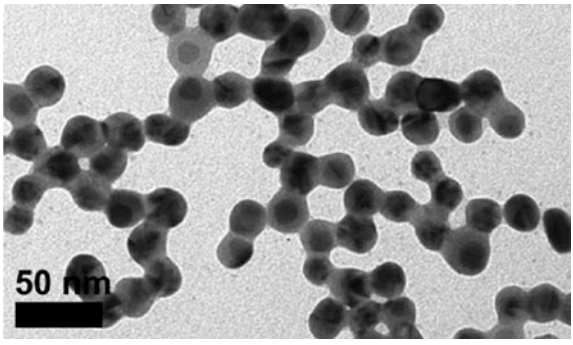

Fig. 2 TEM image of Au@Ag core–shell NPs obtained from citrate-stabilized Au NPs. Reprinted with the permission from Samal et al. (2013)

sedimentation time of the particles is emphasized. For medical diagnosis-based applications, particles that present super-paramagnetic behavior along with a maintained colloidal stability of pH 7 in a physiological environment are preferred.

Magnetite (Fe_3O_4) is one of the most widely used magnetic nanoparticles for its commendable super-paramagnetic properties, but easy oxidation and agglomeration are its disadvantageous factors. Thus, several binary and ternary nanocomposites like core–shell architectures consisting of inorganic coatings are preferred to overcome easy oxidation and agglomeration.

2.2.1 Synthesis of Shape- and Size-Controlled Core–Shell Magnetic Nanoparticle

Synthesis of iron oxide–gold core–shell nanoparticle of three different shapes (sphere, popcorn, and star) with controlled sizes (70–250 nm) was done by Kwizera et al. (2016). Magnetic and optical properties are tunable for the corresponding magnetic nanoparticles as the shape and size of the iron oxide core and gold shell can be engineered as required. The IO–Au nanostars showed strong and distinct redshifted localized surface plasmon resonance compared to IO–Au nanopopcorns and nanospheres. The synthesis procedure of the hybrid structures is carried out in three steps as explained below:

Synthesis of IO NPs

Iron oxide NPs of octahedral shape were synthesized in an oxygen-free environment at 90º centigrade using the method described by Goon et al. (2009) with some modifications. A reaction mixture of 2.5 ml of 1 M of NaOH, 2.5 ml of 2 M of KNO_3, 5 ml of 8 mg/ml polyethylenimine (PEI), and 175 mg of $FeSO_4$ were added to the nitrogen-free ultrapure water. The solution mixture was continuously stirred for 2 h. The formation of iron oxide particulates can be noted with an appearance of an observable color change from blue to black. Further, purification of magnetic nanoparticles was done using magnetic separation and redispersing of the same in ultrapure water after five cycles.

Preparation of IO–Au Core–Shell Nanospheres, Nanostars, and Nanopopcorns

As per the traditional chemical reduction method, the preparation of the IO–Au core–shell nanospheres, nanopopcorns, and nanostars is divided into two levels. Firstly, the preparation of seed solution is followed by the addition of the seed solution to the growth solution. Initial step requires the formation of Au-seeded iron oxide nanoparticles so that the shape of the Au shell can be further varied during the growth step resulting in diversified shell structures. Au-seeded IO NPs were simply prepared by citrate reduction method. A 25 mM of $HAuCl_4$ was reduced using 0.2 M of sodium borohydride and 0.85 mM of sodium citrate. Previously prepared IO NPs stabilized with PEI were now functionalized using these citrate-reduced Au seeds via electrostatic adsorption. This was performed by mixing 55 μL of PEI stabilized IO NPs to 5 mL of Au seed solution. The reaction mixture was

continuously stirred for 45 min. The freshly prepared Au-seeded IO NPs were further purified using three cycles of magnetic separation and washing, followed by redispersing the same in 2.5 ml of 15 mg/ml aqueous PEI for 3 h in a heated environment of 60 °C. Once the purification procedure is complete, the seeded Au–IO NPs were stored by redispersing them in ultrapure water. The variation in structures is performed mainly by modulating the concentration of reagents used in growth solution. Growth solution is prepared by mixing 10 mM of $HAUCl_4$ and 5 ml of 0.1 M aqueous CTAB for 5 min. An addition of 32 μL of 10 mM of ascorbic acid is made to reduce from $HAuCL_4$ to $HAuCl_2$. Different amounts of seeded Au–IO NPs ranging from 100 to 800 μL are added to the growth solution to obtain IO–Au core–shell nanospheres. A similar procedure is followed to synthesize nanostars but with an addition of 30 μL of 10 mM $AgNO_3$. Similarly to obtain nanopopcorn structures, the amount of $AgNO_3$ is kept unchanged but the amount of ascorbic acid is increased to 90 μL in the growth solution. The TEM images of the respective nanostructures are shown in Fig. 3.

2.3 *Polymeric Nanoparticles*

Polymeric nanoparticles are colloidal particles with a size ranging from 10 to 1000 nm. Polymeric nanoparticles (PNPs) synthesized for biosensing or diagnostic purposes are generally prepared using biocompatible and biodegradable polymers. The structural and surface properties of PNPs are optimized depending upon the area of application or the bioanalyte to be sensed. Thus, the way of synthesis plays vital role for designing PNPs for medical diagnosis or sensing application. Various methods of preparation of polymeric nanoparticles from the dispersion of pre-formed polymers include solvent evaporation, nanoprecipitation, emulsification/solvent diffusion, salting out. Polymeric nanoparticles are also synthesized by polymerization of monomers using preparation methods like emulsion, mini-emulsion, micro-emulsion, interfacial polymerization.

Several conducting polymers and consequent hybrids have gained significant applications in the field of biosensors and biomimetic electronic systems. Some of

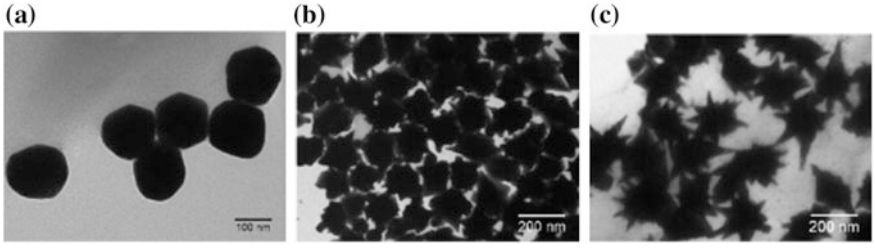

Fig. 3 TEM images of different IO–Au core–shell: **a** nanospheres, **b** nanopopcorns, and **c** nanostars. Reprinted with the permission from Kwizera et al. (2016)

the important conducting polymers reported by Park et al. (2016) are polypyrrole, polyaniline, and poly(3,4-ethylenedioxythiophene). Carboxylated polypyrrole nanotubes were used for developing bioelectronic nose by Song et al. (2013). One of the major areas of application of nanoparticles is as peroxidase mimetics or H_2O_2 sensors which are also explored using polymeric nanoparticles. Polypyrrole-coated silver nanostrip bundles were explored to detect H_2O_2 by Mahmoudian et al. (2014). Similarly, a hybrid structure of polyaniline layer with entrapped glucose oxidase and gold nanoparticles was developed by Nia et al. (2016) for glucose sensing in contrast to use of various (1-D) nanostructures of poly (3,4-ethylenedioxythiophene), such as nanorods, nanotubes, and nanowires.

Some of the synthesis procedures of polymeric nanomaterial of varying shapes and structures are discussed below (Kim et al. 2014).

Synthesis of Spherical Polymeric Nanoparticles

An amount of 0.508 kg of hexane is charged to a reaction environment with 57 °C inside the reactor. Simultaneously, a blend of 1.043 kg of butadiene (22% wt.) and hexane is added maintaining the reaction temperature at 57 °C. Once the temperature was stabilized, 5 ml of 1.6 M n-butyllithium was added to initiate the polymerization process. After 2 h, a reaction mixture of 0.66 kg of styrene (33% wt.) and hexane was added to the reactor. Again after 2 h, a reaction blend of 1.81 kg of hexane and 50 ml of divinylbenzene was added. 57 °C was maintained for the entire process of polymerization. Finally, the product was dropped into 2-propanol and butylated hydroxytoluene solution and dried in a vacuum environment to obtain micelle nanoparticles.

Synthesis of Flower-Type Nanoparticles

As above like in the case of spherical nanoparticles, a reaction mixture of 0.52 kg of hexane and 1 kg of butadiene (22% wt.) and hexane blend was added to a reactor and preheated at the same temperature. The reactor design was chosen with provision of both external jacket heating and internal agitation. As soon as a stable temperature was reached, 16 mL of 0.5 M solution of the dilithium was added to initiate the process of polymerization. A blend of styrene (33% wt.) and hexane was added after 2 h of the polymerization reaction. Again after an interval of 2 h, 50 mL of divinylbenzene and 2.8 kg of hexane were charged into the reactor maintaining the reactor temperature at the same 57 °C. Lastly, the reaction product was dispersed into a 95:5:1 blend of acetone, 2-propanol, and butylated hydroxytoluene, followed by vacuum drying.

3 Nanomaterial-Based Diagnostics

As discussed in previous section, biologists and chemists have been continuously involved in development of organic, inorganic, and hybrid nanomaterials, which can be used in development of nanoanalytical and diagnostic techniques such as

biolabeling, nanobiosensors, DNA tagging, biobarcoding of micro-assays (Rajasundari and Ilamurugu 2011; Kamal et al. 2011).

3.1 Nanoparticles as Part of Biosensors

A biosensor is a chemical sensor (as shown in Fig. 4) which primarily consists of a biological (responsible for sampling) and a physical element (a transducer, which transmits sampling results for further processing). The biosensors utilize biochemical mechanisms for recognition or sensing of target analytes which are mainly biological in nature. Ability to identify and locate particular type of cells or areas in the body with higher sensitivity makes nanomaterial-based chemical and biological sensors very useful.

Biosensors are classified according to the biological element or the mode of signal transduction or the combination of both. Kubik et al. (2005) provided in brief the types of different sensors based on these classifications. Nanomaterial-based sensing uses antigen/antibody, cellular- or DNA-based biological elements which are in sync with the type of recognition element that is used. The signal transduction is done either optically, electrochemically, or thermally.

Based on difference in volume, concentration, displacement, velocity, gravitational properties, electrical and magnetic properties, ambient pressure and temperature of cells, etc., these nanosensors can distinguish and recognize different types of cells at molecular levels in order to monitor their development or growth and to deliver medicines at required times within them. One such example is use of fluorescence properties of cadmium selenide zero-dimensional particles also known as quantum dots used to recognize and uncover tumor cells within the human body. When injected into the body, due to certain nature of the tumor cells, these dots get accumulated on them and get illuminated due to fluorescence properties giving an idea of their presence. Cadmium selenide being toxic has slowly prompted researchers to use alternate coatings of other materials such as zinc sulfide and various other lanthanide elements for similar use (Rajasundari and Ilamurugu 2011).

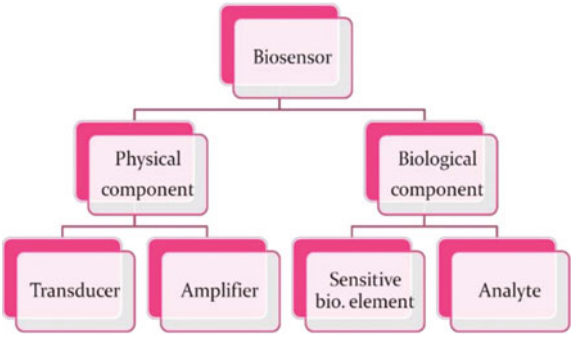

Fig. 4 Components of a biosensor

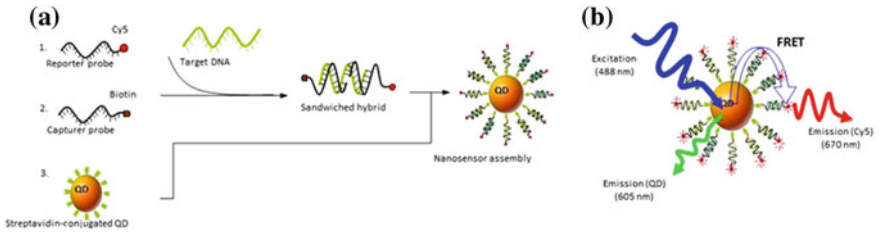

Fig. 5 Scheme for the design of a single QD-based DNA nanosensor system. **a** Scheme showing the formation of a nanosensor assembly in the presence of targets conceptually. **b** Fluorescence emits caused by FRET between Cy5 acceptors and a QD donor from Cy5 upon illumination on QD in a nanosensor assembly. Reprinted with the permission from Zhang et al. (2005)

These quantum dot sensors are also being used heavily to detect specific DNAs in order to recognize explicit genetic defects in individuals especially with a high risk. Figure 5 shows the mechanism of one such quantum dot (QD)-based DNA nanosensing system.

3.2 Nanobarcodes

Cylindrical nanoparticles with specific patterns and primarily being made of various metal ions having dimensions of 12–15 nm diametrically and 1–50 μm in length can cause differential reflectivity. Alternate black and white stripes cause distinction like barcodes under light or fluorescent microscopy or mass spectrometry and can be used for SNP mapping, coding of multiplexed assays for proteomics, and population diagnostics. Tagging of an individual biomolecule using easily detectable nanobarcodes enables their direct digital counting and quantification. Figure 6b shows one such example of DNA nanobarcode having structure as in Fig. 6a, being used in cytometry-based detection strategy.

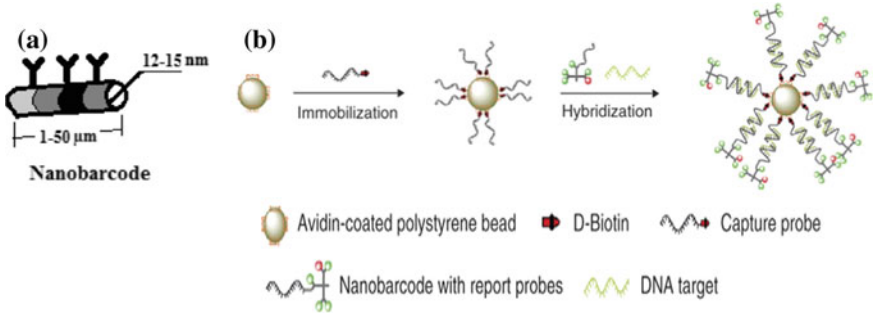

Fig. 6 **a** Scheme of a nanobarcode. **b** A dendrimer-like DNA nanobarcode for use in flow cytometry detection. Reprinted with the permission from Um et al. (2006)

3.3 Nanoparticles Used for Molecular Diagnostics

Many nanoparticles such as gold nanoparticles, magnetic nanoparticles, and quantum dots are heavily deployed in molecular diagnostics.

Gold Nanoparticles for diagnostics

Gold particles of size around 15 nm acting as labels on a variety of molecules are attached with DNA strands which in presence of a complementary target get assembled on the sensor surface. Multiple DNA strands patterned on a sensor surface using this technique can be used for simultaneous detection of millions of target DNA sequences. Current limit of detection of target molecules is in the range of 20 fmol/L.

Quantum dots

QDs are markers of inorganic fluorophores which have significant advantages over conventionally used fluorescent markers. Some of the widely used QDs are made of CdSe (cadmium selenide, 200–1000 atoms wide with zero-dimensional nanoassembly) with or without another stability coating of ZnS (zinc sulfide) as shown in Fig. 7a. The emission frequency is determined by the size of the dots as it is irradiated with a low intensity and low wavelength light. Figure 7b shows the fluorescence versus the wavelength shift for each sized dot.

QDs such as CdSe–ZnS nanoassemblies do not emit in near-infrared regions [biological window] and hence cannot be used in analysis of blood. QD's high sensitivity, stable fluorescence, a simplistic excitation without use of a laser, and

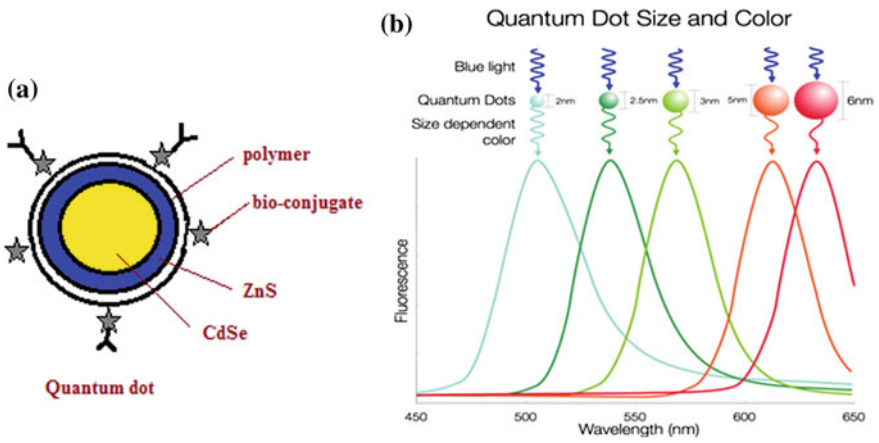

Fig. 7 **a** Scheme of a quantum dot nanoassembly. **b** Fluorescence spectra of CdTe quantum dots of various sizes. Reprinted with the permission from Physics Open Lab (2015)

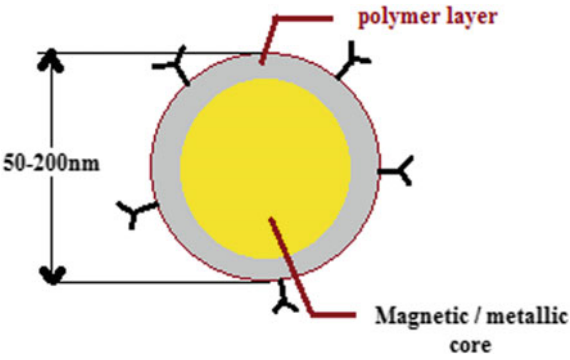

Fig. 8 Scheme of a magnetic or metallic nanoparticle/bead

very broad excitation spectra enables potential application of these for cancer diagnosis.

Magnetic Particles

Iron particles of size of 15–20 nm possessing saturation magnetization properties can be synthesized and embedded in a copolymer bead of styrene and glycidyl methacrylate with an overall diameter of 100–200 nm as shown in Fig. 8. These super-paramagnetic nanoparticles are very useful in tracking of cells and calcium sensing. Also, these nanoparticles having size of 2–3 nm are used in conjunction with MRI to reveal small, undetectable lymph node metastases. A dextran-coated IO NP enhances visualization for more than 24 h of intracranial tumors in an MRI.

3.4 Nanodiagnostics for Infectious Diseases

Most conventional diagnostic methods lack ultrasensitivity with delay in results. Rapid and sensitive detection of disease causing agents like pathogenic bacteria, viruses, and spores at the patient's bedside is an extremely important need of the diagnostics industry. Development of various nanoparticles has helped in enhancing detection speed and sensitivity so that quick detection of a variety of different biological species like different viruses and bacteria can be carried out with optical, spectral, thermal, or electrochemical means without use of any artificially imposed enhancements or manipulations. These methods are highly inexpensive specially as they involve trace sample volumes and are easily reproducible as the degree of instrumentation deployed is quite complex and has a very high sensitivity.

Nanoparticles are increasingly being used for analysis of anthrax pathogenicity genetically, spectral analysis of viruses, and viral strains with gene deletion in biological media, etc. A SERS-based spectroscopic assay using silver nanorods which can significantly amplify the signals is being developed to detect and trace various levels of viruses with a very high degree of sensitivity and specificity (Shanmukh et al. 2006).

3.5 *Nanoparticles for Detection of Cholesterol, Glucose Sensing, and Other Point-of-Care Sensing*

One of the emerging areas for use of nanomaterials is the point-of-care and faster diagnostics of cholesterol, uric acid, albumin, and other blood-related analytes of patients. Rick et al. discussed and summarized nicely the various nanomaterials used for sensing of glucose, H_2O_2, and cholesterol sensing, their sensitivities and specific applications (Rick et al. 2015). Lot of work is reported in this area as conventional techniques require lot of infrastructure, have less sensitivity and specificity, and take longer durations for providing results.

Zhang et al. (2016) and many other authors have reported use of Au@Ag core–shell nanoparticles for detection of glucose and cholesterol in human fluids. Figure 9a shows the evolution of Au@Ag core–shell particle and how colorimetric changes occur after reaction with H_2O_2 and glucose/cholesterol. Gold nanoparticles under UV–vis absorption spectra show peak at 520 nm (wine red color), whereas the peak shifts to 375 nm (orange color) for Au@Ag nanoparticles (Fig. 9b). In the presence of H_2O_2 or cholesterol, a reaction occurs and Ag is reduced leaving only AuNPs in the solution, thus shifting back the peak near to 520 nm. The peak shift and absorbance spectra formed are according to concentrations of H_2O_2 or the cholesterol present in the fluid and type of Au@Ag nanoparticle used.

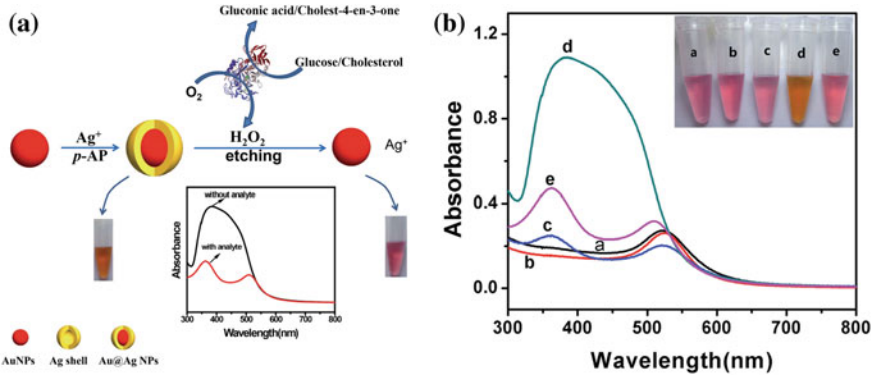

Fig. 9 **a** Illustration showing formation of Au@Ag Nps and its application in colorimetric detection of H_2O_2 and glucose/cholesterol, **b** UV–vis absorption spectra: (*a*) AuNPs, (*b*) AuNPs + $AgNO_3$, (*c*) AuNPs + *p*-AP, (*d*) AuNPs + $AgNO_3$ + p-AP (Au@Ag NPs), (*e*) Au@Ag NPs + H_2O_2. Inset shows corresponding color solutions. Reprinted with the permission from Zhang et al. (2016)

3.6 Nanoparticles as Drug Delivery Agents

Monitoring, repairing, construction, and control using engineered nanodevices and nanostructures of the human biological systems at molecular levels is a widely used step in field of nanoparticle research which has resulted in the concept of targeted nanoparticle based drug delivery. Targeting tissues with a certain physiological constitution and delivery of drug molecules to localized tissues is a very important aspect of drug delivery technology. The advantage of nanoparticles such as liposomes over conventional dosage forms includes ability of protecting the drug from degradation, targeting the drug on the site of required action and also reduces the toxicity and side effects toward other parts of the body. These systems are classified according to the physical form and the functional properties (Kubik et al. 2005).

4 Advantages and Disadvantages of Nanomaterial-Based Diagnostic Techniques

Introduction of nanomaterials in field of diagnostics and sensing has brought out a revolution and has several advantages over conventional methods.

Advantages:

1. Faster response times, better sensitivity, and specificity.
2. Point-of-care diagnostics.
3. Higher surface-to-volume ratios implying greater reach.
4. Nanobiosensors work at atomic levels with highest efficiency and can even detect single virus particles or ultralow concentration of substances that can be harmful.
5. Nanoparticles can also be used for repairing, control, and construction of human biological systems at molecular levels.
6. Target point delivery of drugs or other chemicals and enzymes for sensing and treatment purposes.
7. Various ways of sensing using optical, electrochemical, and thermal properties of the materials can be done. Colorimetric and fluorescence-based techniques are most commonly used methods for diagnostics.
8. Faster results, ease of use, and cheaper diagnostics have resulted in their use as lab on chips for daily use purposes like cholesterol and glucose level testing.
9. More efficient in sensing and tracking of cancerous cells and tumors than traditional techniques.
10. Helps in integration of diagnostics and therapeutics with development in personalized care.

Disadvantages:

1. Most of the nanomaterials used are inorganic agents, which can cause toxicity or other side effects inside the body if used in vivo or may as such cause apoptosis while being used in vitro or in vivo. Thorough investigation for same is required. One such example is of CdSe which is highly toxic but use of ZnS coating has reduced the toxicity levels. Still longer stay of these materials in body can cause various health hazards.
2. Disposal of these nanomaterials after sensing or diagnostic use is of serious concern especially when used for detecting infectious diseases. Also, disposal of waste after fabrication of these particles may be a serious environmental concern.
3. Physical, thermal, and chemical properties of NPs depend on type of process being used to generate these particles, and its handling has very large effect on it sensitivity and specificity.
4. Research is still being done to study the health hazards, if any, when these nanomaterials or agents remain in body for long durations of time.
5. Concerns are also present for nanomaterials of 20 nm or less sizes as these can penetrate into cells.

5 Future Prospects

Medical sensing, diagnosis, proper and efficient delivery of drugs, and the development of artificial cells are some the fields in medicine, where the nanoparticles and nanomaterials have found a great practical utility. The application of nanotechnology in medical and nanomedical fields includes three molecular technologies which are mutually overlapping and progressively powerful.

There are various nanoscale materials and devices that can be fabricated which have shown great promise in advanced diagnostics, biosensing, targeted drug delivery, and immunoisolation therapies, which are significant milestones in the domain of clinical diagnostics.

Biotechnology which offers the benefits of molecular medicines using artificially engineered microbes, proteomics, and genomics has also benefitted from this rapid development of nanoscale technologies.

Molecular machine systems and nanobots in longer terms will allow instantaneous diagnosis and on-site termination of pathogens and perform chromosome replacements and individual cell surgeries and repair in vivo, thereby augmenting and improving natural physiological functions of cellular assemblies and tissues.

With development in nanoscale chemical sensors and molecular electronics, detection of chemical and drug flow patterns in a fluid such as blood could be done which can then be used to study performance of the chemicals for localized treatments.

Another application can be in detection using fluorescence and colorimetric schemes. As the size decreases, the signal intensity decreases too but some nanomaterials have shown better optical signals. Still work is being carried out to search for materials which are non-toxic and do not cause any health hazard or safety issues.

DNA detection assay, biomarker discovery, cancer, and tumor diagnosis are the current important applications of nanomaterial technology in clinical studies. It will enable point-of-care diagnosis and therapeutics, thus providing personalized care and generally elevating the quality of life.

References

Akbarzadeh A, Samiei M, Davaran S (2012) Magnetic nanoparticles: preparation, physical properties, and applications in biomedicine. Nanoscale Res Lett 7(1):144. https://doi.org/10.1186/1556-276X-7-144

Cao S et al (2013) Electrochemistry of cholesterol biosensor based on a novel Pt-Pd bimetallic nanoparticle decorated graphene catalyst, Talanta. Elsevier 109:167–172. https://doi.org/10.1016/j.talanta.2013.02.002

Che X et al (2009) Hydrogen peroxide sensor based on horseradish peroxidase immobilized on an electrode modified with DNA-L-cysteine-gold-platinum nanoparticles in polypyrrole film. Microchim Acta 167(3–4):159–165. https://doi.org/10.1007/s00604-009-0237-0

Goon IY et al (2009) Fabrication and dispersion of gold-shell protected magnetite nanoparticles: systematic control using polyethylenimine. Chem Mater 21(2):673–681

http://physicsopenlab.org/2015/11/20/quantum-dots-a-true-particle-in-a-box-system/

Kamal R, Khan K, Khan MF (2011) Application of nanotechnology in medical diagnosis. In: International Conference on Innovations in Engineering and Technology, vol 2(3), pp 22–34

Kim BH et al (2014) Synthesis, characterization, and application of ultrasmall nanoparticles (pp 499–508). https://doi.org/10.1021/cm402225z

Kubik T, Bogunia-Kubik K, Sugisaka M (2005) Nanotechnology on duty in medical applications. Curr Pharm Biotechnol 6(1):17–33. https://doi.org/10.2174/1389201053167248

Kwizera EA et al (2016) Size- and shape-controlled synthesis and properties of magnetic-plasmonic core-shell nanoparticles. J Phys Chem C 120(19):10530–10546. https://doi.org/10.1021/acs.jpcc.6b00875

Mahmoudian MR et al (2014) Synthesis of polypyrrole coated silver nanostrip bundles and their application for detection of hydrogen peroxide. J Electrochem Soc 161(9):H487–H492. https://doi.org/10.1149/2.0571409jes

Nia PM, Meng WP, Alias Y (2016) One-step electrodeposition of polypyrrole-copper nano particles for H_2O_2 detection. J Electrochem Soc 163(3):B8–B14. https://doi.org/10.1149/2.0481603jes

Park CS, Lee C, Kwon OS (2016) Conducting polymer based nanobiosensors. Polymers 8(7):1–18. https://doi.org/10.3390/polym8070249

Rajasundari K, Ilamurugu K (2011) Nanotechnology and its applications in medical diagnosis. J Basic Appl Chem 1(2):26–32

Rick J, Tsai M-C, Hwang B (2015) Biosensors incorporating bimetallic nanoparticles. Nanomaterials 6(1):5. https://doi.org/10.3390/nano6010005

Safavi A, Farjami F (2011) Electrodeposition of gold-platinum alloy nanoparticles on ionic liquid-chitosan composite film and its application in fabricating an amperometric cholesterol biosensor. Biosens Bioelectron 26(5):2547–2552. https://doi.org/10.1016/j.bios.2010.11.002

Samal AK et al (2013) Size tunable Au@Ag core-shell nanoparticles: synthesis and surface-enhanced raman scattering properties, Langmuir. Am Chem Soc 29(48):15076–15082. https://doi.org/10.1021/la403707j

Sau TK, Murphy CJ (2004) Room temperature, high-yield synthesis of multiple shapes of gold nanoparticles in aqueous solution. J Am Chem Soc 126(28):8648–8649. https://doi.org/10.1021/ja047846d

Shanmukh S et al (2006) Rapid and sensitive detection of respiratory virus molecular signatures using a silver nanorod array sers substrate, nano letters. Am Chem Soc 6(11):2630–2636. https://doi.org/10.1021/nl061666f

Song HS et al (2013) Human taste receptor-functionalized field effect transistor as a human-like nanobioelectronic tongue. Nano Lett 13(1):172–178. https://doi.org/10.1021/nl3038147

Um SH et al (2006) Dendrimer-like DNA-based fluorescence nanobarcodes. Nat Protocols. Nature Publishing Group, 1(2):995–1000. Available at: http://dx.doi.org/10.1038/nprot.2006.141

Yu Y et al (2011) Size-controllable gold-platinum alloy nanoparticles on nine functionalized ionic-liquid surfaces and their application as electrocatalysts for hydrogen peroxide reduction. Chem Eur J 17(40):11314–11323. https://doi.org/10.1002/chem.201100010

Zhang C-Y et al (2005) Single-quantum-dot-based DNA nanosensor. Nat Mater 4(11):826–831. Available at: http://dx.doi.org/10.1038/nmat1508

Zhang X et al (2016) Sensitive colorimetric detection of glucose and cholesterol by using Au@Ag core–shell nanoparticles. RSC Adv R Soc Chem 6(41):35001–35007. https://doi.org/10.1039/C6RA04976A

Chapter 12
Designing of a Low-Cost Optical Density Meter for Medical Applications

Ankit Sharma, Pratyush K. Patnaik, Seemadri Subhadarshini, Suraj K. Nayak, Sirsendu S. Ray, D. N. Tibarewala and Kunal Pal

Abstract Detection of analytes (biological markers) is an important process for the confirmation of some disease and/or overdose of drugs. Without the detection of the analytes, the treatment of the patients cannot be initiated immediately. In this regard, various detection methodologies have been proposed. One such method is the colorimetric estimation of the analytes. This chapter discusses the advancements made in the field of devising of instruments for colorimetric estimation. Keeping a view of above, a case study to device a low-cost colorimetric instrument, capable of measuring the optical density (OD) of a solution, has also been reported. The suitability of the developed device for estimating rhodamin-B dye and potassium indigo sulphate and salicylic acid was ascertained by making a standard curve plot. The results suggested that the developed device can be used with great efficiency in estimating analytes by colorimetric assays.

Keywords Optical density · Light-dependent resistor · Light-emitting diode Microcontroller · MATLAB® · Graphical user interface

1 Introduction

In the last few decades, there has been a significant development in the field of electronic and sensing devices (Swisher et al. 2015). These advancements not only have helped in improving the quality of the electronic consumer products (e.g. television, refrigerator, air conditioner), but also has provided significant knowledge, which can be used to develop devices of clinical importance (McPherson and Pincus 2016). The clinical devices can be broadly divided into two groups, namely diagnostic devices and therapeutic devices (Liedtke and Loerwald 2014; Allen and Adjani 2016). Diagnostic devices are usually analytical instruments with high

A. Sharma · P. K. Patnaik · S. Subhadarshini · S. K. Nayak · S. S. Ray
D. N. Tibarewala · K. Pal (✉)
Rourkela, India
e-mail: kpal.nitrkl@gmail.com

S. Bhattacharya et al. (eds.), *Environmental, Chemical and Medical Sensors*, Energy, Environment, and Sustainability, https://doi.org/10.1007/978-981-10-7751-7_12

sensitivity and are used for the sensing of the clinical markers, which may provide information about the health condition of a patient (Kittipanyangam et al. 2016). A common example of this category of devices includes the blood sugar measurement instrument (Shen and Zipes 2014). The blood sugar measurement instrument has now nearly become a household diagnostic consumer product. This instrument is used for the measurement of the blood sugar level of the diabetic patients. On the contrary, the therapeutic devices are the electronic instruments, which are used for the treatment of the clinical conditions of a patient. A common example of the therapeutic device is iontophoretic drug delivery device (Sanderson and Deriel 1988). This device uses electrical waveforms for injecting drugs (of therapeutic use) within the systemic circulation of the body, which was conventionally achieved by injecting drugs via an intravenous route. The iontophoretic drug delivery device pushes bioactive agents within the systemic circulation in a non-invasive manner through the skin (Sanderson and Deriel 1988). This technology has allowed the administration of the drug with the minimal training of the users. A commercial iontophoretic device is already there in the market, which delivers insulin within the systemic circulation (Ita 2016). Apart from the aforementioned clinical devices (diagnostic and therapeutic), there are certain devices which may use a combination of both of these devices to achieve clinical therapeutic efficacy. An artificial pancreas is a common example of this type of device (Albisser et al. 1974; Breton et al. 2012). An artificial pancreas consists of a biosensor, which is usually implanted in a subcutaneous layer of the skin and measures the blood sugar level within the body. Based on the signals perceived from the biosensor, a microcontroller-based device makes a decision to inject sufficient amount of insulin, kept within an insulin reservoir, into the human body (Cetin et al. 2014). This allows the device (artificial pancreas) to maintain the blood sugar level of the diabetic patients.

From the above discussion and a thorough literature review, it is quite evident that point-of-care diagnostic devices have gained much importance in the last decade. These devices are cheap, easy to use and can be easily portable. Amongst many of the devices, portable spectrophotometers have gained much attention (Zuotao et al. 1999; Kittipanyangam et al. 2016). This is because spectrophotometers not only have wide clinical applications but also have been reported to have applications in environmental science (Pinto et al. 2004). Hence, in this study, a very simple OD meter using LDR as the detector and LED as the light source has been proposed (Poole 2014; Held 2016). Commercially available acrylic cuvettes can be used with the proposed device (Suovaniemi 1984). The device is capable of determining analytes (biological or environmental), whose variation in the concentration in a solution results in the alteration in the OD.

2 Literature Review

In this current world of cut-throat competition, where everybody is busy toiling hard round the clock to achieve everyday goals, the time and the effort dedicated for maintenance of a healthy body are near to nil. The increasing environmental pollution, exponentially rising stress due to huge workload, improper nutritional intake etc. expose the body to various diseases. Diagnosis of the diseases, most often, requires the analysis of the patient's samples. The analysis of the patient's samples can be performed in two major ways. One way is the manual transportation of the samples collected from the patient's body to the laboratory for analysis, and the other being the use of in situ sample analysis devices. The first method is relatively costly, time consuming and cumbersome. The sample's viability is often compromised during the entire process of transportation, storage and analysis (Ho et al. 2005). This entails the very need for the development of the on-site sample analysis systems, which are robust, portable and provide better accuracy than the typical laboratory sampling methods by minimizing the risk of contamination of samples due to transportation. Further, the use of such devices can be cost-effective (Lau et al. 2006) and the results can be viewed then and there, which is much faster and reliable (Marle and Greenway 2005). Due to the above-mentioned reasons, these miniaturized in situ sample analysis devices have gained massive importance and huge demand in today's world. In the last few decades, various techniques were used for the production of these miniaturized biosensors, the prominent ones being the microfluidics and the absorbance-based optical sensing devices.

When the construction of the in situ monitoring systems started, microfluidics was among the first effective strategies to be employed (Sequeira et al. 2002). The advances in the nanotechnology and the microfluidics detection systems led to the development of microfluidics-based portable lab-on-a-chip (LOC) systems for fast, sensitive and accurate detection of numerous pathogens (Schwarz and Hauser 2001; Kuswandi et al. 2007). In such devices, the optimum control of nanolitre volumes of fluids was achieved with the integration of various bioassay operations that allowed the device to rapidly sense pathogenic agents for environmental monitoring (Dutse and Yusof 2011). After that, luminescence-based detectors became quite popular, which used light-emitting diodes (LEDs). These were used for various purposes such as measuring of the concentration of the gaseous oxygen and the dissolved oxygen in water (Watkins et al. 1998).

Use of the advanced detection techniques like spectrophotometry (Gros 2005) and colorimetry as the optoelectronic components in the microfluidics system (Dasgupta et al. 2003; Liu and Dasgupta 1994) allowed the reduction in size, cost and errors due to refractive index and turbidity. These were coupled with small-sized LEDs, which provided exceptional stability, low-power consumption and robustness to the device. The LEDs were further integrated with the photodiode arrays (PDAs), photomultiplier tubes (PMTs), phototransistors (PTs) and photodiodes (PDs) that acted as the detectors for the measurement of the intensity of the

light after it passes the sample (Chen et al. 2003; dos Santos et al. 2002; Lau et al. 2004). Further, the LDRs were used as detectors in reflectometric methods (Tubino and Queiroz 2007) because of their small size, inexpensiveness, small power consumption and low-voltage operation. Copper present in urine and water samples were also detected using LED-based colorimeter (Sorouraddin and Saadati 2010).

LEDs provide the most energy-efficient way for the production of monochromatic light and are used not only in the analytical instruments but also for general illumination in optical sensors. They find application in LED-based absorbance measurements, titrations, field and process analysis, capillary electrophoresis (CE), liquid–liquid extraction systems, film- and drop-based analytical systems and liquid core waveguides (LCWs). Nowadays, LED-based fluorescence and spectroelectrochemical detection systems are widely used (Dasgupta et al. 2003). With further advances, dual beam LED optical sensors (Suzuki et al. 2005; Zagatto et al. 1990) have been developed that allows the detection in colour change, refractive index (RI) or turbidity (Eom and Dasgupta 2006; Worsfold et al. 1987). Multi-LEDs-based systems (Hauser et al. 1995; Fonseca and Raimundo 2004) have also been developed that simultaneously or individually cover a wide range of the electromagnetic spectrum without manually changing the LEDs (Beach 1997; Fonseca and Raimundo 2007). Finally, bi/tricolour LEDs have been proposed as light sources (red, green and yellow) (Huang et al. 1992) that offer a compact, rugged, multi-wavelength spectrophotometer source that can enable multi-component analysis and identify sample artifacts like the presence of turbidity (Gros 2007). LEDs can also be used as light detectors (Lau et al. 2004; O'Toole et al. 2005). LED-based chemical sensors have found numerous applications in health sector such as detection of inhaled air pollutants [like particulate matter (PM) (Kawamura et al. 2006), pesticides and volatile organic compounds (VOCs) (Smiddy et al. 2002)], monitoring of food products (Pacquit et al. 2006, 2007), medical diagnosis (Mitrani et al. 1991; Teshima et al. 2005). They have also found applications for security purposes like detection of explosive materials (Pamula et al. 2005), location of mines (Lee et al. 1982), anti-terrorist activities and forensics (O'Toole and Diamond 2008a).

Biomarkers are indicators that can be measured aptly and can give an idea about the severity or the presence of certain diseases or disease-carrying pathogens. Many studies have been conducted, and research is still ongoing to detect cancer biomarkers in the serum samples with the help of surface plasmon resonance and quartz crystal microbalance sensors with nanoparticle signal amplification (Uludag and Tothill 2012). Tothill et al. (2009) have come up with an optical biosensor that can detect the biomarkers and provides an increased scope for diagnostics (Tothill 2009). Sumriddetchkajorn et al. (2014) have proposed the development of a mobile platform-based colorimeter for the detection of chlorine concentration in water (Sumriddetchkajorn et al. 2014). Yeh et al. (2016) have suggested the applications of chemical sensing devices integrated with LEDs in the range between UV and IR (247–3800 nm). These chemical sensors are not only used to detect heavy metals, toxins and toxic gases, environmental nutrients but also to detect biochemicals and biohazard-related compounds (Yeh et al. 2016). Liu et al. (2016) have reported the

development of a small on-chip colorimeter for detecting the concentration of nitrogen, phosphorus and potassium (NPK) in soil samples and is useful for precision agriculture (Liu et al. 2016). Clippard et al. (2016) have developed and characterized a compact and low-cost colorimeter that can analyse the concentration of various analytes such as food dyes and salicylic acid (Clippard et al. 2016).

In this study, an optical sensor has been developed using LED, LDR and a microcontroller that can measure optical density of the sample in order to detect biomarkers present in biological samples. The developed device detects analytes by measuring the absorbance by the biomarkers (present in the serum) due to the reaction with the analysing reagent. This, in turn, increases the accuracy of the sensor, as the targeted biomarkers can now be identifiable and their amount is easily measurable. The circuitry has been designed using low-power consuming components and developed on a printed circuit board (PCB), which makes the device portable. The sensor is interfaced with a computer. This innovation is distinctive, marks the advancement in the ongoing research trends and is ready for mass commercial production.

3 Materials and Methods

3.1 Requirements

LED (5 mm, 400–700 nm wavelength), LDR (10 KΩ), resistors (10 KΩ and 470 Ω), single-sided copper clad board, Arduino UNO, Arduino 1.0.5 IDE (Arduino, Italy), Multisim 13.0 (National Instruments, USA), Ultiboard 13.0 (National Instruments, USA) and acrylic cuvettes were used in this study. MATLAB® (2014a, MathWorks, USA) was used to develop a graphical user interface (GUI) for easy operation of the device.

3.2 Development of the Device

A simple LED-based OD meter was developed as per the method described by Sorouraddin and Saadati with modifications (Sorouraddin and Saadati 2010). The designing aspects of the developed device have been shown in the schematic diagram (Fig. 1a). The device essentially consisted of LDR and LED, which were placed at 180° (i.e. in front of each other). The distance between LDR sensing surface and the LED tip was 16 mm. The placement of LED and LDR was such that the distance between the centre of the sample holder and LED and distance between the centre of the sample holder and the LDR were equal. This LED–LDR arrangement allowed the measurement of the optical density in the transmission mode (Kittipanyangam et al. 2016).

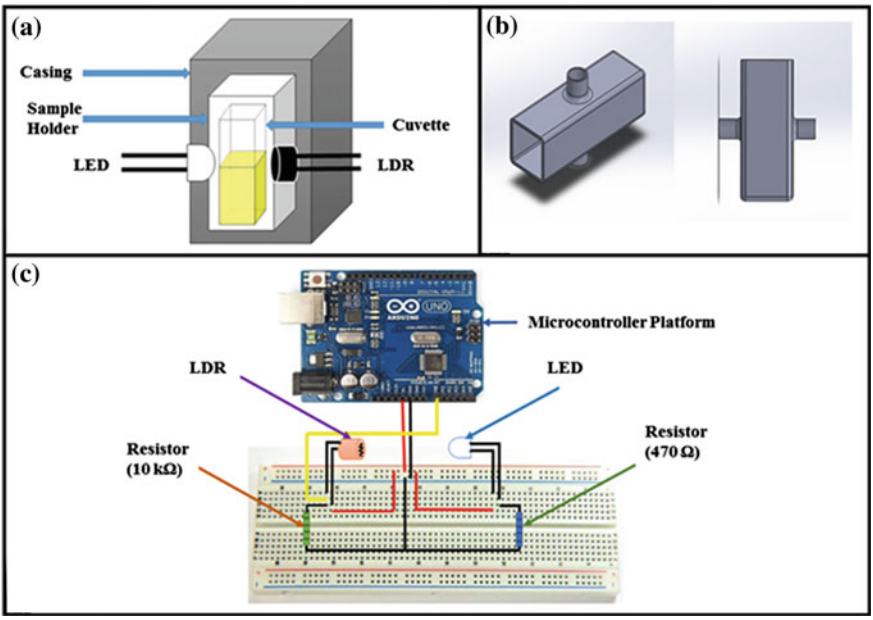

Fig. 1 **a** Schematic diagram of LED–LDR arrangement in the proposed device. **b** Schematic diagram of the sample holder designed in SolidWorks. **c** Schematic diagram of the circuit

The sample holder design was developed in SolidWorks (Shih 2014). The schematic diagram of the model has been shown in Fig. 1b. A 3D printed physical model of the SolidWorks design was developed using a 3D printer (Tran 2016). The sample holder consisted of two slots for housing LED and LDR.

LED was powered using 5 V DC voltage from the Arduino UNO microcontroller platform. LDR was connected in series with a resistor of 10 KΩ. The series combination of LDR and resistor was also supplied with 5 V DC voltage from the Arduino UNO microcontroller. The connection was made such that the free connection terminal of LDR was connected with 5 V, whereas the free connection terminal of the resistor was connected to the analog ground of the Arduino UNO microcontroller. The output from LDR-resistor circuit was measured from LDR-resistor junction. The schematic diagram of the circuit has been shown in Fig. 1c. The Arduino UNO microcontroller was connected to a laptop using the USB interface. This allowed powering of the Arduino UNO microcontroller using the 5 V power supply of the USB terminal, and at the same time transferred the voltage output from LDR-resistor circuit to the laptop via serial communication port. The processing and the display of the signals were done in the laptop by developing a GUI-based program. A printed circuit board (PCB) design layout was made in Ultiboard software (Kim et al. 2016). For this purpose, the circuit diagram was made using the Multisim software (Kalyani and Arya 2014). The circuit design

was subsequently transferred to the Ultiboard for developing PCB layout (Kim and Schubert Jr 2016). Based on the layout, PCB was developed using a single-sided copper clad board. PCB was developed by carbon transfer copper etching method (McClure et al. 2014; Hoinkis et al. 2015).

3.3 Designing of the GUI

GUI was developed using a MATLAB® interface (Lent 2013). GUI was developed such that it acquired signals from the LDR-resistor circuit. Initially, when GUI was started, a provision was made to calibrate the proposed device (Raj et al. 2016). The calibration was achieved by sequentially inserting the blank sample and a black opaque sample and subsequently measuring the voltage drops across the resistor attached to LDR. The calibration voltage signals were stored in a temporary memory created within GUI, which could be available for the computational purpose during that particular session of operation of GUI. After the calibration process was completed, the test samples were analysed (Konieczka and Namiesnik 2016). Thereafter, the ratio of the transmitted light intensity (I) and the incident light intensity (I_0) was calculated using Eq. 1. Absorbance value of the test sample was calculated using Eq. 2 (Sorouraddin and Saadati 2010). The flow chart summarizing the working principle of GUI has been shown in Fig. 2.

$$\frac{I}{I_0} = \frac{V_{\text{test}} - V_{\text{negative}}}{V_{\text{transparent}} - V_{\text{negative}}} \tag{1}$$

where

V_{test} is the voltage when the test sample is placed in the cuvette
$V_{\text{transparent}}$ is the voltage when the transparent liquid (blank solvent) is placed in the cuvette

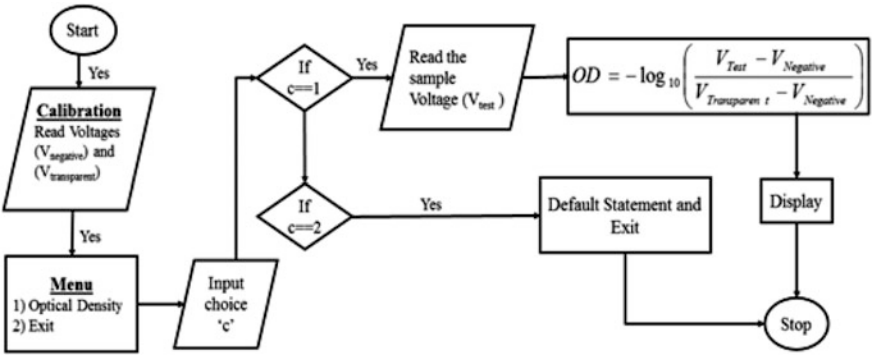

Fig. 2 Flow chart of GUI working process

$V_{negative}$ is the voltage when the black opaque object is placed in the cuvette holder

$$A = -\log_{10}\left(\frac{I}{I_0}\right) \tag{2}$$

where "A" is absorbance.

3.4 Testing of the Device

The testing of the device was carried out using the solutions of rhodamine-B azo dye, potassium indigo sulphate and salicylic acid. For the preparation of the standard curve of rhodamine-B azo dye and potassium indigo sulphate, a stock solution of the dye (500 µg/ml) was made. The stock solution of salicylic acid was prepared by dissolving 100 mg of salicylic acid in 2 ml of ethanol and making the solution up to 100 ml with distilled water in a volumetric flask. The dilution of 10 ml of this stock solution to 100 ml with distilled water resulted in 100 µg/ml salicylic acid stock solution. The ferric chloride reagent was prepared by mixing 100 mg of $FeCl_3$ to 100 ml of 1% HCl. The stock solutions were then serially diluted to obtain different known concentrations of the dye solution (Strijbosch et al. 1988). Thereafter, the diluted solution was tested. This allowed to obtain absorbance values for the solutions of known dye concentration (Kittipanyangam et al. 2016). This information was used to manually plot a standard curve in an excel sheet. In the plot, a linear regression line (Eq. 3) was plotted and the coefficients were determined. This coefficient can be used to calculate the concentration of the unknown test solution using Eq. 4.

$$Y = a + bX \tag{3}$$

$$X = \left(\frac{Y - a}{b}\right) \tag{4}$$

where

Y is the absorbance of the known solution.
X is the concentration of the known solution "a" (intercept) and "b" (slope) is the constants.

4 Results and Discussion

4.1 Designing of the Device and GUI

The schematic diagram of the complete proposed device is shown in Fig. 3a. The 3D printed sample holding unit along with LED and LDR slot has been shown in Fig. 3b (O'Toole and Diamond 2008b). The sample holder was able to accommodate the commercially available acrylic cuvettes. The calibration of the device was done by interfacing the developed device with the laptop in which the in-lab developed GUI program was being operated. The picture of the complete setup has been provided in Fig. 3c. As GUI program was initiated, calibration of the sensor was needed to be carried out (Lent 2013). This could be done by clicking the "Start" button under the "Calibration" tab. As the start button was clicked, a pop-up message, instructing the user to put the black opaque sample was displayed. After the user put the opaque object in the sample holder and clicked "OK" in the dialogue box, V_{negative} was calculated and stored in a temporary memory file. Subsequently, another pop-up message was generated, instructing the user to put the transparent solution in the sample holder. After the placement of the transparent solution, the user needed to click "OK". This resulted in the calculation of the $V_{\text{transparent}}$ value, which was stored in another temporary memory file. The V_{negative} and $V_{\text{transparent}}$ values were displayed on the numerical indicator under the "Calibration" tab. Once the calibration step was completed, the device was ready to use. Thereafter, the test sample was placed within the sample holder and the user needed to click the "Calculate" button. This allowed the measurement of the V_{test}, and the subsequent calculation of the absorbance values as per Eqs. 1 and 2 was carried out.

4.2 Testing of the Device

In order to test the performance of the proposed device, the standard curves of the dye solutions (i.e. rhodamine-B azo, potassium indigo sulphate and salicylic acid) were constructed by determining the absorbance of the diluted rhodamine-B azo dye solution, potassium indigo sulphate solution and salicylic acid solution (Zhi and Zaini 2017; Bhutta et al. 2014). The points of the standard curves were fitted with a linear regression line in an excel sheet (Fig. 4a–c). A correlation coefficient (R^2) > 0.99 was accepted. The intercept "*a*" and the slope of the line "*b*" were calculated from the plot. The "*a*" and the "*b*" values for the rhodamine-B were 0.0018 and 0, respectively. For potassium indigo sulphate, their values were 0.0021 and 0, respectively. Lastly, the "*a*" and the "*b*" values for salicylic acid were 0.0027 and 0, respectively. The "*a*" and the "*b*" values were used to calculate the

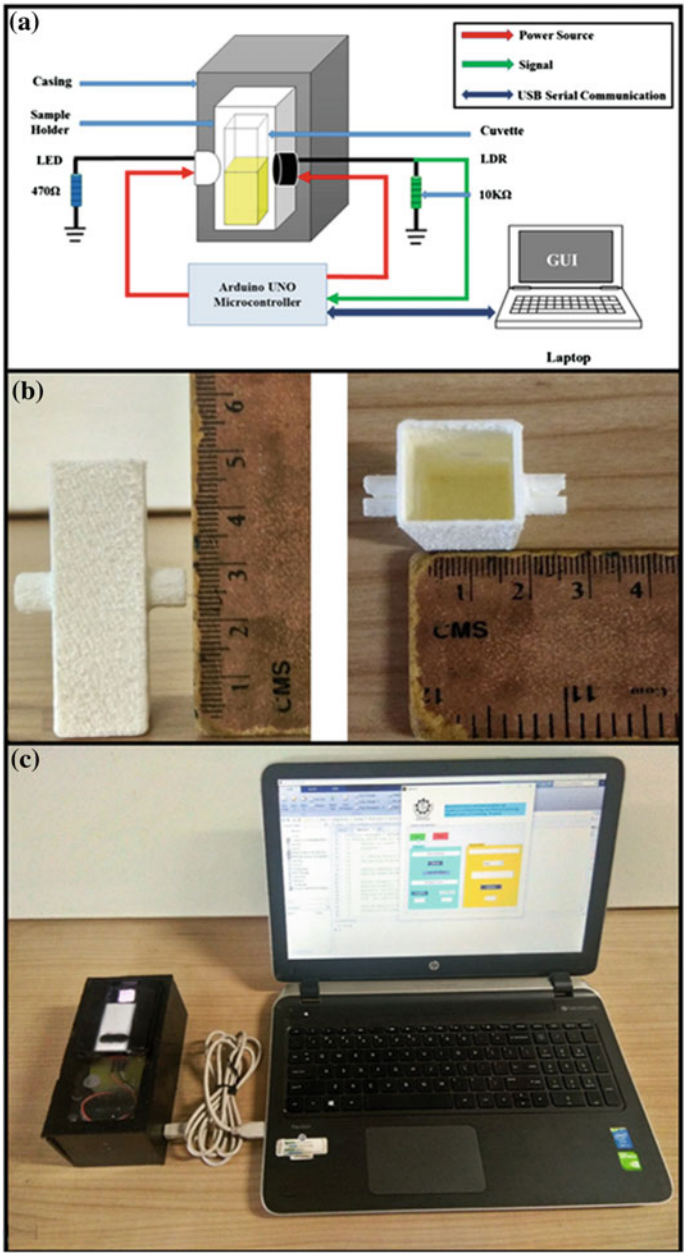

Fig. 3 **a** Schematic diagram of the proposed device. **b** 3D printed sample holder. **c** Picture of the developed device

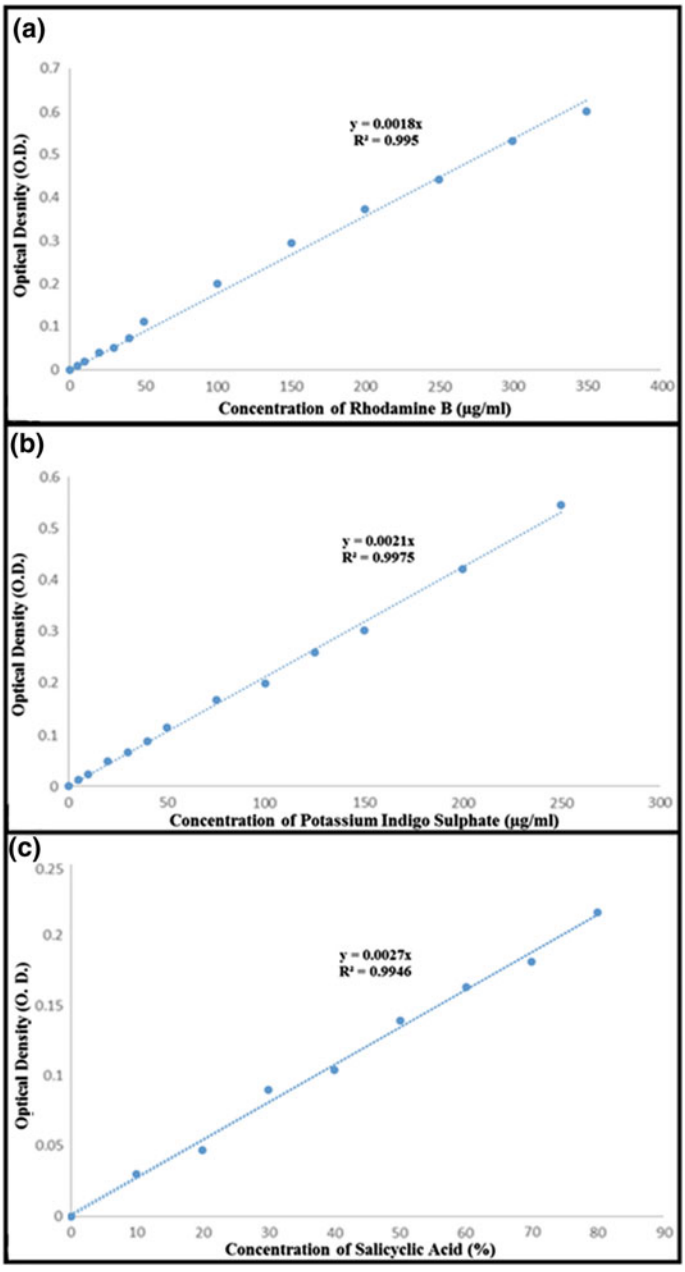

Fig. 4 Standard curve of **a** rhodamine-B, **b** potassium indigo sulphate and **c** salicylic acid

concentration of the test sample. The percentage error between the instrument obtained values and the theoretical values was <5% (Zienkiewicz and Zhu 1987). This confirmed the suitability of the proposed device for the measurement of OD values of different types of analytes.

5 Conclusion

In recent years, the use of colorimeters for determining the concentrations of the analytes is gaining popularity. Colorimeters have been explored for monitoring the concentrations of environmental parameters, food dyes, soil nutrients, etc. apart from the clinical biomarkers. The current study proposes the development and the successful testing of an optical sensing-based colorimeter for the calculation of OD values of analytes. The device was developed using LED, LDR and a microcontroller making it low cost and portable. The interfacing of the device with computer facilitated the fast calculation of the OD values. The performance of the device was tested by drawing the standard curves of the solutions of rhodamine-B azo dye, potassium indigo sulphate and salicylic acid. The results suggested that the device was able to measure the OD values with an acceptable accuracy (<5% error), and hence, can be used for determining the concentration of various types of analytes of medical importance.

References

Albisser AM, Leibel B, Ewart T, Davidovac Z, Botz C, Zingg W, Schipper H, Gander R (1974) Clinical control of diabetes by the artificial pancreas. Diabetes 23(5):397–404

Allen S, Adjani A (2016) Therapeutic device and method. Google Patents

Beach J (1997) A LED light calibration source for dual-wavelength microscopy. Cell Calcium 21(1):63–68

Bhutta MR, Hong K-S, Kim B-M, Hong MJ, Kim Y-H, Lee S-H (2014) Note: three wavelengths near-infrared spectroscopy system for compensating the light absorbance by water. Rev Sci Instrum 85(2):026111

Breton M, Farret A, Bruttomesso D, Anderson S, Magni L, Patek S, Dalla Man C, Place J, Demartini S, Del Favero S (2012) Fully integrated artificial pancreas in type 1 diabetes. Diabetes 61(9):2230–2237

Cetin AE, Coskun AF, Galarreta BC, Huang M, Herman D, Ozcan A, Altug H (2014) Handheld high-throughput plasmonic biosensor using computational on-chip imaging. Light Sci Appl 3(1):e122

Chen S-J, Chen M-J, Chang H-T (2003) Light-emitting diode-based indirect fluorescence detection for simultaneous determination of anions and cations in capillary electrophoresis. J Chromatogr A 1017(1):215–224

Clippard CM, Hughes W, Chohan BS, Sykes DG (2016) Construction and characterization of a compact, portable, low-cost colorimeter for the chemistry lab. J Chem Educ 93(7):1241–1248

Dasgupta PK, Eom I-Y, Morris KJ, Li J (2003) Light emitting diode-based detectors: absorbance, fluorescence and spectroelectrochemical measurements in a planar flow-through cell. Anal Chim Acta 500(1):337–364

dos Santos SRB, de Araújo MCU, Barbosa RA (2002) An automated FIA system to determine alcoholic grade in beverages based on Schlieren effect measurements using an LED-photocolorimeter. Analyst 127(2):324–327

Dutse SW, Yusof NA (2011) Microfluidics-based lab-on-chip systems in DNA-based biosensing: an overview. Sensors 11(6):5754–5768

Eom I-Y, Dasgupta PK (2006) Frequency-selective absorbance detection: refractive index and turbidity compensation with dual-wavelength measurement. Talanta 69(4):906–913

Fonseca A, Raimundo IM (2004) A multichannel photometer based on an array of light emitting diodes for use in multivariate calibration. Anal Chim Acta 522(2):223–229

Fonseca A, Raimundo IM (2007) A simple method for water discrimination based on an light emitting diode (LED) photometer. Anal Chim Acta 596(1):66–72

Gros N (2005) A new type of a spectrometric microtitration set up. Talanta 65(4):907–912

Gros N (2007) A novel type of tri-colour light-emitting-diode-based spectrometric detector for low-budget flow-injection analysis. Sensors 7(2):166–184

Hauser PC, Rupasinghe TW, Cates NE (1995) A multi-wavelength photometer based on light-emitting diodes. Talanta 42(4):605–612

Held G (2016) Introduction to light emitting diode technology and applications. CRC Press, Boca Raton

Ho CK, Robinson A, Miller DR, Davis MJ (2005) Overview of sensors and needs for environmental monitoring. Sensors 5(1):4–37

Hoinkis M, Yan C, Miyazoe H, Joseph E (2015) Copper residue chamber clean. Google Patents

Huang J, Liu H, Tan A, Xu J, Zhao X (1992) A dual-wavelength light-emitting diode based detector for flow-injection analysis process analysers. Talanta 39(6):589–592

Ita K (2016) Transdermal iontophoretic drug delivery: advances and challenges. J Drug Target 24(5):386–391

Kalyani V, Arya A (2014) Design and simulation of VFA and CFA based integrator and differentiator using NI multisim and their comparison. Int J Adv Res Electron Commun Eng (IJARECE) 3

Kawamura K, Ishiyama M, Nagatani N, Hashiba T, Tamiya E (2006) Development of a novel hand-held toluene gas sensor: possible use in the prevention and control of sick building syndrome. Measurement 39(6):490–496

Kim EM, Schubert TF Jr (2016) A low-cost design experience for junior-level electronics circuits laboratories through emulation of industry-printed circuit board design practice. Int J Electr Eng Edu:0020720916673650

Kim H-K, Cho S-H, Chil-Woo K, Chung Y-K, Going-Sik K (2016) Printed circuit board. Google Patents

Kittipanyangam S, Abe K, Eguchi K (2013) Design of a measurement device explaining the relationship between the concentration of solution and the light absorbance for chemical education. In: 2016 13th international conference on electrical engineering/electronics, computer, telecommunications and information technology (ECTI-CON), pp 1–6, 28 June 2016–1 July 2016. doi:https://doi.org/10.1109/ECTICon.2016.7561271

Konieczka P, Namiesnik J (2016) Quality assurance and quality control in the analytical chemical laboratory: a practical approach. CRC Press, Baco Raton

Kuswandi B, Huskens J, Verboom W (2007) Optical sensing systems for microfluidic devices: a review. Anal Chim Acta 601(2):141–155

Lau K-T, Baldwin S, O'Toole M, Shepherd R, Yerazunis WJ, Izuo S, Ueyama S, Diamond D (2006) A low-cost optical sensing device based on paired emitter–detector light emitting diodes. Anal Chim Acta 557(1):111–116

Lau KT, Baldwin S, Shepherd RL, Dietz PH, Yerzunis WS, Diamond D (2004) Novel fused-LEDs devices as optical sensors for colorimetric analysis. Talanta 63(1):167–173

Lee R, Aldis D, Garrett D, Lai F (1982) Improved diagnostics for determination of minimum explosive concentration, ignition energy and ignition temperature of dusts. Powder Technol 31(1):51–62
Lent CS (2013) Learning to program with MATLAB. Wiley, Hoboken
Liedtke S, Loerwald D (2014) Diagnostic device. Google Patents
Liu H, Dasgupta PK (1994) Dual-wavelength photometry with light emitting diodes. Compensation of refractive index and turbidity effects in flow-injection analysis. Anal Chim Acta 289(3):347–353
Liu R-T, Tao L-Q, Liu B, Tian X-G, Mohammad MA, Yang Y, Ren T-L (2016) A miniaturized on-chip colorimeter for detecting NPK elements. Sensors 16(8):1234
Marle L, Greenway GM (2005) Microfluidic devices for environmental monitoring. TrAC Trends Anal Chem 24(9):795–802
McClure SR, Banko JD, Ternus JP (2014) Printed circuit board. Google Patents
McPherson RA, Pincus MR (2016) Henry's clinical diagnosis and management by laboratory methods. Elsevier Health Sciences, Amsterdam
Mitrani AA, Gonzalez ML, O'Connell MT, Guerra J, Harwood RB, Gardner LB (1991) Detection of clinically suspected deep vein thrombosis using light reflection rheography. Am J Surg 161(6):646–650
O'Toole M, Diamond D (2008) Absorbance based light emitting diode optical sensors and sensing devices. Sensors 8(4):2453–2479
O'Toole M, Lau KT, Diamond D (2005) Photometric detection in flow analysis systems using integrated PEDDs. Talanta 66(5):1340–1344
Pacquit A, Frisby J, Diamond D, Lau KT, Farrell A, Quilty B, Diamond D (2007) Development of a smart packaging for the monitoring of fish spoilage. Food Chem 102(2):466–470
Pacquit A, Lau KT, McLaughlin H, Frisby J, Quilty B, Diamond D (2006) Development of a volatile amine sensor for the monitoring of fish spoilage. Talanta 69(2):515–520
Pamula V, Srinivasan V, Chakrapani H, Fair R, Toone E (2005) A droplet-based lab-on-a-chip for colorimetric detection of nitroaromatic explosives. In: 18th IEEE International Conference on Micro Electro Mechanical Systems (MEMS 2005), IEEE, pp 722–725
Pinto JJ, Moreno C, García-Vargas M (2004) A very sensitive flow system for the direct determination of copper in natural waters based on spectrophotometric detection. Talanta 64(2):562–565. doi:https://doi.org/10.1016/j.talanta.2004.03.009
Poole I (2014) Light dependent resistor, photo resistor, or photocell. Radio-Electronics com
Raj JR, Rahman S, Anand S (2016) Microcontroller USB interfacing with MATLAB GUI for low cost medical ultrasound scanners. Eng Sci Technol Int J 19(2):964–969
Sanderson JE, Deriel SR (1988) Method and apparatus for iontophoretic drug delivery. Google Patents
Schwarz MA, Hauser PC (2001) Recent developments in detection methods for microfabricated analytical devices. Lab Chip 1(1):1–6
Sequeira M, Bowden M, Minogue E, Diamond D (2002) Towards autonomous environmental monitoring systems. Talanta 56(2):355–363
Shen MJ, Zipes DP (2014) Role of the autonomic nervous system in modulating cardiac arrhythmias. Circ Res 114(6):1004–1021
Shih R (2014) Introduction to finite element analysis using solidworks simulation 2014. SDC publications
Smiddy M, Papkovskaia N, Papkovsky D, Kerry J (2002) Use of oxygen sensors for the non-destructive measurement of the oxygen content in modified atmosphere and vacuum packs of cooked chicken patties; impact of oxygen content on lipid oxidation. Food Res Int 35(6):577–584
Sorouraddin M, Saadati M (2010) Determination of copper in urine and water samples using a simple led-based colorimeter. J Anal Chem 65(4):423–428
Strijbosch LW, Does RJ, Buurman WA (1988) Computer aided design and evaluation of limiting and serial dilution experiments. Int J Biomed Comput 23(3–4):279–290

Sumriddetchkajorn S, Chaitavon K, Intaravanne Y (2014) Mobile-platform based colorimeter for monitoring chlorine concentration in water. Sens Actuators B Chem 191:561–566

Suovaniemi OA (1984) Set of cuvettes. Google Patents

Suzuki A, Kondoh J, Matsui Y, Shiokawa S, Suzuki K (2005) Development of novel optical waveguide surface plasmon resonance (SPR) sensor with dual light emitting diodes. Sens Actuators B Chem 106(1):383–387

Swisher SL, Lin MC, Liao A, Leeflang EJ, Khan Y, Pavinatto FJ, Mann K, Naujokas A, Young D, Roy S, Harrison MR, Arias AC, Subramanian V, Maharbiz MM (2015) Impedance sensing device enables early detection of pressure ulcers in vivo. Nat Commun 6:6575. doi:https://doi.org/10.1038/ncomms7575. https://www.nature.com/articles/ncomms7575#supplementary-information

Teshima N, Li J, Toda K, Dasgupta PK (2005) Determination of acetone in breath. Anal Chim Acta 535(1):189–199

Tothill IE (2009) Biosensors for cancer markers diagnosis. In: Seminars in cell & developmental biology, vol 1. Elsevier, Amsterdam, pp 55–62

Tran P (2016) Solidworks 2016 Advanced Techniques. SDC Publications

Tubino M, Queiroz CA (2007) Flow injection visible diffuse reflectance quantitative analysis of nickel. Anal Chim Acta 600(1):199–204

Uludag Y, Tothill IE (2012) Cancer biomarker detection in serum samples using surface plasmon resonance and quartz crystal microbalance sensors with nanoparticle signal amplification. Anal Chem 84(14):5898–5904

Watkins AN, Wenner BR, Jordan JD, Xu W, Demas JN, Bright FV (1998) Portable, low-cost, solid-state luminescence-based O_2 sensor. Appl Spectrosc 52(5):750–754

Worsfold PJ, Clinch JR, Casey H (1987) Spectrophotometric field monitor for water quality parameters: the determination of phosphate. Anal Chim Acta 197:43–50

Yeh P, Yeh N, Lee C-H, Ding T-J (2016) Applications of LEDs in optical sensors and chemical sensing device for detection of biochemicals, heavy metals, and environmental nutrients. Renew Sustain Energy Rev 75:461–468

Zagatto E, Arruda M, Jacintho A, Mattos I (1990) Compensation of the Schlieren effect in flow-injection analysis by using dual-wavelength spectrophotometry. Anal Chim Acta 234:153–160

Zhi LL, Zaini MAA (2017) Adsorption properties of cationic rhodamine B dye onto metals chloride-activated castor bean residue carbons. Water Sci Technol 75(4):864–880

Zienkiewicz OC, Zhu JZ (1987) A simple error estimator and adaptive procedure for practical engineerng analysis. Int J Numer Meth Eng 24(2):337–357

Zuotao Z, McCreedy T, Townshend A (1999) Flow-injection spectrophotometric determination of gold using 5-(4-sulphophenylazo)-8-aminoquinoline. Analytica Chimica Acta 401(1–2):237–241. doi:https://doi.org/10.1016/S0003-2670(99)00498-5

Chapter 13
Flexible Sensors for Biomedical Application

Ankur Gupta and Pramod Pal

Abstract The research paradigm for biosensing devices has been focussed to explore flexible sensors. Here, the term "flexible" is indicative of the substrate which has sufficient degree of deformability so that it could be suitably placed at any place. Advances in flexible sensing technologies can be observed by the number of smart products in the market as well as with the number of publications exponentially coming out every year in which diversified development in terms of device operation and performance have been explored. However, as is the case for most new developments, there are several challenges and opportunities which this relatively newfangled field is facing, both in the basic and applied aspects. These challenges and opportunities basically lie in three broad areas, namely design, fabrication, and integration of the developed flexible systems to improve the purpose-oriented sensing capabilities, such as sensing characteristics, functionality, so and so forth. In this chapter, fundamental aspect of various sensing films and associated mechanism has been illustrated. With this article, state-of-the-art work on the promising flexible sensing platforms for biomedical applications is also discussed.

Keywords Flexible · Biosensor · Flexible substrate · Flexible sensor

1 Introduction to Flexible Sensor

In order to develop our understanding towards flexible sensors, we must first understand the terms "flexibility" and "sensors" explicitly. The word "sensor" can be defined as a device which is used to detect the analyte of interest and provide selective signal for the identification and quantification of analyte. The word "flexible" can be defined as property of any material/substrate which has

A. Gupta (✉) · P. Pal
School of Mechanical Sciences, Indian Institute of Technology Bhubaneswar, Bhubaneswar 752050, Odisha, India
e-mail: ankurgupta@iitbbs.ac.in

S. Bhattacharya et al. (eds.), *Environmental, Chemical and Medical Sensors*, Energy, Environment, and Sustainability, https://doi.org/10.1007/978-981-10-7751-7_13

considerable amount of deformability so that it could be fitted in any place. Being flexible, a sensor can acquire the shape of the surface where it has to sense. It is a very useful property required in biomedical sensing, physical sensing, chemical sensing, etc. As an example, ability of bending of strain gauge facilitates us to put it on non-uniform sensing area. Considering the enormous possibilities related to its application, flexibility of sensors may assist in the manufacturing of sensor garments, sensing skin, real-time healthcare monitoring. It may also protect from getting damage due to impact load as well as may lead to adjustability in lesser space, accuracy of sensor gets improved. It not only provides outstanding amount of deformability but also freedom to formulate various sensing surfaces or films with a variety of geometries (Li et al. 2014).

If we have wearable sensor then we can perform long-term sensing which will provide more data and helps in improving health monitoring of the body part without any difficulty. In developing countries, where the healthcare facilities are still in development phase these biomedical sensors provide in situ detection which helps in preventing the spoilage of the subject, and also it reduces the cost of transportation. Flexible sensor can be a possible solution as it will provide us the freedom in motion as we can wear them and do our work. During fever, sometimes it becomes very difficult to keep thermometer stagnant in child's body. In such situation, we may think of attaching a flexible sensor to monitor the temperature of the body, and in this way, our problem to take care about their body motion may be solved.

The biomedical flexible sensors are mainly non-invasive, and we can detect the disease or symptom of disease by detecting the composition, deficiency, or abundance of specific constituent in the subject of interest like skin, saliva, blood and its pressure, tear, urine, neural activity, and several other things. In past recent years, so many ways of sensing these things have been developed. In wearable biomedical flexible sensors like strain sensor, pressure sensor, skin sensor, heart rate sensor, temperature sensor, transduction principle is used where any physical entity is detected. With the change in their electrical behaviour, conversion of these physical entities into readable electrical signals takes place which can be further calibrated by using known values of the physical input and the sensor output. In general, MEMS device requires less energy to operate, less vulnerable to ambient vibration, fast reaction, requires very less volume of fluids to detect.

The accuracy of the sensor is increased by enhancing the sensing area and the resolution of the sensor for which miniaturization is a powerful tool, i.e., we have to go to micro- and nanoscale. Going to micro- and nanoscale, the sensing area increases which allows more analyte to sit on the sensor in molecular level which would provide us very high resolution

2 Substrate for Flexible Sensor

Substrate is a base for sensor on which sensing ability and electrical connection are developed. For making any sensor flexible, flexibility of its substrate is utmost important step. Different kind of flexible substrate has been developed. Some are naturally flexible (paper, some polymer, etc.) and some are artificially made flexible (modified silicon film, thin plastic sheets, etc.). Metal foils are generally of high cost and have rough surface but it can sustain high temperature. The emphasis on developing the biosensor is on making them cheap, so that it could be available for onsite application and for those people to who developed medical facility is not available. Therefore, plastic and paper-based substrates are considered most suitable for developing the bio sensors.

A substrate used for sensing applications should possess following properties:

- Dimensional stability
- Low coefficient of thermal expansion
- Biocompatibility
- It should not react with the environment
- Effect of ambient vibration should not be there otherwise it will bring error in electrical signal
- Thermal, electrical, mechanical stability
- Geometry
- Life span
- Solubility with different chemicals and body fluids.

As of now, following substrates have been used for flexible sensors.

2.1 Paper as a Substrate

Paper as a substrate is simple to fabricate, inexpensive, lightweight, disposable. They have one unique feature to self-drive the liquid (capillary action), which means it does not need any external mechanism to drive the liquid. By simply adding compounds, its properties can be changed (Lemaire et al. 2015). Further, fabricating electrodes for establishing electrical connection is also relatively simple as compared to those fabricated in hard substrates. As an example, very simple graphite on paper piezoresistive device is shown in Fig. 1 in which graphite is utilized as a sensing element. In this work, test result revealed that resistance is directly proportional to the applied force; therefore by calibrating the resistance to force, sensor is developed in this case (Ren et al. 2012).

Paper has been used in making microfluidic devices where in most cases, the fluid which contains the analyte of interest is exposed to the paper and it automatically travel through the paper towards the detection site where the analyte of interest is sensed of the solution. Use of the paper has been observed in many fields.

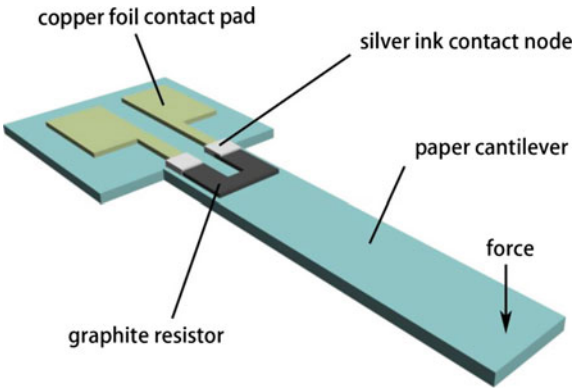

Fig. 1 Shows the schematic for a paper-based sensor for the detection of force. Graphite is here utilized as the sensing element (Ren et al. 2012)

Natural wicking action of the paper vanishes the additional equipment requirement to drive the fluid in microfluidic sensors. In biomedical applications, paper sensors have been emerged out as powerful tool. One of the current developed technologies is commercially available pregnancy test kid which provides signal in the form of change in colour based on human chorionic gonadotropin (hCG) concentration present in the urine. Actual cost of the paper-based sensor is much lower than PDMS-based or silicon-based devices. Some researchers, viz. Whiteside group, Paul Yager's group, etc., have contributed in paper-based sensors and brought the technology to a newer level. They have utilized basic concept of fluid transport which generally obeys Darcy's laws of flow through porous media.

2.2 Polymeric Substrates

Generally, polymeric substrates used in flexible sensors are polyethylene terephthalate (PET), polyethylene napthalate (PEN) along with other various amorphous polymer substrates which are polycarbonate (PC), polyethersulphone (PES), polyimide (PI), and conductive polymer like polyaniline (PANI) etc. (Choi et al. 2008; Trung et al. 2014). Nowadays, biodegradable polymers are used in resorbable surgical sutures.

Most often, coefficient of thermal expansion for thermoplastic semi-crystalline polymers such as PET and PEN and PI are low. Thermoplastics such as PET and PEN have certain characteristics such as high transparency, low coefficient of thermal expansion (CTE), superior moisture adsorption, considerable resistance towards chemical, and low price as well. But drawback of these thermoplastics is that they are not suitable for high temperature and have low surface smoothness (Fig. 2).

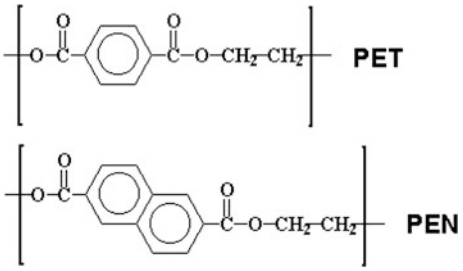

Fig. 2 Molecular structures of polyethylene terephthalate and polyethylene naphthalate (Lechat et al. 2006)

2.2.1 Polyethylene Terephthalate (PET) Plastic Flexible Substrate

PET is a thermoplastic semi-crystalline polymer which is combination of ethylene glycogel and terephthalic acid. And it can be formed as thermoplastic semi-crystalline polymer or amorphous (transparent) by thermal processing It acts as a barrier to water and water vapour, due to its non-polar molecular structure (Lechat et al. 2006). Figure 3 shows how a PET substrate can be used for the development of sensor array; it also shows the transparency of the substrate. It is cheap, lightweight and can be recycled.

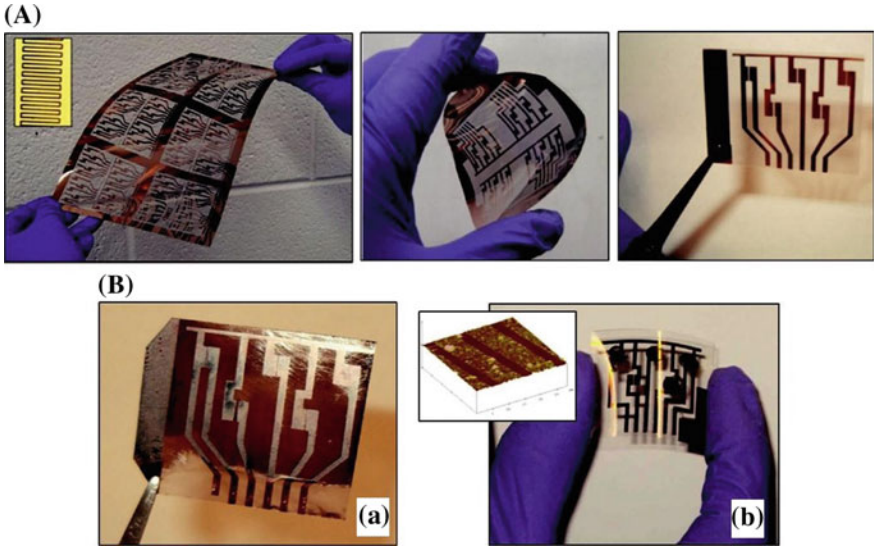

Fig. 3 **A** Shows the images of chemiresistor arrays developed over polyethylene terephthalate substrates of two dissimilar shapes, (insert depicts the detailed aspects of the interdigitated microelectrodes). **B** Pictures showing two examples of sensor arrays which are coated with nanoparticle thin film. In figure **B**, **a** nanoparticle thin films assembled on four of the active interdigitated microelectrode areas, respectively, **b** (insert shows an AFM image of the nanoparticle thin film pattern on gold/mica substrate developed with the help of microcontact printing). (Reproduced with kind permission from Wang et al. 2010)

2.2.2 Polyethylene Naphthalene (PEN) Plastic Flexible Substrates

PEN is polymer of dimethyl naphthalene dicarboxylate and ethylene glycol. It is similar to polyethylene terephthalate (PET) but more temperature resistant. It is more chemically stable towards water vapour, oxygen and can work at higher temperature relative to PET. PEN fibres are much stiffer in comparison to PET fibres; this is due to the fact that PEN fibres have two aromatic rings in its molecular structure (Lechat et al. 2006). It is lightweight, transparent, low cost. Figure 4 is showing how different component can be mounted on the PEN substrate.

2.2.3 Polyimide as Substrate (PI)

Polyimide is a kind of amorphous polymer made up of imide monomers. Kapton is a polyimide which is formed by the condensation of pyromellitic dianhydride and 4,4′-oxydianiline. They have low optical transparency, high glass transition temperature which makes it appropriate to be used at higher temperature, These substrates are lightweight, flexible, resistant to heat, and chemicals (Wright and Hallden-Abberton 2002). Figure 5 shows the flexible sensor made up with the combination of polyimide and aluminium oxide film over polyimide substrate. Flexibility in the sensor can be easily observed in the figure itself (Fig. 6).

2.2.4 Polycarbonate

Polycarbonate is a well explored polymer which is most often being utilized in a various optical applications. It has chemical stability, good optical, and mechanical properties. However, because of its poor surface characteristics, such as low hardness, low resistance to abrasion along with low surface energy, this polymeric substrate generally leads to low wettability and offers very less adhesion to the sensing films deposited over it (Kitova et al. 2005).

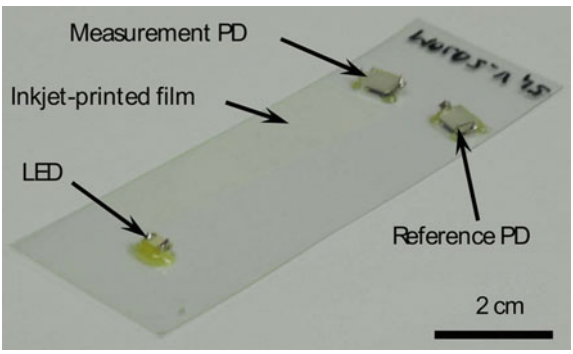

Fig. 4 Shows the sensor assembly developed on PEN substrate. This is an ammonia optical gas sensor used as waveguide with mounted LED and photodetectors (PD) along with inkjet printing sensing film (Courbat et al. 2011)

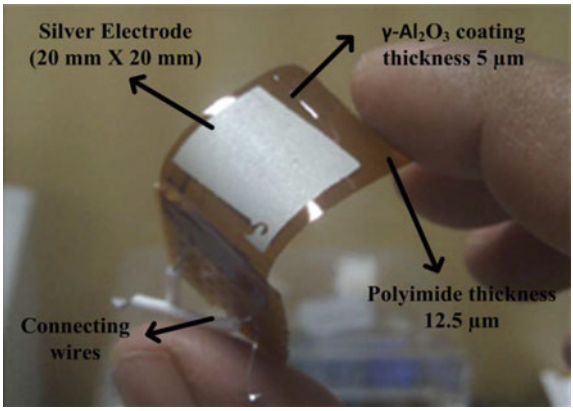

Fig. 5 Photograph of the sensor having combined polyimide-Al_2O_3 dielectric films (Islam et al. 2015)

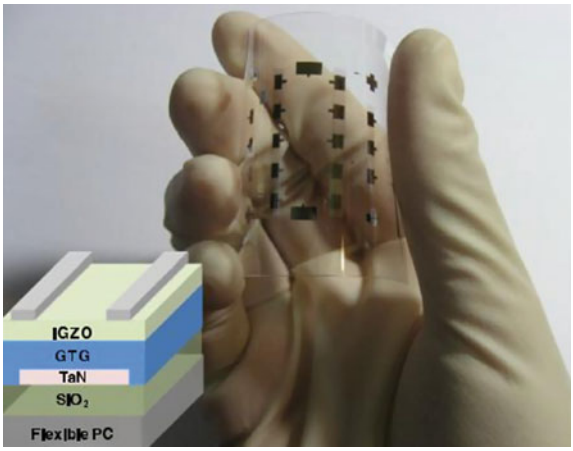

Fig. 6 Shows the photograph of IGZO TFT with GeO_2/TiO_2/GeO_2 dielectric on flexible polycarbonate (PC). (Reproduced with kind permission from Hsu et al. 2013)

2.2.5 Polydimethylsiloxane (PDMS)

PDMS is a visco-elastic polymer being used widely in the development of microfluidics platform. It is a commercially available silicon rubber; initially it exists in liquid form but it can be converted into any size and shape with the help of come chemical and thermal treatment. Generally, PDMS is poured in a mould and cured at 60 °C for 1 h to get the desired shape. It has Si–O–Si, Si–CH_3 linkages in its composition. Presence of methyl group in its structure makes it somewhat hydrophobic in nature. Sensing elements like functionalized nanowires, nanotubes can be embedded on the PDMS sheet to make it suitable for sensing application. PDMS is one of the most extensively used polymers for soft lithography. Beauty of this polymer is that it can be transformed irrespective of any size and shape present in solid substrate, by double inversion technique. It is mostly chosen for fabricating microfluidic chips because of its excellent transparency, exceptional elastic

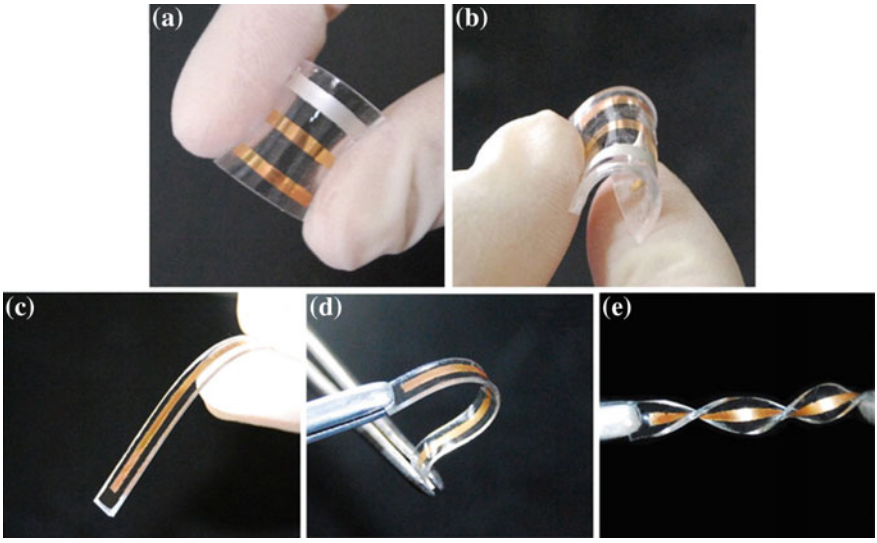

Fig. 7 Depicts the pictures of the flexible PDMS-based electrode sensor. Working electrode: gold, reference electrode: silver and counter electrode: gold. Top view (**a**) and side view (**b**) of the three-electrode sensor, straight (**c**), bend (**d**), and twist (**e**) of the working electrode. (Reproduced with kind permission from Wu et al. 2010)

behaviour, superior thermal stability, and ease of fabrication with various materials. (Wu et al. 2010). It is chemically inert, permeable to gases, trouble-free to manipulate, exhibits isotropic, and homogeneous properties as well as lower cost than silicon. It can conform to submicron features to develop microstructures as well. As an example, Fig. 7 shows the PDMS-based device in which three electrodes have been placed, namely gold as working electrode, silver as reference electrode, and again gold as counter electrode. As can be observed from Fig. 7c–e, sensor can be bent, twist, and straightened according to the requirement.

2.2.6 Polyaniline (PANI)

Polyaniline is composed of '*n*' number of reduced benzenoid diamine and '*m*' number of oxidized quinoid diamine repeating units, where value of *m* defines the oxidation state. The main advantage of using PANI conducting polymer as its properties like conductivity, electrochemical behaviour, electrochromism, and porosity are tunable (Dhand et al. 2011). This unique feature makes PANI to be used in a variety of application like gas sensing, anticorrosive coatings, electrocatalytic devices, energy storage systems. It is unproblematic to deposit it on the sensor electrode. It is structurally flexible, of low cost and can be used as immobilization platform (Fig. 8).

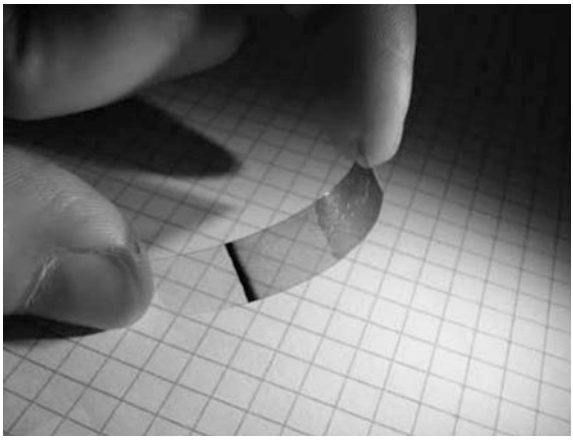

Fig. 8 Shows the transparent and flexible CNT/PANI pH sensors (Kaempgen and Roth 2006)

3 Sensing Element Used in Flexible Sensors

The sensing material is one of the most important elements of any sensor. These are embedded on the flexible template and electrical connections are made through electrode. The signal transducer is responsible for the sensitivity of a sensor by investigating recognition event. This can be analyzed by converting recognition event into an signal which can be in the form of electrical signal or can be done with the help of optical, electrochemical, pressure, thermal means, etc. Common transducers used include amperometric electrodes, optical waveguides, mass sensitive piezoelectric crystals. There are many ways through which we can convert the physical input to the sensing element into readable electrical signal output. The variation in the electrical parameters, such as piezoelectricity (Li et al. 2008; Bu et al. 2007; Hwang et al. 2015), triboelectricity (Yang et al. 2013, 2015), capacitance (Nie et al. 2014; Lipomi et al. 2011), or resistance (Chossat et al. 2013; Jeon and Ha 2016), are used to detect and express physical data, including pressure and temperature (Yeo and Lim 2016).

Depending on the types of active sensing elements experiencing changes in its material properties, category of all types of sensors may be largely classified into solid-state and liquid-state sensing devices (Yeo and Lim 2016). Description of each of them is provided as follows.

3.1 Solid-State Sensing Device Element

In the solid-state sensing device, the active sensing element is in solid state. Some of the example is as follows:

- Carbon nanotubes, graphene
- Metallic particles
- Metallic nanowires (e.g., Ag, Au, Cu, Al, Mn, Zn)
- Polymer nanofibers.

Nanostructured materials such as nanoparticles, nanotubes, nanofibers chosen are the functional part of the sensor. They increase the surface area which in turns increases the sensitivity, sensing resolution and are used as a transducer, chemical reaction site, antigen holder, and from here electrical connection is made to get the desired electrical signal.

3.2 Liquid-State Sensing Device Element

Sensors based on liquid-state sensing element has some advantage in flexible sensor fabrication as the conductive liquid encapsulated in flexible substrate is naturally flexible, and also liquid acquires the shape of its mould. Therefore, it is possible to make complex shape sensor, some other advantages of using liquid element are, that it provides high sensitivity, low cost of fabrication, low sample quantity and requires very small working fluid. These devices triumph over the limitation of solid-state devices in terms of plastic deformation, fracture, and adaptability. These devices are generally based on microfluidics in which the electrical signal varies as the shape of the geometry of encapsulated volume varies with the variation in the length, width, and height, for example, when the strain is applied in the device its length will increase and the concentration of working fluid per unit length will decrease which in turn decreases the conductivity of path and therefore shows less current. In these type of devices, the active sensing elements are taken as liquid such as ionic and metallic liquid.

4 Working Principle on Which Flexible Sensor Works

There are number of working principles explored for sensing and developing biomedical devices. In general, flexible physical sensors comprise two discrete building blocks, i.e., the flexible template materials and the active sensing elements, which may get either solid or liquid form. The fundamental sensing mechanism of the flexible and wearable sensors is based on the mechanical deformations such as bending, pressing, stretching, and twisting faced by the sensing devices. Emerging applications of flexible sensors specially in the area of healthcare and biomedical fields include artificial electronic skins, physiological monitoring and assessment systems, and creation of drug delivery platforms (Yeo and Lim 2016) (Fig. 9).

Flexible sensors-based microfluidic principles are gaining momentum and plethora of research is going on to find novel ways of detecting analyte of interest, this

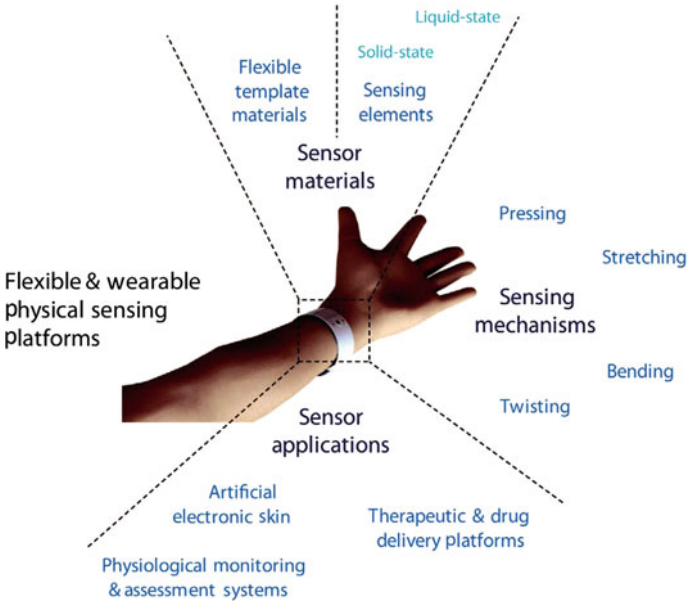

Fig. 9 Shows the outline for flexible and wearable sensing platforms which is mostly suitable for healthcare and biomedical domain (Yeo and Lim 2016)

all has become possible because of the property of paper-based devices. They are cheap, easily fabricated and can be printed easily. They are hydrophilic, disposable and can be burned. Their stiffness can be increased by some modification. Following are the working principles explored so far on which flexible sensors work:

- Colorimetric detection
- Chemiluminescence
- Electrochemiluminescence
- Fluorescence
- Nanoparticles interaction-based sensing
- Electrochemical sensing.

Colorimetric Detection

This is the most simple and easy technique to detect the analyte. In order to use this technique for flexible sensor, the common procedure used may be as follows: hydrophilic channels are created on the paper substrate and the channels are separated by hydrophobic lines which helps the sample to flow in definite (hydrophilic channel) path. Detection zones are created at the end of the hydrophilic lines where the immobilized reagents (enzymes, dye and acid–base) are kept, and the sample after travelling through the channels react with the reagents and colour change takes place. The intensity of colour can inform about the concentration of analyte in

sample. Readouts can be made with the help of calibration chart. Glucose sensing can be performed on the basis of the following steps. Hydrophilic channels can be created by photolithography method on chromatography paper which were separated by hydrophobic lines, two detection zones can be created: one as circular (with glucose assay regent for glucose detection) and second rectangular (protein assay reagent for protein detection). The device is exposed to the sample and colour change takes place. The glucose assay may be based on the enzymatic oxidation of iodide to iodine. Herein, colour transformation from clear to brown is linked with the occurrence of glucose. The protein assay is based on the colour change of tetrabromophenol blue (TBPB) when ionization and binding to proteins take place; a confirmatory result in this case is indicated by a colour change from yellow to blue (Peele et al. 1977; Pugia et al. 1999).

Figure 10 shows the flexible sensor based on chromatography paper. It can be visualized from the figure that the detection is colorimetric. Herein, Fig. 10a shows that darker lines are cured photoresist, whereas the lighter areas are unexposed paper. Patterned paper is formed after absorbing Waterman red ink (5 mL) with the help of capillary action. The central channel absorbs the sample by capillary action and the pattern gives direction to the sample into three split test areas. Figure 10c shows the assay after spotting the reagents. The square region on the right in the figure is the protein test and the circular region which is on the left is the glucose test. The circular region on the top was used as a control well. On left side, negative control for glucose and on right side protein is shown by using an artificial urine solution (5 mL). Figure 10d depicts the positive assay for glucose on left side and protein on right side by using a solution that contained $\sim$550 mm glucose and 75 mm BSA in an artificial urine solution (5 mL). The control well was spotted with the potassium iodide solution, but not with the enzyme solution. A similar control containing the enzyme solution, but not the iodide, gave matching results. Figure 10e shows the glucose and protein detection assays by varying concentrations of glucose and BSA.

The result with different concentration and their corresponding colour intensity is shown in Fig. 10.

Chemiluminescence

Principle of chemiluminescence is to detect the emission of light which comes out during chemical reaction. When two reactants react with each other in the presence of catalyst one of the reactant gets oxidized and it decays to a lower energy level, which gives out light emission with some by product.

As an example, researchers developed microfluidic paper biosensor for simultaneous determination of glucose and uric acid based on chemiluminescence principle. In this device, both uric acid and glucose are detected simultaneously on the principle of chemiluminescence. The paper used for making device is Whatman chromatography paper. The device consists of 3 layer. The middle layer consists of sample injection area from where sample is injected by pipette, two bio active channels on which enzymes (glucose oxidase, red and urate oxidase, green) were immobilized are created, and last part is chemiluminescence detection area which

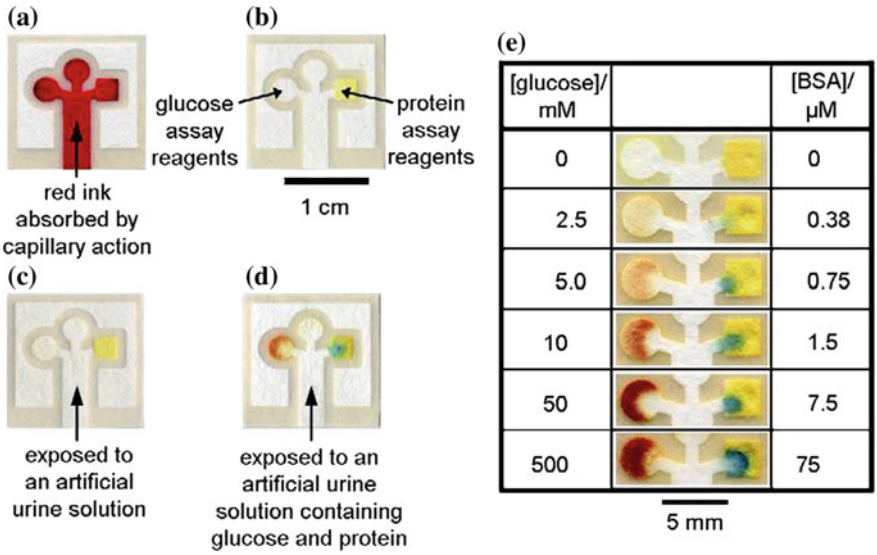

Fig. 10 Shows the flexible sensor based on chromatography paper. **a** Patterned paper after absorbing Waterman red ink (5 mL) by capillary action. **b** Complete assay after spotting the reagents. **c** Negative control for glucose (left) and protein (right) by using an artificial urine solution (5 mL). **d** Positive assay for glucose (left) and protein (right) by using a solution that contained 550 mm glucose and 75 mm BSA in an artificial urine solution (5 mL). **e** Glucose and protein detection assays by using varying concentrations of glucose and BSA. (Reprinted with kind permission from Martinez et al. 2007)

gets prepared by dipping the paper into the M4NRASP anhydrous alcohol solution for few minutes, and dried at normal temperature in air. The whole centre part is covered by water impermeable single-sided adhesive tape, on the up tape rectangular contour is made for sample injection. Now the sample with known concentration of uric acid and glucose is dropped on the sample injection area, and this sample is carried forward by the channels to detection area where the chemiluminescence signals are measured using a computerized ultra-weak luminescence analyzer.

Electrochemiluminescence

Limitation of existing colorimetric methods used in flexible sensors is that they have very low sensitivity and high detection limit. Because of which it becomes difficult to compete with the existing conventional analytical chip. In this case, electrochemiluminescence (ECL) may be the possible alternative to use. The working principle of electrochemiluminescence can be understood on the basis of the work performed by Yan et al. (2012). In this work, two papers A on which screen-printed carbon working electrode was developed and B on which screen-printed carbon counter electrode and Ag/AgCl reference electrode were developed for electrical connection as shown in Fig. 11. Firstly, for the incubation of the carcinoembryonic antigen (CEA), which is a biomarker for oesophagus

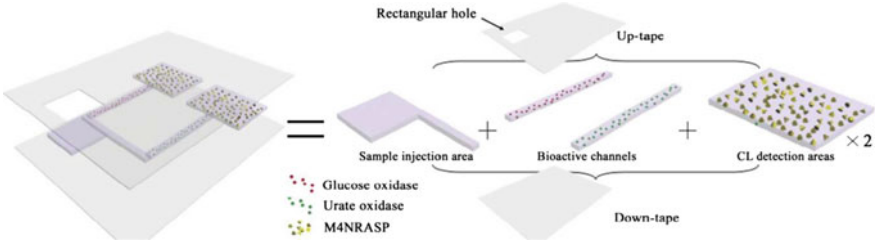

Fig. 11 Schematic representation of the microfluidic paper-based chemiluminescence analytical device (Yu et al. 2011)

cancer on the carbon working electrode, the CAE capturing antibody was made immobilized with the help of chitosan coating and glutaraldehyde (GA) cross linking. And then two antibodies formulate a sandwich complex with the antigen for its incubation (shown in Fig. 11d). After that the paper is kept into the device holder as shown in Fig. 11 and then tris-(bipyridine)–ruthenium [$Ru(bpy)_3^{2+}$]–tri-n-propylamine (TPA) is provided on to the surface and then voltage is applied to bring out ECL reaction. The TPA radical acts as a reducing agent which enables ruthenium to return to its lower energy level that emits photon packet. This cycle continues as long as the voltage is applied. And the emitted light is detected by the instrument. Intensity of light detected is proportional to the target analyte (Yan et al. 2012).

Figure 12 shows the schematic representation of the paper-based ECL device. In this work, first, the paper sheets were patterned by using a wax printer. Then, the electrodes were screen printed onto two sheets, i.e., A and B. At last, sheet-A and sheet-B from bulk were cut to paper-A and paper-B, respectively, with the same size (15.0–25.0 mm).

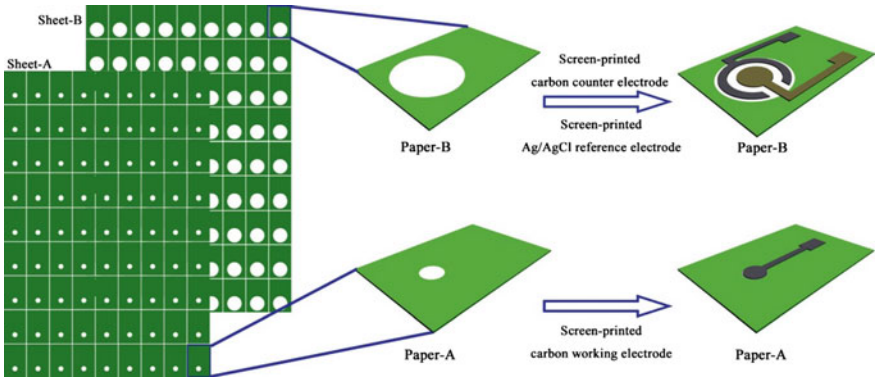

Fig. 12 Shows the schematic representation of the fabrication of the paper-based ECL 3D device. (Reproduced with permission from Yan et al. 2012)

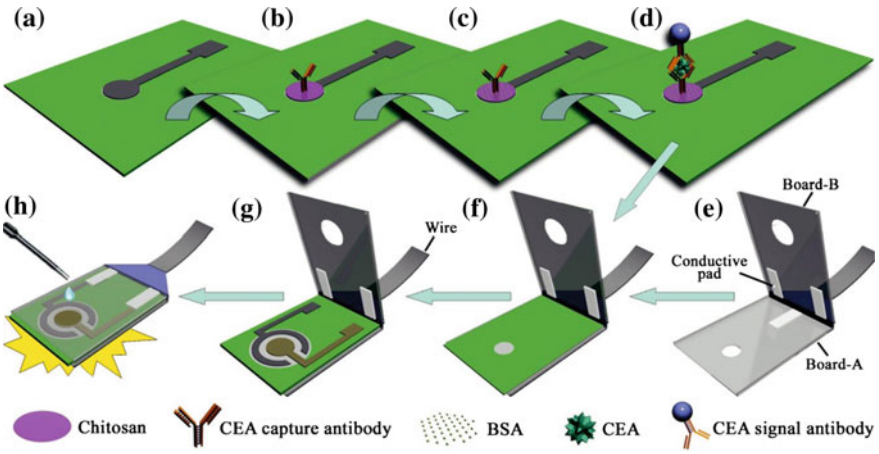

Fig. 13 Shows the schematic representation of the fabrication procedure for the paper-based ECL 3D immunodevice. **a** SPWPE; **b** after modification with chitosan and CEA capture antibody; **c** after blocking and washing; **d** after capture, incubation with signal antibodies, and washing; **e** the facile device-holder; **f** paper-A was placed face down onto board-A; **g** paper-B was placed face up onto paper-A; **h** after clamping the device holder. (Reproduced with permission from Yan et al. 2012)

In the similar work, paper-based electrochemiluminescence (ECL) 3D immunodevice was fabricated. Figure 13 shows the schematic representation of the fabrication and assay procedure for the paper-based ECL 3D immunodevice. Figure 13a shows the screen-printed working paper electrode (SPWPE), Fig. 13b shows the status after modification with chitosan and CEA capture antibody, whereas Fig. 13c shows the image after blocking and washing, Fig. 13d shows condition after capturing and incubating with signal antibodies and washing. Figure 13e shows the facile device-holder, whereas Fig. 13f depicts that paper-A was placed face down onto board-A and Fig. 13g is showing that paper-B was placed face up onto paper-A; Fig. 13h shows status after clamping the device holder, TPA was added to trigger the ECL reaction.

Fluorescence

Fluorescence phenomenon can be understood on the basis of Jablonski diagram as depicted below in Fig. 14. Franck-Condon principle states that absorption process happens so rapidly that there remains negligible time for the movement of molecules during the absorption process. Absorption occurs in the time span it takes a photon to travel the length of a photon.

In an example, flexible sensor had been developed in which detection of DNA was reported using paper strips immobilized with synthetic DNA oligonucleotides, coupled with common biochemical techniques of DNA ligation, and DNA amplification. Illustration of the work is depicted in the Fig. 15 (Ali et al. 2009).

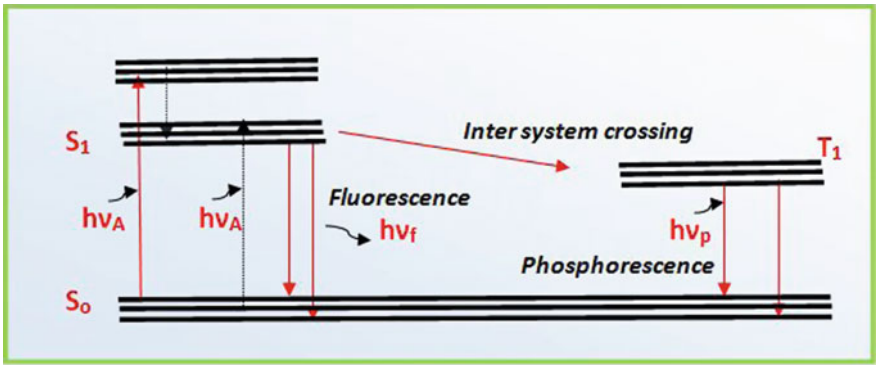

Fig. 14 Shows the Jablonski diagram to explain fluorescence mechanism (Lakowicz 1999)

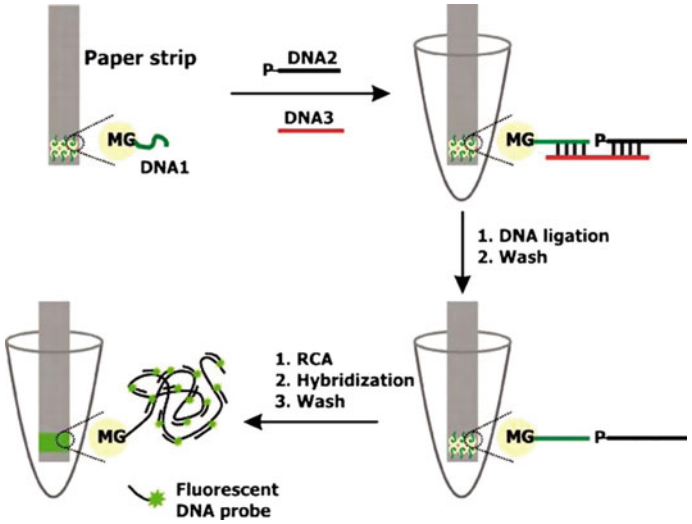

Fig. 15 Shows the DNA detection scheme on a paper strip via DNA ligation, RCA, and DNA hybridization. DNA3 is the intended DNA target. (MG stands for microgel) (Ali et al. 2009)

Nanoparticle-Based Sensing

Nanoparticles (NPs)-based detection has lots of advantage due to its size and large surface area for detection. They have been used in biosensing as they have good electrical, chemical, and physical properties. Some of the examples are metal nanoparticles of group II–VI present in the periodic table, compound semiconductors like CdSe, ZnSe, CdTe also called quantum dots (QDs) as well as gold nanoparticles (AuNPs), silver nanoparticles, etc. (Zhu et al. 2009). Any of the particles having at least one of its dimension lying within 100 nm range is known as nanoparticles. Depending on the dimensions, nanoparticles can be classified as

quantum dots, nanowires, nanotubes, etc. Out of all the nanostructures, QDs are extremely fluorescent and brighter in comparison with organic dyes such as rhodamine (Murphy 2002). These QDs are also stable against photobleaching. QDs are ~1–10 nm size particle of semiconductor like CdSe, ZnSe, CdTe, and can be used for fluorescence, photonics, and electrochemical application (Dickey et al. 2008; Guerfi et al. 2010; Chen et al. 2015).

The binding capabilities of the nanoparticles can be improved with the help of surface modification, doping, and by manufacturing the composites with the NPs. The NPs have also been used for increasing the conductivity of the sensing area where the NPs fill the gap of the metal electrode and hence increase the conductivity. It has been used for the strain sensing. When strain is applied on the electrode the spacing between the NPs increases and thus the conductivity decreases, this brings out relation between the strain and a resistance. Basic principle used in nanoparticle that they are used to bind the specific biomolecules on their surface which attracts the target analyte. The target analyte then react with the biomolecules which brings the changes. And then by obtaining that change in terms of electrical, optical, chemical, physical properties of the sensor, we can sense the analyte of interest. The selection of the nanoparticle for biosensing is based on the application, analyte to be detected, and the principle of detection used for sensing.

Electrochemical Sensing

These sensor works by reacting with the analyte of interest and producing an electrical output signal. This output signal is proportional to the concentration of the analyte present in the solution. These sensing devices consist of three electrodes namely: working electrode, counter electrode, and reference electrode. The working electrodes are made up of such material so that it catalyzed the reaction to the specific analyte which we want to sense. Reference electrode has great importance; it is used to maintain the stable and constant potential at the working electrode, which do not remain constant during constant electrochemical reaction. The analyte react at the working electrode and the current start flowing between the working electrode and the counter electrode which is proportional to the concentration of the analyte. By dropping the solution of known concentration of the analyte, we can obtain the connection between the current flow and the concentration of the analyte.

5 Flexible Sensor for Biomedical Applications

5.1 Solid-State Flexible Sensor

5.1.1 Flexible Enzymatic Glucose Biosensor Based on ZnO Nanowires Supported on a Gold-Coated Polyester Substrate

ZnO being a wide band gap semiconducting material provides excellent properties with a high isoelectric point (of 9.5). This property assists in the easier

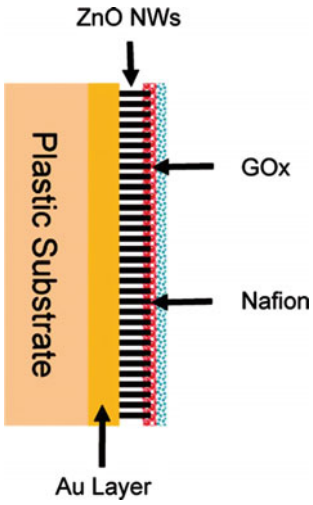

Fig. 16 Shows the schematic diagram of flexible biosensor made up of GO_x/ZnO-NWs/Au/PET bioelectrode which is used in the present study for glucose monitoring (Pradhan et al. 2010)

immobilization of an enzyme (with a low isoelectric point) through electrostatic interaction. Furthermore, its biocompatibility along with high electron transfer capability make ZnO a promising material for building an enzymatic sensor by immobilizing the suitable biological entities without any electron mediators. GO_x can be immobilized by making ZnO nanowires which has been used to act as a catalyst to promote the reaction in glucose which will give the amperometric response and will be proportional to the amount of glucose present in the blood. Nafion provides protection to the network and provides biocompatibility to the enzymes without interacting the sensor.

In a work based on flexible enzymatic glucose biosensor, GO_x/ZnO-NWs/Au/PET bioelectrode was used. Figure 16 shows the schematic of the mentioned flexible biosensor. The Au-coated PET substrate was deposited with ZnO nanowires (NWs) immobilized with glucose oxidase (GO_x) in a phosphate buffer saline solution mixed with Nafion (Pradhan et al. 2010).

5.1.2 Flexible Pressure Sensor with Gold Nanowires

In this work, flexible sensor has been made with the help of PDMS (as a flexible substrate) and Au nanowires coating over it. Schematic of this work is illustrated in Fig. 17. Sensing mechanism is based on the pressing action which was performed on the force-dependent contact between Au nanowires and interdigitated electrode arrays. Unlike a bulk rigid planar metal, soft tissue paper has porous and rough surfaces with hairy AuNWs. The number of AuNWs bridging finger electrode pairs depended on the external forces applied. On applying an external pressure, a small compressive deformation of tissue paper enabled more Au nanowires in contact with finger, i.e., interdigitated electrodes, leading to more conductive pathways

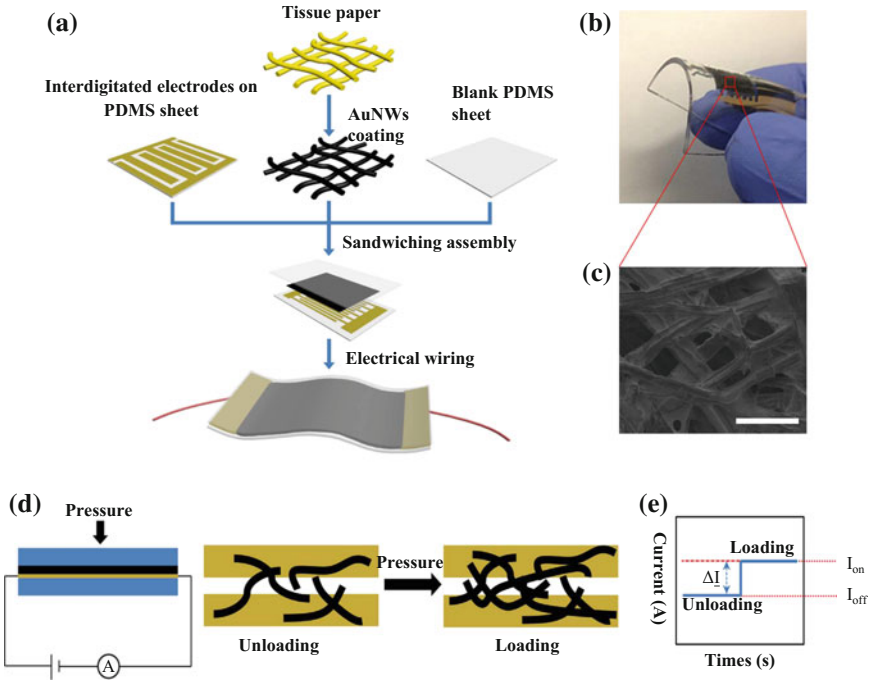

Fig. 17 **a** Shows schematic representation of a flexible sensor fabrication. **b** Shows the bendability of the sensor. **c** Scanning electron microscopy image of the morphology of gold nanowires-coated tissue fibres (scale bar: 100 mm). **d** Schematic illustration of the sensing mechanism. **e** Current changes in responses to loading and unloading (I_{off}: unloading, I_{on}: loading). (Reproduced with kind permission from Gong et al. 2014)

(Fig. 17d). This caused an increase in current when a fixed voltage of 1.5 V was applied as shown in Fig. 17e. On unloading, both PDMS and tissue paper recovered to their original shapes, reducing the amount of AuNWs bridging the finger electrode pairs, therefore, leading to the decrease of the current (Gong et al. 2014).

5.1.3 Flexible Glucose Sensor with Cu Nanowires Modified Graphene Transparent Electrode

Another flexible sensor was developed for glucose monitoring (Fan et al. 2013). In this work, Graphene has been utilized as an electrode. Graphene has high electrical conductivity, huge unit surface area, superior mechanical strength, chemical stability. And when it gets deposited on the polyethylene terephthalate (PET), the whole assembly exhibits good flexibility, transparency, and good conductivity.

Further Cu nanowires provide higher specific surface area, faster electron transfer along the unidirection, more superior catalytic ability, and better sensing responses in comparison to other explored nanoarchitectures. Additionally, it is

much convenient for fabricating in a scalable method. Therefore, copper nanowires are being adopted as optimal choice for possible application in non-enzymatic glucose sensor. The non-enzymatic glucose sensors are based on the current response of the glucose oxidation directly on the electrode surface which enhances their sensitivity (Liu et al. 2012). In general, electrochemical activities can be investigated with cycle voltametry.

5.1.4 Flexible Sensors Based on MnO_2 Nanowires on Graphene Paper

In order to realize a flexible substrate-based sensor, graphene oxide paper can be utilized and coated with manganese oxide (MnO_2). This nanohybrid film can be obtained with the help of single step electrochemical reduction of graphene oxide (GO) paper and electrodeposition of MnO_2 nanowires on electrochemical reduced GO (ERGO) paper. MnO_2-graphene nanocomposites will enhance the specific surface area, conductivity, and catalytic activity. MnO_2–ERGO paper demonstrates high electrocatalytic activity towards the redox of H_2O_2 as well as excellent stability, selectivity, and reproducibility. MnO_2–ERGO paper electrode is used for the real-time tracking H_2O_2 secretion by live cells macrophages. When H_2O_2 is injected onto electrode at an applied voltage of −0.5 V, the electrochemical performance is enhanced towards the non-enzymatic H_2O_2 detection. The sensing is based on electrochemical sensing here the MnO_2 nanowire will act as catalyst which will trigger the reaction in the presence of specific analyte H_2O_2. The reduction H_2O_2 will release the electron and hence the current will start flowing proportional to the analyte taking part in the reaction (Dong et al. 2015) (Fig. 18).

5.1.5 Wearable Strain Sensors

In one of the works related to the flexible sensor development for biomedical applications, wearable strain sensor has also been explored. In this work, silver nanoparticles and carbon nanotubes composite are used for strain sensing of skin. These sensors can be attached to the skin for the non-invasive sensing. The CNT is used because it increases the surface area of sensing, chemically, mechanically stable, and compatible with flexible substrate like PDMS and PI. Silver nanoparticles are used as it increases the conductivity and sensitivity more, relatively to other like gold, copper nanoparticles. When the strain is applied on the sensor the distance between the nanoparticles increases, with that the path to travel for the electron increases and the conductance decreases. So we can have the relation between the applied strain and the resistance change. The sensitivity of the sensor can be calculated by estimating the ratio of change in resistance between the initial and final resistance to the initial resistance. This sensitivity can further be tuned by changing the concentration of the Ag nanoparticles in CNT (Jeon and Ha 2016). Measurement circuit using a straightforward switching method was used to characterize the e-bandage as a human-interactive sensor. The input voltage from the

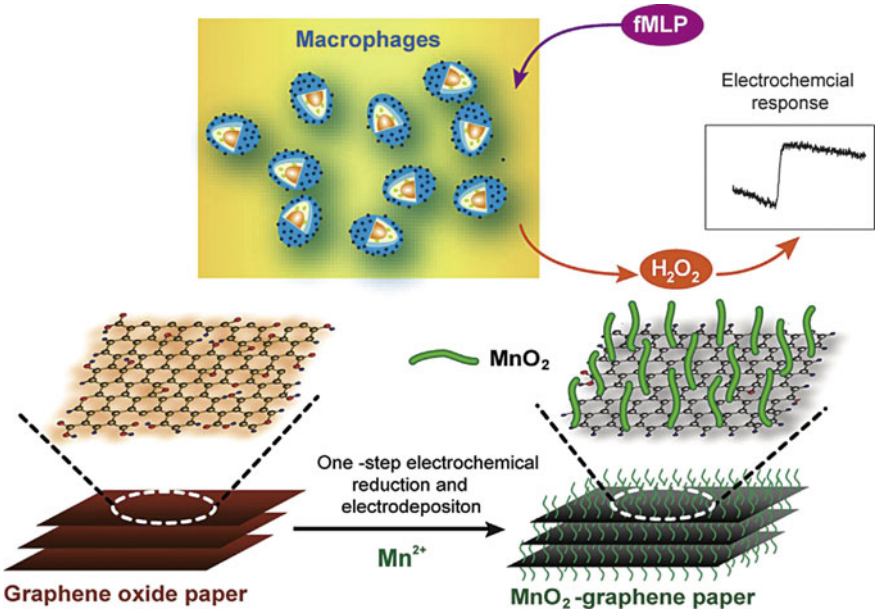

Fig. 18 Illustrates flexible sensor made up of the MnO_2–ERGO paper electrode for the non-enzymatic sensing of hydrogen peroxide released by live cells. (Reproduced with kind permission from Dong et al. 2015)

power supply was applied to the e-bandage connected to the simple circuit consisting of the resistance and the capacitor which were modulated by the change in resistor of the e-bandage at the attached position. When the strain was applied (the finger was bent), the resistance in the e-bandage increased and the output voltage was connected to the ground. When the strain was released, the resistance in the e-bandage decreased and the output voltage was connected to the input voltage. By using DAQ board, the output voltage was in real-time displayed on a screen. A strain profile for the sensitivity as a function of the bending angle provides additional information to consider the design periphery of sensitivity with the real degree of strain (Figs. 19 and 20).

5.2 Liquid-State-Based Sensor

In order to resolve issues of certain limitations with rigid materials (such as silicon, copper) utilized in conventional electronics, there is immense scope of "liquid metals" as a future replacement in flexible sensors. Low melting temperature alloys mostly contain Ga, In, Zn, or Sn. Ga is as commonly used as Li, Pb, and As, Hg, W, and Bi. However, the price of Ga remains high because it has to be extracted from

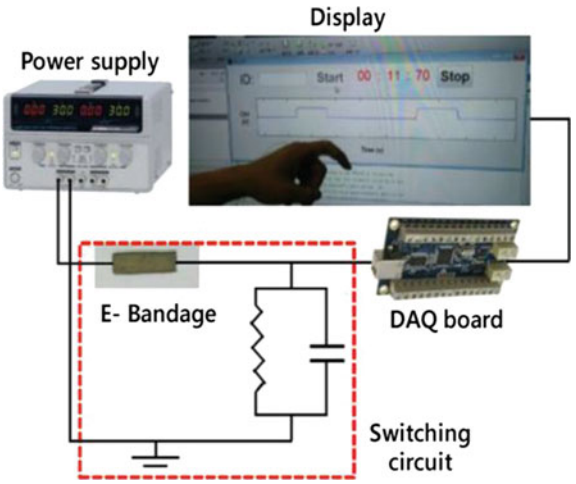

Fig. 19 Shows the illustration of the measurement circuit using a simple switching method to characterize the e-bandage as a human-interactive sensor, and the operation of the e-bandage for wearable motion sensors. (Reproduced with kind permission from Jeon and Ha 2016)

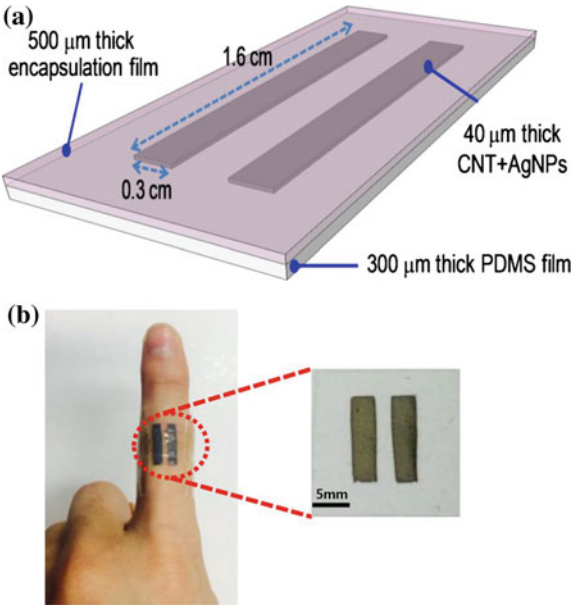

Fig. 20 **a** Device architecture of the e-bandage for wearable strain sensors by employing a sandwich structure and **b** The optical image of the e-bandage directly attached to human skin. (Reproduced with kind permission from Jeon and Ha 2016)

Al with low production rates (~ 80 tons per year). Pure Ga was not preferred as sole material to be used in flexible sensors because it is a solid at room temperature (30 °C melting point). Both eGaIn and Ga have low bulk viscosities (which is nearly two times than that of water) and high electrical conductivities (3.4×10^4 S cm^{-1}). Ga is used primarily in semiconductors (e.g., GaAs), special lubricants, mirrors, and thermometers and also as a substrate to grow nanostructures. So, the ability to shape

the liquid metal holds enormous promise in various applications including various kinds of sensors, microfluidics, flexible electronics.

5.2.1 Soft Strain Sensor Based on Ionic and Metal Liquids

There are few sensors which have been developed based on the liquid-state substrate. Eutectic gallium indium is one of the kinds of liquid-state substrate. The metallic alloy of eutectic gallium indium eGaIn has a high conductivity, similar to copper (Lakowicz 1999). It is also a non-toxic alternative to mercury. Several studies have shown that the electrically conductive, low viscosity liquid metallic alloy eGaIn can be put as electrodes and utilized for pressure sensing and can robustly withstand a high degree of strain. In a particular work, the ionic liquid of NaCl in glycerol solution, which has higher resistivity, was used as the active sensing element in the strain-sensitive part of the sensor. The metallic liquid eGaIn, with lower resistivity, meanwhile, served as the soft wires routing the electrical signal to external electrical circuits. With this arrangement, the soft sensor was highly specific and sensitive only to the prosthetic hand-induced strains while remaining largely insensitive to strains generated elsewhere.

In work illustrated in Fig. 21, due to the unstructured nature of the environment in which a prosthetic hand will be used, it is obvious that soft wires located on the back of the hand will be subjected to occasional stresses such as contact with an object. Therefore, in order to make the whole glove sensitive only to strain applied at the desired measurement area, channels filled with ionic liquid are used as sensing elements while eGaIn channels are dedicated to routing the electrical signal as soft wires to a flexible printed circuit board (PCB) located at the wrist.

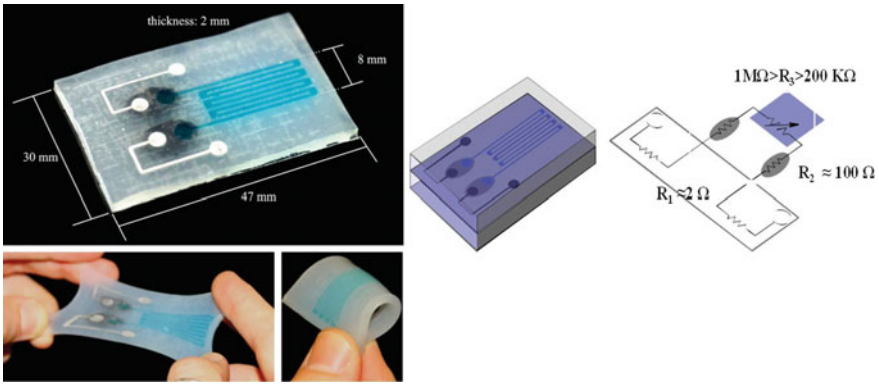

Fig. 21 Shows the image of the hybrid soft strain sensor prototype. Right side image shows the schematic of the sensor and its equivalent electrical circuit. R_1, R_2, and R_3, respectively, being the eutectic gallium indium (eGaIn) resistance, the silicon-doped interfaces resistance, the ionic solution resistance (Chossat et al. 2013)

5.2.2 Iontronic Microdroplet Array for Flexible Tactile Sensing

Three types of ionic fluids have been considered, such as aqueous electrolytes (e.g., NaCl electrolyte solution), organic solvent solutions (e.g. $KClO_4$–PEO), and ionic liquids, which are generally investigated in electrochemical processes. The droplet sensing fluid has to satisfy several design criteria, including high conductivity (providing ultrahigh EDL capacitance and low electrical loss), low viscosity (ensuring short response time), electrochemical stability (no electrochemical reaction under the operating voltage) and environmental stability (maintaining the physical properties over the operating period) (Guerfi et al. 2010).

Aqueous and solvent-based electrolytes are typically highly evaporative under ambient conditions and it becomes really challenging to maintain constant electrical performance, as both the volume and the physical properties change over time (Chen et al. 2015). As an emerging alternative, ionic liquids, consisting of an organic anion or cation, demonstrate high electrical conductivity, low volatility, and tunable viscosity (Fernicola et al. 2006; Zhang et al. 2009). In addition to their wide electrochemical window, ionic liquids are ideal candidates for microdroplet sensors. For manufacturing ionic liquid-based flexible sensor, one idea may be to sandwich nanolitre droplets between two polymeric membranes with patterned transparent electrodes which would formulate electrical double layers with remarkable unit area capacitance. Under external loading, the membrane deformation may result in the circumferential expansion at the highly elastic droplet–electrode contact, which certainly will offer an entirely new capacitive sensing scheme with a remarkable increase in sensitivity. Generally, the direct ionic droplet–electrode contact immediately establishes the electric double layer (EDL), which possesses a remarkable interfacial capacitance (of the order of 10 $\mu F\ cm^{-2}$). Under external loads, the flexible surfaces experience mechanical deformations, resulting in circumferential expansion of the droplet–electrode contact. The corresponding capacitive change over the improved contact area can be detected electronically. This new EDL sensing mechanism is the latest addition to the conventional capacitive sensing principle, principally configured in parallel plates or interdigitated comb drives (Kim et al. 2011).

The measurable capacitive change (ΔC) can be related to the contact pressure applied (ΔP). Relation between them can be derived from the interfacial capacitive sensing principle

$$\Delta C \approx C_0 \times \left[\frac{\Delta P}{K} + \left(\frac{\Delta P}{K}\right)^2\right]$$

where C_0 denotes initial capacitance, $K = 5ET^3h/(1 - \upsilon^2)a^4$ is a constant derived from the design parameters, including the width (a) and height (h) of each sensing cell, and the membrane properties, including Young's modulus E, thickness T, and Poisson ratio υ. The gravitational effect has been neglected in our consideration, as the microdroplet dimensions are considerably less than the capillary length (of $\sim$1.8 mm) (De Gennes et al. 2013).

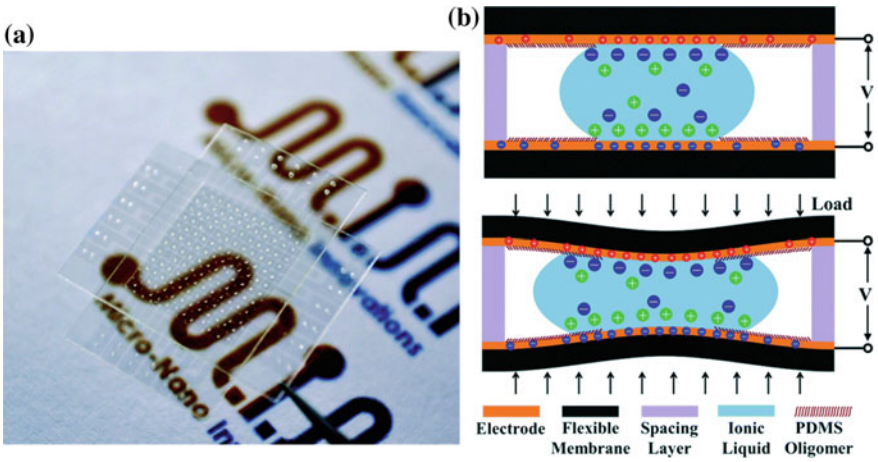

Fig. 22 Shows the image and sensing principle of the iontronic microdroplet sensing device. **a** A photograph of an IMA sensor array indicating the high level of transparency. **b** A cross-sectional sketch of the interfacial capacitive sensing principle. (Reproduced with kind permission from Zhao et al. 2007)

Figure 22 depicts sensing principle of the iontronic microdroplet sensing device. Iontronic microdroplet sensor array of 12 × 12 elements is made with a spatial resolution of 1 mm. The EDL capacitance is simultaneously established at the ionic droplet–electrode contact (top). The interfacial contact area expands circumferentially, which is caused by the mechanical deformation of the membrane under external loads and results in an increase in the EDL capacitance (bottom) (Zhao et al. 2007).

6 Challenges and Future Scope

Major challenges in the field of flexible sensor specially utilized in biomedical application can be defined and categorized into several domains such as its design, fabrication, biocompatibility, integration of device, and its cost. Apart from considering these basic factors, several other aspects, namely sensitivity of the sensor, its selectivity towards a target analyte, its response time, stability, reproducibility of the result, needs to be considered at the initial stage of the development of the sensor. Challenge here is to select right sensing element, substrate, dimensions of the sensors. Many a times the required goals are achieved by performing experiments, which consumes much of the time. While designing a sensor, its fabrication should also be considered we should see whether its fabrication is possible or not. Miniaturization has brought a lot of challenges in the sensor development. In today's modern world, the manufacturing technology has evolved and is able to

manufacture miniature structures. As we go smaller and smaller the accuracy of the sensor or we can say the resolution of the sensor will increase which is the need of modern sensor. The advancement in the fabrication process to fabricate in nano/microscale with precession is highly required. Further, integration of the device is a challenging task. Integration of different sensing devices and processing units to a single device becomes very important as it requires sophisticated fabrication technique and high precession work. With this, it also requires the integration of the device with data processing and wired or wireless transmission system. Biocompatibility is one the important issues in the fabrication of flexible sensors for biomedical applications. A sensor which is interacting with the body should be biocompatible, if it is not then it will become injurious to health as the antibodies will become active and the particular area will be adversely affected so it is very important to use only biocompatible material.

Most of the biomedical sensors are made for in situ sensing which will reduce degradation of analyte and to make them available in remote locations where to avail modern technology and well equipped laboratory facilities is difficult. It should be inexpensive and can be used without any help from expert. For that paper as a substrate has been used. Researchers are exploring new materials for sensing which has low cost and high sensitivity. Sometimes to make sensing device more efficient it should sense multiple stimuli. Such as if we want to mimic electronic skin it should integrate temperature, humidity, tactile sensing, etc. Flexible sensing devices should not get affected by the surrounding environment variations. Many a times the properties of the sensor got affected by the environmental changes like temperature and humidity variation. Sensitivity should be towards specific point of interest and do not get influenced by deformation and other environmental changes. So, in nut shell, challenge is to make flexible sensor inexpensive, accurate, and reliable at the same time.

References

Ali MM, Aguirre SD, Xu Y, Filipe CD, Pelton R, Li Y (2009) Detection of DNA using bioactive paper strips. Chem Commun 43:6640–6642

Bu N, Ueno N, Fukuda O (2007) Monitoring of respiration and heartbeat during sleep using a flexible piezoelectric film sensor and empirical mode decomposition. In: Engineering in Medicine and Biology Society, 2007. EMBS 2007. 29th annual international conference of the IEEE 22 Aug 2007, pp 1362–1366. IEEE

Chen Y, Lu B, Chen Y, Feng X (2015) Breathable and stretchable temperature sensors inspired by skin. Scientific reports, p 5

Choi MC, Kim Y, Ha CS (2008) Polymers for flexible displays: from material selection to device applications. Prog Polym Sci 33(6):581–630

Chossat JB, Park YL, Wood RJ, Duchaine V (2013) A soft strain sensor based on ionic and metal liquids. IEEE Sens J 13(9):3405–3414

Courbat J, Briand D, Wöllenstein J, De Rooij NF (2011) Polymeric foil optical waveguide with inkjet printed gas sensitive film for colorimetric sensing. Sens Actuators B: Chem 160(1): 910–915

De Gennes PG, Brochard-Wyart F, Quéré D (2013) Capillarity and wetting phenomena: drops, bubbles, pearls, waves. Springer Science & Business Media, Berlin, 20 Mar 2013
Dhand C, Das M, Datta M, Malhotra BD (2011) Recent advances in polyaniline based biosensors. Biosens Bioelectron 26(6):2811–2821
Dickey MD, Chiechi RC, Larsen RJ, Weiss EA, Weitz DA, Whitesides GM (2008) Eutectic gallium-indium (EGaIn): a liquid metal alloy for the formation of stable structures in microchannels at room temperature. Adv Func Mater 18(7):1097–1104
Dong S, Xi J, Wu Y, Liu H, Fu C, Liu H, Xiao F (2015) High loading MnO 2 nanowires on graphene paper: facile electrochemical synthesis and use as flexible electrode for tracking hydrogen peroxide secretion in live cells. Anal Chim Acta 1(853):200–206
Fan Z, Liu B, Liu X, Li Z, Wang H, Yang S, Wang J (2013) A flexible and disposable hybrid electrode based on Cu nanowires modified graphene transparent electrode for non-enzymatic glucose sensor. Electrochim Acta 30(109):602–608
Fernicola A, Scrosati B, Ohno H (2006) Potentialities of ionic liquids as new electrolyte media in advanced electrochemical devices. Ionics 12(2):95–102
Gong S, Schwalb W, Wang Y, Chen Y, Tang Y, Si J, Shirinzadeh B, Cheng W (2014) A wearable and highly sensitive pressure sensor with ultrathin gold nanowires. Nat commun 4:5
Guerfi A, Dontigny M, Charest P, Petitclerc M, Lagacé M, Vijh A, Zaghib K (2010) Improved electrolytes for Li-ion batteries: mixtures of ionic liquid and organic electrolyte with enhanced safety and electrochemical performance. J Power Sources 195(3):845–852
Hsu HH, Chang CY, Cheng CH, Yu SH, Su CY, Su CY (2013) Fully room-temperature IGZO thin film transistors adopting stacked gate dielectrics on flexible polycarbonate substrate. Solid-State Electron 30(89):194–197
Hwang GT, Byun M, Jeong CK, Lee KJ (2015) Flexible piezoelectric thin-film energy harvesters and nanosensors for biomedical applications. Adv Healthcare Mat 4(5):646–658
Islam T, Mahboob MR, Khan SA (2015) A simple MOX vapor sensor on polyimide substrate for measuring humidity in ppm level. IEEE Sens J 15(5):3004–3013
Jeon JY, Ha TJ (2016) Waterproof electronic-bandage with tunable sensitivity for wearable strain sensors. ACS Appl Mater Interfaces 8(4):2866–2871
Kaempgen M, Roth S (2006) Transparent and flexible carbon nanotube/polyaniline pH sensors. J Electroanal Chem 586(1):72–76
Kim HK, Lee S, Yun KS (2011) Capacitive tactile sensor array for touch screen application. Sens Actuators, A 165(1):2–7
Kitova S, Minchev M, Danev G (2005) RF plasma treatment of polycarbonate substrates. J Optoelectron Adv Mat 7(5):2607–2612
Lakowicz JR (1999) Principles of fluorescence spectroscopy, 2nd ed, pp 1–23. Springer, Berlin
Lechat C, Bunsell AR, Davies P, Piant A (2006) Mechanical behaviour of polyethylene terephthalate & polyethylene naphthalate fibres under cyclic loading. J Mat Sci 41(6): 1745–1756
Lemaire E, Moser R, Borsa CJ, Shea H, Briand D (2015) Green paper-based piezoelectric material for sensors and actuators. Procedia Eng 1(120):360–363
Li C et al (2008) Flexible dome and bump shape piezoelectric tactile sensors using PVDF-TrFE copolymer. J Microelectromech Syst 17(2):334–341
Li R, Nie B, Digiglio P, Pan T (2014) Microflotronics: a flexible, transparent pressure-sensitive microfluidic film. Adv Funct Mat 24(39):6195–6203
Lipomi DJ, Vosgueritchian M, Tee BC, Hellstrom SL, Lee JA, Fox CH, Bao Z (2011) Skin-like pressure and strain sensors based on transparent elastic films of carbon nanotubes. Nat Nanotechnol 6(12):788–792
Liu G, Zheng B, Jiang Y, Cai Y, Du J, Yuan H, Xiao D (2012) Improvement of sensitive CuO NFs–ITO nonenzymatic glucose sensor based on in situ electrospun fiber. Talanta 15(101): 24–31
Martinez AW, Phillips ST, Butte MJ, Whitesides GM (2007) Patterned paper as a platform for inexpensive, low-volume, portable bioassays. Angew Chem Int Ed 46(8):1318–1320
Murphy CJ (2002) Peer reviewed: optical sensing with quantum dots, pp 520-A

Nie B, Li R, Brandt JD, Pan T (2014) Iontronic microdroplet array for flexible ultrasensitive tactile sensing. Lab Chip 14(6):1107–1116
Peele JD, Gadsden RH, Crews R (1977) Semi-automated vs. visual reading of urinalysis dipsticks. Clin Chem 23(12):2242–2246
Pradhan D, Niroui F, Leung KT (2010) High-performance, flexible enzymatic glucose biosensor based on ZnO nanowires supported on a gold-coated polyester substrate. ACS Appl Mater Interfaces 2(8):2409–2412
Pugia MJ, Lott JA, Profitt JA, Cast TK (1999) High-sensitivity dye binding assay for albumin in urine. J Clin Lab Anal 13(4):180–187
Ren TL, Tian H, Xie D, Yang Y (2012) Flexible graphite-on-paper piezoresistive sensors. Sensors 12(5):6685–6694
Trung TQ, Tien NT, Kim D, Jang M, Yoon OJ, Lee NE (2014) A flexible reduced graphene oxide field-effect transistor for ultrasensitive strain sensing. Adv Func Mater 24(1):117–124
Wang L, Luo J, Yin J, Zhang H, Wu J, Shi X, Crew E, Xu Z, Rendeng Q, Lu S, Poliks M (2010) Flexible chemiresistor sensors: thin film assemblies of nanoparticles on a polyethylene terephthalate substrate. J Mater Chem 20(5):907–915
Wright WW, Hallden-Abberton M (2002) "Polyimides" in Ullmann's encyclopedia of industrial chemistry. Wiley, Weinheim. doi:https://doi.org/10.1002/14356007.a21_253
Wu WY, Zhong X, Wang W, Miao Q, Zhu JJ (2010) Flexible PDMS-based three-electrode sensor. Electrochem Commun 12(11):1600–1604
Yan J, Ge L, Song X, Yan M, Ge S, Yu J (2012) Paper-based electrochemiluminescent 3D immunodevice for lab-on-paper, specific, and sensitive point-of-care testing. Chem-A Eur J 18 (16):4938–4945
Yang Y, Zhang H, Lin ZH, Zhou YS, Jing Q, Su Y, Yang J, Chen J, Hu C, Wang ZL (2013) Human skin based triboelectric nanogenerators for harvesting biomechanical energy and as self-powered active tactile sensor system. ACS Nano 7(10):9213–9222
Yang PK, Lin ZH, Pradel KC, Lin L, Li X, Wen X, He JH, Wang ZL (2015) Paper-based origami triboelectric nanogenerators and self-powered pressure sensors. ACS Nano 9(1):901–907
Yeo JC, Lim CT (2016) Emerging flexible and wearable physical sensing platforms for healthcare and biomedical applications. Microsyst Nanoeng 26(2):16043
Yu J, Ge L, Huang J, Wang S, Ge S (2011) Microfluidic paper-based chemiluminescence biosensor for simultaneous determination of glucose and uric acid. Lab Chip 11(7):1286–1291
Zhang S, Lu X, Zhou Q, Li X, Zhang X, Li S (2009) Ionic liquids: physicochemical properties. Elsevier, Netherlands, 13 Jun 2009
Zhao W, Chiuman W, Brook MA, Li Y (2007) Simple and rapid colorimetric biosensors based on DNA aptamer and noncrosslinking gold nanoparticle aggregation. ChemBioChem 8(7): 727–731
Zhu S, Du C, Fu Y (2009) Fabrication and characterization of rhombic silver nanoparticles for biosensing. Opt Mater 31(6):769–774

Chapter 14
Low-cost Paper Analytical Devices for Environmental and Biomedical Sensing Applications

H. Manisha, P. D. Priya Shwetha and K. S. Prasad

Abstract Over the last decade, the fabrication of analytical devices utilizing microfluidic structures and lab-on-a-chip platforms has shown breakthrough advancements, both for environmental and biological applications. The ASSURED criteria (affordable, sensitive, specific, user-friendly, robust, equipment-free, delivered), developed by the WHO for diagnostics devices, point towards the need of paper-based analytical devices (PAD) for diagnostics. On the other hand, cost-effective PADs owing the great advantage of affordable applicability in both resource-rich and -limited settings are recently employed for on-site environmental monitoring. In this book chapter, we will discuss about the brief history of paper analytical devices, fabrications, need, and its environmental and biomedical applications.

Keywords Paper analytical device · Point-of-care · Biomarkers
Pesticides · Organic pollutants · Sensing

1 Paper Analytical Devices

Microfluidic devices provide innovative solutions to logistical problems, affording the advantages of high sensitivity, low cost, low reagent usage, small size, and several established fabrication techniques (Sackmann et al. 2014). Plethora of these devices has been used as a lab-on-chip type sensor for many biologically important molecules (Cate et al. 2014; Tomazelli Coltro et al. 2014). Among the developed microfluidic devices, PADs have tremendous amount of research attention due to their simplicity, capillary-based pumping ability, and low cost and easiness in

H. Manisha and P. D. Priya Shwetha: Equal contribution by these two authors.

H. Manisha · P. D. Priya Shwetha · K. S. Prasad (✉)
Nanomaterials Research Laboratory (NMRL), Nano Division—Yenepoya Research Centre, Yenepoya University, Deralakatte, Mangalore 575018, India
e-mail: ksprasadnair@yenepoya.edu.in

S. Bhattacharya et al. (eds.), *Environmental, Chemical and Medical Sensors*, Energy, Environment, and Sustainability, https://doi.org/10.1007/978-981-10-7751-7_14

availability to resource-limited settings (Yetisen et al. 2013; Pelton 2009; Hu et al. 2014; Martinez et al. 2009). On the other hand, the capability of filtering the samples to remove the particles and aggregates, helpful surface chemistry for easy modification, biocompatible nature and ability for a safe disposal by incineration makes the PAD as the holy grail in POC diagnostic devices (Cate et al. 2014; Pelton 2009). The PADs are usually incorporated with suitable transduction methods like optical and electrochemical techniques for quantitative analysis. Mostly, the PADs for diagnostics purpose utilize colorimetric, electrochemical, chemiluminescence, electrochemiluminescence, electrical conductivity, and surface enhanced Raman spectroscopy techniques (Cate et al. 2014; Yetisen et al. 2013). Among these, visual identification of the results through naked-eye colorimetric determination is promising, while considering the resource-limited set-up as it does not require a sophisticated instrument or a skilled person. Perhaps the requirement of a higher analyte concentration, and only the yes or no results, makes the colorimetric system unsuitable for ultrasensitive detection. To overcome such limitation and bottlenecks, much sensitive electrochemical detection and signal amplifications strategies are useful (Taton et al. 2000). Müller and Clegg (1949) used an embossing tool to form patterns of hydrophobic and hydrophilic domains on a piece of paper in 1949 to develop two-dimensional PADs. Nevertheless, paper-based devices got much attention after the advent of George Whiteside's group at Harvard, on construction of microfluidic paper-based device for chemical analysis in 2007 (Martinez et al. 2007). A patterned paper platform by employing photolithography technique has been used to develop colorimetric sensor for glucose and protein in urine. After the introduction, there has been a surge in the paper-based diagnostics research. Paper-based indirect ELISA also has been developed (Cheng et al. 2010).

2 Fabrication of Paper Analytical Device

For developing paper-based devices, various types of papers are used and they can be nitrocellulose, cellulose paper, etc. The selection of the paper for fabricating the devices depends upon the procedure and the field of application of the particular fabricated platform (Fig. 1).

Even though different grades of paper exist, very few have been used for the fabrication of microfluidic PADs. Whatman brand filter and chromatography papers, in particular, have developed "gold standard" status in the field. A recent evaluation by Charls Mace group had noted that Whatman grade 1 has been used in most of the PADs. However, it should be noted that interestingly some of them did not identify the exact type of the paper used for PADs (Fernandes et al. 2017). In various fields of application, cellulose paper has been used by the researchers since it is easily available, capillary movement of the liquids through it, and the hydrophilic properties (Apilux et al. 2010). Since the paper substrates are highly porous in nature, electrodes can also be developed by screen printing and can be used for the development of electrochemical sensors (Nie et al. 2010). Nitrocellulose paper,

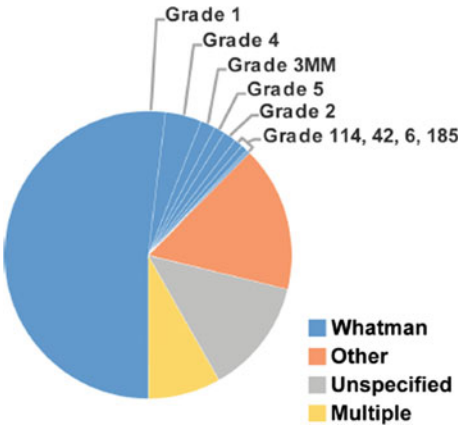

Fig. 1 Types and grades of paper used to fabricate paper analytical device (Fernandes et al. 2017)

which is hydrophobic in nature, can also be used as a paper substrate for the fabrication of PADs. It has a smooth surface and with a uniform pore sizes (0.45 μm) which makes it as a good substrate for stable liquid flow. Also these papers have the provision for immobilizing DNA, since they have huge non-specific binding affinity towards biological entities (Cretich et al. 2010). In addition, paper has been used as a substrate because of its white background which allows the colour changes to be detected by naked eyes, and also it allows the uniform distribution of the samples through the capillary action. In addition, after patterning paper could be used as a substrate for sample development, purification, product formation, and other reactions may also take place without any contamination issues. Different designing approaches are used for fabricating paper devices. Generally paper is treated with polymers or SU8 for developing designs or patterns, and stacking of reagents on the surfaces of paper substrate can be achieved by inkjet etching or printing, wax printing, screen printing, and flexography printing. Among others, the principle approaches used for incorporating chemical alteration of the paper surface is by plasma treatment and inkjet printing (Dou et al. 2015). All these designing approaches have their own merits and demerits, and the selection depends on the application. Figure 2 depicts the various fabrication methods involved with PADs by using handcrafted devices fabricated using (A) wax drawing, (B) polymer ink drawing or stamping, or (C) wax stamping. Masks were used to protect hydrophilic regions for (D) wax dipping, (E) photolithography, and (F) wax screen-printing. Fabrication techniques with ink addition printers used either (G) wax printing, (H) inkjet etching, (I) inkjet printing, or (J) flexographic printing. Cutting or shaping air boundaries or etching channels were performed by a (K) craft cutter or (L) laser cutter (Cate et al. 2014; Martinez et al. 2008).

Blocking of pores in paper substrates can be done by physical approaches, and photolithography technique has been used for designing a paper-based microfluidic gadget, which requires a copier machine or an inkjet printer, UV light, and a hotplate. Also, time taken to complete this action is less than 30 min (Martinez et al. 2008).

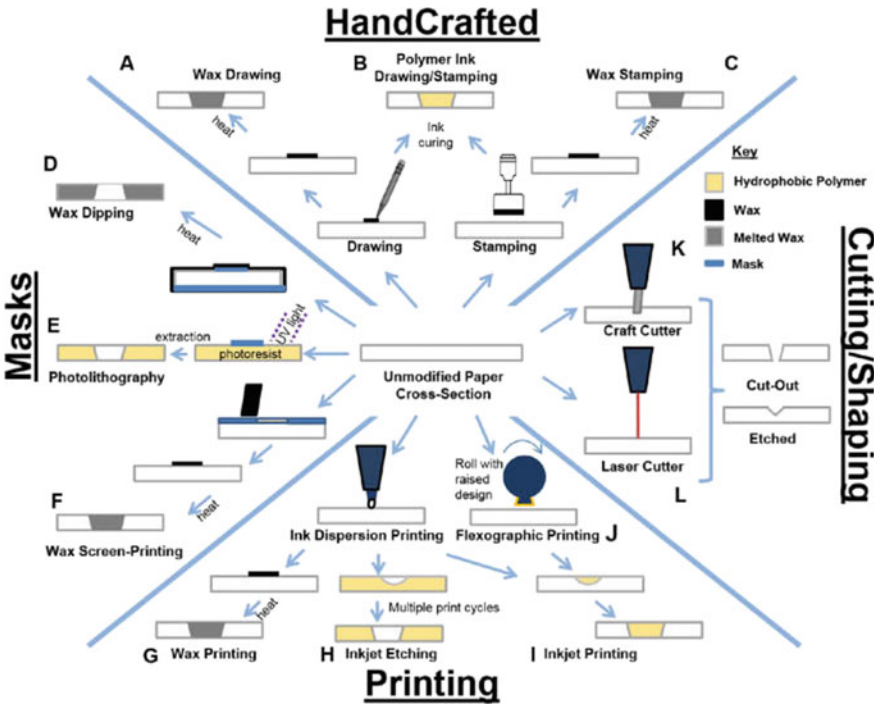

Fig. 2 Different ways of hydrophobic barrier fabrications (Cate et al. 2014)

Photolithography relies on UV exposure through a photomask of photoresist (SU-8 or PDMS)-saturated paper. The photolithography procedure requires natural and organic solvents during developing, and during the usage of these solvents there may be chances of harming the inherent properties of the paper substrate, hence making the manufactured paper devices less flexible and may end up in collapsing or bending. So when compared with the multistep photolithographic method, plotting or printing is a way to characterize hydrophobic designs on paper by printing the hydrophobic polymer. PDMS is ordinarily utilized as a part of the plotting procedure since it is affordable and less toxic. The use of PDMS was first examined by Bruzewicz et al. (2008) and used a plotter to print a hexane solution of PDMS on the filter paper as hydrophobic hindrances. The above said particular approach will not harm inherent properties or flexibility of the paper, but a time consuming approach will not allow a controllable penetration of PDMS. Nevertheless, cost of photoresist and the potential for background reactivity makes photolithography fabrication method less desirable.

Another method to create barriers in paper itself is wax printing method. When compared with the multistep photolithography technique, wax printing has many advantages like they are less complex, more affordable, and more adaptable for various changes. Whitesides' group proposed wax as another hydrophobic material

for fluidic obstructions or blocking the pores on the paper (Carrilho et al. 2009). It is also cost effective, easily available, non-harmful, easily degradable, water insoluble, and also flexible at ambient temperature. The procedure is also quick (5 min) and does not require any solvents. Parafilm was one of the earliest materials used to pattern paper for simple colorimetric metal spot tests using a heated metal stamp (Yagoda 1937). Though wax is convenient to use, it has some limitations, like the softened wax spreads easily in every direction by capillarity, which make the designs poorly characterized and also off colour in high resolution. But the spreading distance is consistent for a given heating time at a specific temperature (Lu et al. 2009). The use of vacuum could limit parallel spreading of the wax through the paper substrate. It should be noted that wax is water insoluble yet dissolvable in non-polar organic solvents; thus, PADs could disintegrate in organic solvents if it is fabricated by wax printing. Alternative barrier materials can provide a wider range of chemical compatibility. Jahanshahi-Anbuhi et al. (2015) used pullulan, a polysaccharide polymer, as a barrier to organic solvents in tandem with wax barriers to fabricate omniphobic devices. Variety of hydrophobic materials have been used in designing microfluidic PADs, with fluoropolymer (Chen et al. 2013) and octadecyltrichlorosilane (He et al. 2013). Barriers made from the aforementioned materials contain water and variety of organic solvents, so the worry of disintegrate in organic solvents is negligible. Microfluidic PADs developed using hydrophobic methylsilsesquioxane showed resistance to pH-induced hydrolysis and also was found to be compatible with cell lysis solutions used, which has been reported by Wang et al. (2014).

Screen printing is simpler and sufficient method for developing nations when compared with wax printing, due to the high cost occupied with wax printers and the accessibility. Screen printing system needs a mesh. Strong or solid wax can be traded within the mesh while it is squeezed. The wax used for printing purpose was dissolved and moulded into the paper surface to form hydrophobic hindrances or the barriers with the help of a hot plate. Wax screen-printing is a minimal cost, straightforward, and quick technique for creating paper-based microfluidic gadgets which is published by Dumgchai et al. (2011). In addition, with simplicity in mind, a single-method screen-printing strategy for designing hydrophobic polystyrene could be used to create barriers. The solution of polystyrene is applied on the screen, infiltrates through the paper, and hence forms a 3D hydrophobic hindrance or barrier, forming a hydrophilic detection zone (Sameenoi et al. 2014).

Flexographic printing is also another method that designs or patterns polystyrene barriers onto chromatographic paper, enabling roll-to-roll channel patterning. Polystyrene is important among the most prevalent hydrophobic agent utilized as a part of this system because of its biocompatibility and the advantage of having not the requirement of heat treatment. Polystyrene patterns are shaped on the surface of paper with polystyrene ink of strength 5%, which incompletely enters the paper of interest. On the rear end of the paper, uniform layer of polystyrene is applied, which serves as a waterproof layer to the whole paper used for fabrication purpose (Olkkonen et al. 2010).

Selective removal or modification of the hydrophobic material after deposition has also been investigated in processes such as inkjet etching and plasma treatment.

To turn the exposed area of hydrophobized paper made with alkyl/alkenyl ketene dimer to hydrophilic, plasma treatment has been used (Li et al. 2008, 2010). Salentijn et al. (2016) showed this as well as subsequent regeneration of hydrophilic behaviour in the paper after oxygen plasma treatment.

Other techniques like laser printing and paper cutting are the techniques used for developing hydrophobic regions on the paper substrates. Easier strategy to manufacture PADs is paper cutting and taping. Cutting approach is fast, requires only scissors, and may be also PC-based gear or laser cutter. Cutting is reasonable for shape formation during manufacturing and is also perfect with cellulosic substrates (Martinez et al. 2008). Craft cutter has been developed and used to form paper boundaries, then by overlaying the paper with films of thermoplastic by Fan group (Liu et al. 2013). Cutting/lamination approach has been used to develop laminated paper-based analytical devices (LPADs) and is fundamentally the same as developing any card proofs and also has important added advantages like non-tedious and also rough help. Transporter or carrier sheet is used as a conciliatory layer and also enables slicing to be done in a solitary stride or in a one-step approach without damaging the paper used for fabrication. This method does not make use of costly laser cutting equipment and also is widely adaptable compared to special craft punch. In the case of laser-based patterning, the hydrophobic barriers are established by the polymerization of the photopolymer. In addition, it is possible to cut a strip of paper using laser as indicated by pre-designed patterns. Laser direct writing (LDW) techniques have also been shown to form hydrophobic barriers by polymerizing photopolymer-impregnated filter paper, and this approach has been applied to fabricate time delay barriers. It is also possible to create delay barriers in filter paper by adjusting the write speed of a laser to control the barrier height, which resulted in the delayed flows of different solutions throughout the device (He et al. 2015). Creating or developing economical microfluidic designs on paper utilizing laser method was reported by Chitnis et al. Those papers developed using hydrophobic surface covering layers (e.g. wax, parchment, and palette) are utilized for creating cost-effective microfluidic patterns. The structure and the properties (hydrophobic to hydrophilic) of these papers used for fabricating devices were modified selectively by utilizing a laser which is of CO_2 (Chitnis et al. 2011). Owing to its advantages, the laser patterning is not so feasible considering the cost associated with it.

Stamps, to impress a particular pattern using hydrophobic ink, also are used to make hydrophobic barriers onto paper. However, it should be noted that stamping method could jeopardize the quality of PAD, since the possibility of spreading of hydrophilic ink (Carrilho et al. 2009). Stamp with geometry of hydrophobic PDMS barrier along with images of side-by-side comparison showing advantage of PDMS barriers with respect to wax is reported by Dornelas et al. (2015). By heating and applying pressure to transfer hydrophobic materials onto PAD could be done by employing embossing technique. Different hydrophobic materials could be used for embossing along with “ink paper”, otherwise by employing laser-induced forward transfer (Jiang and Fan 2016).

3 PADs for Environmental Analysis

Cheap and best, quick, versatile, selective, and specific gadgets are important for on-site environmental checking. For developing such gadgets, PADs are considered as suitable due to the following aspects: (a) it is amazingly cheap and commercially accessible; (b) fluids can be transported by capillary strengths, and along these lines it does not require outside force or an external pump; (c) it is easy to be designed; and (d) it comprises of permeable cellulosic fibre systems that make it bio-friendly. Biological elements (proteins, antibodies, bacteriophages, and aptamers) are the well-known recognition components widely used for the development of PAD-based biosensors, since it shows high selectivity towards target sample of interest. In this manner development of bioactive PADs found great degree of use as efficient and modest sensors.

Despite, most of the developments in PADs are focused more onto health care related diagnostics and are focused to reduce the cost, and to have more benefits to common man. Nowadays other fields such as environmental monitoring, explosives detection, and screening for food and beverage contamination are also found applications of PADs. As of late, more efforts have been put to utilize PADs for environmental monitoring. Accurate and low-cost monitoring is important for environmental applications, where routine testing is conducted for the analysis of river, soil and air contaminants. Herein, we are giving a glimpse of the paper analytical sensors reported for the environmental monitoring of metals and non-metals, organic molecules, pesticides, and microorganisms.

3.1 Metals and Non-metals

Environmental metal contamination is common in three sources, air (aerosols), water, and soil, and many paper analytical devices have been developed for metal detection because of their known toxicity. Metals such as Fe, Cu, Cr, and Co are redox active and have capacity for creating free radicals, which further produce oxidative stress in life forms. On the other hand, Pb and Cd are known for their neurotoxicity (Meredith et al. 2016). Exposure to hazard metals causes numerous health issues; however, progressing endeavours to recognize sources of exposure is impeded due to high cost of estimation, which bringing about restricted tests or monitoring options. Since 2010, PADs for metal detection have got great consideration due to the fact that coloured metal–ligand complexes are effectively able to recognize by naked eyes and measured cheaply using other optical patterns. Microfluidic PAD-based measurement of metals such as Fe, Cu, and Ni in n airborne particulate matter was reported by Mentele et al. (2012) with a detection limits of 1–1.5 μg for each analyte. In addition, the same device has been used to detect Cr and Cr (VI) from ash and welding fumes (Rattanarat et al. 2013). Despite the development in colorimetric detection methods, the detection limits of having

"ppm" levels make these methods undesirable, where a "ppb" level of detection is required for much better sensitive assay. Interestingly paper gadgets by colorimetric means have been fabricated for measuring other toxic metals such as Zn, Cu, Ag, Cd, Pb, Ni, Hg, and Cr (VI) utilizing metal-to-ligand charge-exchange chemistry (Meredith et al. 2016). In order to circumvent the bottleneck of having less sensitivity and ppm levels of detection, electrochemical assay methods are used and it has the ability to quantify metals at sub-ppb levels. So a combination of colorimetric and electrochemical detection is found to be an answer for the less sensitive colorimetric methods (Apilux et al. 2010). A paper sensor by combining both electrochemical and colorimetric detection for the rapid screening of Au (III) has been developed. Interestingly, the sensor could detect Au (III) in industrial waste with the presence of a common interference, Fe (III). As can be observed from Fig. 3, both electrochemical and colorimetric detection zones are patterned onto the paper substrate.

A three-dimensional microfluidic PAD for quantifying Ni, Cu, Fe, Pb, Cr, and Cd has been developed for contaminants that exhibit in airborne particulate matter (Rattanarat et al. 2013). Herein, colorimetric and electrochemical recognition on particular layers has been employed. The colorimetric detection methods are involved for the quantification of Cu, Ni, Fe, and total Cr. However, Pb and Cd are quantified electrochemically. Minimized cross-contamination and distinct reaction chemistry (e.g. agent masking, pH adjustments) are the added advantage of the reported three-dimensional microfluidic PAD with separate layers. This technique also enhances the analyte selectivity and sensitivity. Fabrication of a "lab-on-paper sensor" through inkjet printing with solgel entrapped β-galactosidase for heavy metal sensor by colorimetric visualization was reported. The developed paper assay was able to detect Hg, Ag, Cu, Cd, Pb, Cr, and Ni individually or in mix within 10 min (Hossain and Brennan 2011).

On the other hand, the vulnerability to numerous non-metal inorganic complexes has prompted environmental controls and approaches for building up allowable

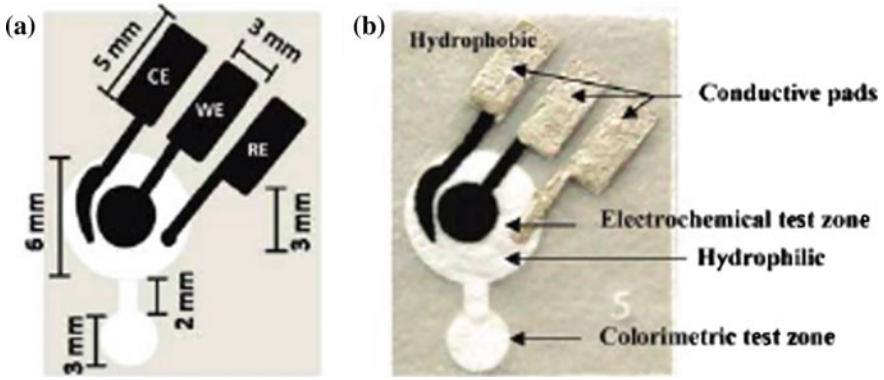

Fig. 3 Dual electrochemical and colorimetric paper sensor (Apilux et al. 2010)

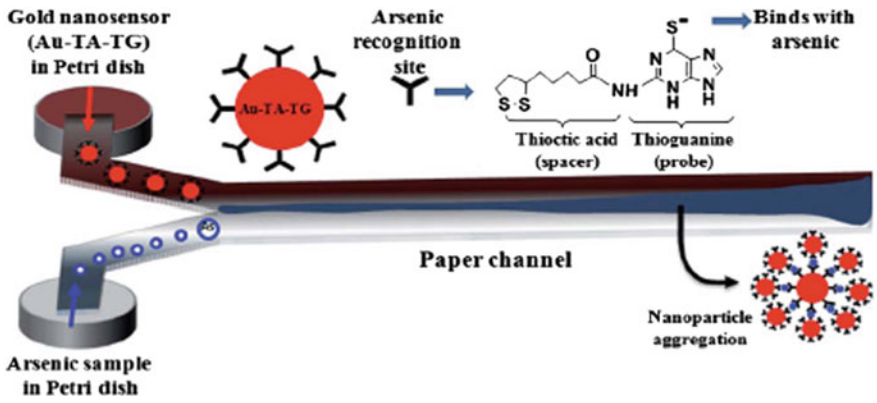

Fig. 4 Microfluidic PAD for arsenic detection (Nath et al. 2014)

exposure concentrations. The main pathway for inorganic pollutants into the environment is by combustion by-product or agricultural run-off or other specimen matrices from animal production facilities. Various low-cost microfluidic PADs have been reported for monitoring inorganic materials in the environment. Microfluidic PAD with colorimetric detection of phosphate, nitrate, nitrite, ammonia, arsenic, and cyanide has been reported and beautifully arranged in a review article by Henry Group (Meredith et al. 2016). Electrochemical recognition of iodide, bromide, chloride, potassium, and ammonium has been shown on a μPAD utilizing potentiometry. Among these, Nirpen chanda et al. had successfully developed a rapid gold nanosensor for arsenic; the gold nanosensor was prepared by stepwise chemical conjugation of gold nanoparticles (AuNPs) with thioctic acid (TA) followed by thioguanine (TG) molecules. A visible bluish-black colour precipitate due to the formation of gold nanoparticle aggregates through transverse diffusive mixing of Au–TA–TG with As^{3+} ions on a paper device depicts the successful detection of arsenic (Nath et al. 2014) (Fig. 4).

Usual methods require an extra reader to quantify the concentration of target analytes in the sample, thus increasing the costs of using microfluidic PADs. However, a novel method for detection or readout has been developed recently. Interestingly, Lewis et al. reported a simple way to quantify the level of mercury and lead with respect to the "time" by noting from the "start" and "stop" (Lewis et al. 2014) (Fig. 5).

Jayawardane et al. proposed a paper device to test the presence of nitrite and nitrate in drinking water (Jayawardane et al. 2014) under optimal conditions and allowed the user to measure concentrations as low as 1 and 19 μM for nitrite and nitrate. Recently, detection of CeO_2 or ceria nanoparticle through paper-based assay has been reported by employing redox-active ligands containing o-dihydroxy functionality, enabling multivalent binding, surface retention, and formation of charge transfer complexes between the grafted ligand and the ceria nanoparticles.

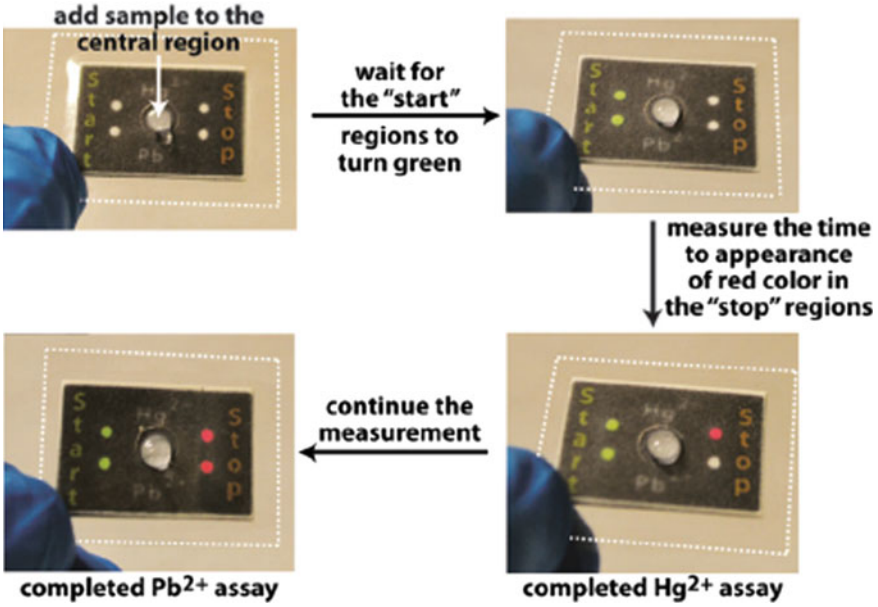

Fig. 5 Paper assay for the concurrent detection of mercury and lead (Lewis et al. 2014)

Using this strategy, paper-based and microarray-printed platforms with NP-capture ability involving either catechol or ascorbic acid as ligands were successfully fabricated (Othman et al. 2017).

3.2 Organic Molecules

Organic contaminants have various antagonistic health impacts relying upon the mechanism of activity or the affected organs. Because of their toxicological effects and hazard nature to human health, sensors to detect volatile organic compounds (VOCs) got much attention. However, most of the fabrication of sensors involves complicated procedures, and the need of additional equipment for detection is required. Hence, PAD-based sensors have been accounted for VOCs' recognition.

Yoon et al. (2013) reported inkjet-printed paper-based VOC sensor strips imaged with polydiacetylenes. Bisurethane-substituted diacetylene monomer, 5,7-dodecadiyne-1,12-diol bis[((butoxycarbonyl) methyl)urethane] (4BCMU) have been inkjet printed on paper substrate, which under UV exposure displayed a blue colour and upon in the presence of chloroform, exhibited an yellow colour.

A reagent less, self-integrated paper assay with colorimetric method has been reported in 2015 for the detection of bisphenol A using the enzyme tyrosinase (Alkasir et al. 2015). Gas-separation microfluidic PADs without membranes are

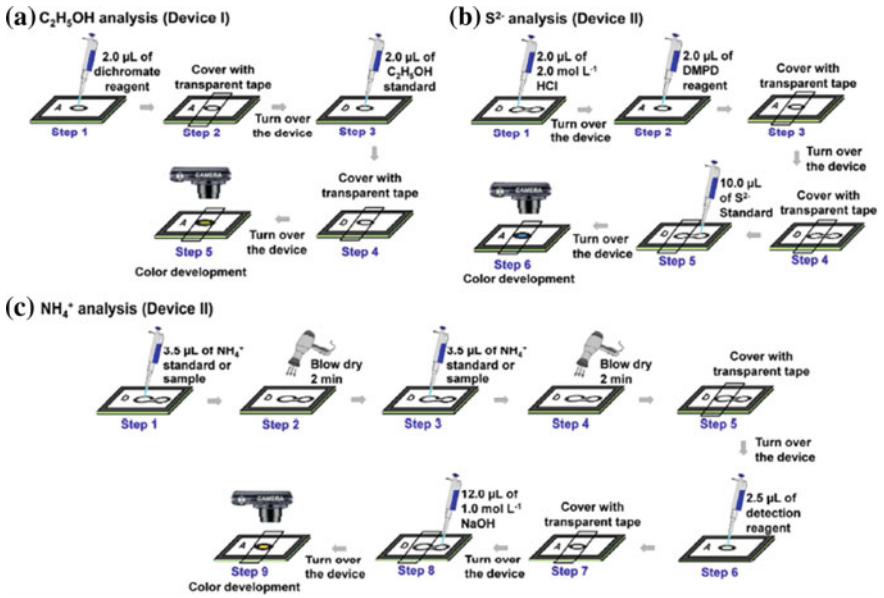

Fig. 6 MBL-GS µPADs for **a** ethanol analysis, **b** sulphide analysis, and **c** ammonium analysis (Phansi et al. 2016)

utilized for quantification of all sorts of materials, and compounds have been reported, and in this case, the authors use different layers, three in number like: "spacer", "donor", and "acceptor layer". The two layers, acceptor and donor, are composed of paper (filter) which has a pattern printed on it. These two layers are stacked one over the using another layer called spacer in the middle of the two. Spacer layer is having a two-faced stacking tape, which is 0.8 mm thick, having a disc which is apparently small and is made open for the diffusion of the gas molecules from the donor layer to the acceptor layer (Fig. 6). Diffusion of the gas can be identified by the colour change which is resulted by the reaction of the gas molecules with the reagent which is present in the acceptor zone. The colour intensity is quantified by utilizing ImageJ software (Phansi et al. 2016).

3.3 Pesticides

Current advances in environmental paper analytical devices applications include the determination of toxic contaminants released or leftover from insecticides or pesticides. Air, water, soil, food, and feed products are always contaminated with pesticides. By means of ingestion, inhalation, and dermal assimilation, pesticide toxicity can happen and is related with neurotoxicity, hepatotoxicity, renal harmfulness, dermatitis, and cancer. Microfluidic PADs offer cost-effective, practical

methods for quickly examining food items for pesticides. Hossain et al. (2009) reported the detection of pesticides in beverage and food samples with a reagent-less bidirectional lateral flow bioactive paper sensor. The sensor consisted of acetyl cholinesterase (AChE) enzyme and indophenyl acetate reagent for the assay where the combination of the two created a blue colour. The pesticides presence was noticed by change in the blue colour intensity and analysed using a digital camera. The same group recently developed much more sensitive device using smartphone application for on-site quantification of colorimetric visual records to monitor organophosphate pesticides using the previously developed microfluidic PADs (Sicard et al. 2015). Recently by using nanoceria-coated paper device, simple, low-cost, and rapid detection of organophosphate (OP) pesticides employing an enzyme inhibition assay with AChE and choline oxidase (ChOX) was reported. When acetylcholine is present in the medium, AChE and ChOX will react and enhance the production of H_2O_2 and is identified colorimetrically using gadget which is coated by nanoceria, which will help in the development of colour (yellow). When it is allowed to react with OP pesticides, it can be seen that the activity of AChE was terminated, leading to the decreased production of H_2O_2, and henceforth a strong decrease in the intensity of the yellow colour produced. This method of detection can be used to detect various OP pesticides such as, methyl-paraoxon and chlorpyrifos-oxon, and hence limits the use of highly established methods and equipments (Nouanthavong et al. 2016). Pentachlorophenol was detected on a microfluidic PAD by utilizing molecular imprinting technique along with photoelectrochemical (PEC) sensing platform was reported by Sun et al. Herein, gold and polypyrrole-functionalized ZnO nanoparticles were found to be the main key for detection (Sun et al. 2014). Colorimetric bioassay on paper for paraxon was proposed based on AChE-catalysed enlargement of gold nanoparticle co-entrapped with the enzyme in a solgel-based silica material (Luckham and Brennan 2010). Both the acetylthiocholine containing test solution and Au (III) salt were spotted on paper decorated previously with 3 nm gold nanoparticles. Hydrolysis of the enzyme substrate generates thiocholine, which further reduces the Au (III) onto gold nanoparticles, inducing the nanoparticles growth, which results in an increase in colour intensity. The colour change produced was correlated with enzyme inhibition by paraxon. A potable bioactive paper for the detection of the degradation products of organophosphorus pesticides with an LOD of 2.5 ppm of malathion was also reported by Kavruk et al. (2013).

3.4 Warfare

Explosives can be any unstable molecules which are organic and also are composed of oxygen and nitrogen atoms along with hydrogen and carbon; whereas hydrogen and oxygen are highly oxidizable compounds, and they play a role as fuels during explosion. A new method has been developed to detect, identify, and distinguish the major explosives like triacetone triperoxide (TATP), 4-amino-2-nitrophenol

(4A2NP), nitrobenzene (NB), picric acid, and hexamethylene triperoxide diamine (HMTD) utilizing paper-based devices, mobile phones, and chemometric equipments. Semi-quantitative quantification and analysis are also possible if the explosives are in less quantity, i.e. less than 0.2 μg. These paper-based sensors are incorporated with agents or chemicals, which will produce or assure a colour which is an important marker for the detection of each explosive. The colour pattern developed for each explosive can be quantified utilizing smartphones; software's developed to serve the purpose and also using a chamber which is closed to overcome the problems of illumination, which is an important limitation in commonly used paper sensors or gadgets (Salles et al. 2014). μPAD design has been developed for detecting 1,3,5-trinitrobenzene (TNB), 2,4,6-trinitrotoluene (TNT), and 2,4,6-trinitrophenylmethylnitramine (tetryl) in explosive residue (Pesenti et al. 2014). Here, potassium peroxide acts as a complexing reagent, and analyte transfer occurs via a swab or by wiping a contaminated surface with the device. Violet colour is produced due to the reaction of methoxide or hydroxide ions (Janowski reaction) with trinitro aromatic compound. μPADs with five different lanes were fabricated and wax printed using filter paper (chromatography) to develop hydrophobic lanes which will be helpful in the identification of explosives like nitrite, nitrate, perchlorate, and chlorate oxidizers, also ammonium. Explosives used in military like RDX and TNT, and also strong explosives like nitrates and urea, are also detected using paper sensors. Paper sensors are also capable of detecting peroxide compounds like TATPs and the hydrogen peroxide precursors (Peters et al. 2015). Very recently, a paper sensors strips were also employed to quantify mustard gas concentrations, a chemical warfare agent. The detection is based on sulphur mustard gas decomposition in the presence of mediator haloalkane dehalogenase which is also followed by pH change in the local medium. The alteration in the pH is identified or detected by the use of pH strips, wherein the colour change is from bluish green to yellow, and the colour change is attained in 10 min (Bidmanova et al. 2016). A microfluidic PAD has been developed by Dubey et al. to detect the presence of vesicant and nerve agents. Here in this method, the procedure for detection of the compounds was relied on the mechanism of their action with *para*-nitrobenzyl pyridine and rhodamine hydroxamate, developing blue and red colours (Pardasani et al. 2012). A rapid and sensitive strip-based quick test for nerve agents like Tabun, Sarin, and Soman are detected rapidly utilizing strip-based devices incorporated with BODIPY-altered silica compounds and were reported by Climent et al. (2016) These strips were made up of spots of hybrid material, which act as an indicator, which consists of a fluorescent BODIPY compound covalently bonded to the lanes of mesoporous SBA silica particles. The change in the fluorescence or the fluorescence quenching will help in the sensitive and selective identification of chemical-based warfare agents.

4 Paper Analytical Devices for Biomedical Applications

In the last decade, paper-based microfluidics field has encountered fast development. Microfluidic PADs were initially created for point-of-care (POC) medicinal diagnostics in resource-poor scenarios and are presently connected to diverse territories. Paper sensors are cost effective and also demonstrate extraordinary guarantee for on-field analysis.

Biomedical applications going from medication, delivery and infection analysis to POC gadgets, and tissue designing have got expanding consideration in the recent decade. Regular biomedical strategies however frequently confront expanding challenges in various biomedical applications, for example, high cost, moderate determination, costly instrumentation, low drug delivery efficiency, and high disappointment rates in medication discovery because of the inconsistency between 2D cells-based assays and living tissues. Furthermore, many instances of worldwide maladies (e.g. intestinal sickness, tuberculosis, or TB, meningitis and hepatitis B) occur in high poverty zones, for example, rural areas and developing countries which regularly cannot manage the cost of costly and high-precise instruments. For example, as per World Health Organization (WHO), one million instances of bacterial meningitis are evaluated to happen and 200,000 loss of life in every year due to meningitis. All these pose great difficulties to regular biomedical strategies.

Long patient hold up and constrained options to analysis and treatment are currently common in health care sector, because of the interminable underfunding of human health care services. In this scenario, a low-cost POC for diagnostics purpose is need of the hour. Low-cost, versatile, and simple analytical devices could be the alternative for essential therapeutic and equipments accessible for underdeveloped countries (Yager et al. 2006). In addition, even the developing countries with built up healthcare insurance frameworks could also find benefits in POC-based diagnostics. Moreover, POC diagnostic devices for on-field utilization could find importance in military, forensic, and space operations. Paper-based POC offers a simple way for detection and are designed for single use and also can be disposed off easily. Hence they are widely used for point-of-care applications.

While considering the tremendous developments in PAD based diagnostics methods in the last decade, the most known strip based pregnancy test, have the benefits like effortlessness, biodegradability, and low cost for manufacturing and fabrication. Having said that, paper-based devices when compared with chip-based microfluidic devices, the later still linger behind when the logical affectability, multiplexing capacity, and shelf life issues are concerned (Yeo et al. 2011).

4.1 Applications of PADs in Medical Diagnostics

Health of an individual can be assessed by testing the biomarkers or the pathogens or the agents that are responsible for the deteriorating affects in health. Biomarkers could be nucleic acids, proteins, lipids, or metabolites. Biomarkers could be nucleic acids, proteins, lipids, or metabolites and are specific to particular diseases, which could be utilized for analyzing different diseases precisely (Li et al. 2002; Jin et al. 2003; Li and Jin 2002). For instance, to monitor and screen prostate disease, prostate specific antigen (PSA) has been generally used (Thompson et al. 2004). Ideally, the biomarker of interest for screening any disease should be exact, specific, and easily available for testing. In general, biomarkers are found in saliva, urine, serum, and tissue samples. However, more non-invasive samples are desirable for analysis. Paper-based devices, as specified some time recently, are a solid and cheap contender for detection of any clinically important analytes. Herein, some of the advances made in paper-based bioassays for human well-being diagnostics are discussed.

4.1.1 Detection of Nucleic Acids

The detection of nucleic acid is important in various fields like, molecular biology, plant pathology, diary, and medical diagnostics. It is also helpful in recognizing the aetiological agents of disease specifically with the specimens available from clinics that will help to monitor unculturable or picky pathogens. In addition, by utilizing amplified microbial DNA/RNA one can detect these disease making pathogens (Liu et al. 2011). With the intensification or amplification step, biomarkers based on nucleic acid in ultra-low levels could be detected (Poppert et al. 2005). As an inexpensive, compact, dispensable, and rapid nucleic acid identification technique, microfluidic PADs for nucleic acid hybridization have generated incredible enthusiasm in the scientist community.

Paper-based activated microfluidic device which was bound with Cy3-tagged test DNA which is single-stranded (ssDNA) has been used for fast recognition of the target by Araújo et al. By utilizing the cheap and promptly accessible connecting reagent which is bifunctional, 1,4-phenylenediisothiocyanate helps in the enactment of Whatman No. 1 filter paper, allowing it agreeable to form conjugation of Cy3-marked ssDNA. As a result of the inborn capillary action of the paper grid, which encourages fast specimen movement along the different test DNA, which in further helps the hybridization process to be completed within 2 min. The paper-based microfluidic strips can be used for fast, specific, and sensitive DNA detection in diagnosis and was also accomplished by the segregation of the amplified products produced from animal (dogs) and human genomic and mitochondrial DNA in forensics (Araújo et al. 2012). A low-cost paper-based microfluidic gadget has also been developed by Cunningham et al. for recognition of the oligonucleotide and protein. The detection was based on the “target-induced

conformational switching" of an aptamer connected to an electrochemically active reporter (Cunningham et al. 2014). A piece of paper combined with reverse transcription loop-mediated isothermal amplification for detecting dengue virus ribonucleic acid has been discovered in 2012. The colorimetric method gave a molecular level monitoring of dengue fever within a short time (60 min) while comparing to the conventional polymerase chain reaction techniques (Lo et al. 2012). A photoelectrochemical (PEC) device on a paper strategy has been utilized to selectively and sensitively detect or sense the presence of DNA, utilizing graphene-based permeable Au-paper as the working electrode for the photoelectrochemical reactions (Wang et al. 2013). Measurement component is depended on the ability of the novel paper supercapacitor (PS) to charge, which is built on a stage by produced photocurrent. A two distinctive supramolecular designs for impedance-based determination of DNA hybridization with respect to paper electrodes has been designed by Ihalainen et al. (2014). The primary design includes formation of self-assembled monolayer on gold nanoparticles decorated electrodes and further formation of streptavidin and biotin conjugated DNA. The second was based on the mixed thiol/DNA probe monolayer's (Ihalainen et al. 2014). Further surface plasmon resonance and impedance parameters showed the apparent changes with respect to the DNA hybridization (Fig. 7).

Very recently, a paper-based colorimetric assay for DNA detection based on pyrrolidinyl peptide nucleic acid (acpcPNA)-induced nanoparticle aggregations reported as an alternative to traditional colorimetric approaches. PNA probes are an attractive alternative to DNA and RNA probes because they are chemically and biologically stable, easily synthesized, and hybridize efficiently with the complementary DNA strands. The multiplex colorimetric PAD was developed for concurrent monitoring of DNA associated with diseases due to bacterial and viral infections, including Middle East Respiratory Syndrome Corona Virus (MERS-CoV), Mycobacterium tuberculosis (MTB), and human papillomavirus (HPV) (Teengam et al. 2017).

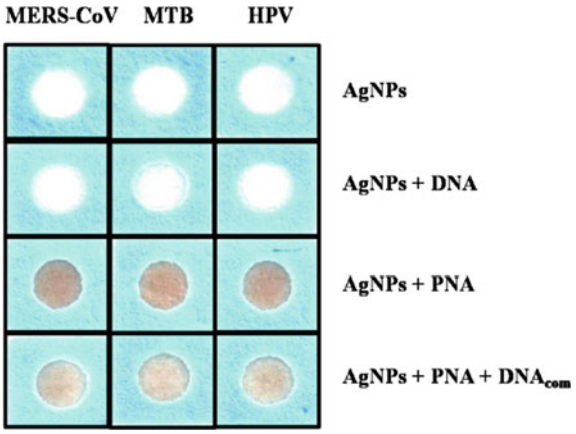

Fig. 7 Image of visual colour changes obtained from detection of MERS-CoV, MTB, and HPV in the presence of DNA (Teengam et al. 2017)

Regardless of the great execution of the paper-based nucleic acid hybridization for nucleic acid recognition, most of the time DNA hybridization depends on nucleic acid amplification process, which is often conducted off-chip and frequently requires costly massive hardware in the research facility. It is as yet difficult to coordinate DNA amplification ventures on paper-based devices because of the issues on fluid dissipation and heating component necessities.

4.1.2 Detection of Proteins

For early detection of a disease or preventions, it is imperative to analyse biomarkers. Mostly proteins also act as major biomarkers, important for research in medicine and medical diagnostics. The molecular biology techniques currently used are time-consuming to perform, expensive, require sophisticated instrumentation and also skilled persons are required to handle it. Hence, there is also an extraordinary need to manufacture or fabricate less expensive, fast, and basic POC detection methodologies with better feasibility and sensitivity, irrespective of resource-rich or less settings. Various paper-based microfluidic devices have been fabricated utilizing colorimetric, fluorescence, electrochemiluminescence, colorimetric, and electrochemical detection techniques for different clinically important biomarkers. Colorimetry-based immunoassay technique is a standout among the most generally utilized methods. The assay mostly depends on the colour change because of compound response between the bio-catalysts/catalyst connected to analyte of interest and the reagent added. The very well-known basic patterned paper device reported by Whitesides group beautifully explains the initial breakthroughs of microfluidic PADs for protein detection (Martinez et al. 2007). The authors used a known method of change in colour from yellow to blue while protein bind with tetrabromophenol blue (TBPB). The fabricated device exhibited the new possibilities available for the detection of bovine serum albumin in the clinically important concentrations. A paper-based microfluidic device to separate plasma from the blood comprised of blood partition film joined with patterned paper has been developed (Songjaroen et al. 2012). The whole plasma protein analysis through colorimetric assay further showed the greater efficiency of the method. It is worth to note that paper-based immunoassay utilizing polymerization-based amplification (PBA) for rapid monitoring of *Plasmodium falciparum* histidine-rich protein 2 (Pf HRP2) in malaria has been recently reported (Badu-Tawiah et al. 2015). Interestingly, the same group have tried another method for the signal amplification assessed performances of different amplification methods, like enzymatic amplification using HRP and alkaline phosphatase (ALP), PBA and also silver enhancement (SE) on AuNPs has been performed for PfHRP2 immunoassays on paper and its limit of detection (LOD) were found to be an order of magnitude lower than assays when compared with PBA or SE/AuNPs (Lathwal and Sikes 2016). 96-microzone paper-based device (P-ELISA) was reported by Whitesides group. The as developed device was easy to build and considering its biodegradable nature makes it more suitable than the common 96-well plates.

ELISA was performed utilizing alkaline phosphatase and BCIP/NBT (5-bromo-4-chloro-3-indolyl phosphate and nitrobluetetrazolium). Since the yellow colour BCIP/NBT reacts with enzyme and produces a colour change to purple, which can be easily visualized without any background colour interferences. The authors demonstrated the detection of rabbit IgG and specific antibodies from serums of HIV-1 positive patients. Even though the human serum samples were diluted to longer ranges, i.e. 10 times dilution, the test showed good results (Cheng et al. 2010). Human performance biomarker Neuropeptide Y detection was performed by using P-ELISA, and the authors were able to detect the analyte of interest in pico moles range (Murdock et al. 2013).

Sensitive and selective chemiluminescence ELISA (CL-ELISA) for the high throughput, rapid, stable, and reusable assay for cancer biomarkers were reported. Herein, chitosan and glutaraldehyde cross-linking were used for the entrapment of capture antibodies. The chemiluminescence was produced after the reaction between luminol-P-iodophenol and H_2O_2 with horseradish peroxidase (HRP)-marked antibodies. Paper-based CL-ELISA exhibited good detection limit for α-fetoprotein, CA-125, and CEA, (Wang et al. 2012). Colorimetric biosensing with respect to the colour change produced after the cross-linking of siloxane, 3-aminopropyltriethoxysilane, and glutaraldehyde onto paper was used for the monitoring of prostate-specific antigen (PSA). Herein, the authors immobilized anti-PSA antibody (Ab1) onto the paper surface and using GOx modified gold nanorod (GNR) as detection anti-PSA antibody (Ab2) label. The detection of PSA was achieved via the liberated H_2O_2 when the GOx label reacted with glucose. The colorimetric detection was based on the visual colour changes happened during the reaction of 3-aminopropyltriethoxysilane–glutaraldehyde complex reaction in presence of H_2O_2 (Zhou et al. 2014).

In general, most of the microfluidic PADs avail the washing procedure to completely remove the loosely binded to non-specific binding protein. But this technique is not so suitable in some cases hence it will interfere the assay procedure. To avoid these troubles, a novel washing procedure based on a ring-oven technique was proposed by Liu et al. Because of the capillary force and the continuous flow of washing solution, the non-specific binding proteins were moved to waste zone (ring area in Fig. 8a), thus making a low background for the detection (Liu et al. 2015). The authors further successfully showed the sensitive detection of carcinoembryonic antigen through TMB-H_2O_2 chemistry using the newly developed ring-oven washing technique (Fig. 8b).

Recently, hybrid microfluidic/paper microplate for ELISA has been reported. The microplate was fabricated by creating micro-wells in a poly(methyl methacrylate) (PMMA) chip and further insertion of wells with porous paper. The proof of concept was demonstrated by detecting immunoglobulin G (IgG) and hepatitis B surface antigen (HBsAg) in human serum samples. The paper/PMMA-based ELISA results could be observed with naked eye (Fig. 9). The porous paper in micro-wells not only helped in the successful immobilization of bio-reagents, but also avoided the tedious steps involved during the washing and modification procedure involved in the conventional ELISA (Sanjay et al. 2016).

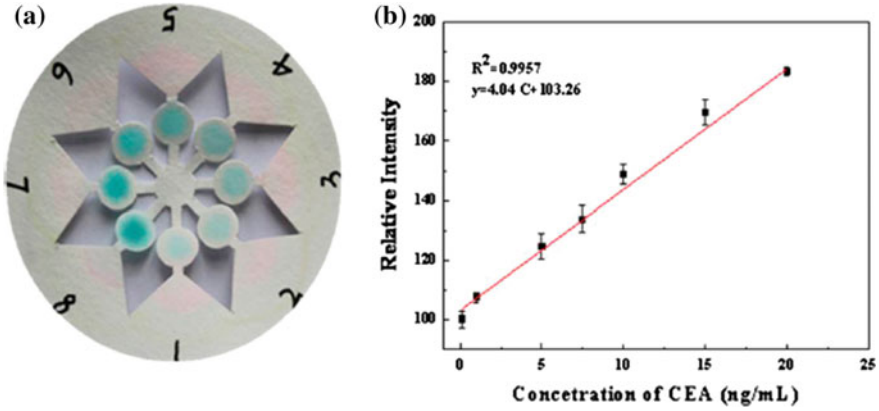

Fig. 8 **a** Image of visual colour changes obtained for different concentration of CEA and **b** corresponding calibration curve (Liu et al. 2015)

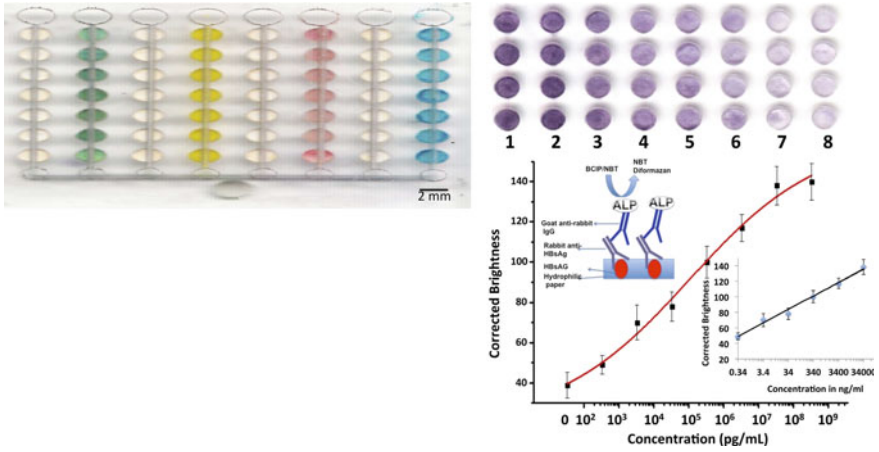

Fig. 9 Hybrid microfluidic microplate based on paper/PMMA chip for ELISA (Sanjay et al. 2016)

4.1.3 Detection of Cells

With improved specificity and affectability, sensing and diagnosis of tumour cells and other sorts of mammalian cells which are clinically significant have been materialized by using paper devices coupled with chemiluminescence, fluorescence, electrochemical, electrochemiluminescence, and colorimetric approaches. Thus, fabrication of inexpensive and simple, cheap microfluidic paper-based sensors for cell detection provides empowering opportunity to scale down the use of sophisticated instruments and also to increase the efficient point-of-care multiple screening methods.

By combining the techniques of electrochemistry and chemiluminescence in an origami principle based microfluidic PAD has been developed to analyze the tumour cells. The device consists of 3D macroporous Au conjugated with specific aptamers for the precise capture of cancer cells such as, MCF-7, HL-60, CCRF-CEM and K562 (Wu et al. 2015). Moreover the combination of a bimetallic gold and palladium nanoparticles decorated with concanavalin-A has been employed as a probe for cell recognition. The detection of human acute promyelocytic leukaemia cells and screening of anticancer drugs using a paper-based electrochemical device has been developed. The device is constructed with combination of gold nanoparticles-aptamer conjugates and enzyme catalysis onto paper device by employing origami and kirigami principles (Su et al. 2014). A differential pulse voltammogram (DPV) and fluorescence response gave a sensitive detection. Additionally, the same group employed the device they developed for the detection of K562 cells and to study the expression of glycans (Su et al. 2015). The Shevkoplyas group developed a microfluidic PAD for diagnosis of sickle-cell disease. This device enables differentiation of healthy patients from those carrying genes encoding for mutations in the structure of haemoglobin that lead to sickle-cell trait or sickle-cell disease. Lysing RBCs in a solution containing sickle dex caused structurally altered haemoglobin to polymerize, which, unlike normal haemoglobin, is insoluble and unable to be transported through paper by wicking. This approach provides a means of performing a diagnosis via visual inspection of the device (Yang et al. 2013). The impact of softwood and hardwood derived paper on microfluidic PAD for the mobility of red blood cells (RBCs) is reported by Li et al. The authors discovered that hardwood strands with low premise weight and higher porosity permitted the simple mobility of RBCs and indicated high clarity blood-typing assays. On the other hand, softwood filaments with more perplexing pore structure made RBCs mobility more troublesome and produced low clarity (Li et al. 2014). However, it is indeed worrisome that, without continuous perfusion, cell cultures based on paper devices can be only implemented by immersing the entire paper device in the cell culture medium and then applying nutrient or drug stimulation in sequence. Also, a technical drawback of creating a cell culture based on paper is the fluorescent interference caused by the paper fibre when both the cells and the paper fibres were stained. Nevertheless, multi-branched hybridization chain reaction (mHCR) and concanavalin-A (ConA) have been integrated for developing a colorimetric or fluorescence-based dual model paper-based device. Final product obtained due to mHCR process was altered to PtCu nanochains that were used as colorimetric signal, and the graphene quantum dot was utilized as fluorescence signal. These were used as such, unaltered, and were used potentially for analysing N-gleeman expression, which is a cell surface marker and can be used for analyzing the cells. These Au–Ag paper gadgets were used or enhanced the active sites and surface areas for accompanying aptamers in larger loads, and this strategy can further efficiently and specifically capture more cancer cells in larger amounts. In addition, the paper background fluorescence was effectively decreased by using this strategy. The device showed excellent fluorescence and colorimetric signals for the detection of breast cancer cell lines with a detection limit range between 25 and 35

cells per mL (Liang et al. 2016). In addition, bacteria cells were also detected by using paper analytical devices. A one-stage chromatographic paper-based test for the rapid sensing of *Salmonella typhi* in human serum utilizing gold nanoparticles was reported. The test was established through simple antigen and antibody interaction of S. *typhi* on nitrocellulose layer, and the authors then compared the test with respect to the dot blot assay and found that the immunochromatographic test is better and showed shorter time requirement for conducting the test. In addition, the paper test had longer shelf life (30 days) (Preechakasedkit et al. 2012).

4.1.4 Microorganisms

Recently much attention has been devoted for bacterial contamination detection particularly in food and water through microfluidic PADs with goals of providing diagnostic tools that are faster to answer and lower in cost than traditional methods such as culture analysis and polymerase chain reaction (PCR). In general, food-borne bacteria detection was accomplished by measuring the colour change occurring in a PAD, which is decorated with an enzyme associated with a pathogen of interest and further biochemical reaction. The chromogenic substrate used by the authors is β-galactosidase with chlorophenol red β-galactopyranoside (CPRG) for *Escherichia coli*; phosphatidylinositol-specific phospholipase C (PI-PLC) with 5-bromo-4-chloro-3-indolylmyo-inositol phosphate (X-InP) for *Listeria monocytogenes*; and esterase with 5-bromo-6-chloro-3-indolyl caprylate (magenta caprylate) for *Salmonella enteric* detection (Jokerst et al. 2012). Sensitive biosensing on a piece of paper was developed to detect of *E. coli.* through nanoparticle aggregation strategy that was reported by Shafiee et al.; here, AuNPs were modified with lipopolysaccharide binding protein (LBP) to recognize bacteria (Shafiee et al. 2015). A hybrid microfluidic device with the combination of paper and polydimethylsiloxane coupled with loop-mediated isothermal amplification was reported by Dou et al. for the rapid, sensitive detection *Neisseria meningitides* (Dou et al. 2014). Smartphone-based detection of *Salmonella* was investigated by Yoon group by employing anti-*S. Typhimurium*-conjugated sub-microparticles modified paper for immunoagglutination and further scattering measurements (San Park et al. 2013). The whole detection process was done by using smartphone application, which helps to avoid the use of sophisticated instruments. In addition, while comparing with other smartphone based assay, here holder for the phone and sensor is not required. An economically feasible microfluidic PAD for *Salmonella* live cell detection based on quantification of adenosine triphosphate (ATP) has been developed (Jin et al. 2015); however, the technique is not selective since many other cell types such as mammal, plant, and yeast cells also release ATP. Rapid detection of influenza A H1N1 and H3N2 viruses was reported by Lei et al. By using a paper assay method, interestingly the same could be used for sub-typing also. By evaluating the internal structural protein, nucleoprotein (NP), and outer surface glycoproteins, H1 and H3, of the influenza viruses, a sensitive and specific test has been established through colorimetric sandwich immunoassay. The detection limits

for H1 virus were found to be 2.7×10^3 (particle forming units) pfu/assay and 2.7×10^4 pfu/assay for H3. The as developed test was able to detect the viruses in the clinical samples and infected cell lysates (Lei et al. 2015).

5 Conclusion

Since PADs are simple, cost effective, easy to handle and give on-site results, many paper sensors are fabricated for wide range of applications worldwide. These devices could be useful in rural areas and for developing countries where individuals find difficulty in bearing the cost of expensive instrumentation for diagnosis purpose as well as environmental monitoring. Researchers have shown new advantages that are obtained from paper-based hybrid microfluidic stages. Various identification systems such as colorimetric, fluorescence, chemiluminescence, ECL, and electrochemical location have been utilized as a part of microfluidic PADs investigation. Electrochemical discovery is additionally attractive for paper-based microfluidic devices, yet it is massive and costly. Albeit compact potentiostats are industrially accessible, the cost is still genuinely high. Colorimetric identification is exceptionally perfect with the way of ease to examine in resource-poor settings, yet affectability and quantitation are regularly bargained. In the most recent decades, advanced mobile phones have grown significantly. May the integration of technology and other electronic readers (e.g. glucometers) with PADs could give awesome effects on social insurance and ecological observing. For reliable PADs, it is essential to investigate the analytical performance under different test conditions (e.g. temperature, humidity, ambient light, complexity of the sample matrixes), perform stability studies (especially when sensitive reagents or materials are involved in the device architecture), and carry out interference studies.

Acknowledgements The authors are grateful to research grant from Department of Biotechnology, Government of India, and Yenepoya University.

References

Alkasir RS, Rossner A, Andreescu S (2015) Portable colorimetric paper-based biosensing device for the assessment of bisphenol A in indoor dust. Environ Sci Technol 49(16):9889–9897

Apilux A, Dungchai W, Siangproh W, Praphairaksit N, Henry CS, Chailapakul O (2010) Lab-on-paper with dual electrochemical/colorimetric detection for simultaneous determination of gold and iron. Anal Chem 82(5):1727–1732

Araújo AC, Song Y, Lundeberg J, Ståhl PL, Brumer H III (2012) Activated paper surfaces for the rapid hybridization of DNA through capillary transport. Anal Chem 84(7):3311–3317

Badu-Tawiah AK, Lathwal S, Kaastrup K, Al-Sayah M, Christodouleas DC, Smith BS, Whitesides GM, Sikes HD (2015) Polymerization-based signal amplification for paper-based immunoassays. Lab Chip 15(3):655–659

Bidmanova S, Steiner MS, Stepan M, Vymazalova K, Gruber MA, Duerkop A, Damborsky J, Prokop Z, Wolfbeis OS (2016) Enzyme-based test strips for visual or photographic detection and quantitation of gaseous sulfur mustard. Anal Chem 88(11):6044–6049

Bruzewicz DA, Reches M, Whitesides GM (2008) Low-cost printing of poly (dimethylsiloxane) barriers to define microchannels in paper. Anal Chem 80(9):3387–3392

Carrilho E, Martinez AW, Whitesides GM (2009) Understanding wax printing: a simple micropatterning process for paper-based microfluidics. Anal Chem 81(16):7091–7095

Cate DM, Adkins JA, Mettakoonpitak J, Henry CS (2014) Recent developments in paper-based microfluidic devices. Anal Chem 87(1):19–41

Chen B, Kwong P, Gupta M (2013) Patterned fluoropolymer barriers for containment of organic solvents within paper-based microfluidic devices. ACS Appl Mater Interfaces 5(23):12701–12707

Cheng CM, Martinez AW, Gong J, Mace CR, Phillips ST, Carrilho E, Mirica KA, Whitesides GM (2010) Paper-based ELISA. Angew Chem Int Ed 49(28):4771–4774

Chitnis G, Ding Z, Chang CL, Savran CA, Ziaie B (2011) Laser-treated hydrophobic paper: an inexpensive microfluidic platform. Lab Chip 11(6):1161–1165

Climent E, Biyikal M, Gawlitza K, Dropa T, Urban M, Costero AM, Martínez-Máñez R, Rurack K (2016) A rapid and sensitive strip-based quick test for nerve agents Tabun, Sarin, and Soman using BODIPY-modified silica materials. Chem A Eur J 22(32):11138–11142

Cretich M, Sedini V, Damin F, Pelliccia M, Sola L, Chiari M (2010) Coating of nitrocellulose for colorimetric DNA microarrays. Anal Biochem 397(1):84–88

Cunningham JC, Brenes NJ, Crooks RM (2014) Paper electrochemical device for detection of DNA and thrombin by target-induced conformational switching. Anal Chem 86(12):6166–6170

Dornelas KL, Dossi N, Piccin E (2015) A simple method for patterning poly (dimethylsiloxane) barriers in paper using contact-printing with low-cost rubber stamps. Anal Chim Acta 858:82–90

Dou M, Dominguez DC, Li X, Sanchez J, Scott G (2014) A versatile PDMS/paper hybrid microfluidic platform for sensitive infectious disease diagnosis. Anal Chem 86(15):7978–7986

Dou M, Sanjay ST, Benhabib M, Xu F, Li X (2015) Low-cost bioanalysis on paper-based and its hybrid microfluidic platforms. Talanta 145:43–54

Dungchai W, Chailapakul O, Henry CS (2011) A low-cost, simple, and rapid fabrication method for paper-based microfluidics using wax screen-printing. Analyst 136(1):77–82

Fernandes SC, Walz JA, Wilson DJ, Brooks JC, Mace CR (2017) Beyond wicking: expanding the role of patterned paper as the foundation for an analytical platform. Anal Chem 89(11):5654–5664

He Q, Ma C, Hu X, Chen H (2013) Method for fabrication of paper-based microfluidic devices by alkylsilane self-assembling and UV/O_3-patterning. Anal Chem 85(3):1327–1331

He PJW, Katis IN, Eason RW, Sones CL (2015) Engineering fluidic delays in paper-based devices using laser direct-writing. Lab Chip 15(20):4054–4061

Hossain SZ, Brennan JD (2011) β-galactosidase-based colorimetric paper sensor for determination of heavy metals. Anal Chem 83(22):8772–8778

Hossain SZ, Luckham RE, McFadden MJ, Brennan JD (2009) Reagentless bidirectional lateral flow bioactive paper sensors for detection of pesticides in beverage and food samples. Anal Chem 81(21):9055–9064

Hu J, Wang S, Wang L, Li F, Pingguan-Murphy B, Lu TJ, Xu F (2014) Advances in paper-based point-of-care diagnostics. Biosens Bioelectron 54:585–597

Ihalainen P, Pettersson F, Pesonen M, Viitala T, Määttänen A, Österbacka R, Peltonen J (2014) An impedimetric study of DNA hybridization on paper-supported inkjet-printed gold electrodes. Nanotechnology 25(9):94

Jahanshahi-Anbuhi S, Pennings K, Leung V, Kannan B, Brennan JD, Filipe CDM, Pelton RH (2015) Design rules for fluorocarbon-free omniphobic solvent barriers in paper-based devices. ACS Appl Mater Interfaces 7(45):25434–25440

Jayawardane BM, Wei S, McKelvie ID, Kolev SD (2014) Microfluidic paper-based analytical device for the determination of nitrite and nitrate. Anal Chem 86(15):7274–7279

Jiang X, Fan ZH (2016) Fabrication and operation of paper-based analytical devices. Ann. Rev. Anal. Chem. 9:203–222

Jin W, Li X, Gao N (2003) Simultaneous determination of tryptophan and glutathione in individual rat hepatocytes by capillary zone electrophoresis with electrochemical detection at a carbon fiber bundle—Au/Hg dual electrode. Anal Chem 75(15):3859–3864

Jin SQ, Guo SM, Zuo P, Ye BC (2015) A cost-effective Z-folding controlled liquid handling microfluidic paper analysis device for pathogen detection via ATP quantification. Biosens Bioelectron 63:379–383

Jokerst JC, Adkins JA, Bisha B, Mentele MM, Goodridge LD, Henry CS (2012) Development of a paper-based analytical device for colorimetric detection of select foodborne pathogens. Anal Chem 84(6):2900–2907

Kavruk M, Özalp VC, Öktem HA (2013) Portable bioactive paper-based sensor for quantification of pesticides. J Anal Methods Chem 2013:8

Lathwal S, Sikes HD (2016) Assessment of colorimetric amplification methods in a paper-based immunoassay for diagnosis of malaria. Lab Chip 16(8):1374–1382

Lei KF, Huang CH, Kuo RL, Chang CK, Chen KF, Tsao KC, Tsang NM (2015) Paper-based enzyme-free immunoassay for rapid detection and subtyping of influenza A H1N1 and H3N2 viruses. Anal Chim Acta 883:37–44

Lewis GG, Robbins JS, Phillips ST (2014) A prototype point-of-use assay for measuring heavy metal contamination in water using time as a quantitative readout. Chem Commun 50(40):5352–5354

Li XJ, Jin WR (2002) Monitoring homovanillic acid and vanillylmandelic acid in human urine by capillary electrophoresis with electrochemical detection. Chin Chem Lett 13(9):874–876

Li X, Jin W, Weng Q (2002) Separation and determination of homovanillic acid and vanillylmandelic acid by capillary electrophoresis with electrochemical detection. Anal Chim Acta 461(1):123–130

Li X, Tian J, Nguyen T, Shen W (2008) Paper-based microfluidic devices by plasma treatment. Anal Chem 80(23):9131–9134

Li X, Tian J, Shen W (2010) Progress in patterned paper sizing for fabrication of paper-based microfluidic sensors. Cellulose 17(3):649–659

Li L, Huang X, Liu W, Shen W (2014) Control performance of paper-based blood analysis devices through paper structure design. ACS Appl Mater Interfaces 6(23):21624–21631

Liang L, Lan F, Li L, Ge S, Yu J, Ren N, Liu H, Yan M (2016) Paper analytical devices for dynamic evaluation of cell surface N-glycan expression via a bimodal biosensor based on multibranched hybridization chain reaction amplification. Biosens Bioelectron 86:756–763

Liu P, Li X, Greenspoon SA, Scherer JR, Mathies RA (2011) Integrated DNA purification, PCR, sample cleanup, and capillary electrophoresis microchip for forensic human identification. Lab Chip 11(6):1041–1048

Liu W, Cassano CL, Xu X, Fan ZH (2013) Laminated paper-based analytical devices (LPAD) with origami-enabled chemiluminescence immunoassay for cotinine detection in mouse serum. Anal Chem 85(21):10270–10276

Liu W, Guo Y, Zhao M, Li H, Zhang Z (2015) Ring-oven washing technique integrated paper-based immunodevice for sensitive detection of cancer biomarker. Anal Chem 87 (15):7951–7957

Lo SJ, Yang SC, Yao DJ, Chen JH, Cheng CM (2012) Molecular-level dengue fever diagnostics: developing a combination of RT-LAMP and paper-based devices. IEEE Nanatechnol Mag 6 (4):26–30

Lu Y, Shi W, Qin J, Lin B (2009) Fabrication and characterization of paper-based microfluidics prepared in nitrocellulose membrane by wax printing. Anal Chem 82(1):329–335

Luckham RE, Brennan JD (2010) Bioactive paper dipstick sensors for acetylcholinesterase inhibitors based on sol–gel/enzyme/gold nanoparticle composites. Analyst 135(8):2028–2035

Martinez AW, Phillips ST, Butte MJ, Whitesides GM (2007) Patterned paper as a platform for inexpensive, low-volume, portable bioassays. Angew Chem Int Ed 46(8):1318–1320

Martinez AW, Phillips ST, Carrilho E, Thomas SW III, Sindi H, Whitesides GM (2008a) Simple telemedicine for developing regions: camera phones and paper-based microfluidic devices for real-time, off-site diagnosis. Anal Chem 80(10):3699–3707

Martinez AW, Phillips ST, Whitesides GM (2008b) Three-dimensional microfluidic devices fabricated in layered paper and tape. Proc Natl Acad Sci 105(50):19606–19611

Martinez AW, Phillips ST, Whitesides GM, Carrilho E (2009) Diagnostics for the developing world: microfluidic paper-based analytical devices. Anal Chem 82(1):3–10

Mentele MM, Cunningham J, Koehler K, Volckens J, Henry CS (2012) Microfluidic paper-based analytical device for particulate metals. Anal Chem 84(10):4474–4480

Meredith NA, Quinn C, Cate DM, Reilly TH, Volckens J, Henry CS (2016) Paper-based analytical devices for environmental analysis. Analyst 141(6):1874–1887

Müller RH, Clegg DL (1949) Automatic paper chromatography. Anal Chem 21(9):1123–1125

Murdock RC, Shen L, Griffin DK, Kelley-Loughnane N, Papautsky I, Hagen JA (2013) Optimization of a paper-based ELISA for a human performance biomarker. Anal Chem 85(23):11634–11642

Nath P, Arun RK, Chanda N (2014) A paper based microfluidic device for the detection of arsenic using a gold nanosensor. RSC Adv 4(103):59558–59561

Nie Z, Nijhuis CA, Gong J, Chen X, Kumachev A, Martinez AW, Narovlyansky M, Whitesides GM (2010) Electrochemical sensing in paper-based microfluidic devices. Lab Chip 10(4):477–483

Nouanthavong S, Nacapricha D, Henry CS, Sameenoi Y (2016) Pesticide analysis using nanoceria-coated paper-based devices as a detection platform. Analyst 141(5):1837–1846

Olkkonen J, Lehtinen K, Erho T (2010) Flexographically printed fluidic structures in paper. Anal Chem 82(24):10246–10250

Othman A, Andreescu D, Karunaratne DP, Babu SV, Andreescu S (2017) Functional paper-based platform for rapid capture and detection of CeO_2 nanoparticles. ACS Appl Mater Interfaces 9(14):12893–12905

Pardasani D, Tak V, Purohit AK, Dubey DK (2012) μ-PADs for detection of chemical warfare agents. Analyst 137(23):5648–5653

Pelton R (2009) Bioactive paper provides a low-cost platform for diagnostics. TrAC Trends Anal Chem 28(8):925–942

Pesenti A, Taudte RV, McCord B, Doble P, Roux C, Blanes L (2014) Coupling paper-based microfluidics and lab on a chip technologies for confirmatory analysis of trinitro aromatic explosives. Anal Chem 86(10):4707–4714

Peters KL, Corbin I, Kaufman LM, Zreibe K, Blanes L, McCord BR (2015) Simultaneous colorimetric detection of improvised explosive compounds using microfluidic paper-based analytical devices (μPADs). Anal Methods 7(1):63–70

Phansi P, Sumantakul S, Wongpakdee T, Fukana N, Ratanawimarnwong N, Sitanurak J, Nacapricha D (2016) Membraneless gas-separation microfluidic paper-based analytical devices for direct quantitation of volatile and nonvolatile compounds. Anal Chem 88(17):8749–8756

Poppert S, Essig A, Stoehr B, Steingruber A, Wirths B, Juretschko S, Reischl U, Wellinghausen N (2005) Rapid diagnosis of bacterial meningitis by real-time PCR and fluorescence in situ hybridization. J Clin Microbiol 43(7):3390–3397

Preechakasedkit P, Pinwattana K, Dungchai W, Siangproh W, Chaicumpa W, Tongtawe P, Chailapakul O (2012) Development of a one-step immunochromatographic strip test using gold nanoparticles for the rapid detection of Salmonella typhi in human serum. Biosens Bioelectron 31(1):562–566

Rattanarat P, Dungchai W, Cate DM, Siangproh W, Volckens J, Chailapakul O, Henry CS (2013) A microfluidic paper-based analytical device for rapid quantification of particulate chromium. Anal Chim Acta 800:50–55

Sackmann EK, Fulton AL, Beebe DJ (2014) The present and future role of microfluidics in biomedical research. Nature 507(7491):181–189

Salentijn GI, Hamidon NN, Verpoorte E (2016) Solvent-dependent on/off valving using selectively permeable barriers in paper microfluidics. Lab Chip 16(6):1013–1021

Salles MO, Meloni GN, de Araujo WR, Paixão TRLC (2014) Explosive colorimetric discrimination using a smartphone, paper device and chemometrical approach. Anal Methods 6(7):2047–2052

Sameenoi Y, Nongkai PN, Nouanthavong S, Henry CS, Nacapricha D (2014) One-step polymer screen-printing for microfluidic paper-based analytical device (μPAD) fabrication. Analyst 139 (24):6580–6588

San Park T, Li W, McCracken KE, Yoon JY (2013) Smartphone quantifies Salmonella from paper microfluidics. Lab Chip 13(24):4832–4840

Sanjay ST, Dou M, Sun J, Li X (2016) A paper/polymer hybrid microfluidic microplate for rapid quantitative detection of multiple disease biomarkers. Sci Rep 6:30474

Shafiee H, Asghar W, Inci F, Yuksekkaya M, Jahangir M, Zhang MH, Durmus NG, Gurkan UA, Kuritzkes DR, Demirci U (2015) Paper and flexible substrates as materials for biosensing platforms to detect multiple biotargets. Sci Rep 5:8719

Sicard C, Glen C, Aubie B, Wallace D, Jahanshahi-Anbuhi S, Pennings K, Daigger GT, Pelton R, Brennan JD, Filipe CD (2015) Tools for water quality monitoring and mapping using paper-based sensors and cell phones. Water Res 70:360–369

Songjaroen T, Dungchai W, Chailapakul O, Henry CS, Laiwattanapaisal W (2012) Blood separation on microfluidic paper-based analytical devices. Lab Chip 12(18):3392–3398

Su M, Ge L, Ge S, Li N, Yu J, Yan M, Huang J (2014) Paper based electrochemical cyto-device for sensitive detection of cancer cells and in situ anticancer drug screening. Anal Chim Acta 847:1–9

Su M, Ge L, Kong Q, Zheng X, Ge S, Li N, Yu J, Yan M (2015) Cyto-sensing in electrochemical lab-on-paper cyto-device for in-situ evaluation of multi-glycan expressions on cancer cells. Biosens Bioelectron 63:232–239

Sun G, Wang P, Ge S, Ge L, Yu J, Yan M (2014) Photoelectrochemical sensor for pentachlorophenol on microfluidic paper-based analytical device based on the molecular imprinting technique. Biosens Bioelectron 56:97–103

Taton TA, Mirkin CA, Letsinger RL (2000) Scanometric DNA array detection with nanoparticle probes. Science 289(5485):1757–1760

Teengam P, Siangproh W, Tuantranont A, Vilaivan T, Chailapakul O, Henry CS (2017) Multiplex paper-based colorimetric DNA sensor using pyrrolidinyl peptide nucleic acid-induced AgNPs aggregation for detecting MERS-CoV, MTB, and HPV oligonucleotides. Anal Chem 89 (10):5428–5435

Thompson IM, Pauler DK, Goodman PJ, Tangen CM, Lucia MS, Parnes HL, Minasian LM, Ford LG, Lippman SM, Crawford ED, Crowley JJ (2004) Prevalence of prostate cancer among men with a prostate-specific antigen level ≤ 4.0 ng per milliliter. N Engl J Med 350(22):2239–2246

Tomazelli Coltro WK, Cheng CM, Carrilho E, Jesus DP (2014) Recent advances in low-cost microfluidic platforms for diagnostic applications. Electrophoresis 35(16):2309–2324

Wang S, Ge L, Song X, Yu J, Ge S, Huang J, Zeng F (2012) Paper-based chemiluminescence ELISA: lab-on-paper based on chitosan modified paper device and wax-screen-printing. Biosens Bioelectron 31(1):212–218

Wang Y, Ge L, Wang P, Yan M, Ge S, Li N, Yu J, Huang J (2013) Photoelectrochemical lab-on-paper device equipped with a porous Au-paper electrode and fluidic delay-switch for sensitive detection of DNA hybridization. Lab Chip 13(19):3945–3955

Wang J, Monton MRN, Zhang X, Filipe CD, Pelton R, Brennan JD (2014) Hydrophobic sol–gel channel patterning strategies for paper-based microfluidics. Lab Chip 14(4):691–695

Wu L, Ma C, Ge L, Kong Q, Yan M, Ge S, Yu J (2015) Paper-based electrochemiluminescence origami cyto-device for multiple cancer cells detection using porous AuPd alloy as catalytically promoted nanolabels. Biosens Bioelectron 63:450–457

Yager P, Edwards T, Fu E, Helton K, Nelson K, Tam MR, Weigl BH (2006) Microfluidic diagnostic technologies for global public health. Nature 442(7101):412–418

Yagoda H (1937) Applications of confined spot tests in analytical chemistry: preliminary paper. Ind Eng Chem Anal Ed 9(2):79–82

Yang X, Kanter J, Piety NZ, Benton MS, Vignes SM, Shevkoplyas SS (2013) A simple, rapid, low-cost diagnostic test for sickle cell disease. Lab Chip 13(8):1464–1467

Yeo LY, Chang HC, Chan PP, Friend JR (2011) Microfluidic devices for bioapplications. small 7(1):12–48

Yetisen AK, Akram MS, Lowe CR (2013) Paper based microfluidic point-of-care diagnostic devices. Lab Chip 13(12):2210–2251

Yoon B, Park IS, Shin H, Park HJ, Lee CW, Kim JM (2013) A litmus-type colorimetric and fluorometric volatile organic compound sensor based on inkjet-printed polydiacetylenes on paper substrates. Macromol Rapid Commun 34(9):731–735

Zhou M, Yang M, Zhou F (2014) Paper based colorimetric biosensing platform utilizing cross-linked siloxane as probe. Biosens Bioelectron 55:39–43

Chapter 15
DNA-Based Sensors

Geeta Bhatt and Shantanu Bhattacharya

Abstract Sensing and detection for clinical diagnostic can be accomplished through various routes. Additionally what and how of sensing is critically optimized to meet individual needs. Diagnostics is carried out with various types of sensors out of which the electrochemical sensors are most used due to their unique ability to couple seamlessly with electronic circuitry. The DNA sensor is one of the most common types of sensors which is majorly deployed to perform expression monitoring, transcription profiling, etc., for example, the products developed by Affymetrix and Nanogen. This chapter is a consolidated review of the various aspects of DNA sensors, like the principle of detection, various ways of sensing and detection, applications of such DNA-based sensing. It looks at the various principles that are utilized for gene mapping like dielectrophoresis, polymerase chain reaction (PCR), real-time PCR or quantitative PCR (better known as q-PCR), hybridization, solid-phase PCR, droplet-based PCR, etc. It also reviews various sensing/detection strategies for sensing DNA like electrophoresis, impedance spectroscopy, colorimetric sensing, optical sensing and inertial sensing. The chapter provides a state-of-the-art review of basic techniques, sensing methodologies and applications for DNA-based diagnostics as carried out by industry.

Keywords DNA-based sensing · Fluorescence · Impedance spectroscopy PCR · q-PCR · Electrophoresis · Dielectrophoresis · Microcantilevers Electrochemical sensing

G. Bhatt (✉)
Microsystems Fabrication Laboratory, Department of Mechanical Engineering, Indian Institute of Technology, Kanpur, India
e-mail: geetabht@iitk.ac.in

S. Bhattacharya
Design Program, Indian Institute of Technology, Kanpur, India

S. Bhattacharya et al. (eds.), *Environmental, Chemical and Medical Sensors*, Energy, Environment, and Sustainability, https://doi.org/10.1007/978-981-10-7751-7_15

1 Introduction

The field of biosensing deals with the development of a sensory platform (generally equipped electrodes) to sense multiple analytes in various samples (e.g., deoxyribonucleic acid (DNA), ribonucleic acid (RNA), bacteria/microorganisms, chemical analytes) to pick up specific targets in those samples which would give important diagnostic information. The sensing is carried out by generating an equivalent signal of various kinds (optical, colorimetric, fluorescence, impedance, etc.) generated differentially from the different chemical arrangements of bases on a DNA which may furnish specific molecular address for the recognition of biological entities. DNA-based sensors are very prominently used in diagnostics/detection purpose, be it disease detection, expression monitoring, transcription profiling, or DNA sequencing. In almost all DNA-based sensors, the detection is carried out through a mediating known sequence of a DNA molecule which detects target DNA that is otherwise present in the sample. There are various principles associated with such detection which may either involve the selective bonding of a base pair sequence of a DNA or an RNA to another similar molecule or molecules (better known as hybridization) or simple copying of the DNA or RNA molecules through an in vitro copying process similar to in vivo processes which keeps happening as cells grow and divide within living systems (better known as PCR). Detection can be carried out further by immobilizing concentrated molecules acting as probes over a small region or by simply trapping the biological constituents in one place from the bulk solution and generating an enhanced signal from this concentrated or trapped sample to enable sensitive detection. There are several techniques developed by researchers which will aid one or more steps of detection as briefed earlier as follows:

1. Dielectrophoretic capture of biological entities containing DNA molecules or molecules themselves.
2. PCR where copying of a specific sequence or sequences is carried out in vivo and detection is carried out simultaneously as the sample gets copied multiple times. Further, the types of phases where this can be carried out are the following:
   (a) Solid-phase PCR
   (b) Liquid-phase PCR with or without the real-time detection capabilities of the copying process
   (c) Droplet-based PCR, etc.
3. Electrophoresis wherein separation of various lengths is achieved by sieving molecules through gelatinous substances with highly porous networks.
4. Immobilization of molecules in a concentrated manner on a substrate which will perform capture and localization followed by tagging of a fluorophore molecule which may result in enabling DNA detection.

5. Sensing of the electrochemical impedance by using the strategy mentioned in step 4 above with a change of the optical label/tag to electrochemical label (e.g., Ferro-cyanide label)
6. Sensing the whole DNA molecule as such by looking at the impedance signal of the solution which contains DNA, etc.

Dielectrophoretic capture deals with manipulation of neutral particles while these particles are kept in varying field intensity. An electrical force is exerted on neutral particles of a certain dielectric constant immersed in a medium of a different dielectric constant particularly as the particle is guided into a non-uniform electric field. This concept can be used to pre-concentrate at a certain place neutrally charged particles and can be used to trap, separate, count, etc., while PCR deals with amplification of DNA to make it detectable. A lot of variants to the conventional well-based PCR system are developed for enhancing the processing rapidity and accuracy. The variants are developed by looking at microchip-based solutions for conducting PCR/real-time PCR (RT-PCR), solid-phase PCR and droplet-based PCR. This is mainly done to miniaturize sample volume so that the overall reaction becomes inexpensive while the limit of detection can be reduced and sensitivity of the system can be greatly improvised. Apart from these techniques, the basic hybridization techniques have been included in sensing/detection technique section. Among the various sensing techniques, the following are discussed in detail in this chapter:

(i) Electrophoresis.
(ii) Electrochemical impedance spectroscopy (EIS).
(iii) Colorimetric sensing.
(iv) Optical sensing.
(v) Inertial sensing.

Electrophoresis is a standard technique for sieving the molecules under the effect of electric field according to their size. The particles get arranged as per their size (larger molecules at the top and so) while the solution travels through the agarose gel which is connected to uniform electric field. This is also used as a confirmation test for conventional PCR. It is the most basic technique which uses dye to visualize the location. The colorimetric sensing and optical sensing can also be considered to be very conventional in nature. In the colorimetric sensing technique, a change in the wavelength is used for detection. In optical sensing technique, either fluorescence or overall sample absorption is used to perform detection. As colorimetric detection and optical detection involve expensive instrumentation, there is an emergent trend in utilization of some other non-optical/non-colorimetric routes like electrochemical impedance-based detection (popularly known as EIS) and inertial/mass-based detection. In impedance sensing route, the impedance (a combination of resistance/capacitance/inductance under alternating electric field) change of the solution containing the sample is observed so that the analyte can be detected. Both the electrical techniques have a niche among the contemporary processes as they are compatible with electronic systems and are easily integrable with

microelectromechanical systems. In inertial sensing approach as developed initially by IBM (Lang et al. 1999), a small array of microcantilevers are used with reference and signal measurements. The signal comes from deflection of the cantilevers owing to small surface stresses due to binding. There are other techniques apart from EIS techniques which are also deployed although not so frequently to perform biological detection. These include amperometric (change in current) and conductometric (change in conductivity) detection which are generally carried out in order to detect traces of chemical species, e.g., nickel oxide-based glucose sensor (Mu et al. 2011) and monitoring the condition of lubricating oil (Latif and Dickert 2011), etc., and generally may not be a good proposition for doing standalone DNA detection.

2 Principles of DNA-Based Biosensors

DNA-based biosensors deal with sensing of different biological analytes by carrying out identification of these analytes through the genetic route. A variety of analytes that are normally detected through these sensors can be purified DNA, RNA samples, other biological entities (e.g., viruses and microorganisms or spores), various drugs, various organic and inorganic particles, chemical elements, etc. The concept of detection in these sensors remains more or less same; the analyte is taken close to the sensory surface, and a chemical/biochemical change is initiated which results in a transduced signal which may be able to reveal information about the basic molecular DNA/RNA, etc. Interaction of the analyte with the sensory surface can be carried out through direct immobilization, adhesion, or partial hybridization to the surface. One of the easiest routes of direct detection of analytes like DNA/drug molecules or organic/inorganic nanoparticles happens through direct adhesion or capturing of the analyte on the substrate. Sometimes, it is even preferable to deploy a technique that may concentrate and accumulate the analyte over the sensory surface. A very effective technique that was developed by Pohl (1951) exists which is popularly called dielectrophoresis (DEP). The other way of accumulating a target sequence of DNA over a surface is to copy the target sequence in vitro through the PCR route while keeping the overall volumes for the PCR very less and enhancing the sensitivity of the system multifolds.

2.1 Dielectrophoretic (DEP) Capture

DEP is a particle manipulation technique in which an external force is exerted on otherwise neutrally charged particles as they are influenced by a of non-uniform electric field. The external force generated tends to alter the motion of these particles, and depending on the relative polarizability of these particles in reference to the medium in which they are immersed, they show different characteristic

behaviours. The limit to which particles are polarized depends on various factors like electrical field strength, frequency of the input voltage, the shape and size of particles, and the medium/particle/free space permittivity. The concept of DEP was shown long back (Pohl 1951) by Pohl and was computed from the Maxwell equation by the famous Clausius–Mossotti projections (Morgan et al. 2007). The magnitude of the DEP force that is felt by a particle in an electric field is given by Eq. 1,

$$F_{\mathrm{DEP}} = 2\pi r^3 \varepsilon_m \mathrm{Re}\left\{\frac{\varepsilon_p^* - \varepsilon_m^*}{\varepsilon_p^* + 2\varepsilon_m^*}\right\} \nabla |E_{\mathrm{rms}}|^2; \quad \varepsilon_i^* = \varepsilon_i - \frac{j\sigma_i}{2\pi f} \quad i = p, m \tag{1}$$

where r is the radius of neutral particle which experiences the DEP force; ε_p is the electrical permittivity of suspended particle; ε_m is the electrical permittivity of the medium in which the particle is suspended; ε_p^* is the complex permittivity of particle; ε_m^* is the complex permittivity of medium; $\left\{\frac{\varepsilon_p^* - \varepsilon_m^*}{\varepsilon_p^* + 2\varepsilon_m^*}\right\}$ is better known as the Clausius–Mossotti factor; E_{rms} is the root-mean-square value of electric field; σ_p is the conductivity of the particle; σ_m is the conductivity of the medium; and f is the frequency of the electric field. Clausius–Mossotti factor is a measure of the polarizability of particles and depends on particle permittivity and medium permittivity. DEP can be applied to a variety of purposes like particle capture, particle manipulation, particle sorting (depending on the size/type of the particles), etc. Depending upon the extent of polarizability, the particles are captured at different instances at different positions during their traverse across microfluidic chips.

Depending on the nature of influence of the external electric fields upon the capture behaviour of particles, DEP can be categorized into two different forms, viz., positive DEP and negative DEP. If the particles are captured in the direction of increasing field strength, it is regarded as positive DEP, and if particles are captured in the direction of diminuting electric fields, it is regarded as negative DEP. Figure 1 explains the effect of uniform and non-uniform external electric field on neutral particles crossing such field. Figure 1a depicts no movement behaviour of neutral particle under the effect of uniform field, while its position is altered in case of non-uniform field (Fig. 1b). Figure 1b shows the concept of negative and positive DEP effects. Since biological cells are mostly neutral, DEP finds wide application in manipulating cells that can be very useful for medical diagnostics, drug delivery, cell therapeutics, etc. DEP can also be classified based on the type of electrode that is deployed. It can be performed through metal electrodes (most common type of electrodes), insulating structures working as field splitters, liquid electrodes (Demierre et al. 2007), carbon electrodes (Jaramillo et al. 2010), light-induced electrodes (Hoeb et al. 2007), etc.

DEP has proved very effective in manipulating cells. In this light, use of DEP using pin and plate electrodes for separating dead and live yeast cells (Pohl and Hawk 1966) has been observed in great detail and it has further been shown that live cells get concentrated on the pin electrode while dead cells remain in the

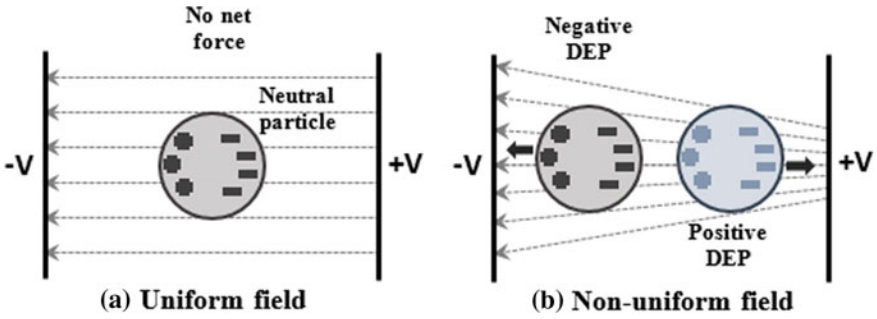

Fig. 1 Behaviour of particle under **a** uniform field; **b** non-uniform field: concept of DEP

solution. Manipulation of bacteria (*Bacillus globigii spores* and *Erwinia herbicola* bacteria) for concentrating and purifying samples (Miles et al. 1999) reduces the level of cross-contamination among samples that may otherwise induce through manual handling processes particularly within microfluidic chips. As compared to electrode-based DEP, electrodeless DEP also utilizes a relatively higher voltage to show capture/manipulation as two electrodes are placed at two extreme ends having symmetric/asymmetric insulator array in between. DEP-based manipulation/separation of cells and polystyrene beads has also been carried out (Saucedo-Espinosa et al. 2016) using insulating posts. The research has also elaborated how surface topology plays a significant role in the process of bacteria (*Escherichia coli*) capture on printed circuit board (PCB) with non-uniform FR4 zone in interelectrode gap (IEG) of copper interdigitated electrodes (IDEs), and it is shown that as compared to the planar surface, rough surface enhances capture efficiency as it adds advantage of both metal electrode-based DEP and insulating DEP (Bhatt et al. 2017).

DEP has also proven its worth in processing direct DNA apart from cells and bacteria. Even though DNA carries overall negative charge and possesses permanent dipole, it is observed that the DNA gets polarized by getting rotated around the major axis (Takashima 1966). DNA polarization is also specific to frequency range and is majorly dependent on the size of the strand. DNA has been shown to be rapidly concentrated over IDEs (Miles et al. 1999). While increasing the degree of miniaturization among the tool providing the non-homogenous electric fields, the input voltage requirement reduces substantially as a very high value of electric field can be achieved through a smaller voltage operating over electrodes spaced through smaller distances. This advantage has been used well while performing DEP capture on carbon nanotube electrodes (Tuukkanen et al. 2006). It has also been observed that carbon nanotube-based platforms are more effective than the lithographically prepared metallic electrodes with nanometric length scales. DNA with very low overall size has been successfully captured over carbon nanotube electrodes. Microarrays of platinum electrodes have been used for separating DNA and delivering drug particles with nanometric dimensions (Sonnenberg et al. 2012) from

blood cells in whole blood samples. It has been observed that both DNA molecules and nanoparticles undergo positive DEP and hence get accumulated in high electric fields while blood cells undergo negative DEP and get collected in the low field zones. A simple wash step introduced leads to the collection of DNA and nanoparticles in the above work from blood cells. In yet another work the DEP capture of DNA copied through a PCR process and labelled with microbeads is observed on castle-walled interdigitated microelectrodes (Kasahara et al. 2015). This paper has also studied well the concept of crossover frequency (frequency over which DEP behaviour changes) in manipulating single DNA molecules, and it is observed that positive DEP (capture in IEG) occurs below crossover frequencies while negative DEP (capture at electrodes) occurs above crossover frequency. The crossover frequency is further seen depending on the length of DNA molecules.

Various other microstructures are also used for capturing DNA. One of them is a nanostructured tip (Yeo et al. 2009). It was observed in this work that initially the DNA and other biological entities were attracted towards the nanotip with DEP and subsequently a size-specific capture was facilitated using capillary action to complete the whole specific capture process. Electrodeless traps are also used to trap and hence concentrate single- as well as double-stranded DNA molecules (Chou et al. 2002). It was observed that DEP force increases rapidly with increase in the size of the DNA strand and additionally DNA is seen to respond well in audio frequency range.

2.2 Polymerase Chain Reaction

PCR is DNA copying/amplification technique in which multiplication of DNA takes place in a particular environment. PCR is carried out in solution phase which contains DNA that is copied/multiplied through PCR technique (using a mix which comprises of various deoxy nucleotide triphosphates (dNTPs) like adenine (A), thymine (T), cytosine (C) and guanine (G); buffer solution; Mg^{2+} ions and *Taq* polymerase) and primers. The mix is thermally cycled across three different temperatures so that the target DNA can copied. The various steps of the thermal cycle include a 94–96 °C heating step for a relatively long time (5 min or so) for activating the *Taq* polymerase enzyme followed by a denaturation step (carried out by heating the mix at 95 °C for 30 s), in which double-stranded DNA (dsDNA) gets unzipped into two single-stranded DNA molecules (ssDNA). This is followed by another thermal step better known as annealing where the sample is cooled and maintained at 55 °C for 45 s, where binding of the primer from the solution to the 3' end of the ssDNA takes place. The primer starts binding from alternate ends of both single strands obtained in the last step. Thus, the primers are really complementary to the end sequences of the molecular sequence being identified. The identified sequence is a part of whole DNA molecule and corresponds to defining the molecular address of a biological entity where it is uniquely present, and such a sequence may not be present is another biological entity. In fact, such sequences are

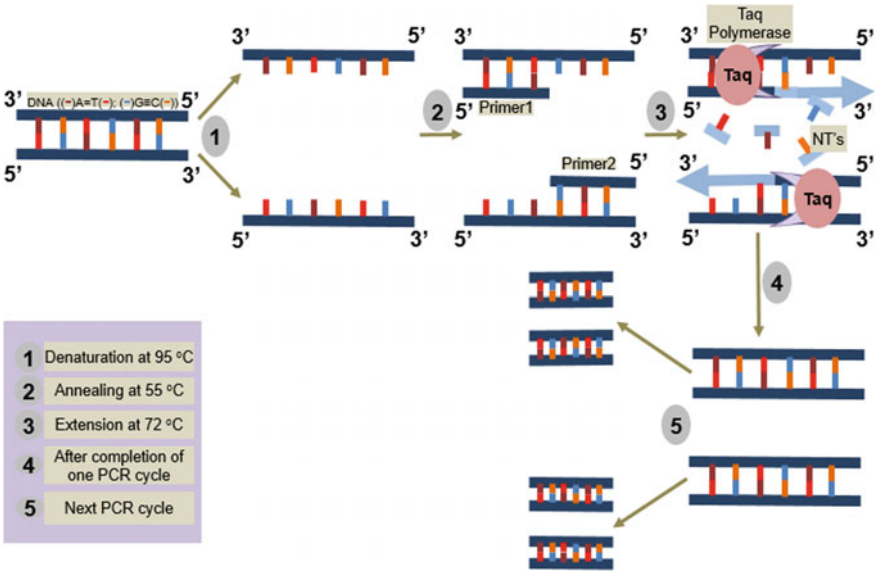

Fig. 2 PCR steps

recognized from the fact that each DNA will be responsible within the host cell to transcribe and translate protein structures and proteins provide functionality and response to a large extent to the living cells and there may a functionality or response associated uniquely with each cell. In this way, PCR continues from 5′ to 3′ direction. Then, the another third step is followed in sequence where the mix is reheated back to 72 °C and held for 90 s corresponding to which an extension in the primer hybridized DNA takes place through action of the initiated *Taq* enzyme. The *Taq* enzyme is highly efficacious and performs the copying action with high accuracy making one mistake in about 10^9 bases that are being sutured to the growing strands of the DNA molecule. The PCR process in this way is a highly stringent process and relatively error-free. Finally, the mix after repeating many thermal cycles as detailed above is cooled at 4 °C for some time and the whole process is evaluated using a separate step of gel electrophoresis. Figure 2 shows the major steps involved in carrying out the thermal cycling related to the PCR process (NT's denotes nucleotides in Fig. 2). The number of copies of the target sequence of the template DNA at the end of number of such thermal cycles is estimated by a product of the initial concentration of the template DNA with 2^n, (where n is the number of cycles). If RNA is subjected to the same process, the RNA template first undergoes a reverse transcription to get the corresponding double-stranded DNA sequence and then the usual thermal cycle is applied to copy the dsDNA obtained from the RNA (Gouvea et al. 1990). As such this process is better known as reverse transcriptase PCR. The RNA/DNA sample of a particular gene can also be extracted directly from the analyte sample for carrying out PCR. The PCR although is a liquid-state reaction carrying out the molecular templating; an copying process is by

itself unable to provide an update on the amplification and thus needs to have a coupled step to generate a transduced signal as the process goes on so that a readable signature generated through the transduced signal can give a fair idea for successfully carrying out the amplification step. The way of looking at the success of the amplification process is to resolve the amplified product using a gelatinous material (process better known as electrophoresis) which may have achieved a certain peak concentration and which may have been cleaved and sized during the PCR process to a unique size as determined by the primer sequences (both forward and reverse primers).

Thus, the normal PCR process is not self-sufficient if operated standalone to perform identification and detection. One way of identifying the sequence DNA is to design a known sequence of a primer assuming that the primer molecules will bind to the target sequence if the target is really present in the sample. So, if we know in advance the sequence that we may have to look for as we are looking for a specific molecular address related to a biological entity (remember each entity has its own unique molecular address), then we may design the primers in accordance and the success of the amplification process determines that the target was present. The different ways of knowing the success of the amplification process are through electrophoresis, q-PCR (using TAQ man assays, molecular beacons or fluorescent dyes).

For carrying out the entire PCR process, thermal cyclers are commercially available in markets, where amplification is performed over many different wells using multiple samples. Conventional cyclers though high throughput have additional complexity in terms of poor heat transfer and extended ramping up/down times, and therefore, if the same were to be done over a thin film orientation would prove out to be a much rapid alternative. Additionally, the time taken to complete the whole process is high as well as the final confirmation is done through gel electrophoresis at the end only which is a cumbersome task in itself. So keeping all this in mind, the shortcomings are eliminated by producing extremely thin chambers (amounting to a few hundred microns width) and carrying out rapid thermal cycling of a lesser amount of thermal mass having lower thermal inertia. In this case, generally fluorescence-based detection is implemented in PCR for evaluating the progress of PCR in real time and the process is better known as RT-PCR. RT-PCR focuses on studying fluorescence level of PCR sample after every amplification cycle, mainly in case when amplification is done on chip rather than well. Microchips with characteristics of either confining the PCR mix or continuously flowing it have been designed, fabricated (using silicon technology) and tested. Continuous flow systems are particularly fast due to their sufficiency to perform thermal cycling without any ramping up or down of the temperature. Such systems are based on flowing of solution drops over three differentially heated zones maintained at different temperatures and as such the rapidity of oscillations of the droplet over the varied thermal zones determines the rapidity of the amplification process. PCR/RT-PCR is performed on large scale involving miniscule volumes of reagents so that huge reaction data can be collected in real time in step-by-step manner and recorded to maintain the reaction statistics of several samples consistently.

Various in-house manufacturing techniques have been utilized to produce inexpensive microfluidic chips for performing DNA amplification (Bhattacharya et al. 2007). A silicon base with printed platinum heaters is utilized to carry out PCR over an intermediary spin- on glass-coated layer irreversibly bonded to another replicated polydimethylsiloxane (PDMS) chamber with inlet and outlet channels. A top-mounted thermocouple is used to acquire thermal data of the chamber, and an electronic instrumentation developed is utilized to rapid heat/cool the chamber. Figure 3 shows the assembled chip for carrying out PCR. The chip has further shown little or no non-specific adhesion of DNA strands during the PCR process enabling the microchip to perform amplification in very lean template mixtures going up to a few femtograms per microlitres. The PCR products extracted at the end of the thermal cycling process are further run through gel for electrophoresis-based identification of the molecular length of amplified sample [details of electrophoresis given later].

The chip fabrication process is further extended towards developing on chip systems for carrying out capture of bacteria (*Listeria monocytogenes* V7) and subsequent PCR using silicon-glass platform having channels, chamber and electrodes with the whole assay mounted over a printed circuit board (PCB) (Bhattacharya et al. 2008). The PCB is enabled with a set of embedded heaters and the instrumentation is realized by assembling a set of programmable power supplies and digital millimetres which can sense the temperature varying resistivity of a thin platinum film printed over the silicon substrate in the microchip. Both DEP-based pre-concentration of the inflowing microorganisms and the PCR process are performed in the same microchip to achieve a higher detection efficiency/detection limit.

Figure 4 shows the basic schematic of the designed chip. This chip is designed in a way to comprise of two chambers, one for DEP-based diversion and second for carrying out PCR by rapid thermal cycling. This system detects the amplification through a mapping of the products of the PCR by means of fluorescent labels which

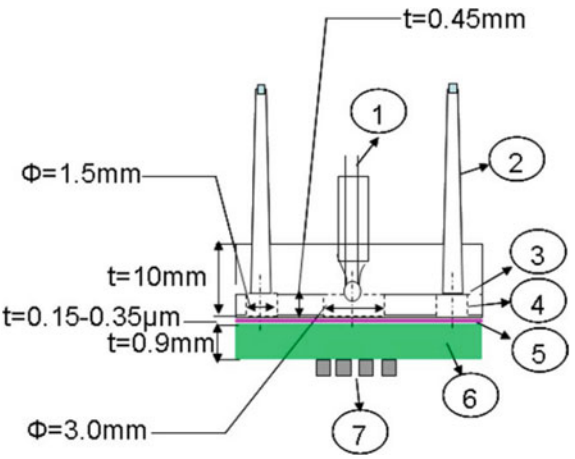

Fig. 3 Schematic of the silicon PDMS cassette. (1) glass-housed thermocouple, (2) epoxied inlet/outlet ports, (3) PDMS channels, (4) inlet/outlet reservoirs, (5) SOG layer, (6) thermally oxidized silicon wafer, (7) heaters. Reprinted with permission from Bhattacharya et al. (2007)

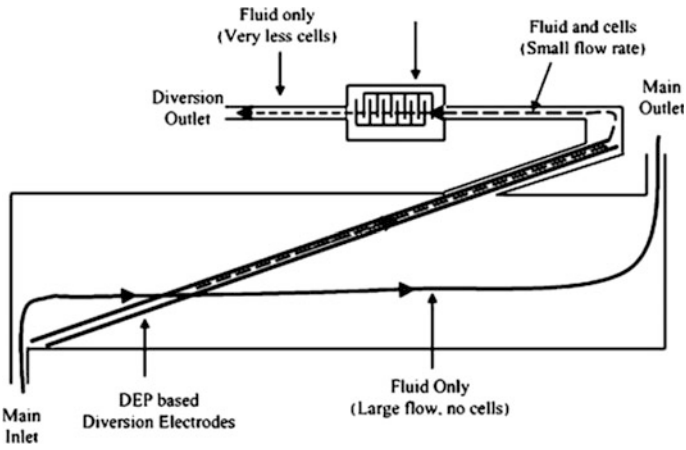

Fig. 4 Principle of operation of the DEP-based diversion and capture of cells. Reprinted with permission from Bhattacharya et al. (2008)

are intercalated into the DNA structure as the amplification is carried out. The dye SYBR green is utilized for this intercalation. The fluorescent signal is investigated through an epi-fluorescence microscope with a solid-state photomultiplier tube (PMT) and through acquired data coming out of the PMT module. Fluorescence increases first linearly due to the diffusional limitations towards the beginning of the thermal cycle and then exponentially as the molecules are able to migrate into every corner of the chamber, thus making the mix homogenous followed by a plateaued growth due to the fall in concentrations of the primer. The low limit of detection is also achieved through simultaneously sorting, concentrating and replicating lean samples of microorganisms (Nayak et al. 2013). Figure 5 presents the plots depicting fluorescence increase during the RT-PCR of normal cells at different number of cycles corresponding to different starting microorganism concentrations in multiple runs in this study. The high sensitivity is further assured through another antibody-based recognition step in a separate work where the DEP is carried out on antibody-/nanoparticle-mediated capture process from the solution phase prior to PCR.

In order to increase the sensitivity of the detection process, DEP and PCR combination is again used for first removing PCR inhibitors and carrying out PCR at higher efficiency (Perch-Nielsen et al. 2003). PCR inhibitors can be removed in various conventional ways like filtration and centrifugation, but with DEP, the main advantage is miniscule manual intervention which helps prevent sample cross-contamination. Separation of haemoglobin and heparin (which act as inhibitors) from whole blood samples has been carried out with DEP to leave only cells behind for replication helping in increasing PCR efficiency. Different methods for controlling thermal cycling in PCR are also proposed. One of them is by using Joule heating effect (Hu et al. 2006). Joule heating effect can be generated in the electro-kinetically driven microfluidic channels by making current to flow through

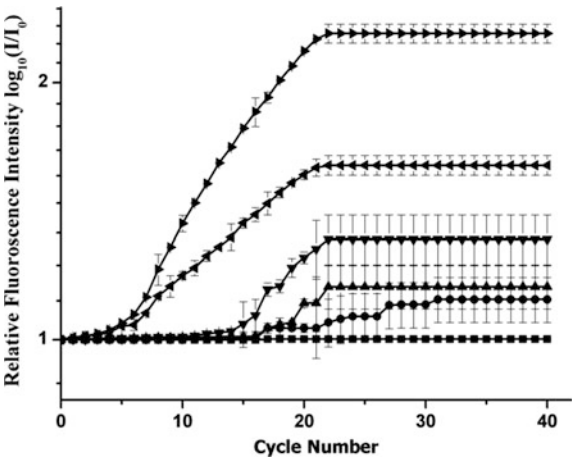

Fig. 5 Plots depicting the trend in fluorescence increase during RT-PCR with time for normal cells black circle—10^2cfu/mL; black diamond suit—10^3 cfu/mL; black up-pointing triangle—10^4 cfu/mL; black down-pointing triangle—10^7 cfu/mL; black right-pointing pointer—10^9 cfu/mL; black square—control. Reprinted with permission from Nayak et al. (2013)

the buffer solution which contains the PCR mix. It removes the need of using external heating component in the system and gets rid of the huge thermal inertia that is being offered by the thermal mass of the chip. This type of chip has successfully shown the amplification of DNA fragment from *E. coli* strains. Similar to RT-PCR or q-PCR, there are also some modifications/advancements offered by changing the environment in which the PCR is being carried out or in the terms of how various constituents of PCR are handled, either as that of the normal liquid PCR or in some alternate way. These modifications are the following:

(i) Solid-phase PCR.
(ii) Droplet-based PCR.

(i) Solid-Phase PCR

Solid-phase (SP) PCR is carried out with either primer or DNA immobilized on a substrate surface instead of being in solution state along with the other reactants. Various methods to attach primers through the 5' end on glass substrates are proposed for the SP-PCR technique (Adessi et al. 2000). It has been observed that for glass substrates, the best immobilization method is obtained through 5′-thiol-modified primers attached to amino-silanised glass surfaces. The reaction can be detected through fluorescent tags or radiolabeling. In this case, as primers are attached to the substrate, two types of amplification occur: one which takes place on the interface between the solution and the glass and the other one on the surface. Initially, the primer hybridization takes place at the surface-attached primers and this is followed by the floating DNA getting attached to this surface layer and gets further multiplied and after that requisite phase gets back to the solution once again. Such phenomena are better known as interfacial amplification. Additionally, the strand for which amplification is completed at the immobilized primer end also takes part in the next amplification cycle after being attached to the surface immobilized primers (remember, the PCR process is about hybridization of a

forward and reverse primers). This near surface multiplication is better known as surface amplification. The single point mutation of *Harvey RAS* gene has also been detected through microring-based SP-PCR and isothermal recombinase polymerase multiplication (Shin et al. 2013). In this work, the primers were attached on the surface via amine modification and the detection was carried out through optical wavelength shift in a silicon-fabricated microring resonator. The optical ring resonator is an optical tool where the surface immobilization of molecules can be transduced into a change in wavelength by light–matter interaction while the scanning beam is being confined into a resonator. The sensitivity in this case was recorded to be around 100 times more than conventional PCR. Another variety of SP-PCR, in which the target DNA from the sample is attached to a membrane after lysis of the containing cells, have also shown better results as compared to those of the culture-based method for detection particularly for airborne microorganisms (example in detection of *E. coli* DH1) (Alvarez et al. 1994). In this case, cell lysis and immobilization of lysed DNA on a membrane are done and subsequently the replication is done on the immobilized lysates using PCR.

(ii) **Droplet-based PCR**

Further extending continuous flow PCR concepts, the droplet-based PCR is executed within microchips. In case of on-chip PCR, the cross-contamination problem (through adsorption of sample on the chip surface) can ruin the efficacy of the PCR process. As it may be a good idea to explore multiple sample amplification on the same microchip, the reusability of the same chip can create cross-contamination between alternate runs and may increase error rates. So keeping this fact in mind, a continuous flow system is designed which may take care of cross-contamination. There has also been the design of wash steps as reported by some groups to explore the multiple usability of the same microchip. The continuous droplet-based PCR is designed by keeping the water/oil immiscibility in mind where a water-based PCR solution is inserted in a flowing stream of oil drop by drop and the drops of PCR mix are further circulated across of different zones maintained at different temperatures without touching the microchip surface. This way the amplification takes place in the particular droplet only leaving the microchip surface uncontaminated and clean. Various working conditions for droplet-based PCR are optimized in term of chip design requirement, thermal mass, thermal resistance, and flow rate needed (Mohr et al. 2007). Figure 6 shows basic concept of droplet-based PCR and one proposed design.

It is observed that low thermal mass for carrier fluid is a desirable condition to achieve heating/cooling of the droplet in a minimum time. A proper dilution to have optimum reaction contents is needed and a desirable flow rate is needed to be maintained uniformly to attain good results. Droplet-based PCR with oscillating flows is also studied (Wang et al. 2005). A silicon-based microchip manufactured in a way so that it has three zones kept at different temperatures as needed by the PCR process for amplification. Single droplet is flown over these in an oscillatory manner over all three zones. Slab gel electrophoresis methods are used to identify the results in one of the shortest times achieved for amplification of samples. For a

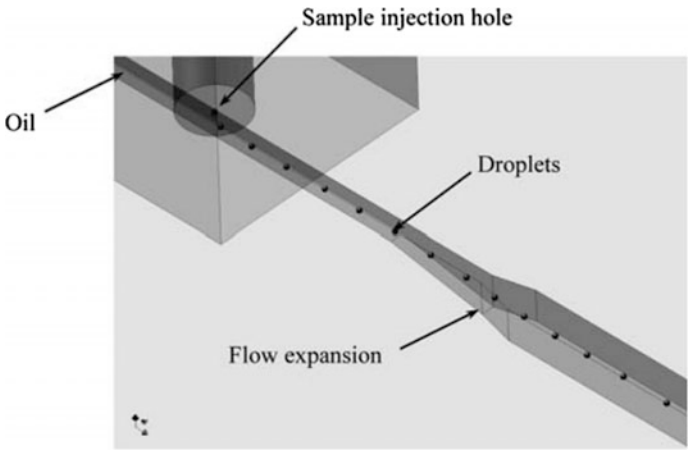

Fig. 6 Concept of droplet-based PCR. Reprinted with permission from Mohr et al. (2007)

similar method, a different technique for transporting the reaction mixture through three different temperature zones is also observed wherein hydrophilic magnetic beads are mixed with the PCR droplet and the movement of droplet is controlled thereby through a magnetic field setup at the bottom of the tray-type reactor (Ohashi et al. 2007).

3 Sensing and Detection Techniques Involved in DNA-Based Biosensors

When analyte becomes detectable in some way, it has to be sensed via multiple strategies. These sensing/detection routes can be varied depending upon the conditions of the system. This section discusses various techniques for carrying out sensing/detection like electrophoresis, EIS, colorimetric sensing, optical sensing, inertial sensing, etc.

3.1 Electrophoresis

Electrophoresis is a detection technique in which particles move under the effect of uniform electric field and the particles are separated on the basis of their respective size. Depending on the field strength, the particles move at some speed towards oppositely charged electrodes, smaller particles travelling at higher speed and vice versa. Electrophoresis can be divided in three categories depending upon the

medium through which particles are passed, and these are gel electrophoresis, surface electrophoresis and capillary electrophoresis.

Gel electrophoresis uses porous gelatinous structure for separating the particles. The gel structure used is agarose (polysaccharide polymer material), with two extreme ends connected to oppositely charged electrodes. The pore size is usually very small that only particles of size of the order of DNA can be passed through this gel; hence, it is mainly used for separating differently sized DNA (Schwartz and Cantor 1984). Electrophoresis is most widely used method for detecting PCR products since long. It works like a confirmation test for PCR. If PCR products contain fluorophore attached to the strands, the total number of molecules present can also be estimated correctly through electrophoresis by just counting. Electrophoresis is also helpful in detecting single base mismatch (Ganguly et al. 1993). Gel electrophoresis is also used for detecting DNA polymorphism (Orita et al. 1989) which is done by digesting DNA through restricting endonucleases and denaturing it in alkaline solution and consecutive electrophoresis.

While separating DNA through gel electrophoresis, size becomes a critical constraint as it is very tough to separate DNA sizes of above than 10 kilo base pair. Hence in such cases, a modified technique for fractionation of DNA is proposed, where DNA travels on the surface rather than through the gel block as in case of gel electrophoresis. This technique works on the similar principle as that of gel electrophoresis. The surface on which DNA travels can be of different types, one being PDMS with channel fabricated on the top through LASER machining (Ghosh et al. 2011). Figure 7 shows the schematic of one such chip fabricated to carry out surface electrophoresis.

In capillary electrophoresis technique, single capillary is used for making DNA to travel from one end to the other. Microchips comprising of capillary have also been fabricated through micromachining process to separate fluorescein and calcein (Harrison et al. 1992) on planar glass substrate.

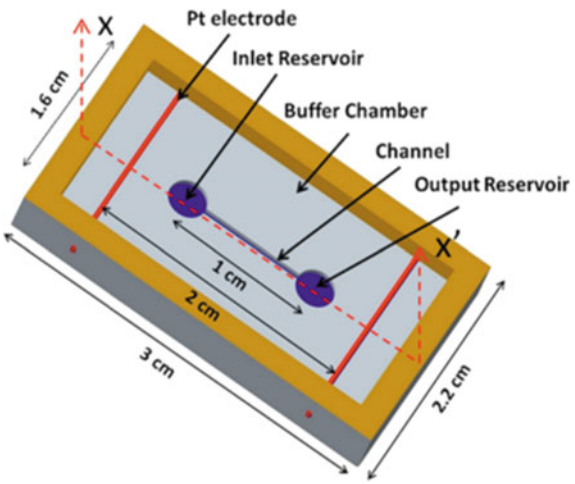

Fig. 7 Schematic of chip to carry out surface electrophoresis (dimensions: reservoirs diameter = 3 mm, width of channel = 400 μm, depth of features = 250 μm). Reprinted with permission from Ghosh et al. (2011)

3.2 Electrochemical Impedance Spectroscopy

EIS is an analysis technique which is used to detect the presence of genes through a change in the overall AC impedance of the medium containing the genes. It has been found that the charge transport phenomena within a solution get significantly altered due to the presence of DNA in this medium. Various DNA lengths further may have different signature impedances. This behaviour can be studied as a electrochemical reaction at the electrode/electrolyte interface, which can be further elaborated using an electrical equivalent circuit (EEC) model, as proposed by Randles (1952). The concept of ion transport in the electrode/electrolyte interface and corresponding equivalent circuit have been illustrated in Fig. 8.

In this figure, the abbreviation IHP expresses inner Helmholtz plane and the abbreviation OHP expresses outer Helmholtz plane. The figure explains the concept of formation of a diffusion layer when the interaction of electrodes occurs while the electrode comes in contact with the electrolyte solution. In this condition, the current level is affected by various factors contributing to the overall ion transport. These components will ultimately lead to the change of impedance. One component is a faradaic component (due to electron transfer across the IHP/OHP interface during the reaction as the electron transfer takes place by crossing over the activation barrier), which determines the polarization resistance, R_p, and solution resistance, R_s. Other component is the non-faradaic part, which comprises of the double-layer capacitor, C_d (due to charging), and gets affected by a change in dielectric constant or thickness of the double layer (Saby et al. 1993). The other non-faradaic part is the Warburg impedance Z_w (due to mass transport of reactant and product across the dual layer).

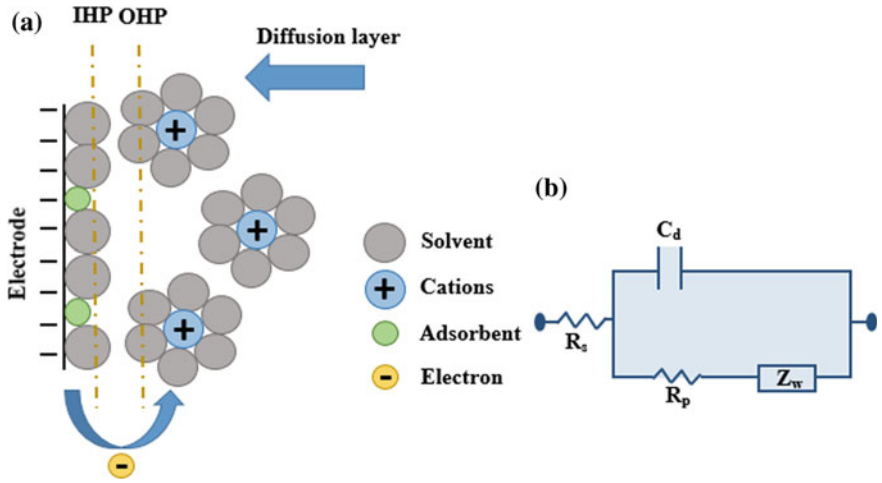

Fig. 8 **a** Interaction of electrode with electrolyte solution. Concept of ion transport. **b** An idealized Randles electrical equivalent circuit for the interface

Identification using EIS technique mainly focuses on identification of molecules with or without the labels attached on the molecule. Measurement techniques have several other aspects, either impedance of molecules can be directly measured while floating in solution or can be done by immobilization on a substrate with appropriate bonding method. In either case, the mechanism is same, but the number of prior steps is different. Various researchers have worked in this field of impedance measurement of molecules immobilised on the substrate surface. Various antibodies, antigens, DNA/proteins, and heavy metal ions are detected by immobilising them on electrode surfaces modified with self-assembled monolayers (SAM) (Berggren et al. 2001). In this assembly, the capacitive sensing has been used for detecting molecules up to a detection limit of 10^{-15} M. In the same context, various bacteria like *E. coli* and *Salmonella typhimurium* are detected on gold IDEs functionalised by biotinylated polyclonal anti-*E. coli* antibodies to neutrAvidin-coated surfaces of the electrode (Laczka et al. 2008). Among the most significant results in this case, a decrease in capacitance was observed due to a decrease in effective dielectric constant of the interface. Application of impedance spectroscopy for detection of *Listeria innocua/monocytogenes* and *E. coli* cells has been elaborated by some groups (Gómez et al. 2002). Impedance measurements are made with the help of micropatterned platinum IDEs on the crystalline silicon substrates. Significant differences in the signal for live and dead cells for even the small order of range 0–20 (limit of detection limit: 1–10 cells/nL) have been observed. Two kinds of suspension media have been used, one where there is lesser ionic content (Tris-Gly-Dext) and the other with high ionic content (LB broth). Significant differences in the impedance have been observed in case of *L. innocua* and *E. coli* suspended in Tris-Gly-Dext for number of cells of the order of 100. No difference in sensitivity has been observed in the two suspension mediums, but LB broth was found to be the preferred medium in two as it did not stress the cells. Impedance curves obtained were examined to show different behaviour for the live and dead cells in this work.

Interfacial interactions between immobilized DNA probes and DNA-specific sequence binding drugs using impedance measurement techniques based on the charge transfer kinetics of the label $[Fe(CN)_6]^{3-/4-}$ were studied (Li et al. 2005). In this both the immobilization of DNA and the DNA drug interaction on the surface of an electrode altered the overall capacitance and interfacial electron resistance and thus removed charge transfer kinetics by preventing redox species from approaching the electrode. A gold nanoparticle-deposited surface has shown higher sensitivity, higher detection limit and thus higher impedance increase after hybridization as compared to pure gold substrates. Sensing and analysis of Tay–Sachs mutants is studied using impedance spectroscopy in sensing and analysis (Bardea et al. 1999) using gold electrodes used for immobilization. The assembly comprised of three components. Initially, a strand of oligonucleotide (with thiophosphate tags) with some part complementary to Tay-Sachs mutant is immobilized in which Tay–Sachs mutant is hybridized, which is further immobilized with another biotinylated oligonucleotide. Finally, avidin is immobilized on this assembly. Nyquist plot showed that the impedance value increases with each

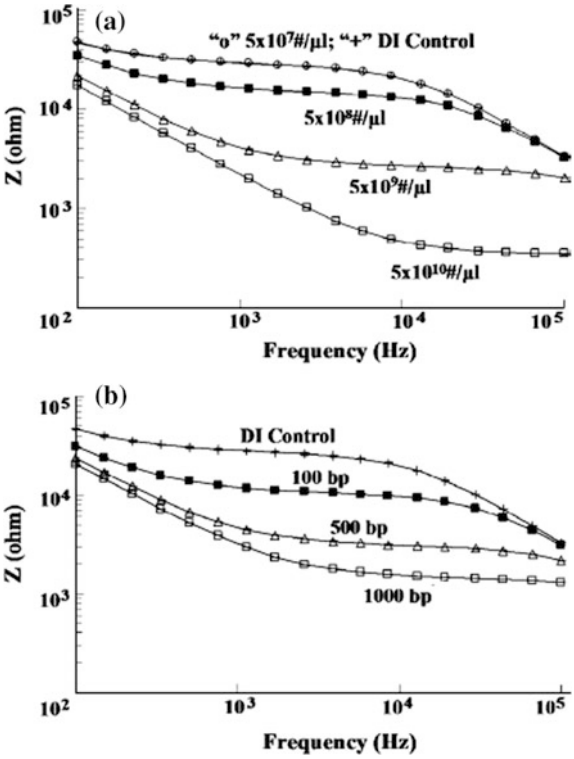

Fig. 9 Impedance magnitude as a function of frequency for a variation in concentration of 400 bp dsDNA molecule and b variation in size of dsDNA where concentration of each molecule was 10^9 molecules/µL. Reprinted with permission from Liu et al. (2008)

immobilization step and reaches a maximum with the addition of the avidin. This identification is specific as no impedance increase was seen with any other combination of the attaching molecules. The study dealing with change in impedance in fluids to examine the effect of length and concentration of free floating dsDNA molecules (Liu et al. 2008) has also been done. Figure 9 depicts the effect of variation of concentration and number of base pair on impedance change.

DNA floating in the fluid generates electrical response under the effect of applied electrical fields due to formation and relaxation of the induced dipole moment. The impedance magnitude was found to decrease as the concentration of dsDNA was increased. Additionally, the impedance magnitude was found to decrease as the length of dsDNA molecule was increased. DNA-based detection using PCR/DEP sensed by impedance measurement has also been extensively carried out (Nakano et al. 2014). In this, the PCR product was immobilized on microbeads and these microbeads were captured on the IDEs, which was sensed by a change in the overall impedance of the system. Microbead-tagged DNA strands have shown positive DEP pattern, which was negative DEP in case of only microbeads. Impedance-based system has shown good sensitivity in a manner to differentiate between various concentrations.

3.3 Colorimetric Sensing

Colorimetric sensing is the most common type of sensing technique in which detection is done through a colour change as a result of change of wavelength of the DNA containing solution. Colour change can be either through direct adhesion or some kind of hybridization. The colour-based detection generally deals with interaction of nanoparticles with DNA in some form.

Colorimetric detection is also observed using hybridization chain reaction (HCR). Two hairpin auxiliary ssDNA probes as immobilized on gold nanoparticles let the gold nanoparticle solutions remain stabilized in a manner so that they do not form aggregates as the salt concentration is increased. But as soon as the target DNA hybridizes with the auxiliary hair pin auxiliary probe, the gold nanoparticles start to aggregate under the effect of similar salt concentrations changing the colour from red to purple because of size effect (Liu et al. 2013). Figure 10a shows a change in colour when hybridization was carried out. It shows how colour varies with different concentrations of (0–6.0 nM) target DNA. Figure 10b shows that with an increase in the DNA constituent in the gold solution the absorbance decreases with an increase in the concentration.

Sensitive DNA detection is also carried out using gold nanoparticles along with asymmetric PCR (Deng et al. 2012). In this technique, selective hybridization takes place on the DNA attached to gold nanoparticles, when correct target DNA is put in

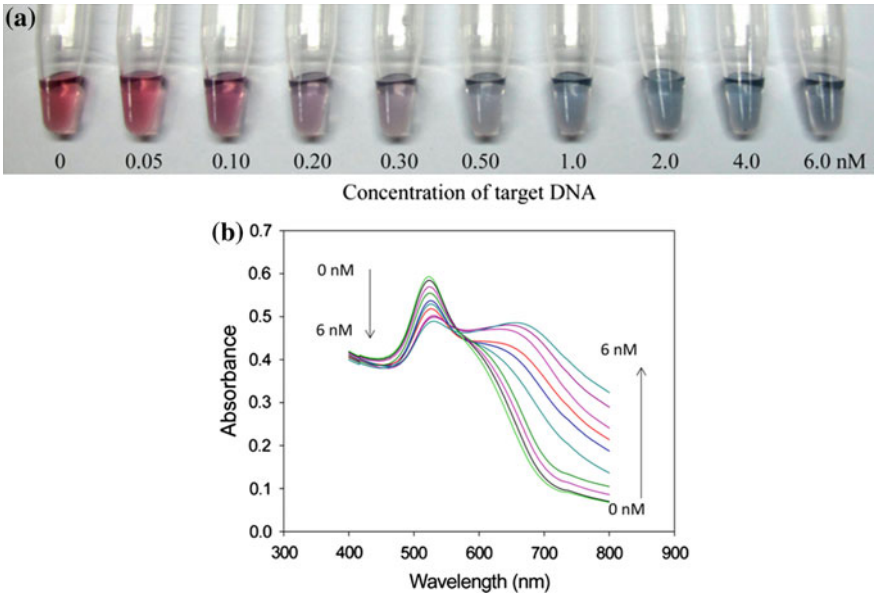

Fig. 10 Photograph showing **a** colorimetric responses of detection system in the presence of various concentrations of target DNA; **b** corresponding absorbance plot. Reprinted with permission from Liu et al. (2013)

the solution, which further aggregates the gold solution and changes its colour from ruby red to purplish blue in the presence of the salt. This aggregation is usually highly specific in nature. Some internally modified DNA sequences incorporated with strands of dATP and dCTP nucleotides using standard NIAK-translation protocol with labelled biotin are also used to test the target DNA (Gebeyehu et al. 1981). It was seen to get detected by streptavidin and calf intestinal alkaline phosphate conjugates in Southern blot of mammalian DNA. Standard colour scheme has been devised to detect the solution concentration in different aspects. DNA-gold nanoparticle conjugated systems can also be used further to detect various ions like mercury (Lee et al. 2007). This is a temperature controlled process and additionally it's an enzyme free process. Depending upon the concentration of the Hg^{2+} ions, the colour change was observed. The Hg^{2+} ions are directly immobilized on the DNA-gold nanoparticle assembly, which is an easy and affordable route of detection. This technique of detecting ions on DNA-gold nanoparticle hybrids can also be used for other ions like silver. These all protocols deal with functionalising gold nanoparticle with some probe DNA in a manner so as to detect the target DNA. Single-strand probe DNA, unmodified gold nanoparticle and water soluble positively charged conjugated polyelectrolyte combinations have been generalized to produce a universal biosensor for detecting various targets like proteins, DNA and small molecules like ions. (Xia et al. 2010). This universal sensor is based on the mechanism of conjugated polyelectrolyte to prevent ability of ssDNA to avoid gold nanoparticle aggregation which is not the case in case of dsDNA. These modification-based techniques have been further simplified by removing the need of immobilizing probe DNA on the nanoparticle surface. Rather direct adhesion of target ssDNA or dsDNA on the gold nanoparticle through electrostatic means has also shown different colour change in the solution showing aggregation (Li and Rothberg 2004). This colour-based detection has shown temperature dependence. Hybridization conditions are different for different type of strands which are to be optimized separately.

3.4 Optical Sensing

Optical sensing needs sophisticated instruments because of the accuracy needs in recording optical data. Therefore the instrumentation deployed should be critically calibrated for better results. In case of optical sensing, the preliminary sensing mechanism is a change in optical properties due to analyte/analyte interaction in the presence of a biocatalyst enabling the sensing to be carried out (Bhattacharya et al. 2007). These optical properties can be changes in fluorescence, reflectance (wavelength/intensity), UV-Vis absorption, chemiluminescence and so on.

Change in fluorescence is a key element for carrying out detection in optical sensing. For sensing of DEP captured molecules, the major sensing technique still remains fluorescence-based sensing. DNA/cells are stained with fluorescent dyes like Acridine Orange which is excited through a specific wavelength (≈502 nm).

And while doing PCR the SYBR green dye is used which shares a similar visibility condition. Various authors have worked with fluorescence-based detection for characterizing the DEP capture process (Saucedo-Espinosa et al. 2016; Bhatt et al. 2017; Tuukkanen et al. 2006; Sonnenberg et al. 2012) and PCR (Kasahara et al. 2015; Bhattacharya et al. 2008; Nayak et al. 2013; Perch-Nielsen et al. 2003). Figure 5 shows the fluorescence intensity increase corresponding to a RT-PCR process with respect to carrying out of the different cycles. It is observed that initially the fluorescence increase is linear and then exponential followed by plateauing for reasons mentioned earlier.

TaqMan probes are also used for rapidly detecting PCR via fluorescence route as TaqMan probe consists of covalently bonded fluorophore at 5′ end and quencher at 3′ end of primer and produces fluorescence at the annealing step in PCR. Quencher restricts fluorophore from producing fluorescence when is present in proximity but during annealing *Taq* polymerase breaks bond between fluorophore and primer and thus gets released to produce fluorescence in a manner to detect the correct bonding. TaqMan assay helps in detection of viruses like West Nile from clinical samples (Lanciotti et al. 2000). Apart from TaqMan probe, molecular beacons also help in detecting PCR product through fluorescence route, like *Adinovirus* (Poddar 1999) amplification has been studied through this route. Apart from fluorescence-based detection, other optical sensing techniques are also devised. SP-PCR techniques based on microring-based silicon devices combining recombinase polymerase amplification has been devised to identify single point mutation of *Harvey RAS*. In this the identification has been done through measurement of optical wavelength shifting in a microring resonator (Shin et al. 2013). Figure 11 shows the shift in resonant wavelength for amplification as compared to the control samples. It can be clearly observed from the figure that the resonant frequency shift is more prominent as time progresses.

Nanopore-optofluidic chip has been characterized for detection of ssDNA using patch clamp technology (Liu et al. 2015). Optical signals generated while passing

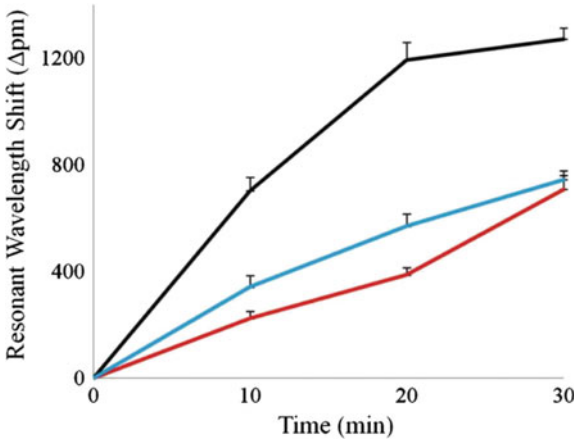

Fig. 11 Resonance wavelength shift shows the results of the amplification of HRAS gene containing 5 ng/μl of human genomic DNA (black) in the ISAD device. Negative controls; (I) distilled water (red), (II) rat genomic DNA from INS-1 cells (light blue) instead of human genomic DNA. Reprinted with permission from Shin et al. (2013)

DNA through nanopores have been further verified by electrical measurement taken consequently. Fluorescent intensity changes for DNA at different positions is plotted and is compared with the corresponding electrical response.

Optical fibres are also heavily used for detecting DNA. These fibres are used as optofluidic devices in which DNA detection is carried out by measuring the shift in reflected Infrared light wavelength (Bertucci et al. 2015). In this the optical fibre containing microchannel and Bragg grating additionally functionalized with peptide nucleic acid (PNA) specific to the gene being detected is used for DNA detection.

3.5 *Inertial Sensing*

Inertial or mass-based sensing is a mechanical sensing platform. As mechanical loads are applied on thin overhanging structures there is a deflection; the magnitude of which can be used to quantitate the force applied. A similar concept is followed while performing inertial sensing. The hanging structures could be vertically growing nano/microstructures or cantilevers. The size scale of micro or nano is particularly explored to perform high sensitivity detection of miniscule targets particularly as the inertial loads of such structures are also miniscule and does not create noise while sensing of deflection is carried out. As some force/load is applied on the cantilever, it deflects and the limit of deflection can be quantitated considering the mathematical formulation as below. The cantilever deflection, □ can approximated using the Eq. 2 (Sader 2001):

$$\delta \cong \frac{3(1-v)L^2}{Et^2}(\Delta\sigma_1 - \Delta\sigma_2) \tag{2}$$

where E is the Young's modulus; v is the Poisson's ratio; t is the thickness; L is the length of beam and $(\Delta\sigma_1 - \Delta\sigma_2)$ is the differential surface stress. Hence while working with the cantilevers, either defection or the resonant frequency with which cantilever vibrates becomes measure for detection. Since Atomic Force Microscopy (AFM) (Binnig and Quate 1986) has been in market, cantilevers have evolved as one of the major biosensors. As in AFM, a tip is used to indent the sample and corresponding force between tip and sample is measured by measuring deflection in tip or change in frequency at which tip vibrates. Hence the frequency at which cantilever vibrates completely depends on the mass/load/force which is exerted on the cantilever. Shift of cantilever resonant frequency (measurements are carried out in a dynamic mode (vibrating cantilevers) is considered in many ways. A specific DNA sequence can be detected by hybridizing it on the capture DNA which is further immobilized by the probe DNA immobilized on the gold nanoparticle (Su et al. 2003). Binding event tends to change the resonating frequency of cantilever and this detection strategy can detect very low concentrations as weight of cantilevers goes down substantially. This platform also provides facility of detecting various DNA by immobilizing various capture DNA on the cantilevers and

comparing the resonating frequency of individual cantilevers. Microcantilever-based optical detection has been devised for detecting DNA mismatch (Hansen et al. 2001). For this purpose, a gold coated Silicon-based cantilever immobilised with thiolated probes are used with no other external labelling. This assembly further exposed to the target DNA resulted in the deflection. Hybridization of one or two mismatch nucleotides produced net negative deflection while correct matching of approximately 10 nucleotide produced net positive deflection providing a base pair wise comparison of individual mismatches while conducting hybridization. Figure 12 shows the design of triangular micromechanical cantilever and corresponding deflection of cantilever when one or two mismatch or 9 or 10 correct matches occurred while carrying out hybridization. The net negative and positive deflection caused is depicted in the figure.

Polymer-based cantilevers have been also heavily utilized for the detection of DNA. Standard spin coating and UV exposure technique is used for fabricating SU8 (photosensitive polymer)-based cantilevers (Calleja et al. 2005). As Young's modulus of SU8 is 40 times lower than that of Silicon, hence sensitivity enhancement by a factor of six is achieved in case of SU8-based cantilevers. These cantilevers have shown a noticeable response for adsorption of ssDNA and subsequent interstitial adsorption of spacer particle.

As a concluding remark, a comparison table (Table 1) is devised to compare various sensing/detection techniques, their advantages/disadvantages and limit of detection in the available literature (limit of detection related to *E. coli* detection).

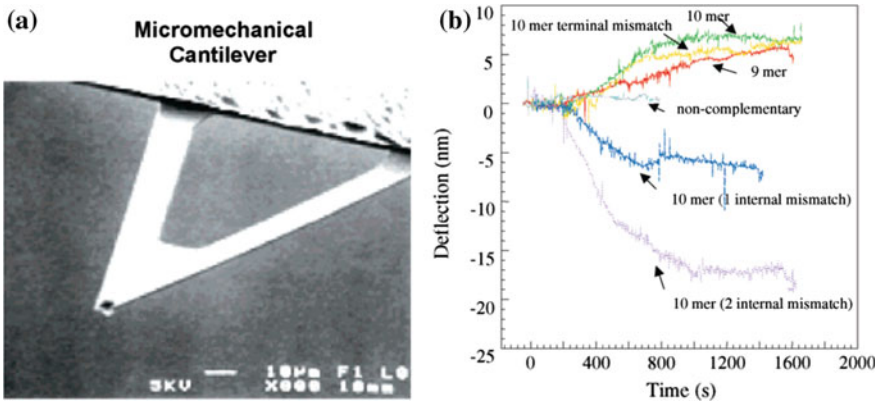

Fig. 12 **a** Structure of micromechanical cantilever; **b** deflection produced through hybridization. Reprinted with permission from Hansen et al. (2001)

Table 1 Comparison table showing limit of detection, advantages, and disadvantages of various sensing/detection techniques

S. No.	Sensing/detection technique	Limit of detection (cfu/ml)	Advantages	Disadvantages
1	Electrophoresis	1000	• Lesser cost involved	• Time-consuming process
2	Electrochemical impedance Spectroscopy	39 Dastider et al. (2016)	• Easy detection • Real-time sensing • Single- or multiple-analyte detection possible • Portable instrumentation • Lesser cost involved	• Low sensitivity
3	Colorimetric sensing	5 Hossain et al. (2012)	• Simple/rapid detection • Portable chips • Cost effective	• Limited quantification detection (only yes/no type, not real time)
4	Optical sensing	5 Fu et al. (2005)	• Real-time sensing • Higher sensitivity	• Most expensive technology • Sophisticated instrumentation required • Instrument is not portable
5	Inertial sensing	100 Leahy and Lai (2017)		• Complicated fabrication procedure • Instrument is not portable

4 Conclusions

The chapter therefore summarizes all DNA detection techniques as utilized for a sensitive DNA diagnostics. A comparison table has been provided to briefly identify the limit of detection, advantages and disadvantages of various sensing methods. The chapter discusses various aspects related to DNA-based diagnostics and applicable area in detail. It also details various principles in DNA detection like DEP, PCR and immobilization and also discusses in detail the various sensing and detection techniques like electrophoresis, impedance-based sensing, colorimetric sensing, optical sensing and inertial sensing. By and large among all diagnostics the DNA-based diagnostics still formulates a vast share of the market and one of the reasons in the sensitivity aspect related to the molecular detection strategies as exist in the DNA-based diagnostic technologies. In fact the DNA-based detection solutions mostly carried out at the molecular levels is still an industry gold standard for diagnostics.

References

Adessi C, Matton G, Ayala G et al (2000) Solid phase DNA amplification: characterisation of primer attachment and amplification mechanisms. Nucleic Acids Res 28:E87. https://doi.org/10.1093/nar/28.20.e87

Alvarez AJ, Buttner MP, Toranzos GA et al (1994) Use of solid-phase PCR for enhanced detection of airborne microorganisms. Appl Environ Microbiol 60:374–376

Bardea A, Patolsky F, Dagan A, Willner I (1999) Sensing and amplification of oligonucleotide-DNA interactions by means of impedance spectroscopy: a route to a Tay–Sachs sensor. Chem Commun 21–22. https://doi.org/10.1039/a808319c

Berggren C, Bjarnason B, Johansson G (2001) Capacitive biosensors. Electroanalysis 13:173–180. https://doi.org/10.1002/1521-4109(200103)13:3<173:AID-ELAN173>3.0.CO;2-B

Bertucci A, Manicardi A, Candiani A et al (2015) Detection of unamplified genomic DNA by a PNA-based microstructured optical fiber (MOF) Bragg-grating optofluidic system. Biosens Bioelectron 63:248–254. https://doi.org/10.1016/j.bios.2014.07.047

Bhattacharya S, Gao Y, Korampally V et al (2007a) Optimization of design and fabrication processes for realization of a optimization of design and fabrication processes for realization of a PDMS-SOG-silicon. J Microelectromech Syst 16(2):404–410

Bhattacharya S, Jang J, Yang L et al (2007b) Biomems and nanotechnology-based approaches for rapid detection of biological entities. Rapid detection of biological entities. J Rapid Methods Autom Microbiol 15:1–32

Bhattacharya S, Salamat S, Morisette D et al (2008) PCR-based detection in a micro-fabricated platform. Lab Chip 8:1130. https://doi.org/10.1039/b802227e

Bhatt G, Kant R, Mishra K et al (2017) Impact of surface roughness on dielectrophoretically assisted concentration of microorganisms over PCB based platforms. Biomed Microdevices 19:28. https://doi.org/10.1007/s10544-017-0172-5

Binnig G, Quate CF (1986) Atomic force microscope. Phys Rev Lett 56:930–933. https://doi.org/10.1103/PhysRevLett.56.930

Calleja M, Nordstrom M, Alvarez M et al (2005) Highly sensitive polymer-based cantilever-sensors for DNA detection. Ultramicroscopy 105:215–222. https://doi.org/10.1016/j.ultramic.2005.06.039

Chou C-F, Tegenfeldt JO, Bakajin O et al (2002) Electrodeless dielectrophoresis of single- and double-stranded DNA. Biophys J 83:2170–2179. https://doi.org/10.1016/S0006-3495(02)73977-5

Dastider SG, Barizuddin S, Yuksek N et al (2016) Impedance biosensor for rapid detection of low concentration of *E. coli* 0157:H7. In: Proceedings of international conference on micro electro mechanical systems, pp 302–306

Demierre N, Braschler T, Muller R, Renaud P (2007) Focusing and continuous separation of cells in a microfluidic device using lateral dielectrophoresis. TRANSDUCERS EUROSENSORS '07—4th International Conference on Solid-State Sensors, Actuators Microsystems, vol 132, pp 1777–1780. https://doi.org/10.1109/SENSOR.2007.4300498

Deng H, Xu Y, Liu Y et al (2012) Gold nanoparticles with asymmetric polymerase chain reaction for colorimetric detection of DNA sequence. Anal Chem 84:1253–1258. https://doi.org/10.1021/ac201713t

Fu Z, Rogelj S, Kieft TL (2005) Rapid detection of *Escherichia coli* O157:H7 by immunomagnetic separation and real-time PCR. Int J Food Microbiol 99:47–57. S0168-1605(04)00400-3 [pii]\rhttps://doi.org/10.1016/j.ijfoodmicro.2004.07.013

Ganguly A, Rock MJ, Prockop DJ (1993) Conformation-sensitive gel electrophoresis for rapid detection of single-base differences in double-stranded PCR products and DNA fragments: evidence for solvent-induced bends in DNA heteroduplexes. Proc Natl Acad Sci U S A 90:10325–10329. https://doi.org/10.1073/pnas.91.11.5217a

Gebeyehu G, Rao PY, SooChan P et al (1981) Novel biotinylated nucleotide—analogs for labeling and colorimetric detection of DNA. Nucl Acids Res 9:85–93. https://doi.org/10.1093/nar/16.5.2269

Ghosh A, Patra TK, Kant R et al (2011) Surface electrophoresis of ds-DNA across orthogonal pair of surfaces. Appl Phys Lett 98:2009–2012. https://doi.org/10.1063/1.3565238

Gómez R, Bashir R, Bhunia AK (2002) Microscale electronic detection of bacterial metabolism. Sensors Actuators B Chem 86:198–208. https://doi.org/10.1016/S0925-4005(02)00175-2

Gouvea V, Glass RI, Woods P et al (1990) Polymerase chain reaction amplification and typing of rotavirus nucleic acid from stool polymerase chain reaction amplification and typing of rotavirus nucleic acid from stool specimens. J Clin Microbiol 28:276–282

Hansen KM, Ji HF, Wu G et al (2001) Cantilever-based optical deflection assay for discrimination of DNA single-nucleotide mismatches. Anal Chem 73:1567–1571. https://doi.org/10.1021/ac0012748

Harrison DJ, Manz A, Fan Z et al (1992) Capillary electrophoresis and sample injection systems integrated on a planar glass chip. Anal Chem 64:1926–1932. https://doi.org/10.1021/ac00041a030

Hoeb M, Rädler JO, Klein S et al (2007) Light-induced dielectrophoretic manipulation of DNA. Biophys J 93:1032–1038. https://doi.org/10.1529/biophysj.106.101188

Hossain SMZ, Ozimok C, Sicard C et al (2012) Multiplexed paper test strip for quantitative bacterial detection. Anal Bioanal Chem 403:1567–1576. https://doi.org/10.1007/s00216-012-5975-x

Hu G, Xiang Q, Fu R et al (2006) Electrokinetically controlled real-time polymerase chain reaction in microchannel using Joule heating effect. Anal Chim Acta 557:146–151. https://doi.org/10.1016/j.aca.2005.10.021

Jaramillo MDC, Torrents E, Martínez-Duarte R et al (2010) On-line separation of bacterial cells by carbon-electrode dielectrophoresis. Electrophoresis 31:2921–2928. https://doi.org/10.1002/elps.201000082

Kasahara H, Ding Z, Nakano M, Suehiro J (2015) Effect of DNA length on dielectrophoretic characteristics of DNA-labeled microbeads. In: Proceedings of IEEE international conference on industrial technology 2015, pp 3341–3346. https://doi.org/10.1109/ICIT.2015.7125593

Laczka O, Baldrich E, Muñoz FX, Del Campo FJ (2008) Detection of *Escherichia coli* and *Salmonella typhimurium* using interdigitated microelectrode capacitive immunosensors: the importance of transducer geometry. Anal Chem 80:7239–7247. https://doi.org/10.1021/ac800643k

Lanciotti RS, Kerst AJ, Nasci RS et al (2000) Rapid detection of west nile virus from human clinical specimens, field-collected mosquitoes, and avian samples by a TaqMan reverse transcriptase-PCR assay. J Clin Microbiol 38(11):4066–4071

Lang HP, Baller MK, Berger R et al (1999) An artificial nose based on a micromechanical cantilever array. Anal Chim Acta 393:59–65. https://doi.org/10.1016/S0003-2670(99)00283-4

Latif U, Dickert FL (2011) Conductometric sensors for monitoring degradation of automotive engine oil. Sensors 11:8611–8625. https://doi.org/10.3390/s110908611

Leahy S, Lai Y (2017) A cantilever biosensor based on a gap method for detecting *E. coli* in real time. Sens Actuators, B Chem 246:1011–1016. https://doi.org/10.1016/j.snb.2017.02.144

Lee JS, Han MS, Mirkin CA (2007) Colorimetric detection of mercuric ion (Hg^{2+}) in aqueous media using DNA-functionalized gold nanoparticles. Angew Chem Int Ed 46:4093–4096. https://doi.org/10.1002/anie.200700269

Li H, Rothberg L (2004) Colorimetric detection of DNA sequences based on electrostatic interactions with unmodified gold nanoparticles. Proc Natl Acad Sci U S A 101:14036–14039. https://doi.org/10.1073/pnas.0406115101

Li CZ, Liu Y, Luong JHT (2005) Impedance sensing of DNA binding drugs using gold substrates modified with gold nanoparticles. Anal Chem 77:478–485. https://doi.org/10.1021/ac048672l

Liu Y-S, Banada PP, Bhattacharya S et al (2008) Electrical characterization of DNA molecules in solution using impedance measurements. Appl Phys Lett 92:143902. https://doi.org/10.1063/1.2908203

Liu P, Yang X, Sun S et al (2013) Enzyme-free colorimetric detection of DNA by using gold nanoparticles and hybridization chain reaction amplification. Anal Chem 85:7689–7695. https://doi.org/10.1021/ac4001157

Liu S, Wall TA, Ozcelik D et al (2015) Electro-optical detection of single λ-DNA. Chem Commun 51:2084–2087. https://doi.org/10.1039/C4CC07591A

Miles R, Belgrader P, Bettencourt K, Hamilton J, Nasarabadi S (1999) Dielectrophoretic manipulation of particles for use in microfluidic devices. Micro-Mech Syst 1:497–501

Mohr S, Zhang YH, Macaskill A et al (2007) Numerical and experimental study of a droplet-based PCR chip. Microfluid Nanofluidics 3:611–621. https://doi.org/10.1007/s10404-007-0153-8

Morgan H, Sun T, Holmes D et al (2007) Single cell dielectric spectroscopy. J Phys D Appl Phys 40:61–70. https://doi.org/10.1088/0022-3727/40/1/S10

Mu Y, Jia D, He Y et al (2011) Nano nickel oxide modified non-enzymatic glucose sensors with enhanced sensitivity through an electrochemical process strategy at high potential. Biosens Bioelectron 26:2948–2952. https://doi.org/10.1016/j.bios.2010.11.042

Nakano M, Ding Z, Kasahara H, Suehiro J (2014) DNA detection using microbeads-based dielectrophoretic impedance measurement. In Sensors 2014 IEEE 1010–1013.

Nayak M, Singh D, Singh H et al (2013) Integrated sorting, concentration and real time PCR based detection system for sensitive detection of microorganisms. Sci Rep 3:3266. https://doi.org/10.1038/srep03266

Ohashi T, Kuyama H, Hanafusa N, Togawa Y (2007) A simple device using magnetic transportation for droplet-based PCR. Biomed Microdevices 9:695–702. https://doi.org/10.1007/s10544-007-9078-y

Orita M, Iwahana H, Kanazawa H et al (1989) Detection of polymorphisms of human DNA by gel electrophoresis as single-strand conformation polymorphisms. Proc Natl Acad Sci 86:2766–2770. https://doi.org/10.1073/pnas.86.8.2766

Perch-Nielsen IR, Bang DD, Poulsen CR et al (2003) Removal of PCR inhibitors using dielectrophoresis as a selective filter in a microsystem. Lab Chip 3:212–216. https://doi.org/10.1039/B304549H

Poddar SK (1999) Detection of adenovirus using PCR and molecular beacon. J Virol Methods 82:19–26. https://doi.org/10.1016/S0166-0934(99)00074-9

Pohl HA (1951) The motion and precipitation of suspensoids in divergent electric fields. J Appl Phys 22:869–871. https://doi.org/10.1063/1.1700065

Pohl HA, Hawk I (1966) Separation of living and dead cells by dielectrophoresis. Science 80 (152):647–649. https://doi.org/10.1126/science.152.3722.647

Randles JEB (1952) Kinetics of rapid electrode reactions. Discuss Faraday Soc 48:828–832. https://doi.org/10.1039/df9470100011

Saby C, Jaffrezic-Renault N, Martelet C et al (1993) Immobilization of antibodies onto a capacitance silicon-based transducer. Sensors Actuators B Chem 16:458–462. https://doi.org/10.1016/0925-4005(93)85228-3

Sader JE (2001) Surface stress induced deflections of cantilever plates with applications to the atomic force microscope: rectangular plates. J Appl Phys 89:2911–2921. https://doi.org/10.1063/1.1342018

Saucedo-Espinosa MA, Lalonde A, Gencoglu A et al (2016) Dielectrophoretic manipulation of particle mixtures employing asymmetric insulating posts. Electrophoresis 37:282–290. https://doi.org/10.1002/elps.201500195

Schwartz DC, Cantor CR (1984) Separation of yeast chromosome-sized DNAs by pulsed field gradient gel electrophoresis. Cell 37:67–75. https://doi.org/10.1016/0092-8674(84)90301-5

Shin Y, Perera AP, Kim KW, Park MK (2013) Real-time, label-free isothermal solid-phase amplification/detection (ISAD) device for rapid detection of genetic alteration in cancers. Lab Chip 13:2106. https://doi.org/10.1039/c3lc50129a

Sonnenberg A, Marciniak JY, Krishnan R, Heller MJ (2012) Dielectrophoretic isolation of DNA and nanoparticles from blood. Electrophoresis 33:2482–2490. https://doi.org/10.1002/elps.201100700

Su M, Li S, Dravida VP (2003) Microcantilever resonance-based DNA detection with nanoparticle probes. Appl Phys Lett 82:3562–3564. https://doi.org/10.1063/1.1576915

Takashima S (1966) Dielectric dispersion of Deoxyribonucleic Acid. II[1]. J Phys Chem 70:1372–1380. https://doi.org/10.1021/j100877a006

Tuukkanen S, Toppari JJ, Kuzyk A et al (2006) Carbon nanotubes as electrodes for dielectrophoresis of DNA. Nano Lett 6:1339–1343. https://doi.org/10.1021/nl060771m

Wang W, Li Z-X, Luo R et al (2005) Droplet-based micro oscillating-flow PCR chip. J Micromech Microeng 15:1369–1377. https://doi.org/10.1088/0960-1317/15/8/001

Xia F, Zuo X, Yang R et al (2010) Colorimetric detection of DNA, small molecules, proteins, and ions using unmodified gold nanoparticles and conjugated polyelectrolytes. Proc Natl Acad Sci 107:10837–10841. https://doi.org/10.1073/pnas.1005632107

Yeo WH, Chung JH, Liu Y, Lee KH (2009) Size-specific concentration of DNA to a nanostructured tip using dielectrophoresis and capillary action. J Phys Chem B 113:10849–10858. https://doi.org/10.1021/jp900618t

Chapter 16
The Microflow Cytometer

Ravindra S. Gaikwad and A. K. Sen

Abstract Integrated optical detection in a microfluidic platform recently got an immense attention, on such integrated platforms light and fluids are engineered synergistically to implement highly sensitive and portable lab-on-chip biochemical sensors. Integrated optofluidic platforms were successfully demonstrated in last few years for various applications such as controlling liquid motion using light, sunlight-based fuel-production, and flow cytometry. Various microflow analyzers were developed for different applications including counting and studying biological cells, bacteria, molecular biology, and cellular DNA. Microflow cytometer is an instrument, which interrogates a small volume of fluid to detect and sort biological cells/samples present in a sample fluid. Presently, the flow cytometry is the state of the art for biological sample analysis due to its capability for detailed analysis. However, conventional flow cytometers are very expensive and thus are available only in centralized research facilities and major health care centers. Similarly, due to its complexity, regular maintenance and skilled expertise are required to operate the machine, analyze data, and make reports. In the last few years, several research works have been carried out to design cost-effective and portable microflow cytometer by employing the advancements in the field of microfluidic and microfabrication technology. However, the complicated techniques required for three-dimensional focusing of biological cells flowing inside the microchannel and controlling inter distance between them in the optical window are the primary hindrances in the development of a microflow cytometer. Another challenge in the development of microflow cytometer is the isolation of target cells downstream after detection. In literature, various techniques have been reported to achieve the sorting of target cells. Therefore, development of microflow cytometers is mainly concentrated on focusing of samples in a microchannel, miniaturization of optical

R. S. Gaikwad · A. K. Sen (✉)
Department of Mechanical Engineering, IIT Madras, Chennai 600036, India
e-mail: ashis@iitm.ac.in

R. S. Gaikwad
e-mail: ravi.sg32@gmail.com

R. S. Gaikwad
Department of Electrical Engineering, IIT Madras, Chennai 600036, India

S. Bhattacharya et al. (eds.), *Environmental, Chemical and Medical Sensors*, Energy, Environment, and Sustainability, https://doi.org/10.1007/978-981-10-7751-7_16

and supporting flow systems, integration of electronics on the same chip, and development of optimal sorting technique. Hence, by incorporating above mentioned developments, microflow cytometer can be used successfully to focus, detect, and sort the particles with a high throughput which can lead to a proper analysis of biological samples.

Keywords Flow cytometry · Optofluidic platforms · Microfabrication Sorting · Biological cells

1 Introduction

Onset of disease directly affects the mechanical, electrical (Cole et al. 2017; Petchakup et al. 2017; Huh et al. 2005; Schwan 1957), and optical (Antfolk and Laurell 2017) properties of the cell, which can act as a biomarker. Importance of studying different cells and sampling of biological fluids have increased, which forces researchers to analyze single cells individually (Petchakup et al. 2017). Analysis of single cell is very useful in drug discovery application by studying blood containing rare cells such as fetal cells (Fiddler 2014), circulating tumor cells (CTC) (Zhang et al. 2016), and stem cells; also, it is useful in immunological research. Bulk analysis of the cell sample and extraction of the information for single cell using probabilistic approach (as followed previously) does not provide accurate information (Wang and Bodovitz 2010). Here, the probabilistic analysis means instead of studying the cells individually; a stochastic average of the bulk measurement is considered to collect the information about the single cell. In contrast, analyzing single cells based on their optical and electrical properties gives a clearer picture. The conventional methods are available to analyze single cells but they have some limitations such as the conventional cell analysis method uses a large volume of samples to analyze the cells which is very crucial for the cases where low volume of samples is available (Preckel 2010a). Also, it is difficult to automate the analysis processes in the conventional methods (Preckel 2010b). The microfluidics technique uses small structures comparable to the biological cells which gives explicit control over the cells. This precise control leads to a better isolation of cells based on the targeted properties (Dittrich and Schwille 2003), but this explicit control over cells is missing in conventional methods. The conventional methods take long analysis time that may affect the viability and usefulness of the cells (Antfolk and Laurell 2017). Microfluidic technique looks promising to overcome the limitations present in the conventional methods. As microfluidic techniques depend on the intrinsic cell properties rather than traditional biomarkers (Antfolk and Laurell 2017). Microfluidic concepts like a lab-on-chip and micrototal analysis system bring more sophisticated tool for analyzing single cells (Yin and Marshall 2012).

Microflow cytometer is a very powerful microfluidic tool because of its ability to differentiate group of cells in a heterogeneous mixture (Guo et al. 2015). Recent development in the microflow cytometer has given the ability to analyze thirteen

parameters simultaneously, which leads researcher to find well-defined interesting biological subsets in biofluids. Flow cytometry is also helpful for diagnosis of hematological disorders (Huh et al. 2005; Sobti and Krishan 2003). Flow cytometry is able to characterize cells or particle based on their optical, fluorescence (Ibrahim and van den Engh 2007), and electrical properties (Cheung et al. 2010). In a cytometer, particles are allowed to pass through a light beam in a moving fluid and produce a scatter or fluorescence signal (Etcheverry et al. 2017). Then, the signal analysis gives the information about biochemical and biophysical aspects of the particle. The scattering signal tells about size and structure of the particle or cell, whereas fluorescence signal is related to the cellular components (Brown and Wittwer 2000). Flow cytometers are divided into two types based on their ability to sort particles. First one is sorting type, and second one is non-sorting type flow cytometers. Sorting-based flow cytometers are capable of sorting particles from the heterogeneous mixture based on fluorescence and scatter signal. FACS (Fluorescence-activated cell sorter) is an example of sorting type flow cytometer (Fig. 1) (Adan et al. 2016). A flow cytometry consists of fluidic system, optical system, sorting system, and electronics system (Weaver 2000). Fluidic system is responsible to transport the particles in a channel to the interrogation zone. Optical system consists of a light source, optical filters, optical components, detectors, and electronic system, which is useful in converting a detected light signal into an electronic signal (Cho et al. 2010). Some flow cytometer uses electronics to create sorting mechanisms.

It is very important to analyze the particles accurately by the flow cytometer. To accurately analyze the individual particle, it is necessary to have single particle in the interrogation zone (Ateya et al. 2008). To achieve this condition, the flow-focusing techniques are used, where the sample fluid is focused to a single file

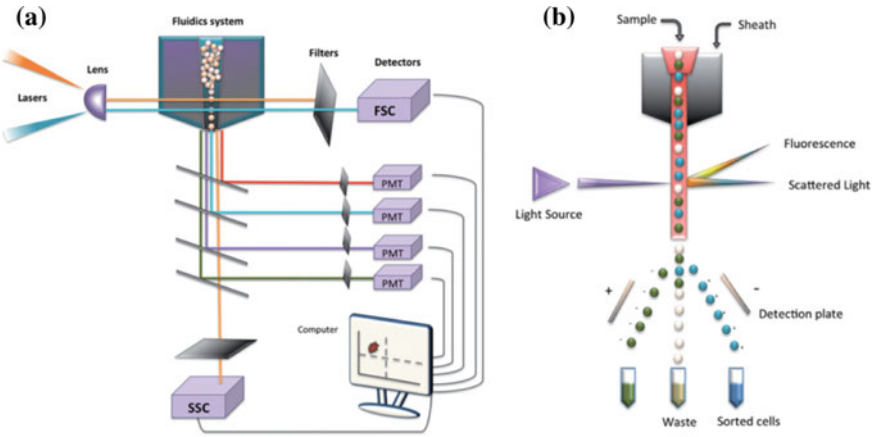

Fig. 1. **a** Schematic of a FACS (*PMT* photomultiplier tube, *SSC* represent side scatter, and *FSC* forward scatter), **b** Schematic of sorting system of a FACS. Reprinted by permission of the publisher Taylor & Francis Ltd., http://www.tandfonline.com (Adan et al. 2016)

stream. Then, these particles are analyzed by the optical components, and based on this light signal, particles are sorted. In this chapter, we discuss each system in detail. The Fig. 1 shows the schematic of a flow cytometer.

2 Fluidic System

It is very important to have single file stream of a sample fluid to get accurate information of scattered, fluorescence signal, and impedance value in optical and impedance-based flow cytometer, respectively. The focusing of the sample fluid is important to ensure single file stream condition in a microchannel, and the use of a narrow channel may lead to clogging as well as microparticles may adhere to walls of a microchannel and may not be useful for a sample containing different size of particles. There are different techniques available to converge sample fluid in a microchannel such as hydrodynamic flow focusing, droplet generation, acoustophoresis, dielectrophoresis (DEP), and electrokinetic focusing (Fu et al. 2004).

3 Hydrodynamic Focusing

The hydrodynamic focusing is the one where sample fluid is focused by using a sheath flow. The focused sample fluid width is adjusted such that a narrow width is comparative to the size of the particle in a channel. The width of a focused sample is a function of relative flow rates (Lee et al. 2006). In a microchannel, hydrodynamic focusing is extensively used. There are two types of hydrodynamic flow focusing, two dimensional (2-D) and three dimensional (3-D). The general concept of these flow-focusing methods is described with a schematic diagram shown in Fig. 2.

The 2-D focusing channel fabrication is easy compare to 3-D flow focusing. The 3-D flow-focusing channel fabrication requires multilayer fabrication process. In a 2-D focusing channel, the sample fluid is focused horizontally within the center with the help of two sheaths. The increase in the flow rate of a sample and keeping the flow rate of a sheath constant causes broadening of the sample width and inversely by keeping the flow rate of a sample constant and increasing the sheath flow rate leads to a narrowing of a sample width. Basically, by changing the sheath flow rate to the sample flow rate ratio, the width of the sample fluid is varied. The same experimental study has done by Lee et al. (2006) on variation of sample width in a microchannel of width 250 μm and height 445 μm by varying flow rate ratio; the Fig. 3 shows the experimental result.

The analytical model of 2-D hydrodynamic flow focusing can be derived by assuming uniform, steady and laminar flow in a channel, also consider the fluid is Newtonian fluid. The pressure variation along the y and z directions (Fig. 2) is zero,

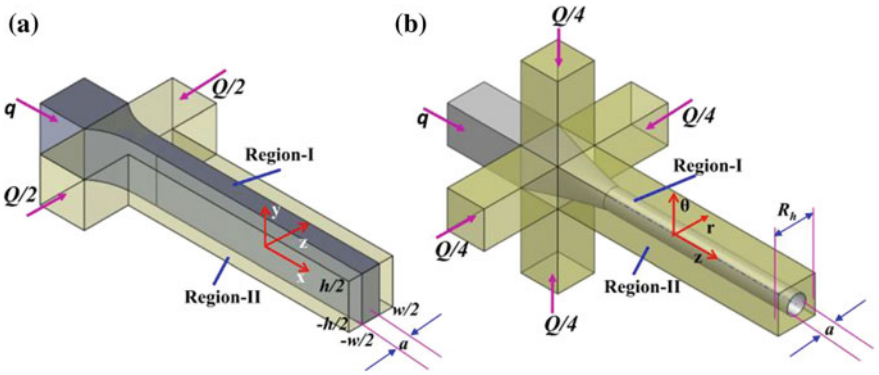

Fig. 2. Schematics of **a** 2-D hydrodynamic focusing (q flow rate of a sample, $Q/2$ one side sheath flow rate in a channel, w width and h height, a focused sample width) **b** four sheath inlet 3-D hydrodynamic flow focusing (q flow rate of a sample, $Q/2$ one side sheath flow rate in a channel, w width and h height, a focused sample width). Reproduced from Shivhare et al. (2016), With permission of Springer

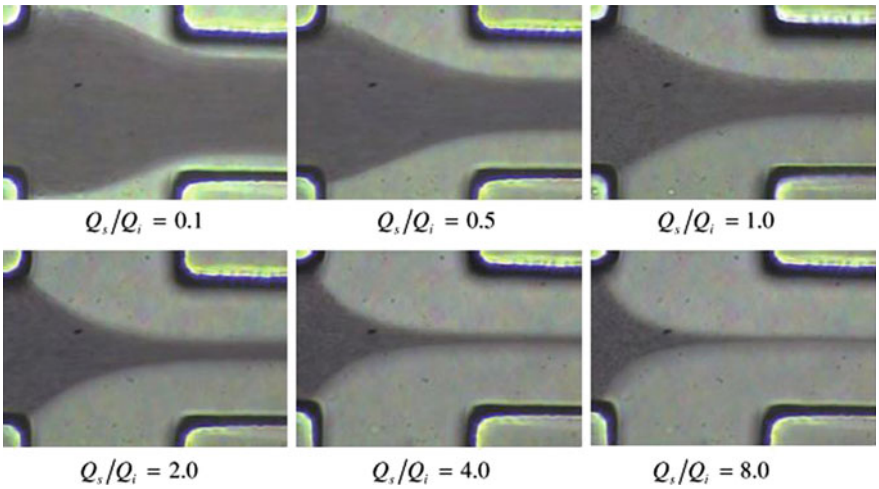

Fig. 3. Experimental images of 2-D flow focusing with different flow rate ratio (Q_s and Q_i are one side sheath flow rate and flow rate of a sample, respectively) in microchannel with aspect ratio of 1.78 (Lee et al. 2006)

and the sample and sheath fluid interface is assumed to be flat. Therefore, the Navier–Stokes equation for the considered assumptions can be written as follow

$$\frac{\partial^2 u}{\partial y^2} + \frac{\partial^2 u}{\partial z^2} = \frac{1}{\mu}\frac{\partial p}{\partial x} \tag{1}$$

where u is fluid velocity, and μ represents the dynamic viscosity of the fluid. To make the analytical model dimensionless, it is required to introduce dimensionless parameters such as $\hat{u} = u/u_0$, $\hat{y} = y/w$, $\hat{z} = z/h$ and $\hat{x} = x/L$, where L, w, and h represent length, width, and height of a channel. Hence, the equation becomes

$$\alpha^2 \frac{\partial^2 \hat{u}}{\partial \hat{y}^2} + \frac{\partial^2 \hat{u}}{\partial \hat{x}^2} = P \tag{2}$$

where, $P = \frac{h^2}{u_0 uL} \frac{\partial p}{\partial x}$ and $\alpha = h/w$.

As shown in the Fig. 2 there are two regions, region-I is representing sample fluid, and region-II represents sheath fluid. By applying above equation to these regions and solving those equations for $\hat{u}$, hence $\hat{u}$ becomes

$$\hat{u}_1 = \sum_{n=0}^{\infty} \left[\frac{-4P}{((2n-1)\pi)^3} + A \cos h\left(\frac{(2n-1)\pi}{\alpha}\hat{y}\right) + B \sin h\left(\frac{(2n-1)\pi}{\alpha}\hat{y}\right) \right] \sin(2(2n-1)\pi\hat{z}) \tag{3}$$

and

$$\hat{u}_2 = \sum_{n=0}^{\infty} \left[\frac{-4P}{((2n-1)\pi)^3} + C \cos h\left(\frac{(2n-1)\pi}{\alpha}\hat{y}\right) + D \sin h\left(\frac{(2n-1)\pi}{\alpha}\hat{y}\right) \right] \sin(2(2n-1)\pi\hat{z}) \tag{4}$$

where A, B, C, and D can be find by applying boundary conditions. The sheath flow rate (Q) and sample flow rate (q) are then find by integrating corresponding velocity field over a cross section. The mathematical expressions for these flow rates are as given below

$$q = 4 \times \sum_{n=1}^{\infty} \left[\frac{-2Pb}{((2n-1)\pi)^4} + \frac{\mathrm{A}\alpha}{((2n-1)\pi)^2} \sin h\left(\frac{(2n-1)\pi}{2\alpha} b\right) \right] \tag{5}$$

$$Q = 4 \times \sum_{n=1}^{\infty} \left[\frac{-2P(1-b)}{((2n-1)\pi)^4} + \frac{\alpha}{((2n-1)\pi)^2} (C \times X + D \times Y) \right] \tag{6}$$

where, $X = \left[\sin h\left(\frac{(2n-1)\pi}{2\alpha}\right) - \sin h\left(\frac{(2n-1)\pi b}{2\alpha}\right) \right]$ and $Y = \left[\cos h\left(\frac{(2n-1)\pi}{2\alpha}\right) - \cos h\left(\frac{(2n-1)\pi b}{2\alpha}\right) \right]$.

Stiles et al. (2005) have demonstrated an alternate method to create a 2-D flow focusing by creating a relative change in a hydraulic flow resistance that has been created by maintaining the outlet at negative pressure and with a geometry which supports flow rate difference (Stiles et al. 2005). Another way to produce 2-D flow

focusing is the use of air as a sheath flow. Producing a two-phase flow in a channel, air sheath from two side is use to focus sample in a channel (Huh et al. 2002). In a two-dimensional flow focusing, sample is focused horizontally not vertically. The sample is still in touch with the top wall and bottom wall of a channel which gives parabolic velocity profile in vertical direction. The parabolic profile means particles will experience different velocities at different location in a microchannel which may cause two or more particle in interrogation zone. The 2-D focusing is minimizing the problem rather eliminating it completely. Hence, it is important to focus the sample in all direction.

The Fig. 2b shows the schematic of a 3-D focusing, and the sample fluid is allow to focus at the center, where the sheath flow is forcing the sample from four directions. The flow rate ratio is modulated to get the required sample width like 2-D focusing. Shivhare et al. (2016) had done set of experiments by varying the flow rate ratio and validated it with simulation results. The graph shown in Fig. 4 shows the sample width variation with flow rate ratio.

There are different ways to obtain 3-D focusing in the channel. Howell et al. made a chevron-shaped groove at the top wall and at the bottom wall of a channel as shown in Fig. 5a. These grooves are helping to surround the sample with a sheath flow. Lee et al. (2009) had studied contraction and expansion microchannel in a series to create a 3-D focusing of a sample fluid. Basically, the fluid entering from expansion region to contraction region at the entrance creates a counter-rotating fluid flow field due to centrifugal forces. These secondary counter-rotating flow fields enclose sample fluid with a sheath flow. The schematic diagram of a contraction and expansion array is shown in Fig. 5b. The advantage of this 3-D focusing method is that it uses only one sheath flow and requires one layer of fabrication.

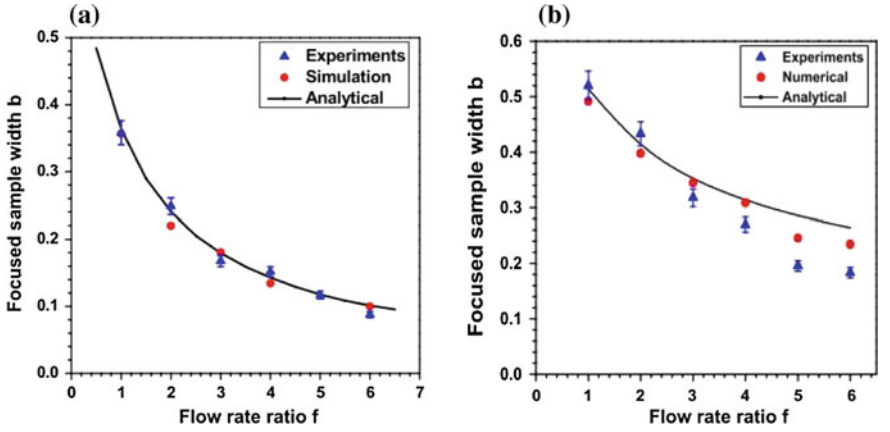

Fig. 4. **a** Variation of sample width *b* (non-dimensional) with flow rate (*f*) in 2-D focusing channel, **b** Variation of sample width *b* (non-dimensional) with flow rate (*f*) in 3-D focusing channel. Reproduced from Shivhare et al. (2016), with permission of Springer

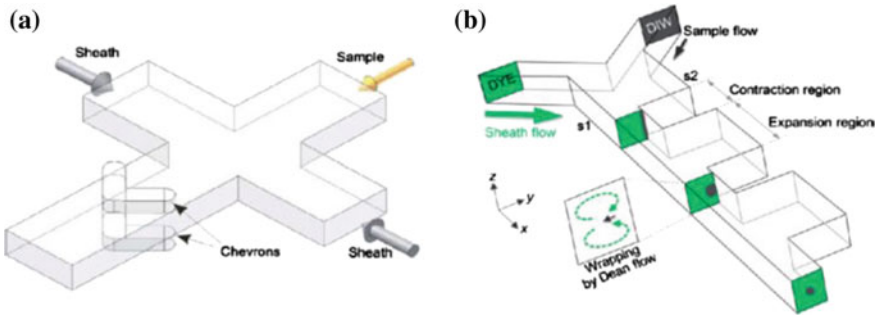

Fig. 5. Schematic of **a** chevron-shaped grooves 3-D focusing channel **b** contraction and expansion-based 3-D flow focusing. Reproduced from Lee et al. (2009) with permission of The Royal Society of Chemistry

Frankowski et al. (2013) had demonstrated two different concepts of 3-D hydrodynamic flow focusing, and those are cascade focusing and spin focusing. These methods produce very stable and fully controlled focusing of a sample flow. The schematics of these techniques are shown below (Fig. 6).

Frankowski et al. (2013) have discussed two stage cascade focusing method which uses only single inlet for the sheath fluid. In this approach, each stage has different size of a sheath channel and sample channel. The flow channel dimensions can be changed gradually by using high precision milling. The typical dimensions of a first stage sheath channel are 300 μm width and 1000 μm height, and for the second stage, width is 270 μm for a height of 1000 μm, and for the sample channel, first stage is of 125 μm × 125 μm and the corresponding second stage having a dimensions of 200 μm × 200 μm. In a cascaded channel, the particles get focused better than the single stage focusing mechanisms due to successive acceleration in a sample flow and sheath flow. The schematic of a cascaded focusing channel is shown in the Fig. 6a. In a spin focusing channel, the sample flow is focused perpendicular to the plane joining two sheath flows. Sheath flows which are flowing in two different parallel planes merge at the point where sample flow is getting injected into a channel. This particular geometry creates a vortex in the channel

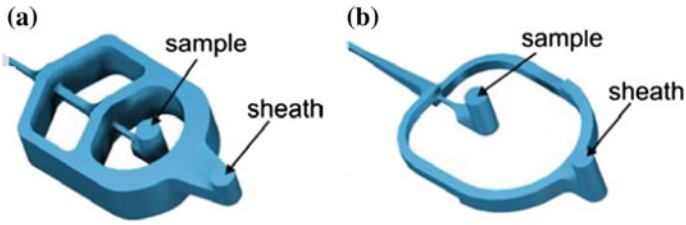

Fig. 6. Schematic of **a** two cascade focusing **b** spin focusing (Frankowski et al. 2013)

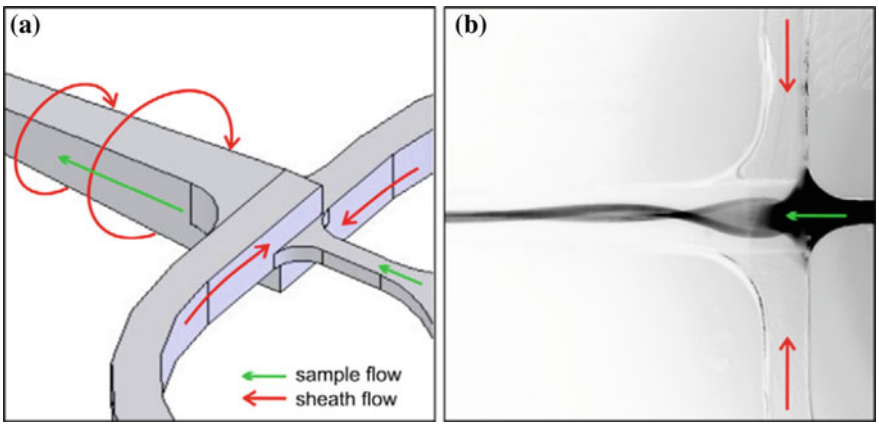

Fig. 7 **a** Schematic diagram of a spin focusing principle **b** experimental fluorescence image taken with a rhodamine dye 6G as a sample fluid (Frankowski et al. 2013)

enclosing sample fluid at the center. The principle of this spin focusing is explained with the help of a schematic diagram in Fig. 7a and supported by experimental image of spin focusing channel in Fig. 7b.

4 Sheath Less Particle Focusing

The sheath-based flow-focusing devices use complicated fluidic systems for precise control over the relative flow rates, and sometimes sheath fluid may dilute the sample. To overcome these limitations, sheath less focusing is emerged. Sheath less focusing is divided into two major types. First is field-based techniques in which particles are focused with the help of external forces. Second is flow-assisted methods in which particles are guided with the help of microstructures or microchannel.

(A) **Dielectrophoresis (DEP)**

A dielectric particle experiences a force in a non-uniform electric field. Basically, this technique is used to sort the different microparticles in a sample. The experienced dielectrophoretic force by the particles is given by the following mathematical equation.

$$F_{\mathrm{DEP}} = 2\pi a^3 \varepsilon_m \mathrm{Re}\{\mathrm{CM}\} \nabla |\bar{E}|^2 \tag{7}$$

Where the particle radius is a, a medium permittivity ε_m, the applied electric field is $\bar{E}$, and the real part of Clausius–Mossotti factor is Re{CM}. The sign of CM factor decides the force experienced by the particle. The CM factor depends on

conductivity of the particle, medium, and applied electric field frequency. Based on these factors, the particle will move toward high electric field region or toward minimum, and based on this, it is named as positive DEP and negative DEP, respectively. The electric field is generated in a microchannel with the help of planar electrodes. Holmes et al. (2006) developed a DEP focusing channel by placing two electrodes onto the top and bottom of a microchannel. The Fig. 8 shows the schematic diagram and experimental image.

(B) **Acoustic force**

In acoustophoresis, the particles suspended in a medium experience a force which is induced by creating standing waves. Acoustic radiation force (Eq. 2) is mainly responsible for manipulation of particles. This acoustic radiation force transports the particle into pressure nodes or antinodes depending on acoustic contrast factor (Eq. 3) which depends on a difference in density and compressibility of particle and medium. When particles are dense, they possess positive contrast factor, which leads them into nodes and vice versa.

$$F_{\text{rad}} = 4\Pi a^3 \phi k_y E_{\text{ac}} \sin(2k_y y) \tag{8}$$

where,

$$\phi = \frac{\kappa_o - \kappa_p}{3\kappa_o} + \frac{\rho_p - \rho_o}{2\rho_p + \rho_o} \tag{9}$$

And a is particle radius, Φ is the acoustic contrast factor, E_{ac} is the acoustic energy density, k_y is the wave number, distance from wall is y, κ_p and κ_o are the particle isothermal compressibility and the isothermal compressibility of a fluid, respectively, ρ_o and ρ_p are the densities of the fluid and the particles, respectively.

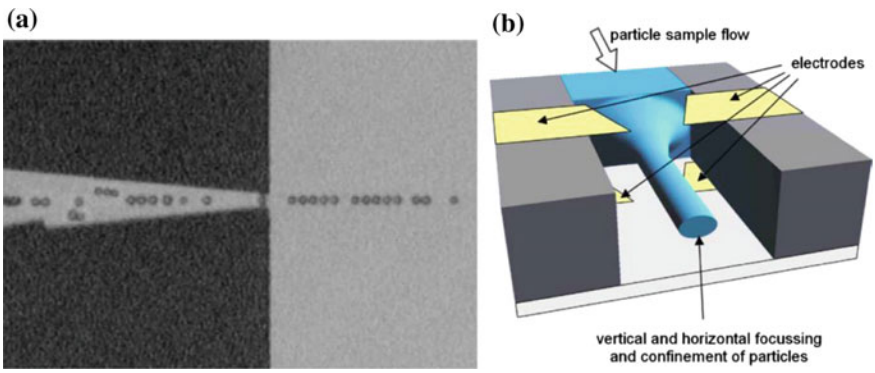

Fig. 8 **a** Experimental image showing focusing of 6 μm particles by electrodes **b** schematics of a 3-D flow focusing with the help of a two pair of electrodes. Reprinted from Holmes et al. (2006), with permission from Elsevier

Jakobsson et al. (2015) demonstrated acoustic actuated fluorescence activated cell sorter in which the particles are focused with a single acoustic actuation and further downstream they are sorted by small acoustic bursts based on the fluorescence signal. The schematic of the working principle of this device is shown in Fig. 9. The prefocusing zone uses the acoustic waves with the frequency 4 and 6 MHz for particle focusing, and sorting zone uses 2 MHz acoustic burst (Jakobsson et al. 2015).

Other than these two-field-based flow-focusing methods, the third is optical focusing. In optical focusing, the scattering forces are used to deviates the particles in a stream. The optical forces depend on a square of a particle diameter; hence while designing the device, consideration of size of the particle is very important. Also, it helps in selecting the optical sources and components. This sheathless flow focusing has some advantages as well as disadvantages. The sheathless flow focusing is very much particle size dependent. In many flow cytometry applications, the size dependence creates a problem in maintaining a stable flow focusing of the particles.

(C) **Inertial focusing**

There are passive and active techniques for the particle focusing in a microchannel. One of the passive techniques is inertial focusing, where particles are focused at different equilibrium positions along the straight channel based on the channel aspect ratio at moderate Reynolds number flow. Equilibrium position of a particle is determined by the balance of shear gradient lift force and the wall lift force which counteracts each other in a channel. Basically, the shear gradient lift force comes in a picture because of parabolic velocity profile of a fluid in a channel which tries to force the particle away from the center of a channel, and the wall lift force acts away from the wall which is because of interaction between the wall and a particle.

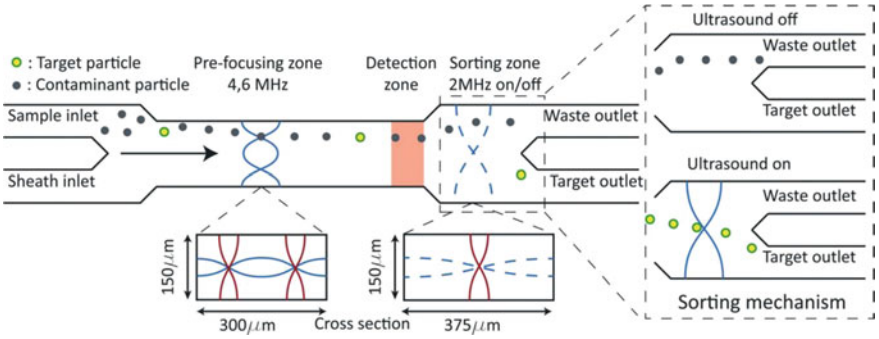

Fig. 9. Schematic of the working principle of AFACS. Reproduced from Jakobsson et al. (2015) with permission of The Royal Society of Chemistry

Though this particle focusing technique is popular in the recent time but it has some drawbacks such as it needs a long length of a channel to achieve equilibrium position for the particles, also the particle focusing is a function of a channel aspect ratio and at the same time we can have different equilibrium positions in a channel. These limitations of the inertial focusing can be eliminated by introducing secondary flow in a channel. The secondary flow exerts drag force on the particles. The secondary flow can be generated by incorporating geometrical changes in a channel. Zhao et al. (2017) demonstrated a high-throughput inertial focusing with arc-shaped grooves on the channel surface. The schematics of the arc-shaped groove array channel are as shown in Fig. 10.

The pressure gradient generated in a channel in the transverse direction because of groove structures tends to trap fluid which results in a secondary flow. This secondary flow forms vorticity in a channel cross section, forcing the fluid to move in a lateral direction along the vorticity rotation. The rotational direction movement of fluid exerts secondary flow drag force on a particle forcing them to move laterally. The particle simultaneously experiences the shear gradient lift force and the wall lift force. The equilibrium position of a particle is determined by the balance of all these forces. Here, the drag force is counteracting with inertial lift forces. This counteraction sets the particle in the equilibrium position at the upper corner of a channel. It has demonstrated in the same work that the strong secondary drag force can be generated by keeping approximately the same height of a curve-shaped groove and the channel. This method even shows the better focusing of the particles with different sizes and hence can be used effectively in a microflow cytometer.

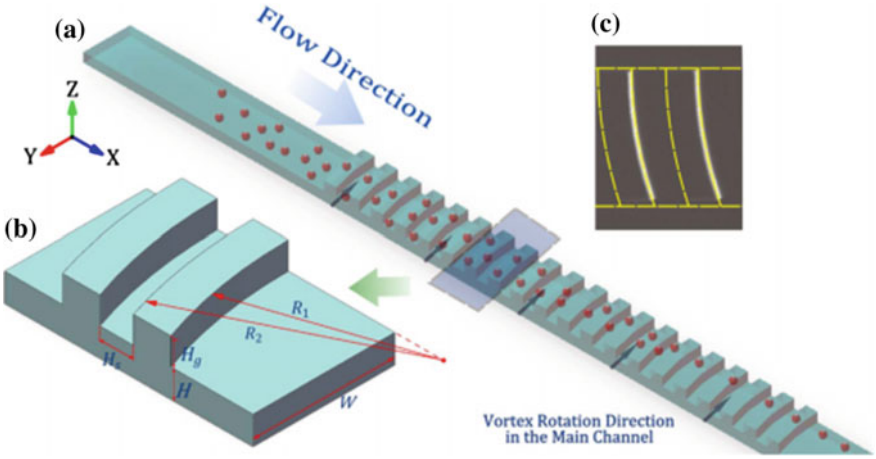

Fig. 10 **a** Schematic of a microchannel with curve grooves on the top of the channel and focusing of the particles **b** zoom in section of a microchannel with grooves with size parameters **c** CCD camera captured image of a channel (Zhao et al. 2017)

5 Optical System

The second most important part of a flow cytometry is an optical system. The focused particles are then allowed to pass through an interrogation zone. The optical system provides a means by which particles are classified and detected. There are two main signals which help in analyzing the particles; they are scatter signal and fluorescence signal. The optical detection based on the fluorescence is used mostly because of its advantages such as high selectivity and sensitivity. The incident beam of light is focused into the observation window using different optical components. The particles after illumination of light produces scatter and florescence light signal. These light signals are then passed through the filters to the photodetectors to generate corresponding electrical signals. Traditionally, in a flow cytometer, bulky light sources such as mercury or xenon lamps and other bulky optical components are used, but to develop a miniaturized flow cytometer, it is very important to integrate optical components on-chip.

Waveguides are important to guide the light signals from a light source to the interrogation zone and from interrogation zone to the detectors. There are different ways to do this—either inserting optical fibers tip available in the market into the aligned groves in a microchannel chip (Wu et al. 2007) or fabricating optical waveguides with in a chip. When a laser beam hits the cell flowing in a microchannel, part of a light beam gets deflected, and this deflected light is called as scattering of light. There are mainly two types of scattering, forward scattering (FSC) and side scattering (SSC). The cell structure, size, membrane, and nucleus decide the scattering of the light signal (Adan et al. 2016). FSC is collected from front side of an exciting fiber at a small angle (0.5°–20°) (Guo et al. 2015) (Fig. 11). FSC signal tells about size of a particle or cell, whereas SSC signal which is collected at large angle (15°–150°) to the axis of excitation fiber gives information about cell/particle granularity, and internal complexity of a cell. To separate the particles from a heterogeneous mixture, FSC and SSC signals are very useful (Reggeti and Bienzle 2010).

A fluorescence signal is very important in the flow cytometer. A compound which has fluorescence ability absorbs a light over a specific range of wavelengths and emits the light over another range of wavelengths. Basically, by absorbing light, in an atom, electrons go to excited state, and when they come back to original ground state after sometime, during this transition, they emits an energy. That energy is called as fluorescence. The fluorescence-based flow cytometry required staining of cells with fluorochromes, because numbers of intrinsically fluorescent compounds in a cell are less. The staining of cells is useful in many applications such as cell sorting, finding nucleic acid, and immune phenotyping.

To detect the light signals generated in the flow cytometry, photodetectors are used. The photodetector converts light signal to a voltage waveform. There are two photo detectors, photodiode (PD) and photomultiplier tubes (PMT). They are widely used based on the required sensitivity. PMT is more sensitive than PD; hence, to detect SSC signal, PMT is used, and for FSC detection, PD is used. To detect fluorescence signal, PMT is used with different optical filters.

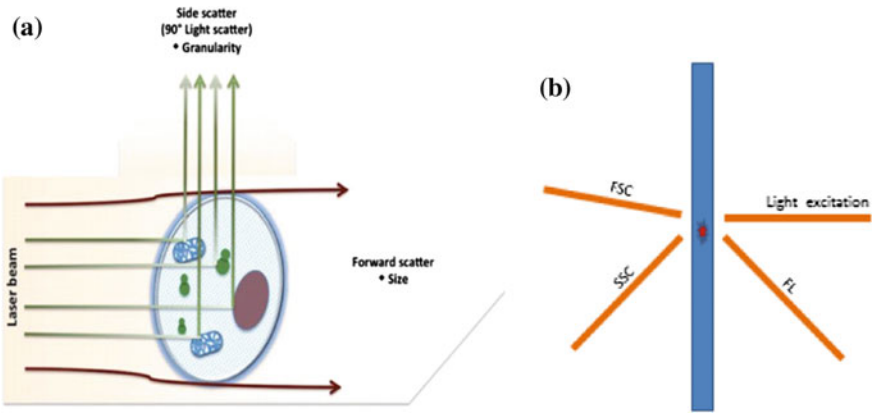

Fig. 11. **a** Schematics of FSC and SSC signal from a cell. Reprinted by permission of the publisher Taylor & Francis Ltd., http://www.tandfonline.com (Adan et al. 2016), **b** schematic diagram showing different groves location corresponds to SSC, FSC, FL (fluorescence) and excitation light fiber in a microchip

6 Sorting Systems

As discussed earlier there are two types of flow cytometer, the one which incorporates sorting mechanisms and the second which do not have sorting mechanisms. Sorting mechanism in a flow cytometry gives additional advantage to the flow cytometry. There are different mechanisms to sort focused particles such as electrokinetic flow switching, hydrodynamic flow switching using on-chip or off-chip valves, etc. Sorting system is activated based on optical signal. Dittrich and Schwille have demonstrated electro-osmotic induced particle separation mechanisms. The proposed device is capable of deflecting particles based on the applied voltage polarity to the electrodes (Fig. 12) (Dittrich and Schwille 2003). Wang et al.

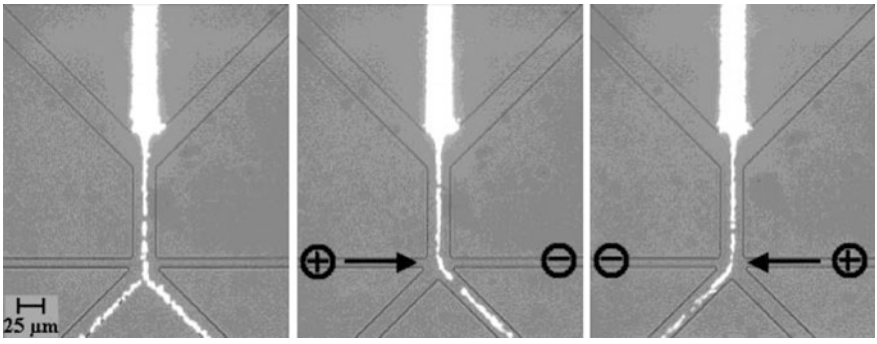

Fig. 12. Electro-osmotic particle sorting by changing the applied voltage polarity. Reprinted with permission from Dittrich and Schwille (2003)

(2005) demonstrated the sorting of the focused particles by switching optical forces (Wang et al. 2005). Jakobsson et al. (2015) demonstrated acoustic actuated fluorescence activated cell sorter in which particles are sorted with the help of acoustic radiation (Fig. 9).

7 Electronic System

Electronics and data analysis software are very important for flow cytometry applications. The electronics and analysis software convert optical signals into a meaningful data. Incorporating electronics in the flow cytometry increases the efficiency and functionality of the system and makes the system more autonomous. Analog circuit amplifiers are widely used to amplify the signals generated by the photodetectors, which increases the sensitivity of a device. Also, the signal generated by the devices should have less noise content. One can improve the SNR (signal to noise ratio) by using analog and digital filters. In many applications, real time analysis of data is very important. Hence, to process such real time data micro controller and microprocessors with digital signal processing techniques can be used. There is a lot of opportunity to make a very sophisticated flow cytometer by incorporating electronics in it.

8 Conclusion

Flow cytometer has a potential to analyze a large number of individual biological particles within a short span of time by utilizing mainly light scattering, and fluorescence. This device is capable of determining ample parameters related to cells or particles. The use of less volume of a sample and the high efficiency to separate rare particles or cells in the sample are some advantages of flow cytometry. By adopting different focusing approaches which are discussed in this chapter, they are able to meet the condition of single cell at a time in the interrogation region. Integration of optical and electronics components in the microflow cytometer is very important to miniaturize the system. In this chapter, we have discussed methods to incorporate these components which lead to the device miniaturization. The sensitivity and the sorting capabilities of the device can further be increased by incorporating more robust electronics on the chip. Because of all these developments, microflow cytometer holds the potential to secure a place in all cell analysis laboratories.

References

Adan A, Alizada G, Kiraz Y, et al (2016) Flow cytometry: basic principles and applications. Crit Rev Biotechnol 0:1–14. https://doi.org/10.3109/07388551.2015.1128876

Antfolk M, Laurell T (2017) Continuous flow microfluidic separation and processing of rare cells and bioparticles found in blood??? A review. Anal Chim Acta 965:9–35. https://doi.org/10.1016/j.aca.2017.02.017

Ateya DA, Erickson JS, Howell PB et al (2008) The good, the bad, and the tiny: a review of microflow cytometry. Anal Bioanal Chem 391:1485–1498. https://doi.org/10.1007/s00216-007-1827-5

Brown M, Wittwer C (2000) Flow cytometry: principles and clinical applications in hematology. Clinic Chem 46(8):1221–29

Cheung KC, Berardino MD, Schade-Kampmann G et al (2010) Microfluidic impedance-based flow cytometry. Cytom Part A 77:648–666

Cho SH, Godin JM, Chen C-H et al (2010) Review article: recent advancements in optofluidic flow cytometer. Biomicrofluidics 4:1–23. https://doi.org/10.1063/1.3511706

Cole NJ, Richardson AM, Abdul-Hafiz A (2017) Development of a multi frequency impedance measurement system for use in MEMS flow cytometers. Microsyst Technol. https://doi.org/10.1007/s00542-017-3359-z

Dittrich PS, Schwille P (2003) An integrated microfluidic system for reaction, high-sensitivity detection, and sorting of fluorescent cells and particles. Anal Chem 75:5767–5774. https://doi.org/10.1021/ac034568c

Etcheverry S, Faridi A, Ramachandraiah H et al (2017) High performance micro-flow cytometer based on optical fibres. Sci Rep 7:5628. https://doi.org/10.1038/s41598-017-05843-7

Fiddler M (2014) Fetal cell based prenatal diagnosis: perspectives on the present and future. J Clin Med 3:972–985. https://doi.org/10.3390/jcm3030972

Frankowski M, Theisen J, Kummrow A et al (2013) Microflow cytometers with integrated hydrodynamic focusing. Sensors (Basel) 13:4674–4693

Fu LM, Yang RJ, Lin CH et al (2004) Electrokinetically driven micro flow cytometers with integrated fiber optics for on-line cell/particle detection. Anal Chim Acta 507:163–169. https://doi.org/10.1016/j.aca.2003.10.028

Guo J, Liu X, Kang K et al (2015) A compact optofluidic cytometer for detection and enumeration of tumor cells. J Light Technol 33:3433–3438. https://doi.org/10.1109/JLT.2015.2407397

Holmes D, Morgan H, Green NG (2006) High throughput particle analysis: combining dielectrophoretic particle focussing with confocal optical detection. Biosens Bioelectron 21:1621–1630. https://doi.org/10.1016/j.bios.2005.10.017

Huh D, Tung Y-C, Wei H-H et al (2002) Use of air-liquid two-phase flow in hydrophobic microfluidic channels for disposable flow cytometers. Biomed Microdevices 4:141–149

Huh D, Gu W, Kamotani Y et al (2005) Microfluidics for flow cytometric analysis of cells and particles. Physiol Meas 26:R73–R98. https://doi.org/10.1088/0967-3334/26/3/R02

Ibrahim SF, van den Engh G (2007) Flow Cytometry and Cell Sorting. Springer, Berlin, Heidelberg, pp 19–39

Jakobsson O, Grenvall C, Nordin M, et al (2015) Correction: acoustic actuated fluorescence activated sorting of microparticles. Lab Chip 15:4625–4625. https://doi.org/10.1039/C5LC90123E

Lee G-B, Chang C-C, Huang S-B, Yang R-J (2006) The hydrodynamic focusing effect inside rectangular microchannels. J Micromech Microeng 16:1024–1032

Lee MG, Choi S, Park J-K (2009) Three-dimensional hydrodynamic focusing with a single sheath flow in a single-layer microfluidic device. Lab Chip 9:3155. https://doi.org/10.1039/b910712f

Petchakup C, Li KHH, Hou HW (2017) Advances in single cell impedance cytometry for biomedical applications. Micromachines. https://doi.org/10.3390/mi8030087

Preckel T (2010a) Analysis of Single cells using lab-on-a-chip systems. In: The microflow cytometer. Pan Stanford Publishing

Preckel T (2010b) Analysis of single cells using lab-on-a-chip systems. In: The microflow cytometer. Pan Stanford Publishing

Reggeti F, Bienzle D (2010) Flow cytometry in veterinary oncology. Vet Pathol 48:223–235. https://doi.org/10.1177/0300985810379435

Schwan HP (1957) Electrical properties of tissue and cell suspensions. Adv Biol Med Phys 5:147–209

Shivhare PK, Bhadra A, Sajeesh P et al (2016) Hydrodynamic focusing and interdistance control of particle-laden flow for microflow cytometry. Microfluid Nanofluidics. https://doi.org/10.1007/s10404-016-1752-z

Sobti RC, Krishan A (2003) Advanced flow cytometry: applications in biological research. Springer, Netherlands

Stiles T, Fallon R, Vestad T et al (2005) Hydrodynamic focusing for vacuum-pumped microfluidics. Microfluid Nanofluidics 1:280–283. https://doi.org/10.1007/s10404-005-0033-z

Wang D, Bodovitz S (2010) Single cell analysis: the new frontier in "Omics". Trends Biotechnol 28:281–290

Wang MM, Tu E, Raymond DE et al (2005) Microfluidic sorting of mammalian cells by optical force switching. Nat Biotechnol 23:83–87. https://doi.org/10.1038/nbt1050

Weaver JL (2000) Introduction to flow cytometry. Methods 21(3):199–201

Wu M-H, Wang J, Taha T, Cui Z, Urban J, Cui Z (2007) Study of on-line monitoring of lactate based on optical fibre sensor and in-channel mixing mechanism. Biomed Microdevices 9:167–174, 8p

Yin H, Marshall D (2012) Microfluidics for single cell analysis. Curr Opin Biotechnol 23:110–119. https://doi.org/10.1016/j.copbio.2011.11.002

Zhang J, Chen K, Fan ZH (2016) Circulating tumor cell isolation and analysis. Adv Clin Chem 75:1–31. https://doi.org/10.1016/bs.acc.2016.03.003

Zhao Q, Yuan D, Yan S et al (2017) Flow rate-insensitive microparticle separation and filtration using a microchannel with arc-shaped groove arrays. Microfluid Nanofluidics 21:1–11. https://doi.org/10.1007/s10404-017-1890-y

Chapter 17
Microfluidic Sensors for Mechanophenotyping of Biological Cells

A. Raj and A. K. Sen

Abstract The mechanical properties of cells have been considered as biomarkers to indicate the presence of various diseases and changes in cell states. In literature, various conventional techniques have been established for studying cell mechanics such as atomic force microscopy (AFM), optical tweezers (OT), micropipette aspiration (MA), and cell stretching. Traditional techniques are time consuming and produce low throughput which is inadequate for time-sensitive analysis as well as has lesser clinical relevance. Toward this, microfluidic techniques provide attractive and suitable platform for cell phenotyping because of comparatively higher throughput, requirement of small sample volume, integration capability, biocompatibility, fast response, and dimensional match with biological cells. In the last few years, various microfluidic techniques have been developed for studying the mechanics of single cells. In this chapter, we present some of the recently developed microfluidic techniques and explain their benefit over the traditional techniques.

Keywords Mechanophenotyping · Cell phenotyping · Biophysical characterization · Mechanical property of biological cells · Disease diagnosis Microfluidic sensors

1 Introduction

Cells being the basic functional unit of life are well known to sense the biochemical as well as mechanical cues present in vicinity. In order to perform their various functions, cells control a number of intracellular and extracellular actions many times with the influence of the external forces experienced by them (Suresh 2007; Hervy 2010). The source of external forces varies for different kinds of cells

A. Raj · A. K. Sen (✉)
Department of Mechanical Engineering, Indian Institute of Technology Madras, Chennai 600036, India
e-mail: ashis@iitm.ac.in

S. Bhattacharya et al. (eds.), *Environmental, Chemical and Medical Sensors*, Energy, Environment, and Sustainability, https://doi.org/10.1007/978-981-10-7751-7_17

in vivo. For example, vascular cells have to face the shear stress from the blood flow and tension force because of the blood pressure (Hervy 2010). Similarly, pulmonary cells are subjected to cyclic stretching because of respiration (Hervy 2010).

A major part of functioning in biology and physiology involves cell mechanics. Structural integrity of the cell keeps the shape intact and often cell shape is responsible for its actions (Kamm et al. 2010). For example, the biconcave shape of the red blood cell provides them comparatively large surface-to-area ratio which helps in a better gas exchange (such as exporting oxygen to different organs). Also, the spherical shape of white cells or leukocytes makes them capable to roll along the blood vessel endothelium wall before adhering and migrating into the tissue. Leukocytes have excess membranes in the form of microvilli which enable them to deform at constant volume while migration. Moreover, the organization of the cytoskeletal structure of the muscle cells is such that they can actively generate forces and are able to sustain large strains. Thus, internal structure of the cell keeps the shape maintained to perform various functions.

Cell migration is one of the major parts of physiological processes, which is not only important in the early development (such as embryo development) but also to sustain life in the fully differentiated organism. For example, in the case of wound repair, healthy cells migrate into the wound. Also, angiogenesis (generation of new blood vessels) and combating infections in which immune cells migrate to the infected tissues by crossing the blood vessel wall are few other examples which show the importance of cell migration. Thus, optimal level of cell mechanical property is crucial for healthy functioning of the human body.

An optimal level of mechanical property (i.e., the structural integrity, deformability, and shape) of the cells as well as arterial walls is crucial for the healthy functioning of the body. Any alteration in the mechanical property can cause a disruption toward the functioning of the body leading to a diseased state. For example, any damage in the contractility of heart muscle cells gives rise to a high possibility of heart failure (Fung 1993). Malaria-infected red blood cells are known to loosen their deformability which affects the efficiency of the oxygen transport process and may cause an abnormal blood flow (Shelby et al. 2003). This stiffening causes vessel blockage which may lead the patients to coma and finally death. Likewise, the stiffening and increased viscosity of the erythrocytes have been reported for the case of sickle cell anemia which leads to obstruction of small vasculature and causes clinical vasco-occlusion events (Lemonne et al. 2013). Similarly, in the case of asthma, due to stiffening of airway smooth muscle cells, pulmonary airway constricts during breathing (Kamm et al. 2010). Also, during traumatic brain injury, excessive stretching of the axon of neural cells may cause cell death (Morrison et al. 1998). Cancerous cells have been reported to be softer than their normal counterpart, which is one of the major causes of cancer progression leading to death of the patient (Cross et al. 2007). Literature reports alterations in the concentration of cytoskeletal structure and contents from an ordered and rigid structure to a more irregular and compliant state is the main

reason of the increased deformability for the cancerous cells (Suresh 2007; Li et al. 2008). Thus, onset of disease directly leads to the anomalies in the structural and physical characteristics of the cells due to the alteration in the cytoskeleton structure. Hence, the mechanical property of the cells can act as an effective label-free biomarker for the detection of the diseases (Di Carlo 2012).

Having understood the importance of cell mechanical property as a biomarker, a highly competent and clinically relevant technique to characterize the mechanical property of the cells is demanded. The basic approach to characterize the mechanical property (deformability in the present case) of the cell is to deform the cell with the application of force and extract the deformability by relating the force applied, the resulted deformation, and the deformability of the cell in terms of its elastic properties. Since the cells are deformable in nature, an applied force little more the threshold deforms the cell. Also, the availability of 80–100% excess area in terms of wrinkles and folds in the cell membrane allows the cells to deform under an applied load (Schmid-Schonbein et al. 1980). In this chapter, we will be presenting traditional as well as the microfluidic techniques available in the literature for the characterization of the cell mechanical property. Firstly, major traditional techniques such as atomic force microscopy (AFM), micropipette aspiration (MA), and optical tweezer (OT) are explained briefly. Then, some of the recently developed microfluidic techniques (basically of three types: Fluid induced, Structure induced and Aspiration induced) are described.

2 Traditional Techniques of Cell Mechanophenotyping

2.1 Micropipette Aspiration

This is one of the most popular traditional techniques till date being utilized to characterize the mechanical properties of a cell. The first time usage of the micropipette aspiration technique dates back to the year 1954, when Mitchison and Swann (1954) had demonstrated the usage of this technique to measure the elastic property of sea urchin eggs. In this technique, the whole cell is aspirated into the glass pipette (sizes smaller than the cell size) with the application of small negative pressure (see Fig. 1a). Under the influence of negative pressure, the cell protrudes into the pipette with a certain leading edge length L_p which is a function of the suction pressure applied. The leading edge movement at various suction pressures

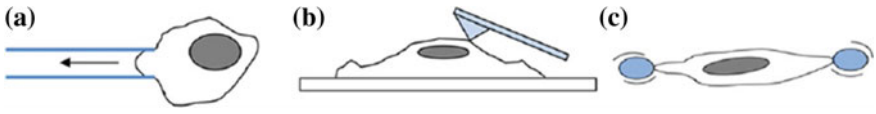

Fig. 1 **a** Micropipette aspiration, **b** Atomic force microscopy, **c** Optical tweezers. (Adapted from Ahmad et al. (2014) with the permission from Springer)

is tracked by recording the video on an optical microscope which is further translated into various quantitative mechanical properties of the cell using suitable models. By assuming the cell as a homogenous continuum solid, Young's modulus (E) can be determined for known value of suction pressure L_p and the inner radius of the pipette (Hochmuth 2000). However, if the cell is assumed to be a viscous solid, the viscosity can be deduced with the input of the radius of spherical portion of the cell outside the pipette and the rate of progression of the leading L_p with time (Hochmuth 2000). Also, the cortical tension value of the cell is related to Young's modulus E and the internal radius R_p of the pipette, which can be utilized to find out the cortical tension value. For a detailed description of the approaches, please refer to the extensive review on micropipette aspiration by Hochmuth (2000). This technique has been utilized to measure the mechanical property of various types of cells such as leukocytes (Evans and Yeung 1989; Herant 2005; Ting-Beall et al. 1993), red blood cells (Hochmuth 1993), chondrocytes (Trickey et al. 2006), platelets (McGrath et al. 2011), and cancer cells (Lee and Liu 2015). Although MA is conceptually simple, the following are the challenges. It requires specialized equipments and involves delicate procedures which demand highly skilled operation. Since conventional instruments are prone to mechanical vibration, temperature, humidity fluctuations, and noise offsets, producing precise negative pressure is difficult (Ahmad and Ahmad 2014). One single-cell measurement takes 10 min, which limits the throughput drastically (Lee and Liu 2015). Further, liquid evaporation from the reservoir affects the accuracy of the applied negative pressure in an open atmosphere. Also, it needs periodic recalibration to eliminate the effect of drifting baseline (Ahmad and Ahmad 2014).

2.2 *Atomic Force Microscopy*

Atomic force microscopy (AFM) is another classical technique which has been serving the community very well since last few decades. Originally, AFM technique was founded by Binnig et al. back in 1986 for characterizing the atomic and surface properties of materials for electronic devices (Binnig and Quate 1986). Later, it has been utilized for biological specimens such as cells. AFM technique utilizes a probe tip attached to a flexible cantilever to indent on the surface of the cell (see Fig. 1b). The tip is directed downward toward the cell surface by a piezoelectric stage which has a precision of (sub-) nanometer range. This applies a small indentation force (typically in the range of $10\,\text{pN}-100\,\text{nN}$) onto the cell surface, and the deflection of the flexible cantilever is measured by tracking the tip displacement using laser. Further, the deflection of the cantilever is used to deduce the value of indentation depth and calculate the applied force. Once the force-indentation curve is plotted, the mechanical property (Young's modulus or shear modulus) of the cell is determined by suitably fitting the experimental curve with the one generated using Hertz model (or with some modifications) assuming

cell as a linear, elastic, and isotropic material (Radmacher et al. 1994). More detailed description of measurement and the post-processing of the data can be found from our previous work (Sajeesh et al. 2016). Our group has utilized atomic force microscopy to extract Young's modulus value of various cell lines (MCF-7, MDAMB-231, HL60, and HeLa) (Sajeesh et al. 2016).

AFM is a non-destructive technique and can be utilized to all eukaryotic cells. AFM has been used not only for probing the mechanical property of the whole cell, but also to investigate their mechanotransductive response to the applied force (Charras et al. 2001; Charras and Horton 2002). Nevertheless, following are the challenges associated with the technique. Using this technique, only one cell can be probed at a time, which increases the time required to probe large number of cells, often desirable for the cases like this because of the inherent heterogeneity present in the biological systems. The measurement can get influenced by the experimental conditions such as indenting force, AFM tip geometry, and operating temperature; hence, multiple trials on the same cell are required to achieve repeatable data. Also, it has bulky experimental apparatus and is difficult to handle. Moreover, this technique is not suitable for non-adherent cells because these kinds of cells are not stable on the substrate under the application of load due to absence of adherence. However, there are studies in which non-adherent cells are immobilized in a microwell and characterized using AFM (Rosenbluth et al. 2006).

2.3 Optical Tweezers (OT)

Optical tweezers (OT) is an optical technique which utilizes photon trapping to manipulate cells. Originally, this technique was developed for trapping individual atoms, viruses, and bacteria by Arthur Ashkin of Bell Telephone laboratories (Ashkin 1970). It works on the principle of conservation of photon momentum. Two dielectric beads (50–1000 nm), one attached to the glass slide and another in control of infrared laser, are utilized to trap a single cell for manipulation (see Fig. 1c). The laser photons are directed toward the beads with the help of high-powered microscope. The laser beam changes its direction because of the presence of beads (depending upon the refractive index of the bead), which causes an alteration in the momentum of the beam developing a force onto the beads. This way, laser beams can trap the beads at its central spot. The beads used here are coated with ECM proteins like fibronectin which bind with the cell's integrin by forming focal adhesion complexes (Rodriguez et al. 2013). Then, the trapping force (typically in range $0.01-1000\,\text{pN}$) is applied to the cell by adjusting the central portion of the laser beam. With the application of force, the cells deform three dimensionally reducing the diameter in the transverse direction and increasing the diameter in the direction of force application. The deformation of the cell is monitored with the function of applied stretching force, and the deformation behavior is further translated to the elastic property of the cell or shear modulus of the cell membrane using various constitutive relations. For more details regarding

the theoretical and computational module utilized for the extraction of mechanical property using optical tweezer method, please refer to the work by Dao et al. (2003). The resulting deformation of the cell between the two beads is monitored. This technique has been utilized to probe various types of cells such as red blood cells (Dao et al. 2003; Lim et al. 2004), fibroblasts (Ananthakrishnan et al. 2006), tumor cell (Guck et al. 2005), and epithelial cells (Guck et al. 2005).

Since this technique does not involve any contact between cells and the force producing and sensing mechanism, it eliminates contamination from the system (Rodriguez et al. 2013). However, the maximum force that can be applied with the technique is <1 nN because higher force needs high-power laser which can excessively heat the cell leading to death. Also, the maximum force is often small for producing large-scale cellular deformation, especially in the case of stiffer cells (Kamm et al. 2010).

3 Microfluidic Techniques

Although all the traditional techniques are accurate, it requires sophisticated instruments and skilled operations. Moreover, the issues of low throughput and tedious operations make them clinically irrelevant (Suresh 2007; Lee and Lim 2007). Toward this, microfluidics provides an attractive platform for cellular property characterization as an alternative mainly due to its small length scale, reduced sample volume needed, and well-developed fabrication techniques (Zheng et al. 2013). Microfluidic devices are mainly fabricated using silicon, glass, and transparent polymeric materials [such as poly-dimethylsiloxane (PDMS)]. PDMS is a biocompatible material, and because of its transparency, it is suitable for most imaging techniques. Moreover, since the microenvironment can mimic the physiological environments, microfluidics is able to provide us a platform where studies on cellular responses to mechanical (or chemical) stimulus can be carried out. Further, the throughput of the measurement is much higher than the traditional techniques. Most importantly, it is integration capability with other platforms such as imaging and data acquisition enables us for real-time analysis of diseases which makes it clinically relevant (Hou et al. 2011).

In this section, we will be presenting few of the recently developed microfluidic techniques. The techniques are categorized basically in three types: fluid induced, structure induced, and aspiration induced depending upon the basic approach taken to induce the deformation to the cells.

3.1 Aspiration Induced Technique

This technique is the reproduction of the traditional MA technique using microfluidic device with additional benefits associated with microfluidics. The principle

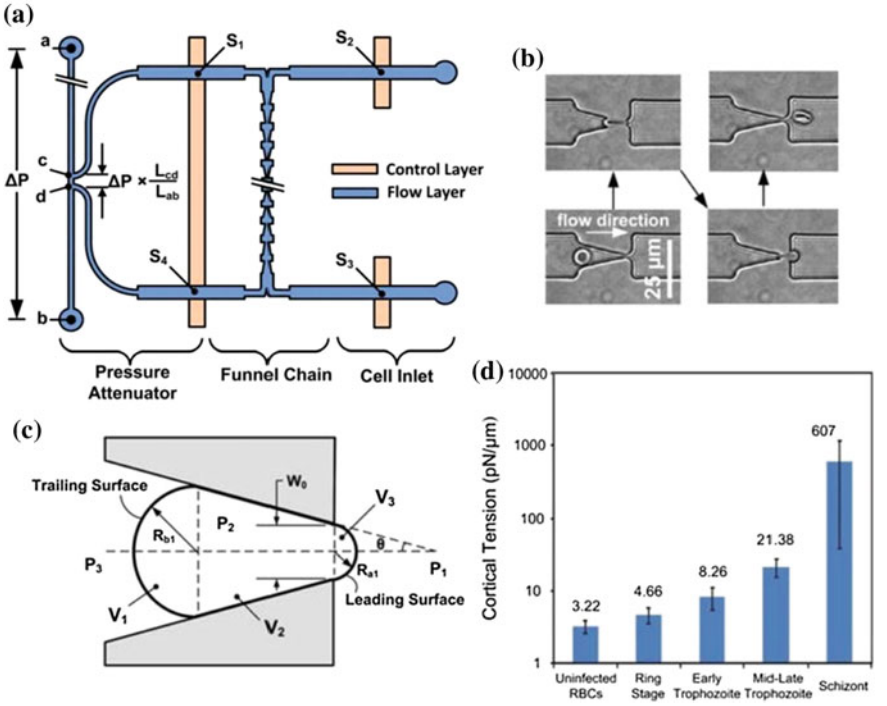

Fig. 2 **a** Infrastructure of the microfluidic device. **b** Micrograph showing the deformation of RBC while migrating through the funnel-shaped constriction. **c** Schematic showing the different notations utilized in the theoretical model with a cell deformed at the mouth of the funnel constriction. **d** Predicted cortical tension value of the RBCs parasitized with *Plasmodium falciparum* at different stages. (Reproduced from Guo et al. (2012) with the permission from Royal Society of chemistry)

of MA is utilized on the microfluidic device to probe the mechanical property of the cell. In place of cylindrical pipette, a microchannel with rectangular cross section is utilized to aspirate the single cell under a pressure gradient. Once the single cell migrates into the microchannel, the kinetics of cell shape deformation during entry is utilized to extract the cellular mechanical property by using suitable model. There are many works on this principle (Lee and Liu 2015; Guo et al. 2012). Guo et al. (2012) have reported a microfluidics device which utilizes a funnel-shaped constriction microchannel to deform the cell under an applied pressure gradient across it. Figure 2a shows the infrastructure of the microfluidic device. A single cell is flown into the constriction at a precisely controlled hydrodynamic pressure. Once the cell moves into the mouth of the funnel constriction, the pressure gradient is increased slowly till the point the cell moves across the constriction. Sequence of images showing cell moving across the funnel constriction is shown in Fig. 2b. This gives the threshold pressure needed for the cell to successfully transit the constriction. Now, assuming the cell as a liquid drop with constant volume and

persistent cortical tension, the threshold pressure is related to the cortical tension of the cell membrane T_c (Intrinsic mechanical property of the cell) and the radii of curvatures (R_{a1} & R_{b1} as shown in Fig. 2c) by utilizing Young–Laplace equation (Hochmuth 2000) as shown in Eq. (1).

$$P_3 - P_1 = T_c\left(\frac{1}{R_{a1}} - \frac{1}{R_{b1}}\right) \tag{1}$$

Please refer to Fig. 2c for the notations which show the deformed cell while it is entering into the funnel constriction. Once the threshold pressure $(P_3 - P_1)$ and radii of curvatures are extracted from the experiments, Eq. (1) is utilized to determine the cortical tension value of the aspirated cell. This technique could successfully show the contrast in the predicted cortical tension value for RBCs parasitized with Plasmodium falciparum at different stages as shown in Fig. 2d. Figure 2d clearly shows the cortical tension which essentially indicates the stiffness of the cell, increases with the progression of different stages (ring, early trophozoite, late trophozoite, and schizont being the last stage) of malaria infection.

There is another microfluidic device recently presented named as microfluidic pipette array device (μFPA), which utilizes a microfluidic device with a number of parallel constriction channels (sizes lesser than the cells) (Fig. 3a) (Lee and Liu 2015). Single Cell is trapped in the constriction post, and the pressure gradient is applied across the constriction. Because of the device infrastructure, any infused flow of the cell sample distributes itself into parts at the constriction post junction. This produces variable pressure gradient across the different posts. Also, as the input flow rate is changed, the pressure gradient across the posts modifies. Once cell sample is infused into the device, single cells automatically get trapped in the constriction post which has certain pressure gradient across it. Similar to micropipette aspiration technique, at a certain pressure gradient, the single cell protrudes into the constriction channel (hydraulic radius R_p) with a protrusion length L_p which is tracked using a microscope. Now, input flow rate to the microfluidic device is increased which accordingly increases the pressure gradient across the trapped cell resulting to a new L_p. Figure 3b shows the microscopic image of the progression of cell's leading edge (indicated by the yellow arrow) for two different kinds of cells (MDAMB-231 and MCF-10A) with the variation in the pressure gradient. Thus, a number of data points are obtained for L_p at various pressure differences Δp across the cell and are plotted as shown in Fig. 3c.

Further, assuming cell as a homogeneous elastic solid, Young's modulus of the single cell E can be given as (Theret et al. 1988)

$$E = \left[\frac{\frac{3\Delta p \Phi}{2\pi}}{\frac{L_p}{R_p}}\right] \tag{2}$$

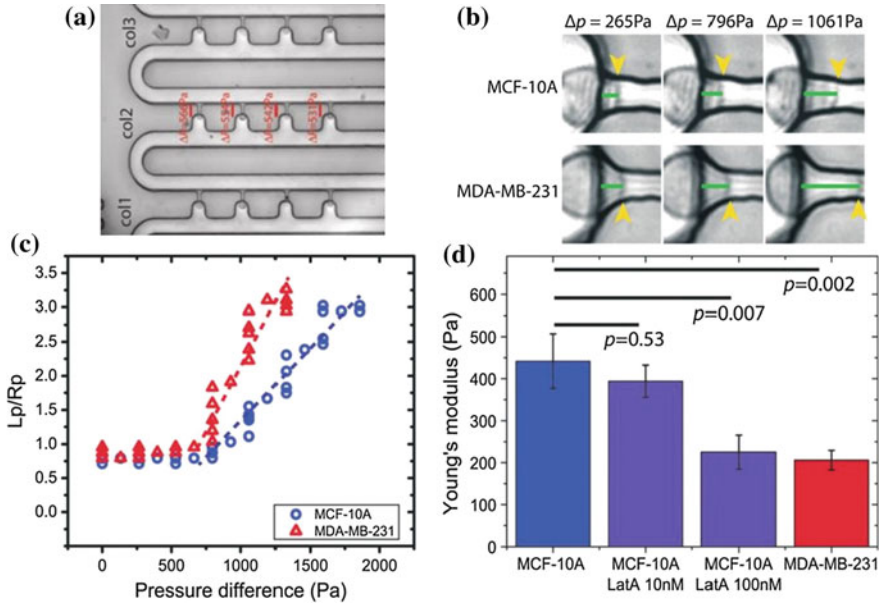

Fig. 3 **a** Infrastructure of microfluidic pipette aspiration device. **b** Micrograph showing the progression of cell leading edge into the microconstriction channel with the increase in the applied pressure gradient. **c** Experimentally measured protrusion length at various applied pressure gradients. **d** Predicted Young's modulus of the cells using μFPA. (Reproduced from Lee et al. (Lee and Liu 2015) with the permission from Royal Society of chemistry)

where Φ is a constant dependent on the geometry of the micropipette and typically takes a value of 2.1. To determine Young's modulus of the aspirated cell, the advancing linear portion of the protrusion curve (Fig. 3c) is fitted with a linear regression (Hochmuth 2000). The slope of the fitted line is utilized to extract Young's modulus of the aspirated cell by incorporating into Eq. (2). This technique could predict Young's modulus of normal breast epithelial cell lines MCF-10A and cancerous breast cell line MDAMB-231 (As shown in Fig. 3d) which are in good agreement with the micropipette aspiration data tested by Lee and Liu (2015). Also, the technique was tested to detect the decrease in the stiffness of the cell because of the treatment with Latrunculin-A [microfilament disrupting chemical (Vargas-Pinto et al. 2013)] and could sense the variation in stiffness for treatment with two distinct concentrations of Latrunculin-A solution as shown in Fig. 3d. Also, *p*-values are indicated in Fig. 3d from student's t test, which clearly shows a significant difference between the measured data for four different cell lines.

3.2 *Fluid Induced Techniques*

These are another type of microfluidic techniques which utilize the converging streamlines to induce force on the cells. Since in this technique force is applied purely by flow, the direct contact between cell and the microstructures is eliminated. This demands the size of the microchannel to be bigger than the cell sizes. The deformability of the cell is characterized in terms of deformation index or stretch ratio which is captured using high-speed imaging. Less-stiff cells like RBCs can be deformed under fluid shear stress by flowing them through simple, straight microchannels as studied by many earlier literature (Forsyth et al. 2010; Tsukada et al. 2001). Apart from straight microchannels, hyperbolic converging microchannels have also been utilized for probing mechanical property of RBCs (Lee et al. 2009). However, low magnitude of fluid shear is not sufficient for other stiffer cells (Zheng et al. 2013). Toward this, Gossett et al. (2012) have developed a hydrodynamic-stretching microfluidic device (refer to Fig. 4). In this technique, the cells are focused at the center of the microchannel and then brought to a junction of two orthogonal microchannels at high flow rate where cells deform as shown in Fig. 4a. The cell deformation is captured using high-speed camera, and images are evaluated to measure the deformation index (DI) and the cell volume. Figure 4b shows the close-up view of a deformed cell, where the diameter of the deformed cell is measured in longitudinal (shown by b) and transverse direction (shown by a). Figure 4c shows the deformation of a single MCF-7 cell with time as it approaches toward the junction of two orthogonal microchannels. The deformability of the cell was defined as a/b and was measured for cells (a total number of $N = 9{,}740$) of various initial non-deformed diameters d as shown in Fig. 4d.

The technique could show a clear contrast between the DI and volume measured for cancerous cells as compared to benign cells. The throughput observed for this technique is $\sim$2000 cells s^{-1} which is quite higher than most of the other techniques and hence proves itself to be a good candidate for clinical applications. Also, recently, Guillou et al. (2016) have presented an analytical model which can

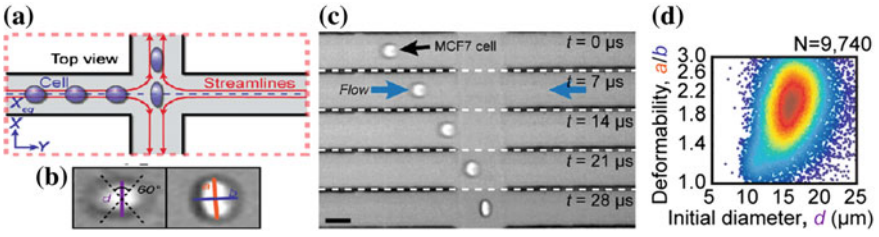

Fig. 4 **a** Schematic of the hydrodynamic-stretching microfluidic device showing the stretching of the cell at the junction of two orthogonal channels, **b** experimental micrograph showing the deformed shape of the cell at the junction. **c** Process of deformation of single MCF-7 cell with time while moving toward the junction. **d** Scatter plot showing the deformability of human embryonic stem cells of various non-deformed diameters (Gossett et al. 2012)

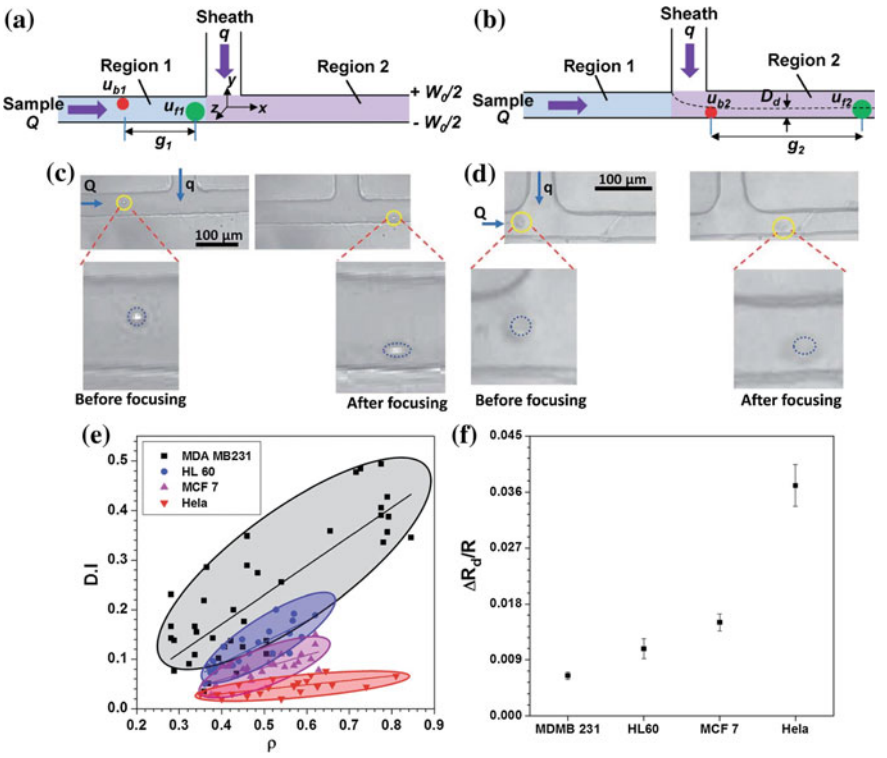

Fig. 5 **a**–**b** Schematic of working principle of the focusing and spacing control module; before T-junction (**a**) and after T-junction (**b**), micrograph showing hydrodynamic stretching of MDAMB-231 cells (**c**) and HeLa cells (**d**) at flow rate ratio f_p = 1.5 (ratio of the sheath fluid flow rate q to the sample fluid flow rate Q), **e** Comparison of deformability index for various cells at different size ratios; f_p = 1.5, **f** induced hydrodynamic resistance offered by various cells at fixed size ratio (ratio of the cell diameter to the channel hydraulic diameter) ρ_c = 0.7. (Reproduced from Sajeesh et al. (2016) with the permission from Royal Society of chemistry)

incorporate the deformation of the cells in these kinds of characterization techniques and predict the shear modulus of the cells. Also, they have validated the developed analytical model to predict the shear modulus of 3T3 fibroblast cell and could obtain data in the same order of MA technique (experimented by them) as well as the presented data in the earlier published work by Evans and Lips (1990).

Our group has also developed a focusing and spacing control module microfluidic device (Sajeesh et al. 2015), which was later utilized to characterize the mechanical property of various cells (Sajeesh et al. 2016). Figure 5a, b shows the working principle of spacing and focusing control module device. Cells randomly distributed across the cross section (in the region 1) are modified as a flow with cells moving in a single file along the side wall of the channel (in the region 2 of Fig. 5a) by adding the sheath fluid with flow rate q to the mainstream channel. The sheath fluid applies shear to the surface of the cells moving in single file along the side

wall and thus deforms the cells as shown in Fig. 5c, d. The deformability index as defined in our previous work (Sajeesh et al. 2014) is measured by analyzing the videos and images captured using high-speed imaging. Figure 5c shows the deformability index of highly malignant breast cancer cell line MDAMB-231 is much higher than HeLa cells (Fig. 5d) which is well supported by Young's modulus reported for the two cell lines (Sajeesh et al. 2016). Figure 5e shows the deformability index measured for various cell lines which follows a trend visible in Young's modulus data measured using AFM (Sajeesh et al. 2016). Softer cell shows higher deformability index than the stiffer cells.

Further, the induced hydrodynamic resistance offered by a single cell while flowing through the microchannel also acts as an indirect measure of the stiffness of the cell.

Induced hydrodynamic resistance offered by the cell was measured and compared (Sajeesh et al. 2016) at various size ratios. Stiffer cells offer higher induced hydrodynamic resistance than the softer cells. Under an applied shear, the softer cells deform more increasing the thickness of liquid film between cell surface and the channel wall. This increased film thickness decreases the viscous dissipation and thus contributes to a lesser pressure drop across the microchannel. Figure 5f shows the induced hydrodynamic resistance offered by cells of varying stiffness. Thus, it becomes clear fluid induced deformation techniques can provide various indirect and direct measures of mechanical property of the cell.

In fluid induced deformation technique, as the channel dimensions are larger than cell diameters, the effect of adhesion between cell and channel wall is eliminated.

Despite of all the benefits, the fluid induced probing technique has a drawback. It requires the use of high-speed imaging (tens of kHz) for measuring DI. High-speed cameras are often costly, and along with optical microscope, it makes the overall microfluidic system bulky (Zheng et al. 2013).

3.3 Structure Induced Techniques

These techniques are inspired from the process of microcirculation in which blood cells migrate through the microcapillaries. As explained in the introduction section, onset of diseases like malaria or sickle cell anemia results in the blockage of small vasculatures which show a method to sense the deformability of the cell. In order to test the mechanical property, microcapillary alike microchannels are utilized in these techniques (see Fig. 6a).

Single cell is pressurized to migrate through the constriction microchannel and the resulting deformation as well as passage behaviors is utilized to characterize the mechanical property. Under an applied pressure gradient, the cells squeeze themselves and pass through the constriction microchannels. Various parameters such as entry time (time taken by a single cell to squeeze into the constriction), extension ratio

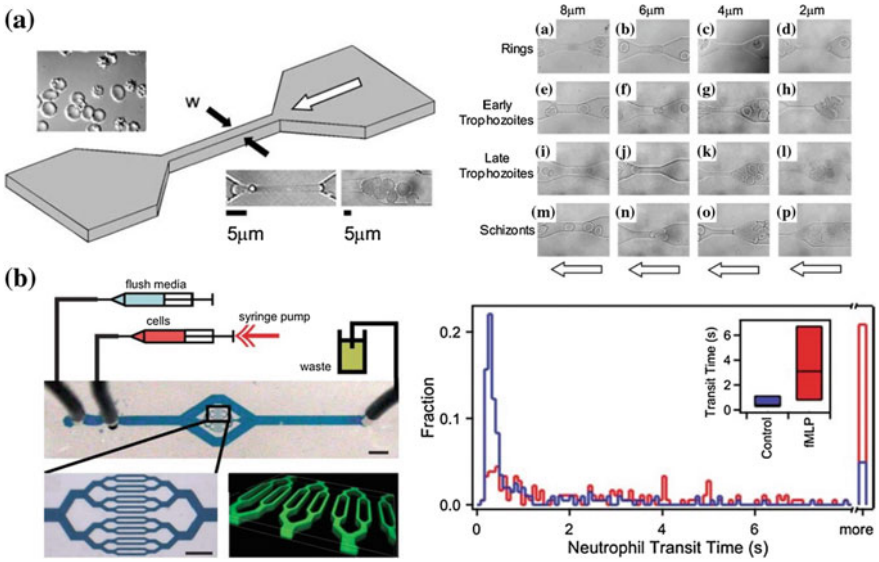

Fig. 6 **a** Left—infrastructure of single constriction microchannel and right—micrographs showing the migration of malaria-infected RBCs at different stages. The early trophozoite and late trophozoite could squeeze through 8 and 6 μm constriction channels but blocked the 4 and 2 μm. Schizoint stage cells blocked all the channels except 8 μm. On the other hand, ring stage cell could migrate through all the constrictions; Shelby et al. (2003) (Xue et al. 2015) **b** Left—infrastructure of the microfluidics device presented by Rosenbluth et al. (2008) and right—experimentally measured transit time for healthy neutrophil and fMLP-exposed neutrophils; fMLP is the inflammatory mediator involved in sepsis; (Reproduced from Rosenbluth et al. (2008) with the permission from Royal society of chemistry)

(ratio of deformed cell length in the constriction to undeformed diameter of the cell), and passage time or velocity act as an indirect measure of the deformability of the cell.

First time, the utility of constriction microchannel (fabricated using PDMS) was demonstrated by Shelby et al. (2003). The constriction microchannels of various hydraulic diameters were exploited to study the migration of healthy as well as malaria-parasitized RBCs of different stages (early ring stage, early trophozoite, late trophozoite, and schizont) (see Fig. 6a—right image). The results demonstrate the deformability of RBCs decreases with the progression of parasite stage, and infected RBCs block the channel. However, the healthy RBCs transit the constriction channel easily. Later, Rosenbluth et al. (2008) have designed a microfluidic device with a network of 64 constriction channels (Fig. 6b), which solve the issue of clogging of the device and increase the throughput making it clinically relevant. The device was tested for white blood cells of sepsis and leukostasis patients, and the transit time was found to be higher than the healthy cells (see Fig. 6b right). Our group has also developed a microfluidic device with multi-constrictions which solves the issue of clogging and allows the

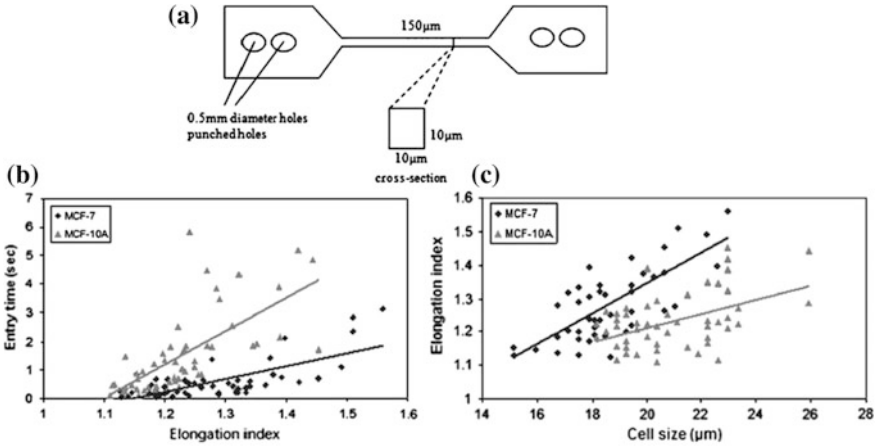

Fig. 7 **a** Schematic of the single constriction device used by Hou et al. (2009) **b** entry time variation with the elongation index **c** variation of elongation index for various cell sizes; (Reproduced from Hou et al. (2009) with the permission of Springer)

characterization of mechanical property of cells in high throughput manner (Raj and Sen 2016). Further, a clear contrast in the entry time between breast cancerous cell line MCF-7 and normal breast epithelial cell line MCF-10A has been reported (Hou et al. 2009). It was concluded this technique can be utilized to distinguish different cell types by investigating the contrast of scatter plots of cell volume and entry time. Figure 7a shows the schematic of the setup used by Hou et al. (2009). Elongation index (ratio of deformed cell length to the non-deformed cell diameter) is dependent on the cell diameter (Fig. 7b) which shows a clear separate scatter plot for two different cell lines. Also, entry time dependency over the elongation index is shown in Fig. 7c. Thus, the scatter plot for cell size and entry time is utilized to distinguish between the two different cells.

Further, Byun et al. (2013) have investigated the role of friction and the deformability of the cell in the metastatic potential using a constricted microchannel in the suspended microchannel resonator device. It was found changing the deformability by alteration in the cytoskeleton changes the entry time, and alteration in the surface friction mainly changes the transit velocity. Hence, transit velocity alone does not give the complete picture of the deformability of the cell.

There have been efforts to extract the mechanical property of the cells by utilizing entry time of the cell (Leong et al. 2011; Luo et al. 2014). Leong et al. (2011) have presented a numerical model which can be used along with the experimental entry time to predict the apparent cytoplasmic viscosity of the cells. The apparent cytoplasmic viscosity predicted by the numerical model for normal breast epithelial cell line MCF-10A (6.4 Pa s) falls in the same order with the reported values using MA studies. Further, Luo et al. (2014) have developed a numerical model assuming the cell to be a visco-hyperelastic solid, which utilizes the cell entry process into the constriction channel to extract the instantaneous Young's modulus of the cell.

With the support of high-speed imaging, constriction channel devices are capable to achieve higher throughput than most of the techniques. Moreover, it can be integrated with optical stretcher (Lee et al. 2007) as well as electrical impedance measurement system (Zheng et al. 2012) in order to improve the sensitivity and the reliability. However, one issue with these kinds of devices are the adhesion between the cell membrane and the channel wall which effects the measurements. The undesirable adhesions are generally avoided by coating the PDMS microchannel walls with a diluted solution of bovine serum albumin (BSA; 4 wt%) (Hou et al. 2009).

3.4 Integration Capability of Microfluidics Techniques

Till now, we have discussed the microfluidic techniques for cell mechanophenotyping, which has naturally higher throughput than the traditional techniques because of presence of the fluid flow networks and dimensional similarity with the biological cell. However, to further improve the speed of measurement and analysis, there have been various techniques developed to capture and post-process the data actively and provide the quantitative or qualitative measure of the mechanical property of the cell. Toward this, the integration capability of the microfluidic device with electrode and optical fibers plays a vital role, which is explained further in detail below.

Adamo et al. have demonstrated the incorporation of electrodes on both sides of the constriction microchannel (Please see Fig. 8a) and utilized it to track the migration (Transit) behavior of the cells through the constriction microchannel (Adamo et al. 2012). The electrical resistance between the electrodes was monitored actively. As a single cell traverses through the narrow constriction, the overall electrical impedance increases which becomes visible in terms of a sudden rise in the electrical signal of the resistance, and the width of the bulging in the signal (sudden rise) (see Fig. 8a) is exploited to find out the transit time of the cell. Thus, using the electrodes, it is possible to monitor the passage time of each single cell online, which otherwise needed the post-analysis of the captured high-speed imaging microscopic migration videos of the cells. Further, microfluidics device provides a decent service to the investigations involving biology-related processes too such as exocytosis. Gao et al. (2009) have utilized a dam-like structure to trap single cell in the proximity of electrodes, and the resulting amperometric current from the exocytosis of catecholamine is recorded using electrodes for further analysis (see Fig. 8b). Figure 8b shows the infrastructure of the microfluidic device utilized by Gao et al. (2009). Cell sample is filled into the inlet reservoir and a negative pressure is applied at the exit reservoir which pumps the cell sample through the device. As the cell traverses through the bigger channel (20–70 μm) (see the right upper image of Fig. 8b), single cells get trapped in the cell docking sites which are the small (3 μm) channels in the side wall of the main channel and are connected to the exit reservoir as shown in the cross-sectional view (bottom

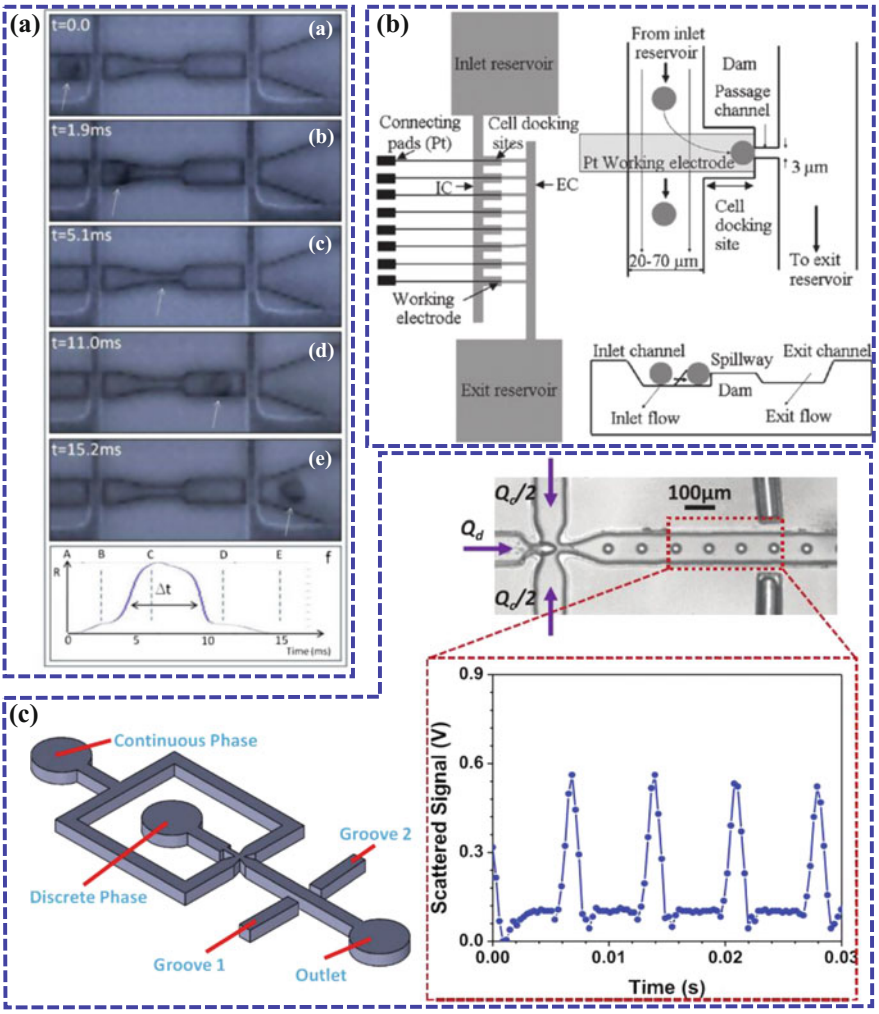

Fig. 8 Integration capability of microfluidics devices **a** electrodes incorporated on both sides of constriction microchannel; Once a single cell crosses the region between two electrodes, sudden rise in electrical resistance is visible as shown in the bottommost image; width of the rising region of signal Δt gives the transit time value of the cell. Reproduced from Adamo et al. (2012) with the permission from American Chemical Society. **b** Infrastructure of the device used by Gao et al. (2009); left image shows the overall layout of the device, right upper image shows the zoomed view of a single cell docking site with electrode near to it, right (down) image shows the cross-sectional view of the device with cell docking channel shown as dam. Reproduced from Gao et al. (2009, 2012) with the permission from Royal Society of chemistry. **c** Schematic of the optical fiber integrated microfluidic device used by Shivhare et al. (2017) (left), micrographic image of the droplet generation and detection using the optical system with graph showing the scattered signal of the droplets (Shivhare et al. 2017). Reproduced from Shivhare et al. (2017) with the permission from Institute of physics publishing

right image of Fig. 8b). Electrodes are installed close to the cell docking sites such that single cell anchored at the docking site touches the electrode. Once exocytosis is initiated, the amperometric current is monitored with the help the corresponding electrode touching the cell. Thus, in a single run, a number of cells are anchored at the docking sites, and exocytosis is performed in a high throughput manner with the data directly recorded.

Further, optical fibers are easily incorporated in the microfluidic device. In our previous work, we have utilized two optical fibers embedded into the grooves to predict the droplet size and frequency (Shivhare et al. 2017). Figure 8c (left) shows the schematic of the optical fiber integrated device. Focused illumination beam (of size ~ 10 μm) was used to obtain the forward-scattered signals which were processed through various optical interrogation techniques to predict the droplet size. Figure 8c (right) shows the obtained scattered signal of the droplet. The sudden peak in the signal shows the presence of droplet in the sensing zone between two optical fibers. The results obtained (droplet size and frequency) were in good agreement (with 10–13% error) with the conventional microscopy technique, which needs extra time to post-process the data in order to measure the droplet diameter and the frequency. Further, recently, Pedrol et al. (2017) have utilized the similar arrangement of optical fibers into the microfluidic device to detect the presence of circulating tumor cells in a sample. Thus, we find the microfluidic devices increase the speed of measurement and analysis by incorporating various electrical and optical platforms.

4 Conclusion

In this chapter, first of all, we have explained the importance of cellular mechanical property in the healthy functioning of the body and its role as a biomarker in the diagnosis of the disease. Then, few major traditional techniques (AFM, MA and OT) for cell mechanical property characterization were described briefly. Further, few of the recently developed microfluidic techniques were presented and discussed. Following are the main concluding remarks of the chapter:

- Despite being accurate and robust, traditional techniques for cell mechanophenotyping lack in the speed of the measurement and need sophisticated equipment which make them clinically irrelevant for time-sensitive analysis.
- Microfluidics provides an attractive platform to assess the mechanical property of the cells giving higher throughput as well as the measurement speed compared to the traditional techniques.
- The integration capability of the microfluidic devices with data acquisition systems and possibility of real-time analysis makes them a good candidate for time-sensitive diagnostic tests.

References

Adamo A, Sharei A, Adamo L, Lee B, Mao S, Mao S, Jensen KF (2012) Microfluidic based assessment of cell deformability. Anal Chem 84:417–428

Ahmad IL, Ahmad MR (2014) Trends in characterizing single cell's stiffness properties. Micro Nano Syst Lett 2:1–11

Ananthakrishnan R, Guck J, Wottawah F, Schinkinger S, Lincoln B, Romeyke M, Moon T, Käs J (2006) Quantifying the contribution of actin networks to the elastic strength of fibroblasts. J Theor Biol 242:502–516

Ashkin A (1970) Acceleration and trapping of particles by radiation pressure. Phys Rev Lett 24:156–159

Binnig G, Quate CF (1986) Atomic force microscope. Phys Rev Lett 56:930–933

Byun S, Son S, Amodei D, Cermak N, Shaw J, Kang JH, Hecht VC, Winslow MM, Jacks T, Mallick P, Manalis SR (2013) Characterizing deformability and surface friction of cancer cells. Proceedings of the National Academy of Sciences of the United States of America, 110(19), 7580–5

Charras GT, Horton MA (2002) Single cell mechanotransduction and its modulation analyzed by atomic force microscope indentation. Biophys J 82:2970–2981

Charras GT, Lehenkari PP, Horton MA (2001) Atomic force microscopy can be used to mechanically stimulate osteoblasts and evaluate cellular strain distributions. Ultramicroscopy 86:85–95

Cross SE, Jin YS, Rao J, Jk G (2007) Nanomechanical analysis of cells from cancer patients. Nat Nanotechnol 2(12):780–783

Dao M, Lim CT, Suresh S (2003) Mechanics of the human red blood cell deformed by optical tweezers. J Mech Phys Solids 51:2259–2280

Di Carlo D (2012) A mechanical biomarker of cell state in medicine J Lab Autom, 17(1):32–42

Evans ID, Lips A (1990) Concentration dependence of the linear elastic behaviour of model. Online 86:3413–3417

Evans E, Yeung A (1989) Apparent viscosity and cortical tension of blood granulocytes determined by micropipet aspiration. Biophy J 56:151–160

Forsyth AM, Wan J, Ristenpart WD, Stone HA (2010) The dynamic behavior of chemically "stiffened" red blood cells in microchannel flows. Microvasc Res 80:37–43

Fung YC (1993) Biomechanics: mechanical properties of living tissues, vol 9. Springer, Berlin, pp 1007

Gao Y, Bhattacharya S, Chen X, Barizuddin S, Gangopadhyay S, Gillis KD (2009) A microfluidic cell trap device for automated measurement of quantal catecholamine release from cells. Lab Chip 9:3442–3446

Gossett DR, Tse HTK, Lee SA, Ying Y, Lindgren AG, Yang OO, Rao J, Clark AT, Di Carlo D (2012) Hydrodynamic stretching of single cells for large population mechanical phenotyping. Proc Natl Acad Sci 109:7630–7635

Guck J, Schinkinger S, Lincoln B, Wottawah F, Ebert S, Romeyke M, Lenz D, Erickson HM, Ananthakrishnan R, Mitchell D, Käs J, Ulvick S, Bilby C (2005) Optical deformability as an inherent cell marker for testing malignant transformation and metastatic competence. Biophys J 88:3689–3698

Guillou L, Dahl JB, Lin JMG, Barakat AII, Husson J, Muller SJ, Kumar S (2016) Measuring cell viscoelastic properties using a microfluidic extensional flow device. Biophys J 111:2039–2050

Guo Q, Reiling SJ, Rohrbach P, Ma H (2012) Microfluidic biomechanical assay for red blood cells parasitized by Plasmodium falciparum. Lab Chip 12:1143

Herant M (2005) Mechanics of neutrophil phagocytosis: behavior of the cortical tension. J Cell Sci 118:1789–1797

Hervy M (2010) Modulation of cell structure and function in response to substrate stiffness and external forces. J Adhes Sci Technol 24:963–973

Hochmuth RM (1993) Measuring the mechanical properties of individual human blood cells. J Biomech Eng 115:515–519
Hochmuth RM (2000) Review: micropipette aspiration of living cells. J Biomech 33:15–22
Hou HW, Li QS, Lee GYH, Kumar AP, Ong CN, Lim CT (2009) Deformability study of breast cancer cells using microfluidics. Biomed Microdevices 11:557–564
Hou HW, Lee WC, Leong MC, Sonam S, Vedula SRK, Lim CT (2011) Microfluidics for applications in cell mechanics and mechanobiology. Cell Mol Bioeng 4:591–602
Kamm R, Lammerding J, Mofrad M (2010) Cellular nanomechanics. In: Springer Handbook of Nanotechnology. Springer, Berlin, pp 1171–1200
Lee GYH, Lim CT (2007) Biomechanics approaches to studying human diseases. TRENDS Biotechnol 25:111–118
Lee LM, Liu AP (2015) A microfluidic pipette array for mechanophenotyping of cancer cells and mechanical gating of mechanosensitive channels. Lab Chip 15:264–273
Lee WG, Bang H, Yun H, Lee J, Park J, Kim JK, Chung S, Cho K, Chung C, Han D-C, Chang JK (2007) On-chip erythrocyte deformability test under optical pressure. Lab Chip 7:516
Lee SS, Yim Y, Ahn KH, Lee SJ (2009) Extensional flow-based assessment of red blood cell deformability using hyperbolic converging microchannel. Biomed Microdevices 11:1021–1027
Lemonne N, Lamarre Y, Romana M, Mukisi-Mukaza M, Hardy-Dessources M-D, Tarer V, Mougenel D, Waltz X, Tressières B, Lalanne-Mistrih M-L, Etienne-Julan M, Connes P (2013) Does increased red blood cell deformablity raise the risk for osteonecrosis in sickle cell anemia. Blood 121:3054
Leong FY, Li Q, Lim CT, Chiam KH (2011) Modeling cell entry into a micro-channel. Biomech Model Mechanobiol 10:755–766
Li QS, Lee GYH, Ong CN, Lim CT (2008) AFM indentation study of breast cancer cells. Biochem Biophys Res Commun 374:609–613
Lim CT, Dao M, Suresh S, Sow CH, Chew KT (2004) Large deformation of living cells using laser traps. Acta Mater 52:1837–1845
Luo YN, Chen DY, Zhao Y, Wei C, Zhao XT, Yue WT, Long R, Wang JB, Chen J (2014) A constriction channel based microfluidic system enabling continuous characterization of cellular instantaneous Young's modulus. Sens Actuators B Chem 202:1183–1189
McGrath B, Mealing G, Labrosse MR (2011) A mechanobiological investigation of platelets. Biomech Model Mechanobiol 10:473–484
Mitchison J, Swann M (1954) The mechanical properties of the cell surface II. The unfertilized sea-urchin egg. J Exp Biol 31:461–472
Morrison B, Saatman KE, Meaney DF, Mcintosh TK (1998) In vitro central nervous system models of mechanically induced trauma: a review. J Neurotrauma 15:911–928
Pedrol E, Garcia-Algar M, Massons J, Nazarenus M, Guerrini L, Martínez J, Rodenas A, Fernandez-Carrascal A, Aguiló M, Estevez LG, Calvo I, Olano-Daza A, Garcia-Rico E, Díaz F, Alvarez-Puebla RA (2017) Optofluidic device for the quantification of circulating tumor cells in breast cancer. Sci Rep 7:3677
Radmacher M, Cleveland JP, Fritz M, Hansma HG, Hansma PK (1994) Mapping interaction forces with the atomic force microscope. Biophys J 66:2159–2165
Raj A, Sen AK (2016) Constriction based microfluidic device for cell phenotyping. In: 20th International conference for miniaturized systems for chemistry and life sciences, 9–13 October, Dublin, Ireland
Rodriguez ML, McGarry PJ, Sniadecki NJ (2013) Review on cell mechanics: experimental and modeling approaches. Appl Mech Rev 65:60801
Rosenbluth MJ, Lam WA, Fletcher DA (2006) Force microscopy of nonadherent cells: a comparison of leukemia cell deformability. Biophys J 90:2994–3003
Rosenbluth MJ, Lam A, Fletcher DA (2008) Analyzing cell mechanics in hematologic diseases with microfluidic biophysical flow cytometry. Lab Chip 8. doi:https://doi.org/10.1039/b802931h

Sajeesh P, Doble M, Sen AK (2014) Hydrodynamic resistance and mobility of deformable objects in microfluidic channels. Biomicrofluidics 8:54112

Sajeesh P, Manasi S, Doble M, Sen AK (2015) A microfluidic device with focusing and spacing control for resistance-based sorting of droplets & Cells. Lab Chip 15:3738–3748

Sajeesh P, Raj A, Doble M, Sen AK (2016) Characterization and sorting of cells based on sti ff ness contrast in a micro fluidic channel. RSC Adv 6:74704–74714

Schmid-Schonbein GW, Shih YY, Chien S (1980) Morphometry of human leukocytes. Blood 56:866–876

Shelby JP, White J, Ganesan K, Rathod PK, Chiu DT (2003) A microfluidic model for single-cell capillary obstruction by Plasmodium falciparum-infected erythrocytes. Proc Natl Acad Sci USA 100:14618–14622

Shivhare P, Prabhakar A, Sen AK (2017) Optofluidics based lab on chip device for in situ measurement of mean droplet size and droplet size distribution of an emulsion. J Micromech Microeng 27:035003(9pp)

Suresh S (2007) Biomechanics and biophysics of cancer cells. Acta Biomater 3:413–438

Theret DP, Levesque MJ, Sato M, Nerem RM, Wheeler LT (1988) The application of a homogeneous half-space model in the analysis of endothelial cell micropipette measurements. J Biomech Eng 110:190

Ting-Beall HP, Needham D, Hochmuth RM (1993) Volume and osmotic properties of human neutrophils. Blood 81:2774–2780

Trickey WR, Baaijens FPT, Laursen TA, Alexopoulos LG, Guilak F (2006) Determination of the Poisson's ratio of the cell: recovery properties of chondrocytes after release from complete micropipette aspiration. J Biomech 39:78–87

Tsukada K, Sekizuka E, Oshio C, Minamitani H (2001) Direct measurement of erythrocyte deformability in diabetes mellitus with a transparent microchannel capillary model and high-speed video camera system. Microvasc Res 61:231–239

Vargas-Pinto R, Gong H, Vahabikashi A, Johnson M (2013) The effect of the endothelial cell cortex on atomic force microscopy measurements. Biophys J 105:300–309

Xue C, Wang J, Zhao Y, Chen D, Yue W, Chen J (2015) Constriction channel based single-cell mechanical property characterization. Micromachines 6:1794–1804

Zheng Y, Shojaei-Baghini E, Azad A, Wang C, Sun Y (2012) High-throughput biophysical measurement of human red blood cells. Lab Chip 12:2560

Zheng Y, Nguyen J, Wei Y, Sun Y (2013) Recent advances in microfluidic techniques for single-cell biophysical characterization. Lab Chip 13:2464–2483

Author Index

S. Bhattacharya et al. (eds.), *Environmental, Chemical and Medical Sensors*, Energy, Environment, and Sustainability, https://doi.org/10.1007/978-981-10-7751-7